AN ABSTRACT OF A DISSERTATION

ON-GRID DOUBLY-FED INDUCTION GENERATOR WIND TURBINE WITH NINE-SWITCH CONVERTER AS GRID SIDE CONVERTER FOR LOW VOLTAGE RIDE-THROUGH

Kennedy Adinbo Aganah

Doctor of Philosophy in Engineering

Utility codes for grid-connected Wind Energy Conversion Systems (WECS) have become a standard feature since they are becoming a significant portion of the power grid. However, Doubly-Fed Induction Generators (DFIGs) which make up the bulk of all wind power installations are known to be susceptible to grid disturbances such as voltage sags. In the literature, one of the most robust low voltage ride-through (LVRT) solution for both balanced and unbalanced sags is based on the principle of series voltage compensation used extensively in dynamic voltage restorers (DVRs) and unified power quality conditioner (UPQC) systems. However, the voltage compensation LVRT is expensive as an additional converter is required. This converter however is underutilized idling during normal grid conditions but increases the complexity, cost, size and losses of the entire system.

The component saving topological feature of the Nine-switch converter fits well into this type of application as it reduces cost, size and losses compared to using two classical grid side converters. A detailed mathematical model of the Nine-switch converter is needed to fully utilize the performance advantages of this converter which is virtually nonexistent.

The mathematical model of this converter is derived and its space vector and carrier-based pulse-width modulation methodologies are developed. In addition, as an extension of this converter topology, the model of the generalized 3n+3-switch converter is also presented. It is shown that injecting the neutral voltages of the converter into the modulation signals has a dual role of shaping the modulation scheme as well as ensuring that the switching function constraints of the converter are not violated.

The Nine-switch converter so developed is used for the proposed LVRT for a grid-connected DFIG wind turbine to serve the dual role of parallel grid side and series grid side converters. The principle of ride-through, sag detection, and controllers are described. The controllers are designed based on the stationary reference frame using hybrid proportional and resonance controllers. Operation is demonstrated through simulation and verified by experimentation using a laboratory scale 5-hp wound rotor induction machine and a 5-hp DC machine as the wind turbine emulator.

ON-GRID DOUBLY FED INDUCTION GENERATOR WIND TURBINE WITH

NINE-SWITCH CONVERTER AS GRID SIDE CONVERTER FOR LOW

VOLTAGE RIDE-THROUGH

———————————————————————

A Dissertation

Presented to

the Faculty of the Graduate School

Tennessee Technological University

by

Kennedy Adinbo Aganah

———————————————————————

In Partial Fulfillment

of the Requirements for the Degree

DOCTOR OF PHILOSOPHY

Engineering

———————————————————————

August 2013

CERTIFICATE OF APPROVAL OF DISSERTATION

ON-GRID DOUBLY-FED INDUCTION GENERATOR WIND TURBINE WITH

NINE-SWITCH CONVERTER AS GRID SIDE CONVERTER FOR LOW

VOLTAGE RIDE-THROUGH

by

Kennedy Adinbo Aganah

Graduate Advisory Committee:

_____ _____
Joseph Olorunfemi Ojo, Chairperson　　　Date

_____ _____
Ghadir Radman　　　　　　　　　　　Date

_____ _____
Omar Elkeelany　　　　　　　　　　　Date

_____ _____
Yung-way Liu　　　　　　　　　　　　Date

_____ _____
Ahmed Kamal　　　　　　　　　　　　Date

Approved for the Faculty:

_____
Francis Otuonye
Associate Vice President
for Research and Graduate Studies

_____
Date

DEDICATION

This dissertation is dedicated to my parents, my wife Fawzy, my son Boma, and my brothers Gamel, Tito and Benedict. Thank you for all your support.

ACKNOWLEDGEMENTS

TABLE OF CONTENTS

LIST OF FIGURES

LIST OF TABLES

CHAPTER 1

GENERAL INTRODUCTION

1.1 Background

In time past when wind energy share in the electric power grids were relatively low and insignificant, there were no stringent rules required to connect wind energy conversion systems (WECS) to the grid. In the event of network disturbances, it was acceptable then to disconnect WECS from the grid to protect the wind turbine and the power electronic converters. In doubly-fed induction generator (DFIG) based WECS, this has been achieved by diverting the rotor overcurrent away from the rotor side converter (RSC) using a crowbar circuit connected to the rotor slip ring terminals [1]. However, the past decade has seen rapid development of WECS and its share of the electric grid can no longer be ignored. For example, by the end of 2010, wind power in Denmark covered about 26 percent of total electricity consumption, by far the largest share of any country in the world. Demark is followed by Portugal and Spain with 15 percent, Ireland 13 percent, and Germany 8 percent [2]. In the U.S., wind plants contribute a little over 2 percent of electricity supply but this is expected to reach about 20 percent by 2030 [3]. Figure 1.1 illustrates the wind energy's share of national electricity demand by country.

The rapid increase of installed wind capacity in transmission systems necessitates that WECS stay connected to grid in the event of network disturbances and contribute to system stability after fault clearance [4],[5],[6]. For this reason, regulatory bodies in countries with significant WECS penetrations have issued new grid codes that invariably

require that wind farms remain online during grid disturbances down to a certain percentage of the nominal grid voltage and for a specified time period otherwise known as Low Voltage Ride-Through (LVRT) codes. In the U.S., the Federal Energy Regulatory Commission (FERC) set forth the LVRT requirements depicted graphically in Figure 1.2 [4].
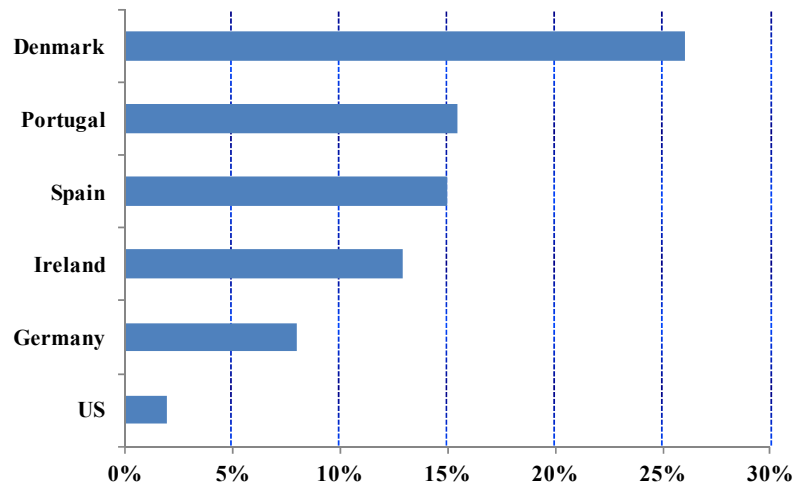
Figure 1.1. Wind energy's share of national electricity demand at end of 2010
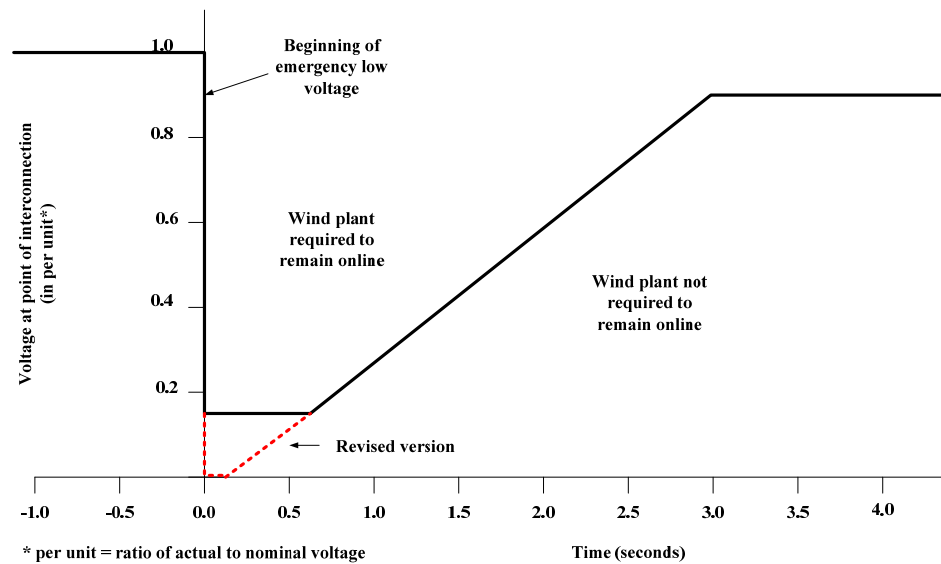
Figure 1.2. U.S. low voltage ride-through standard

However, a joint report of the North American Electric Reliability Council (NERC) and the American Wind Energy Association (AWEA) recommended some revisions to the FERC's LVRT provisions, requiring wind plants to ride-through low voltage sags down to zero up to 9 cycles [5]. Grid code requirements also include fast active and reactive output power restoration to the pre-fault values, after the system voltage returns to normal levels. Most grid codes also impose increased reactive current generation by the wind turbines during the disturbance, in order to support the system voltage [6].

1.2 Wind Turbine Electrical Drivetrain Topologies

Wind turbine systems can be categorized by the type of generator (including power electronics) and by the method of power control into three types: fixed speed (one or two speeds), variable speed with DFIG, and variable speed with synchronous generator and full rated converter. While the market is largely dominated by the DFIG topology, the full converter topology is increasingly gaining ground [7]. The primary reason for the paradigm shift is the advantage of the full converter in grid code compliance and optimized power generation at low wind speeds [8]. A more detailed overview of the three topologies are given in the following subsections.

1.2.1. Fixed Speed Squirrel-Cage Induction Generator

The concept is based on a 'squirrel-cage' induction generator (SCIG) shown in Figure 1.3 (a). The generator rotor is driven by the wind turbine and its stator is directly connected to the grid. The rotation speed can only vary slightly (between 1% and 2%), which is almost "fixed speed" in comparison with other wind turbine concepts. The concept exists both in single speed and double speed versions by changing the number of poles of the stator winding. This type of wind turbine requires part or full reactive power compensation to improve the power factor and the mechanical power may be regulated through an inherent aerodynamic stall characteristic of blades or with active control of blade pitch.

1.2.2. Doubly Fed-Induction Generator (DFIG)

The DFIG topology delivers power to the grid via both the stator and rotor of a wound rotor generator as shown in Figure 1.3 (b). Typically, the generator feeds two-thirds of the nominal power via the directly connected stator and one-third through the rotor connected to the grid via a partially rated power electronic converter. Compared to fixed speed turbines, it enables variable speed operation resulting in an increased kilowatt-hour production. Because of the power electronic converter is rated about one-third of the nominal power, it offers a lower cost solution compared with the full converter topology.
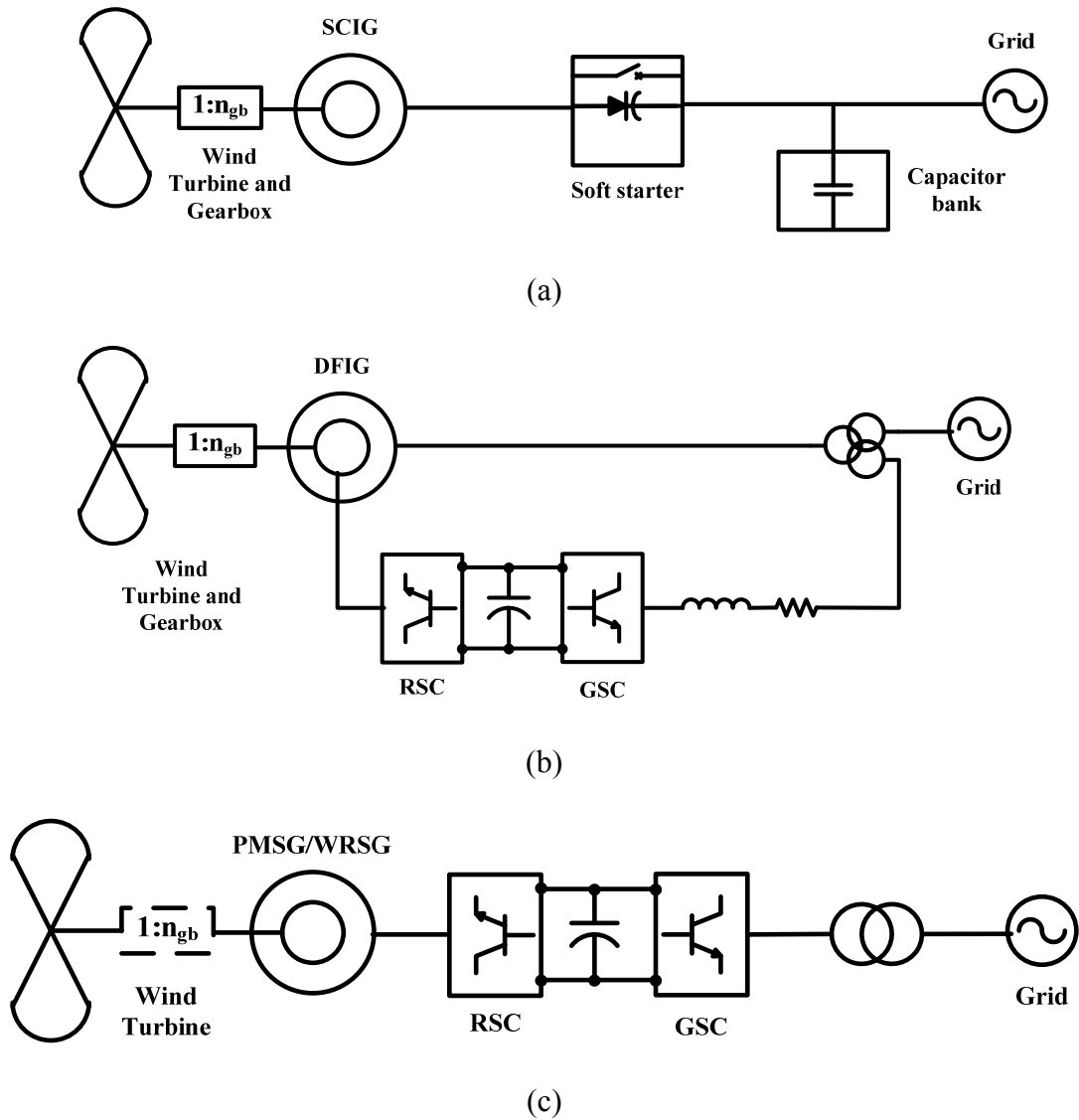
Figure 1.3. Wind turbine electrical drive train topologies: (a) squirrel-cage induction generator, (b) doubly fed-induction generator , and (c) synchronous generator

In terms of grid code compliance, this topology is very sensitive to grid disturbances since the stator is directly connected to the grid and is the primary reason manufacturers are shifting to the full converter topology. The DFIG concept is the main theme in this research.

1.2.3. Synchronous Generator with Full Rated Converter

Various types of generators are being used namely: synchronous generators with wound rotors, and permanent magnet generators as shown in Figure 1.3(c). In this topology the stator is connected to the grid via a full rated power electronic converter and the rotor has excitation windings or permanent magnets. Being completely decoupled from the grid, it can provide an even more wide range of operating speeds than the DFIG type and has a broader range of reactive power and voltage control capabilities.

1.3 Motivation and Objectives

Variable-speed wind turbines equipped with DFIGs are very sensitive to grid disturbances since the stator of the DFIG is directly connected to the grid. Severe grid voltage dips may cause overvoltages and overcurrents in the generator rotor windings that could destroy the partial scale power electronic converter if no external protection schemes are implemented.

In the past before the grid codes were implemented, it was the norm for wind turbine manufacturers to connect an external circuit with anti-parallel thyristors and resistors, known as a "crowbar", to the rotor winding. The crowbar protection then immediately disconnects the rotor-side converter from the rotor winding when grid fault is detected. Therefore, the induced high transient rotor current is diverted through the crowbar circuit away from the converter, protecting it from damage.

This classical rotor crowbar solution does not meet the new grid codes which require wind turbines to ride-through grid faults up to certain minimum time and depth. Moreover, tripping wind turbines by the crowbar may actually worsen the fault condition and contribute to its eventual collapse since DFIG in that configuration acts as a typical squirrel cage induction generator drawing reactive power from the grid.

Several LVRT solutions that meet grid codes with varying degree of success abound in the literature. Most of these ride-through solutions are however suited for balanced and/or shallow sags but fall short when the sag is deep, and/or unbalanced. In practice unbalanced sags occur more frequently than balanced sags, it is therefore imperative to seek solutions for these types of grid sags. One solution that is gaining prominence is the use of voltage source compensators to inject voltage to the DFIG stator immediately sag is detected. It has been found to be a very robust LVRT solution capable of riding through long deep and/or unbalanced sags. A major setback though is the added cost, size and complexity of an extra converter, transformer and other accessories.

The focus of this work is on the use of the Nine-switch converter as a parallel and series connected grid side converter to enable the DFIG wind turbine to ride-through severe balanced and unbalanced voltage sags. The advantages of the Nine-switch converter compared with using the classical topology of two 2-level, three phase converters are its reduced device count and better utilization of converter during normal and sag conditions.

In particular, this dissertation will examine three main research objectives:

- Develop an elaborate mathematical model of the Nine-switch and 12-switch converters;

- Propose a control algorithm that utilizes the Nine-switch converter to assist the DFIG wind turbine to ride-through grid faults;

- Implement the proposed topology and control scheme using a laboratory scale experimental rig.

The first objective is to develop a mathematical model of the Nine-switch converter which will be used as the grid side converter in DFIG-based wind turbine. Detailed space vector pulse-width modulation and carrier-based pulse-width modulation schemes of the Nine-switch converter will be explored. The second objective seeks to prepare an elaborate dynamic model and control scheme of the proposed DFIG-based wind turbine using the Nine-switch converter as the grid side converter. Finally, a laboratory hardware demonstration of the proposed setup would be implemented to validate the theoretical analysis.

1.4 Organization of the Dissertation

The overall structure of this dissertation takes the form of eight (8) chapters, including this introductory chapter. Chapter 2 summarizes the literature review of the state of the art grid voltage ride-through solutions for DFIG-based wind turbine systems. In Chapter 3, the behavior of grid-connected DFIG wind turbine is studied. Vector control and steady-state characteristics are presented.

Chapter 4 looks at the DFIG wind turbine grid interactions and its stability profile. Also presented in this chapter are the effects of errors in machine parameters and angle measurements/estimates on the vector controlled DFIG system. The detail mathematical

modeling of the Nine-switch converter proposed in this dissertation for low voltage ride-through is presented in Chapter 5. The model proposes a space vector and carrier-based pulse-width modulation methods for the converter. This is followed by the model of the 12-switch converter which is an extension of the Nine-switch converter in Chapter 6. As with the Nine-switch, a space vector and carrier-based pulse-width modulation schemes for the converter are derived. The final part of Chapter 6 generalizes the 3n+3-switch converter topology based on the models of the Nine-switch and 12-switch converters.

In Chapter 7, a detailed vector control scheme of a Nine-switch voltage low voltage ride-through of a grid connected DFIG wind turbine is presented. The conclusions and contributions of this dissertation are presented in Chapter 8. Some suggestions for future work are also provided.

CHAPTER 2

LITERATURE REVIEW

2.1 Grid Faults

The Doubly-Fed Induction Generator (DFIG) has been the dominant player in the wind power industry but is recently losing its place in new installations primarily due to its vulnerability to grid disturbances. For the avoidance of doubt, this study will focus on faults that originate from the grid. The main causes of voltage dips at the terminals of wind power plant are short circuits or overload somewhere in the grid. These short circuits may be caused by lightning strikes, falling objects, animals, fire, explosions, ice, etc.

In a three-phase power system, a number of different fault types can occur: single-phase-to-ground, phase-to-phase, two-phase-to-ground and three-phase faults. The faults may be balanced or unbalanced depending on the cause. If the remnant three phase voltages are equal in magnitude with the phase angles shifted by 120° as in the normal grid conditions, then a balanced (symmetrical) fault is the result. These types of faults are usually the result of a three-phase fault. It can be shown that this type of fault has the most severe effect on the grid but has the least effect on the wind plant [4]. It therefore makes sense that grid codes requirements are based on symmetrical three phase faults even though statistics show that they constitute only about 3-5% of all grid faults [13].

On the other hand, in the majority of faults the individual phase voltages are different or the phase relationship is other than 120°, and are therefore considered

unbalanced (asymmetrical). The majority of these faults are caused by single-phase-to-ground faults and in some cases by phase-to-phase, or two-phase-to-ground faults. Statistics show that unbalanced faults constitute about 74 - 95% of all fault types and their effects on the grid are less severe but are however much more detrimental to the wind plant when compared to balanced three-phase faults [13].

References [8] and [9] show that voltage sags experienced by three-phase loads can be classified into four types, denoted as A, B, C, and D. The phasor expressions of each type are given below where h ($0 \leq h \leq 1$) is the sag magnitude or depth and V is the nominal pre-fault voltage. Sag type A is symmetrical, whereas types B, C and D are unsymmetrical sags. For sag type B only one phasor drops in magnitude. For sag types C and D, two phasors drop in magnitude and change in phase angle.

Type A : $v_a = hV$, $v_b = -\frac{1}{2}hV - j\frac{\sqrt{3}}{2}hV$, $v_c = -\frac{1}{2}hV + j\frac{\sqrt{3}}{2}hV$

Type B : $v_a = hV$, $v_b = -\frac{1}{2}V - j\frac{\sqrt{3}}{2}V$, $v_c = -\frac{1}{2}V + j\frac{\sqrt{3}}{2}V$

Type C : $v_a = V$, $v_b = -\frac{1}{2}V - j\frac{\sqrt{3}}{2}hV$, $v_c = -\frac{1}{2}V + j\frac{\sqrt{3}}{2}hV$

Type D : $v_a = V$, $v_b = -\frac{1}{2}hV - j\frac{\sqrt{3}}{2}V$, $v_c = -\frac{1}{2}hV + j\frac{\sqrt{3}}{2}V$

In this research, both balanced and unbalanced sags appearing at the point of common coupling (PCC) would be considered.

2.2 State of the Art DFIG Wind Turbine Low Voltage Ride-Through

As pointed out in the previous section, actual grid codes only specify for symmetrical faults because they affect more severely the grid stability but are known to occur least frequently [4]. On the other hand, asymmetrical faults are more problematic particularly for the DFIGs even if they are less severe on the grid [11].

The magnetic flux of an induction machine may be divided into two components; "forced flux" that rotates at synchronous speed and is related to the stator voltage and the "natural flux" that only appears during voltage transients [12]. The natural flux unlike the forced flux does not rotate and has been shown to be the cause of high overcurrents (and overvoltages) in the rotor if the control system is unable to deal effectively with it [12], [13], and [14]. In the event of a sudden dip in the stator voltage, stator flux being a state variable cannot change instantaneously and so the natural flux (or DC flux) appears to guarantee that there are no discontinuities. The rotor however keeps running and high slip is generated that causes overvoltage and overcurrent in the rotor circuits due to the effect of speed and voltage. Asymmetrical faults create higher over-current and over-voltages in the rotor because a negative sequence component exists in the stator voltage and the slip of this negative sequence is very high [15], [16], [17]. The excess current may damage the power converters and the overvoltage may damage the rotor of the generator. A protection scheme is imperative to protect the power converter connected to the rotor from these overvoltages and overcurrents. The excess current in the rotor also increases the voltage in the DC bus [17], [18] as well as increases oscillations in the active and reactive power of the machine [15], [18].

12

Several researchers have proposed different techniques to meet LVRT requirements. However, majority of these techniques rely on a rotor crowbar circuit that creates a by-pass to divert the high rotor currents from the power electronics converters. More recent LVRT solutions rely on modifications to the Rotor Side Converter (RSC) controller to limit the rotor currents while others employ voltage compensation to meet LVRT requirements. These solutions are discussed in the ensuing sections.

2.2.1. Rotor Crowbar

The rotor crowbar circuit shown in the Figure 2.1 is the simplest technique used to protect the rotor side converter (RSC) during grid disturbances. The crowbar is basically used to divert rotor over currents away from the RSC upon detection of grid fault. However, new grid code requirements for LVRT means it is no longer acceptable to just direct over currents away from the RSC, and thereby disenabling the RSC control. Not only is the active and reactive power control lost, the DFIG in such configuration runs as a squirrel cage machine absorbing reactive power from the grid. This is counterproductive as it worsens the fault condition. Several modifications have therefore been made to the simple crowbar circuit to comply with LVRT requirements [18], [19], [20], and [21].

In [22], the authors propose a three-phase resistive by pass circuit connected to the rotor circuit via thyistors to limit high current in the rotor. This topology is shown to be capable of riding through a 15% voltage dip for 200ms. The authors in [20] demonstrate that low crowbar resistance leads to high electrical torque, overcurrents, and
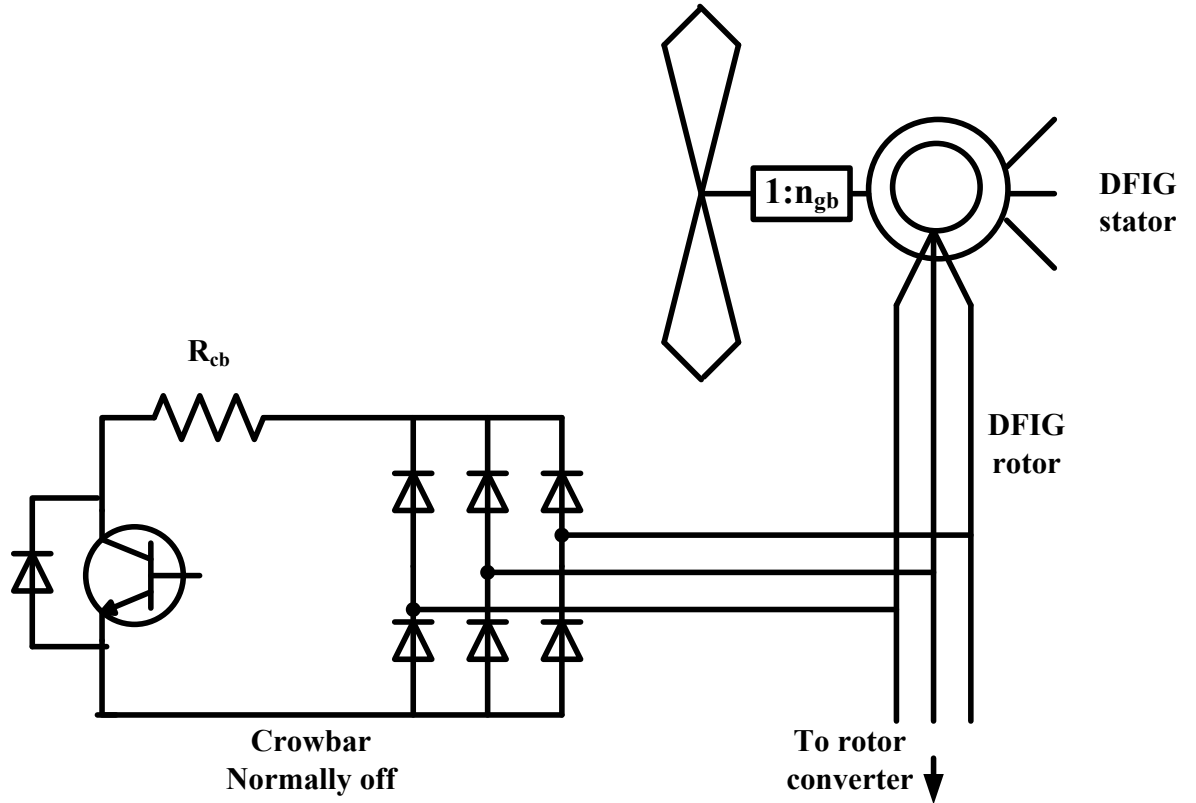
Figure 2.1. Crowbar circuit ([21])

low rotor voltage whereas, high crowbar resistance results in lower electrical torque and rotor currents but also higher rotor voltage.

Reference [20] therefore proposes an optimal crowbar of approximately 200 times the normal rotor resistance. Notwithstanding, the optimal crowbar resistance still results in torque pulsations of the order of 5 p.u. and anytime the crowbar engages the DFIG runs as a squirrel-cage machine absorbing reactive power from the grid and thereby worsening the fault condition. In such a situation, one would have expected the Grid Side Converter (GSC) to provide the required reactive power to support the grid. Unfortunately however, the GSC is limited in the amount of reactive power it can generate and may not generate adequate reactive power needed. Other modifications of

the crowbar can be found in [18], [19],[21]. In [19] the crowbar thyristors are replaced with PWM modulated IGBT bridge enabling the DC bus control. Simulations of this control algorithm shows it can withstand 80 percent voltage dip for 500 ms. G. Pannell et.al [21] improves the LVRT performance of a 7.5 kW DFIG-Based wind turbine by minimizing the crowbar application periods to about 11-16 ms and experimental results show the LVRT technique is capable of riding through a 15 percent voltage for 500 ms and a zero percent voltage for 140 ms.

2.2.2. Modified Rotor Side Converter Control

Increasingly, more LVRT approaches focus on limiting the rotor currents during grid disturbances by modifying the RSC control without additional hardware components. In [23], and [24], the RSC is protected by using measured stator currents as references for the rotor current controllers. The LVRT solution presented in [23] is shown to support a 12.5% symmetrical voltage dip of 400ms duration. The limitation of the stator current feedback solution lies in the fact that the RSC voltage must be at least be as high as the maximum rotor voltage during voltage dip to maintain current controllability, otherwise in the event of deep voltage dips, additional hardware protection is required. Lima et al. [24] demonstrated that the maximum voltage dip that can be withstood by the WECS without exceeding the rotor voltage limit depends on the machine slip and the depth of the voltage dip. Thus it is possible to predict the performance of the DFIG under various faults situations, a requisite of most grid codes.

Other modified RSC control schemes propose injecting a current into the rotor that is 180 degrees out of phase with the natural stator flux in other to weaken its effect on the rotor [13], [25]. In [13], the rotor current is used to cancel both the DC and the negative sequence components of the stator flux linkage. The authors recommend canceling 60% of the negative sequence component of the stator flux linkage and the remainder of the current capability is used to deal with the DC component in the stator flux linkage. The control objective is to constrain the instantaneous rotor current to below 2.0 p.u., while the converter DC link voltage is also maintained below the device's voltage rating thus producing a feasible DFIG ride-through region. Increased machine leakage inductances broaden these feasible ride-through regions. However, these feasible regions are system specific and have to be revised when systems have different current and voltage ratings.

In the conventional RSC control, if the stator resistance is considered to be small (especially true for large generators), the angle between stator-flux and stator voltage orientations is extremely small and can be neglected [33]. This assumption is quite satisfactory for decoupled active and reactive power control purposes in normal operating conditions. However, under grid faults, this assumption fails and any control based on the above assumption is bound to be erroneous. Liang et al. [24], based on the DFIG transient model, propose an additional feed-forward stator transient term added to the output of the RSC current controller. This feed-forward injection of the transient terms reflects in minimum transient current in the rotor circuit. The authors demonstrate with a 3.6 MW, 4.16 kV DFIG experimental rig that this method is able to ride-through a 0.15 p.u. for 625 ms.

2.2.3. Passive Impedance Network

This method offers a simple, low cost LVRT technology. A passive impedance network is connected in series with the stator circuit during grid disturbances to suppress undesirable stator flux transients [25], [26] and [27]. The WECS connected to the grid may be thought of as two separate Thevenin's equivalent circuits connected to each other through an impedance representing transformer and line impedance as illustrated in Figure 2.2. In the event of a grid fault, an equivalent impedance can be inserted in series with the stator instantaneously. Ideally, the stator flux, stator and rotor currents as well as the torque will stay the same. The inserted impedance is designed as a constant value and should provide ride-though capabilities for all fault types and up to zero volts at the PCC. Ideally, this topology should compensate for the sag as long as it lasts.
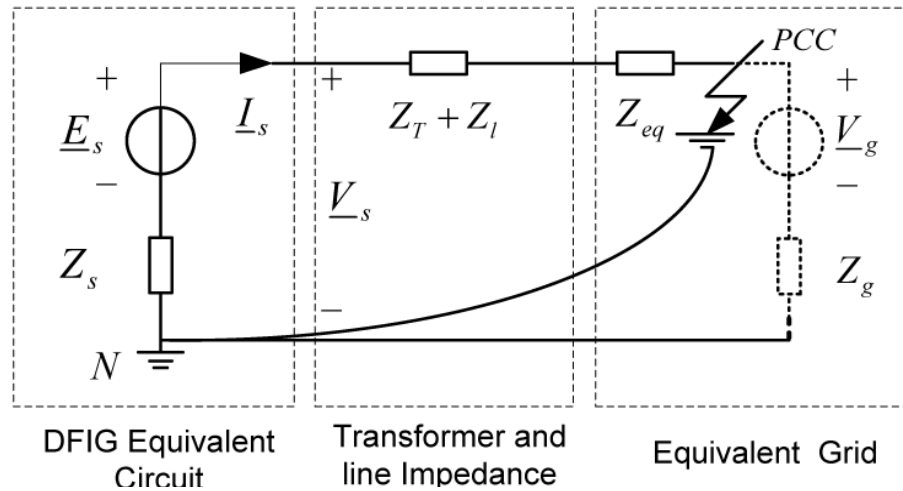
Figure 2.2. Single-phase simplified equivalent circuit of DFIG wind turbine with passive-impedance networks [26]

2.2.4. Voltage Compensation

A perfect solution for a sensitive load (DFIG in this case) during grid disturbances would be to isolate the load from the disturbance. One such solution is to compensate for the voltage dip almost instantaneously. This can be done using series converters such as dynamic voltage restorers (DVRs) [23], [30]-[34]. DVRs are basically voltage source converters (VSCs) that add voltage at the point where they are connected in order to compensate for the voltage dip.

Traditionally, the GSC is connected to the grid in a shunt configuration also known as Parallel Grid Side Converter (PGSC) as illustrated in Figure 2.3(a). What this shunt configuration does is to inject current into the grid. On the other hand, if the GSC is connected in series with the grid (known as Series Grid Side Converter, SGSC) as shown in Figure 2.3(b), the generator stator voltage is effectively the sum of the grid and converter voltages. In the event of a grid disturbance, the series converter voltage is utilized to compensate for the stator flux. This was first proposed for LVRT in DFIG-based WECS in [35] and revealed an excellent LVRT potential but suffers from increased power losses and thus reduced power processing efficiency. A number of modifications have been made to this topology. In [36], the authors present a unified (series- and shunt-connected GSCs) configuration that is extremely robust to balanced voltage dips to as much as 100 percent dip that lasts for 150 ms. A similar unified converter topology is reported in [37] for unbalanced voltage dips and the system shows good tolerance to grid disturbances. A modified version of the unified topology presented in [36],[37] is proposed in [32]. Liao et al. [32] argue that, the solution for unbalanced voltage dips

presented in [37] is insufficient for large megawatt turbines with large stator time constants. During severe voltage dips, [37] proposed controlling the negative sequence component of the stator flux to zero to reject the undesirable effect on the rotor side while the positive sequence component of the stator flux is scaled in proportion to the positive component of the remaining grid flux to eliminate the transient DC flux component and prevent excess active power flowing into the DC bus.

(a)

(b)
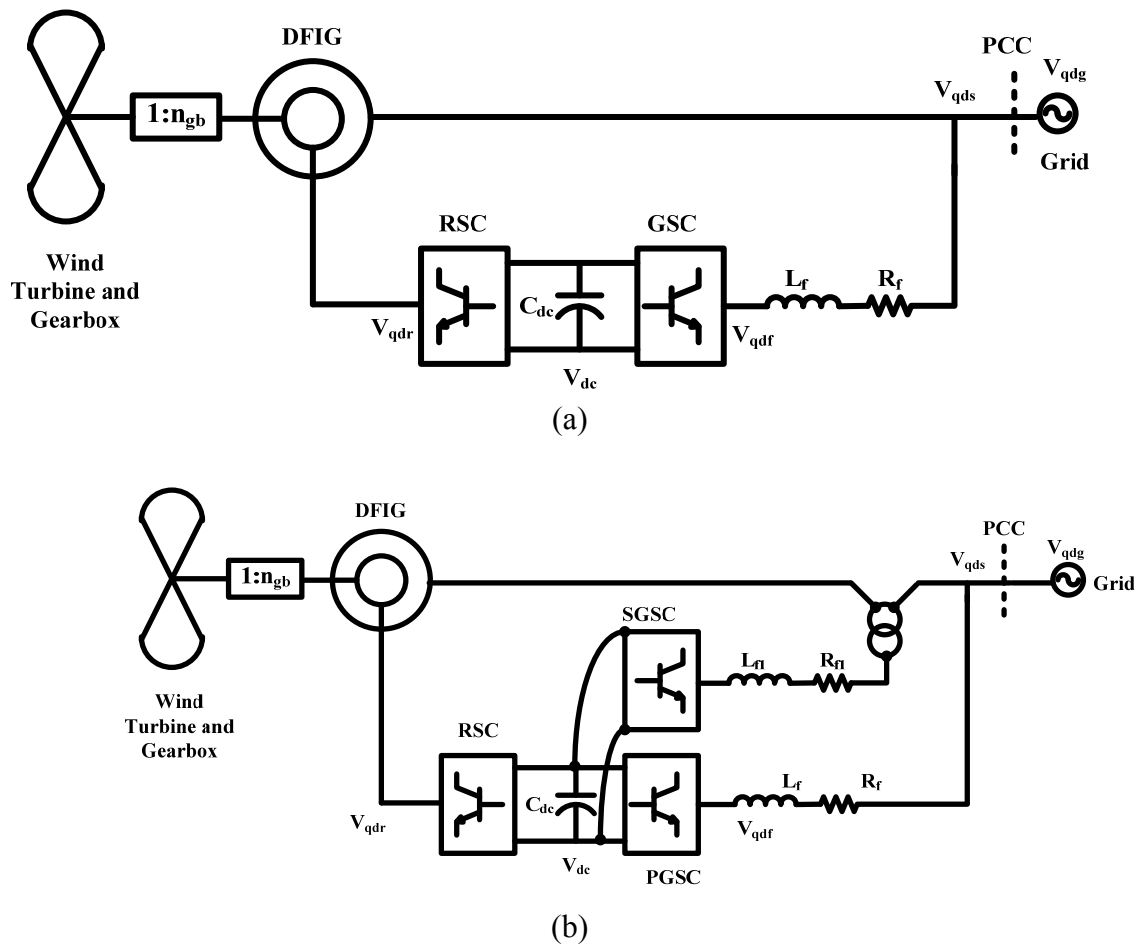
Figure 2.3. Parallel- and series-connected converters for DFIG-based WECS

However, since the transient DC flux is not directly controlled and requires a properly tuned stator flux controller to avoid its appearance, once it appears (due to an improperly tuned controller), it can only be damped with the stator time constant which in relatively large wind turbines may be in the order of 1000ms. To overcome this drawback, the authors in [32] propose a direct control of the transient DC flux component to zero. In addition, the active power output of the DFIG is controlled to zero through the RSC to maintain the DC link voltage within its safe limit and to further reduce the stator and rotor currents.

While the above solutions result in robust performance of the system during deep sags, it ultimately adds to the cost and complexity of the system. The extra series converter is underutilized since it is idling most of the time and it is only activated when a grid fault is detected.

It is obvious that the longer (and deeper) the voltage sag, the larger the compensator energy storage capacity required resulting in expensive and bulky energy storage element. As pointed out in [14], the power rating of SGSC converter is sized bigger (about 15 percent) than its shunt counterpart in order to meet ride-through requirements of the worst case sags. Hence it becomes important to consider solutions that will reduce the size of the energy storage element and injection transformer that are usually used to interface SGSC to the grid.

Recently, some researchers have shown that the stator voltage need not be 100 percent compensated during the entire period of the fault. Abdal-Baqi et al. [38],[39] demonstrated this using a decaying injected voltage and with time constant less than the stator time constant while still keeping rotor currents within its limits. Zhang et al. [33]

adopted ramp function injection method for the series compensator. Since the energy that is being delivered during the short circuit is proportional to the stator voltage, the required size of the energy storage capacitor (along with converter power rating and series transformer size) is decreased due to smaller stator voltage. This is achieved by keeping the frequency of the exponentially decaying compensated voltage the same as the grid frequency during the short circuit. This allows for the stator flux to rotate with its initial speed during the short circuit and results in keeping the rotor circuit voltage due to the stator flux same as its value during normal operation. Another solution to reduce the power rating of the DVR is to reduce the stator power reference during faults in addition to using pitch angle control system to counter generator over-speeding and stabilize operation of wind turbine system[31]. The drawback is the response time of pitch angle system is very slow in comparison with the electrical control system.

A limitation of the DVR solution is the assumption of an ideal injection transformer. A series injection transformer may suffer from magnetic flux saturation [40], leading to overcurrents. Voltage compensation as described above is done using the conventional back-to-back Voltage Source Converters (VSCs) configuration shown in Figure 2.4 (a). In spite of their popularity, DVRs with the back-to-back VSCs are extremely underutilized even though they offer independent control of two decoupled converters.

Recently some researchers have shown keen interest in the Nine-switch converter shown in Figure 2.4(b) as an alternative to the conventional back-to-back VSC. It has shown good performance in the independent control of two three-phase AC loads [43], [44], [45], [46] and has been used as a unified power quality conditioner (UPQC) in [47]

21

(a)

(b)
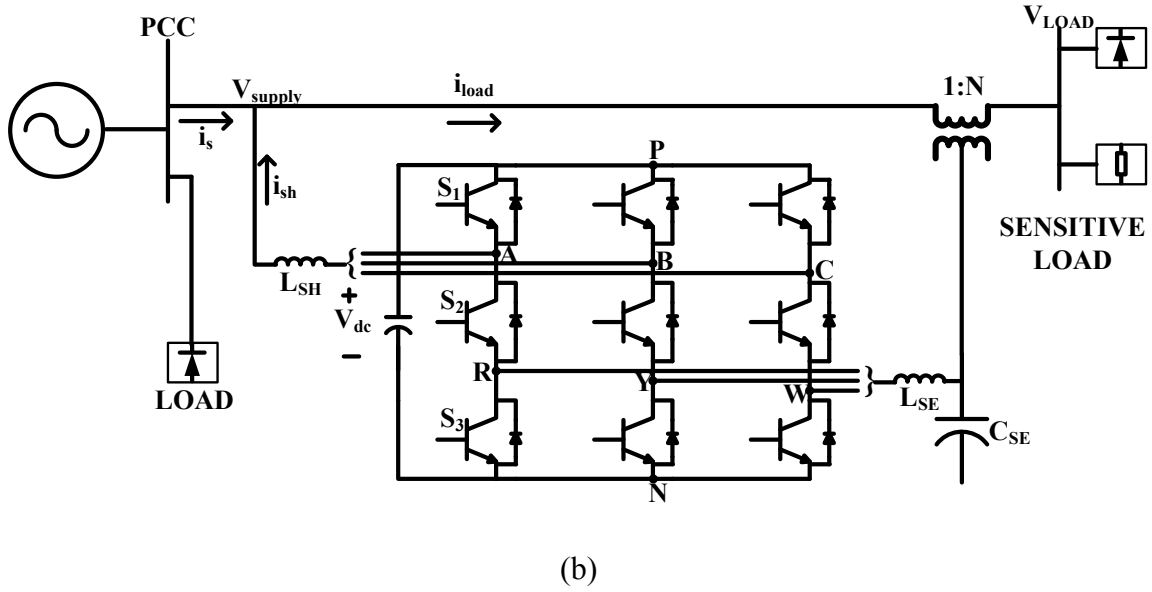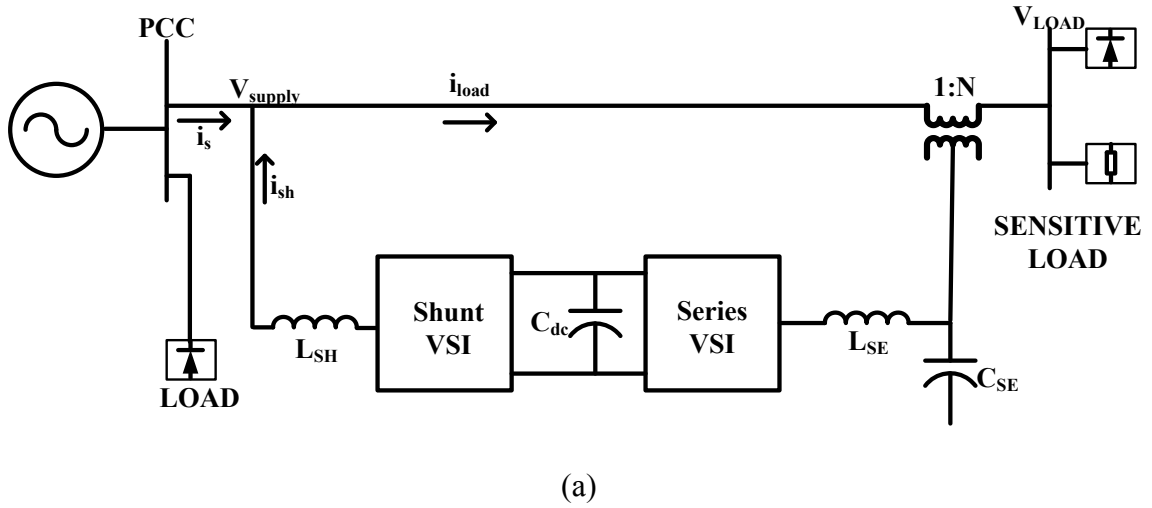
Figure 2.4. Schematics of power conditioner system using (a) back-to-back converters and (b) Nine-switch converter.

and [48]. The Nine-switch converter has the advantage of reduced switch count compared to the conventional back-to-back VSCs. However, it requires a higher rated DC bus capacitor to produce the same output voltages compared to using two 2-level VSCs [43], [47].This might over shadow the gains that come with its reduced component count as the switching devices may be unduly over stressed. The advantage in the Nine-switch

converter lies in its auto-complementary tuning of the shunt and series converters under both normal and sag operating conditions. That is under normal operating conditions, the shunt converter is modulated to give its maximum output and the complementary series converter output is kept almost zero. On the other hand, in voltage sag conditions, a larger output voltage is needed at the series converter output and therefore it can be modulated to give a higher output voltage and consequently a small complementary voltage appears at the shunt output.

Experimental results in [48] show that a load protected by this UPQC is very immune to 20% balanced voltage sag and the DC bus voltage is merely 8% higher than that of the back-to-back converter. So far, however, there has been little discussion on the theoretical foundation of the Nine-switch converter and its application to LVRT in wind applications to the best of author's knowledge has not been investigated. The main thrust in this research is therefore to investigate the application of the Nine-switch converter for DFIG wind turbine LVRT.

CHAPTER 3

MODELING THE BEHAVIOUR OF ON-GRID DFIG WIND TURBINE

3.1 DFIG Wind Turbine Model

The Doubly-Fed Induction Generator (DFIG) is currently the most widely installed generator type for WECS. It has the advantage of sizing the power converter to handle only a fraction of the wind turbine power. This lowers the size, cost, and losses of the power converter compared to using a full rated converter in the case of a synchronous generator. A typical DFIG-based WECS comprises, the wind turbine (including gearbox), DFIG, and power electronics converters connected to the grid as shown in Figure 3.1. In the following sections, detailed mathematical models of each component are described.
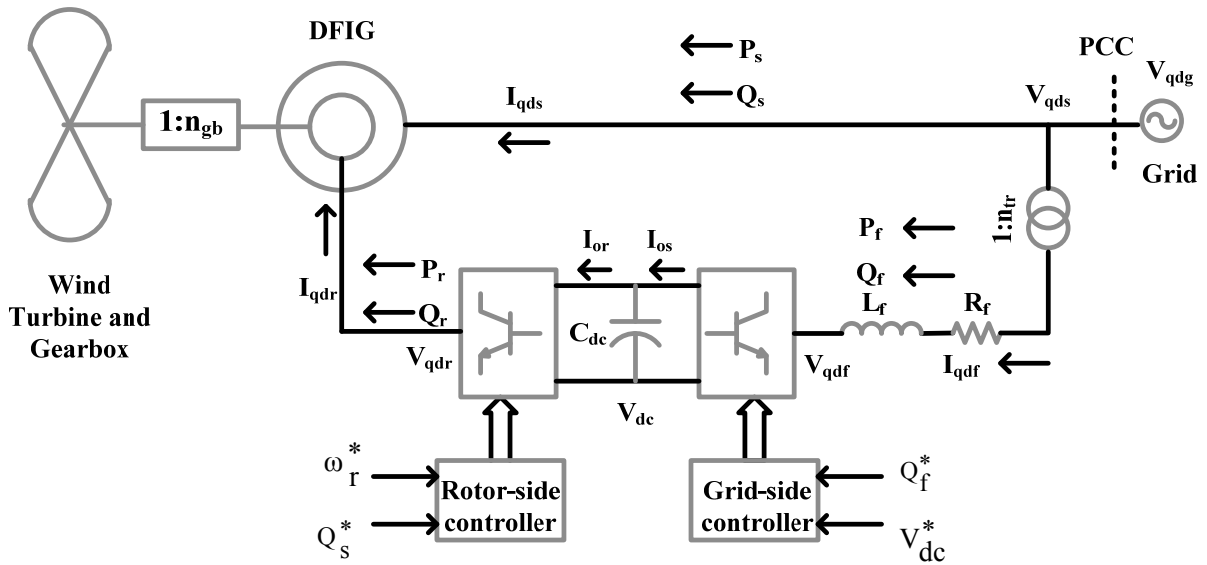
Figure 3.1. Schematic of on-grid DFIG wind turbine system

3.1.1. Wind Turbine Drive Train

A brief introduction of the basics of the mechanics of vibrations is outlined here to help understand the dynamics of the wind turbine. The simplest model of rotary oscillation due to torsional deformation of a shaft is shown in Figure 3.2 (a), in which an elastic circular shaft is rigidly attached to a support at one end and carries an inertia disk at the other end. An equivalent representation of this model, Figure 3.2 (b), consists of a spring (a means of storing potential energy), a mass or inertia (a means of storing kinetic energy), and a damper (a means of dissipating energy) [58].

When an external force is applied to the disk, an equal and opposite internal reaction torque exists due to the torsional shear-stress in the shaft. If the external force is suddenly removed, the system will oscillate back and forth transferring its potential energy into kinetic energy and vice versa and in the process dissipate some of its energy in the form of heat, sound, etc. By considering the free-body diagram of the system,
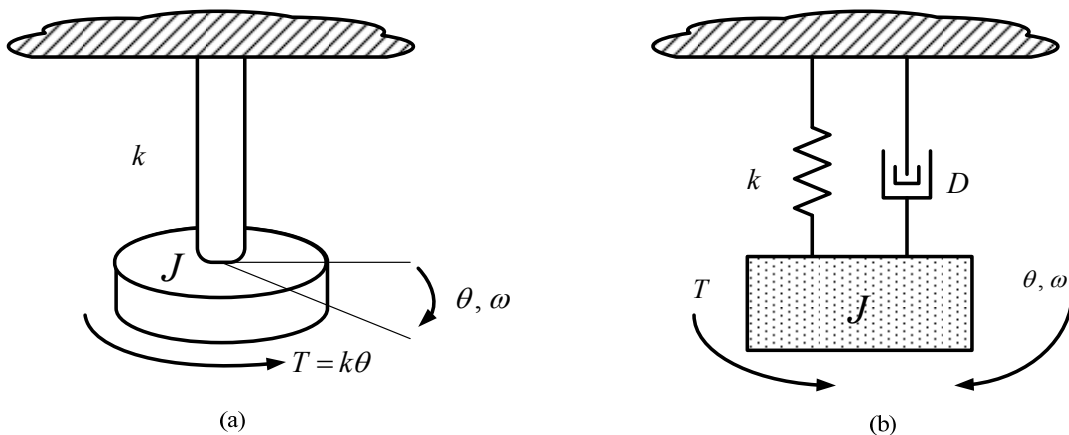
Figure 3.2. Elementary parts of a vibrating system

Figure 3.2, the equation of motion is obtained by applying Newton's second law of motion:

$$Jp\omega = f(t) - k\theta - D\omega$$
$$p\theta = \omega$$

(3.1)

where J is the moment inertia of the disk, k is the spring torsional constant or stiffness, ω is the angular frequency of vibration, θ represents the angle of twist of the shaft, D is the damping coefficient, $p = \dfrac{d}{dt}$ and $f(t)$ is the externally applied force.

The model of the single mass system above can be extended to 'n' interconnected rotating masses. To model such a system, we first look at the equivalent system in terms of spring stiffness and the damping coefficients. When two springs are connected in parallel, as shown in Figure 3.3 (a), their equivalent stiffness is given by [59]

$$k_{eq} = k_1 + k_2,$$

(3.2)

In general, when there are n springs in parallel, Figure 3.3 (b), each of stiffness k_j, their equivalent spring stiffness is given by their summation, that is

$$k_{eq} = \sum_{j=1}^{n} k_j = k_1 + k_2 + k_3 + \ldots + k_n,$$

(3.3)

If however, the springs are connected in series, Figure 3.3 (c), the expression of their equivalent spring stiffness is represented by

$$\frac{1}{k_{eq}} = \sum_{i=1}^{n} \frac{1}{k_i} = \frac{1}{k_1} + \frac{1}{k_2} + \frac{1}{k_3} + \ldots + \frac{1}{k_n},$$

(3.4)

It can be shown that the equivalent dampers act in the same way as the springs. That is, the equivalent parallel and series n-connected dampers are respectively given by (3.5) and (3.6).

$$D_{eq} = \sum_{j=1}^{n} D_j = D_1 + D_2 + D_3 + \dots + D_n \qquad (3.5)$$

$$\frac{1}{D_{eq}} = \sum_{i=1}^{n} \frac{1}{D_i} = \frac{1}{D_1} + \frac{1}{D_2} + \frac{1}{D_3} + \dots + \frac{1}{D_n}, \qquad (3.6)$$

In mechanical systems, gears are frequently used to increase, or reduce shaft speed. When a torsional system is interconnected by a set of gears, Figure 3.4, the inertia disks do not operate at the same angular speed throughout the system. In that case, the actual inertias, spring constants, damping coefficients, etc, would have to be referred to one reference speed of rotation. It can be shown that this transformation is given by [60]

$$\frac{\omega_1}{\omega_2} = \frac{T_2}{T_1} = \frac{n_2}{n_1} = n_{gb}, \qquad \frac{J_1'}{J_1} = \frac{k_1'}{k_1} = \frac{D_1'}{D_1} = \frac{1}{n_{gb}^2}, \qquad (3.7)$$

where , the apostrophe (') indicates referred variables and those without the apostrophe indicates actual variables; n_1, n_2 are the number of teeth of input and output gears; T_1, T_2 are the corresponding torques applied to the gears.
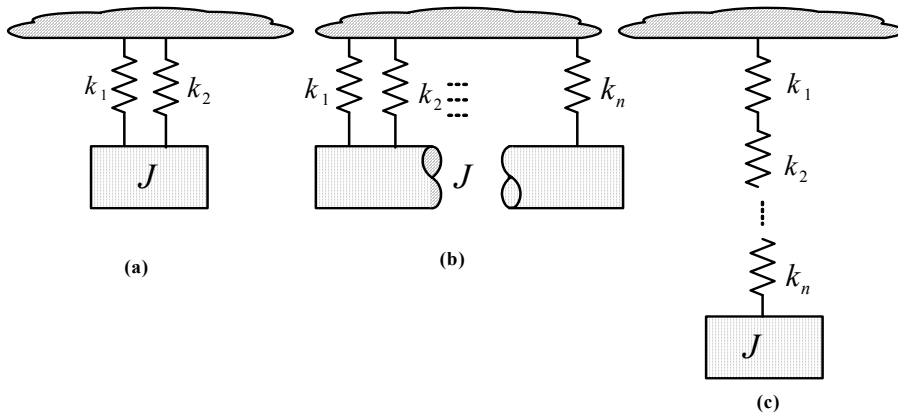
Figure 3.3. Equivalent model of n-connected springs (a) parallel, and (b) series
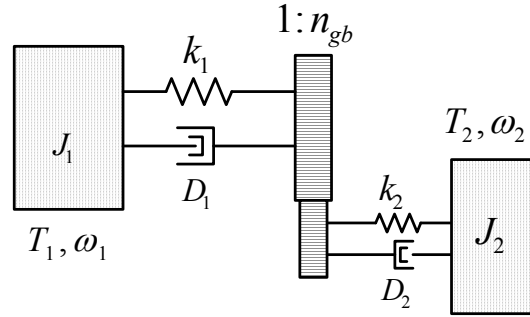
Figure 3.4. Schematic diagram of two inertias interconnected by gears

The wind turbine drive train is a much more complex interconnected system than the examples described above but can simplified into a six-lumped mass model as shown in Figure 3.5 [72]. It consists of the blades, hub, low-speed shaft, gearbox, high-speed shaft and generator rotor. However, the six-mass equivalent is unwieldy and not suitable for control algorithms. The rotating mass may be further lumped into three-lumped, two-lumped or one-lumped mass equivalent models as shown in Figure 3.6. In the three-mass model, the first mass represents the rotor blades; the second represents the hub while the third mass represents the lumped mass of the generator including gearbox, high-speed shafts and generator shaft. The three-mass model can be reduced to a two-mass model by considering an equivalent system with an equivalent stiffness and damping factor.

The moment of inertia for the shafts and the gearbox wheels can be neglected because they are small compared with the moment of inertia of the wind turbine or generator. Therefore the resultant model is essentially a two mass model connected by a flexible shaft. Only the gearbox ratio has influence on the new equivalent system. When the stiffness and the damping factor are neglected, the two-mass model can be reduced to a one-mass model. The dynamic equations describing these equivalent models are given by (3.8) - (3.16).
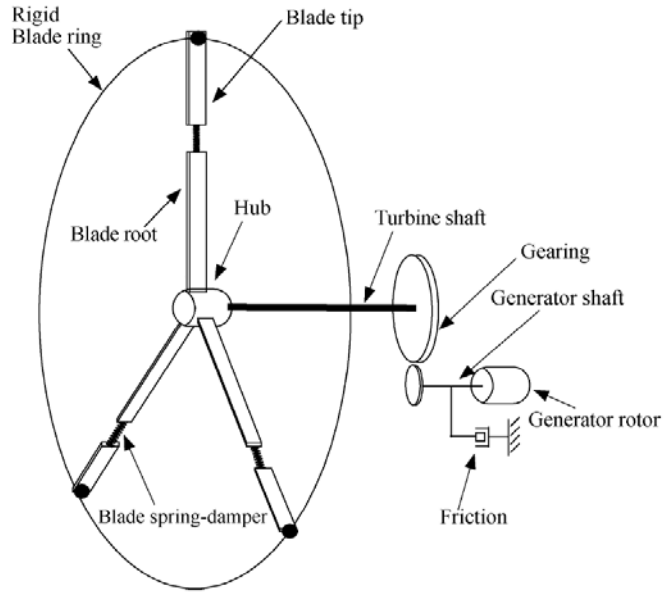
Figure 3.5. Schematic of DFIG wind turbine drive train [72]

(a)

(b)

(c)
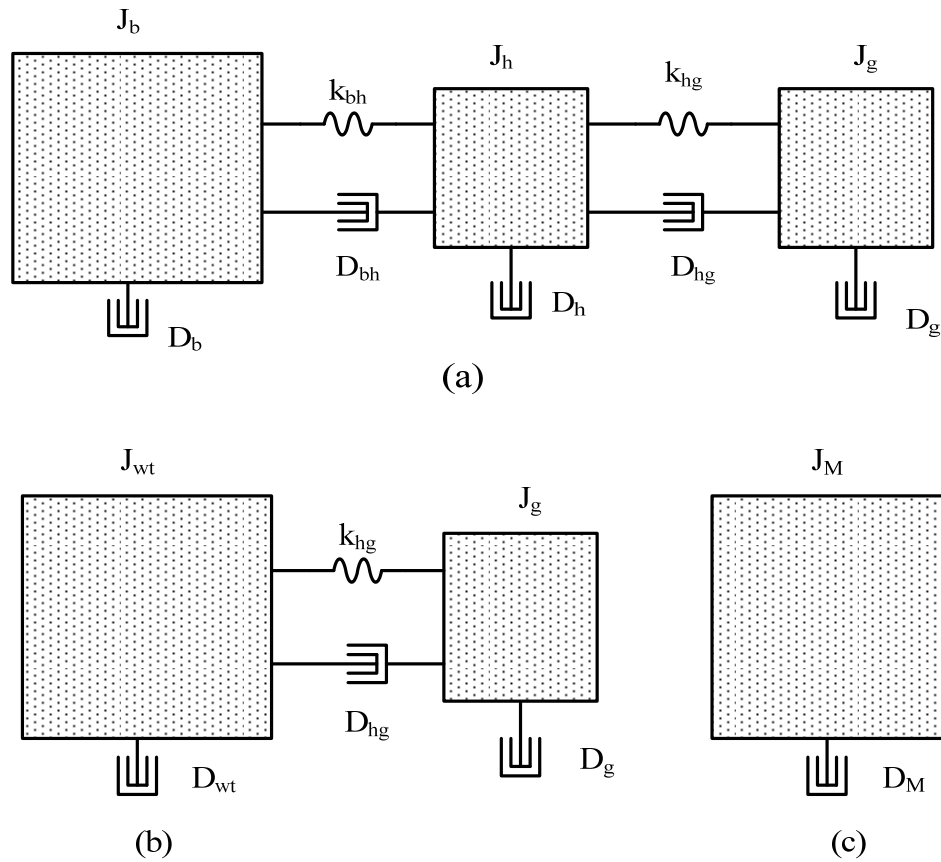
Figure 3.6. Schematic diagram of the equivalent (a) three-mass, (b) two-mass, and (c) one-mass DFIG wind turbine drive train

The dynamic equations of the three-mass model, Figure 3.6 (a), with the low speed side variables referred to the high speed side are as follows [72]:

$$J_b' p\omega_b' = T_m' - k_{bh}' \theta_{bh}' - D_{bh}' (\omega_b' - \omega_h') - D_b' \omega_b' \;,$$
(3.8)

$$J_h' p\omega_h' = k_{bh}' \theta_{bh}' - k_{hg}' \theta_{hg}' + D_{bh}' (\omega_b' - \omega_h') - D_{hg}' (\omega_h' - \omega_g) - D_h' \omega_h'$$
(3.9)

$$J_g p\omega_g = k_{hg}' \theta_{hg}' - T_e + D_{hg}' (\omega_h' - \omega_g) - D_g \omega_g$$
(3.10)

$$p\theta_{bh}' = (\omega_b' - \omega_h')$$
(3.11)

$$p\theta_{hg}' = (\omega_h' - \omega_g)$$
(3.12)

where

$$J_b' = J_b / n_{gb}^2, \; J_h' = J_h / n_{gb}^2, \; k'_{bh} = k_{bh} / n_{gb}^2, \; k'_{hg} = k_{hg} / n_{gb}^2,$$

$$D'_{bh} = D_{bh} / n_{gb}^2, \; D'_b = D_b / n_{gb}^2, \; D'_h = D_h / n_{gb}^2, D'_{hg} = D_{hg} / n_{gb}^2$$

$$\theta_{bh}' = n_{gb} \theta_{bh}, \; \theta_{hg}' = n_{gb} \theta_{hg}, \; \omega_b' = n_{gb} \omega_b, \; \omega_h' = n_{gb} \omega_h, \; T'_m = T_m / n_{gb}$$

In (3.8) – (3.12) above ω_b, ω_h, ω_g are the blade, hub and generator angular speeds respectively; J_b, J_h, J_g are the equivalent inertias of the blade, hub and generator rotor respectively; D_b, D_h, D_g are the damping coefficient of the blade, hub and generator rotor respectively; θ_{bh} is the angle between the blade and hub and θ_{hg} is the angle between the hub and generator rotor; k_{bh}, k_{hg} are the stiffness of the blade and low-speed shaft respectively; T_m is the aerodynamic torque; and T_e is the electromagnetic torque. The apostrophe indicates variables that are referred to the high speed shaft.

The differential equations for the two-mass model, Figure 3.6 (b), are:

$$J_{wt}' p\omega_{wt}' = T_m' - k_{hg}' \theta_{hg}' - D_{hg}' (\omega_{wt}' - \omega_g) - D_{wt}' \omega_{wt}'$$
(3.13)

$$J_g p\omega_g = k_{hg}' \theta_{hg}' - T_e + D_{hg}' (\omega_{wt}' - \omega_g) - D_g \omega_g$$
(3.14)

$$p\theta_{hg}' = \omega_0 (\omega_{wt}' - \omega_g)$$
(3.15)

where $J_{wt} = J_b + J_h$ is the wind turbine inertia and ω_{wt} is the wind turbine rotor speed. k and D are the relevant drive train stiffness and damping coefficients respectively.

The commonly used one-mass model lumps all rotating masses into one equivalent mass for the drive train. The differential equation is given by

$$J'_M \, p\omega'_M = T'_m - T_e - D'_M \omega'_M \qquad (3.16)$$

where $J_M = J_b + J_h + J_g$ is the equivalent inertia for all rotating masses; ω_M and D_M are respectively the rotor speed and damping coefficient of the equivalent mass. The aerodynamic torque, T_m and the wind turbine power coefficient are defined by the following expressions [72]:

$$T_m = \frac{1}{2} \frac{\rho \pi R^2 C_p(\lambda, \beta) V_w^3}{\omega_b} \qquad (3.17)$$

$$C_p(\lambda, \beta) = c_1 \left[\frac{c_2}{\lambda_i} - c_3 \beta - c_4 \right] e^{-c_5/\lambda_i} + c_6 \lambda \qquad (3.18)$$

$$\frac{1}{\lambda_i} = \frac{1}{\lambda - c_7 \beta} - \frac{c_8}{\beta^3 + 1} \qquad (3.19)$$

$$\lambda = \frac{\omega_b R_b}{V_w} \qquad (3.20)$$

where C_p, λ, β and V_w represent the turbine power coefficient, the blade pitch angle, and wind speed respectively; R_b represent the blade swept radius; c_1 to c_8 are constants for the turbine and their values are listed in Appendix.

3.1.2. Induction Generator

The *q-d* axis model of an induction machine with the reference axis rotating at an arbitrary reference frame as set forth in [57] is given below. The motor convention is adopted here meaning the machine currents flow into the machine and the real and

reactive powers are positive when the machine consumes power from the grid. The machine stator and rotor voltages are given as:

$$V_{qs} = r_s I_{qs} + p\lambda_{qs} + \omega\lambda_{ds}$$ (3.21)

$$V_{ds} = r_s I_{ds} + p\lambda_{ds} - \omega\lambda_{qs}$$ (3.22)

$$V_{qr} = r_r I_{qr} + p\lambda_{qr} + (\omega - \omega_r)\lambda_{dr}$$ (3.23)

$$V_{dr} = r_r I_{dr} + p\lambda_{dr} + (\omega - \omega_r)\lambda_{qr}$$ (3.24)

The stator and rotor fluxes are expressed by the following equations:

$$\lambda_{qs} = L_s I_{qs} + L_m I_{qr}$$ (3.25)

$$\lambda_{ds} = L_s I_{ds} + L_m I_{dr}$$ (3.26)

$$\lambda_{qr} = L_m I_{qs} + L_r I_{qr}$$ (3.27)

$$\lambda_{dr} = L_m I_{ds} + L_r I_{dr}$$ (3.28)

and the active and reactive power of stator and rotor are defined as:

$$P_s = \frac{3}{2}\left(V_{qs} I_{qs} + V_{ds} I_{ds}\right)$$ (3.29)

$$Q_s = \frac{3}{2}\left(-V_{ds} I_{qs} + V_{qs} I_{ds}\right)$$ (3.30)

$$P_r = \frac{3}{2}\left(V_{qr} I_{qr} + V_{dr} I_{dr}\right)$$ (3.31)

$$Q_r = \frac{3}{2}\left(-V_{dr} I_{qr} + V_{qr} I_{dr}\right)$$ (3.32)

The generator electromagnetic torque is given by

$$T_e = \frac{3P}{2}\left(\lambda_{ds} I_{qs} - \lambda_{qs} I_{ds}\right)$$ (3.33)

In the equations above, the notation for subscripts $'d'$, $'q'$ refer to d-axis and q-axis components while $'s'$, $'r'$ mean variables associated with stator and rotor circuits respectively. V_{qs}, V_{ds}, V_{qr} and V_{dr} are the stator and rotor voltages while I_{qs}, I_{ds}, I_{qr} and I_{dr} are the corresponding currents; $\lambda_{qs}, \lambda_{ds}, \lambda_{qr}$ and λ_{dr} are the stator and rotor fluxes linkages; P is the number of poles of the induction machine; L_s, L_r, and L_m are

respectively the machine stator, rotor, and magnetizing inductances; r_s and r_r are the stator and rotor resistances; ω is the angular frequency of the arbitrary reference frame; ω_r is the rotor electrical speed and $p = d/dt$.

3.1.3. Power Electronics Converter

The power converter circuit consists of a rotor-side converter (RSC) and a grid-side converter (GSC) connected back-to-back as shown in Figure 3.1. Their dynamics including that of the DC-bus capacitor, according to Kirchhoff's voltage and current laws is governed by the following voltage and current equations:

$$V_{qr} = r_r I_{qr} + p\lambda_{qr} + (\omega - \omega_r)\lambda_{dr} = \frac{M_{qr}}{2}V_{dc} \tag{3.34}$$

$$V_{dr} = r_r I_{dr} + p\lambda_{dr} - (\omega - \omega_r)\lambda_{qr} = \frac{M_{dr}}{2}V_{dc} \tag{3.35}$$

$$C_{dc} p V_{dc} = I_{or} - I_{os} \tag{3.36}$$

$$I_{or} = \frac{3}{4}\left(M_{qr}I_{qr} + M_{dr}I_{dr}\right) \tag{3.37}$$

$$I_{os} = \frac{3}{4}\left(M_{qf}I_{qf} + M_{df}I_{df}\right) \tag{3.38}$$

$$V_{qf} = r_f I_{qf} + L_f p I_{qf} + \omega L_f I_{df} + V_{qg} = \frac{M_{qf}}{2}V_{dc} \tag{3.39}$$

$$V_{df} = r_f I_{df} + L_f p I_{df} - \omega L_f I_{qf} + V_{dg} = \frac{M_{df}}{2}V_{dc} \tag{3.40}$$

where M_{qr}, M_{dr} are the modulation indices of the RSC; M_{qf}, M_{df} are the modulation indices of the GSC; V_{qf}, V_{df} are the voltages at the output of the GSC and I_{qf}, I_{df} are the corresponding currents injected into the grid; V_{dc} is the DC bus voltage; C_{dc} is the DC bus

capacitance; r_f, L_f are the resistance and inductance of the filter at the GSC output; and

V_{qg}, V_{dg} represent the grid voltages as shown in Figure 3.1.

3.2 DFIG Wind Turbine Vector Control

Vector control methods of the DFIG wind turbine allow decoupled control of active and reactive powers injected into the grid. In this work, the stator-flux oriented rotor current control is adopted to decouple the active and reactive powers.

3.2.1. Rotor Side Converter Control

The objective of the Rotor Side Converter (RSC) controller is to regulate the stator active and reactive powers injected into grid. It consists of two cascaded controllers; the inner current loops regulating the *q*- and *d*-axis rotor currents (I_{qr} and I_{dr}) and the outer decoupled active and reactive power loops as shown in Figure 3.7. The reference frame is chosen such that it rotates synchronously with respect to the stator flux linkage, with the d-axis aligned with the stator flux. That is $\lambda_{qs} = 0$ and the DFIG stator voltage equations in (3.21) and (3.22) reduce to (3.41) and (3.42). The corresponding stator currents are given by (3.43) and (3.44).
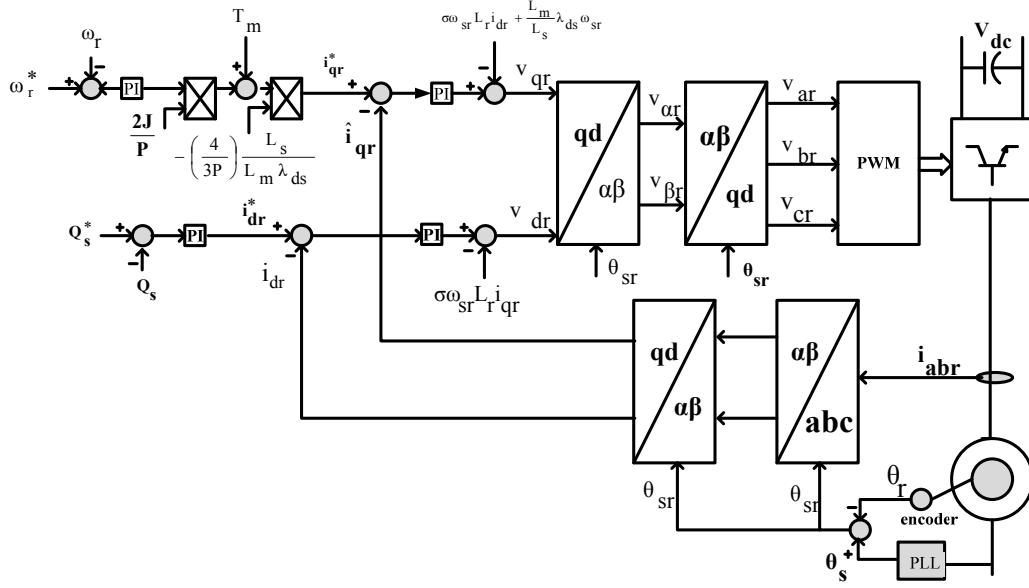
Figure 3.7. Detailed schematic diagram of a typical RSC vector control

$$V_{qs} = r_s I_{qs} + \omega \lambda_{ds} \tag{3.41}$$

$$V_{ds} = r_s I_{ds} + p\lambda_{ds} \tag{3.42}$$

$$I_{qs} = -\frac{L_m}{L_s} I_{qr} \tag{3.43}$$

$$I_{ds} = \left(\frac{1}{L_s} \lambda_{ds} - \frac{L_m}{L_s} I_{dr} \right) \tag{3.44}$$

The rotor flux linkages can be rewritten by substituting (3.43) and (3.44) into (3.27) and

(3.28). That is:

$$\lambda_{qr} = \sigma L_r I_{qr}, \quad \sigma = \left(1 - \frac{L_m^2}{L_s L_r} \right) \tag{3.45}$$

$$\lambda_{dr} = \frac{L_m}{L_s} \lambda_{ds} + \sigma L_r I_{dr} \tag{3.46}$$

Substituting (3.45) and (3.46) into (3.23) and (3.24), the rotor voltage equations can be

rewritten as:

$$V_{qr} = r_r I_{qr} + \sigma L_r p I_{qr} + \omega_{so} \left(\frac{L_m}{L_s} \lambda_{ds} + \sigma L_r I_{dr} \right) \tag{3.47}$$

$$V_{dr} = r_r I_{dr} + \sigma L_r p I_{dr} - \omega_{so} \sigma L_r I_{qr} \tag{3.48}$$

35

and the electromagnetic torque in (3.33) reduces to:

$$T_e = \frac{3}{2}\frac{P}{2}\lambda_{ds}I_{qs} = -\frac{3}{2}\frac{P}{2}\frac{L_m}{L_s}\lambda_{ds}I_{qr} \qquad (3.49)$$

Substituting for the stator current expressions from (3.43) and (3.44) into (3.29) and (3.30), the expressions of active and reactive powers can be written as:

$$P_s = \frac{3}{2}\left(-\frac{L_m}{L_s}V_{qs}I_{qr} + V_{ds}\left(\frac{1}{L_s}\lambda_{ds} - \frac{L_m}{L_s}I_{dr}\right)\right) \qquad (3.50)$$

$$Q_s = \frac{3}{2}\left(V_{ds}\frac{L_m}{L_s}I_{qr} + V_{qs}\left(\frac{1}{L_s}\lambda_{ds} - \frac{L_m}{L_s}I_{dr}\right)\right) \qquad (3.51)$$

A legitimate claim can be that the stator resistance (r_s) is negligible which is particularly true for large megawatt generators. With this assumption and the fact that the *d*-axis stator flux linkage remains approximately constant, the *d*-axis stator voltage is approximately zero. That is:

$$r_s \approx 0, \qquad p\lambda_{ds} \approx 0, \qquad V_{ds} = r_sI_{ds} + p\lambda_{ds} = 0 \qquad (3.52)$$

So if the *d*-axis stator voltage is zero, the expressions of the stator active and reactive powers in (3.50) and (3.51) reduces to (3.53) and (3.54) respectively.

$$P_s = -\frac{3}{2}\frac{L_m}{L_s}V_{qs}I_{qr} \qquad (3.53)$$

$$Q_s = \frac{3}{2}V_{qs}\left(\frac{1}{L_s}\lambda_{ds} - \frac{L_m}{L_s}I_{dr}\right) \qquad (3.54)$$

Equations (3.53) and (3.54) show that the stator active and reactive powers can be regulated independently by the stator *qd*-axis currents.

3.2.1.1.**Outer power control loops.** The outer power loops are needed to produce the reference qd-axis rotor currents required by the inner loops. To obtain the reference q-axis rotor current, the torque expression in (3.49) is relevant as it contains I_{qr}. Since

maximum power point tracking (MPPT) is usually sought, an appropriate MPPT scheme is to use the optimal torque control technique. In this work, a speed control loop is used to obtain the torque reference and consequently the reference q-axis rotor current. Substituting the electromagnetic torque expression in (3.49) into the speed dynamics (3.16) assuming a damper-free system, the resulting expression is given by (3.55) and the reference q-axis rotor current, I_{qr}^*, is given by (3.56).

$$p\omega_r = -\frac{P}{2J}\left(\frac{3}{2}\frac{P}{2}\frac{L_m}{L_s}\lambda_{ds}I_{qr}^* + T_m\right) \tag{3.55}$$

$$I_{qr}^* = -\left(\frac{2J}{P}p\omega_r + T_m\right)K_{Te}, \qquad K_{Te} = -\frac{3}{2}\frac{P}{2}\frac{L_m}{L_s}\lambda_{ds} \tag{3.56}$$

The mechanical torque may be taken as a disturbance in the design of the speed regulator using the classical Propotional-Integral (PI) controller design. Thus it can be modeled as:

$$p\omega_r = \sigma_{\omega_r} = K_{\omega_r}\left(\omega_r^* - \omega_r\right) = \left(k_{p\omega_r} + \frac{k_{i\omega_r}}{p}\right)\left(\omega_r^* - \omega_r\right) \tag{3.57}$$

from which the speed transfer function is obtained as :

$$\frac{\omega_r}{\omega_r^*} = \frac{pk_{p\omega_r} + k_{i\omega_r}}{p^2 + pk_{p\omega_r} + k_{i\omega_r}} \tag{3.58}$$

where σ_{ω_r} is the output of the speed controller; $k_{p\omega_r}$ and $k_{i\omega_r}$ are the proportional and integral gains respectively and ω_r^* is the reference rotor electrical speed. The PI controller gains, $k_{p\omega_r}$ and $k_{i\omega_r}$, are determined by comparing the denominator of the speed transfer function given by (3.58) to the Butterworth polynomial [61]:

$$p^2 + pk_{p\omega_r} + k_{i\omega_r} \equiv p^2 + \sqrt{2}\omega_{o\omega_r}p + \omega_{o\omega_r}^2$$
$$k_{p\omega_r} = \sqrt{2}\omega_{o\omega_r}, \qquad k_{i\omega_r} = \omega_{o\omega_r}^2 \tag{3.59}$$

37

The reactive power loop is used to obtain the reference d-axis rotor current I_{dr}^*.

The time derivative of the stator reactive power may be obtained by differentiating (3.54) to obtain (3.60). In (3.60), the expression for the time derivative of the d-axis rotor current, I_{dr} may be obtained from (3.48) and is given in (3.61).

$$pQ_s = -\frac{3}{2}V_{qs}\frac{L_m}{L_s}pI_{dr}$$

(3.60)

$$pI_{dr} = \frac{1}{\sigma L}(V_{dr} - r_r I_{dr} + \omega_{so}\sigma L_r I_{qr})$$

(3.61)

Substituting (3.61) into (3.60), the time derivative of the stator reactive power is given by (3.62) from which the reference d-axis rotor current I_{dr}^* is obtained as in (3.63).

$$pQ_s = \frac{3}{2}V_{qs}\frac{L_m}{\sigma L_r L_s}\left(r_r I_{dr} - \omega_{so}\sigma L_r I_{qr} - V_{dr}\right)$$

(3.62)

$$I_{dr}^* = \frac{1}{r_r}\left(\frac{1}{\eta_{Q_s}}pQ_s + \omega_{so}\sigma L_r I_{qr} + V_{dr}\right), \qquad \eta_{Q_s} = \frac{3}{2}V_{qs}\frac{L_m}{\sigma L_r L_s}$$

(3.63)

The stator reactive power controller can be modeled as:

$$pQ_s = \sigma_{Q_s} = K_{Q_s}\left(Q_s^* - Q_s\right) = \left(k_{pQ_s} + \frac{k_{iQ_s}}{p}\right)\left(Q_s^* - Q_s\right)$$

(3.64)

and the transfer function of the stator reactive power is obtained as:

$$\frac{Q_s}{Q_s^*} = \frac{pk_{pQ_s} + k_{iQ_s}}{p^2 + pk_{pQ_s} + k_{iQ_s}}$$

(3.65)

where σ_{Q_s} is the output of the reactive power controller; k_{pQ_s} and k_{iQ_s} are its proportional and integral gains respectively and Q_s^* is the reference reactive power. Similarly, the PI controller gains, k_{pQ_s} and k_{iQ_s}, are determined by comparing the denominator of the stator reactive power speed transfer function ,(3.65), to the Butterworth polynomial:

38

$$p^2 + pk_{pQ_s} + k_{iQ_s} \equiv p^2 + \sqrt{2}\omega_{oQ_s}p + \omega_{oQ_s}^2$$

$$k_{pQ_s} = \sqrt{2}\omega_{oQ_s}, \qquad k_{iQ_s} = \omega_{oQ_s}^2 \tag{3.66}$$

3.2.1.2.**Inner current control loops.** The rotor current can be regulated by means of rotor voltage expression given in (3.47) and (3.48). The reference q- and d- rotor voltages can be expressed as:

$$V_{qr}^* = \sigma_{qr} + \omega_{so}\left(\frac{L_m}{L_s}\lambda_{ds} + \sigma L_r I_{dr}\right) \tag{3.67}$$

$$V_{dr}^* = \sigma_{dr} - \omega_{so}\sigma L_r I_{qr} \tag{3.68}$$

where the controller outputs are defined as:

$$\sigma_{qr} = r_r I_{qr} + \sigma L_r p I_{qr} \tag{3.69}$$

$$\sigma_{dr} = r_r I_{dr} + \sigma L_r p I_{dr} \tag{3.70}$$

The last terms in (3.67) and (3.68) are cross-coupling terms and are normally added to the output of the PI controller as shown in Figure 3.7. The controller gains are found similar to the power loops derived above by finding the transfer functions of the rotor currents. The q- and d-axis current controller may be modeled as in (3.71) and (3.72) respectively. The corresponding transfer functions are given in (3.73) and (3.74).

$$\sigma_{qr} = r_r I_{qr} + \sigma L_r p I_{qr} = \left(k_{pqr} + \frac{k_{iqr}}{p}\right)\left(I_{qr}^* - I_{qr}\right) \tag{3.71}$$

$$\sigma_{dr} = r_r I_{dr} + \sigma L_r p I_{dr} = \left(k_{pdr} + \frac{k_{idr}}{p}\right)\left(I_{dr}^* - I_{qr}\right) \tag{3.72}$$

$$\frac{I_{qr}}{I_{qr}^*} = \frac{\frac{1}{\sigma L_r}\left(pk_{pqr} + k_{iqr}\right)}{p^2 + \frac{1}{\sigma L_r}\left(k_{pqr} + r_r\right)p + \frac{1}{\sigma L_r}k_{iqr}} \tag{3.73}$$

$$\frac{I_{dr}}{I_{dr}^*} = \frac{\frac{1}{\sigma L_r}\left(pk_{pdr} + k_{idr}\right)}{p^2 + \frac{1}{\sigma L_r}\left(k_{pdr} + r_r\right)p + \frac{1}{\sigma L_r}k_{idr}} \tag{3.74}$$

where σ_{qr} and σ_{dr} are the outputs of the q- and d-axis current controllers; k_{pqr} and k_{idr} are its proportional and integral gains respectively and I_{qr}^* and I_{dr}^* are the reference rotor currents.

The current controller parameters are calculated by comparing the Butterworth polynomial with the denominator of the transfer functions to obtain the following:

$$p^2 + \frac{1}{\sigma L_r}\left(k_{pqr} + r_r\right)p + \frac{k_{iqr}}{\sigma L_r} \equiv p^2 + \sqrt{2}\omega_{oqr}p + \omega_{oqr}^2$$

$$k_{pqr} = \sqrt{2}\omega_{oqr}\sigma L_r - r_r, \qquad k_{iqr} = \sigma L_r \omega_{oqr}^2 \tag{3.75}$$

$$p^2 + \frac{1}{\sigma L_r}\left(k_{pdr} + r_r\right)p + \frac{k_{idr}}{\sigma L_r} \equiv p^2 + \sqrt{2}\omega_{odr}p + \omega_{odr}^2$$

$$k_{pdr} = \sqrt{2}\omega_{odr}\sigma L_r - r_r, \qquad k_{idr} = \sigma L_r \omega_{odr}^2 \tag{3.76}$$

Generally, as a design rule, the inner loop controller should have a value of the desired closed loop bandwidth frequency $\omega_{oqr} = \omega_{odr} = \omega_{or}$ about 10 times higher than the one in the outer control loop [62].

3.2.2. Grid-Side Converter And DC-Link Voltage Control

The control objective of the grid side converter (GSC) is to regulate the DC-bus voltage and the reactive power injected into the grid from the GSC. Figure 3.8 shows the control scheme of the GSC. As in the case of the RSC controller, there are two cascaded q- and d-axis control loops. These are discussed below.

3.2.2.1. **Outer power control loop.** The outer loops involve the DC-bus voltage and the GSC reactive power whereas the inner loops are for current control. In large DFIG systems, the stator resistance is negligible and can be ignored to simplify the

control scheme. With this assumption, the d-axis grid voltage can be approximated to zero, that is:

$$V_{qg} = V_g$$
$$V_{dg} = 0 \qquad (3.77)$$

The dynamics of the GSC represented in (3.36)-(3.40) can be rewritten as follows:

$$C_{dc} p V_{dc}^2 = \frac{3}{2}(V_{qr} I_{qr} + V_{dr} I_{dr} - V_{qf} I_{qf}) = P_r - \frac{3}{2} V_{qf} I_{qf} \qquad (3.78)$$

$$V_{qf} = r_f I_{qf} + L_f p I_{qf} + \omega L_f I_{df} + V_{qg} = \frac{M_{qf}}{2} V_{dc} \qquad (3.79)$$

$$V_{df} = r_f I_{df} + L_f p I_{df} - \omega L_f I_{qf} = \frac{M_{df}}{2} V_{dc} \qquad (3.80)$$

where the modulation indices have been replaced with the corresponding voltages. The active and reactive powers injected into the grid from the GSC are given by

$$P_f = \frac{3}{2} V_{qg} I_{qf} \qquad (3.81)$$

$$Q_f = \frac{3}{2} V_{qg} I_{df} \qquad (3.82)$$

Equation (3.78) can be represented as a second-order linear system (P_r is treated as a disturbance which can be compensated for using a standard PI regulator). Thus the DC- link voltage can be controlled using the q-component of the current, I_{qf}. The corresponding d-component of the GSC current, I_{df} can be used to control the GSC reactive power, Q_f.

41
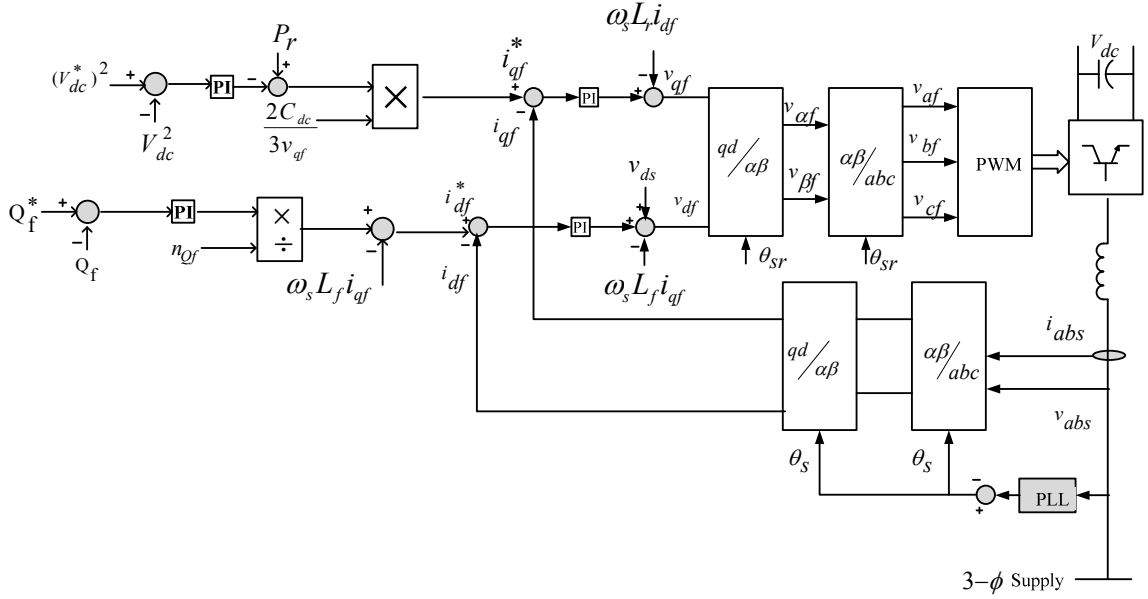
Figure 3.8. Detailed schematic diagram of a typical GSC vector control

The DC-bus controller is modeled as follows:

$$C_{dc} p V_{dc}^2 = -\frac{3}{2} V_{qf} I_{qf} = \sigma_{dc} \tag{3.83}$$

$$C_{dc} p V_{dc}^2 = \sigma_{dc} = K_{dc}\left(V_{dc}^{*2} - V_{dc}^2\right) = \left(k_{pdc} + \frac{k_{idc}}{p}\right)\left(V_{dc}^{*2} - V_{dc}^2\right)$$

$$C_{dc} p V_{dc}^2 = \left(k_{pdc} + \frac{k_{idc}}{p}\right)V_{dc}^{*2} - \left(k_{pdc} + \frac{k_{idc}}{p}\right)V_{dc}^2 \tag{3.84}$$

$$\frac{V_{dc}^2}{V_{dc}^{*2}} = \frac{\dfrac{1}{C_{dc}}\left(p k_{pdc} + k_{idc}\right)}{p^2 + p\dfrac{k_{pdc}}{C_{dc}} + \dfrac{k_{idc}}{C_{dc}}} \tag{3.85}$$

where σ_{dc} is the output of the q-axis DC-bus voltage controller; k_{pdc} and k_{idc} are its

proportional and integral gains respectively and V_{dc}^* is the reference DC-bus voltage. The

PI control parameters are calculated by comparing the denominator of the transfer

function obtained in (3.85) to the Butterworth polynomial. That is:

$$p^2 + p\frac{k_{pdc}}{C_{dc}} + \frac{k_{idc}}{C_{dc}} = p^2 + \sqrt{2}\omega_{odc}p + \omega_{odc}^2$$

(3.86)

$$k_{pdc} = \sqrt{2}\omega_{odc}C_{dc}, \quad k_{idc} = C_{dc}\omega_{odc}^2$$

The GSC reactive power control is modeled by finding the time derivative of (3.82) and substituting for the time derivative of the d-axis GSC current from (3.40). That is:

$$pQ_f = \frac{3}{2}V_{qg}pI_{df}$$

(3.87)

$$pI_{df} = \frac{1}{L_f}\left(V_{df} - r_f I_{df} + \omega L_f I_{qf}\right)$$

(3.88)

$$pQ_f = \frac{3}{2}\frac{1}{L_f}V_{qg}\left(V_{df} - r_f I_{df} + \omega L_f I_{qf}\right)$$

(3.89)

$$I_{df}^* = \frac{1}{r_r}\left(\frac{1}{\eta_{Q_f}}pQ_f - \omega_s L_f I_{qf}\right), \qquad \eta_{Q_f} = \frac{3}{2}V_{qg}\frac{1}{L_f}$$

(3.90)

The GSC reactive power controller can be modeled as:

$$pQ_f = \sigma_{Q_f} = K_{Q_f}\left(Q_f^* - Q_f\right) = \left(k_{pQ_f} + \frac{k_{iQ_f}}{p}\right)\left(Q_f^* - Q_f\right)$$

(3.91)

and its transfer function is obtained from (3.91) as:

$$\frac{Q_f}{Q_f^*} = \frac{pk_{pQ_f} + k_{iQ_f}}{p^2 + pk_{pQ_f} + k_{iQ_f}}$$

(3.92)

where σ_{Q_f} is the output of the GSC reactive power controller; k_{pQ_f} and k_{iQ_f} are its proportional and integral gains respectively and Q_f^* is the reference GSC reactive power. Similarly, the PI controller gains, k_{pQ_f} and k_{iQ_f}, are determined by comparing the denominator of the GSC reactive power transfer function, (3.92) to the Butterworth polynomial:

43

$$p^2 + pk_{pQ_f} + k_{iQ_f} \equiv p^2 + \sqrt{2}\omega_{oQ_f}p + \omega_{oQ_f}^2$$

$$k_{pQ_s} = \sqrt{2}\omega_{oQ_f}, \qquad k_{iQ_f} = \omega_{oQ_f}^2 \tag{3.93}$$

3.2.2.2.**Inner current control loops.** The GSC filter current can be regulated by means of its voltage expression given in (3.39) and (3.40). The implementation of the current controller is shown in Figure 3.8. The reference q- and d-axis rotor voltages can be expressed as:

$$V_{qf} = \sigma_{qf} + \omega L_f I_{df} + V_{qg} \tag{3.94}$$

$$V_{df} = \sigma_{df} - \omega L_f I_{qf} \tag{3.95}$$

where the controller outputs are defined as:

$$\sigma_{qf} = r_f I_{qf} + L_f p I_{qf} = \left(k_{pqf} + \frac{k_{iqf}}{p}\right)\left(I_{qf}^* - I_{qf}\right) \tag{3.96}$$

$$\sigma_{df} = r_f I_{df} + L_f p I_{df} = \left(k_{pdf} + \frac{k_{idf}}{p}\right)\left(I_{df}^* - I_{df}\right) \tag{3.97}$$

The controller gains are found similar to the power loops above. The q- and d-axis current controller may be modeled as in (3.98) and (3.99) respectively. The corresponding transfer functions are given in (3.100) and (3.101).

$$\sigma_{qf} = r_f I_{qf} + L_f p I_{qf} = \left(k_{pqf} + \frac{k_{iqf}}{p}\right)\left(I_{qf}^* - I_{qf}\right) \tag{3.98}$$

$$\sigma_{df} = r_f I_{df} + L_f p I_{df} = \left(k_{pdf} + \frac{k_{idf}}{p}\right)\left(I_{df}^* - I_{df}\right) \tag{3.99}$$

$$\frac{I_{qf}}{I_{qf}^*} = \frac{\frac{1}{L_f}\left(pk_{pqf} + k_{iqf}\right)}{p^2 + \frac{1}{L_f}\left(k_{pqf} + r_f\right)p + \frac{1}{L_f}k_{iqf}} \tag{3.100}$$

$$\frac{I_{df}}{I_{df}^*} = \frac{\frac{1}{L_f}\left(pk_{pdf} + k_{idf}\right)}{p^2 + \frac{1}{L_f}\left(k_{pdf} + r_f\right)p + \frac{1}{L_f}k_{idf}} \tag{3.101}$$

In the expressions above, σ_{qf} and σ_{df} are the outputs of the q- and d-axis current controllers; k_{pqf} and k_{idf} are its proportional and integral gains respectively and I_{qf}^* and I_{df}^* are the reference GSC filter currents.

The current controller parameters are calculated by comparing the Butterworth polynomial with the denominator of the transfer functions to obtain the following:

$$p^2 + \frac{1}{L_f}\left(k_{pqf} + r_f\right)p + \frac{k_{iqf}}{L_f} \equiv p^2 + \sqrt{2}\omega_{of}p + \omega_{of}^2$$
$$k_{pqf} = \sqrt{2}\omega_{of}L_f - r_f, \qquad k_{iqf} = L_f\omega_{of}^2$$
(3.102)

$$p^2 + \frac{1}{L_f}\left(k_{pdf} + r_f\right)p + \frac{k_{idf}}{L_f} \equiv p^2 + \sqrt{2}\omega_{of}p + \omega_{of}^2$$
$$k_{pdf} = \sqrt{2}\omega_{of}L_f - r_f, \qquad k_{iqf} = L_f\omega_{of}^2$$
(3.103)

3.2.2.3.**Design of PI controller gains.** The expressions of the PI controller gains have been derived in the preceeding subsections. Their values are calculated here based on the DFIG wind turbine parameters and the chosen bandwidths. A good approximation in selecting the switching frequency is that it should be at least 5 times the close loop bandwidth [62] and [105]. It is also recommended that the bandwidth of the inner current controllers should be atleast 10 times that of outer loop controllers (rotor speed, reactive power and DC link voltage).

Table 3.1 depicts all the controller gains used in simulations in the proceeding section based on the above descriped design criteria. The converters switching frequency chosen is 1 kHz and the DFIG machine parameters are given in the Appendix. Given that the switching frequency, f_{sw} is 1 kHz, the following design was done for all the bandwidth frequencies:

Table 3.1. Parameters of 5 hp DFIG wind turbine PI controllers

PI Controller	Gain symbol	Value
Rotor Current	$k_{pqr} = k_{pdr}$	1
	$k_{iqr} = k_{idr}$	82
GSC filter current	$k_{pqf} = k_{pdf}$	3
	$k_{iqf} = k_{idf}$	790
Rotor speed	$k_{p\omega r}$	100
	$k_{i\omega r}$	0.1
DC link voltage	k_{pdc}	0.1
	k_{idc}	0.0001

$\omega_{sw} = 2\pi f_{sw} = 6280 \, rad/s$ and the inner and outer bandwith frequencies are respectively,

$\omega_{01} = \dfrac{\omega_{sw}}{10}$ and $\omega_{o2} = \dfrac{\omega_{o1}}{10}$. Thus

$\omega_{o1} = \omega_{0r} = \omega_{of} = 628 \, rad/s$, $\omega_{o2} = \omega_{odc} = \omega_{oQs} = \omega_{oQf} = 62.8 \, rad/s$

3.3 Steady State and Dynamic Simulations

In this section, the steady state operating characteristics of the grid-connected DFIG wind turbine is presented. The dynamic simulations are also presented to verify performance of the vector control and the steady state behavior.

3.3.1. Steady State Characteristics

The DFIG wind turbine dynamic equations as well as its vector control model have been derived in the previous sections. The steady state equations can be obtained by

setting the derivative terms of these dynamic equations to zero. A summary of the steady state equations are:

$$V_{qs} = r_f I_{qf} + \omega\, L_f I_{df} + \frac{M_{qf} V_{dc}}{2} \tag{3.104}$$

$$V_{ds} = r_f I_{df} - \omega\, L_f I_{qf} + \frac{M_{df} V_{dc}}{2} \tag{3.105}$$

$$V_{qr} = r_r I_{qr} + \omega_{so} \frac{L_m}{L_s} \lambda_{ds} + \sigma \omega_{so} L_r I_{dr} \tag{3.106}$$

$$V_{dr} = r_r I_{dr} - \sigma \omega_{so} L_r I_{qr} \tag{3.107}$$

$$C_{dc} p V_{dc} = \frac{3}{4} \left(M_{qf} I_{qf} + M_{df} I_{df} - M_{qr} I_{qr} - M_{dr} I_{dr} \right) \tag{3.108}$$

$$I_{df}^* = \frac{1}{2 V_{ds}} \left(M_{qr} I_{qr} + M_{dr} I_{dr} \right) \tag{3.109}$$

$$I_{qf}^* = -\frac{2 Q_f^*}{3 V_{ds}} \tag{3.110}$$

$$I_{qr}^* = \frac{2}{3} \frac{2}{P} \frac{L_s}{L_m \lambda_{ds}} T_e^* \tag{3.111}$$

$$i_{dr}^* = \frac{1}{L_m} \left(\lambda_{ds} - \frac{2 L_s}{3 v_{qs}} Q_s^* \right) \tag{3.112}$$

The unknown variables are: $M_{qf}, M_{df}, M_{qr}, M_{dr}, \lambda_{ds}, I_{qf}$. Six equations in six unknown variables assuming the electromagnetic torque and stator reactive power are known desirable quantities.

Figures 3.9-3.13 show the results of the steady state solutions after solving the six equations. As shown in Figure 3.9, the reference torque at low to medium wind speeds is given by the mechanical torque assuming maximum power tracking. Above the rated wind speed, the generated torque is limited to its rated value (1 p.u.).
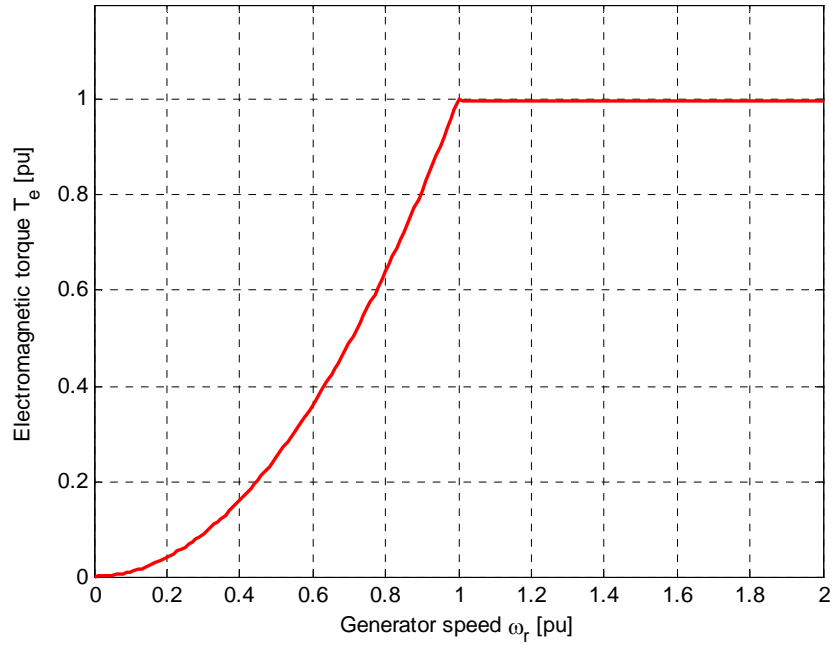
Figure 3.9. Electromagnetic torque at varying generator speed
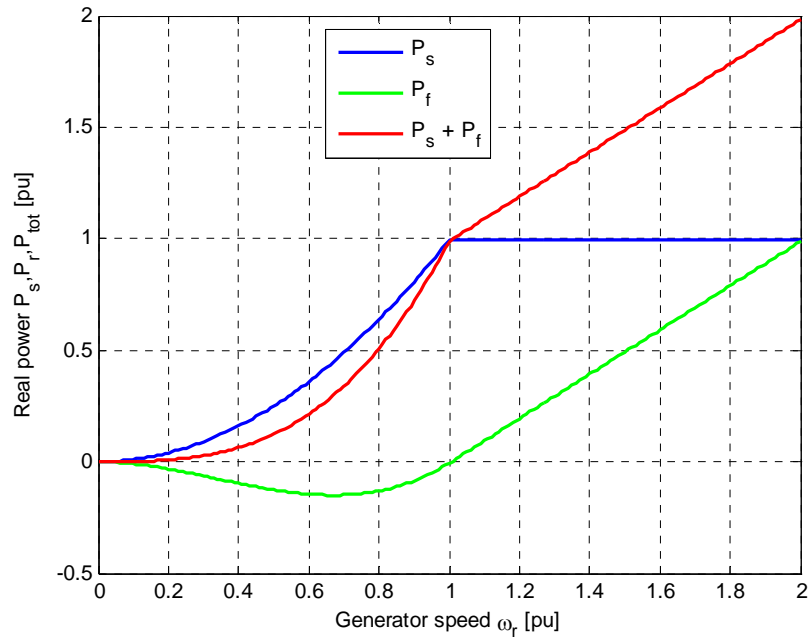
Figure 3.10.   Stator, rotor and total real powers at varying generator speed
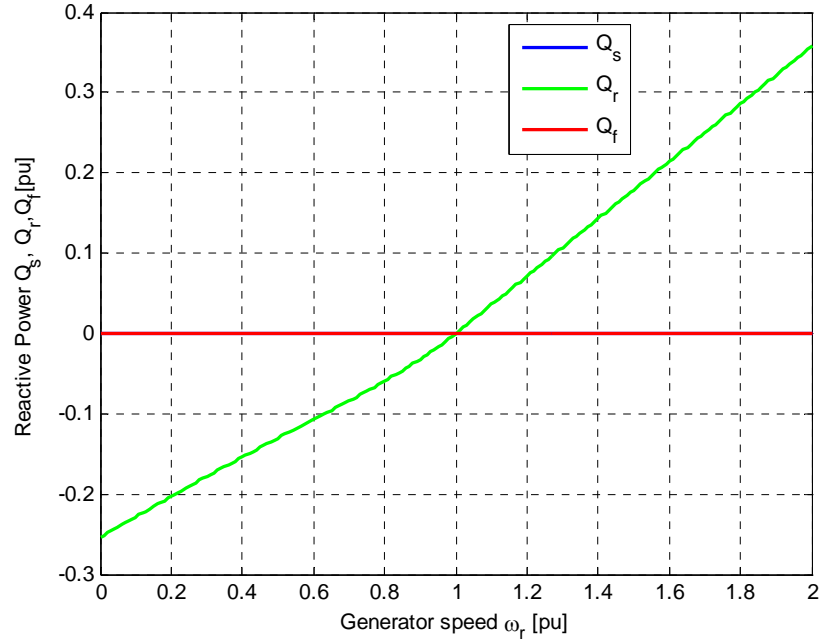
Figure 3.11.   DFIG stator, rotor and powers at varying generator speed
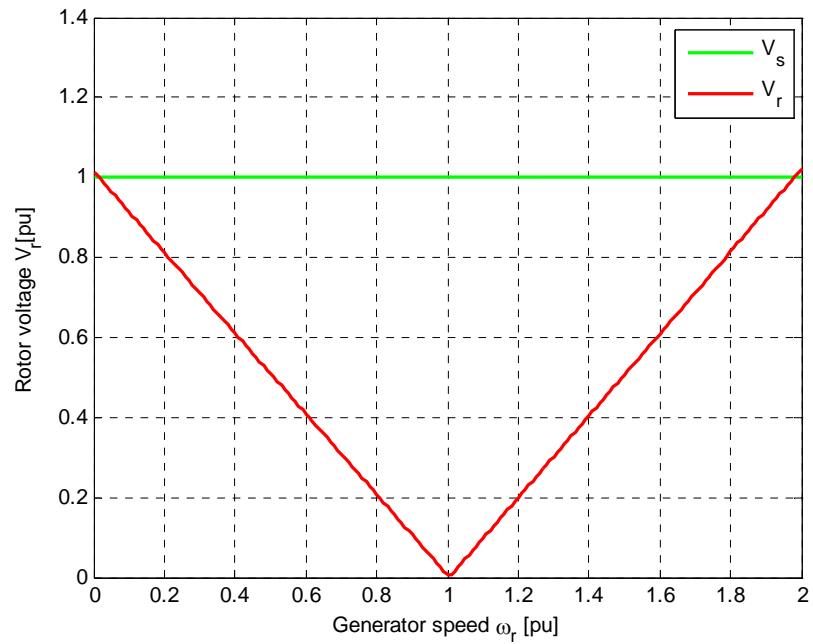
Figure 3.12.   DFIG rotor voltage magnitude at varying generator speed
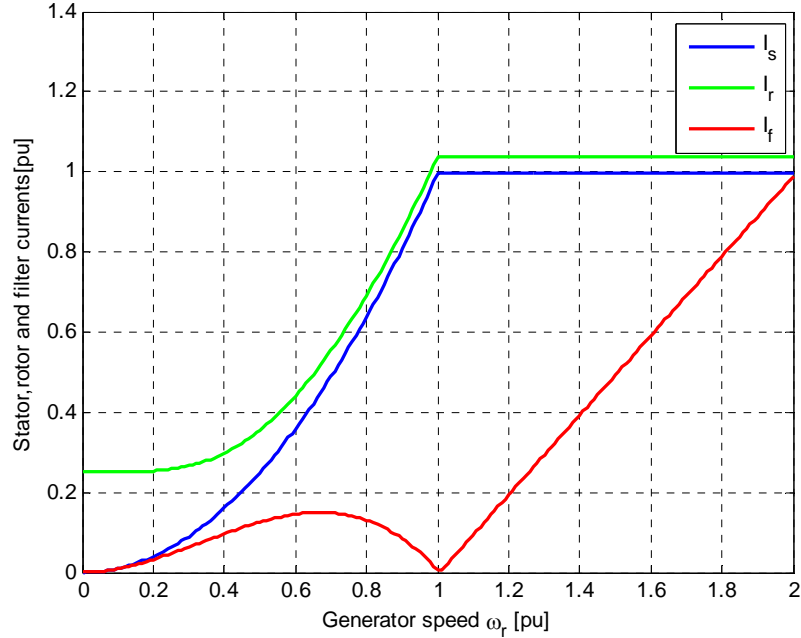
Figure 3.13.   DFIG stator, rotor and GSC filter current magnitudes at varying generator speed

Unlike the behavior of the squirrel-cage induction generator, the DFIG is capable of generating power at both sub-synchronous and super-synchronous rotor speeds as shown in Figure 3.10. At lower wind speeds, the rotor is rotating at sub-synchronous speed ($s > 0$). The stator power increases with rotor speed peaking in at synchronous speed. However, the rotor and converter circuits absorb power from the grid connection to provide excitation for rotor winding. When rotating at the synchronous speed ($s = 0$), the DFIG supplies all the power via the stator winding, with no active power flow in the rotor circuit and converters.

At high wind speed, the rotor speed is regulated to maintain optimum tip-speed ratios and the generator operates at super-synchronous speeds ($s < 0$). Power flows to the grid through both the stator and the rotor windings. The reactive power to the grid is regulated to be null as shown in Figure 3.11. Figure 3.12 illustrates that if stator voltage kept at 1 p.u., the rotor voltage is well within rated values. However, as shown in Figure

3.13, the limiting variable for the DFIG is the magnitude of the rotor current which is above 1 p.u. in the rated power mode region and must be carefully regulated.

3.3.2. Dynamic Simulations

Figures 3.14 – 3.16 show the performance of the of the DFIG vector control to step changes in the rotor speed and dc link voltage. There is a step change of 10 rad/sec (0.03 p.u.) at 2.4 seconds and at 15 rad/s at 3.2 seconds. Additionally, there is also a step change in the dc-link voltage (10 volts) at 2.5 seconds and 15 volts at 3.0 seconds. These overlap of the speed and voltage changes are to enable observation of the response of the various variables to both controllers. Observe in Figure 3.14 that the performance of the real and reactive powers as well as the generator torque respond to changes in the rotor speed and not the dc link voltage. Similarly in Figure 3.15, the rotor current, rotor voltage, rotor flux, and stator flux respond to changes in the rotor speed but remain unchanged to fluctuations in the dc link voltage. However, the GSC filter currents and voltages in Figures 3.15 and 3.16 show they are affected by both rotor speed and dc link fluctuations
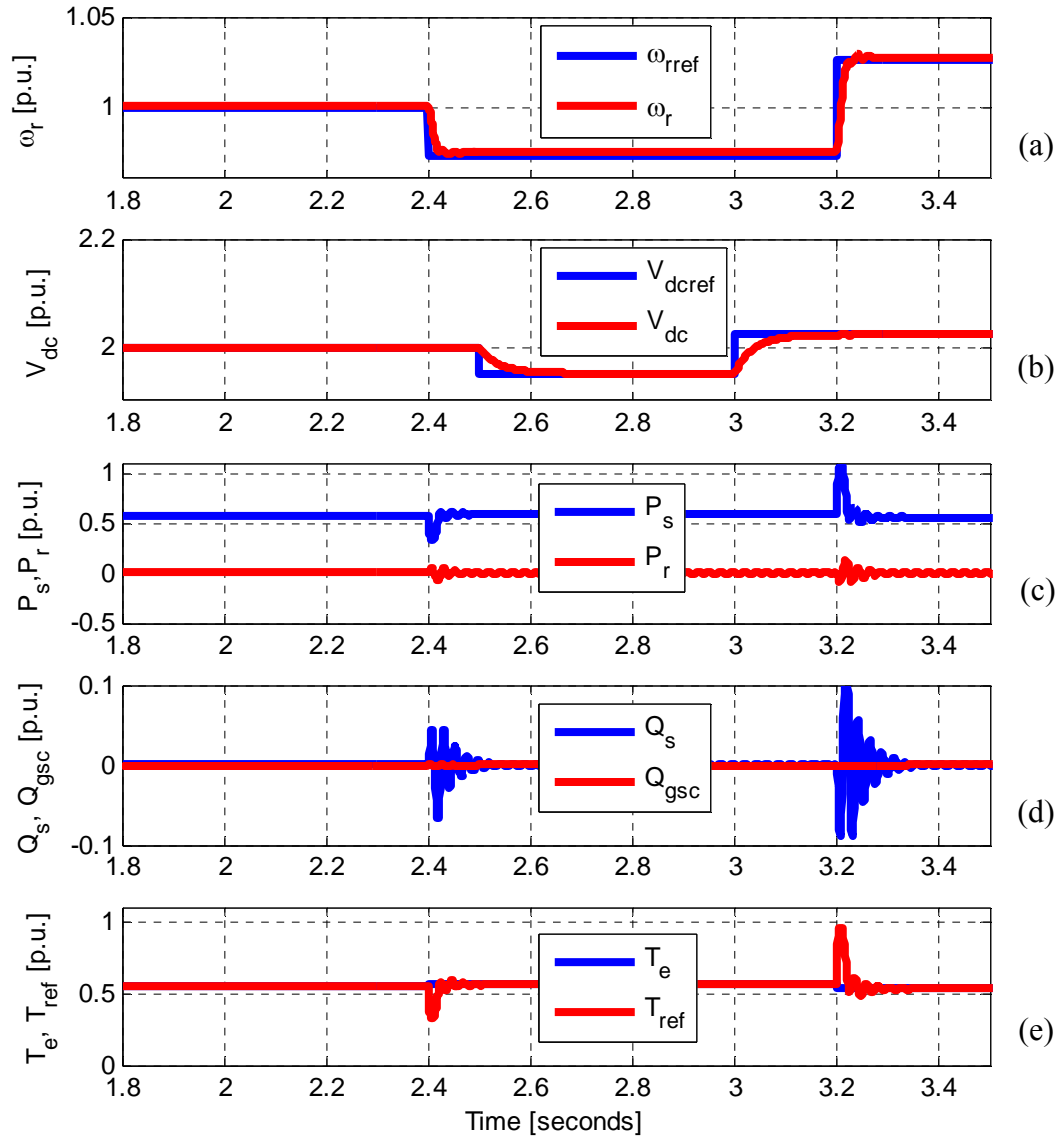
Figure 3.14.   DFIG vector controller performance to step change in rotor speed and dc-link voltage for (a) rotor speed, (b) dc-link voltage, (c) stator a rotor active powers, (d) stator and GSC reactive powers (e) generator torque
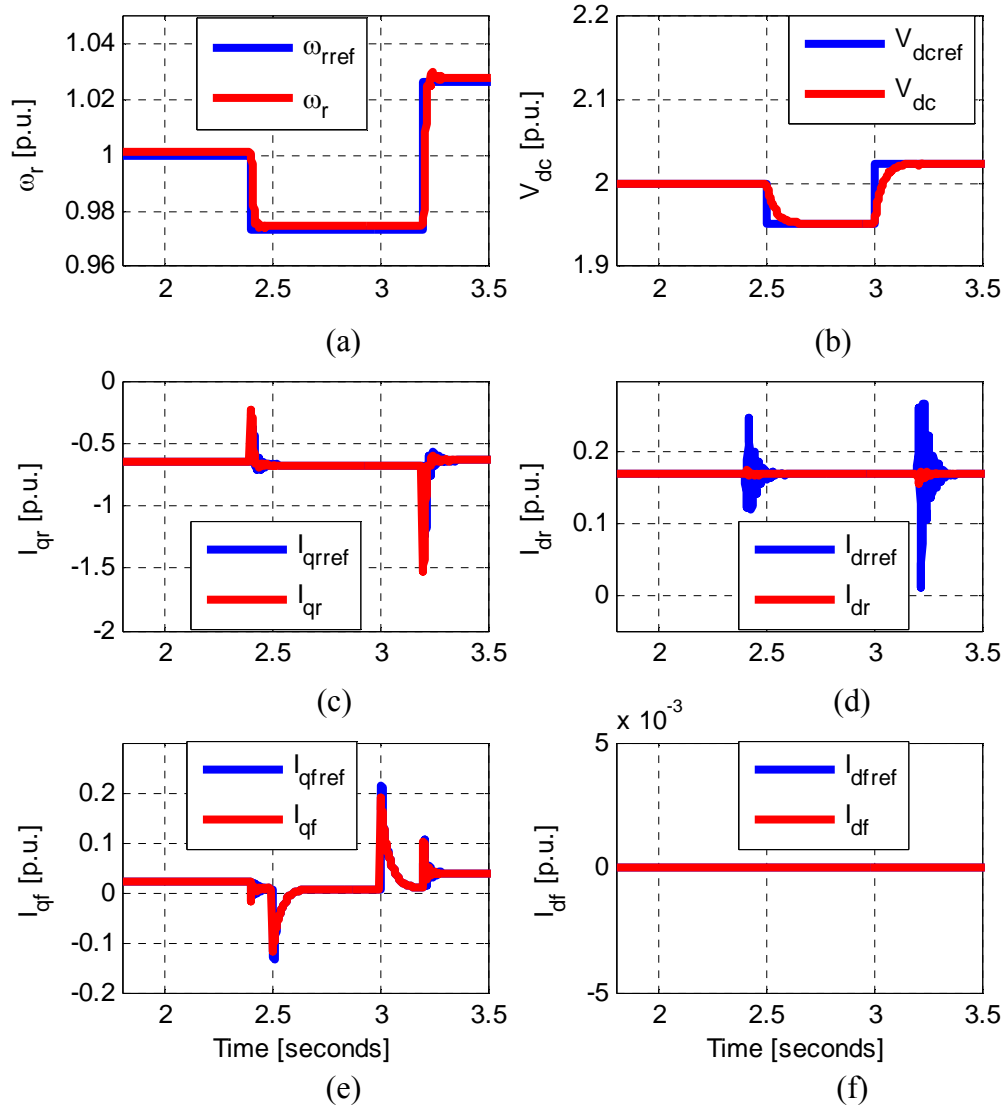
Figure 3.15.   DFIG vector controller performance to step change in rotor speed and dc-link voltage for (a) rotor speed, (b) dc-link voltage, (c) q-axis rotor current, (d) d-axis rotor current (e) q-axis GSC filter current, and (f) d-axis GSC filter current
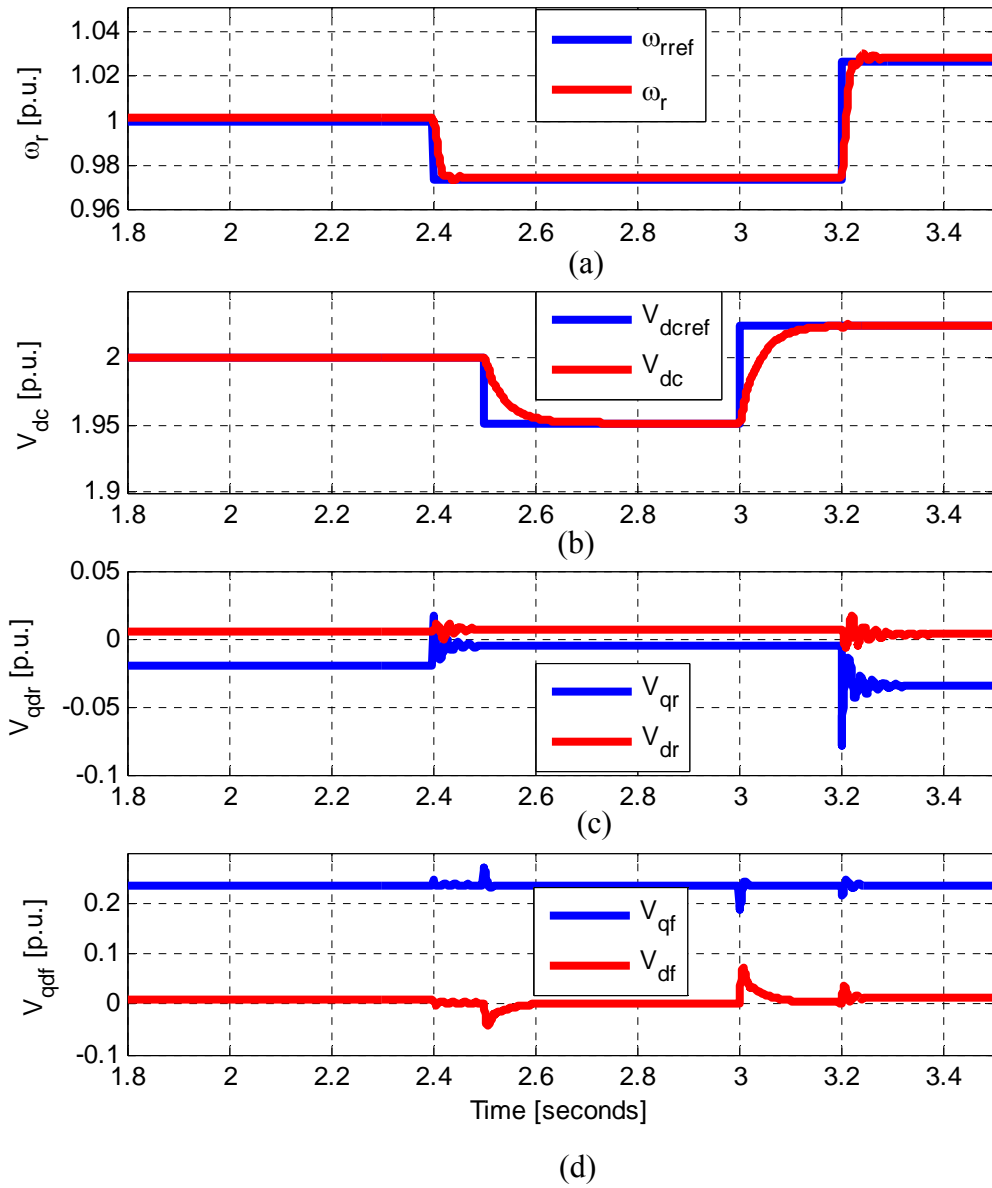
Figure 3.16. DFIG vector controller performance to step change in rotor speed and dc-link voltage for (a) rotor speed, (b) dc-link voltage, (c) qd-axis rotor voltages, and (d) qd-axis GSC voltages
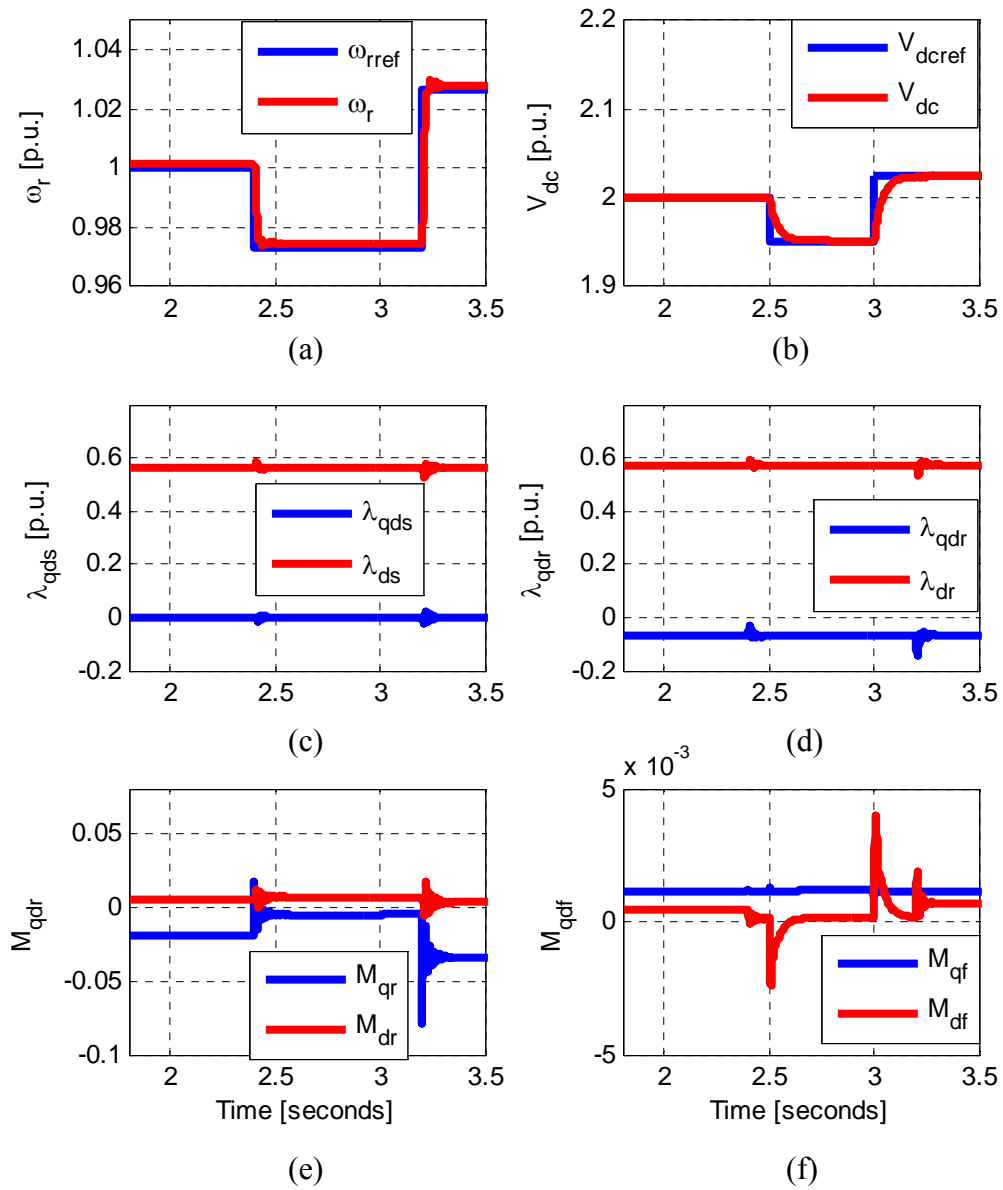
Figure 3.17. DFIG vector controller performance to step change in rotor speed and dc-link voltage for (a) rotor speed, (b) dc-link voltage, (c) qd-axis stator flux linkages, (d) qd-axis rotor flux linkages (e) qd-axis RSC modulation indices, and (f) qd-axis GSC modulation indices

CHAPTER 4

STEADY STATE STABILITY INVESTIGATION OF DFIG WIND TURBINE

4.1 Introduction

Wind energy is increasingly becoming the most viable renewable alternative to the conventional fossil fuels. Generating costs for wind with existing technologies is lower than most other renewable energy sources. It is therefore not surprising that the U.S. Energy Information Administration's Annual Energy Outlook 2011, projects that the installed wind capacity will grow by about 48 percent per year from 2009 through 2016. As more wind farms are integrated into the existing power grids, the chief concern is its ability to provide the required power while remaining relatively stable. Several factors influence the steady-state stability of wind generating systems including wind speed, real and reactive power exchanges with the grid. The situation is even more complicated in variable-speed, variable-pitch wind generator systems.

In variable-speed, variable-pitch wind turbines, the objective is to maximize power extraction at low to medium wind speeds by following the maximum profile of the power coefficient as depicted in Figure 4.1. However, at high wind speeds, below the turbine cut-out speed, blade pitch angle control is usually used to maintain some rated shaft speed and to shed off aerodynamic power so as to maintain a safe operation [46]-[50]. Pitch angle control is very cumbersome because of the highly nonlinear characteristics which add to the complexity of the wind generation control architecture.
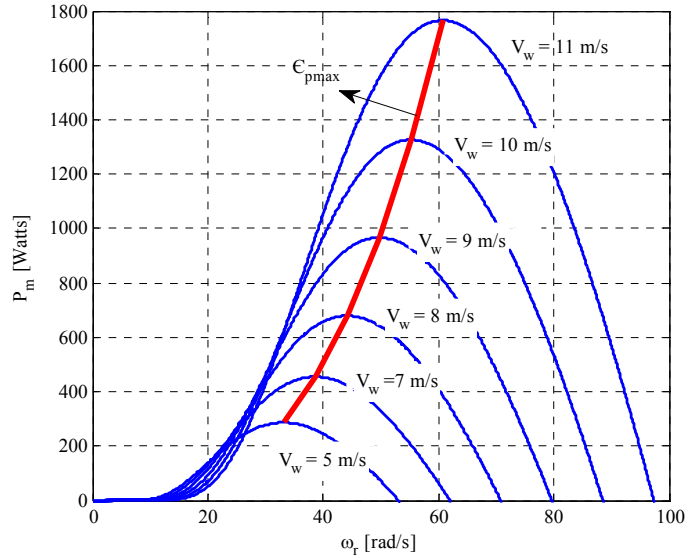
Figure 4.1. Wind turbine mechanical power versus rotor speed at different wind speeds

The aforementioned reasons emphasize the need to investigate the stability of DFIG based wind turbine system.

In DFIG based wind turbine systems, the slip power is limited by the converter ratings in addition to other electro-mechanical limitations. It is therefore crucial to establish the steady state-stability boundaries especially at high wind speeds. Steady-state stability of the doubly-fed induction generator has been evaluated in [46] and [47]. Banakar et al. considers the electrical dynamics by taking the partial derivatives of the electromagnetic torque with respect to the rotor speed, neglecting the mechanical shaft dynamics while Liu et al. considers the shaft dynamics in the form of the derivative of the mechanical torque. In addition, Liu et al. also analyzes the effect of rotor excitation voltage on the steady-state stability. They however do not show the effect of blade pitching at high wind speeds and power regulation at both below and above rated wind speed.

References [48]-[54] investigate the wind turbine in a highly fluctuating wind environment. The control scheme developed by the authors employs pitch control to maintain rated power and rotor speed while keeping the torsional torque to a minimum. Reference [55] investigates the effect of shaft torsional dynamics for a DFIG and flywheel system. A coordinated shaft design and DFIG control using both frequency and time domain techniques so as to avoid torsional resonance, a potential threat to the safety of the system.

In this dissertation, a general expression for the steady-state stability of the DFIG for maximum power tracking (MPT), rated power, and power regulation modes are derived. The derivation takes into account the effects of changes in wind speed, rotor speed, and the blade pitch angle. Simulations results are compared with previous work to show the effects of these added parameters on the DFIG stability region. This research takes a cue from [46] by omitting the DFIG's external controls and other connections and only focusing on the intrinsic causes of instability of the system. In the second part of this chapter, the DFIG stability in the presence of measurement errors is investigated. In particular, a vector controlled DFIG system with machine parameters and rotor position estimation errors are considered.

4.2 DFIG Steady-State Stability Criterion

The DFIG wind turbine interaction is governed by the behavior of the rotor shaft dynamics. Assuming the simplified single mass system and neglecting frictional losses, the shaft dynamics is given by

$$pw_r = \frac{P}{2J}(T_e - T_m) = f(\omega_r, V_w, \beta) \tag{4.1}$$

where J is the equivalent inertia of the turbine-generator system, T_m is the turbine mechanical torque, and T_e, is the generator electromagnetic torque. The shaft speed, wind speed and the blade pitch angle are respectively ω_r, V_w, and β and $f(.)$ stands for 'a function of.'

The linearized model of (4.1) at an operating point say, $op(\omega_{r0}, V_{w0}, \beta_0)$, can be approximated using the Taylor series expansion and neglecting higher order terms [48]. The resulting equations are given by (4.2)-(4.4). From (4.4), the transfer functions in (4.5) and (4.6) can be obtained.

$$p\Delta\omega_r = \frac{\partial f}{\partial \omega_r}\bigg|_{op}\Delta\omega_r + \frac{\partial f}{\partial u}\bigg|_{op}\Delta V_w + \frac{\partial f}{\partial \beta}\bigg|_{op}\Delta\beta \tag{4.2}$$

$$p\Delta\omega_r = \frac{P}{2J}\left[\frac{\partial T_e}{\partial \omega_r}\bigg|_{op}\Delta\omega_r - \frac{\partial T_m}{\partial \omega_r}\bigg|_{op}\Delta\omega_r - \frac{\partial T_m}{\partial u}\bigg|_{op}\Delta V_w - \frac{\partial T_m}{\partial \beta}\bigg|_{op}\Delta\beta\right] \tag{4.3}$$

$$\left(p - \frac{P}{2J}\frac{\partial T_e}{\partial \omega_r}\bigg|_{op} + \frac{P}{2J}\frac{\partial T_m}{\partial \omega_r}\bigg|_{op}\right)\Delta\omega_r = -\frac{P}{2J}\left(\frac{\partial T_m}{\partial u}\bigg|_{op}\Delta V_w + \frac{\partial T_m}{\partial \beta}\bigg|_{op}\Delta\beta\right) \tag{4.4}$$

$$\frac{\Delta\omega_r}{\Delta V_w}\bigg|_{\Delta\beta=0} = \frac{-\dfrac{P}{2J}\dfrac{\partial T_m}{\partial u}\bigg|_{op}\Delta V_w}{\left(p - \dfrac{P}{2J}\dfrac{\partial T_e}{\partial \omega_r}\bigg|_{op} + \dfrac{P}{2J}\dfrac{\partial T_m}{\partial \omega_r}\bigg|_{op}\right)} \tag{4.5}$$

$$\frac{\Delta\omega_r}{\Delta\beta}\bigg|_{\Delta V_w=0} = \frac{-\dfrac{P}{2J}\dfrac{\partial T_m}{\partial \beta}\bigg|_{op}}{\left(p - \dfrac{P}{2J}\dfrac{\partial T_e}{\partial \omega_r}\bigg|_{op} + \dfrac{P}{2J}\dfrac{\partial T_m}{\partial \omega_r}\bigg|_{op}\right)} \tag{4.6}$$

59

Finally, the denominator of transfer functions in (4.5) and (4.6) determine the stability of the system. Thus the system is stable if its poles are located in the left hand plane. That is:

$$p = \frac{P}{2J}\left(\frac{\partial T_e}{\partial \omega_r} - \frac{\partial T_m}{\partial \omega_r}\right) < 0$$

or

$$\left.\frac{\partial T_e}{\partial \omega_r}\right|_{op} - \left.\frac{\partial T_m}{\partial \omega_r}\right|_{op} < 0 \tag{4.7}$$

4.2.1. Partial Derivatives of the Wind Turbine Torque

The stability criterion of the DFIG wind turbine has been established by (4.7). The immediate task then is to find the torque expressions and their corresponding partial derivatives. The turbine mechanical torque is given by (4.8) from which the derivatives in (4.3) are given by (4.9), (4.10), and (4.11) [48].

$$T_m = \frac{P_m}{\omega_r} = \frac{1}{2}\frac{\rho\pi R^2 C_p(\lambda,\beta) V_w^3}{\omega_r} \tag{4.8}$$

$$\frac{\partial T_m}{\partial \omega_r} = \frac{\rho\pi R^2}{2\omega_r}V_w^2\left(-C_p\frac{V_w}{\omega_r} + R\frac{\partial C_p}{\partial \lambda}\right) \tag{4.9}$$

$$\frac{\partial T_m}{\partial V_w} = \frac{\rho\pi R^2}{2}V_w\left(3C_p\frac{V_w}{\omega_r} - R\frac{\partial C_p}{\partial \lambda}\right) \tag{4.10}$$

$$\frac{\partial T_m}{\partial \beta} = \frac{\rho\pi R^2}{2\omega_r}V_w^3\frac{\partial C_p}{\partial \beta} \tag{4.11}$$

where

60

$$C_p(\lambda, \beta) = c_1 \left[\frac{c_2}{\lambda_i} - c_3 \beta - c_4 \right] e^{-c_5/\lambda_i} + c_6 \lambda \tag{4.12}$$

$$\frac{1}{\lambda_i} = \frac{1}{\lambda - c_7 \beta} - \frac{c_8}{\beta^3 + 1} \tag{4.13}$$

$$\lambda = \frac{\omega_r R}{V_w} \tag{4.14}$$

In (4.8)-(4.14), the variables are defined as follows: P_m is the turbine mechanical power, ρ is the air density, R is radius of rotor blade, C_p is the power coefficient given by (4.12) and λ is the blade tip speed ratio defined in (4.14). The symbols c_1 to c_8 are constants for a given turbine type and are listed in Appendix. Substituting (4.13) into (4.12), and differentiating, the partial derivatives of the power coefficient with respect to the tip speed ratio and pitch angle are shown respectively in (4.15) and (4.16).

$$\frac{\partial C_p}{\partial \lambda} = \frac{c_1}{(\lambda - c_7 \beta)^2} e^{-\frac{c_5}{\lambda_i}} \left\{ \frac{c_2 c_5}{\lambda_i} - c_3 c_5 \beta - c_4 c_5 - c_2 \right\} + c_6 \tag{4.15}$$

$$\frac{\partial C_p}{\partial \beta} = \left\{ c_1 e^{-\frac{c_5}{\lambda_i}} \left(\begin{array}{c} \dfrac{c_2 c_7}{(\lambda - c_7 \beta)^2} + \dfrac{3 c_2 c_8 \beta^2}{(\beta^3 + 1)^2} - c_3 + \\[2mm] - \left(\dfrac{c_1 c_2 c_5}{\lambda_i} - c_1 c_3 c_5 \beta - c_1 c_4 c_5 \right) \left(\dfrac{c_7}{(\lambda - c_7 \beta)^2} + \dfrac{3 c_8 \beta^2}{(\beta^3 + 1)^2} \right) \end{array} \right) \right\} \tag{4.16}$$

4.2.2. Partial Derivative of the Electromagnetic Torque

The steady-state generator voltage and electromagnetic torque equations in complex form are given by [57]:

$$
\begin{bmatrix} V_{qds} \\ V_{qdr} \end{bmatrix} = \begin{bmatrix} r_s - j\omega L_s & -j\omega L_s \\ -j(\omega - \omega_r) & r_r - j(\omega - \omega_r)L_r \end{bmatrix} \begin{bmatrix} I_{qds} \\ I_{qdr} \end{bmatrix}
\tag{4.17}
$$

$$
T_e = k \operatorname{Im}(\lambda_{qds} I_{qds}^*) \equiv k \operatorname{Im}(L_m I_{qdr} I_{qds}^*)
\tag{4.18}
$$

where, $k = 3P/4$; P is the number of poles of the induction machine; L_m is the machine magnetizing inductance; I_{qds} and I_{qdr} represent the stator and rotor q-d axis currents respectively; V_{qds} and V_{qdr} are respectively the stator and rotor q-d voltages; r_s and r_r are the stator and rotor resistances ; ω is the stator frequency and Im( ) is the imaginary part of a complex variable.

From the generator stator and rotor voltages in (4.17), we can obtain the corresponding currents given respectively by (4.19) and (4.20). The derivative (with respect to the rotor speed) of the electromagnetic torque is obtained by substituting (4.19) and (4.20) into (4.18) and differentiating. The resulting equations are given respectively by (4.22) and (4.23).

$$
I_{qds} = \frac{1}{\Delta}[(r_r - j\omega_{so}L_r)V_{qds} + j\omega L_m V_{qdr}]
\tag{4.19}
$$

$$
I_{qdr} = \frac{1}{\Delta}[j\omega_{so}L_m V_{qds} + (r_s - j\omega L_s)V_{qdr}]
\tag{4.20}
$$

$$
\Delta = (r_r - j\omega_{so}L_r)(r_s - j\omega L_s) + \omega L_m^2 \omega_{so}
\tag{4.21}
$$

$$
T_e = \frac{kL_m}{|\Delta|^2} \left\{ \begin{array}{l} \omega_{so}L_m r_r |V_{qds}|^2 - \omega L_m r_s |V_{qdr}|^2 + (r_r r_s + \omega_{so}L_r \omega L_s)\operatorname{Im}(V_{qds}^* V_{qdr}) + \\ + \omega L_m^2 \omega_{so} \operatorname{Im}(V_{qds} V_{qdr}^*) - (\omega L_s r_r - \omega_{so}L_r r_s)\operatorname{Re}(V_{qds}^* V_{qdr}) \end{array} \right\}
\tag{4.22}
$$

$$\frac{dT_e}{d\omega_r} = \frac{L_m k}{|\Delta|^4} \begin{bmatrix} |\Delta|^2 \begin{Bmatrix} -L_m r_r |V_{qds}|^2 - L_r \omega L_s (V_{qs} V_{dr} - V_{ds} V_{qr}) - \omega L_m^2 (V_{ds} V_{qr} - V_{qs} V_{dr}) + \\ + L_r r_s (V_{qs} V_{qr} + V_{ds} V_{dr}) \end{Bmatrix} \\ - \begin{Bmatrix} \omega_{so} L_m r_r |V_{qds}|^2 - \omega L_m r_s |V_{qdr}|^2 + \\ + (r_r r_s + \omega_{so} L_r \omega L_s)(V_{qs} V_{dr} - V_{ds} V_{qr}) + \\ + \omega L_m^2 \omega_{so} (V_{ds} V_{qr} - V_{qs} V_{dr}) + \\ - (\omega L_s r_r - \omega_{so} L_r r_s)(V_{qs} V_{qr} + V_{ds} V_{dr}) \end{Bmatrix} \times \begin{Bmatrix} 2(\omega L_s L_r - \omega L_m^2) \begin{pmatrix} r_s r_r + \\ - \omega L_s \omega_{so} L_r \\ + \omega L_m^2 \omega_{so} \end{pmatrix} \\ - 2L_r r_s (\omega L_s r_r + \omega_{so} L_r r_s) \end{Bmatrix} \end{bmatrix} \qquad (4.23)$$

The slip speed is $\omega_{so} = \omega - \omega_r$.

4.3 Mapping the DFIG Stability Boundaries

4.3.1. Maximum Power Point Tracking Mode

At low to medium wind speeds, the objective of the wind turbine control is to track the maximum power coefficient profile as shown in Figure 4.1. Under this consideration, the partial derivative of the power coefficient (4.12) with respect to the tip speed ratio is null and (4.9) reduces to:

$$\frac{\partial T_m}{\partial \omega_r} = -\frac{\rho \pi R^2}{2} \frac{C_p}{\omega_r^2} V_w^3 \qquad (4.24)$$

Substituting (4.23) and (4.24) into (4.7), the criteria for the DFIG steady-state stability when operating in MPT mode is obtained.

Figure 4.2 shows the stability profile of a 5 hp wind turbine (parameters are given in Appendix) as a function of the rotor speed, ω_r and rotor voltage angle , ϕ at different peak rotor voltages, V_r when operating in the MPT mode using the criteria given in (4.7). For comparison purposes, the stability profile by the conventional approach. That is using

(4.23) and neglecting the partial derivative of the mechanical torque with respect to rotor speed, is also depicted in Figure 4.3. The contour in Figure 4.2 shows that when compared with the conventional approach, the method proposed in this dissertation reveals a significant narrowing of the stability region in the sub-synchronous region (synchronous speed is 125.67 rad/s) but shows a much milder effect in the super-synchronous region. This is a significant result since it shows that incorporating the effect of the mechanical defines a more accurate region of operation of the DFIG wind turbine system.
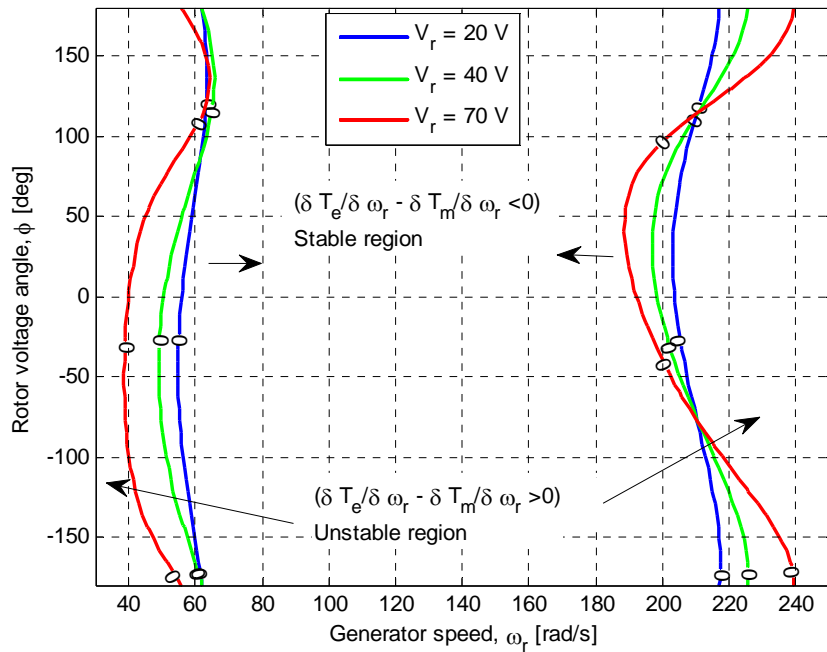
Figure 4.2. Steady-state stability region for the MPT mode (proposed approach)
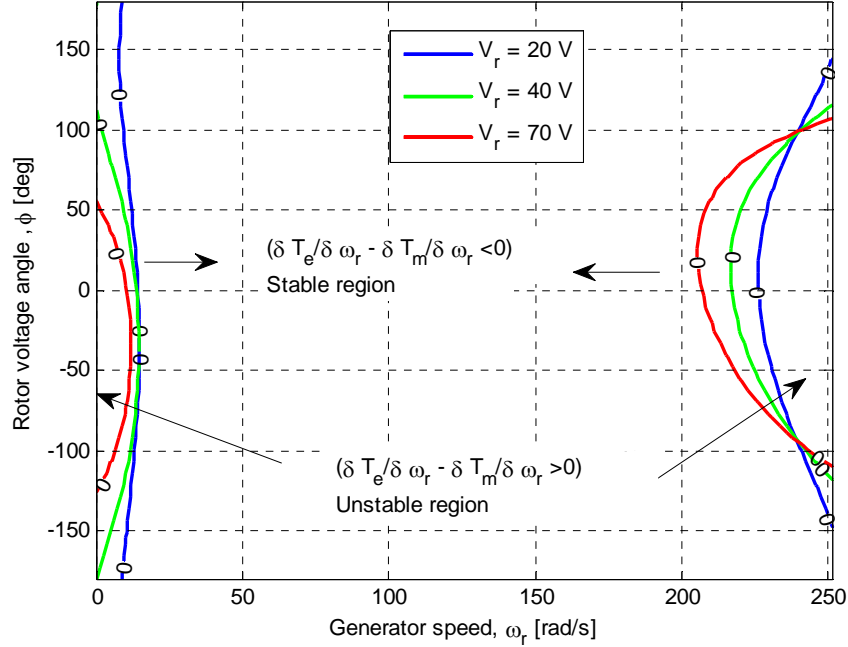
Figure 4.3. Steady-state stability region for the MPT mode (conventional approach)

4.3.2. Rated Power Mode

At high wind speeds, blade pitch angle control is used to limit the wind turbine power to its rated value. With the output power controlled to the rated value, the power coefficient C_p is shown to be a cubic function of the wind speed as given by (4.25). Equation (4.9) can then be rewritten for rated power mode by differentiating (4.25) and substituting the obtained derivative into (4.9) to obtain (4.27). Alternatively, substituting (4.15) into (4.9) introduces the pitch angle explicitly into the stability criteria as given by (4.28). The effect of both (4.27) and (4.28) will be explored.

$$C_p(\lambda, \beta) = \frac{\gamma}{V_w^3} \qquad (4.25)$$

$$\gamma = 2P_{m,\text{rated}} \frac{1}{\rho \pi R^2} \tag{4.26}$$

$$\frac{\partial T_m}{\partial \omega_r} = 2P_{m,\text{rated}} \frac{1}{\omega_r^2} \tag{4.27}$$

$$\frac{\partial T_m}{\partial \omega_r} = \frac{\rho \pi R^2}{2\omega_r} V_w^2 \left(\begin{array}{l} -C_p \dfrac{V_w}{\omega_r} + \dfrac{Rc_1}{(\lambda - c_7\beta)^2} \times \\[2mm] e^{-\frac{c_5}{\lambda_i}} \left\{ \dfrac{c_2 c_5}{\lambda_i} - c_3 c_5 \beta - c_4 c_5 - c_2 \right\} + c_6 \end{array} \right) \tag{4.28}$$

In the above equations, $P_{m,\text{rated}}$ is the wind turbine rated output power.

At any rotor speed, ω_r, the tip speed ratio is given by (4.14) and power coefficient, $C_p(\lambda, \beta)$, can be found from (4.25). In this situation the only unknown term is the pitch angle β required to maintain the rated power. The roots of the exponential function in (4.12) or its equivalent polynomial using curve-fitting gives the corresponding pitch angle, β.

Figure 4.4 illustrates the contour of the DFIG stability region corresponding to the rated output power mode using (4.27). As in the MPT mode, the stability region is much wider in the super-synchronous region. However, in the sub-synchronous region, the stability profile is narrower and varies for various combinations of the rotor voltage magnitude and phase angle.

Equation (4.12) can be used to depict the contour of the power coefficient as shown in Figure 4.5. One can infer from this contour that at lower tip speed ratios (about $\lambda < 10$), the power coefficient is less sensitive to changes in the pitch angle than at higher tip speed ratios (about $\lambda > 10$). In the rated power mode, the wind speed is inversely proportional to the turbine power coefficient. Therefore in Figure 4.5, increasing contour

lines means decreasing wind speed. For a given wind speed for example, Figure 4.5 shows there are infinite number combinations of λ and β to obtain a fixed C_p.

Combining (4.12) and (4.25) and solving, results in the solution of β for varying λ as shown in Figure 4.6. It should be mentioned that some of the solutions of β may turn out to be very large or negative and have been dropped for obvious practical considerations.
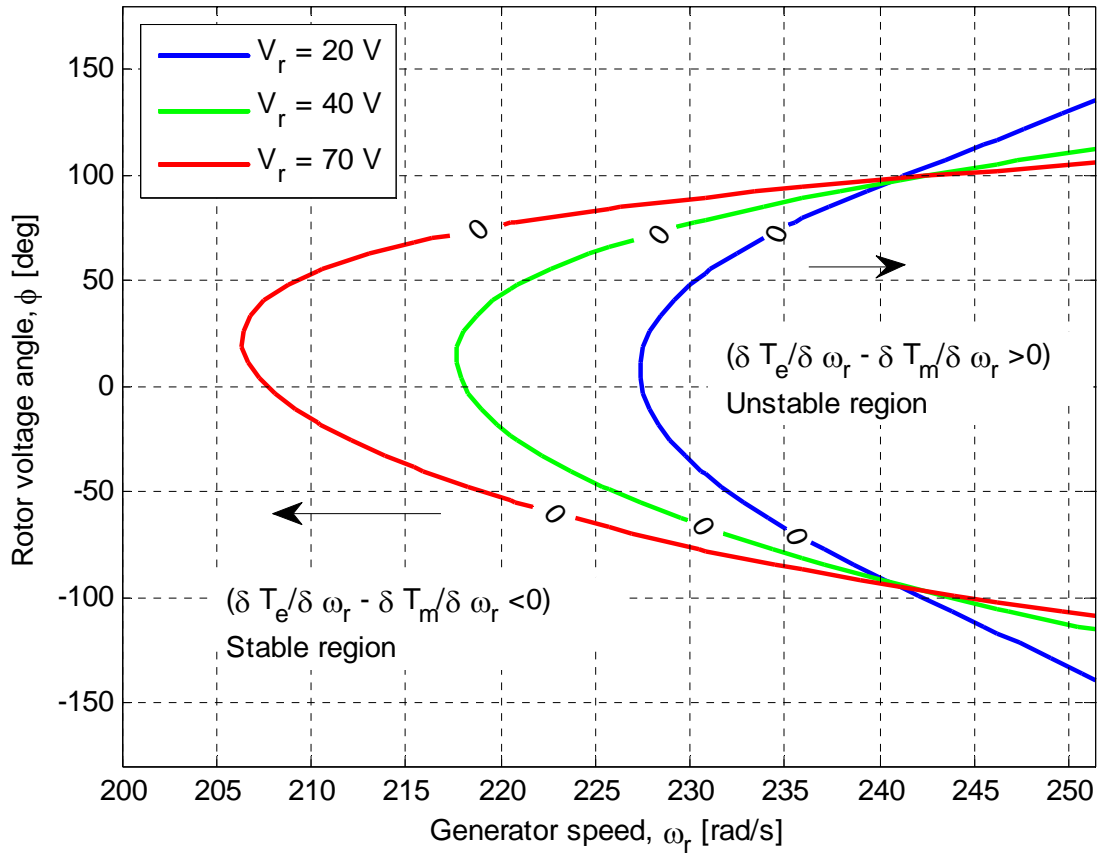
Figure 4.4. Steady- state stability region for the DFIG in rated power mode (proposed approach)
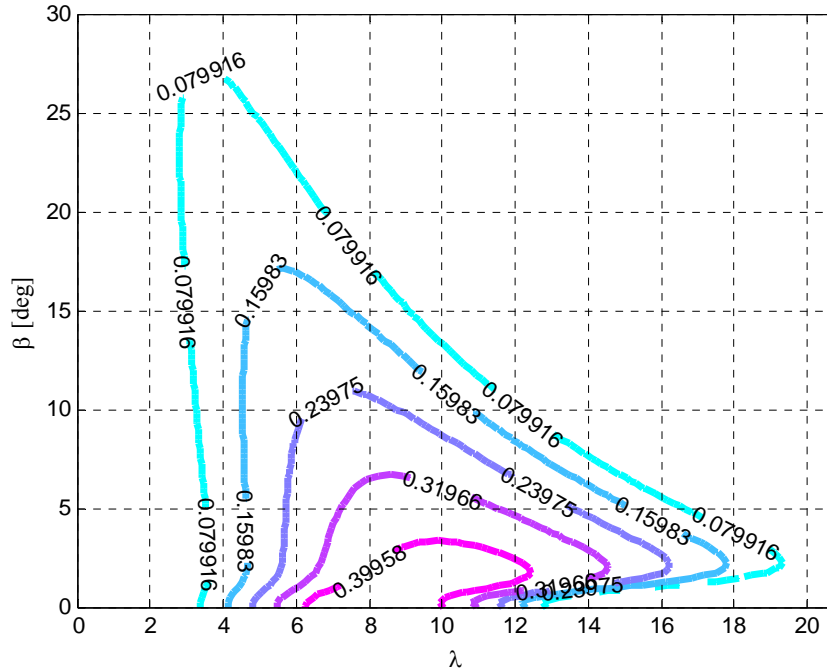
Figure 4.5. The Contour of the power coefficient as a function of the tip speed ratio, λ and pitch angle, β
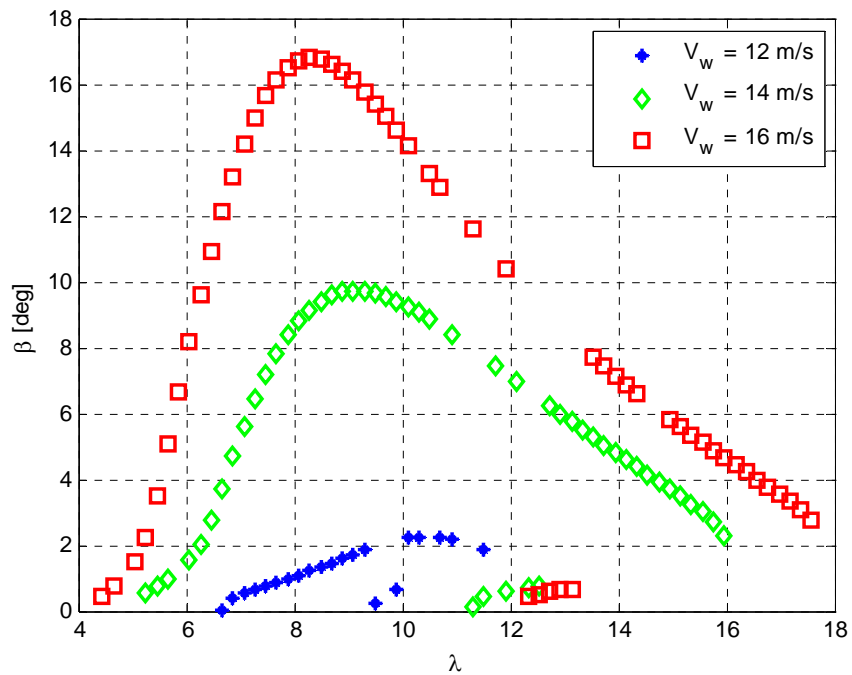
Figure 4.6. The blade pitch angle β and the tip speed ratio λ at various wind speeds

The solutions of β and λ shown in Figure 4. 6 show that in order to maintain a constant power, while varying rotor speed, the range of λ is very limited. At lower wind speeds above the rated speed, the range of λ is small, increasing as the wind speed moves towards the cut-out speed. Figure 4.7 shows the contour of the DFIG wind turbine in the rated power mode evaluated using the solutions of β and λ found in Figure 4. 6. This compares with a similar contour depicted in Figure 4.4. It shows that the sub-synchronous stability boundary has been significantly narrowed by the effect of the pitch angle regulation. Figure 4.8 shows the same pattern as the wind speed is changed. It can be seen that the sub-synchronous region is heavily affected as the speed changes but the super-synchronous regions remain fairly constant.
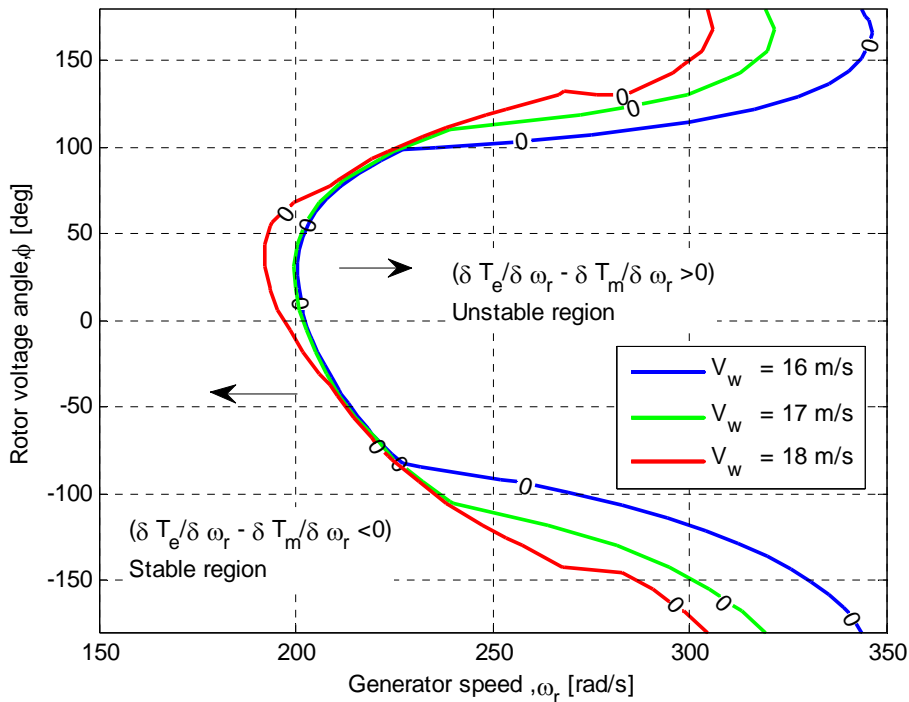
Figure 4.7. Contour of the stability region at selected wind speeds showing the effect of blabe pitching
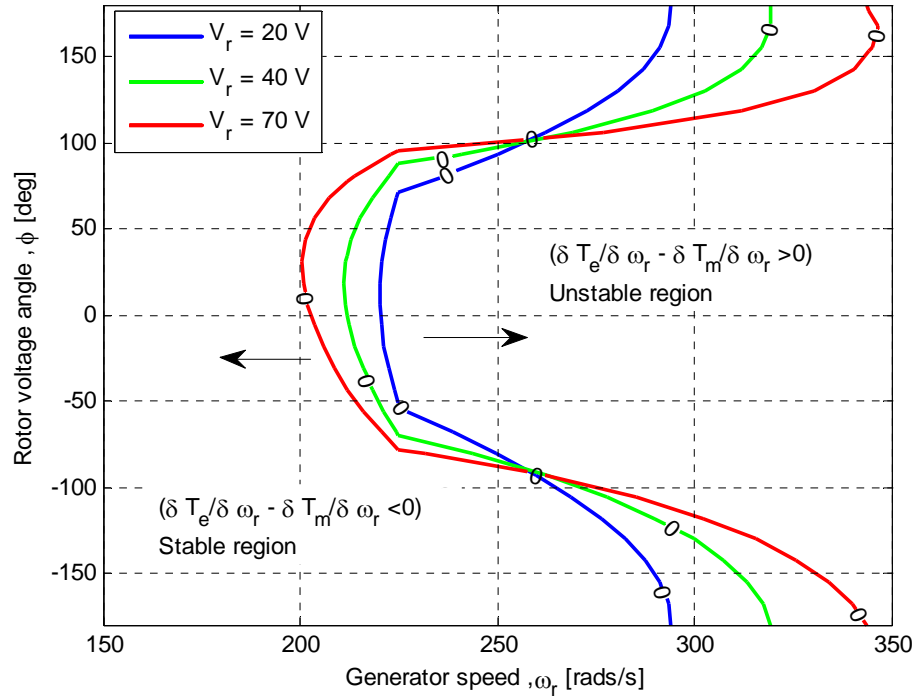
Figure 4.8. Contour of the stability region at selected rotor voltages showing the effect of pitching ($V_w = 16m/s$)

4.3.3. Power Regulation Mode

4.3.3.1.**Wind speed less than rated speed.** With increased penetration level of wind power in power system, it is not accurate to assume that the wind turbine operates in the MPT and rated output power modes only. For maintaining regulated frequency and voltage in the power system, the generated power should be equal to the demanded power. Hence in that condition, the variable-speed, variable-pitch wind turbine should be operated in the power regulation mode whenever necessary. When the wind speed is less than the rated speed, the pitch angle is always kept as zero and the power output of turbine varies with rotor speed. Figure 4.9 is used as the reference to obtain the stability profiles shown in Figures 4.11 and 4.12. Figures 4.11 and 4.12 depict that there is no

significant effect on the stability profile as the power level varies. However, as in the case of MPT, increased rotor voltage magnitude reduces the stability region.

4.3.3.2.**Wind speed greater than rated speed.** If the wind speed is more than rated speed, then the turbine speed is maintained at rated turbine speed and the blade is pitched to extract less mechanical power from the wind for safe operation of the wind generator. However, when the load decreases, the power output from the turbine should be reduced to match the load. Figure 4.10. shows the variation of the blade pitch angle with wind speed during power regulation operation mode. Power regulation above rated speed can be done by a combination of pitch angle and/or rotor speed variations. From the power speed curve shown in Figure 4.1, increasing the rotor speed gives a faster response to lowering the power than using decreasing rotor speed. This means that $\frac{\partial T_m}{\partial \omega_r} < 0$ and since at any operating, point considering losses, $T_e < T_m$ and thus the stability criteria given in (4.7) is negative and the system is always stable for λ and β shown in Figure 4.10.
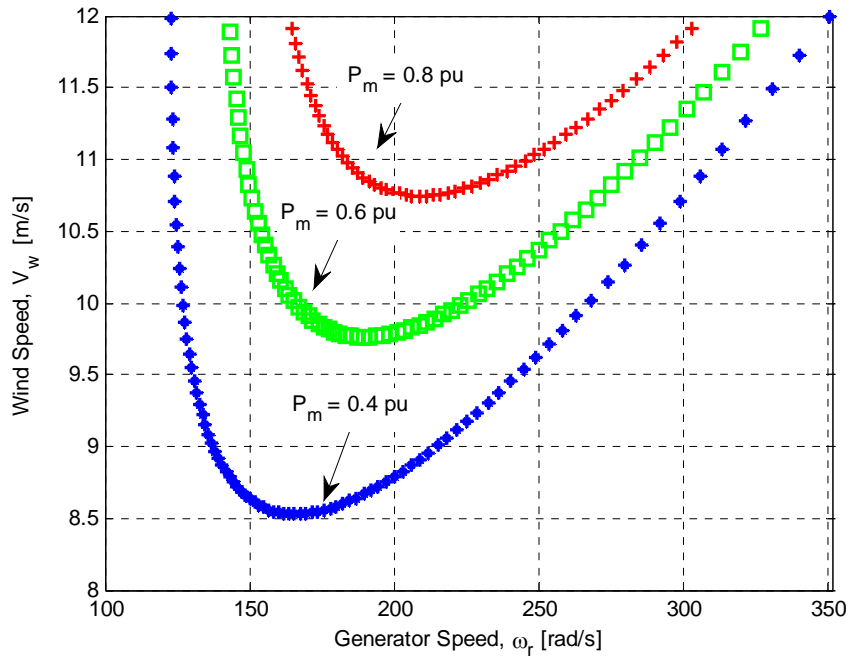
Figure 4.9. Wind speed, V_w (below rated wind speed) versus rotor speed ω_r, at various turbine output power levels
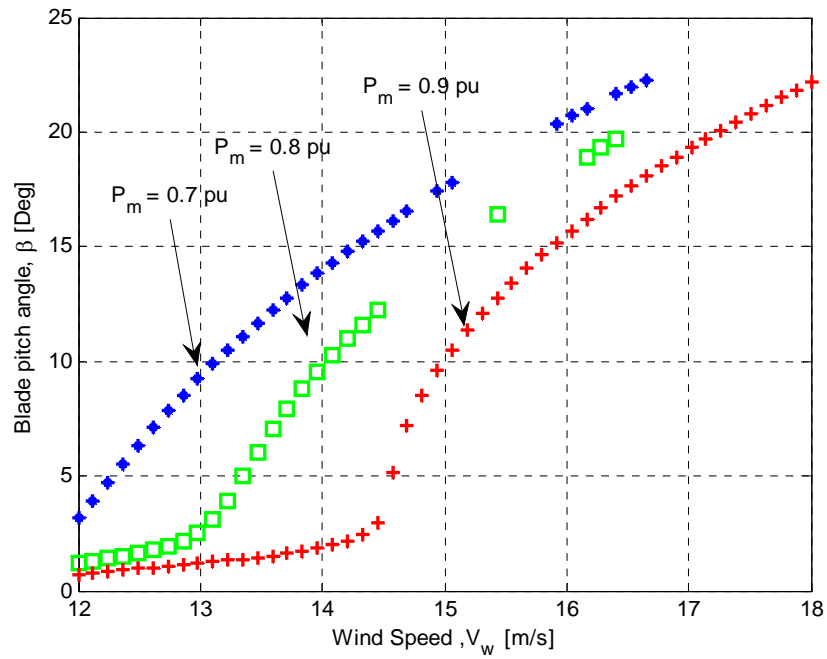
Figure 4.10.   Wind speed, V_w (above rated wind speed) versus pitch angle β, at various turbine output power levels

72
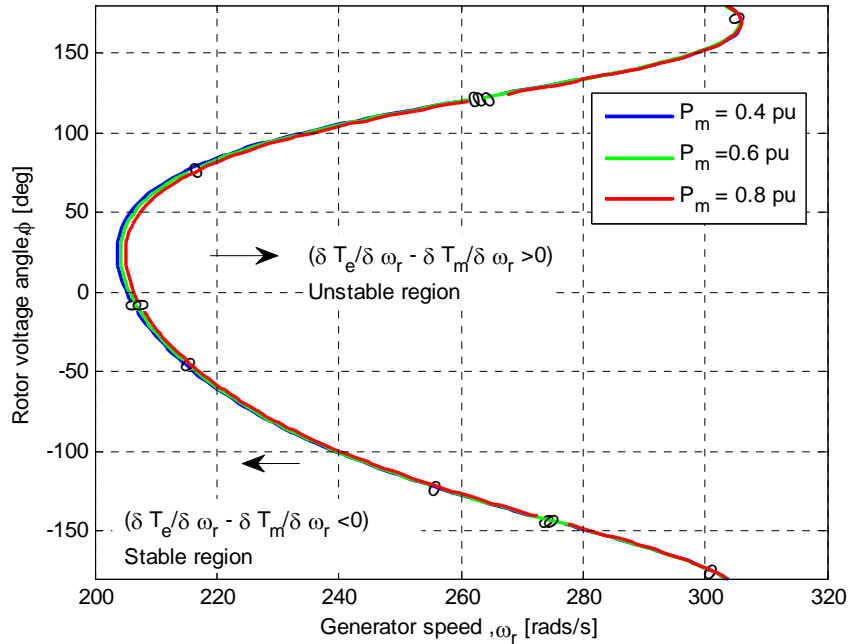
Figure 4.11.   Stability region in power regulation mode for wind speed less than rated speed at various turbine output powers
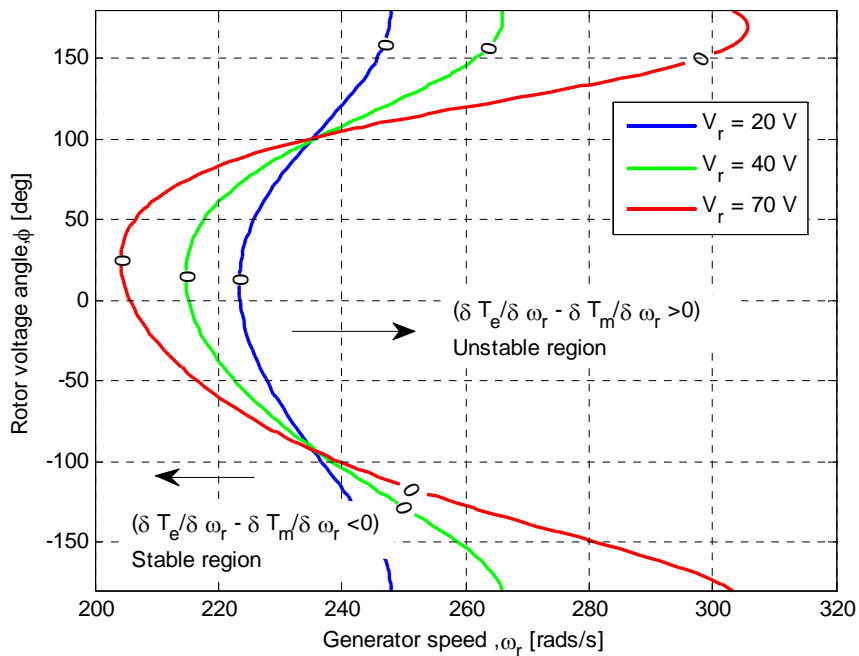
Figure 4.12.   Stability region in power regulation mode for wind speed less than rated speed at various rotor voltage magnitudes

4.4 Effects of Machine Parameters and Rotor Position Errors on the Stability of Vector Controlled DFIG

The typical control schemes used to control the flow of active and reactive powers to and from the grid include Direct Power Control (DPC) [73], [74], Direct Torque control (DTC) [75], and vector control [76]-[78]. Both DPC and DTC have the advantage of having a simpler structure and less dependence on machine parameters. The drawbacks of the DTC are the variable switching frequency structure and torque ripple.

This section does not attempt to establish the pros and cons of the various control schemes but specifically tries to investigate the conventional vector control scheme as applied to DFIG wind turbine systems. In vector control, decoupling of active and reactive is usually achieved by aligning the *d*-axis on either the stator flux vector position [77], [78] or the stator voltage vector position [76]. Figure 4.13 shows a typical vector control scheme for the rotor-side converter (RSC) utilizing coordinate transformation. These transformations depend on accurate knowledge of the rotor position as well as stator flux/voltage angle. Therefore, any error in angle measurements/estimates will result in inaccurate reference signals (voltages, currents, speed and power).

Reference [77] investigates the effects of errors in slip angle while [78] and [79], examines the sensitivity of the vector control system to errors in estimating machine parameters such as the stator, rotor and their mutual inductance as well as the rotor position error [78] for a sensorless DFIG model. In this research, the combined effect of the inaccuracies in machine inductances and rotor position for the RSC control system shown in Figure 4.13 is investigated.

74

4.4.1. Induction Machine Model

The induction machine can be modeled by the following *q-d* equations in the synchronous reference frame. The voltage, flux, electromagnetic torque and speed equations are respectively:

$$\begin{cases} v_{qs} = -r_s i_{qs} + p\lambda_{qs} + \omega_e \lambda_{ds} \\ v_{ds} = -r_s i_{ds} + p\lambda_{ds} - \omega_e \lambda_{qs} \\ v_{qr} = r_r i_{qr} + p\lambda_{qr} + (\omega_e - \omega_r)\lambda_{dr} \\ v_{dr} = r_r i_{dr} + p\lambda_{dr} + (\omega_e - \omega_r)\lambda_{qr} \end{cases} \tag{4.29}$$

$$\begin{cases} \lambda_{qs} = -L_s i_{qs} + L_m i_{qr} \\ \lambda_{ds} = -L_s i_{ds} + L_m i_{dr} \\ \lambda_{qr} = -L_m i_{qs} + L_r i_{qr} \\ \lambda_{dr} = -L_m i_{ds} + L_r i_{dr} \end{cases} \tag{4.30}$$

$$T_e = \frac{3}{2}\frac{P}{2}\left(\lambda_{ds} i_{qs} - \lambda_{qs} i_{ds}\right) \tag{4.31}$$

$$p\omega_r = \frac{P}{2J}(T_e - T_m) \tag{4.32}$$

In (4.29) – (4.32), the machine parameters are the stator resistance r_s, the rotor resistance r_r, the stator inductance L_s, rotor inductance L_r, and their mutual inductance L_m. The stator and rotor $d-q$ voltages, currents and flux linkages are respectively $v_{ds}, v_{qs}, v_{dr}, v_{qr}$; $i_{qs}, i_{ds}, i_{qr}, i_{dr}$ and $\lambda_{qs}, \lambda_{ds}\ \lambda_{qr}, \lambda_{dr}$. The variables ω_e, ω_r, T_e, T_m, P and J are respectively the synchronous angular speed, rotor angular speed, electromagnetic torque, mechanical torque, number of poles and inertia of combined turbine-generator
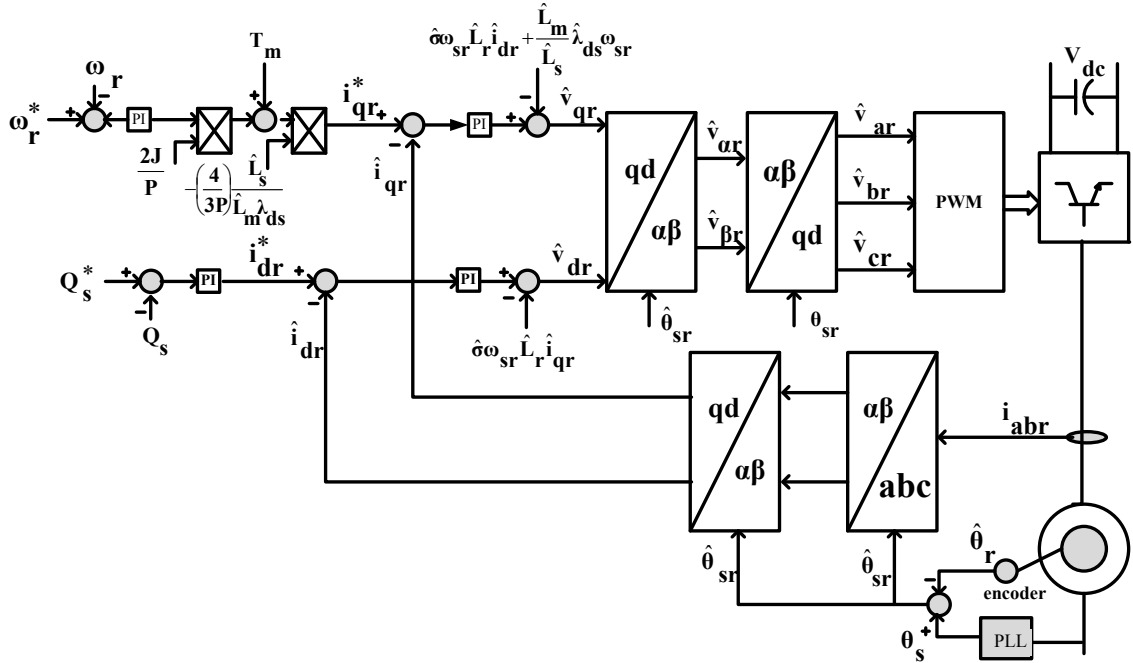
Figure 4.13.   Rotor side converter control structure

system. The subscript s and r refer to stator and rotor variables and $p = \dfrac{d}{dt}$ represent the time derivative operator.

In the stator flux-oriented control, the d – axis is aligned with the stator flux enabling decoupled control of the active and reactive powers. That is:

$$\lambda_{qs} = 0 \quad and \quad \lambda_{ds} = \lambda_s \approx \text{constant} \tag{4.33}$$

Substituting (4.33) into (4.30) and solving for the stator currents results in (4.34) and (4.35). Subsequent substitution of (4.34) and (4.35) into the rotor voltage equations in (4.30) gives (4.36) and (4.37).

$$i_{qs} = \frac{L_m}{L_s} i_{qr} \tag{4.34}$$

76

$$i_{ds} = -\frac{1}{L_s}\lambda_{ds} + \frac{L_m}{L_s}i_{dr} \tag{4.35}$$

$$\lambda_{qr} = \sigma L_r i_{qr} \tag{4.36}$$

$$\lambda_{dr} = \frac{L_m}{L_s}\lambda_{ds} + \sigma L_r i_{dr} \tag{4.37}$$

$$p\begin{bmatrix} i_{qr} \\ i_{dr} \end{bmatrix} = A\begin{bmatrix} i_{qr} \\ i_{dr} \end{bmatrix} + B\begin{bmatrix} v_{qr} \\ v_{dr} \end{bmatrix} + D \tag{4.38}$$

where

$$A = \begin{bmatrix} -\dfrac{r_r}{\sigma L_r} & \omega_{sr} \\[2ex] -\omega_{sr} & -\dfrac{r_r}{\sigma L_r} \end{bmatrix} \tag{4.39}$$

$$B = \begin{bmatrix} \dfrac{1}{\sigma L_r} & 0 \\[2ex] 0 & \dfrac{1}{\sigma L_r} \end{bmatrix} \tag{4.40}$$

$$D = \begin{bmatrix} 0 \\ -\dfrac{L_m}{L_s}\omega_{sr}\lambda_{ds} \end{bmatrix} \tag{4.41}$$

$$\sigma = 1 - \frac{L_m^2}{L_r L_s}, \quad \omega_{sr} = \omega_e - \omega_r \tag{4.42}$$

4.4.2. Sources of Errors

In Figure 4.13 of the vector control architecture, two sources of errors can readily be identified; rotor position/speed measurement errors and machine parameter errors. The

co-ordinate transformations blocks involve the use of rotor and stator angles (slip angle). That is:

$$\begin{bmatrix} i_{\alpha r} \\ i_{\beta r} \end{bmatrix} = \begin{bmatrix} \cos\theta_{sr} & -\sin\theta_{sr} \\ \sin\theta_{sr} & \cos\theta_{sr} \end{bmatrix} \begin{bmatrix} i_{dr} \\ i_{qr} \end{bmatrix} \tag{4.43}$$

$$\begin{bmatrix} v_{dr} \\ v_{qr} \end{bmatrix} = \begin{bmatrix} \cos\theta_{sr} & \sin\theta_{sr} \\ -\sin\theta_{sr} & \cos\theta_{sr} \end{bmatrix} \begin{bmatrix} v_{\alpha r} \\ v_{\beta r} \end{bmatrix} \tag{4.44}$$

where $\theta_{sr} = \theta_s - \theta_r$ is the slip angle. and θ_s, θ_r are the stator supply and rotor angles respectively.

As can be observed from (4.43) and (4.44), any error in either the phase-locked loop (PLL) or the encoder, introduces errors into the transformation blocks. That is:

$$\Delta\theta_{sr} = \theta_{sr} - \hat{\theta}_{sr} \tag{4.45}$$

where θ_{sr} and $\hat{\theta}_{sr}$ represent the actual and observed slip angles respectively. Thus from (4.43) and (4.44), the observed currents and voltages are given by [77]:

$$\begin{bmatrix} \hat{i}_{dr} \\ \hat{i}_{qr} \end{bmatrix} = \begin{bmatrix} \cos\hat{\theta}_{sr} & \sin\hat{\theta}_{sr} \\ -\sin\hat{\theta}_{sr} & \cos\hat{\theta}_{sr} \end{bmatrix} \begin{bmatrix} i_{\alpha r} \\ i_{\beta r} \end{bmatrix} \tag{4.46}$$

$$\begin{bmatrix} v_{\alpha r} \\ v_{\beta r} \end{bmatrix} = \begin{bmatrix} \cos\hat{\theta}_{sr} & \sin\hat{\theta}_{sr} \\ -\sin\hat{\theta}_{sr} & \cos\hat{\theta}_{sr} \end{bmatrix} \begin{bmatrix} \hat{v}_{dr} \\ \hat{v}_{qr} \end{bmatrix} \tag{4.47}$$

Substituting (4.43) into (4.46) and (4.44) into (4.47), together with (4.45), we have:

$$\begin{bmatrix} \hat{i}_{dr} \\ \hat{i}_{qr} \end{bmatrix} = \begin{bmatrix} \cos\Delta\theta_{sr} & -\sin\Delta\theta_{sr} \\ \sin\Delta\theta_{sr} & \cos\Delta\theta_{sr} \end{bmatrix} \begin{bmatrix} i_{dr} \\ i_{qr} \end{bmatrix} \tag{4.48}$$

$$\begin{bmatrix} v_{dr} \\ v_{qr} \end{bmatrix} = \begin{bmatrix} \cos\Delta\theta_{sr} & \sin\Delta\theta_{sr} \\ -\sin\Delta\theta_{sr} & \cos\Delta\theta_{sr} \end{bmatrix} \begin{bmatrix} \hat{v}_{dr} \\ \hat{v}_{qr} \end{bmatrix} \tag{4.49}$$

In matrix form (4.48) and (4.49) can be rewritten as:

$$\begin{bmatrix} i_{dr} \\ i_{qr} \end{bmatrix} = T^{-1} \begin{bmatrix} \hat{i}_{dr} \\ \hat{i}_{qr} \end{bmatrix}$$

(4.50)

$$\begin{bmatrix} v_{dr} \\ v_{qr} \end{bmatrix} = T^{-1} \begin{bmatrix} \hat{v}_{dr} \\ \hat{v}_{qr} \end{bmatrix}$$

(4.51)

where

$$T = \begin{bmatrix} \cos \Delta \theta_{sr} & -\sin \Delta \theta_{sr} \\ \sin \Delta \theta_{sr} & \cos \Delta \theta_{sr} \end{bmatrix}$$

(4.52)

Substituting (4.50) and (4.51) into (4.38), results in

$$p \begin{bmatrix} \hat{i}_{dr} \\ \hat{i}_{qr} \end{bmatrix} = TAT^{-1} \begin{bmatrix} \hat{i}_{dr} \\ \hat{i}_{qr} \end{bmatrix} + TBT^{-1} \begin{bmatrix} \hat{v}_{dr} \\ \hat{v}_{qr} \end{bmatrix} + TD$$

(4.53)

4.4.3. Modeling the Effects of Errors

4.4.3.1. **Inner current control loop.** The $d-q$ axes current controller in Figure 4.13 can be modeled as:

$$px_1^c = i_{dr}^* - \hat{i}_{dr}$$

(4.54)

$$px_2^c = i_{qr}^* - \hat{i}_{qr}$$

(4.55)

$$v_{qr}^* = \left(k_{p2}^c + \frac{k_{i2}^c}{p} \right) \left(i_{qr}^* - \hat{i}_{qr} \right)$$

(4.56)

$$v_{dr}^* = \left(k_{p1}^c + \frac{k_{i1}^c}{p} \right) \left(i_{dr}^* - \hat{i}_{dr} \right)$$

(4.57)

where k_{p1}^c, k_{i1}^c and k_{p2}^c, k_{i2}^c are the PI controller gains for the d-axis and q-axis rotor

current controllers. The asterix ($*$) superscript refer to reference variables.

Expanding (4.56) and (4.57) as well as substituting for (4.54) and (4.55), we obtain (4.58)

and (4.59) respectively.

$$v_{qr}^* = k_{p2}^c i_{qr}^* - k_{p2}^c \hat{i}_{qr} + k_{i2}^c x_2^c \tag{4.58}$$

$$v_{dr}^* = k_{p1}^c i_{dr}^* - k_{p1}^c \hat{i}_{dr} + k_{i1}^c x_1^c \tag{4.59}$$

From (4.38), (4.58), and (4.59), the observed rotor voltage equations can be written as:

$$\hat{v}_{qr} = k_{p2}^c i_{qr}^* - k_{p2}^c \hat{i}_{qr} + k_{i2}^c x_2^c + \hat{\sigma}\hat{\omega}_{sr}\hat{L}_r i_{dr} + \frac{\hat{L}_m}{\hat{L}_s}\lambda_{ds}\hat{\omega}_{sr} \tag{4.60}$$

$$\hat{v}_{dr} = k_{p1}^c i_{dr}^* - k_{p1}^c \hat{i}_{dr} + k_{i1}^c x_1^c - \hat{\omega}_{sr}\hat{\sigma}\hat{L}_r i_{qr} \tag{4.61}$$

In matrix form, (4.54) – (4.55) and (4.60) – (4.61) can be rewritten respectively as:

$$p\begin{bmatrix} x_1^c \\ x_2^c \end{bmatrix} = -I_{2\times 2}\begin{bmatrix} \hat{i}_{dr} \\ \hat{i}_{qr} \end{bmatrix} + I_{2\times 2}\begin{bmatrix} i_{dr}^* \\ i_{qr}^* \end{bmatrix} \tag{4.62}$$

$$\begin{bmatrix} \hat{v}_{dr} \\ \hat{v}_{qr} \end{bmatrix} = K_i^c\begin{bmatrix} x_1^c \\ x_2^c \end{bmatrix} + \hat{K}_p^c\begin{bmatrix} \hat{i}_{dr} \\ \hat{i}_{qr} \end{bmatrix} + K_p^c\begin{bmatrix} i_{dr}^* \\ i_{qr}^* \end{bmatrix} + \hat{D} \tag{4.63}$$

where $K_i^c = \begin{bmatrix} k_{i1}^c & 0 \\ 0 & k_{i2}^c \end{bmatrix}$, $\hat{K}_p^c = \begin{bmatrix} -k_{p1}^c & -\hat{\sigma}\hat{\omega}_{sr}\hat{L}_r \\ \hat{\omega}_{sr}\hat{\sigma}\hat{L}_r & -k_{p2}^c \end{bmatrix}$, $K_p^c = \begin{bmatrix} k_{p1}^c & 0 \\ 0 & k_{p2}^c \end{bmatrix}$ and $\hat{D} = \begin{bmatrix} 0 \\ -\dfrac{\hat{L}_m}{\hat{L}_s}\hat{\omega}_{sr}\lambda_{ds} \end{bmatrix}$

Substituting (4.63) into (4.52), gives (4.64). A fourth-order dynamic system is obtained

by combining (4.62) and (4.64) as in (4.65).

$$p\begin{bmatrix} \hat{i}_{dr} \\ \hat{i}_{qr} \end{bmatrix} = \begin{bmatrix} TAT^{-1}\begin{bmatrix} \hat{i}_{dr} \\ \hat{i}_{qr} \end{bmatrix} + TBT^{-1}K_i^c\begin{bmatrix} x_1^c \\ x_2^c \end{bmatrix} + \\ TBT^{-1}\hat{K}_p^c\begin{bmatrix} \hat{i}_{dr} \\ \hat{i}_{qr} \end{bmatrix} + TBT^{-1}K_p^c\begin{bmatrix} i_{dr}^* \\ i_{qr}^* \end{bmatrix} + TBT^{-1}\hat{D} + TD \end{bmatrix} \tag{4.64}$$

$$px = A^c x + B^c u + E^c \tag{4.65}$$

where $A^c = \begin{bmatrix} TAT^{-1} + TBT^{-1}\hat{K}_p^c & TBT^{-1}K_i^c \\ -I_{2\times2} & 0 \end{bmatrix}$, $B^c = \begin{bmatrix} TBT^{-1}K_p^c \\ I_{2\times2} \end{bmatrix}$, $E^c = \begin{bmatrix} 0 \\ -TBT^{-1}D + TD \end{bmatrix}$,

$x^T = \begin{bmatrix} \hat{i}_{dr} & \hat{i}_{qr} & x_1^c & x_2^c \end{bmatrix}$, and $u^T = \begin{bmatrix} i_{dr}^* & i_{qr}^* \end{bmatrix}$.

For simplicity, it is reasonable to assume that the d- and q-axes PI controller gains are equal resulting in (4.66) - (4.68):

$$k_{p1}^c = k_{p2}^c = k_p^c \quad , \quad k_{i1}^c = k_{i2}^c = k_i^c \tag{4.66}$$

$$K_i^c = k_i^c I_{2\times2}, \quad K_p^c = k_p^c I_{2\times2} \tag{4.67}$$

$$A^c = \begin{bmatrix} TAT^{-1} + TBT^{-1}\hat{K}_p^c & TBT^{-1}k_i^c \\ -I_{2\times2} & 0 \end{bmatrix} \tag{4.68}$$

Finally, substituting all the sub matrices in (4.68) results in (4.69).

$$A^c = \begin{bmatrix} -\dfrac{r_r + k_p^c}{\sigma L_r} & \omega_{sr} - \dfrac{\hat{\sigma}\hat{\omega}_{sr}\hat{L}_r}{\sigma L_r} & \dfrac{1}{\sigma L_r}k_i^c & 0 \\[3mm] -\omega_{sr} + \dfrac{\hat{\sigma}\hat{\omega}_{sr}\hat{L}_r}{\sigma L_r} & -\dfrac{r_r + k_p^c}{\sigma L_r} & 0 & \dfrac{1}{\sigma L_r}k_i^c \\[3mm] -1 & 0 & 0 & 0 \\[3mm] 0 & -1 & 0 & 0 \end{bmatrix} \tag{4.69}$$

4.4.3.2.**Stability analysis of current loop.** Using the Routh-Hurwitz criteria for a fourth-order polynomial, the conditions for system stability can be established with the characteristic equation is given by

$$AD(s) = \left| sI_{4\times4} - A^c \right| = 0 \tag{4.70}$$

$$D(s) = a_4 s^4 + a_3 s^3 + a_2 s^2 + a_1 s + a_0 \tag{4.71}$$

where $a_0 = \left(\dfrac{k_i^c}{\sigma L_r}\right)^2$, $a_1 = \dfrac{2k_i^c(r_r + k_p^c)}{\sigma^2 L_r^2}$, $a_3 = \dfrac{2(r_r + k_p^c)}{\sigma L_r}$, $a_4 = 1$, and

$$a_2 = \frac{1}{\sigma^2 L_r^2}\left(2r_r k_p^c + 2\sigma L_r k_i^c + (\omega_{sr}\sigma\, L_r - \hat{\omega}_{sr}\hat{\sigma}\, \hat{L}_r)^2 + (k_p^c)^2 + r_r^2\right).$$

According to the Routh-Hurwitz stability criteria for a fourth-order system, the system is said to be stable if and only if the following inequalities are simultaneously satisfied:

$$
\begin{aligned}
&a_4 > 0, \quad a_3 > 0, \quad a_2 > 0 \quad a_1 > 0, \quad a_0 > 0 \\
&a_3 a_2 > a_4 a_1 \\
&a_1(a_3 a_2 - a_4 a_1) - a_3^2 a_0 > 0
\end{aligned}
\tag{4.72}
$$

An important observation of the system matrix A^c is that it does not contain any slip angle terms. Thus the stability of the current controller is unaffected by error in the rotor position. From the coefficients of the characteristic equation (4.71), all the coefficients $a_4, a_3, a_2, a_1,$ and a_0 are guaranteed to be positive provided the controller gains are positive (i.e. $k_p^c > 0$ and $k_i^c > 0$) satisfying the the first condition. The second and third conditions are found below.

Second Routh-Hurwitz inequality, $a_3 a_2 > a_4 a_1$:

$$a_3 a_2 = \frac{2(r_r + k_p^c)}{\sigma L_r}\frac{1}{\sigma^2 L_r^2}\left(2\sigma L_r k_i^c + (\omega_{sr}\sigma\, L_r - \hat{\omega}_{sr}\hat{\sigma}\, \hat{L}_r)^2 + (r_r + k_p^c)^2\right)$$

$$a_3 a_2 = \frac{4k_i^c(r_r + k_p^c)}{\sigma^2 L_r^2} + \frac{2(r_r + k_p^c)^3}{\sigma L_r}\frac{1}{\sigma^2 L_r^2} + \frac{2(r_r + k_p^c)}{\sigma L_r}\frac{1}{\sigma^2 L_r^2}(\omega_{sr}\sigma\, L_r - \hat{\omega}_{sr}\hat{\sigma}\, \hat{L}_r)^2$$

and

$$a_4 a_1 = a_1 = \frac{2k_i^c(r_r + k_p^c)}{\sigma^2 L_r^2}$$

It implies

$$a_3 a_2 = 2a_1 + \frac{2(r_r + k_p^c)^3}{\sigma L_r} \frac{1}{\sigma^2 L_r^2} + \frac{2(r_r + k_p^c)}{\sigma L_r} \frac{1}{\sigma^2 L_r^2} (\omega_{sr} \sigma \ L_r - \hat{\omega}_{sr} \hat{\sigma} \ \hat{L}_r)^2$$

$$a_3 a_2 = 2a_1 + X$$

Where $X = \dfrac{2(r_r + k_p^c)^3}{\sigma L_r} \dfrac{1}{\sigma^2 L_r^2} + \dfrac{2(r_r + k_p^c)}{\sigma L_r} \dfrac{1}{\sigma^2 L_r^2} (\omega_{sr} \sigma \ L_r - \hat{\omega}_{sr} \hat{\sigma} \ \hat{L}_r)^2$

Since X is positive, it can be concluded that $a_3 a_2 > a_4 a_1$

Third Routh-Hurwitz inequality, $a_1 (a_3 a_2 - a_4 a_1) - a_3^2 a_0 > 0$:

$$a_3 a_2 = 2a_1 + \frac{2(r_r + k_p^c)^3}{\sigma L_r} \frac{1}{\sigma^2 L_r^2} + \frac{2(r_r + k_p^c)}{\sigma L_r} \frac{1}{\sigma^2 L_r^2} (\omega_{sr} \sigma \ L_r - \hat{\omega}_{sr} \hat{\sigma} \ \hat{L}_r)^2$$

$$a_3 a_2 = 2a_1 + \frac{a_3^3}{4} + a_3 \frac{1}{\sigma^2 L_r^2} (\omega_{sr} \sigma \ L_r - \hat{\omega}_{sr} \hat{\sigma} \ \hat{L}_r)^2$$

$$a_1 (a_3 a_2 - a_4 a_1) = a_1 (2a_1 + \frac{a_3^3}{4} + a_3 \frac{1}{\sigma^2 L_r^2} (\omega_{sr} \sigma \ L_r - \hat{\omega}_{sr} \hat{\sigma} \ \hat{L}_r)^2 - a_1)$$

$$a_1 (a_3 a_2 - a_4 a_1) = a_1 (a_1 + \frac{a_3^3}{4} + a_3 \frac{1}{\sigma^2 L_r^2} (\omega_{sr} \sigma \ L_r - \hat{\omega}_{sr} \hat{\sigma} \ \hat{L}_r)^2)$$

$$a_3^2 a_0 = \frac{4(r_r + k_p^c)^2}{\sigma^2 L_r^2} \left(\frac{k_i^c}{\sigma L_r} \right)^2 = \frac{2a_1}{k_i^c} \left(\frac{k_i^c}{\sigma L_r} \right)^2 = \frac{2a_1 k_i^c}{\sigma^2 L_r^2}$$

and

$$a_1 (a_1 + \frac{a_3^3}{4} + a_3 \frac{1}{\sigma^2 L_r^2} (\omega_{sr} \sigma \ L_r - \hat{\omega}_{sr} \hat{\sigma} \ \hat{L}_r)^2) > \frac{2a_1 k_i^c}{\sigma^2 L_r^2} \tag{4.73}$$

Statisfying the third inequality.Thus the the positive PI controllers ensures the current control loop is always stable.

4.4.3.3.**Speed and Power Loop.** The rotor speed dynamics, electromagnetic torque and stator reactive power are given respectively by (4.74), (4.75) and (4.76). The state equations of the rotor speed and reactive power controllers can be written as (4.77)-(4.80).

$$p\omega_r = z = \frac{P}{2J}\left(T_e - T_m\right) \tag{4.74}$$

$$T_e = \frac{3}{2}\frac{P}{2}\frac{L_m}{L_s}\lambda_{ds}i_{qr} \tag{4.75}$$

$$Q_s = \frac{3}{2}v_{qs}\left(\frac{\lambda_{ds}}{L_s} - \frac{L_m}{L_s}i_{dr}\right) \tag{4.76}$$

$$px_1^\omega = z^* - \hat{z} \tag{4.77}$$

$$px_2^q = Q_s^* - \hat{Q}_s \tag{4.78}$$

$$i_{qr}^* = \left(k_p^\omega + \frac{k_i^\omega}{p}\right)\left(z^* - \hat{z}\right) \tag{4.79}$$

$$i_{dr}^* = \left(k_p^q + \frac{k_i^q}{p}\right)\left(Q_s^* - \hat{Q}_s\right) \tag{4.80}$$

where k_p^ω, k_i^ω and k_p^q, k_i^q are respectively the PI controller gains for the speed and reactive power controllers.

Expanding (4.79), (4.80) and then substituting for (4.77) and (4.78), we have:

$$i_{qr}^* = k_i^\omega x_1^\omega - k_p^\omega \hat{z} + k_p^\omega z^* \tag{4.81}$$

$$i_{dr}^* = k_i^q x_2^q - k_p^q \hat{Q}_s + k_p^q Q_s^* \tag{4.82}$$

From (4.50), (4.74), (4.75), and (4.76) the observed rotor angular speed dynamics $\hat{z}$ and stator reactive power are given by (4.83) and (4.84) respectively:

$$\hat{z} = \frac{P}{2J}\left(\frac{3}{2}\frac{P}{2}\frac{\hat{L}_m}{\hat{L}_s}\lambda_{ds}T^{-1}\hat{i}_{qr} - T_m\right)$$

(4.83)

$$\hat{Q}_s = \frac{3}{2}\frac{1}{\hat{L}_s}v_{qs}\hat{\lambda}_{ds} - \frac{3}{2}\frac{\hat{L}_m}{\hat{L}_s}v_{qs}T^{-1}\hat{i}_{dr}$$

(4.84)

Substituting (4.83) and (4.84) into (4.77), (4.78), (4.81), and (4.82), we have

$$px_1^{\omega} = z^* - \frac{P}{2J}\left(\frac{3}{2}\frac{P}{2}\frac{\hat{L}_m}{\hat{L}_s}\hat{\lambda}_{ds}T^{-1}\hat{i}_{qr} - T_m\right)$$

(4.85)

$$px_2^q = Q_s^* - \frac{3}{2}\frac{1}{L_s}v_s\hat{\lambda}_{ds} + \frac{3}{2}\frac{\hat{L}_m}{\hat{L}_s}v_{qs}T^{-1}\hat{i}_{dr}$$

(4.86)

$$i_{qr}^* = k_i^{\omega}x_1^{\omega} - k_p^{\omega}\frac{P}{2J}\left(\frac{3}{2}\frac{P}{2}\frac{\hat{L}_m}{\hat{L}_s}\hat{\lambda}_{ds}T^{-1}\hat{i}_{qr} - T_m\right) + k_p^{\omega}z^*$$

(4.87)

$$i_{dr}^* = k_i^q x_2^q - k_p^q\left(\frac{3}{2}\frac{1}{L_s}v_{qs}\hat{\lambda}_{ds} - \frac{3}{2}\frac{\hat{L}_m}{\hat{L}_s}v_{qs}T^{-1}\hat{i}_{dr}\right) + k_p^q Q_s^*$$

(4.88)

Equations (4.85) and (486) can be rewritten in matrix form as:

$$p\begin{bmatrix} x_1^{\omega} \\ x_2^p \end{bmatrix} = -T^{-1}K_m\begin{bmatrix} \hat{i}_{dr} \\ \hat{i}_{qr} \end{bmatrix} + I_{2\times 2}\begin{bmatrix} Q_s^* \\ z^* \end{bmatrix} + D^p$$

(4.89)

where $\quad K_m = \begin{bmatrix} \dfrac{3}{2}\dfrac{\hat{L}_m}{\hat{L}_s}v_{qs} & 0 \\ 0 & \dfrac{3P^2}{8J}\dfrac{\hat{L}_m}{\hat{L}_s}\hat{\lambda}_{ds} \end{bmatrix}$, and $D^p = \begin{bmatrix} -\dfrac{3}{2}v_{qs}\dfrac{\hat{\lambda}_{ds}}{\hat{L}_s} & 0 \\ 0 & \dfrac{P}{2J}T_m \end{bmatrix}$

Similarly, (4.87) and (4.88) can be written as:

$$\begin{bmatrix} i_{qr}^* \\ i_{dr}^* \end{bmatrix} = K_i^{\omega p}\begin{bmatrix} x_1^{\omega} \\ x_2^q \end{bmatrix} - T^{-1}K_m K_p^{\omega q}\begin{bmatrix} \hat{i}_{qr} \\ \hat{i}_{dr} \end{bmatrix} + K_p^{\omega q}\begin{bmatrix} Q_s^* \\ z^* \end{bmatrix} + K_p^{\omega q}D^p$$

(4.90)

where $\quad K_i^{\omega q} = \begin{bmatrix} k_i^q & 0 \\ 0 & k_i^{\omega} \end{bmatrix}, \quad K_p^{\omega q} = \begin{bmatrix} k_p^q & 0 \\ 0 & k_p^{\omega} \end{bmatrix}.$

Substituting (4.90) into (4.62) and (4.64), we obtain (4.91) and (4.92).

$$
p\begin{bmatrix} \hat{i}_{dr} \\ \hat{i}_{qr} \end{bmatrix} = \left\{ \begin{array}{l} \left(\begin{array}{l} TAT^{-1} + TBT^{-1}\hat{K}_p^c \\ -TBT^{-1}K_p^cT^{-1}K_mK_p^{\omega q} \end{array} \right) \begin{bmatrix} \hat{i}_{dr} \\ \hat{i}_{qr} \end{bmatrix} + TBT^{-1}K_i^c \begin{bmatrix} x_1^c \\ x_2^c \end{bmatrix} + \\[2em] TBT^{-1}K_p^cK_i^{\omega q} \begin{bmatrix} x_2^q \\ x_1^\omega \end{bmatrix} + +TBT^{-1}K_p^cK_p^{\omega q} \begin{bmatrix} Q_s^* \\ z^* \end{bmatrix} + \\[2em] TBT^{-1}K_p^cD^{\omega q} + TBT^{-1}D + TD \end{array} \right\} \quad (4.91)
$$

$$
p\begin{bmatrix} x_1^c \\ x_2^c \end{bmatrix} = I_{2\times2}\left(-1 + T^{-1}K_mK_p^{\omega q} \right) \begin{bmatrix} \hat{i}_{dr} \\ \hat{i}_{qr} \end{bmatrix} + I_{2\times2}K_i^{\omega q} \begin{bmatrix} x_2^q \\ x_1^\omega \end{bmatrix} + I_{2\times2}K_p^{\omega q} \begin{bmatrix} Q_s^* \\ z^* \end{bmatrix} + K_p^{\omega q}D^p \quad (4.92)
$$

Combining (4.81), (4.91), and (4.92), the final expression in matrix form is given by

$$
px = A^p x + B^p u + E^p \quad (4.93)
$$

where

$$
A^p = \begin{bmatrix} \left(\begin{array}{l} TAT^{-1} + TBT^{-1}\hat{K}_p^c \\ -TBT^{-1}K_p^cT^{-1}K_mK_p^{\omega q} \end{array} \right) & TBT^{-1}K_i^c & TBT^{-1}K_p^cK_i^{\omega q} \\ -\left(I_{2\times2} + T^{-1}K_mK_p^{\omega q} \right) & 0 & I_{2\times2}K_i^{\omega q} \\ -T^{-1}K_m & 0 & 0 \end{bmatrix} \quad (4.94)
$$

$$
B^p = \begin{bmatrix} TBT^{-1}K_p^cK_p^{\omega q} \\ I_{2\times2}K_p^{\omega q} \\ I_{2\times2} \end{bmatrix} \quad (4.95)
$$

$$
E^p = \begin{bmatrix} TBT^{-1}K_p^cD^{\omega q} + TBT^{-1}D + TD \\ I_{2\times2}D^{\omega q} \\ D^p \end{bmatrix} \quad (4.96)
$$

Expanding for all the entries in A^p above results in (4.97).

$$
A^p = \begin{bmatrix}
a_{11} & a_{12} & a_{13} & 0 & a_{15} & 0 \\
a_{21} & a_{22} & 0 & a_{24} & 0 & a_{26} \\
a_{31} & a_{32} & 0 & 0 & a_{35} & 0 \\
a_{41} & a_{42} & 0 & 0 & 0 & a_{46} \\
a_{51} & a_{52} & 0 & 0 & 0 & 0 \\
a_{61} & a_{62} & 0 & 0 & 0 & 0
\end{bmatrix}
\tag{4.97}
$$

where
$$
\begin{cases}
a_{11} = -\dfrac{r_r + k_p^c}{\sigma L_r} - \dfrac{3}{2}\dfrac{k_p^c k_p^q}{\omega_e \sigma L_r}\dfrac{\hat{L}_m}{\hat{L}_s} v_{qs}\cos(\varDelta\theta_{sr}), \\[4mm]
a_{12} = \omega_{sr} - \dfrac{\hat{\omega}_{sr}\hat{\sigma}\hat{L}_r}{\sigma L_r} - \dfrac{3}{2}\dfrac{k_p^c k_p^\omega}{\sigma L_r}\dfrac{\hat{L}_m}{\hat{L}_s} v_{qs}\sin(\varDelta\theta_{sr}), \\[4mm]
a_{13} = \dfrac{k_i^c}{\sigma L_r}, \quad a_{15} = \dfrac{k_p^c k_i^q}{\sigma L_r},
\end{cases}
$$

$$
\begin{cases}
a_{21} = -\omega_{sr} + \dfrac{\hat{\omega}_{sr}\hat{\sigma}\hat{L}_r}{\sigma L_r} + \dfrac{3P^2}{8}\dfrac{k_p^c k_p^\omega}{\sigma L_r}\dfrac{\hat{L}_m}{\hat{L}_s}\lambda_{ds}\sin(\varDelta\theta_{sr}), \\[4mm]
a_{22} = -\dfrac{r_r + k_p^c}{\sigma L_r} - \dfrac{3P^2}{8J}\dfrac{k_p^c k_p^\omega}{\sigma L_r}\dfrac{\hat{L}_m}{\hat{L}_s}\lambda_{ds}\cos(\varDelta\theta_{sr}), \quad a_{24} = \dfrac{k_i^c}{\sigma L_r}, \\[4mm]
a_{26} = \dfrac{k_p^c k_i^\omega}{\sigma L_r}, \quad a_{31} = -1 - \dfrac{3}{2}\dfrac{k_p^q \hat{L}_m}{\hat{L}_s} v_{qs}\cos(\varDelta\theta_{sr}), \\[4mm]
a_{32} = -\dfrac{3}{2}\dfrac{k_p^q \hat{L}_m}{\hat{L}_s} v_{qs}\sin(\varDelta\theta_{sr}), \quad a_{41} = \dfrac{3P^2}{8J}\dfrac{k_p^\omega \hat{L}_m}{\hat{L}_s}\lambda_{ds}\sin(\varDelta\theta_{sr}) \\[4mm]
a_{35} = k_i^q, \quad a_{42} = -1 + \dfrac{3P^2}{8J}\dfrac{k_p^\omega \hat{L}_m}{\hat{L}_s}\lambda_{ds}\cos(\varDelta\theta_{sr}), \\[4mm]
a_{46} = k_i^\omega, \quad a_{51} = -\dfrac{3}{2}\dfrac{k_p^\omega \hat{L}_m}{\hat{L}_s} v_{qs}\cos(\varDelta\theta_{sr}), \\[4mm]
a_{52} = -\dfrac{3}{2}\dfrac{k_p^\omega \hat{L}_m}{\hat{L}_s} v_{qs}\sin(\varDelta\theta_{sr}), \quad a_{61} = \dfrac{3P^2}{8J}\dfrac{k_p^\omega \hat{L}_m}{\hat{L}_s}\lambda_{ds}\sin(\varDelta\theta_{sr}), \\[4mm]
a_{62} = -\dfrac{3P^2}{8J}\dfrac{k_p^\omega \hat{L}_m}{\hat{L}_s}\lambda_{ds}\cos(\varDelta\theta_{sr}).
\end{cases}
$$

4.4.3.4.**Stability Analysis for the Entire System.** The elements of the system matrix, A^p, in (4.97) contains sinusoidal functions of the slip angle, $\Delta\theta_{sr}$, machine inductance errors, the slip speed, and magnitude of the stator flux linkage. The placement of the eigenvalues of matrix in the complex s-plane is thus affected by these parameters. Figure 4.14 depicts the plot of the real part of the system eigenvalues using the system parameters given in Appendix.
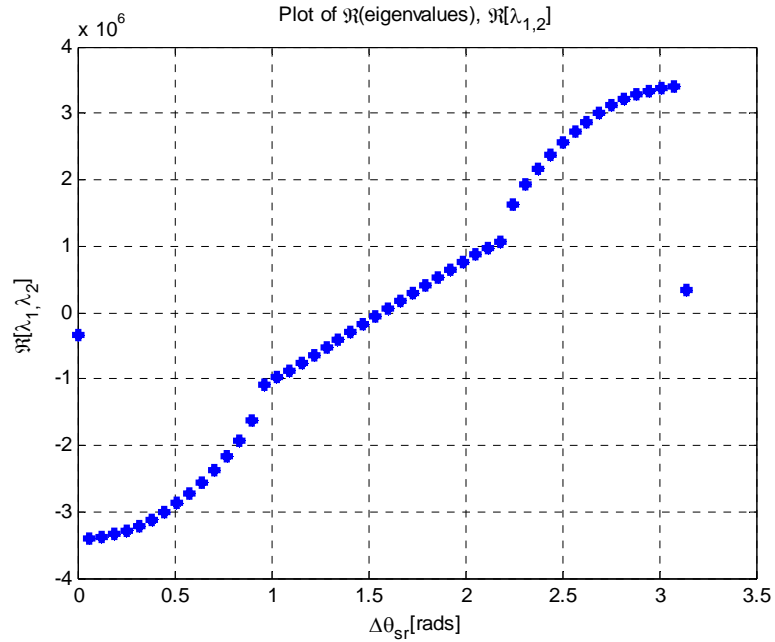
Figure 4.14 (a) plot of the real part of the system eigenvalues $\lambda_{1,2}$
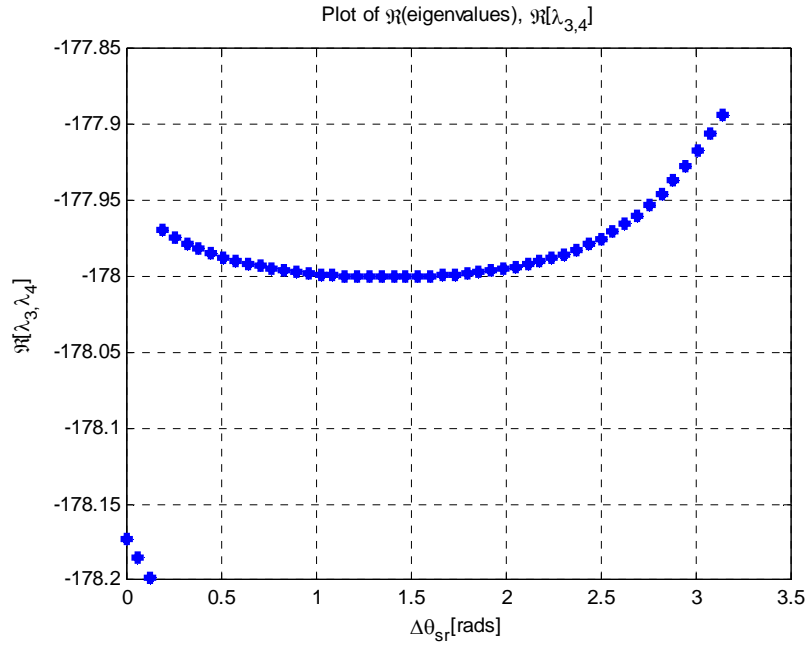
(b)
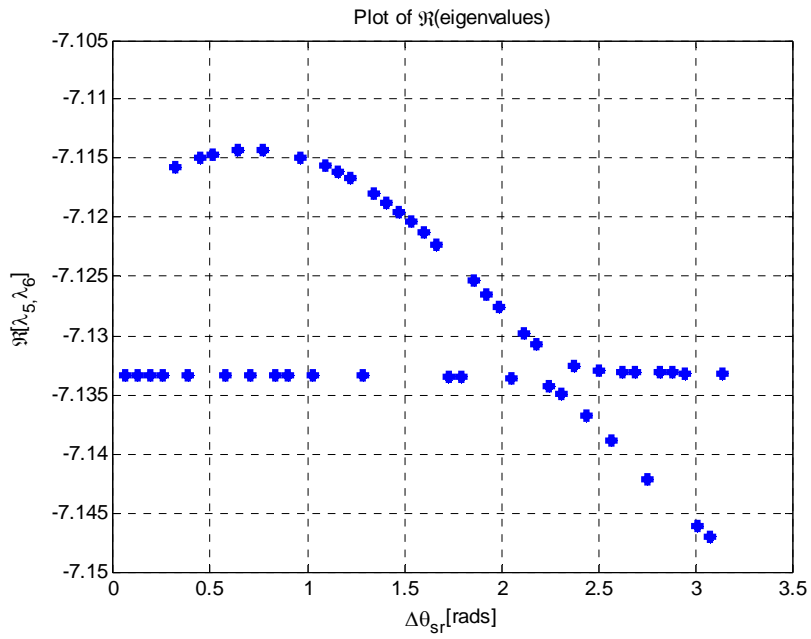
(c)

Figure 4.14. Plot of the real part of the system eigenvalues (a) $\lambda_{1,2}$, (b) $\lambda_{3,4}$; and (c) $\lambda_{5,6}$
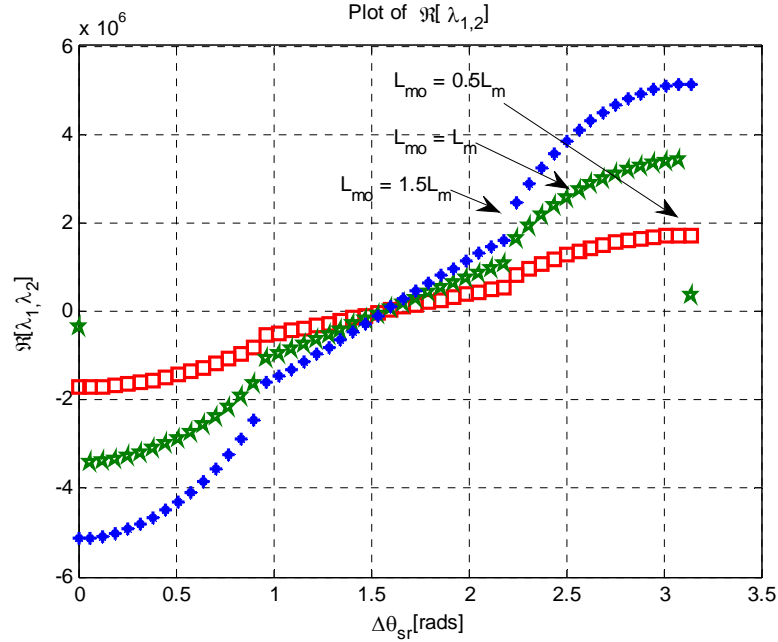
Figure 4.15. Plot of the real part of the eigenvalues λ_1, λ_2 with 3 different errors in L_m (L_{mo} is the erroneous L_m)

Figure 4.14 shows the effect of the slip angle error on the real part of the system eigenvalues while holding the machine inductances constant. There are three pairs of eigenvalues. The first pair $\lambda_{1,2}$ relates to the speed and reactive power controllers, the second pair, $\lambda_{3,4}$ are to the rotor current controller and the last pair $\lambda_{5,6}$ relates to the rotor current. The real part of $\lambda_{3,4}$ and $\lambda_{5,6}$ are effectively insensitive to slip angle and machine inductance errors and do not contribute to any right hand poles. The system becomes unstable at about $\Delta\theta_{sr} \approx 1.55\ rads$ irrespective of the magnitude of inductance mismatches. Such large errors are known to occur in using hardware PLL when there are external disturbances close to the falling edge of the stator voltage [77]. Figure 4.15 show that the effect of the machine parameter errors is placement of the eigenvalues in the left hand plane but does not drive the system to instability (right hand plane).

90

4.5 Summary

A generic expression for the intrinsic stability criteria of a variable-speed, variable-pitch DFIG-based wind turbine system has been derived. The inequality obtained represents the acceptable region of operation of the wind system when it is capturing maximum power at low to medium wind speeds, constant power at high wind speeds and power regulation operation mode.

A number of specific conclusions may be drawn. When the rotor speed, wind speed and pitch angle are taken into account, a more accurate prediction of the stability region is defined. It reveals narrower stability region than the conventional method for both MPT and rated power modes.

The effect of pitch angle regulation shows up more significantly in the sub-synchronous region than in the super-synchronous region. It is also found that there no significant effect of output power variation on the stability region when wind turbine system operating in the power regulation modes.

In the second part of this chapter, the effect of rotor position error and machine parameter inaccuracies on a vector controlled DFIG turbine system has been analyzed. The results show that the error in rotor position has a significant effect on the stability of the entire system. Specifically, the system's eigenvalues related to the speed and power controllers crosses over to the right-hand plane when the slip angle error is at about 1.55 rads. This large error is known to occur when using hardware PLL. It has also been established that for a properly tuned controller gains, machine parameter inaccuracies do

not affect the stability of the system but affects the placement of system poles in the left-hand plane.

CHAPTER 5

NINE-SWITCH CONVERTER

5.1 Introduction

Recently, some researchers have shown keen interest in the Nine-switch converter (NSC) shown in Figure 5.1. It has been used in independent control of two AC loads [41]-[43] and in unified power quality conditioners, [32] and [44]. The NSC has also been used to control the doubly-fed induction generator [63], permanent-magnet synchronous generator [64] and a six-phase machine drive system [65]. Hereinafter, the upper portion of the NSC comprising the upper and middle switches (T_{ap}, T_{bp}, T_{cp} and T_{am}, T_{bm}, T_{cm}) is referred to as *NSC1* whereas the lower portion comprising the middle and lower switches (T_{am}, T_{bm}, T_{cm} and T_{an}, T_{bn}, T_{cn}) is *NSC2*.
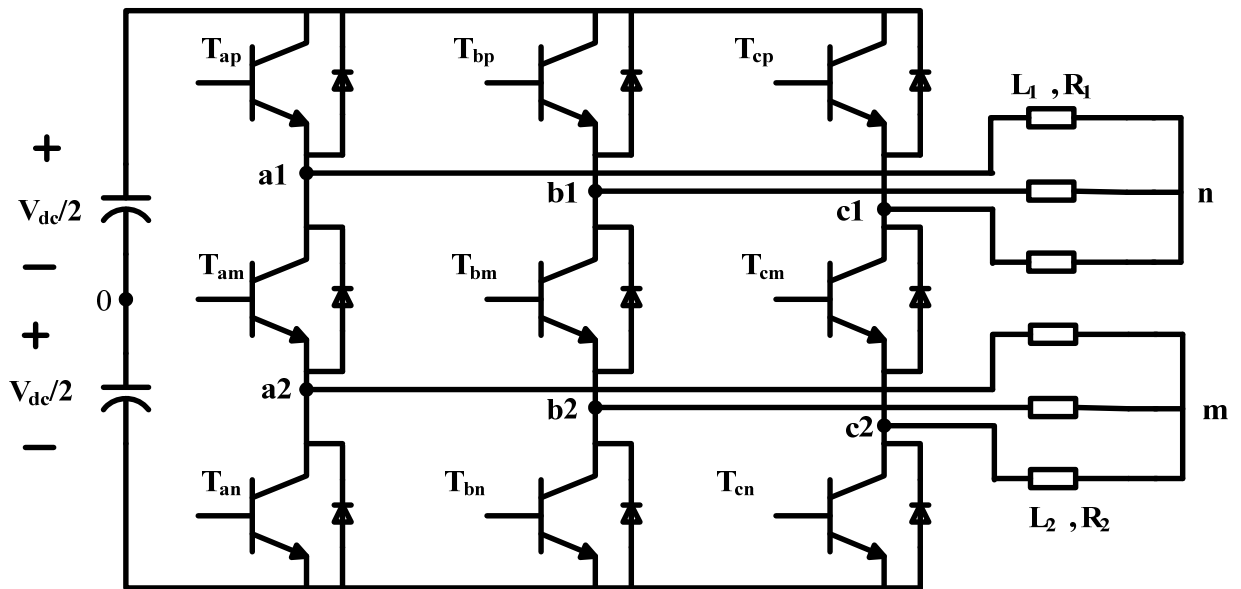
Figure 5.1. Schematic of the Nine-switch converter

93

The NSC topology requires a higher rated DC-link voltage to produce the same output voltages compared to using two of the classical 2-level voltage source converters [41], [42]. This limitation might overshadow the gains that come with its reduced component count as the switches may be unduly overstressed. In the topology shown in Figure 5.1, observe that the middle switches (T_{am}, T_{bm}, T_{cm}) are shared between *NSC1* and *NSC2*. This sharing of devices means that the two outputs depend on each other and thus constrain independent amplitude and frequency operation. To ensure Kirchoff's voltage law (KVL) and Kirchoff's current law (KCL) are not violated during operation, the modulating signals of *NSC1* at any instant must always be greater than the modulating signals of *NSC2* [41], [43], [44]. This has been accomplished in [41], [42], [66] by adding 'appropriate' DC offsets to the two modulating signals. So far, however, the selection of the DC offsets is somewhat arbitrary. For example, whereas [42] adds 1/4 of the DC voltage to upper reference and subtracts same value from the lower reference, [66] selects DC offsets equal to the maximum and the minimum of the phase voltages for upper and lower references, respectively. The goal of this Chapter is to layout the mathematical model of the Nine-switch converter and to provide a method of selecting the offset signals.

In the NSC topology shown in Figure 5.1, there are 2^9 different possible combinations of all 9 switching devices. However, Kirchoffs' current and voltage laws must be obeyed to prevent short-circuiting the DC source and ensure current continuity. Thus, the following constraint on the switching functions must be satisfied:

$$S_{ip} + S_{im} + S_{in} = 2 \tag{5.1}$$

where S_{ip}, S_{im}, S_{in} are, respectively, the switching functions of the upper, middle and bottom switching devices and have a value of unity when they are turned-on and take a value of zero when turned-off. The subscripts $i = a, b, c$ refer to the output phase to which the device is connected; p, m, n refer to the top, middle and bottom devices of the converter leg, respectively. Equation (5.1) reduces the feasible switching states to twenty-seven (27) as listed in Table 5.1.

Table 5.1. Feasible switching states of the Nine-switch converter

Switching State	S_{ap}	S_{an}	S_{bp}	S_{bn}	S_{cp}	S_{cn}
1	0	1	1	0	1	1
2	0	1	1	0	1	1
3	0	1	1	0	1	1
4	0	1	1	1	1	0
5	0	1	1	1	1	0
6	0	1	1	1	1	0
7	0	1	1	1	0	1
8	0	1	1	1	0	1
9	0	1	1	1	0	1
10	1	1	0	0	1	1
11	1	1	0	0	1	1
12	1	1	0	0	1	1
13	1	1	0	1	1	0
14	1	1	0	1	1	0
15	1	1	0	1	1	0
16	1	1	0	1	0	1
17	1	1	0	1	0	1
18	1	1	0	1	0	1
19	1	0	1	0	1	1
20	1	0	1	0	1	1
21	1	0	1	0	1	1
22	1	0	1	1	1	0
23	1	0	1	1	1	0
24	1	0	1	1	1	0
25	1	0	1	1	0	1
26	1	0	1	1	0	1
27	1	0	1	1	0	1

5.2 Modulation Techniques for Nine-switch Converter

In the classical pulse-width modulated voltage source inverters, two (2) main modulation techniques namely; Space Vector Pulse-Width Modulation (SV-PWM) and Carrier-Based Pulse-Width Modulation (CB-PWM) methods are used for controlling the magnitude and frequency of the output AC voltages. In both the SV-PWM and CB-PWM methods, voltage linearity, waveform quality, and switching losses are all influenced by the choice of the zero-state placement [70]. Depending on the placement of these zero vectors, the modulation may be continuous or discontinuous. As discussed extensively by Hava et al. in [71], the continuous PWM (CPWM) methods have superior performance in the low modulation range compared to the discontinuous PWM (DPWM) methods. The reverse is true in the high modulation region. However, each DPWM modulator's performance viz-a-viz switching losses, waveform quality, and voltage linearity characteristics are different in each DPWM and the method of choice depends on the characteristics that are most critical to the designer. In the preceding section detailed SV-PWM and CB-PWM schemes of the Nine-switch converter are discussed.

5.2.1. Space Vector Modulation of the Nine-Switch Converter

The SV-PWM technique is a direct digital PWM method that calculates the conduction times of the switching devices required to synthesize a desired voltage vector. It has been shown that there are twenty-seven (27) feasible switching states of the Nine-

switch converter (see Table 5.1). The converter voltages in natural *abc* reference frame can be transformed to the stationary *qd* reference frame using (5.2) [57].

$$f_{qd0s} = K(\theta)f_{abcs} \tag{5.2}$$

$$K(\theta) = \frac{2}{3} \begin{bmatrix} \cos(\theta) & \cos(\theta - 2\pi/3) & \cos(\theta + 2\pi/3) \\ \sin(\theta) & \sin(\theta - 2\pi/3) & \sin(\theta + 2\pi/3) \\ 1/2 & 1/2 & 1/2 \end{bmatrix} \tag{5.3}$$

where

$f_{qd0s} = \begin{bmatrix} f_{qs} & f_{ds} & f_{0s} \end{bmatrix}^T$, $f_{abcs} = \begin{bmatrix} f_{as} & f_{bs} & f_{cs} \end{bmatrix}^T$ and f_{abcs} may represent voltage, current or flux linkage. The reference transformation angle $\theta = 0°$ for the stationary reference frame. To synthesize the desired three-phase voltages, the natural *abc* voltages are transformed into the *qd* stationary reference frame voltages using (5.4). All the *abc* and the corresponding *qd* voltages are listed in Tables 5.2 and 5.3 for *NSC1* and *NSC2* respectively.

$$V_{qs}^* = \frac{2}{3}\left(v_{as} - \frac{1}{2}v_{bs} - \frac{1}{2}v_{cs} \right)$$

$$V_{qs}^* = \frac{2}{3}\left(-\frac{\sqrt{3}}{2}v_{bs} + \frac{\sqrt{3}}{2}v_{cs} \right) \tag{5.4}$$

$$V_{0s}^* = \frac{2}{3}\left(\frac{1}{2}v_{as} + \frac{1}{2}v_{bs} + \frac{1}{2}v_{cs} \right)$$

The corresponding space vector diagrams for switching states listed in Tables 5.2 and 5.3 are illustrated in Figure 5.2.

The following observations can be deduced from the space vector diagrams:

- The zero states of *NSC1 and NSC2* are, respectively, {1, 14, 15, 17, 18, 23,24, 27} and {1,3,7,9,14,19,21,25,27}

97

Table 5.2. Switching states for *NSC1*

Switching State	S_{ap}	S_{am}	S_{an}	S_{bp}	S_{bm}	S_{bn}	S_{cp}	S_{cm}	S_{cn}	V_{alo} $V_{dc}/2$	V_{blo} $V_{dc}/2$	V_{clo} $V_{dc}/2$	V_{qs1} $V_{dc}/6$	V_{ds1} $V_{dc}\sqrt{3}/6$	V_{no} $V_{dc}/6$
1	0	1	1	0	1	1	0	1	1	-1	-1	-1	0	0	-3
2	0	1	1	0	1	1	1	1	0	-1	-1	1	-2	2	-1
3	0	1	1	0	1	1	1	0	1	-1	-1	1	-2	2	-1
4	0	1	1	1	1	0	0	1	1	-1	1	-1	-2	-2	-1
5	0	1	1	1	1	0	1	1	0	-1	1	1	-4	0	1
6	0	1	1	1	1	0	1	0	1	-1	1	1	-4	0	1
7	0	1	1	1	0	1	0	1	1	-1	1	-1	-2	-2	-1
8	0	1	1	1	0	1	1	1	0	-1	1	1	-4	0	1
9	0	1	1	1	0	1	1	0	1	-1	1	1	-4	0	1
10	1	1	0	0	1	1	0	1	1	1	-1	-1	4	0	-1
11	1	1	0	0	1	1	1	1	0	1	-1	1	2	2	1
12	1	1	0	0	1	1	1	0	1	1	-1	1	2	2	1
13	1	1	0	1	1	0	0	1	1	1	1	-1	2	-2	1
14	1	1	0	1	1	0	1	1	0	1	1	1	0	0	3
15	1	1	0	1	1	0	1	0	1	1	1	1	0	0	3
16	1	1	0	1	0	1	0	1	1	1	1	-1	2	-2	1
17	1	1	0	1	0	1	1	1	0	1	1	1	0	0	3
18	1	1	0	1	0	1	1	0	1	1	1	1	0	0	3
19	1	0	1	0	1	1	0	1	1	1	-1	-1	4	0	-1
20	1	0	1	0	1	1	1	1	0	1	-1	1	2	2	1
21	1	0	1	0	1	1	1	0	1	1	-1	1	2	2	1
22	1	0	1	1	1	0	0	1	1	1	1	-1	2	-2	1
23	1	0	1	1	1	0	1	1	0	1	1	1	0	0	3
24	1	0	1	1	1	0	1	0	1	1	1	1	0	0	3
25	1	0	1	1	0	1	0	1	1	1	1	-1	2	-2	1
26	1	0	1	1	0	1	1	1	0	1	1	1	0	0	3
27	1	0	1	1	0	1	1	0	1	1	1	1	0	0	3

Table 5.3. Switching states for *NSC2*

Switching	S_{ap}	S_{am}	S_{an}	S_{bp}	S_{bm}	S_{bn}	S_{cp}	S_{cm}	S_{cn}	V_{xo} $V_{dc}/2$	V_{yo} $V_{dc}/2$	V_{zo} $V_{dc}/2$	V_{qs2} $V_{dc}/6$	V_{ds2} $V_{dc}\sqrt{3}/6$	V_{mo} $V_{dc}/6$
1	0	1	1	0	1	1	0	1	1	-1	-1	-1	0	0	-3
2	0	1	1	0	1	1	1	1	0	-1	-1	1	-2	2	-1
3	0	1	1	0	1	1	1	0	1	-1	-1	-1	0	0	-3
4	0	1	1	1	1	0	0	1	1	-1	1	-1	-2	-2	-1
5	0	1	1	1	1	0	1	1	0	-1	1	1	-4	0	1
6	0	1	1	1	1	0	1	0	1	-1	1	-1	-2	-2	-1
7	0	1	1	1	0	1	0	1	1	-1	-1	-1	0	0	-3
8	0	1	1	1	0	1	1	1	0	-1	-1	1	-2	2	-1
9	0	1	1	1	0	1	1	0	1	-1	-1	-1	0	0	-3
10	1	1	0	0	1	1	0	1	1	1	-1	-1	4	0	-1
11	1	1	0	0	1	1	1	1	0	1	-1	1	2	2	1
12	1	1	0	0	1	1	1	0	1	1	-1	-1	4	0	-1
13	1	1	0	1	1	0	0	1	1	1	1	-1	2	-2	1
14	1	1	0	1	1	0	1	1	0	1	1	1	0	0	3
15	1	1	0	1	1	0	1	0	1	1	1	-1	2	-2	1
16	1	1	0	1	0	1	0	1	1	1	-1	-1	4	0	-1
17	1	1	0	1	0	1	1	1	0	1	-1	1	2	2	1
18	1	1	0	1	0	1	1	0	1	1	-1	-1	4	0	-1
19	1	0	1	0	1	1	0	1	1	-1	-1	-1	0	0	-3
20	1	0	1	0	1	1	1	1	0	-1	-1	1	-2	2	-1
21	1	0	1	0	1	1	1	0	1	-1	-1	-1	0	0	-3
22	1	0	1	1	1	0	0	1	1	-1	1	-1	-2	-2	-1
23	1	0	1	1	1	0	1	1	0	-1	1	1	-4	0	1
24	1	0	1	1	1	0	1	0	1	-1	1	-1	-2	-2	-1
25	1	0	1	1	0	1	0	1	1	-1	-1	-1	0	0	-3
26	1	0	1	1	0	1	1	1	0	-1	-1	1	-2	2	-1
27	1	0	1	1	0	1	1	0	1	-1	-1	-1	0	0	-3
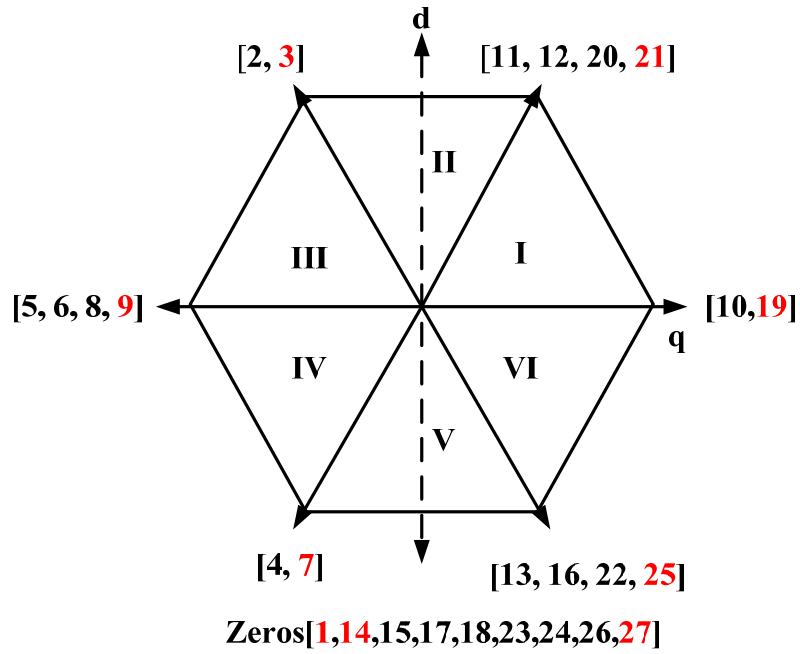
(a)

NSC2
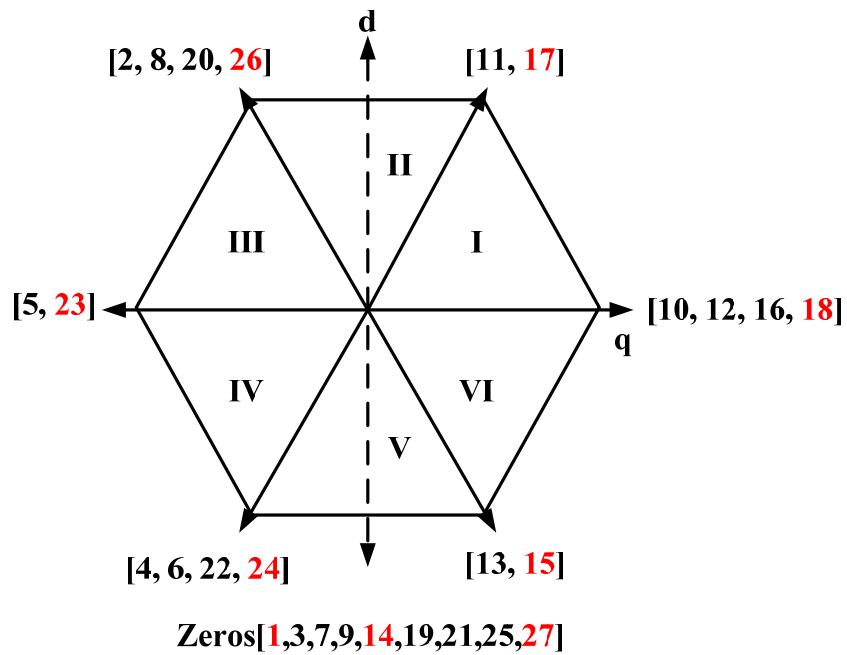
(b)

Figure 5.2. Voltage space vector diagrams for (a) *NSC1*, and (b) *NSC2* for all feasible switching states

(a)

(b)
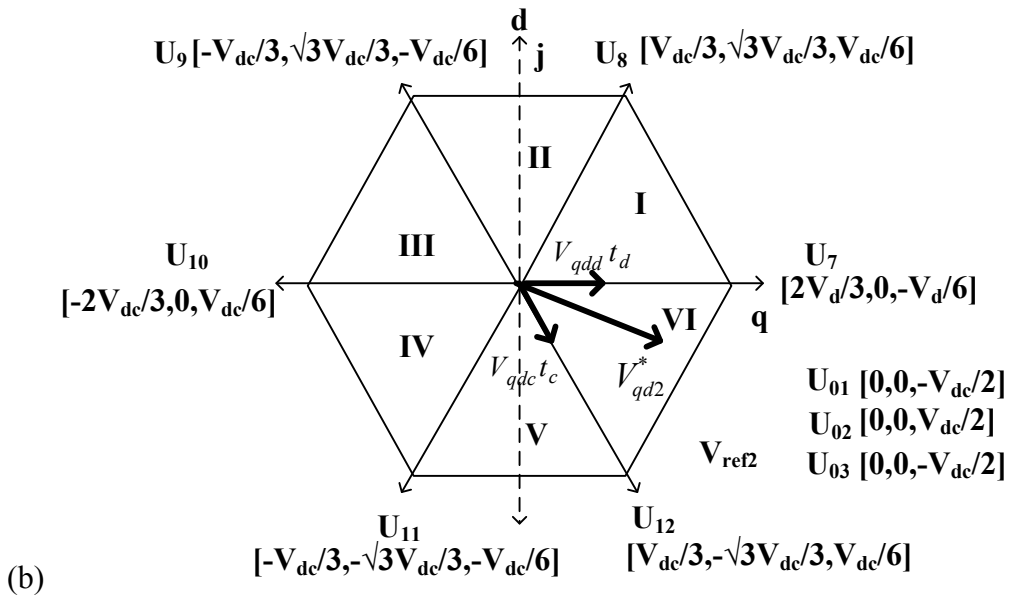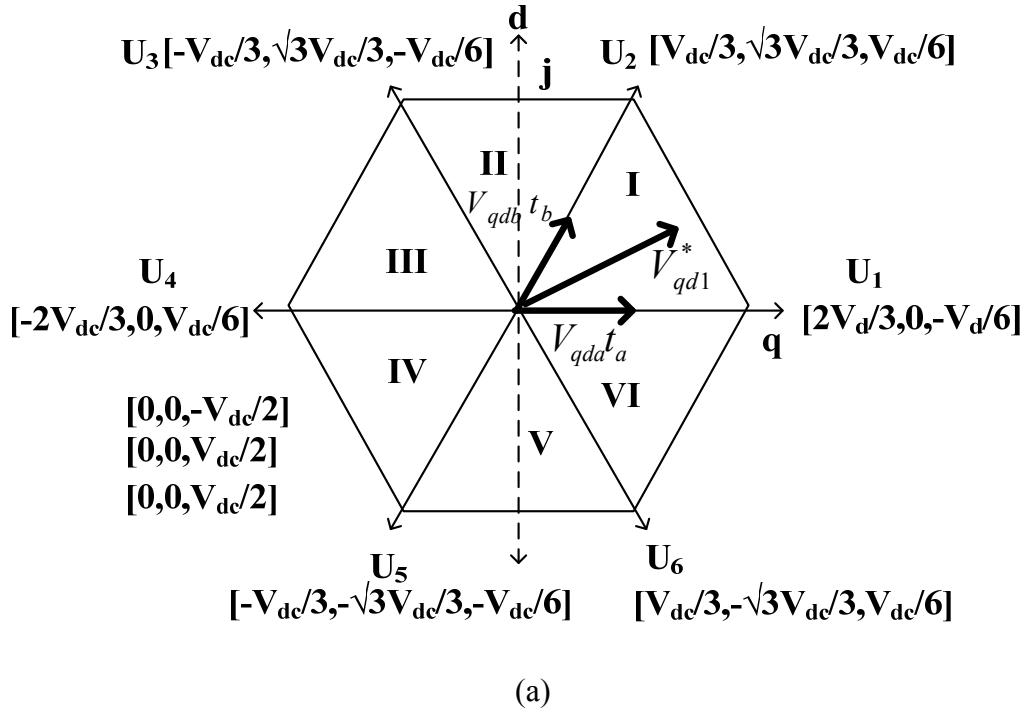
Figure 5.3. Voltage space vector diagrams for (a) *NSC1*, and (b) *NSC2* for selected switching states which ensures their independent control

- The zero states {1, 14, 27} are common to both *NSC1 and NSC2*

- The remaining zero states {15, 17, 18, 23, and 24} of *NSC1* are active states in *NSC2* and the zero states {3, 7, 9, 19, 21, and 25} of *NSC2* produce active states in *NSC1*.

If we desire independent control of the two sets of AC outputs (variable frequency and/or amplitudes), eliminate all the zero states that are not common to both *NSC1 and NSC2*. That is implementing a switching scheme that forbids all switching states that produce:

- active vectors in both *NSC1* and *NSC2* simultaneously and

- zero vectors that are not common to both *NSC1* and *NSC2*.

After eliminating these switching states as mentioned above, an independent control of the converter frequencies is possible since the active states are chosen such that an active state applied to *NSC1* produces a zero state in *NSC2* and vice versa [42]. This leaves fifteen (15) permissible states as shown in Table 5.4 and the corresponding space vector diagrams are shown in Figure 5.3. For example, U_1 has the effect of producing an active vector, U_1 [$2V_d/3$, 0, $-V_{dc}/6$] in *NSC1* but a zero vector, U_1 [0, 0, $-V_{dc}/2$] in *NSC2*. However, U_7 has the opposite effect; producing a zero vector, U_7 [0, 0, $V_{dc}/2$] in *NSC1* but an active vector, U_7 [$2V_d/3$, 0, $-V_{dc}/6$] in *NSC2*. Any two reference three-phase voltage sets expressed in the stationary reference frame , V_{qd1}^*, V_{qd2}^* may be synthesized from their respective immediate adjacent space vectors, V_{qda}, V_{qdb} and V_{qdc}, V_{qdd}, respectively, in addition to the zero vectors V_{qd01}, V_{qd02} and V_{qd03} as shown in Figure 5.3.

Table 5.4. Switching states for both *NSC1 and NSC2* for independent control

Switching State e	S_{ap}	S_{an}	S_{bp}	S_{bn}	S_{cp}	S_{cn}	V_{qs1}	V_{ds1}	V_{qs2}	V_{ds2}	V_{0s1}	V_{os2}
$U_1=19$	1	0	0	1	0	1	$2V_d/3$	0	0	0	$-V_d/6$	$-V_d/2$
$U_2=21$	1	0	0	1	1	0	$V_d/3$	$\sqrt{3}V_d/3$	0	0	$V_d/6$	$-V_d/2$
$U_3=3$	0	1	0	1	1	0	$-V_d/3$	$\sqrt{3}V_d/3$	0	0	$-V_d/6$	$-V_d/2$
$U_4=9$	0	1	1	0	1	0	$-2V_d/3$	0	0	0	$V_d/6$	$-V_d/2$
$U_5=7$	0	1	1	0	0	1	$-V_d/3$	$-\sqrt{3}V_d/3$	0	0	$-V_d/6$	$-V_d/2$
$U_6=25$	1	0	1	0	0	1	$V_d/3$	$-\sqrt{3}V_d/3$	0	0	$V_d/6$	$-V_d/2$
$U_7=18$	1	1	1	0	1	0	0	0	$2V_d/3$	0	$V_d/2$	$-V_d/6$
$U_8=17$	1	1	1	0	1	1	0	0	$V_d/3$	$\sqrt{3}V_d/3$	$V_d/2$	$V_d/6$
$U_9=26$	1	0	1	0	1	1	0	0	$-V_d/3$	$\sqrt{3}V_d/3$	$V_d/2$	$-V_d/6$
$U_{10}=23$	1	0	1	1	1	1	0	0	$-2V_d/3$	0	$V_d/2$	$V_d/6$
$U_{11}=24$	1	0	1	1	1	0	0	0	$-V_d/3$	$-\sqrt{3}V_d/3$	$V_d/2$	$-V_d/6$
$U_{12}=15$	1	1	1	1	1	0	0	0	$V_d/3$	$-\sqrt{3}V_d/3$	$V_d/2$	$V_d/6$
$U_{01}=1$	0	1	0	1	0	1	0	0	0	0	$-V_d/2$	$-V_d/2$
$U_{02}=14$	1	1	1	1	1	1	0	0	0	0	$V_d/2$	$V_d/2$
$U_{03}=27$	1	0	1	0	1	0	0	0	0	0	$V_d/2$	$-V_d/2$
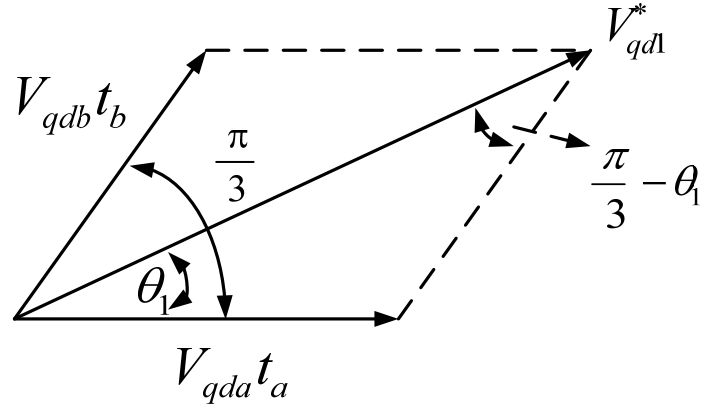
(a)
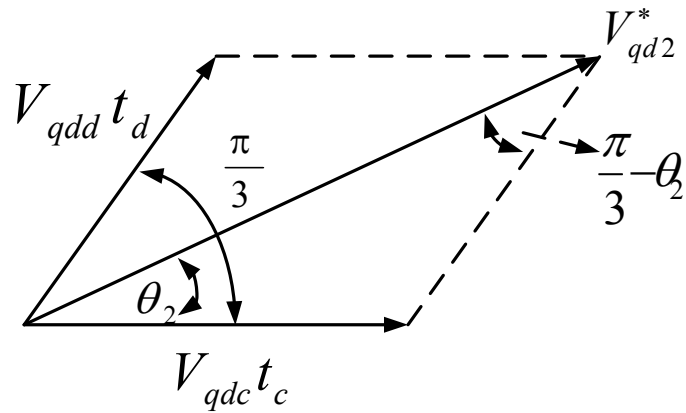
(b)

Figure 5.4. Synthesizing (a) *NSC1* and (b) *NSC2* reference voltages

5.2.1.1.**Calculating the switching times.** Using the space vector diagrams in Figure 5.3, any two reference output voltages V_{qd1}^* and V_{qd2}^* can be synthesized from their respective immediate adjacent space vectors. For *NSC1*, let the two adjacent vectors for synthesizing V_{qd1}^* be given as V_{qda} and V_{qdb} as shown in Figure 5.4(a). Similarly, V_{qdc} and V_{qdd} can be used to synthesize V_{qd2}^*, Figure 5.4(b). Let the normalized times that the

switching devices producing V_{qda}, V_{qdb}, V_{qdc}, V_{qdd}, V_{qd01}, V_{qd02}, and V_{qd03}, are applied are

t_a, t_b, t_c, t_d, t_{01}, t_{02}, and t_{03} respectively.

Hence,

$$\left.\begin{array}{l} V_{qd1}^* = t_a V_{qda} + t_b V_{qdb} + t_{01} V_{qd01} + t_{02} V_{qd02} + t_{03} V_{qd03} \\ V_{qd2}^* = t_c V_{qdc} + t_d V_{qdd} + t_{01} V_{qd01} + t_{02} V_{qd02} + t_{03} V_{qd03} \end{array}\right\} \tag{5.5}$$

where

$$V_{qd1}^* = V_{q1}^* + jV_{d1}^* \qquad V_{qd2}^* = V_{q2}^* + jV_{d2}^* \tag{5.6}$$

Substituting (5.6) into (5.5):

$$\left.\begin{array}{l} V_{qd1}^* = t_a\left(V_{qqa} + jV_{dda}\right) + t_b\left(V_{qqb} + jV_{ddb}\right) \\ V_{qd2}^* = t_c\left(V_{qqc} + jV_{ddc}\right) + t_d\left(V_{qqd} + jV_{ddd}\right) \end{array}\right\} \tag{5.7}$$

Expanding and separating (5.7) into real and imaginary parts:

$$\left.\begin{array}{ll} V_{q1}^* = t_a V_{qqa} + t_b V_{qqb}, & V_{d1}^* = t_a V_{dda} + t_b V_{ddb} \\ V_{q2}^* = t_c V_{qqc} + t_d V_{qqd}, & V_{d2}^* = t_c V_{ddc} + t_d V_{ddd} \end{array}\right\} \tag{5.8}$$

Thus there are four (4) equations in four (4) unknowns and therefore solving these equations simultaneously, the normalized active times are:

$$t_a = \frac{V_{d1}^* V_{qqb} - V_{ddb} V_{q1}^*}{V_{dda} V_{qqb} - V_{ddb} V_{qqa}}, \quad t_b = \frac{V_{q1}^* V_{dda} - V_{qqa} V_{d1}^*}{V_{dda} V_{qqb} - V_{ddb} V_{qqa}}$$

$$t_c = \frac{V_{d2}^* V_{qqd} - V_{ddd} V_{q2}^*}{V_{ddc} V_{qqd} - V_{ddd} V_{qqc}}, \quad t_d = \frac{V_{q2}^* V_{ddc} - V_{qqc} V_{d2}^*}{V_{ddc} V_{qqd} - V_{ddd} V_{qqc}} \tag{5.9}$$

$$t_0 = t_{01} + t_{02} + t_{03}, \quad t_{01} = \alpha t_0, \quad t_{02} = \beta t_0,$$

$$t_{03} = \gamma t_0 = (1 - \alpha - \beta)t_0, \quad \alpha + \beta + \gamma = 1$$

where, α, β and γ are the distribution factors for the zero vectors U_{01}, U_{02} and U_{03} respectively. Note that the zero voltage vectors have no effect on the output voltages and therefore the values of t_a, t_b, t_c, t_d. The expression for the normalized times in (5.9) can be generalized as [69]:

$$t_a = 1.5V_1\left(\cos\theta_1 - \frac{1}{\sqrt{3}}\sin\theta_1\right), \qquad t_b = \sqrt{3}V_1 \sin\theta_1$$

$$\text{(5.10)}$$

$$t_c = 1.5V_2\left(\cos\theta_2 - \frac{1}{\sqrt{3}}\sin\theta_2\right), \qquad t_d = \sqrt{3}V_2 \sin\theta_2$$

where
$$V_1 = mag(V^*_{qd1})/V_{dc}, \quad \chi_1 = angle(V^*_{qd1}) = \pi(n_1-1)/3 + \theta_1$$

$$V_2 = mag(V^*_{qd2})/V_{dc}, \quad \chi_2 = angle(V^*_{qd2}) = \pi(n_2-1)/3 + \theta_2$$

and $mag(\ )$ refers to the magnitude of the variable in the parentheses; the integers n_1, n_2 are the space vector sector numbers (1~6) shown in Figure 5.3. Refering to Figure 5.4, the two reference voltages, V^*_{qd1} and V^*_{qd2} in complex form may be written as:

$$V^*_{qd1} = mag(V^*_{qd1})[\cos\theta_1 + j\sin\theta_1]$$
$$= mag(V_{qda})t_a + mag(V_{qdb})\left(\cos\frac{\pi}{3} + j\sin\frac{\pi}{3}\right)t_b$$

$$\text{(5.11)}$$

$$V^*_{qd2} = mag(V^*_{qd2})[\cos\theta_2 + j\sin\theta_2]$$
$$= mag(V_{qdc})t_c + mag(V_{qdd})\left(\cos\frac{\pi}{3} + j\sin\frac{\pi}{3}\right)t_d$$

Expanding (5.11) and comparing real and imaginary parts on both sides of the equations, the normalized times are given by

$$t_a = \frac{\sqrt{3} mag(V_{qd1}^*)}{V_{dc}} \sin\left(\frac{\pi}{3} - \theta_1\right)$$

$$t_b = \frac{\sqrt{3} mag(V_{qd1}^*)}{V_{dc}} \sin\theta_1$$

$$t_c = \frac{\sqrt{3} mag(V_{qd2}^*)}{V_{dc}} \sin\left(\frac{\pi}{3} - \theta_2\right) \tag{5.12}$$

$$t_d = \frac{\sqrt{3} mag(V_{qd2}^*)}{V_{dc}} \sin\theta_2$$

5.2.1.2.**Constraint on modulation indices.** The sum of the normalized active times in (5.12) must be less than or equal to unity as given in (5.13). Substituting the expressions of the active times given in (5.12) into (5.13), the resulting expression is given by (5.14).

$$t_a + t_b + t_c + t_d \le 1 \tag{5.13}$$

$$\left[\begin{array}{l} \dfrac{\sqrt{3}}{V_{dc}} mag(V_{qd1}^*)\sin\left(\dfrac{\pi}{3} - \theta_1\right) + \dfrac{\sqrt{3}}{V_{dc}} mag(V_{qd1}^*)\sin\theta_1 + \\[2mm] + \dfrac{\sqrt{3}k}{V_{dc}} mag(V_{qd1}^*)\sin\left(\dfrac{\pi}{3} - \theta_2\right) + \dfrac{\sqrt{3}k}{V_{dc}} mag(V_{qd1}^*)\sin\theta_2 \end{array} \right] \le 1 \tag{5.14}$$

where $k = \dfrac{mag(V_{qd2}^*)}{mag(V_{qd1}^*)}$ is the voltage amplitude ratio of the two reference voltages.

Solving for the voltage amplitude ratio from (5.14):

$$k \le \frac{V_{dc} - \sqrt{3} mag(V_{qd1}^*)\sin(\pi/3 + \theta_1)}{\sqrt{3} mag(V_{qd1}^*)\sin(\pi/3 + \theta_2)} \tag{5.15}$$

The voltage ratio k is dependent on the voltage angles θ_1 and θ_2 for given amplitude of the reference voltage, $mag(V_{qd1}^*)$. In the linear operating region, the space vector around the center of the hexagon, Figure 5.3, must lie on or within the boundary of the hexagon. For a given $mag(V_{qd1}^*)$, the combination of θ_1 and θ_2 that gives the

maximum allowed $mag(V_{qd2}^*)$ gives the limiting value of the voltage ratio. In others words, it gives the minimum value of k.

The modulation indices constraint can be determined by taking the partial derivatives of (5.15) with respect to θ_1 and θ_2, and then setting the resulting expressions to zero. That is:

$$\frac{\partial k}{\partial \theta_1} = -\frac{\cos(\pi/3 + \theta_1)}{\sin(\pi/3 + \theta_2)} = 0 \tag{5.16}$$

$$\frac{\partial k}{\partial \theta_2} = \frac{(-V_1 \sin(\pi/3 + \theta_1) + 1)\cos(\pi/3 + \theta_2)}{V_1^2 \sin^2(\pi/3 + \theta_2)} = 0 \tag{5.17}$$

where $V_1 = \dfrac{\sqrt{3}}{V_{dc}} mag(V_{qd1}^*)$.

From (5.16) and (5.17)

$$\cos(\pi/3 + \theta_1) = 0$$

$$(-V_1 \sin(\pi/3 + \theta_1) + 1)\cos(\pi/3 + \theta_2) = 0 \tag{5.18}$$

If $\cos(\pi/3 + \theta_1) = 0$, it implies that $\pi/3 + \theta_1 = \pi/2$ and $\theta_1 = \pi/2 - \pi/3 = \pi/6$. In the second condition, either $(-V_1 \sin(\pi/3 + \theta_1) + 1)$ or $\cos(\pi/3 + \theta_2)$ or both expressions are zero. If $\cos(\pi/3 + \theta_2) = 0$, it means $\theta_2 = \pi/2 - \pi/3 = \pi/6$. However, if $(-V_1 \sin(\pi/3 + \theta_1) + 1) = 0$, it implies $\sin(\pi/3 + \theta_1) = 1/V_1$ and the angle θ_1 is dependent on the amplitude of V_{qd1}^* and therefore is not unique and this solution is dropped. Thus if $\theta_1 = \theta_2 = \pi/6$, then

$$k_{min} = k(\pi/6, \pi/6) = -\frac{V_1 \sin(\pi/3 + \pi/6) - 1}{V_1 \sin(\pi/3 + \pi/6)} = -\frac{V_1 \sin(\pi/2) - 1}{V_1 \sin(\pi/2)} = \frac{1 - V_1}{V_1} \tag{5.19}$$

$$mag(V_{qd2}^*) + \sqrt{3}mag(V_{qd1}) = V_{dc} \tag{5.20}$$

$$\frac{mag(V^*_{qd1})}{V_{dc}} + \frac{mag(V^*_{qd2})}{V_{dc}} = \frac{1}{\sqrt{3}}$$ (5.21)

If the modulation indices are defined by $m_1 = \frac{2}{V_{dc}} mag(V^*_{qd1})$, $m_2 = \frac{2}{V_{dc}} mag(V^*_{qd2})$, the

constraint on the modulation indices can be written as:

$$m_1 + m_2 \leq \frac{2}{\sqrt{3}}$$ (5.22)

5.2.1.3.**Switching patterns for the Nine-switch converter.** In general the dwell

times of the active vectors are less than unity when operating in the linear modulation

region. The remaining time may then be filled by one or more of the zero vectors. In all,

there are thirty-four (34) possible sector combinations between *NSC1* and *NSC2* as listed

in Table 5.5 showing the switching sequence adopted to achieve the desired voltages.

Upon examining Table 5.5, a pattern appears depending on whether the sectors involved

are odd or even. The summary is given in Table 5.6 and the corresponding graphical

displays are shown in Figures 5.5 (a)-(d). The normalized device switching times in terms

of the device *qd* voltages may be calculated from (5.9) and are listed in Table 5.7. Table

5.8 shows the corresponding device turn-on times in terms of the line-to-line voltages.

Table 5.5. Switching sequence for all possible sector combinations

	S_{ap}	S_{bp}	S_{cp}	S_{am}	S_{bm}	S_{cm}	S_{an}	S_{bn}	S_{cn}	Time
Sector (I,I)										
U_{01}	0	0	0	1	1	1	1	1	1	t_{01}
U_a	1	0	0	0	1	1	1	1	1	t_a
U_b	1	0	1	0	1	0	1	1	1	t_b
U_{03}	1	1	1	0	0	0	1	1	1	t_{03}
U_c	1	1	1	1	0	0	0	1	1	t_c
U_d	1	1	1	1	0	1	0	1	0	t_d
U_{02}	1	1	1	1	1	1	0	0	0	t_{02}
Sector (II,I)										
U_{01}	0	0	0	1	1	1	1	1	1	t_{01}
U_b	0	0	1	1	1	0	1	1	1	t_b
U_a	1	0	1	0	1	0	1	1	1	t_a
U_{03}	1	1	1	0	0	0	1	1	1	t_{03}
U_c	1	1	1	1	0	0	0	1	1	t_c
U_d	1	1	1	1	0	1	0	1	0	t_d
U_{02}	1	1	1	1	1	1	0	0	0	t_{02}
Sector (III,I)										
U_{01}	0	0	0	1	1	1	1	1	1	t_{01}
U_a	0	0	1	1	1	0	1	1	1	t_a
U_b	0	1	1	1	0	0	1	1	1	t_b
U_{03}	1	1	1	0	0	0	1	1	1	t_{03}
U_c	1	1	1	1	0	0	0	1	1	t_c
U_d	1	1	1	1	0	1	0	1	0	t_d
U_{02}	1	1	1	1	1	1	0	0	0	t_{02}
Sector (IV,I)										
U_{01}	0	0	0	1	1	1	1	1	1	t_{01}
U_b	0	1	0	1	0	1	1	1	1	t_b
U_a	0	1	1	1	0	0	1	1	1	t_a
U_{03}	1	1	1	0	0	0	1	1	1	t_{03}
U_c	1	1	1	1	0	0	0	1	1	t_c
U_d	1	1	1	1	0	1	0	1	0	t_d
U_{02}	1	1	1	1	1	1	0	0	0	t_{02}

Table 5.5 (Continued)

Sector (V,I)									
	S_{ap}	S_{bp}	S_{cp}	S_{am}	S_{bm}	S_{cm}	S_{an}	S_{bn}	S_{cn}	Time
U_{01}	0	0	0	1	1	1	1	1	1	t_{01}
U_a	0	1	0	1	0	1	1	1	1	t_a
U_b	1	1	0	0	0	1	1	1	1	t_b
U_{03}	1	1	1	0	0	0	1	1	1	t_{03}
U_c	1	1	1	1	0	0	0	1	1	t_c
U_d	1	1	1	1	0	1	0	1	0	t_d
U_{02}	1	1	1	1	1	1	0	0	0	t_{02}

Sector (VI,I)									
	S_{ap}	S_{bp}	S_{cp}	S_{am}	S_{bm}	S_{cm}	S_{an}	S_{bn}	S_{cn}	Time
U_{01}	0	0	0	1	1	1	1	1	1	t_{01}
U_b	1	0	0	0	1	1	1	1	1	t_b
U_a	1	1	0	0	0	1	1	1	1	t_a
U_{03}	1	1	1	0	0	0	1	1	1	t_{03}
U_c	1	1	1	1	0	0	0	1	1	t_c
U_d	1	1	1	1	0	1	0	1	0	t_d
U_{02}	1	1	1	1	1	1	0	0	0	t_{02}

Sector (I,II)									
	S_{ap}	S_{bp}	S_{cp}	S_{am}	S_{bm}	S_{cm}	S_{an}	S_{bn}	S_{cn}	Time
U_{01}	0	0	0	1	1	1	1	1	1	t_{01}
U_a	1	0	0	0	1	1	1	1	1	t_a
U_b	1	0	1	0	1	0	1	1	1	t_b
U_{03}	1	1	1	0	0	0	1	1	1	t_{03}
U_d	1	1	1	0	0	1	1	1	0	t_d
U_c	1	1	1	1	0	1	0	1	0	t_c
U_{02}	1	1	1	1	1	1	0	0	0	t_{02}

Sector (II,II)									
	S_{ap}	S_{bp}	S_{cp}	S_{am}	S_{bm}	S_{cm}	S_{an}	S_{bn}	S_{cn}	Time
U_{01}	0	0	0	1	1	1	1	1	1	t_{01}
U_b	0	0	1	1	1	0	1	1	1	t_b
U_a	1	0	1	0	1	0	1	1	1	t_a
U_{03}	1	1	1	0	0	0	1	1	1	t_{03}
U_d	1	1	1	0	0	1	1	1	0	t_d
U_c	1	1	1	1	0	1	0	1	0	t_c
U_{02}	1	1	1	1	1	1	0	0	0	t_{02}

Table 5.5 (Continued)

	S_{ap}	S_{bp}	S_{cp}	S_{am}	S_{bm}	S_{cm}	S_{an}	S_{bn}	S_{cn}	Time
Sector (III,II)										
U_{01}	0	0	0	1	1	1	1	1	1	t_{01}
U_a	0	0	1	1	1	0	1	1	1	t_a
U_b	0	1	1	1	0	0	1	1	1	t_b
U_{03}	1	1	1	0	0	0	1	1	1	t_{03}
U_d	1	1	1	0	0	1	1	1	0	t_d
U_c	1	1	1	1	0	1	0	1	0	t_c
U_{02}	1	1	1	1	1	1	0	0	0	t_{02}
Sector (IV,II)										
U_{01}	0	0	0	1	1	1	1	1	1	t_{01}
U_b	0	1	0	1	0	1	1	1	1	t_b
U_a	0	1	1	1	0	0	1	1	1	t_a
U_{03}	1	1	1	0	0	0	1	1	1	t_{03}
U_d	1	1	1	0	0	1	1	1	0	t_d
U_c	1	1	1	1	0	1	0	1	0	t_c
U_{02}	1	1	1	1	1	1	0	0	0	t_{02}
Sector (V,II)										
U_{01}	0	0	0	1	1	1	1	1	1	t_{01}
U_a	0	1	0	1	0	1	1	1	1	t_a
U_b	1	1	0	0	0	1	1	1	1	t_b
U_{03}	1	1	1	0	0	0	1	1	1	t_{03}
U_d	1	1	1	0	0	1	1	1	0	t_d
U_c	1	1	1	1	0	1	0	1	0	t_c
U_{02}	1	1	1	1	1	1	0	0	0	t_{02}
Sector (VI,II)										
U_{01}	0	0	0	1	1	1	1	1	1	t_{01}
U_b	1	0	0	0	1	1	1	1	1	t_b
U_a	1	1	0	0	0	1	1	1	1	t_a
U_{03}	1	1	1	0	0	0	1	1	1	t_{03}
U_d	1	1	1	0	0	1	1	1	0	t_d
U_c	1	1	1	1	0	1	0	1	0	t_c
U_{02}	1	1	1	1	1	1	0	0	0	t_{02}

Table 5.5 (Continued)

	S_{ap}	S_{bp}	S_{cp}	S_{am}	S_{bm}	S_{cm}	S_{an}	S_{bn}	S_{cn}	Time
Sector (I,III)										
U_{01}	0	0	0	1	1	1	1	1	1	t_{01}
U_a	1	0	0	0	1	1	1	1	1	t_a
U_b	1	0	1	0	1	0	1	1	1	t_b
U_{03}	1	1	1	0	0	0	1	1	1	t_{03}
U_c	1	1	1	0	0	1	1	1	0	t_c
U_d	1	1	1	0	1	1	1	0	0	t_d
U_{02}	1	1	1	1	1	1	0	0	0	t_{02}
Sector (II,III)										
	S_{ap}	S_{bp}	S_{cp}	S_{am}	S_{bm}	S_{cm}	S_{an}	S_{bn}	S_{cn}	Time
U_{01}	0	0	0	1	1	1	1	1	1	t_{01}
U_b	0	0	1	1	1	0	1	1	1	t_b
U_a	1	0	1	0	1	0	1	1	1	t_a
U_{03}	1	1	1	0	0	0	1	1	1	t_{03}
U_c	1	1	1	0	0	1	1	1	0	t_c
U_d	1	1	1	0	1	1	1	0	0	t_d
U_{02}	1	1	1	1	1	1	0	0	0	t_{02}
Sector (III,III)										
	S_{ap}	S_{bp}	S_{cp}	S_{am}	S_{bm}	S_{cm}	S_{an}	S_{bn}	S_{cn}	Time
U_{01}	0	0	0	1	1	1	1	1	1	t_{01}
U_a	0	0	1	1	1	0	1	1	1	t_a
U_b	0	1	1	1	0	0	1	1	1	t_b
U_{03}	1	1	1	0	0	0	1	1	1	t_{03}
U_c	1	1	1	0	0	1	1	1	0	t_c
U_d	1	1	1	0	1	1	1	0	0	t_d
U_{02}	1	1	1	1	1	1	0	0	0	t_{02}
ector (IV,III)										
	S_{ap}	S_{bp}	S_{cp}	S_{am}	S_{bm}	S_{cm}	S_{an}	S_{bn}	S_{cn}	Time
U_{01}	0	0	0	1	1	1	1	1	1	t_{01}
U_b	0	1	0	1	0	1	1	1	1	t_b
U_a	0	1	1	1	0	0	1	1	1	t_a
U_{03}	1	1	1	0	0	0	1	1	1	t_{03}
U_c	1	1	1	0	0	1	1	1	0	t_c
U_d	1	1	1	0	1	1	1	0	0	t_d
U_{02}	1	1	1	1	1	1	0	0	0	t_{02}

Table 5.5 (Continued)

Sector (V,III)									
	S_{ap}	S_{bp}	S_{cp}	S_{am}	S_{bm}	S_{cm}	S_{an}	S_{bn}	S_{cn}	Time
U_{01}	0	0	0	1	1	1	1	1	1	t_{01}
U_a	0	1	0	1	0	1	1	1	1	t_a
U_b	1	1	0	0	0	1	1	1	1	t_b
U_{03}	1	1	1	0	0	0	1	1	1	t_{03}
U_c	1	1	1	0	0	1	1	1	0	t_c
U_d	1	1	1	0	1	1	1	0	0	t_d
U_{02}	1	1	1	1	1	1	0	0	0	t_{02}

Sector (VI,III)									
	S_{ap}	S_{bp}	S_{cp}	S_{am}	S_{bm}	S_{cm}	S_{an}	S_{bn}	S_{cn}	Time
U_{01}	0	0	0	1	1	1	1	1	1	t_{01}
U_b	1	0	0	0	1	1	1	1	1	t_b
U_a	1	1	0	0	0	1	1	1	1	t_a
U_{03}	1	1	1	0	0	0	1	1	1	t_{03}
U_c	1	1	1	0	0	1	1	1	0	t_c
U_d	1	1	1	0	1	1	1	0	0	t_d
U_{02}	1	1	1	1	1	1	0	0	0	t_{02}

Sector (I,IV)									
	S_{ap}	S_{bp}	S_{cp}	S_{am}	S_{bm}	S_{cm}	S_{an}	S_{bn}	S_{cn}	Time
U_{01}	0	0	0	1	1	1	1	1	1	t_{01}
U_a	1	0	0	0	1	1	1	1	1	t_a
U_b	1	0	1	0	1	0	1	1	1	t_b
U_{03}	1	1	1	0	0	0	1	1	1	t_{03}
U_d	1	1	1	0	1	0	1	0	1	t_d
U_c	1	1	1	0	1	1	1	0	0	t_c
U_{02}	1	1	1	1	1	1	0	0	0	t_{02}

Sector (II,IV)									
	S_{ap}	S_{bp}	S_{cp}	S_{am}	S_{bm}	S_{cm}	S_{an}	S_{bn}	S_{cn}	Time
U_{01}	0	0	0	1	1	1	1	1	1	t_{01}
U_b	0	0	1	1	1	0	1	1	1	t_b
U_a	1	0	1	0	1	0	1	1	1	t_a
U_{03}	1	1	1	0	0	0	1	1	1	t_{03}
U_d	1	1	1	0	1	0	1	0	1	t_d
U_c	1	1	1	0	1	1	1	0	0	t_c
U_{02}	1	1	1	1	1	1	0	0	0	t_{02}

Table 5.5 (Continued)

	S_{ap}	S_{bp}	S_{cp}	S_{am}	S_{bm}	S_{cm}	S_{an}	S_{bn}	S_{cn}	Time
Sector (III,IV)										
U_{01}	0	0	0	1	1	1	1	1	1	t_{01}
U_a	0	0	1	1	1	0	1	1	1	t_a
U_b	0	1	1	1	0	0	1	1	1	t_b
U_{03}	1	1	1	0	0	0	1	1	1	t_{03}
U_d	1	1	1	0	1	0	1	0	1	t_d
U_c	1	1	1	0	1	1	1	0	0	t_c
U_{02}	1	1	1	1	1	1	0	0	0	t_{02}
Sector (IV,IV)										
U_{01}	0	0	0	1	1	1	1	1	1	t_{01}
U_b	0	1	0	1	0	1	1	1	1	t_b
U_a	0	1	1	1	0	0	1	1	1	t_a
U_{03}	1	1	1	0	0	0	1	1	1	t_{03}
U_d	1	1	1	0	1	0	1	0	1	t_d
U_c	1	1	1	0	1	1	1	0	0	t_c
U_{02}	1	1	1	1	1	1	0	0	0	t_{02}
Sector (V,IV)										
U_{01}	0	0	0	1	1	1	1	1	1	t_{01}
U_a	0	1	0	1	0	1	1	1	1	t_a
U_b	1	1	0	0	0	1	1	1	1	t_b
U_{03}	1	1	1	0	0	0	1	1	1	t_{03}
U_d	1	1	1	0	1	0	1	0	1	t_d
U_c	1	1	1	0	1	1	1	0	0	t_c
U_{02}	1	1	1	1	1	1	0	0	0	t_{02}
Sector (VI,IV)										
U_{01}	0	0	0	1	1	1	1	1	1	t_{01}
U_b	1	0	0	0	1	1	1	1	1	t_b
U_a	1	1	0	0	0	1	1	1	1	t_a
U_{03}	1	1	1	0	0	0	1	1	1	t_{03}
U_d	1	1	1	0	1	0	1	0	1	t_d
U_c	1	1	1	0	1	1	1	0	0	t_c
U_{02}	1	1	1	1	1	1	0	0	0	t_{02}

Table 5.5 (Continued)

	S_{ap}	S_{bp}	S_{cp}	S_{am}	S_{bm}	S_{cm}	S_{an}	S_{bn}	S_{cn}	Time
Sector (I,V)										
U_{01}	0	0	0	1	1	1	1	1	1	t_{01}
U_a	1	0	0	0	1	1	1	1	1	t_a
U_b	1	0	1	0	1	0	1	1	1	t_b
U_{03}	1	1	1	0	0	0	1	1	1	t_{03}
U_c	1	1	1	0	1	0	1	0	1	t_c
U_d	1	1	1	1	1	0	0	0	1	t_d
U_{02}	1	1	1	1	1	1	0	0	0	t_{02}
Sector(II,V)										
	S_{ap}	S_{bp}	S_{cp}	S_{am}	S_{bm}	S_{cm}	S_{an}	S_{bn}	S_{cn}	Time
U_{01}	0	0	0	1	1	1	1	1	1	t_{01}
U_b	0	0	1	1	1	0	1	1	1	t_b
U_a	1	0	1	0	1	0	1	1	1	t_a
U_{03}	1	1	1	0	0	0	1	1	1	t_{03}
U_c	1	1	1	0	1	0	1	0	1	t_c
U_d	1	1	1	1	1	0	0	0	1	t_d
U_{02}	1	1	1	1	1	1	0	0	0	t_{02}
Sector (III,V)										
	S_{ap}	S_{bp}	S_{cp}	S_{am}	S_{bm}	S_{cm}	S_{an}	S_{bn}	S_{cn}	Time
U_{01}	0	0	0	1	1	1	1	1	1	t_{01}
U_a	0	0	1	1	1	0	1	1	1	t_a
U_b	0	1	1	1	0	0	1	1	1	t_b
U_{03}	1	1	1	0	0	0	1	1	1	t_{03}
U_c	1	1	1	0	1	0	1	0	1	t_c
U_d	1	1	1	1	1	0	0	0	1	t_d
U_{02}	1	1	1	1	1	1	0	0	0	t_{02}
Sector (IV,V)										
	S_{ap}	S_{bp}	S_{cp}	S_{am}	S_{bm}	S_{cm}	S_{an}	S_{bn}	S_{cn}	Time
U_{01}	0	0	0	1	1	1	1	1	1	t_{01}
U_b	0	1	0	1	0	1	1	1	1	t_b
V_a	0	1	1	1	0	0	1	1	1	t_a
U_{03}	1	1	1	0	0	0	1	1	1	t_{03}
U_c	1	1	1	0	1	0	1	0	1	t_c
U_d	1	1	1	1	1	0	0	0	1	t_d
U_{02}	1	1	1	1	1	1	0	0	0	t_{02}

Table 5.5 (Continued)

Sector (V,V)									
	S_{ap}	S_{bp}	S_{cp}	S_{am}	S_{bm}	S_{cm}	S_{an}	S_{bn}	S_{cn}	Time
U_{01}	0	0	0	1	1	1	1	1	1	t_{01}
U_a	0	1	0	1	0	1	1	1	1	t_b
U_b	1	1	0	0	0	1	1	1	1	t_b
U_{03}	1	1	1	0	0	0	1	1	1	t_{03}
U_c	1	1	1	0	1	0	1	0	1	t_c
U_d	1	1	1	1	1	0	0	0	1	t_d
U_{02}	1	1	1	1	1	1	0	0	0	t_{02}

Sector (VI,V)									
U_{01}	**0**	**0**	**0**	**1**	**1**	**1**	**1**	**1**	**1**	**t_{01}**
U_b	1	0	0	0	1	1	1	1	1	t_b
U_a	1	1	0	0	0	1	1	1	1	t_a
U_{03}	1	1	1	0	0	0	1	1	1	t_{03}
U_c	1	1	1	0	1	0	1	0	1	t_c
U_d	1	1	1	1	1	0	0	0	1	t_d
U_{02}	1	1	1	1	1	1	0	0	0	t_{02}

(I,IV)									
	S_{ap}	S_{bp}	S_{cp}	S_{am}	S_{bm}	S_{cm}	S_{an}	S_{bn}	S_{cn}	Time
U_{01}	0	0	0	1	1	1	1	1	1	t_{01}
U_a	1	0	0	0	1	1	1	1	1	t_a
U_b	1	0	1	0	1	0	1	1	1	t_b
U_{03}	1	1	1	0	0	0	1	1	1	t_{03}
U_d	1	1	1	1	0	0	0	1	1	t_d
U_c	1	1	1	1	1	0	0	0	1	t_c
U_{02}	1	1	1	1	1	1	0	0	0	t_{02}

Sector (II,VI)									
	S_{ap}	S_{bp}	S_{cp}	S_{am}	S_{bm}	S_{cm}	S_{an}	S_{bn}	S_{cn}	Time
U_{01}	0	0	0	1	1	1	1	1	1	t_{01}
U_b	0	0	1	1	1	0	1	1	1	t_b
U_a	1	0	1	0	1	0	1	1	1	t_a
U_{03}	1	1	1	0	0	0	1	1	1	t_{03}
U_d	1	1	1	1	0	0	0	1	1	t_d
U_c	1	1	1	1	1	0	0	0	1	t_c
U_{02}	1	1	1	1	1	1	0	0	0	t_{02}

Table 5.5 (Continued)

	S_{ap}	S_{bp}	S_{cp}	S_{am}	S_{bm}	S_{cm}	S_{an}	S_{bn}	S_{cn}	Time
Sector (III,VI)										
U_{01}	0	0	0	1	1	1	1	1	1	t_{01}
U_a	0	0	1	1	1	0	1	1	1	t_a
U_b	0	1	1	1	0	0	1	1	1	t_b
U_{03}	1	1	1	0	0	0	1	1	1	t_{03}
U_d	1	1	1	1	0	0	0	1	1	t_d
U_c	1	1	1	1	1	0	0	0	1	t_c
U_{02}	1	1	1	1	1	1	0	0	0	t_{02}
Sector (IV,VI)										
U_{01}	0	0	0	1	1	1	1	1	1	t_{01}
U_b	0	1	0	1	0	1	1	1	1	t_b
U_a	0	1	1	1	0	0	1	1	1	t_a
U_{03}	1	1	1	0	0	0	1	1	1	t_{03}
U_d	1	1	1	1	0	0	0	1	1	t_d
U_c	1	1	1	1	1	0	0	0	1	t_c
U_{02}	1	1	1	1	1	1	0	0	0	t_{02}
Sector (V,VI)										
U_{01}	0	0	0	1	1	1	1	1	1	t_{01}
U_a	0	1	0	1	0	1	1	1	1	t_a
U_b	1	1	0	0	0	1	1	1	1	t_b
U_{03}	1	1	1	0	0	0	1	1	1	t_{03}
U_d	1	1	1	1	0	0	0	1	1	t_d
U_c	1	1	1	1	1	0	0	0	1	t_c
U_{02}	1	1	1	1	1	1	0	0	0	t_{02}
Sector (VI,VI)										
U_{01}	0	0	0	1	1	1	1	1	1	t_{01}
U_b	1	0	0	0	1	1	1	1	1	t_b
U_a	1	1	0	0	0	1	1	1	1	t_a
U_{03}	1	1	1	0	0	0	1	1	1	t_{03}
U_d	1	1	1	1	0	0	0	1	1	t_d
U_c	1	1	1	1	1	0	0	0	1	t_c
U_{02}	1	1	1	1	1	1	0	0	0	t_{02}

Table 5.6. Summarized switching sequence for all possible sector combinations

Switching Sequence	V_{qd1}^{*} in	V_{qd2}^{*} in
U_{01}->U_a->U_b->U_{03}->U_c->U_d->U_{02}->U_{02}->U_d->U_c->U_{03}->U_b->U_a ->U_{01}	(I,III,V)	(I,III,V)
U_{01}->U_a->U_b->U_{03}->U_d->U_c->U_{02}->U_{02}->U_c->U_d->U_{03}->U_b->U_a ->U_{01}	(I,III,V)	(II,IV,VI)
U_{01}->U_b->U_a->U_{03}->U_c->U_d->U_{02}->U_{02}->U_d->U_c->U_{03}->U_a->U_b ->U_{01}	(II,IV,VI)	(I,III,V)
U_{01}->U_b->U_a->U_{03}->U_d->U_c->U_{02}->U_{02}->U_c->U_d->U_{03}->U_a->U_b ->U_{01}	(II,IV,VI)	(II,IV,VI)

(a)

119

(b)

(c)

120
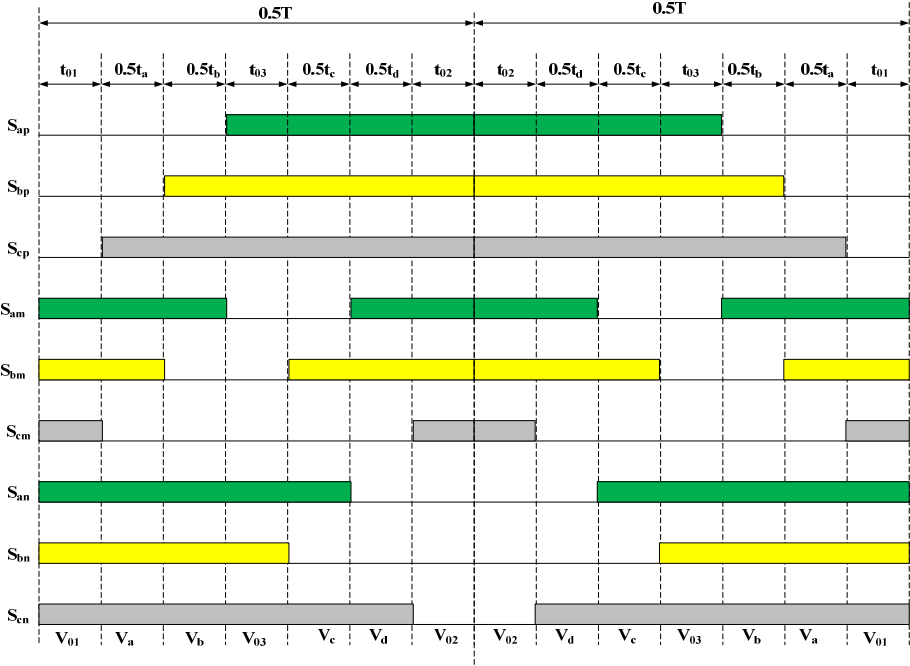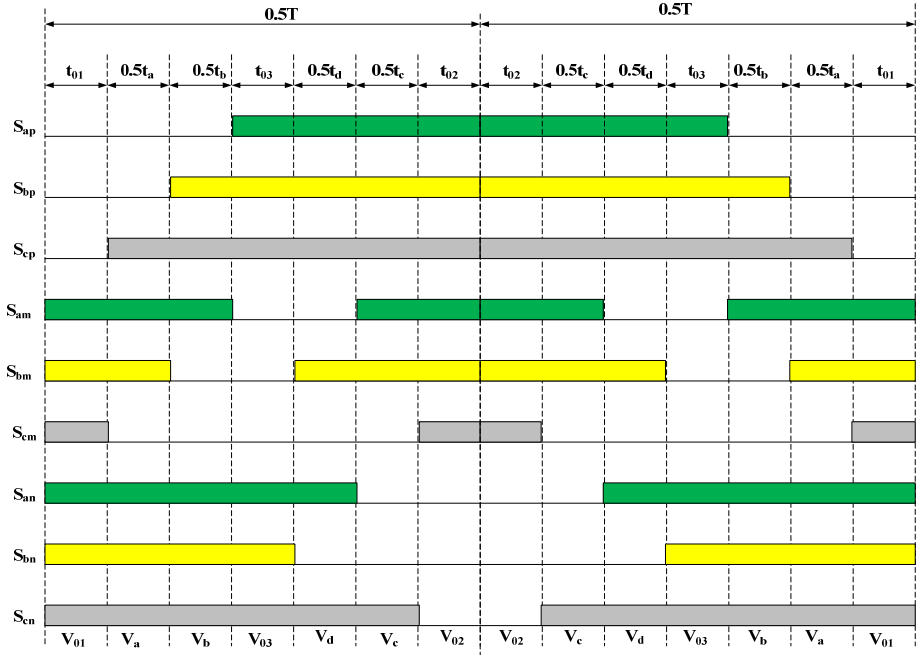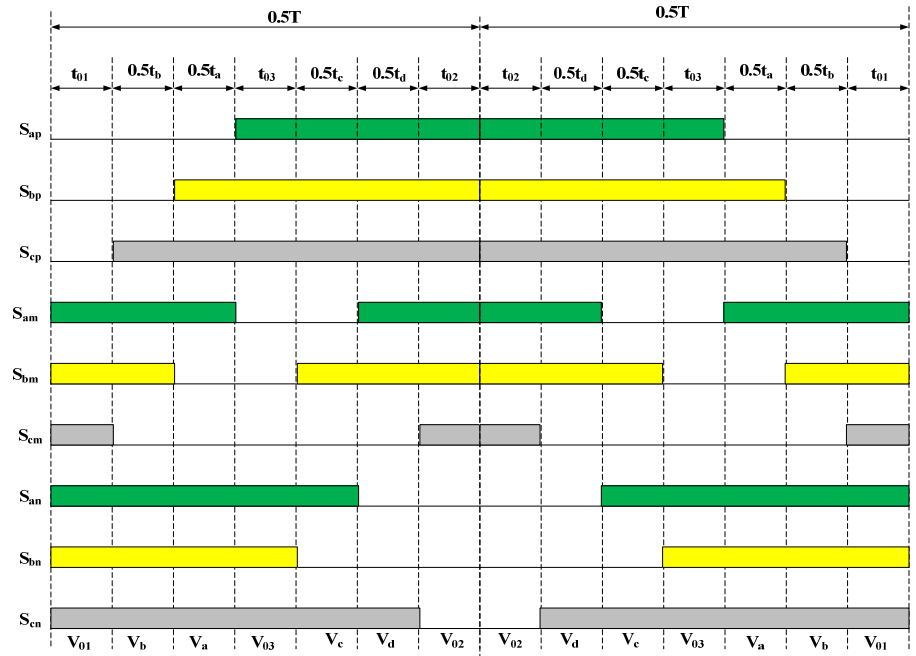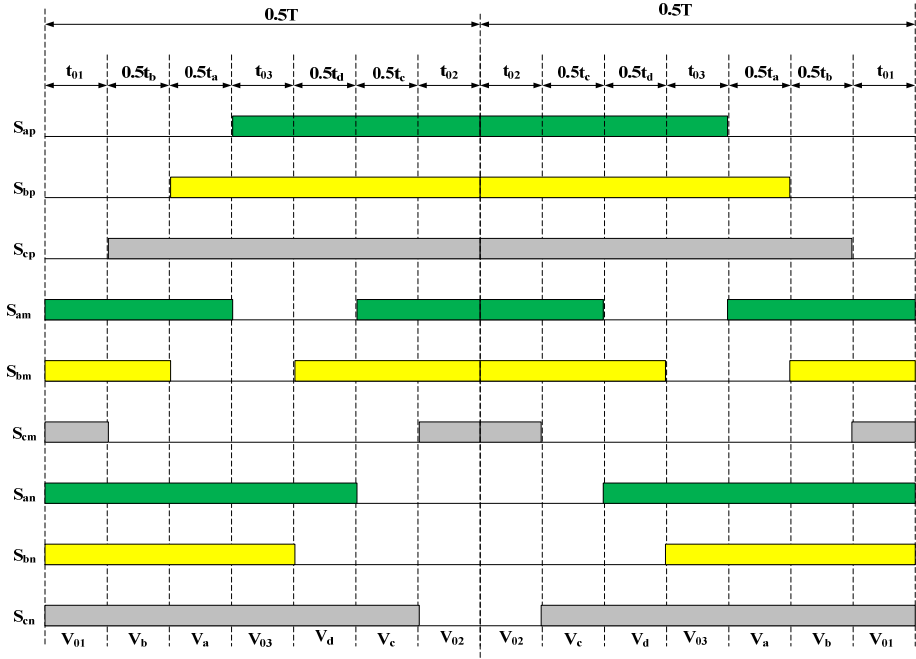
(d)

Figure 5.5. Switching sequence for all possible sector combinations between *NSC1* and *NSC2* outputs where V_{qd1}^*, V_{qd2}^* are located in sector (a) I, III or V and I, III, or V ;(b) I, III or V and II, VI or VI; (c) II, VI or VI and I, III or V and (d) II, VI or VI and II, VI or VI

Table 5.7. Device switching times expressed in terms of the *qd* reference voltages

| | | | NSC2 | | | | | |
			I	II	III	IV	V	VI
NSC1	I	t_a	$\frac{1}{2}(3V_{q1}+\sqrt{3}V_{d1})/V_{dc}$	$\frac{1}{2}(3V_{q1}+\sqrt{3}V_{d1})/V_{dc}$	$\frac{1}{2}(3V_{q1}+\sqrt{3}V_{d1})/V_{dc}$	$\frac{1}{2}(3V_{q1}+\sqrt{3}V_{d1})/V_{dc}$	$\frac{1}{2}(3V_{q1}+\sqrt{3}V_{d1})/V_{dc}$	$\frac{1}{2}(3V_{q1}+\sqrt{3}V_{d1})/V_{dc}$
		t_b	$-\sqrt{3}V_{d1}/V_{dc}$	$-\sqrt{3}V_{d1}/V_{dc}$	$-\sqrt{3}V_{d1}/V_{dc}$	$-\sqrt{3}V_{d1}/V_{dc}$	$-\sqrt{3}V_{d1}/V_{dc}$	$-\sqrt{3}V_{d1}/V_{dc}$
		t_c	$\frac{1}{2}(3V_{q2}+\sqrt{3}V_{d2})/V_{dc}$	$\frac{1}{2}(3V_{q2}-\sqrt{3}V_{d2})/V_{dc}$	$-\sqrt{3}V_{d2}/V_{dc}$	$\frac{1}{2}(-3V_{q2}-\sqrt{3}V_{d2})/V_{dc}$	$\frac{1}{2}(-3V_{q2}+\sqrt{3}V_{d2})/V_{dc}$	$\sqrt{3}V_{d2}/V_{dc}$
		t_d	$-\sqrt{3}V_{d2}/V_{dc}$	$\frac{1}{2}(-3V_{q2}-\sqrt{3}V_{d2})/V_{dc}$	$\frac{1}{2}(-3V_{q2}+\sqrt{3}V_{d2})/V_{dc}$	$\sqrt{3}V_{d2}/V_{dc}$	$\frac{1}{2}(3V_{q2}+\sqrt{3}V_{d2})/V_{dc}$	$\frac{1}{2}(3V_{q2}-\sqrt{3}V_{d2})/V_{dc}$
	II	t_a	$\frac{1}{2}(3V_{q1}-\sqrt{3}V_{d1})/V_{dc}$	$\frac{1}{2}(3V_{q1}-\sqrt{3}V_{d1})/V_{dc}$	$\frac{1}{2}(3V_{q1}-\sqrt{3}V_{d1})/V_{dc}$	$\frac{1}{2}(3V_{q1}-\sqrt{3}V_{d1})/V_{dc}$	$\frac{1}{2}(3V_{q1}-\sqrt{3}V_{d1})/V_{dc}$	$\frac{1}{2}(3V_{q1}-\sqrt{3}V_{d1})/V_{dc}$
		t_b	$\frac{1}{2}(-3V_{q1}-\sqrt{3}V_{d1})/V_{dc}$	$\frac{1}{2}(-3V_{q1}-\sqrt{3}V_{d1})/V_{dc}$	$\frac{1}{2}(-3V_{q1}-\sqrt{3}V_{d1})/V_{dc}$	$\frac{1}{2}(-3V_{q1}-\sqrt{3}V_{d1})/V_{dc}$	$\frac{1}{2}(-3V_{q1}-\sqrt{3}V_{d1})/V_{dc}$	$\frac{1}{2}(-3V_{q1}-\sqrt{3}V_{d1})/V_{dc}$
		t_c	$\frac{1}{2}(3V_{q2}+\sqrt{3}V_{d2})/V_{dc}$	$\frac{1}{2}(3V_{q2}-\sqrt{3}V_{d2})/V_{dc}$	$-\sqrt{3}V_{d2}/V_{dc}$	$\frac{1}{2}(-3V_{q2}-\sqrt{3}V_{d2})/V_{dc}$	$\frac{1}{2}(-3V_{q2}+\sqrt{3}V_{d2})/V_{dc}$	$\sqrt{3}V_{d2}/V_{dc}$

Table 5.7 (Continued)

		I	II	III	IV	V	VI
	t_d	$-\sqrt{3}V_{d2}/V_{dc}$	$\frac{1}{2}(-3V_{q2}-\sqrt{3}V_{d2})/V_{dc}$	$\frac{1}{2}(-3V_{q2}+\sqrt{3}V_{d2})/V_{dc}$	$\sqrt{3}V_{d2}/V_{dc}$	$\frac{1}{2}(3V_{q2}+\sqrt{3}V_{d2})/V_{dc}$	$\frac{1}{2}(3V_{q2}-\sqrt{3}V_{d2})/V_{dc}$
II I	t_a	$-\sqrt{3}V_{d1}/V_{dc}$	$-\sqrt{3}V_{d1}/V_{dc}$	$-\sqrt{3}V_{d1}/V_{dc}$	$-\sqrt{3}V_{d1}/V_{dc}$	$-\sqrt{3}V_{d1}/V_{dc}$	$-\sqrt{3}V_{d1}/V_{dc}$
	t_b	$\frac{1}{2}(-3V_{q1}+\sqrt{3}V_{d1})/V_{dc}$	$\frac{1}{2}(-3V_{q1}+\sqrt{3}V_{d1})/V_{dc}$	$\frac{1}{2}(-3V_{q1}+\sqrt{3}V_{d1})/V_{dc}$	$\frac{1}{2}(-3V_{q1}+\sqrt{3}V_{d1})/V_{dc}$	$\frac{1}{2}(-3V_{q1}+\sqrt{3}V_{d1})/V_{dc}$	$\frac{1}{2}(-3V_{q1}+\sqrt{3}V_{d1})/V_{dc}$
	t_c	$\frac{1}{2}(3V_{q2}+\sqrt{3}V_{d2})/V_{dc}$	$\frac{1}{2}(3V_{q2}-\sqrt{3}V_{d2})/V_{dc}$	$-\sqrt{3}V_{d2}/V_{dc}$	$\frac{1}{2}(-3V_{q2}-\sqrt{3}V_{d2})/V_{dc}$	$\frac{1}{2}(-3V_{q2}+\sqrt{3}V_{d2})/V_{dc}$	$\sqrt{3}/V_{dc}V_{d2}$
	t_d	$-\sqrt{3}V_{d2}/V_{dc}$	$\frac{1}{2}(-3V_{q2}-\sqrt{3}V_{d2})/V_{dc}$	$\frac{1}{2}(-3V_{q2}+\sqrt{3}V_{d2})/V_{dc}$	$\sqrt{3}/V_{dc}V_{d2}$	$\frac{1}{2}(3V_{q2}+\sqrt{3}V_{d2})/V_{dc}$	$\frac{1}{2}(3V_{q2}-\sqrt{3}V_{d2})/V_{dc}$
I V	t_a	$\frac{1}{2}(-3V_{q1}-\sqrt{3}V_{d1})/V_{dc}$	$\frac{1}{2}(-3V_{q1}-\sqrt{3}V_{d1})/V_{dc}$	$\frac{1}{2}(-3V_{q1}-\sqrt{3}V_{d1})/V_{dc}$	$\frac{1}{2}(-3V_{q1}-\sqrt{3}V_{d1})/V_{dc}$	$\frac{1}{2}(-3V_{q1}-\sqrt{3}V_{d1})/V_{dc}$	$\frac{1}{2}(-3V_{q1}-\sqrt{3}V_{d1})/V_{dc}$
	t_b	$\sqrt{3}V_{d1}/V_{dc}$	$\sqrt{3}V_{d1}/V_{dc}$	$\sqrt{3}V_{d1}/V_{dc}$	$\sqrt{3}V_{d1}/V_{dc}$	$\sqrt{3}V_{d1}/V_{dc}$	$\sqrt{3}V_{d1}/V_{dc}$
	t_c	$\frac{1}{2}(3V_{q2}+\sqrt{3}V_{d2})/V_{dc}$	$\frac{1}{2}(3V_{q2}-\sqrt{3}V_{d2})/V_{dc}$	$-\sqrt{3}V_{d2}/V_{dc}$	$\frac{1}{2}(-3V_{q2}-\sqrt{3}V_{d2})/V_{dc}$	$\frac{1}{2}(-3V_{q2}+\sqrt{3}V_{d2})/V_{dc}$	$\sqrt{3}V_{d2}/V_{dc}$
	t_d	$-\sqrt{3}/V_{dc}V_{d2}$	$\frac{1}{2}(-3V_{q2}-\sqrt{3}V_{d2})/V_{dc}$	$\frac{1}{2}(-3V_{q2}+\sqrt{3}V_{d2})/V_{dc}$	$\sqrt{3}V_{d2}/V_{dc}$	$\frac{1}{2}(3V_{q2}+\sqrt{3}V_{d2})/V_{dc}$	$\frac{1}{2}(3V_{q2}-\sqrt{3}V_{d2})/V_{dc}$

Table 5.7 (Continued)

		I	II	III	IV	V	VI
	t_a	$\frac{1}{2}(-3V_{q1}+\sqrt{3}V_{d1})/V_{dc}$	$\frac{1}{2}(-3V_{q1}+\sqrt{3}V_{d1})/V_{dc}$	$\frac{1}{2}(-3V_{q1}+\sqrt{3}V_{d1})/V_{dc}$	$\frac{1}{2}(-3V_{q1}+\sqrt{3}V_{d1})/V_{dc}$	$\frac{1}{2}(-3V_{q1}+\sqrt{3}V_{d1})/V_{dc}$	$\frac{1}{2}(-3V_{q1}+\sqrt{3}V_{d1})/V_{dc}$
	t_b	$\frac{1}{2}(3V_{q1}+\sqrt{3}V_{d1})/V_{dc}$	$\frac{1}{2}(3V_{q1}+\sqrt{3}V_{d1})/V_{dc}$	$\frac{1}{2}(3V_{q1}+\sqrt{3}V_{d1})/V_{dc}$	$\frac{1}{2}(3V_{q1}+\sqrt{3}V_{d1})/V_{dc}$	$\frac{1}{2}(3V_{q1}+\sqrt{3}V_{d1})/V_{dc}$	$\frac{1}{2}(3V_{q1}+\sqrt{3}V_{d1})/V_{dc}$
	t_c	$\frac{1}{2}(3V_{q2}+\sqrt{3}V_{d2})/V_{dc}$	$\frac{1}{2}(3V_{q2}-\sqrt{3}V_{d2})/V_{dc}$	$-\sqrt{3}V_{d2}/V_{dc}$	$\frac{1}{2}(-3V_{q2}-\sqrt{3}V_{d2})/V_{dc}$	$\frac{1}{2}(-3V_{q2}+\sqrt{3}V_{d2})/V_{dc}$	$\sqrt{3}V_{d2}/V_{dc}$
V	t_d	$-\sqrt{3}V_{d2}/V_{dc}$	$\frac{1}{2}(-3V_{q2}-\sqrt{3}V_{d2})/V_{dc}$	$\frac{1}{2}(-3V_{q2}+\sqrt{3}V_{d2})/V_{dc}$	$\sqrt{3}V_{d2}/V_{dc}$	$\frac{1}{2}(3V_{q2}+\sqrt{3}V_{d2})/V_{dc}$	$\frac{1}{2}(3V_{q2}-\sqrt{3}V_{d2})/V_{dc}$
	t_a	$\sqrt{3}V_{d1}/V_{dc}$	$\sqrt{3}V_{d1}/V_{dc}$	$\sqrt{3}V_{d1}/V_{dc}$	$\sqrt{3}V_{d1}/V_{dc}$	$\sqrt{3}V_{d1}/V_{dc}$	$\sqrt{3}V_{d1}/V_{dc}$
	t_b	$\frac{1}{2}(3V_{q1}-\sqrt{3}V_{d1})/V_{dc}$	$\frac{1}{2}(3V_{q1}-\sqrt{3}V_{d1})/V_{dc}$	$\frac{1}{2}(3V_{q1}-\sqrt{3}V_{d1})/V_{dc}$	$\frac{1}{2}(3V_{q1}-\sqrt{3}V_{d1})/V_{dc}$	$\frac{1}{2}(3V_{q1}-\sqrt{3}V_{d1})/V_{dc}$	$\frac{1}{2}(3V_{q1}-\sqrt{3}V_{d1})/V_{dc}$
	t_c	$\frac{1}{2}(3V_{q2}+\sqrt{3}V_{d2})/V_{dc}$	$\frac{1}{2}(3V_{q2}-\sqrt{3}V_{d2})/V_{dc}$	$-\sqrt{3}V_{d2}/V_{dc}$	$\frac{1}{2}(-3V_{q2}-\sqrt{3}V_{d2})/V_{dc}$	$\frac{1}{2}(-3V_{q2}+\sqrt{3}V_{d2})/V_{dc}$	$\sqrt{3}V_{d2}/V_{dc}$
VI	t_d	$-\sqrt{3}V_{d2}/V_{dc}$	$\frac{1}{2}(-3V_{q2}-\sqrt{3}V_{d2})/V_{dc}$	$\frac{1}{2}(-3V_{q2}+\sqrt{3}V_{d2})/V_{dc}$	$\sqrt{3}V_{d2}/V_{dc}$	$\frac{1}{2}(3V_{q2}+\sqrt{3}V_{d2})/V_{dc}$	$\frac{1}{2}(3V_{q2}-\sqrt{3}V_{d2})/V_{dc}$

Table 5.8. Device switching times expressed in terms of the line-to-line voltages

Sector	I	II	III	IV	V	VI
t_a	V_{ab1}/V_{dc}	V_{ac1}/V_{dc}	V_{bc1}/V_{dc}	V_{ba1}/V_{dc}	V_{ca1}/V_{dc}	V_{cb1}/V_{dc}
t_b	V_{bc1}/V_{dc}	V_{ba1}/V_{dc}	V_{ca1}/V_{dc}	V_{cb1}/V_{dc}	V_{ab1}/V_{dc}	V_{ac1}/V_{dc}
t_c	V_{ab2}/V_{dc}	V_{ac2}/V_{dc}	V_{bc2}/V_{dc}	V_{ba2}/V_{dc}	V_{ca2}/V_{dc}	V_{cb2}/V_{dc}
t_d	V_{bc2}/V_{dc}	V_{ba2}/V_{dc}	V_{ca2}/V_{dc}	V_{cb2}/V_{dc}	V_{ab2}/V_{dc}	V_{ac2}/V_{dc}

5.2.1.4.**Generalized neutral voltage.** It has been shown that the placement of the zero space vectors is the fundamental difference between PWM strategies [70]. In this research, it is assumed that all three (3) zero vectors are used in synthesizing the voltages with the distribution factors given in (5.24). The average neutral voltage can be approximated as:

$$<V_{n0}> = V_{oa}t_a + V_{ob}t_b + V_{oc}t_c + V_{od}t_d + V_{o1}t_{01} + V_{o2}t_{02} + V_{o3}t_{03}$$

(5.23)

$$<V_{m0}> = V_{oa}t_a + V_{ob}t_b + V_{oc}t_c + V_{od}t_d + V_{o1}t_{01} + V_{o2}t_{02} + V_{o3}t_{03}$$

$$t_{01} = \alpha t_0$$

$$t_{02} = \beta t_0$$

(5.24)

$$t_{03} = (1 - \alpha - \beta)t_0$$

For example, if the reference voltages are located in sectors (I, I), from the space vector diagram, the voltages in (5.23) are gven by:

$$V_{oa} = -\frac{V_{dc}}{6}, \quad V_{ob} = \frac{V_{dc}}{6}, \quad V_{oc} = \frac{V_{dc}}{2}, \quad V_{od} = \frac{V_{dc}}{2}, \quad V_{o1} = -\frac{V_{dc}}{2}, \quad V_{o2} = \frac{V_{dc}}{2} \quad \text{and} \quad V_{o3} = \frac{V_{dc}}{2} \quad \text{for}$$

NSC1.

$$V_{oa} = -\frac{V_{dc}}{2}, \quad V_{ob} = -\frac{V_{dc}}{2}, \quad V_{oc} = -\frac{V_{dc}}{6}, \quad V_{od} = \frac{V_{dc}}{6}, \quad V_{o1} = -\frac{V_{dc}}{2}, \quad V_{o2} = \frac{V_{dc}}{2} \quad \text{and} \quad V_{o3} = -\frac{V_{dc}}{2}$$

for *NSC2.*

Substituting the above voltages into (5.23), the neutral voltages are given as:

Sector

(I,I):

$$<V_{no}> = \frac{V_{dc}}{2}\left(-t_{01} + t_{02} + t_{03} + t_c + t_d\right) + \frac{V_{dc}}{6}\left(-t_a + t_b\right)$$

$$<V_{mo}> = \frac{V_{dc}}{2}\left(-t_{01} + t_{02} - t_{03} - t_a - t_b\right) + \frac{V_{dc}}{6}\left(-t_c + t_d\right)$$

(5.25)

Similarly, in other sector combinations, the neutral voltages are:

Sector

(I,II):

$$<V_{n0}> = \frac{V_{dc}}{2}\left(-t_{01} + t_{02} + t_{03} + t_c + t_d\right) + \frac{V_{dc}}{6}\left(-t_a + t_b\right)$$

$$<V_{m0}> = -\frac{V_{dc}}{2}\left(t_{01} - t_{02} + t_{03} + t_a + t_b\right) + \frac{V_{dc}}{6}\left(t_c - t_d\right)$$

(5.26)

Sector

(I,III)

$$<V_{n0}> = \frac{V_{dc}}{2}\left(-t_{01} + t_{02} + t_{03} + t_c + t_d\right) + \frac{V_{dc}}{6}\left(-t_a + t_b\right)$$

$$<V_{m0}> = -\frac{V_{dc}}{2}\left(t_{01} - t_{02} + t_{03} + t_a + t_b\right) + \frac{V_{dc}}{6}\left(-t_c + t_d\right)$$

(5.27)

Sector

(I, IV):

$$<V_{n0}> = \frac{V_{dc}}{2}\left(-t_{01} + t_{02} + t_{03} + t_c + t_d\right) + \frac{V_{dc}}{6}\left(-t_a + t_b\right)$$

$$<V_{m0}> = -\frac{V_{dc}}{2}\left(t_{01} - t_{02} + t_{03} + t_a + t_b\right) + \frac{V_{dc}}{6}\left(t_c - t_d\right)$$

(5.28)

Sector

(II, I):

$$<V_{n0}> = \frac{V_{dc}}{2}\left(-t_{01} + t_{02} + t_{03} + t_c + t_d\right) + \frac{V_{dc}}{6}\left(t_a - t_b\right)$$

$$<V_{m0}> = -\frac{V_{dc}}{2}\left(t_{01} - t_{02} + t_{03} + t_a + t_b\right) + \frac{V_{dc}}{6}\left(-t_c + t_d\right)$$

(5.29)

Sector

(II, I):

$$<V_{n0}> = \frac{V_{dc}}{2}\left(-t_{01} + t_{02} + t_{03} + t_c + t_d\right) + \frac{V_{dc}}{6}\left(t_a - t_b\right)$$

$$<V_{m0}> = -\frac{V_{dc}}{2}\left(t_{01} - t_{02} + t_{03} + t_a + t_b\right) + \frac{V_{dc}}{6}\left(t_c - t_d\right)$$

(5.30)

Sector

(II,III):

$$<V_{n0}> = \frac{V_{dc}}{2}\left(-t_{01} + t_{02} + t_{03} + t_c + t_d\right) + \frac{V_{dc}}{6}\left(t_a - t_b\right)$$

$$<V_{m0}> = -\frac{V_{dc}}{2}\left(t_{01} - t_{02} + t_{03} + t_a + t_b\right) + \frac{V_{dc}}{6}\left(-t_c + t_d\right)$$

(5.31)

Sector

(II,IV):

$$<V_{n0}> = \frac{V_{dc}}{2}\left(-t_{01} + t_{02} + t_{03} + t_c + t_d\right) + \frac{V_{dc}}{6}\left(t_a - t_b\right)$$

$$<V_{m0}> = -\frac{V_{dc}}{2}\left(t_{01} - t_{02} + t_{03} + t_a + t_b\right) + \frac{V_{dc}}{6}\left(t_c - t_d\right)$$

(5.32)

In tabular form, all the neutral voltages in the various sector combinations are listed in Table 5.9. It can be deduced from (5.25) - (5.32) or Table 5.9, that the neutral voltages depend on whether a sector is odd or even. Table 5.10 summarizes the neutral voltages in all possible sector combinations in terms of the switching times while Table 5.11 shows the switching times in terms of the line-to-line voltages.

Table 5.9. Calculating the converter neutral voltages

(I,I)	$V_{dc}/6$	$V_{dc}/6$			(I,II)	$V_{dc}/6$	$V_{dc}/6$	
	V_{01}	V_{02}	**Time**			V_{01}	V_{02}	**Time**
$V_1=U_{01}$	-3	-3	t_{01}		$V_1=U_{01}$	-3	-3	t_{01}
$V_{19}=U_a$	-1	-3	t_a		$V_{19}=U_a$	-1	-3	t_a
$V_{21}=U_b$	1	-3	t_b		$V_{21}=U_b$	1	-3	t_b
$V_{27}=U_{03}$	3	-3	t_{03}		$V_{27}=U_{03}$	3	-3	t_{03}
$V_{18}=U_c$	3	-1	t_c		$V_{26}=U_d$	3	-1	t_d
$V_{17}=U_d$	3	1	t_d		$V_{17}=U_c$	3	1	t_c
$V_{14}=U_{02}$	3	3	t_{02}		$V_{14}=U_{02}$	3	3	t_{02}

(II,I)	$V_{dc}/6$	$V_{dc}/6$			(II,II)	$V_{dc}/6$	$V_{dc}/6$	
	V_{01}	V_{02}	**Time**			V_{01}	V_{02}	**Time**
$V_1=U_{01}$	-3	-3	t_{01}		$V_1=U_{01}$	-3	-3	t_{01}
$V_3=U_b$	-1	-3	t_b		$V_3=U_b$	-1	-3	t_b
$V_{21}=U_a$	1	-3	t_a		$V_{21}=U_a$	1	-3	t_a
$V_{27}=U_{03}$	3	-3	t_{03}		$V_{27}=U_{03}$	3	-3	t_{03}
$V_{18}=U_c$	3	-1	t_c		$V_{26}=U_d$	3	-1	t_d
$V_{17}=U_d$	3	1	t_d		$V_{17}=U_c$	3	1	t_c
$V1_4=U_{02}$	3	3	t_{02}		$V_{14}=U_{02}$	3	3	t_{02}

(III,I)	$V_{dc}/6$	$V_{dc}/6$			(III,II)	$V_{dc}/6$	$V_{dc}/6$	
	V_{01}	V_{02}	**Time**			V_{01}	V_{02}	**Time**
$V_1=U_{01}$	-3	-3	t_{01}		$V_1=U_{01}$	-3	-3	t_{01}
$V_3=U_a$	-1	-3	t_a		$V_3=U_a$	-1	-3	t_a
$V_9=U_b$	1	-3	t_b		$V_9=U_b$	1	-3	t_b
$V_{27}=U_{03}$	3	-3	t_{03}		$V_{27}=U_{03}$	3	-3	t_{03}
$V_{18}=U_c$	3	-1	t_c		$V_{26}=U_d$	3	-1	t_d
$V_{17}=U_d$	3	1	t_d		$V_{17}=U_c$	3	1	t_c
$V_{14}=U_{02}$	3	3	t_{02}		$V_{14}=U_{02}$	3	3	t_{02}

Table 5.9. (Continued)

(IV,I)	$V_{dc}/6$	$V_{dc}/6$			(IV,II)	$V_{dc}/6$	$V_{dc}/6$	
	V_{01}	V_{02}	Time			V_{01}	V_{02}	Time
$V_1=U_{01}$	-3	-3	t_{01}		$V_1=U_{01}$	-3	-3	t_{01}
$V_7=U_b$	-1	-3	t_b		$V_7=U_b$	-1	-3	t_b
$V_9=U_a$	1	-3	t_a		$V_9=U_a$	1	-3	t_a
$V_{27}=U_{03}$	3	-3	t_{03}		$V_{27}=U_{03}$	3	-3	t_{03}
$V_{18}=U_c$	3	-1	t_c		$V_{26}=U_d$	3	-1	t_d
$V_{17}=U_d$	3	1	t_d		$V_{17}=U_c$	3	1	t_c
$V_{14}=U_{02}$	3	3	t_{02}		$V_{14}=U_{02}$	3	3	t_{02}

(V,I)	$V_{dc}/6$	$V_{dc}/6$			(V,II)	$V_{dc}/6$	$V_{dc}/6$	
	V_{01}	V_{02}	Time			V_{01}	V_{02}	Time
$V_1=U_{01}$	-3	-3	t_01		$V_1=U_{01}$	-3	-3	t_{01}
$V_7=U_a$	-1	-3	t_a		$V_7=U_b$	-1	-3	t_b
$V_{25}=U_b$	1	-3	t_b		$V_{25}=U_b$	1	-3	t_b
$V_{27}=U_{03}$	3	-3	t_{03}		$V_{27}=U_{03}$	3	-3	t_03
$V_{18}=U_c$	3	-1	t_c		$V_{26}=U_d$	3	-1	t_d
$V_{17}=U_d$	3	1	t_d		$V_{17}=U_c$	3	1	t_c
$V_{14}=U_{02}$	3	3	t_{02}		$V_{14}=U_{02}$	3	3	t_{02}

(VI,I)	$V_{dc}/6$	$V_{dc}/6$			(VI,II)	$V_{dc}/6$	$V_{dc}/6$	
	V_{01}	V_{02}	Time			V_{01}	V_{02}	Time
$V_1=U_{01}$	-3	-3	t_{01}		$V_1=U_{01}$	-3	-3	t_{01}
$V_{19}=U_b$	-1	-3	t_b		$V_{19}=U_b$	-1	-3	t_b
$V_{25}=U_a$	1	-3	t_a		$V_{25}=U_a$	1	-3	t_a
$V_{27}=U_{03}$	3	-3	t_{03}		$V_{27}=U_{03}$	3	-3	t_{03}
$V_{18}=U_c$	3	-1	t_c		$V_{26}=U_d$	3	-1	t_d
$V_{17}=U_d$	3	1	t_d		$V_{17}=U_c$	3	1	t_c
$V_{14}=U_{02}$	3	3	t_{02}		$V_{14}=U_{02}$	3	3	t_{02}

Table 5.9. (Continued)

(I,III)	$V_{dc}/6$	$V_{dc}/6$			(I,IV)	$V_{dc}/6$	$V_{dc}/6$	
	V_{01}	V_{02}	Time			V_{01}	V_{02}	Time
$V_1=U_{01}$	-3	-3	t_{01}		$V_1=U_{01}$	-3	-3	t_{01}
$V_{19}=U_a$	-1	-3	t_a		$V_{19}=U_a$	-1	-3	t_a
$V_{21}=U_b$	1	-3	t_b		$V_{21}=U_b$	1	-3	t_b
$V_{27}=U_{03}$	3	-3	t_{03}		$V_{27}=U_{03}$	3	-3	t_{03}
$V_{26}=U_c$	3	-1	t_c		$V_{24}=U_d$	3	-1	t_d
$V_{23}=U_d$	3	1	t_d		$V_{23}=U_c$	3	1	t_c
$V_{14}=U_{02}$	3	3	t_{02}		$V_{14}=U_{02}$	3	3	t_{02}

(II,III)	$V_{dc}/6$	$V_{dc}/6$			(II,IV)	$V_{dc}/6$	$V_{dc}/6$	
	V_{01}	V_{02}	Time			V_{01}	V_{02}	Time
$V_1=U_{01}$	-3	-3	t_{01}		$V_1=U_{01}$	-3	-3	t_{01}
$V_3=U_b$	-1	-3	t_b		$V_3=U_b$	-1	-3	t_b
$V_{21}=U_a$	1	-3	t_a		$V_{21}=U_a$	1	-3	t_a
$V_{27}=U_{03}$	3	-3	t_{03}		$V_{27}=U_{03}$	3	-3	t_{03}
$V_{26}=U_c$	3	-1	t_c		$V_{24}=U_d$	3	-1	t_d
$V_{23}=U_d$	3	1	t_d		$V_{23}=U_c$	3	1	t_c
$V_{14}=U_{02}$	3	3	t_{02}		$V_{14}=U_{02}$	3	3	t_{02}

(III,III)	$V_{dc}/6$	$V_{dc}/6$			(III,IV)	$V_{dc}/6$	$V_{dc}/6$	
	V_{01}	V_{02}	Time			V_{01}	V_{02}	Time
$V_1=U_{01}$	-3	-3	t_{01}		$V_1=U_{01}$	-3	-3	t_{01}
$V_3=U_a$	-1	-3	t_a		$V_3=U_a$	-1	-3	t_a
$V_9=U_b$	1	-3	t_b		$V_9=U_b$	1	-3	t_b
$V_{27}=U_{03}$	3	-3	t_{03}		$V_{27}=U_{03}$	3	-3	t_{03}
$V_{26}=U_c$	3	-1	t_c		$V_{24}=U_d$	3	-1	t_d
$V_{23}=U_d$	3	1	t_d		$V_{23}=U_c$	3	1	t_c
$V_{14}=U_{02}$	3	3	t_{02}		$V_{14}=U_{02}$	3	3	t_{02}

Table 5.9. (Continued)

(IV,III)	$V_{dc}/6$	$V_{dc}/6$			(IV,IV)	$V_{dc}/6$	$V_{dc}/6$	
	V_{01}	V_{02}	Time			V_{01}	V_{02}	Time
$V_1=U_{01}$	-3	-3	t_{01}		$V_1=U_{01}$	-3	-3	t_{01}
$V_7=U_b$	-1	-3	t_b		$V_7=U_b$	-1	-3	t_b
$V_9=U_a$	1	-3	t_a		$V_9=U_a$	1	-3	t_a
$V_{27}=U_03$	3	-3	t_{03}		$V_{27}=U_{03}$	3	-3	t_{03}
$V_{26}=U_c$	3	-1	t_c		$V_{24}=U_d$	3	-1	t_d
$V_{23}=U_d$	3	1	t_d		$V_23=U_c$	3	1	t_c
$V_{14}=U_{02}$	3	3	t_{02}		$V_{14}=U_{02}$	3	3	t_{02}

(V,III)	$V_{dc}/6$	$V_{dc}/6$			(V,IV)	$V_{dc}/6$	$V_{dc}/6$	
	V_{01}	V_{02}	Time			V_{01}	V_{02}	Time
$V_1=U_{01}$	-3	-3	t_{01}		$V_1=U_{01}$	-3	-3	t_{01}
$V_7=U_b$	-1	-3	t_b		$V_7=U_b$	-1	-3	t_b
$V_{25}=U_b$	1	-3	t_b		$V_{25}=U_b$	1	-3	t_b
$V_{27}=U_{03}$	3	-3	t_{03}		$V_{27}=U_{03}$	3	-3	t_{03}
$V_{26}=U_c$	3	-1	t_c		$V_{24}=U_d$	3	-1	t_d
$V_{23}=U_d$	3	1	t_d		$V_{23}=U_c$	3	1	t_c
$V_{14}=U_{02}$	3	3	t_{02}		$V_{14}=U_{02}$	3	3	t_{02}

(VI,III)	$V_{dc}/6$	$V_{dc}/6$			(VI,IV)	$V_{dc}/6$	$V_{dc}/6$	
	V_{01}	V_{02}	Time			V_{01}	V_{02}	Time
$V_1=U_{01}$	-3	-3	t_{01}		$V_1=U_{01}$	-3	-3	t_{01}
$V_{19}=U_b$	-1	-3	t_b		$V_{19}=U_b$	-1	-3	t_b
$V_{25}=U_a$	1	-3	t_a		$V_{25}=U_a$	1	-3	t_a
$V_{27}=U_{03}$	3	-3	t_{03}		$V_{27}=U_{03}$	3	-3	t_{03}
$V_{26}=U_c$	3	-1	t_c		$V_{24}=U_d$	3	-1	t_d
$V_{23}=U_d$	3	1	t_d		$V_{23}=U_c$	3	1	t_c
$V_{14}=U_{02}$	3	3	t_{02}		$V_{14}=U_{02}$	3	3	t_{02}

Table 5.9. (Continued)

(I,V)	$V_{dc}/6$	$V_{dc}/6$			(I,IV)	$V_{dc}/6$	$V_{dc}/6$	
	V_{01}	V_{02}	Time			V_{01}	V_{02}	Time
$V_1=U_{01}$	-3	-3	t_{01}		$V_1=U_{01}$	-3	-3	t_{01}
$V_{19}=U_a$	-1	-3	t_a		$V_{19}=U_a$	-1	-3	t_a
$V_{21}=U_b$	1	-3	t_b		$V_{21}=U_b$	1	-3	t_b
$V_{27}=U_{03}$	3	-3	t_{03}		$V_{27}=U_{03}$	3	-3	t_{03}
$V_{24}=U_c$	3	-1	t_c		$V_{18}=U_d$	3	-1	t_d
$V_{15}=U_d$	3	1	t_d		$V_{15}=U_c$	3	1	t_c
$V_{14}=U_{02}$	3	3	t_{02}		$V_{14}=U_{02}$	3	3	t_{02}

(II,V)	$V_{dc}/6$	$V_{dc}/6$			(II,VI)	$V_{dc}/6$	$V_{dc}/6$	
	V_{01}	V_{02}	Time			V_{01}	V_{02}	Time
$V_1=U_{01}$	-3	-3	t_{01}		$V_1=U_{01}$	-3	-3	t_{01}
$V_3=U_b$	-1	-3	t_b		$V_3=U_b$	-1	-3	t_b
$V_{21}=U_a$	1	-3	t_a		$V_{21}=U_a$	1	-3	t_a
$V_{27}=U_{03}$	3	-3	t_{03}		$V_{27}=U_{03}$	3	-3	t_{03}
$V_{24}=U_c$	3	-1	t_c		$V_{18}=U_d$	3	-1	t_d
$V_{15}=U_d$	3	1	t_d		$V_{15}=U_c$	3	1	t_c
$V_{14}=U_{02}$	3	3	t_{02}		$V_{14}=U_{02}$	3	3	t_{02}

(III,V)	$V_{dc}/6$	$V_{dc}/6$			(III,VI)	$V_{dc}/6$	$V_{dc}/6$	
	V_{01}	V_{02}	Time			V_{01}	V_{02}	Time
$V_1=U_{01}$	-3	-3	t_{01}		$V_1=U_{01}$	-3	-3	t_{01}
$V_3=U_a$	-1	-3	t_a		$V_3=U_a$	-1	-3	t_a
$V_9=U_b$	1	-3	t_b		$V_9=U_b$	1	-3	t_b
$V_{27}=U_{03}$	3	-3	t_{03}		$V_{27}=U_{03}$	3	-3	t_{03}
$V_{24}=U_c$	3	-1	t_c		$V_{18}=U_d$	3	-1	t_d
$V_{15}=U_d$	3	1	t_d		$V_{15}=U_c$	3	1	t_c
$V_{14}=U_{02}$	3	3	t_{02}		$V_{14}=U_{02}$	3	3	t_{02}

Table 5.9. (Continued)

(IV,V)	$V_{dc}/6$	$V_{dc}/6$			(IV,VI)	$V_{dc}/6$	$V_{dc}/6$	
	V_{01}	V_{02}	Time			V_{01}	V_{02}	Time
$V_1=U_{01}$	-3	-3	t_{01}		$V_1=U_{01}$	-3	-3	t_{01}
$V_7=U_b$	-1	-3	t_b		$V_7=U_b$	-1	-3	t_b
$V_9=U_a$	1	-3	t_a		$V_9=U_a$	1	-3	t_a
$V_{27}=U_{03}$	3	-3	t_{03}		$V_{27}=U_{03}$	3	-3	t_{03}
$V_{24}=U_c$	3	-1	t_c		$V_{18}=U_d$	3	-1	t_d
$V_{15}=U_d$	3	1	t_d		$V_{15}=U_c$	3	1	t_c
$V_{14}=U_{02}$	3	3	t_{02}		$V_{14}=U_{02}$	3	3	t_{02}

(V,V)	$V_{dc}/6$	$V_{dc}/6$			(V,VI)	$V_{dc}/6$	$V_{dc}/6$	
	V_{01}	V_{02}	Time			V_{01}	V_{02}	Time
$V_1=U_{01}$	-3	-3	t_{01}		$V_1=U_{01}$	-3	-3	t_{01}
$V_7=U_b$	-1	-3	t_b		$V_7=U_b$	-1	-3	t_b
$V_{25}=U_b$	1	-3	t_b		$V_{25}=U_b$	1	-3	t_b
$V_{27}=U_{03}$	3	-3	t_{03}		$V_{27}=U_{03}$	3	-3	t_{03}
$V_{24}=U_c$	3	-1	t_c		$V_{18}=U_d$	3	-1	t_d
$V_{15}=U_d$	3	1	t_d		$V_{15}=U_c$	3	1	t_c
$V_{14}=U_{02}$	3	3	t_{02}		$V_{14}=U_{02}$	3	3	t_{02}

	$V_{dc}/6$	$V_{dc}/6$				$V_{dc}/6$	$V_{dc}/6$	
(VI,V)	V_{01}	V_{02}	Time		(VI,VI)	V_{01}	V_{02}	Time
$V_1=U_{01}$	-3	-3	t_{01}		$V_1=U_{01}$	-3	-3	t_{01}
$V_{19}=U_b$	-1	-3	t_b		$V_{19}=U_b$	-1	-3	t_b
$V_{25}=U_a$	1	-3	t_a		$V_{25}=U_a$	1	-3	t_a
$V_{27}=U_{03}$	3	-3	t_{03}		$V_{27}=U_{03}$	3	-3	t_{03}
$V_{24}=U_c$	3	-1	t_c		$V_{18}=U_d$	3	-1	t_d
$V_{15}=U_d$	3	1	t_d		$V_{15}=U_c$	3	1	t_c
$V_{14}=U_{02}$	3	3	t_{02}		$V_{14}=U_{02}$	3	3	t_{02}

Table 5.10. Neutral voltages in terms of the switching times

NSC1			NSC2	
			I,III,V	**II,IV,VI**
	I,III,V	V_{n0}	$(-t_{01}+t_{02}+t_{03}+t_c+t_d)V_{dc}/2+(-t_a+t_b)V_{dc}/6$	$(-t_{01}+t_{02}+t_{03}+t_c+t_d)V_{dc}/2+(-t_a+t_b)V_{dc}/6$
		V_{m0}	$-(t_{01}-t_{02}+t_{03}+t_c+t_d)V_{dc}/2+(-t_c+t_d)V_{dc}/6$	$-(t_{01}-t_{02}+t_{03}+t_c+t_d)V_{dc}/2+(t_c-t_d)V_{dc}/6$
	II,IV,VI	V_{n0}	$(-t_{01}+t_{02}+t_{03}+t_c+t_d)V_{dc}/2+(t_a-t_b)V_{dc}/6$	$(-t_{01}+t_{02}+t_{03}+t_c+t_d)V_{dc}/2+(t_a-t_b)V_{dc}/6$
		V_{m0}	$-(t_{01}-t_{02}+t_{03}+t_c+t_d)V_{dc}/2+(-t_c+t_d)V_{dc}/6$	$-(t_{01}-t_{02}+t_{03}+t_c+t_d)V_{dc}/2+(t_c-t_d)V_{dc}/6$

Table 5.11. Device switching times in terms of the line-to-line voltages

Sector	I	II	III	IV	V	VI
t_a	V_{ab1}/V_{dc}	V_{ac1}/V_{dc}	V_{bc1}/V_{dc}	V_{ba1}/V_{dc}	V_{ca1}/V_{dc}	V_{cb1}/V_{dc}
t_b	V_{bc1}/V_{dc}	V_{ba1}/V_{dc}	V_{ca1}/V_{dc}	V_{cb1}/V_{dc}	V_{ab1}/V_{dc}	V_{ac1}/V_{dc}
V_{max1}	V_{an1}	V_{bn1}	V_{bn1}	V_{cn1}	V_{cn1}	V_{an1}
V_{min1}	V_{cn1}	V_{cn1}	V_{an1}	V_{an1}	V_{bn1}	V_{bn1}
t_c	V_{ab2}/V_{dc}	V_{ac2}/V_{dc}	V_{bc2}/V_{dc}	V_{ba2}/V_{dc}	V_{ca2}/V_{dc}	V_{cb2}/V_{dc}
t_d	V_{bc2}/V_{dc}	V_{ba2}/V_{dc}	V_{ca2}/V_{dc}	V_{cb2}/V_{dc}	V_{ab2}/V_{dc}	V_{ac2}/V_{dc}
V_{max2}	V_{am2}	V_{bm2}	V_{bm2}	V_{cm2}	V_{cm2}	V_{am2}
V_{min2}	V_{cm2}	V_{cm2}	V_{am2}	V_{am2}	V_{bm2}	V_{bm2}

As an example consider the reference voltages in the sector (I, I), the active vectors dwell times are:

$t_a = V_{ab1}/V_{dc};$ $t_b = V_{bc1}/V_{dc};$ $t_c = V_{ab2}/V_{dc};$ $t_d = V_{bc1}/V_{dc}.$

Substituting these expressions into (5.25) for V_{n0}:

$$< V_{no} >= \frac{V_{dc}}{2}(-\alpha t_0 + \beta t_0 + (1-\alpha-\beta)t_{00} + t_c + t_d) + \frac{V_{dc}}{6}(-t_a + t_b)$$

$$< V_{no} >= \frac{V_{dc}}{2}((1-2\alpha)t_0 + t_c + t_d) + \frac{V_{dc}}{6}(-t_a + t_b)$$

$$< V_{no} >= \frac{V_{dc}}{2}((1-2\alpha)(1-t_a-t_b-t_c-t_d) + t_c + t_d) + \frac{V_{dc}}{6}(-t_a + t_b)$$

$$< V_{no} >= \frac{V_{dc}}{2}(1-2\alpha) - \frac{V_{bc1}}{3} - \frac{2V_{ab1}}{3} + \alpha V_{ab1} + \alpha V_{ab2} + \alpha V_{bc1} + \alpha V_{bc2}$$

$$< V_{no} >= \left[\begin{array}{c} \frac{V_{dc}}{2}(1-2\alpha) - \frac{V_{b1}-V_{c1}}{3} - \frac{2(V_{a1}-V_{b1})}{3} + \alpha(V_{a1}-V_{b1}) + \\ + \alpha(V_{a2}-V_{b2}) + \alpha(V_{b1}-V_{c1}) + \alpha(V_{b2}-V_{c2}) \end{array} \right] \qquad (5.33)$$

Similarly for V_{m0}:

$$< V_{mo} >= -\frac{V_{dc}}{2}(t_{01}-t_{02}+t_{03}+t_c+t_d) + \frac{V_{dc}}{6}(-t_c+t_d)$$

$$< V_{mo} >= \frac{V_{dc}}{2}(\alpha t_{00} - \beta t_{00} + (1-\alpha-\beta)t_{00} + t_a + t_b) + \frac{V_{dc}}{6}(-t_c + t_d)$$

$$< V_{mo} >= \frac{V_{dc}}{2}((1-2\beta)t_{00} + t_a + t_b) + \frac{V_{dc}}{6}(-t_a + t_b)$$

$$< V_{mo} >= \frac{V_{dc}}{2}\left((1-2\beta)(1-t_a-t_b-t_c-t_d)+t_a+t_b\right)+\frac{V_{dc}}{6}(-t_a+t_b)$$

$$< V_{mo} >= \frac{V_{dc}}{2}(2\beta-1)+\frac{V_{ab2}}{3}+\frac{2V_{bc2}}{3}-\beta V_{ab1}-\beta V_{ab2}-\beta V_{bc1}-\beta V_{bc2}$$

$$< V_{mo} >= \begin{bmatrix}\dfrac{V_{dc}}{2}(2\beta-1)+\dfrac{V_{a2}-V_{b2}}{3}+\dfrac{2(V_{b2}-V_{c2})}{3}+\\ -\beta(V_{a1}-V_{b1})-\beta(V_{a2}-V_{b2})-\beta(V_{b1}-V_{c1})-\beta(V_{b2}-V_{c2})\end{bmatrix} \qquad (5.34)$$

If $V_{b1} = -V_{a1} - V_{c1}$, $V_{b2} = -V_{a2} - V_{c2}$, then

$$< V_{no} >= \begin{bmatrix}\dfrac{V_{dc}}{2}(1-2\alpha)-\dfrac{-V_{a1}-2V_{c1}}{3}-\dfrac{2(2V_{a1}+V_{c1})}{3}+\alpha(2V_{a1}+V_{c1})+\\ +\alpha(2V_{a2}+V_{c2})+\alpha(-V_{a1}-2V_{c1})+\alpha(-V_{a2}-2V_{c2})\end{bmatrix} \qquad (5.35)$$

$$< V_{mo} >= \begin{bmatrix}\dfrac{V_{dc}}{2}(2\beta-1)+\dfrac{V_{a2}-V_{b2}}{3}+\dfrac{2(V_{b2}-V_{c2})}{3}+\\ -\beta(V_{a1}-V_{b1})-\beta(V_{a2}-V_{b2})-\beta(V_{b1}-V_{c1})-\beta(V_{b2}-V_{c2})\end{bmatrix} \qquad (5.36)$$

In sector (I, I), $V_{a1} = V_{max1}, V_{a2} = V_{max2}, V_{c1} = V_{min1}, V_{c2} = V_{min2}$, therefore

substituting these expressions into (5.35) into (5.36), the neutral voltages are given as:

$$V_{n0} = \frac{V_{dc}}{2}(1-2\alpha)+(\alpha-1)V_{max1}+\alpha V_{max2}-\alpha(V_{min1}+V_{min2})$$

$$V_{m0} = \frac{V_{dc}}{2}(2\beta-1)+(\beta-1)V_{min2}+\beta V_{min1}-\beta(V_{max1}+V_{max2}) \qquad (5.37)$$

Similar mathematical manipulations for all other sector combinations show that (5.37) is the generalized converter neutral voltage.

5.2.2. Carrier-Based Pulse-Width Modulation

5.2.2.1.**Converter voltages.** It has been shown that there are 12 feasible active switching states and on per phase basis, 3 states can be identified as listed in Table 5.12.

Table 5.12. Switching function per phase truth table

State	S_{ip}	S_{im}	S_{in}	V_{j0}	V_{k0}
1	0	1	1	$V_{dc}/2$	$V_{dc}/2$
2	1	0	1	$V_{dc}/2$	$-V_{dc}/2$
3	1	1	0	$-V_{dc}/2$	$-V_{dc}/2$

where V_{j0} and V_{k0} are the phase-leg to midpoint of the DC link voltages; $j = a, b, c$; $k = x, y, z$; V_{dc} is the DC-link voltage. It can be shown that the voltages between the inverter leg and the mid-point '*0*' of the DC supply (Figure 5.1) for *NSC1* and *NSC1* are:

$$v_{ao} = v_{an} + v_{no} = \frac{v_{dc}}{2}\left(S_{ap} - S_{am}S_{an}\right)$$

$$v_{bo} = v_{bn} + v_{no} = \frac{v_{dc}}{2}\left(S_{bp} - S_{bm}S_{bn}\right) \tag{5.38}$$

$$v_{co} = v_{cn} + v_{no} = \frac{v_{dc}}{2}\left(S_{cp} - S_{cm}S_{cn}\right)$$

$$v_{xo} = v_{xm} + v_{mo} = \frac{v_{dc}}{2}\left(S_{ap}S_{am} - S_{an}\right)$$

$$v_{yo} = v_{ym} + v_{mo} = \frac{v_{dc}}{2}\left(S_{bp}S_{bm} - S_{bn}\right) \tag{5.39}$$

$$v_{zo} = v_{zm} + v_{mo} = \frac{v_{dc}}{2}\left(S_{cp}S_{cm} - S_{cn}\right)$$

Or in compact form (5.38) and (5.39) can be written as:

$$v_{j0} = \frac{v_{dc}}{2}\left(S_{ip} - S_{im}S_{in}\right)\Bigg\}$$
$$v_{k0} = \frac{v_{dc}}{2}\left(S_{ip}S_{im} - S_{in}\right)\Bigg\}$$
(5.40)

Based on the Table 5.12, the switching functions of the devices in a leg are related by (5.41) and substituting (5.41) into (5.40), the voltages between the converter legs and the mid-point of the DC-link capacitor are given by (5.42).

$$S_{ip} + S_{im}S_{in} = 1\Bigg\}$$
$$S_{in} + S_{ip}S_{im} = 1\Bigg\}$$
(5.41)

$$V_{j0} = V_{jn} + V_{n0} = V_{dc}(2S_{ip} - 1)/2\Bigg\}$$
$$V_{k0} = V_{km} + V_{m0} = V_{dc}(1 - 2S_{in})/2\Bigg\}$$
(5.42)

Expanding (5.42):

$$v_{a0} = v_{an} + v_{n0} = \frac{v_{dc}}{2}\left(2S_{ap} - 1\right)$$

$$v_{b0} = v_{bn} + v_{n0} = \frac{v_{dc}}{2}\left(2S_{bp} - 1\right)$$
(5.43)

$$v_{c0} = v_{cn} + v_{n0} = \frac{v_{dc}}{2}\left(2S_{cp} - 1\right)$$

$$v_{x0} = v_{xm} + v_{m0} = \frac{v_{dc}}{2}\left(1 - 2S_{an}\right)$$

$$v_{y0} = v_{ym} + v_{m0} = \frac{v_{dc}}{2}\left(1 - 2S_{bn}\right)$$
(5.44)

$$v_{z0} = v_{zm} + v_{m0} = \frac{v_{dc}}{2}\left(1 - 2S_{cn}\right)$$

In a balanced source, the sum of the phase voltages must be zero. That is:

$$v_{an} + v_{bn} + v_{cn} = 0$$
$$v_{xm} + v_{ym} + v_{zm} = 0$$
(5.45)

Summing all the rows of (5.43) and (5.44), the neutral voltages are given by

138

$$v_{n0} = \frac{v_{dc}}{3}\left(S_{ap} + S_{bp} + S_{cp}\right) - \frac{v_{dc}}{2}$$

$$v_{m0} = \frac{v_{dc}}{2} - \frac{v_{dc}}{3}\left(S_{an} + S_{bn} + S_{cn}\right)$$

(5.46)

The expressions for the switching functions, of the top and bottom devices can be obtained from (5.42) as:

$$\left. \begin{array}{l} S_{ip} = (V_{jn} + V_{n0})/V_{dc} + 0.5 \\ S_{in} = -(V_{km} + V_{m0})/V_{dc} + 0.5 \end{array} \right\}$$

(5.47)

5.2.2.2. **Fourier approximation of switching function.** The switching function is a time-varing binary representation of the state of the switching devices. In sinusoidal PWM, the switching function is commonly generated by comparing a reference modulating signal with a high frequncey triangular signal and their intersections give the state of the switch. The switching function generated by this process can be analytically represented by [70]:

$$s(x,y) = \left[\begin{array}{l} \dfrac{A_{00}}{2} + \displaystyle\sum_{n=1}^{\infty}\left[A_{0n}\cos ny + B_{0n}\sin ny\right] + \sum_{m=1}^{\infty}\left[A_{m0}\cos mx + B_{m0}\sin mx\right] \\ + \displaystyle\sum_{m=1}^{\infty}\sum_{\substack{n=-\infty \\ (n\neq 0)}}^{\infty}\left[A_{mn}\cos(mx+ny) + B_{mn}\sin(mx+ny)\right] \end{array} \right]$$

(5.48)

where

$$\overline{C}_{mn} = A_{mn} + jB_{mn} = \frac{1}{2\pi^2}\int_{-\pi}^{\pi}\int_{-\pi}^{\pi}f(x,y)e^{j(mx+ny)}dxdy$$

(5.49)

$x(t) = \omega_c t + \theta_c$, $y(t) = \omega_o t + \theta_o$; ω_c and ω_o are the carrier and modulating waveform frequencies and θ_c and θ_o are the corresponding phase shifts respectively; m and n are

multiples of the carrier and modulating waveform frequencies. The first term in $s(x,y)$ represent the dc offset component of the pulse width-modulated waveform. The first summation term, defines the output fundamental low-frequency synthesized waveform and its baseband harmonics. The second summation corresponds to the harmonics of the carrier frequency and the last term (double summation) represents carrier sidebands. The spectral coefficients A_{mn} and B_{mn} can be evaluated for any given modulation strategy and converter topology.

In the Nine-switch converter, the relationship between the switching functions of the top and bottom devices and their corresponding reference modulating waveforms with zero sequence voltage injection has been shown earlier to be given respectively by:

$$S_{ip} = \frac{1}{V_{dc}}(V_{jn} + V_{no}) + \frac{1}{2} \tag{5.50}$$

$$S_{ip} = -\frac{1}{V_{dc}}(V_{kn} + V_{mo}) + \frac{1}{2} \tag{5.51}$$

In the following analysis, the zero sequence voltage injection is ignored for simplicity without loss of generality. That is:

$$S_{ip} = \frac{V_{jn}}{V_{dc}} + \frac{1}{2} = \frac{V_{p1}}{V_{dc}}\cos y_1 + \frac{1}{2} \tag{5.52}$$

$$S_{in} = -\frac{V_{kn}}{V_{dc}} + \frac{1}{2} = -\frac{V_{p2}}{V_{dc}}\cos y_2 + \frac{1}{2} \tag{5.53}$$

where V_{p1} and V_{p2} are respectively the peak values of the reference voltages of *NSC1* and *NSC2*; $y_1 = \omega_{o1}t + \theta_{o1}$ and $y_2 = \omega_{o2}t + \theta_{o2}$ are their corresponding frequencies. A general expression switching function for top and bottom devices may then be written as:

140

$$S_{iq} = \eta \frac{V_{ph}}{V_{dc}} \cos y_h + \frac{1}{2} \qquad (5.54)$$

where $q = p, n;\ h = 1, 2$ and $\eta = 1$ for $q = p$ and $\eta = -1$ for $q = n$.

The dc offset term in (5.48) is evaluated at $m = n = 0$. That is:

$$\overline{C}_{00} = A_{00} + jB_{00} = \frac{1}{2\pi^2} \int_{-\pi}^{\pi} \int_{-\pi S_{iq}}^{\pi S_{iq}} e^{j(0x+0y)} dx dy_h \qquad (5.55)$$

Evaluating the inner integral:

$$\overline{C}_{00} = A_{00} + jB_{00} = \frac{1}{2\pi^2} \int_{-\pi}^{\pi} [x]_{-\pi S_{iq}}^{\pi S_{iq}} dy_h$$

$$\overline{C}_{00} = A_{00} + jB_{00} = \frac{1}{2\pi^2} \int_{-\pi}^{\pi} 2\pi S_{iq} dy_h$$

$$\overline{C}_{00} = A_{00} + jB_{00} = \frac{1}{\pi} \int_{-\pi}^{\pi} S_{iq} dy_h \qquad (5.56)$$

Substituing for S_{iq} into (5.56) and evaluating the integral:

$$\overline{C}_{00} = A_{00} + jB_{00} = \frac{1}{\pi} \int_{-\pi}^{\pi} \left(\eta \frac{V_{ph}}{V_{dc}} \cos y_h + \frac{1}{2} \right) dy_h$$

$$\overline{C}_{00} = A_{00} + jB_{00} = \frac{1}{\pi} \int_{-\pi}^{\pi} \eta \frac{V_{ph}}{V_{dc}} \cos y_h dy_h + \frac{1}{\pi} \int_{-\pi}^{\pi} \frac{1}{2} dy_h$$

$$\overline{C}_{00} = A_{00} + jB_{00} = \frac{1}{\pi} \eta \frac{V_{ph}}{V_{dc}} \int_{-\pi}^{\pi} \cos y_h dy_h + \frac{1}{2\pi} \int_{-\pi}^{\pi} dy_h$$

$$\overline{C}_{00} = A_{00} + jB_{00} = \frac{1}{2\pi}[y_h]_{-\pi}^{\pi}$$

$$\overline{C}_{00} = A_{00} + jB_{00} = \frac{1}{2\pi}[\pi - (-\pi)] = 1$$

$$A_{00} = 1, \quad B_{00} = 0.$$

The coefficient for the base band harmonics is computed when $m = 0$ and $n > 0$. That is:

$$\overline{C}_{0n} = A_{0n} + jB_{0n} = \frac{1}{2\pi^2}\int_{-\pi}^{\pi}\int_{-\pi S_{iq}}^{\pi S_{iq}}e^{j(0x+ny)}dxdy_h$$

$$\overline{C}_{0n} = A_{0n} + jB_{0n} = \frac{1}{2\pi^2}\int_{-\pi}^{\pi}\left[e^{j(0x+ny)}x\right]_{-\pi S_{iq}}^{\pi S_{iq}}dy_h$$

$$\overline{C}_{0n} = A_{0n} + jB_{0n} = \frac{1}{\pi}\int_{-\pi}^{\pi}e^{j(0x+ny)}S_{iq}dy_h$$

$$\overline{C}_{0n} = A_{0n} + jB_{0n} = \frac{1}{\pi}\int_{-\pi}^{\pi}e^{j(0x+ny)}\left(\eta\frac{V_{ph}}{V_{dc}}\cos y_h + \frac{1}{2}\right)dy_h$$

$$\overline{C}_{0n} = A_{0n} + jB_{0n} = \frac{1}{\pi}\eta\frac{V_{ph}}{V_{dc}}\int_{-\pi}^{\pi}\cos y_h e^{j(0x+ny)}dy_h + \frac{1}{2\pi}\int_{-\pi}^{\pi}e^{j(0x+ny)}dy_h \qquad (5.57)$$

Substituting $\cos y_h = \frac{1}{2}e^{jy_h} + \frac{1}{2}e^{-jy_h}$ into (5.57)

$$\overline{C}_{0n} = A_{0n} + jB_{0n} = \frac{1}{\pi} \eta \frac{V_{ph}}{V_{dc}} \frac{1}{2} \left[\frac{1}{j(n+1)} e^{jy_h(n+1)} + \frac{1}{j(n-1)} e^{jy_h(n-1)} \right]_{-\pi}^{\pi} + \frac{1}{2\pi} \left[\frac{1}{jn} e^{jny_h} \right]_{-\pi}^{\pi}$$

$$\overline{C}_{0n} = A_{0n} + jB_{0n} = \frac{1}{\pi} \eta \frac{V_{ph}}{V_{dc}} \frac{1}{2} \left[\begin{array}{l} \frac{1}{j(n+1)} e^{j\pi(n+1)} + \frac{1}{j(n-1)} e^{j\pi(n-1)} \\ -\frac{1}{j(n+1)} e^{-j\pi(n+1)} - \frac{1}{j(n-1)} e^{-j\pi(n-1)} \end{array} \right] + \frac{1}{jn2\pi} \left[e^{jn\pi} - e^{-jn\pi} \right]$$

$$\overline{C}_{0n} = A_{0n} + jB_{0n} = \frac{1}{\pi} \eta \frac{V_{ph}}{V_{dc}} \int_{-\pi}^{\pi} \left(\frac{1}{2} e^{jy_h} + \frac{1}{2} e^{-jy_h} \right) e^{jny_h} dy_h + \frac{1}{2\pi} \int_{-\pi}^{\pi} e^{j(0x+ny_h)} dy_h$$

$$\overline{C}_{0n} = A_{0n} + jB_{0n} = \frac{1}{\pi} \eta \frac{V_{ph}}{V_{dc}} \frac{1}{2} \int_{-\pi}^{\pi} \left(e^{jy_h} e^{jny_h} + e^{-jy_h} e^{jny_h} \right) dy_h + \frac{1}{2\pi} \int_{-\pi}^{\pi} e^{jny_h} dy_h$$

$$\overline{C}_{0n} = A_{0n} + jB_{0n} = \frac{1}{\pi} \eta \frac{V_{ph}}{V_{dc}} \frac{1}{2} \int_{-\pi}^{\pi} \left(e^{jy_h(n+1)} + e^{jy_h(n-1)} \right) dy_h + \frac{1}{2\pi} \int_{-\pi}^{\pi} e^{jny_h} dy_h$$

$$\overline{C}_{0n} = A_{0n} + jB_{0n} = \frac{1}{\pi} \eta \frac{V_{ph}}{V_{dc}} \frac{1}{2} \int_{-\pi}^{\pi} \left(e^{jy_h(n+1)} + e^{jy_h(n-1)} \right) dy_h + \frac{1}{2\pi} \int_{-\pi}^{\pi} e^{jny_h} dy_h$$

$$\overline{C}_{0n} = A_{0n} + jB_{0n} = \frac{1}{\pi} \eta \frac{V_{ph}}{V_{dc}} \frac{1}{2} \left[\begin{array}{l} \frac{1}{j(n+1)} e^{j\pi(n+1)} - \frac{1}{j(n+1)} e^{-j\pi(n+1)} + \\ +\frac{1}{j(n-1)} e^{j\pi(n-1)} - \frac{1}{j(n-1)} e^{-j\pi(n-1)} \end{array} \right] + \frac{1}{jn2\pi} \left[e^{jn\pi} - e^{-jn\pi} \right]$$

$$\overline{C}_{0n} = A_{0n} + jB_{0n} = \frac{1}{\pi} \eta \frac{V_{ph}}{V_{dc}} \frac{1}{2} \left[\begin{array}{l} \frac{1}{j(n+1)} j2\sin(\pi(n+1)) + \\ \frac{1}{j(n-1)} j2\sin(\pi(n-1)) \end{array} \right] + \frac{1}{jn2\pi} j2\sin(n\pi)$$

$$\overline{C}_{0n} = A_{0n} + jB_{0n} = \eta\frac{V_{ph}}{V_{dc}}\left[\frac{1}{\pi\ (n+1)}\sin(\pi(n+1)) + \frac{1}{\pi\ (n-1)}\sin(\pi(n-1))\right] + \frac{1}{n\pi}\sin(n\pi)$$

$$A_{0n} = \eta\frac{V_{ph}}{V_{dc}}\left[\frac{1}{\pi\ (n+1)}\sin(\pi(n+1)) + \frac{1}{\pi\ (n-1)}\sin(\pi(n-1))\right] + \frac{1}{n\pi}\sin(n\pi)$$

$$A_{0n} = \eta\frac{V_{ph}}{V_{dc}}\left[\frac{\sin(\pi(n+1))}{\pi(n+1)} + \frac{\sin(\pi(n-1))}{\pi(n-1)}\right]$$

Since $\sin(0)/0 = 1$, then for $n = 1$

$$A_{01} = \eta\frac{V_{ph}}{V_{dc}}[0+1] = \eta\frac{V_{ph}}{V_{dc}}, \quad B_{01} = 0$$

and for $n > 1$, $A_{0n} = 0, \quad B_{0n} = 0$.

The coefficient for carrier harmonics computed when $m > 0$ and $n = 0$. That is:

$$\overline{C}_{m0} = A_{m0} + jB_{m0} = \frac{1}{2\pi^2}\int_{-\pi}^{\pi}\int_{-\pi S_{iq}}^{\pi S_{iq}}e^{j(mx+0y)}dxdy$$

$$\overline{C}_{m0} = A_{m0} + jB_{m0} = \frac{1}{j2\pi^2 m}\int_{-\pi}^{\pi}\left[e^{jmx}\right]_{-\pi S_{iq}}^{\pi S_{iq}}dy$$

$$\overline{C}_{m0} = A_{m0} + jB_{m0} = \frac{1}{j2\pi^2 m}\int_{-\pi}^{\pi}\left[e^{jm\pi S_{iq}} - e^{-jm\pi S_{iq}}\right]dy$$

$$\overline{C}_{m0} = A_{m0} + jB_{m0} = \frac{1}{j2\pi^2 m}\left(\int_{-\pi}^{\pi}\left[e^{jm\pi S_{ip}}\right]dy - \int_{-\pi}^{\pi}\left[e^{-jm\pi S_{ip}}\right]\right)$$

$$\overline{C}_{m0} = A_{m0} + jB_{m0} = \frac{1}{j2\pi^2 m}\int_{-\pi}^{\pi}\left[e^{jm\pi(\eta\frac{V_{ph}}{V_{dc}}\cos y+\frac{1}{2})} - e^{-jm\pi(\eta\frac{V_{ph}}{V_{dc}}\cos y+\frac{1}{2})}\right]$$

$$\overline{C}_{m0} = A_{m0} + jB_{m0} = \frac{1}{j2\pi^2 m}\int_{-\pi}^{\pi}\left[e^{(jm\pi\eta\frac{V_{ph}}{V_{dc}}\cos y+jm\pi\frac{1}{2})} - e^{-(jm\pi\eta\frac{V_{ph}}{V_{dc}}\cos y+\frac{1}{2}jm\pi)}\right]$$

$$\overline{C}_{m0} = A_{m0} + jB_{m0} = \frac{1}{j2\pi^2 m}\int_{-\pi}^{\pi}\left[e^{jm\pi\eta\frac{V_{ph}}{V_{dc}}\cos y}\, e^{jm\pi\frac{1}{2}} - e^{-jm\pi\eta\frac{V_{ph}}{V_{dc}}\cos y}\, e^{-\frac{1}{2}jm\pi}\right]$$

$$\overline{C}_{m0} = A_{m0} + jB_{m0} = \frac{1}{j2\pi^2 m}\left(e^{jm\pi\frac{1}{2}}\int_{-\pi}^{\pi}e^{jm\pi\eta\frac{V_{ph}}{V_{dc}}\cos y} - e^{-jm\pi\frac{1}{2}}\int_{-\pi}^{\pi}e^{-jm\pi\eta\frac{V_{ph}}{V_{dc}}\cos y}\right) \tag{5.58}$$

The following integrals based on the Bessel Functions are shown to be given by [70]:

$$\int_{-\pi}^{\pi}e^{j\xi\cos y}dy = \int_{-\pi}^{\pi}e^{-j\xi\cos y}dy = 2\pi J_0(\xi)$$

$$J_0(\xi) = J_0(-\xi) \tag{5.59}$$

Thus the integrals in (5.58) are evaluated as:

$$\overline{C}_{m0} = A_{m0} + jB_{m0} = \frac{1}{j2\pi^2 m} 2\pi J_0\left(m\pi\eta\frac{V_{ph}}{V_{dc}}\right)\left(e^{jm\pi\frac{1}{2}} - e^{-jm\pi\frac{1}{2}}\right)$$

$$\overline{C}_{m0} = A_{m0} + jB_{m0} = \frac{1}{j2\pi^2 m} 2\pi J_0\left(m\pi\eta\frac{V_{ph}}{V_{dc}}\right) j2\sin(m\pi\frac{1}{2})$$

$$\overline{C}_{m0} = A_{m0} + jB_{m0} = \frac{2}{m\pi} J_0\left(m\pi\eta\frac{V_{ph}}{V_{dc}}\right)\sin\left(\frac{1}{2}m\pi\right)$$

$$\overline{C}_{m0} = A_{m0} + jB_{m0} = \frac{2}{m\pi} J_0\left(m\pi\frac{V_{ph}}{V_{dc}}\right)\sin\left(\frac{1}{2}m\pi\right) \qquad (5.60)$$

For $m > 0$ and $n \neq 0$, the sideband harmonics

$$\overline{C}_{mn} = A_{mn} + jB_{mn} = \frac{1}{2\pi^2}\int_{-\pi}^{\pi}\int_{-\pi S_{iq}}^{\pi S_{iq}} e^{j(mx+ny)}\,dxdy$$

$$\overline{C}_{mn} = A_{mn} + jB_{mn} = \frac{1}{2\pi^2}\int_{-\pi}^{\pi}\int_{-\pi S_{iq}}^{\pi S_{iq}} e^{jmx} e^{jny}\,dxdy$$

$$\overline{C}_{mn} = A_{mn} + jB_{mn} = \frac{1}{2\pi^2}\int_{-\pi}^{\pi} e^{jny}\int_{-\pi S_{iq}}^{\pi S_{iq}} e^{jmx}\,dxdy$$

$$\overline{C}_{mn} = A_{mn} + jB_{mn} = \frac{1}{2\pi^2}\int_{-\pi}^{\pi} e^{jny} \frac{1}{jm}\left[e^{jmx}\right]_{-\pi S_{iq}}^{\pi S_{iq}}\,dy$$

$$\overline{C}_{mn} = A_{mn} + jB_{mn} = \frac{1}{2\pi^2 jm}\int_{-\pi}^{\pi} e^{jny}\left[e^{jm\pi S_{iq}} - e^{-jm\pi S_{iq}}\right]dy$$

146

$$\overline{C}_{mn} = A_{mn} + jB_{mn} = \frac{1}{2\pi^2 jm} \int_{-\pi}^{\pi} e^{jny} \left[e^{jm\pi\left(\eta\frac{V_{ph}}{V_{dc}}\cos y + \frac{1}{2}\right)} - e^{-jm\pi\left(\eta\frac{V_{ph}}{V_{dc}}\cos y + \frac{1}{2}\right)} \right] dy$$

$$\overline{C}_{mn} = A_{mn} + jB_{mn} = \frac{1}{2\pi^2 jm} \int_{-\pi}^{\pi} e^{jny} \left[e^{jm\pi\eta\frac{V_{ph}}{V_{dc}}\cos y} e^{jm\pi\frac{1}{2}} - e^{-jm\pi\eta\frac{V_{ph}}{V_{dc}}\cos y} e^{-jm\pi\frac{1}{2}} \right] dy$$

$$\overline{C}_{mn} = A_{mn} + jB_{mn} = \frac{1}{2\pi^2 jm} \int_{-\pi}^{\pi} \left[e^{jny} e^{jm\pi\eta\frac{V_{ph}}{V_{dc}}\cos y} e^{jm\pi\frac{1}{2}} - e^{jny} e^{-jm\pi\eta\frac{V_{ph}}{V_{dc}}\cos y} e^{-jm\pi\frac{1}{2}} \right] dy$$

$$\overline{C}_{mn} = A_{mn} + jB_{mn} = \frac{1}{2\pi^2 jm} \left[\begin{array}{l} e^{jm\pi\frac{1}{2}} \int_{-\pi}^{\pi} \left(e^{jny} e^{jm\pi\eta\frac{V_{ph}}{V_{dc}}\cos y} \right) dy + \\[2mm] - e^{-jm\pi\frac{1}{2}} \int_{-\pi}^{\pi} \left(e^{jny} e^{-jm\pi\eta\frac{V_{ph}}{V_{dc}}\cos y} \right) dy \end{array} \right] \tag{5.61}$$

The expressions for the integrals in terms of the Bessel functions are:

$$\int_{-\pi}^{\pi} e^{j\xi\cos y} e^{jny} dy = \int_{-\pi}^{\pi} e^{-j\xi\cos y} dy = j^n 2\pi J_n(\xi) \tag{5.62}$$

$$\int_{-\pi}^{\pi} e^{j\xi\cos y} e^{jny} dy = \int_{-\pi}^{\pi} e^{-j\xi\cos y} dy = j^n 2\pi J_n(-\xi) \tag{5.63}$$

Thus

$$\overline{C}_{mn} = A_{mn} + jB_{mn} = \frac{1}{2\pi^2 jm} \left[e^{jm\pi\frac{1}{2}} j^n 2\pi J_n\left(m\pi\eta\frac{V_{ph}}{V_{dc}} \right) - e^{-jm\pi\frac{1}{2}} j^n 2\pi J_n\left(-m\pi\eta\frac{V_{ph}}{V_{dc}} \right) \right]$$

$$\overline{C}_{mn} = A_{mn} + jB_{mn} = \frac{1}{2\pi^2 jm} \left[e^{jm\pi\frac{1}{2}} j^n 2\pi J_n\left(m\pi\frac{V_{ph}}{V_{dc}} \right) - e^{-jm\pi\frac{1}{2}} j^n 2\pi J_n\left(-m\pi\frac{V_{ph}}{V_{dc}} \right) \right]$$

$$\overline{C}_{mn} = A_{mn} + jB_{mn} = \frac{2\pi}{2\pi^2 jm} J_n\left(m\pi \frac{V_{ph}}{V_{dc}}\right)\left[e^{jm\pi\frac{1}{2}} j^n - e^{-jm\pi\frac{1}{2}} j^{-n}\right] \tag{5.64}$$

The values of j^n and j^{-n} can be written as: $j^n = e^{jn\frac{\pi}{2}}, j^{-n} = e^{-jn\frac{\pi}{2}}$. Substituting into (5.64):

$$\overline{C}_{mn} = A_{mn} + jB_{mn} = \frac{2\pi}{2\pi^2 jm} J_n\left(m\pi \frac{V_{ph}}{V_{dc}}\right)\left[e^{jm\frac{\pi}{2}} e^{jn\frac{\pi}{2}} - e^{-jm\frac{\pi}{2}} e^{-jn\frac{\pi}{2}}\right]$$

$$\overline{C}_{mn} = A_{mn} + jB_{mn} = \frac{2\pi}{2\pi^2 jm} J_n\left(m\pi \frac{V_{ph}}{V_{dc}}\right)\left[e^{j\frac{\pi}{2}(m+n)} - e^{-j\frac{\pi}{2}(m+n)}\right]$$

$$\overline{C}_{mn} = A_{mn} + jB_{mn} = \frac{2\pi}{2\pi^2 jm} j2J_n\left(m\pi \frac{V_{ph}}{V_{dc}}\right)\sin\left((m+n)\frac{\pi}{2}\right)$$

$$\overline{C}_{mn} = A_{mn} + jB_{mn} = \frac{2}{\pi m} J_n\left(m\pi \frac{V_{ph}}{V_{dc}}\right)\sin\left((m+n)\frac{\pi}{2}\right) \tag{5.65}$$

The complete solution of the switching is formed by substitung the speactral coeffients found above into (5.48) giving the expression for the switching function (5.66)

$$s(x,y) = \begin{bmatrix} \dfrac{1}{2} + \eta\dfrac{V_{ph}}{V_{dc}}\cos y + \dfrac{2}{\pi}\displaystyle\sum_{m=1}^{\infty}\left[\dfrac{1}{m}J_0\left(m\pi\dfrac{V_{ph}}{V_{dc}}\right)\sin\left(m\dfrac{\pi}{2}\right)\cos mx\right] \\[4mm] + \dfrac{2}{\pi}\displaystyle\sum_{m=1}^{\infty}\sum_{\substack{n=-\infty \\ (n\neq 0)}}^{\infty}\left[\dfrac{1}{m}J_n\left(m\pi\dfrac{V_{ph}}{V_{dc}}\right)\sin\left((m+n)\dfrac{\pi}{2}\right)\cos(mx+ny)\right] \end{bmatrix} \tag{5.66}$$

If only the first two terms are considered, the switching fuction can be approximated to:

$$s(x,y) = \frac{1}{2} + \eta \frac{V_{ph}}{V_{dc}} \cos(\omega_o t + \theta_o)$$ (5.67)

Or

$$S_{ip} = \frac{1}{2} + \frac{1}{2} M_{ip}$$ (5.68)

$$S_{in} = \frac{1}{2} - \frac{1}{2} M_{ip}$$ (5.69)

where $M_{ip} = m_1 \cos(\omega_{o1} t + \theta_{o1})$ and $M_{ip} = m_2 \cos(\omega_{o2} t + \theta_{o2})$ are the modulating signals of

the top and bottom devices respectively and $m_1 = \frac{2V_{p1}}{V_{dc}}$ and $m_2 = \frac{2V_{p1}}{V_{dc}}$ are the

modulations indices of the *NSC1* and *NSC2* respectively.

The expressions for the modulating signals from (5.47), (5.68), and (6.69) are

given by

$$M_{ip} = \frac{2V_{jn}^*}{V_{dc}} + \frac{2V_{no}}{V_{dc}}$$ (5.70)

$$M_{in} = -\left(\frac{2V_{jn}^*}{V_{dc}} + \frac{2V_{mo}}{V_{dc}} \right)$$ (5.71)

where M_{ip}, and M_{in} are, respectively, the modulation signals of the upper and bottom

devices, V_{jn}^* and V_{km}^* are the desired (reference) inverter phase voltages ; V_{n0} and V_{m0} are

the neutral voltages of *NSC1* and *NSC2*, respectively. Note that at this instant, these

neutral voltages are unknown and by extension the modulation indices or switching

functions. The generalized neutral voltages, (5.37), found using SV-PWM, are substituted back into the above expressions to determine the modulation indices. That is:

$$M_{ip} = m_{ip} + m_{no} \tag{5.72}$$

$$M_{in} = -\left(m_{in} + m_{mo}\right) \tag{5.73}$$

where

$$m_{ip} = \frac{2V_{jn}^*}{V_{dc}}$$

$$\tag{5.74}$$

$$m_{no} = \frac{2V_{no}}{V_{dc}} = (1 - 2\alpha) + (\alpha - 1)m_{max1}^* - \alpha m_{min1}^* + \alpha\left(m_{max2}^* - m_{min2}^*\right)$$

$$m_{in} = \frac{2V_{kn}^*}{V_{dc}}$$

$$\tag{5.75}$$

$$m_{mo} = (2\beta - 1) + (\beta - 1)m_{min2}^* - \beta m_{max2}^* + \alpha\left(m_{min1}^* - m_{max2}^*\right)$$

5.2.2.3. Fourier series approximation of the zero sequence signals. For the classical 2-level converter, the zero sequence modulation signal is given by [100]:

$$m_o = 1 - 2\alpha + (1 - \alpha)m_{max}^* - \alpha m_{min}^* \tag{5.76}$$

Comparing the zero sequence modulation signals of the Nine-switch converter given in (5.74) and (5.75) to the corresponding 2-level converter given by (5.76), the modulation signals of the Nine-switch converter can be written as:

$$\left.\begin{aligned} m_{no} &= (1 - 2\alpha) + (\alpha - 1)m_{max1}^* - \alpha m_{min1}^* + \alpha\left(m_{max2}^* - m_{min2}^*\right) \\ \\ m_{no} &= m_{o1} + \alpha\left(m_{max2}^* - m_{min2}^*\right) \end{aligned}\right\} \tag{5.77}$$

$$m_{mo} = (2\beta - 1) + (\beta - 1)m^{*}_{\min 2} - \beta m^{*}_{\max 2} + \beta\left(m^{*}_{\min 1} - m^{*}_{\max 2}\right)$$

$$m_{mo} = m_{o2} + \beta\left(m^{*}_{\min 1} - m^{*}_{\max 2}\right)$$

(5.78)

where m_{o1} and m_{o2} are the equivalent normalized zero sequence voltage of the corresponding 2-level converter as given by (5.76).

From the expressions (5.77) and (5.78), it is sufficient to find the Fourier series approximation of zero sequence modulation signal of the 2-level converter and then add the second terms $\alpha\left(m^{*}_{\max 2} - m^{*}_{\min 2}\right)$ and $\beta\left(m^{*}_{\min 1} - m^{*}_{\max 2}\right)$ respectively to obtain the equivalent expressions for the Nine-switch converter.

The Fourier coefficients of α are found considering a number of cases of α using four values of the modulation angle, $\delta_o = 0^0$, 15^0, -15^0, 30^0 and -30^0. The graphical waveforms of the reference modulation signals and α used in the Fourier analysis are given in Figures 5.6 – 5.10.

Case I: $\delta_o = 0^o$

From Figure 5.6, the Fourier coefficients are found as follows:

$$a_o = \frac{1}{2\pi}\left[\int_0^{\frac{\pi}{3}} d\theta + \int_{\frac{2\pi}{3}}^{\frac{3\pi}{3}} d\theta + \int_{\frac{4\pi}{3}}^{\frac{5\pi}{3}} d\theta\right]$$

$$a_o = \frac{1}{2\pi}\left[\left[\theta\right]_0^{\frac{\pi}{3}} + \left[\theta\right]_{\frac{2\pi}{3}}^{\frac{3\pi}{3}} + \left[\theta\right]_{\frac{4\pi}{3}}^{\frac{5\pi}{3}}\right]$$

$$= \frac{1}{2\pi}\left[\left[\frac{\pi}{3} - 0\right] + \left[\frac{3\pi}{3} - \frac{2\pi}{3}\right] + \left[\frac{5\pi}{3} - \frac{4\pi}{3}\right]\right]$$

151

$$a_o = \frac{1}{2\pi}\left[\frac{\pi}{3}+\frac{\pi}{3}+\frac{\pi}{3}\right] = \frac{1}{2\pi}\frac{3\pi}{3} = \frac{\pi}{2\pi} = \frac{1}{2} \tag{5.79}$$

The coefficient a_n is given by

$$a_n = \frac{1}{\pi}\left[\int_0^{\frac{\pi}{3}}\cos n\theta d\theta + \int_{\frac{2\pi}{3}}^{\frac{3\pi}{3}}\cos n\theta d\theta + \int_{\frac{4\pi}{3}}^{\frac{5\pi}{3}}\cos n\theta d\theta\right]$$
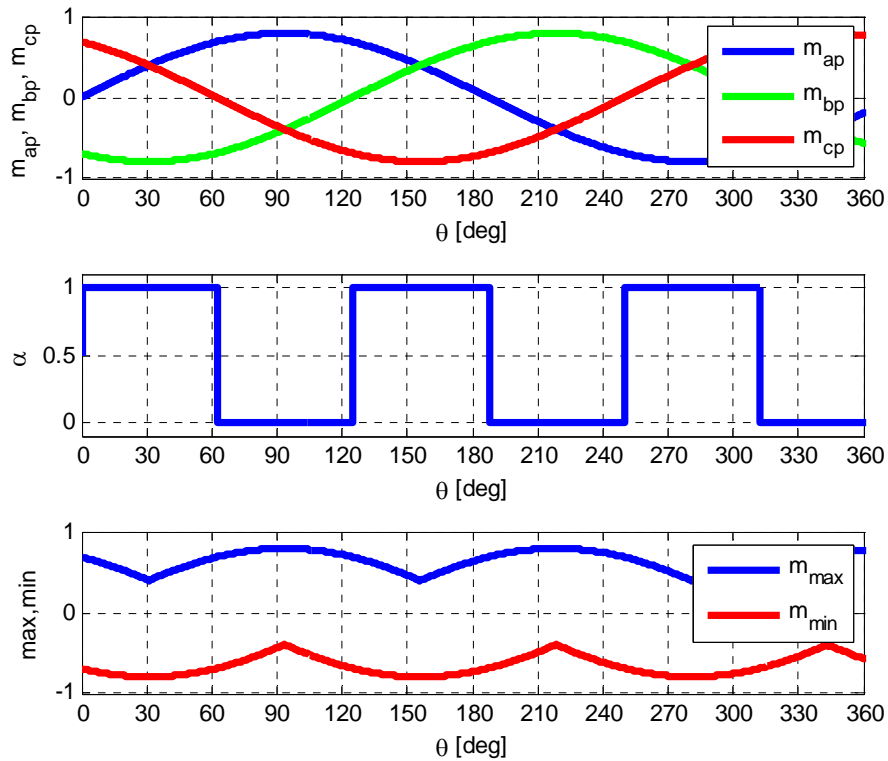
Figure 5.6. Waveform of the reference modulation signals with $\delta_o = 0^0$ showing the maximum and minimum values in the six sectors

$$a_n = \frac{1}{n\pi} \begin{bmatrix} \left[\sin n\frac{\pi}{3} - \sin n0 \right] + \left[\sin n\frac{3\pi}{3} - \sin n\frac{2\pi}{3} \right] \\ + \left[\sin n\frac{5\pi}{3} - \sin n\frac{4\pi}{3} \right] \end{bmatrix}$$

$$a_n = \frac{1}{n\pi} \left[\sin\frac{n\pi}{3} + \sin n\pi - \sin\frac{2n\pi}{3} + \sin\frac{5n\pi}{3} - \sin\frac{4n\pi}{3} \right] \tag{5.80}$$

$$a_n = \frac{1}{n\pi} \left[\sin\frac{n\pi}{3} - \sin\frac{2n\pi}{3} + \sin\frac{5n\pi}{3} - \sin\frac{4n\pi}{3} \right]$$

when n = 1:

$$a_1 = \frac{1}{\pi} \left[\sin\frac{\pi}{3} - \sin\frac{2\pi}{3} + \sin\frac{5\pi}{3} - \sin\frac{4\pi}{3} \right]$$

$$a_1 = \frac{1}{\pi} \left[\sin\frac{\pi}{3} - \sin\frac{\pi}{3} - \sin\frac{\pi}{3} + \sin\frac{\pi}{3} \right] = 0$$

when n = 2:

$$a_2 = \frac{1}{2\pi} \left[\sin\frac{2\pi}{3} - \sin\frac{4\pi}{3} + \sin\frac{10\pi}{3} - \sin\frac{8\pi}{3} \right]$$

$$a_2 = \frac{1}{2\pi} \left[\sin\frac{\pi}{3} + \sin\frac{\pi}{3} - \sin\frac{\pi}{3} - \sin\frac{\pi}{3} \right] = 0$$

when n = 3:

$$a_3 = \frac{1}{3\pi} \left[\sin\frac{3\pi}{3} - \sin\frac{6\pi}{3} + \sin\frac{15\pi}{3} - \sin\frac{12\pi}{3} \right]$$

$$a_3 = \frac{1}{3\pi} \left[\sin\pi - \sin 2\pi + \sin 5\pi - \sin 4\pi \right] = 0$$

The coefficient b_n is given by

153

$$b_n = \frac{1}{\pi}\left[\int_0^{\frac{\pi}{3}} \sin n\theta d\theta + \int_{\frac{2\pi}{3}}^{\frac{3\pi}{3}} \sin n\theta d\theta + \int_{\frac{4\pi}{3}}^{\frac{5\pi}{3}} \sin n\theta d\theta\right]$$

$$b_n = -\frac{1}{\pi n}\left[\left[\cos n\theta\right]_0^{\frac{\pi}{3}} + \left[\cos n\theta\right]_{\frac{2\pi}{3}}^{\frac{3\pi}{3}} + \left[\cos n\theta\right]_{\frac{4\pi}{3}}^{\frac{5\pi}{3}}\right]$$

$$b_n = -\frac{1}{n\pi}\left[\left[\cos n\frac{\pi}{3} - \cos n0\right] + \left[\cos n\frac{3\pi}{3} - \cos n\frac{2\pi}{3}\right] + \left[\cos n\frac{5\pi}{3} - \cos n\frac{4\pi}{3}\right]\right]$$

$$b_n = -\frac{1}{n\pi}\left[\cos\frac{n\pi}{3} - 1 + \cos n\pi - \cos\frac{2n\pi}{3} + \cos\frac{5n\pi}{3} - \cos\frac{4n\pi}{3}\right]$$

when n = 1:

$$b_1 = -\frac{1}{\pi}\left[\cos\frac{\pi}{3} - 1 + \cos\pi - \cos\frac{2\pi}{3} + \cos\frac{5\pi}{3} - \cos\frac{4\pi}{3}\right]$$

$$b_1 = -\frac{1}{\pi}\left[\cos\frac{\pi}{3} - 1 - 1 + \cos\frac{\pi}{3} + \cos\frac{\pi}{3} + \cos\frac{\pi}{3}\right]$$

$$b_1 = -\frac{1}{\pi}\left[\frac{1}{2} - 1 - 1 + \frac{1}{2} + \frac{1}{2} + \frac{1}{2}\right] = 0$$

when n = 2:

$$b_2 = -\frac{1}{2\pi}\left[\cos\frac{2\pi}{3} - 1 + \cos 2\pi - \cos\frac{4\pi}{3} + \cos\frac{10\pi}{3} - \cos\frac{8\pi}{3}\right]$$

$$b_2 = -\frac{1}{2\pi}\left[-\cos\frac{\pi}{3} - 1 + 1 + \cos\frac{\pi}{3} - \cos\frac{\pi}{3} + \cos\frac{\pi}{3}\right] = 0$$

when n = 3:

$$b_3 = -\frac{1}{3\pi}\left[\cos\frac{3\pi}{3} - 1 + \cos 3\pi - \cos\frac{6\pi}{3} + \cos\frac{15\pi}{3} - \cos\frac{12\pi}{3}\right]$$

154

$$b_3 = -\frac{1}{3\pi}\left[\cos\pi - 1 + \cos 3\pi - \cos 2\pi + \cos 5\pi - \cos 4\pi\right]$$

$$b_3 = -\frac{1}{3\pi}\left[-1 - 1 - 1 - 1 - 1 - 1\right] = \frac{1}{3\pi}\left[-6\right] = \frac{6}{3\pi} = \frac{2}{\pi}$$

Thus

$$\alpha = \frac{1}{2} + \frac{2}{\pi}\sin 3\theta \tag{5.82}$$

The coefficient a_o is given by

$$a_o = \frac{1}{2\pi}\left[\int_0^{\frac{\pi}{3}-\delta_o} d\theta + \int_{\frac{2\pi}{3}-\delta_o}^{\frac{3\pi}{3}-\delta_o} d\theta + \int_{\frac{4\pi}{3}-\delta_o}^{\frac{5\pi}{3}-\delta_o} d\theta + \int_{\frac{6\pi}{3}-\delta_o}^{\frac{6\pi}{3}} d\theta\right] \tag{5.83}$$

Case II: $\delta_o = 15^0$
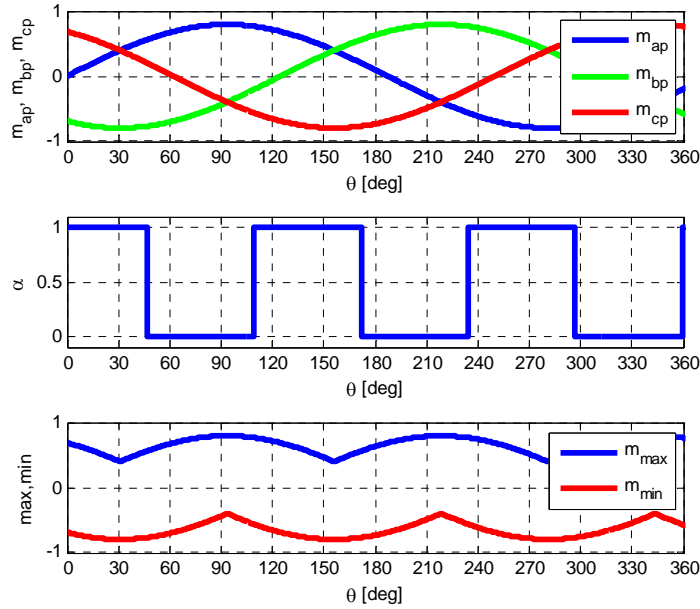
Figure 5.7. Waveform of the reference modulation signals with $\delta_o = 15^0$ showing the maximum and minimum values in the six sectors

$$a_o = \frac{1}{2\pi}\left[[\theta]_0^{\frac{\pi}{3}-\delta_o} + [\theta]_{\frac{2\pi}{3}-\delta_o}^{\frac{3\pi}{3}-\delta_o} + [\theta]_{\frac{4\pi}{3}-\delta_o}^{\frac{5\pi}{3}-\delta_o} + [\theta]_{\frac{6\pi}{3}-\delta_o}^{\frac{6\pi}{3}} \right]$$

$$a_o = \frac{1}{2\pi}\left[\left[\frac{\pi}{3}-\delta_o -0\right] + \left[\frac{3\pi}{3}-\delta_o -\left(\frac{2\pi}{3}-\delta_o\right)\right] + \left[\frac{5\pi}{3}-\delta_o -\left(\frac{4\pi}{3}-\delta_o\right)\right] + \left[\frac{6\pi}{3}-\left(\frac{6\pi}{3}-\delta_o\right)\right] \right]$$

$$a_o = \frac{1}{2\pi}\left[\frac{\pi}{3}-\delta_o +\frac{\pi}{3}+\frac{\pi}{3}+\delta_o \right] = \frac{1}{2}$$

The coefficient a_n is given by

$$a_n = \frac{1}{\pi}\left[\begin{array}{l} \int_0^{\frac{\pi}{3}-\delta_o}\cos n\theta d\theta + \int_{\frac{2\pi}{3}-\delta_o}^{\frac{3\pi}{3}-\delta_o}\cos n\theta d\theta + \\[2ex] \int_{\frac{4\pi}{3}-\delta_o}^{\frac{5\pi}{3}-\delta_o}\cos n\theta d\theta + \int_{\frac{6\pi}{3}-\delta_o}^{\frac{6\pi}{3}}\cos n\theta d\theta \end{array} \right] \qquad (5.84)$$

$$a_n = \frac{1}{n\pi}\left[[\sin n\theta]_0^{\frac{\pi}{3}-\delta_o} + [\sin n\theta]_{\frac{2\pi}{3}-\delta_o}^{\frac{3\pi}{3}-\delta_o} + [\sin n\theta]_{\frac{4\pi}{3}-\delta_o}^{\frac{5\pi}{3}-\delta_o} + [\sin n\theta]_{\frac{6\pi}{3}-\delta_o}^{\frac{6\pi}{3}} \right]$$

$$a_n = \frac{1}{n\pi}\left[\begin{array}{l} \left[\sin\left(\frac{n\pi}{3}-n\delta_o\right)-\sin n0\right] + \left[\sin\left(\frac{3n\pi}{3}-n\delta_o\right)-\sin\left(\frac{2n\pi}{3}-n\delta_o\right)\right] + \\[2ex] \left[\sin\left(\frac{5n\pi}{3}-n\delta_o\right)-\sin\left(\frac{4n\pi}{3}-n\delta_o\right)\right] + \left[\sin\frac{6n\pi}{3}-\sin\left(\frac{6n\pi}{3}-n\delta_o\right)\right] \end{array} \right]$$

$$a_n = \frac{1}{n\pi} \begin{bmatrix} \sin\dfrac{n\pi}{3}\cos n\delta_o - \cos\dfrac{n\pi}{3}\sin n\delta_o - \sin n0 + \\[2mm] + \sin\dfrac{3n\pi}{3}\cos n\delta_o - \cos\dfrac{3n\pi}{3}\sin n\delta_o + \\[2mm] -\left[\sin\dfrac{2n\pi}{3}\cos n\delta_o - \cos\dfrac{2n\pi}{3}\sin n\delta_o\right] + \\[2mm] \sin\dfrac{5n\pi}{3}\cos n\delta_o - \cos\dfrac{5n\pi}{3}\sin n\delta_o \\[2mm] -\left[\sin\dfrac{4n\pi}{3}\cos n\delta_o - \cos\dfrac{4n\pi}{3}\sin n\delta_o\right] + \\[2mm] \sin\dfrac{6n\pi}{3} -\left[\sin\dfrac{6n\pi}{3}\cos n\delta_o - \cos\dfrac{6n\pi}{3}\sin n\delta_o\right] \end{bmatrix}$$

$$a_n = \frac{1}{n\pi} \begin{bmatrix} \sin\dfrac{n\pi}{3}\cos n\delta_o - \cos\dfrac{n\pi}{3}\sin n\delta_o - \sin n0 + \\[2mm] \sin\dfrac{3n\pi}{3}\cos n\delta_o - \cos\dfrac{3n\pi}{3}\sin n\delta_o + \\[2mm] -\sin\dfrac{2n\pi}{3}\cos n\delta_o + \cos\dfrac{2n\pi}{3}\sin n\delta_o + \\[2mm] \sin\dfrac{5n\pi}{3}\cos n\delta_o - \cos\dfrac{5n\pi}{3}\sin n\delta_o \\[2mm] -\sin\dfrac{4n\pi}{3}\cos n\delta_o + \cos\dfrac{4n\pi}{3}\sin n\delta_o + s \\[2mm] in\dfrac{6n\pi}{3} - \sin\dfrac{6n\pi}{3}\cos n\delta_o + \cos\dfrac{6n\pi}{3}\sin n\delta_o \end{bmatrix}$$

$$a_n = \frac{1}{n\pi} \begin{bmatrix} \sin\dfrac{n\pi}{3}\cos n\delta_o - \cos\dfrac{n\pi}{3}\sin n\delta_o - \sin n0 + \\[2mm] \sin n\pi \cos n\delta_o - \cos n\pi \sin n\delta_o + \\[2mm] -\sin\dfrac{2n\pi}{3}\cos n\delta_o + \cos\dfrac{2n\pi}{3}\sin n\delta_o + \\[2mm] \sin\dfrac{5n\pi}{3}\cos n\delta_o - \cos\dfrac{5n\pi}{3}\sin n\delta_o \\[2mm] -\sin\dfrac{4n\pi}{3}\cos n\delta_o + \cos\dfrac{4n\pi}{3}\sin n\delta_o + \\[2mm] \sin 2n\pi - \sin 2n\pi \cos n\delta_o + \cos 2n\pi \sin n\delta_o \end{bmatrix}$$

157

$$a_n = \frac{1}{n\pi} \begin{bmatrix} \sin\dfrac{n\pi}{3}\cos n\delta_o - \cos\dfrac{n\pi}{3}\sin n\delta_o - \cos n\pi \sin n\delta_o \\[2mm] -\sin\dfrac{2n\pi}{3}\cos n\delta_o + \cos\dfrac{2n\pi}{3}\sin n\delta_o + \\[2mm] \sin\dfrac{5n\pi}{3}\cos n\delta_o - \cos\dfrac{5n\pi}{3}\sin n\delta_o + \\[2mm] -\sin\dfrac{4n\pi}{3}\cos n\delta_o + \cos\dfrac{4n\pi}{3}\sin n\delta_o + \sin n\delta_o \end{bmatrix}$$

$$a_n = \frac{1}{n\pi}\left[\begin{array}{l} \left(\sin\dfrac{n\pi}{3} - \sin\dfrac{2n\pi}{3} + \sin\dfrac{5n\pi}{3} - \sin\dfrac{4n\pi}{3}\right)\cos n\delta_o + \\[3mm] \left(-\cos\dfrac{n\pi}{3} - \cos n\pi + \cos\dfrac{2n\pi}{3} - \cos\dfrac{5n\pi}{3} + \cos\dfrac{4n\pi}{3} + 1\right)\sin n\delta_o \end{array} \right]$$

when n = 1:

$$a_1 = \frac{1}{\pi}\left[\begin{array}{l} \left(\sin\dfrac{\pi}{3} - \sin\dfrac{2\pi}{3} + \sin\dfrac{5\pi}{3} - \sin\dfrac{4\pi}{3}\right)\cos \delta_o + \\[3mm] \left(-\cos\dfrac{\pi}{3} - \cos \pi + \cos\dfrac{2\pi}{3} - \cos\dfrac{5\pi}{3} + \cos\dfrac{4\pi}{3} + 1\right)\sin \delta_o \end{array} \right]$$

$$a_1 = \frac{1}{\pi}\left[\begin{array}{l} \left(\sin\dfrac{\pi}{3} - \sin\dfrac{\pi}{3} - \sin\dfrac{\pi}{3} + \sin\dfrac{\pi}{3}\right)\cos \delta_o + \\[3mm] \left(-\cos\dfrac{\pi}{3} + 1 - \cos\dfrac{\pi}{3} - \cos\dfrac{\pi}{3} - \cos\dfrac{\pi}{3} + 1\right)\sin \delta_o \end{array} \right]$$

$$a_1 = 0$$

when n = 2:

$$a_2 = \frac{1}{2\pi} \left[\begin{array}{l} \left(\sin\dfrac{2\pi}{3} - \sin\dfrac{4\pi}{3} + \sin\dfrac{10\pi}{3} - \sin\dfrac{8\pi}{3} \right) \cos 2\delta_o + \\[2mm] \left(-\cos\dfrac{2\pi}{3} - \cos 2\pi + \cos\dfrac{4\pi}{3} - \cos\dfrac{10\pi}{3} + \cos\dfrac{8\pi}{3} + 1 \right) \sin 2\delta_o \end{array} \right]$$

$$a_2 = \frac{1}{2\pi} \left[\begin{array}{l} \left(\sin\dfrac{\pi}{3} + \sin\dfrac{\pi}{3} - \sin\dfrac{\pi}{3} - \sin\dfrac{\pi}{3} \right) \cos 2\delta_o + \\[2mm] \left(\cos\dfrac{\pi}{3} - 1 - \cos\dfrac{\pi}{3} + \cos\dfrac{\pi}{3} - \cos\dfrac{\pi}{3} + 1 \right) \sin 2\delta_o \end{array} \right]$$

$$a_2 = 0$$

when n = 3:

$$a_3 = \frac{1}{3\pi} \left[\begin{array}{l} \left(\sin\dfrac{3\pi}{3} - \sin\dfrac{6\pi}{3} + \sin\dfrac{15\pi}{3} - \sin\dfrac{12\pi}{3} \right) \cos 3\delta_o + \\[2mm] \left(-\cos\dfrac{3\pi}{3} - \cos 3\pi + \cos\dfrac{6\pi}{3} - \cos\dfrac{15\pi}{3} + \cos\dfrac{12\pi}{3} + 1 \right) \sin 3\delta_o \end{array} \right]$$

$$a_3 = \frac{1}{3\pi} \left[\begin{array}{l} \left(\sin\pi - \sin 2\pi + \sin 5\pi - \sin 4\pi \right) \cos 3\delta_o + \\[2mm] \left(-\cos\pi - \cos 3\pi + \cos 2\pi - \cos 5\pi + \cos 4\pi + 1 \right) \sin 3\delta_o \end{array} \right]$$

$$a_3 = \frac{1}{3\pi} \left[(1 + 1 + 1 + 1 + 1 + 1) \sin 3\delta_o \right]$$

$$a_3 = \frac{6}{3\pi} \sin 3\delta_o$$

The coefficient b_n is given by

$$b_n = \frac{1}{\pi} \left[\int_0^{\frac{\pi}{3} - \delta_o} \sin n\theta d\theta + \int_{\frac{2\pi}{3} - \delta_o}^{\frac{3\pi}{3} - \delta_o} \sin n\theta d\theta + \int_{\frac{4\pi}{3} - \delta_o}^{\frac{5\pi}{3} - \delta_o} \sin n\theta d\theta + \int_{\frac{6\pi}{3} - \delta_o}^{\frac{6\pi}{3}} \sin n\theta d\theta \right] \qquad (5.85)$$

159

$$b_n = \frac{1}{\pi}\left[\int_0^{\frac{\pi}{3}-\delta_o} \sin n\theta\, d\theta + \int_{\frac{2\pi}{3}-\delta_o}^{\frac{3\pi}{3}-\delta_o} \sin n\theta\, d\theta + \int_{\frac{4\pi}{3}-\delta_o}^{\frac{5\pi}{3}-\delta_o} \sin n\theta\, d\theta + \int_{\frac{6\pi}{3}-\delta_o}^{\frac{6\pi}{3}} \sin n\theta\, d\theta \right]$$

$$b_n = -\frac{1}{n\pi}\left[[\cos n\theta]_0^{\frac{\pi}{3}-\delta_o} + [\cos n\theta]_{\frac{2\pi}{3}-\delta_o}^{\frac{3\pi}{3}-\delta_o} + [\cos n\theta]_{\frac{4\pi}{3}-\delta_o}^{\frac{5\pi}{3}-\delta_o} + [\cos n\theta]_{\frac{6\pi}{3}-\delta_o}^{\frac{6\pi}{3}} \right]$$

$$b_n = -\frac{1}{n\pi}\left[\begin{array}{l} \left[\cos\left(\frac{n\pi}{3}-n\delta_o\right)-\cos n0\right] + \left[\cos\left(\frac{3n\pi}{3}-n\delta_o\right)-\cos\left(\frac{2n\pi}{3}-n\delta_o\right)\right] + \\[2mm] \left[\cos\left(\frac{5n\pi}{3}-n\delta_o\right)-\cos\left(\frac{4n\pi}{3}-n\delta_o\right)\right] + \left[\cos\frac{6n\pi}{3}-\cos\left(\frac{6n\pi}{3}-n\delta_o\right)\right] \end{array} \right]$$

$$b_n = -\frac{1}{n\pi}\left[\begin{array}{l} \cos\frac{n\pi}{3}\cos n\delta_o + \sin\frac{n\pi}{3}\sin n\delta_o - \cos n0 \\[2mm] + \cos\frac{3n\pi}{3}\cos n\delta_o + \sin\frac{3n\pi}{3}\sin n\delta_o + \\[2mm] -\left[\cos\frac{2n\pi}{3}\cos n\delta_o + \sin\frac{2n\pi}{3}\sin n\delta_o\right] + \\[2mm] \cos\frac{5n\pi}{3}\cos n\delta_o + \sin\frac{5n\pi}{3}\sin n\delta_o \\[2mm] -\left[\cos\frac{4n\pi}{3}\cos n\delta_o + \sin\frac{4n\pi}{3}\sin n\delta_o\right] + \\[2mm] \cos\frac{6n\pi}{3} - \left[\cos\frac{6n\pi}{3}\cos n\delta_o + \sin\frac{6n\pi}{3}\sin n\delta_o\right] \end{array} \right]$$

$$b_n = -\frac{1}{n\pi} \begin{bmatrix} \cos\dfrac{n\pi}{3}\cos n\delta_o + \sin\dfrac{n\pi}{3}\sin n\delta_o - \cos n0 + \\[2mm] \cos n\pi \cos n\delta_o + \sin n\pi \sin n\delta_o + \\[2mm] -\cos\dfrac{2n\pi}{3}\cos n\delta_o - \sin\dfrac{2n\pi}{3}\sin n\delta_o + \\[2mm] \cos\dfrac{5n\pi}{3}\cos n\delta_o + \sin\dfrac{5n\pi}{3}\sin n\delta_o \\[2mm] -\cos\dfrac{4n\pi}{3}\cos n\delta_o - \sin\dfrac{4n\pi}{3}\sin n\delta_o + \\[2mm] \cos 2n\pi - \cos 2n\pi \cos n\delta_o - \sin 2n\pi \sin n\delta_o \end{bmatrix}$$

$$b_n = -\frac{1}{n\pi} \begin{bmatrix} \cos\dfrac{n\pi}{3}\cos n\delta_o + \sin\dfrac{n\pi}{3}\sin n\delta_o - 1 + \cos n\pi \cos n\delta_o + \\[2mm] -\cos\dfrac{2n\pi}{3}\cos n\delta_o - \sin\dfrac{2n\pi}{3}\sin n\delta_o + \cos\dfrac{5n\pi}{3}\cos n\delta_o + \sin\dfrac{5n\pi}{3}\sin n\delta_o \\[2mm] -\cos\dfrac{4n\pi}{3}\cos n\delta_o - \sin\dfrac{4n\pi}{3}\sin n\delta_o + 1 - \cos n\delta_o \end{bmatrix}$$

$$b_n = -\frac{1}{n\pi} \begin{bmatrix} \cos\dfrac{n\pi}{3}\cos n\delta_o + \cos n\pi \cos n\delta_o - \cos\dfrac{2n\pi}{3}\cos n\delta_o + \\[2mm] \cos\dfrac{5n\pi}{3}\cos n\delta_o - \cos\dfrac{4n\pi}{3}\cos n\delta_o + \\[2mm] -\cos n\delta_o + \sin\dfrac{n\pi}{3}\sin n\delta_o - \sin\dfrac{2n\pi}{3}\sin n\delta_o + \\[2mm] \sin\dfrac{5n\pi}{3}\sin n\delta_o - \sin\dfrac{4n\pi}{3}\sin n\delta_o + 1 - 1 \end{bmatrix}$$

$$b_n = -\frac{1}{n\pi} \left[\left(\cos\dfrac{n\pi}{3} + \cos n\pi - \cos\dfrac{2n\pi}{3} + \cos\dfrac{5n\pi}{3} - \cos\dfrac{4n\pi}{3} - 1 \right)\cos n\delta_o + \left(\sin\dfrac{n\pi}{3} - \sin\dfrac{2n\pi}{3} + \sin\dfrac{5n\pi}{3} - \sin\dfrac{4n\pi}{3} \right)\sin n\delta_o \right]$$

when n = 1:

$$b_1 = -\frac{1}{\pi} \left[\left(\cos\dfrac{\pi}{3} + \cos \pi - \cos\dfrac{2\pi}{3} + \cos\dfrac{5\pi}{3} - \cos\dfrac{4\pi}{3} - 1 \right)\cos \delta_o + \left(\sin\dfrac{\pi}{3} - \sin\dfrac{2\pi}{3} + \sin\dfrac{5\pi}{3} - \sin\dfrac{4\pi}{3} \right)\sin \delta_o \right]$$

161

$$b_1 = -\frac{1}{\pi}\left[\begin{array}{l}\left(\cos\frac{\pi}{3}-1+\cos\frac{\pi}{3}+\cos\frac{\pi}{3}+\cos\frac{\pi}{3}-1\right)\cos\delta_o + \\ \left(\sin\frac{\pi}{3}-\sin\frac{\pi}{3}-\sin\frac{\pi}{3}+\sin\frac{\pi}{3}\right)\sin\delta_o\end{array}\right] = 0$$

when n = 2:

$$b_2 = -\frac{1}{2\pi}\left[\begin{array}{l}\left(\cos\frac{2\pi}{3}+\cos 2\pi-\cos\frac{4\pi}{3}+\cos\frac{10\pi}{3}-\cos\frac{8\pi}{3}-1\right)\cos 2\delta_o + \\ \left(\sin\frac{2\pi}{3}-\sin\frac{4\pi}{3}+\sin\frac{10\pi}{3}-\sin\frac{8\pi}{3}\right)\sin 2\delta_o\end{array}\right]$$

$$b_2 = -\frac{1}{2\pi}\left[\begin{array}{l}\left(-\cos\frac{\pi}{3}+1+\cos\frac{\pi}{3}-\cos\frac{\pi}{3}+\cos\frac{\pi}{3}-1\right)\cos 2\delta_o + \\ \left(\sin\frac{\pi}{3}+\sin\frac{\pi}{3}-\sin\frac{\pi}{3}-\sin\frac{\pi}{3}\right)\sin 2\delta_o\end{array}\right] = 0$$

when n = 3:

$$b_3 = -\frac{1}{3\pi}\left[\begin{array}{l}\left(\cos\frac{3\pi}{3}+\cos 3\pi-\cos\frac{6\pi}{3}+\cos\frac{15\pi}{3}-\cos\frac{12\pi}{3}-1\right)\cos 3\delta_o + \\ \left(\sin\frac{3\pi}{3}-\sin\frac{6\pi}{3}+\sin\frac{15\pi}{3}-\sin\frac{12\pi}{3}\right)\sin 3\delta_o\end{array}\right]$$

$$b_3 = -\frac{1}{3\pi}\left[\begin{array}{l}(\cos\pi+\cos 3\pi-\cos 2\pi+\cos\pi-\cos 2\pi-1)\cos 3\delta_o + \\ (\sin\pi-\sin\pi+\sin\pi-\sin 2\pi)\sin 3\delta_o\end{array}\right]$$

$$b_3 = -\frac{1}{3\pi}\left[(-1-1-1-1-1-1)\cos 3\delta_o\right]$$

$$a_3 = \frac{6}{3\pi}\sin 3\delta_o, \ b_3 = \frac{6}{3\pi}\cos 3\delta_o$$

162

Thus in **Case II,**

$$\alpha = \frac{1}{2} + \frac{6}{3\pi}\left[\sin 3\delta_o \cos 3\theta + \cos 3\delta_o \sin 3\theta\right]$$

$$\alpha = \frac{1}{2} + \frac{2}{\pi}\left[\sin 3\theta \cos 3\delta_o + \cos 3\theta \sin 3\delta_o\right] \qquad (5.86)$$

$$\alpha = \frac{1}{2} + \frac{2}{\pi}\left[\sin(3\theta + 3\delta_o)\right]$$

Case III: $\delta_o = -15^0$

The coefficient a_o is given by

Figure 5.8. Waveform of the reference modulation signals with $\delta_o = -15^0$ showing the maximum and minimum values in the six sectors

163

$$a_o = \frac{1}{2\pi}\left[\int_{\delta_o}^{\frac{\pi}{3}+\delta_o} d\theta + \int_{\frac{2\pi}{3}+\delta_o}^{\frac{3\pi}{3}+\delta_o} d\theta + \int_{\frac{4\pi}{3}+\delta_o}^{\frac{5\pi}{3}+\delta_o} d\theta\right] \tag{5.87}$$

$$a_o = \frac{1}{2\pi}\left[[\theta]_{\delta_o}^{\frac{\pi}{3}+\delta_o} + [\theta]_{\frac{2\pi}{3}+\delta_o}^{\frac{3\pi}{3}+\delta_o} + [\theta]_{\frac{4\pi}{3}+\delta_o}^{\frac{5\pi}{3}+\delta_o}\right]$$

$$a_o = \frac{1}{2\pi}\left[\left[\frac{\pi}{3}+\delta_o - \delta_o\right] + \left[\frac{3\pi}{3}+\delta_o - \left(\frac{2\pi}{3}+\delta_o\right)\right] + \left[\frac{5\pi}{3}+\delta_o - \left(\frac{4\pi}{3}+\delta_o\right)\right]\right]$$

$$a_o = \frac{1}{2\pi}\left[\frac{\pi}{3}+\frac{\pi}{3}+\frac{\pi}{3}\right] = \frac{1}{2}$$

The coefficient a_n is given by

$$a_n = \frac{1}{\pi}\left[\int_{\delta_o}^{\frac{\pi}{3}+\delta_o}\cos n\theta d\theta + \int_{\frac{2\pi}{3}+\delta_o}^{\frac{3\pi}{3}+\delta_o}\cos n\theta d\theta + \int_{\frac{4\pi}{3}+\delta_o}^{\frac{5\pi}{3}+\delta_o}\cos n\theta d\theta\right] \tag{5.88}$$

$$a_n = \frac{1}{n\pi}\left[[\sin n\theta]_{\delta_o}^{\frac{\pi}{3}+\delta_o} + [\sin n\theta]_{\frac{2\pi}{3}+\delta_o}^{\frac{3\pi}{3}+\delta_o} + [\sin n\theta]_{\frac{4\pi}{3}+\delta_o}^{\frac{5\pi}{3}+\delta_o}\right]$$

$$a_n = \frac{1}{n\pi}\left[\begin{array}{l}\left[\sin\left(\frac{n\pi}{3}+n\delta_o\right)-\sin n\delta_o\right] + \left[\sin\left(\frac{3n\pi}{3}+n\delta_o\right)-\sin\left(\frac{2n\pi}{3}+n\delta_o\right)\right] + \\ \left[\sin\left(\frac{5n\pi}{3}+n\delta_o\right)-\sin\left(\frac{4n\pi}{3}+n\delta_o\right)\right]\end{array}\right]$$

$$a_n = \frac{1}{n\pi}\left[\begin{array}{l}\sin\frac{n\pi}{3}\cos n\delta_o + \cos\frac{n\pi}{3}\sin n\delta_o - \sin n\delta_o + \sin\frac{3n\pi}{3}\cos n\delta_o + \cos\frac{3n\pi}{3}\sin n\delta_o + \\ -\left[\sin\frac{2n\pi}{3}\cos n\delta_o + \cos\frac{2n\pi}{3}\sin n\delta_o\right] + \sin\frac{5n\pi}{3}\cos n\delta_o + \cos\frac{5n\pi}{3}\sin n\delta_o \\ -\left[\sin\frac{4n\pi}{3}\cos n\delta_o + \cos\frac{4n\pi}{3}\sin n\delta_o\right]\end{array}\right]$$

$$a_n = \frac{1}{n\pi}\left[\begin{array}{l} \sin\dfrac{n\pi}{3}\cos n\delta_o + \cos\dfrac{n\pi}{3}\sin n\delta_o - \sin n\delta_o + \sin\dfrac{3n\pi}{3}\cos n\delta_o + \cos\dfrac{3n\pi}{3}\sin n\delta_o + \\[3mm] -\sin\dfrac{2n\pi}{3}\cos n\delta_o - \cos\dfrac{2n\pi}{3}\sin n\delta_o + \sin\dfrac{5n\pi}{3}\cos n\delta_o + \cos\dfrac{5n\pi}{3}\sin n\delta_o \\[3mm] -\sin\dfrac{4n\pi}{3}\cos n\delta_o - \cos\dfrac{4n\pi}{3}\sin n\delta_o \end{array}\right]$$

$$a_n = \frac{1}{n\pi}\left[\begin{array}{l} \sin\dfrac{n\pi}{3}\cos n\delta_o + \cos\dfrac{n\pi}{3}\sin n\delta_o - \sin n\delta_o + \sin n\pi\cos n\delta_o + \cos n\pi\sin n\delta_o + \\[3mm] -\sin\dfrac{2n\pi}{3}\cos n\delta_o - \cos\dfrac{2n\pi}{3}\sin n\delta_o + \sin\dfrac{5n\pi}{3}\cos n\delta_o + \cos\dfrac{5n\pi}{3}\sin n\delta_o \\[3mm] -\sin\dfrac{4n\pi}{3}\cos n\delta_o - \cos\dfrac{4n\pi}{3}\sin n\delta_o \end{array}\right]$$

$$a_n = \frac{1}{n\pi}\left[\begin{array}{l} \sin\dfrac{n\pi}{3}\cos n\delta_o + \cos\dfrac{n\pi}{3}\sin n\delta_o + \cos n\pi\sin n\delta_o + \\[3mm] -\sin\dfrac{2n\pi}{3}\cos n\delta_o - \cos\dfrac{2n\pi}{3}\sin n\delta_o + \\[3mm] \sin\dfrac{5n\pi}{3}\cos n\delta_o + \cos\dfrac{5n\pi}{3}\sin n\delta_o - \sin\dfrac{4n\pi}{3}\cos n\delta_o + \\[3mm] -\cos\dfrac{4n\pi}{3}\sin n\delta_o - \sin n\delta_o \end{array}\right]$$

$$a_n = \frac{1}{n\pi}\left[\begin{array}{l} \left(\sin\dfrac{n\pi}{3} - \sin\dfrac{2n\pi}{3} + \sin\dfrac{5n\pi}{3} - \sin\dfrac{4n\pi}{3}\right)\cos n\delta_o + \\[3mm] \left(\cos\dfrac{n\pi}{3} + \cos n\pi - \cos\dfrac{2n\pi}{3} + \cos\dfrac{5n\pi}{3} - \cos\dfrac{4n\pi}{3} - 1\right)\sin n\delta_o \end{array}\right]$$

when n = 1:

$$a_1 = \frac{1}{\pi}\left[\begin{array}{l} \left(\sin\dfrac{\pi}{3} - \sin\dfrac{2\pi}{3} + \sin\dfrac{5\pi}{3} - \sin\dfrac{4\pi}{3}\right)\cos\delta_o + \\[3mm] \left(\cos\dfrac{\pi}{3} + \cos\pi - \cos\dfrac{2\pi}{3} + \cos\dfrac{5\pi}{3} - \cos\dfrac{4\pi}{3} - 1\right)\sin\delta_o \end{array}\right]$$

165

$$a_1 = \frac{1}{\pi} \left[\begin{array}{l} \left(\sin\frac{\pi}{3} - \sin\frac{\pi}{3} - \sin\frac{\pi}{3} + \sin\frac{\pi}{3} \right) \cos\delta_o + \\ \left(\cos\frac{\pi}{3} - 1 + \cos\frac{\pi}{3} + \cos\frac{\pi}{3} + \cos\frac{\pi}{3} - 1 \right) \sin\delta_o \end{array} \right]$$

$$a_1 = 0$$

when n = 2:

$$a_2 = \frac{1}{2\pi} \left[\begin{array}{l} \left(\sin\frac{2\pi}{3} - \sin\frac{4\pi}{3} + \sin\frac{10\pi}{3} - \sin\frac{8\pi}{3} \right) \cos 2\delta_o + \\ \left(\cos\frac{2\pi}{3} + \cos 2\pi - \cos\frac{4\pi}{3} + \cos\frac{10\pi}{3} - \cos\frac{8\pi}{3} - 1 \right) \sin 2\delta_o \end{array} \right]$$

$$a_2 = \frac{1}{2\pi} \left[\begin{array}{l} \left(\sin\frac{\pi}{3} + \sin\frac{\pi}{3} - \sin\frac{\pi}{3} - \sin\frac{\pi}{3} \right) \cos 2\delta_o + \\ \left(-\cos\frac{\pi}{3} + 1 + \cos\frac{\pi}{3} - \cos\frac{\pi}{3} + \cos\frac{\pi}{3} - 1 \right) \sin 2\delta_o \end{array} \right]$$

$$a_2 = 0$$

when n = 3:

$$a_3 = \frac{1}{3\pi} \left[\begin{array}{l} \left(\sin\frac{3\pi}{3} - \sin\frac{6\pi}{3} + \sin\frac{15\pi}{3} - \sin\frac{12\pi}{3} \right) \cos 3\delta_o + \\ \left(\cos\frac{3\pi}{3} + \cos 3\pi - \cos\frac{6\pi}{3} + \cos\frac{15\pi}{3} - \cos\frac{12\pi}{3} - 1 \right) \sin 3\delta_o \end{array} \right]$$

$$a_3 = \frac{1}{3\pi} \left[\begin{array}{l} (\sin\pi - \sin 2\pi + \sin 5\pi - \sin 4\pi)\cos 3\delta_o + \\ (\cos\pi + \cos 3\pi - \cos 2\pi + \cos 5\pi - \cos 4\pi - 1)\sin 3\delta_o \end{array} \right]$$

$$a_3 = \frac{1}{3\pi} \left[(-1 - 1 - 1 - 1 - 1 - 1)\sin 3\delta_o \right]$$

$$a_3 = -\frac{6}{3\pi}\sin 3\delta_o$$

The coefficient b_n is given by

$$b_n = \frac{1}{\pi}\left[\int_{\frac{\pi}{3}+\delta_o}^{\frac{\pi}{3}+\delta_o}\sin n\theta d\theta + \int_{\frac{2\pi}{3}+\delta_o}^{\frac{3\pi}{3}+\delta_o}\sin n\theta d\theta + \int_{\frac{4\pi}{3}+\delta_o}^{\frac{5\pi}{3}+\delta_o}\sin n\theta d\theta\right] \qquad (5.89)$$

$$b_n = -\frac{1}{n\pi}\left[\left[\cos n\theta\right]_{\delta_o}^{\frac{\pi}{3}+\delta_o} + \left[\cos n\theta\right]_{\frac{2\pi}{3}+\delta_o}^{\frac{3\pi}{3}+\delta_o} + \left[\cos n\theta\right]_{\frac{4\pi}{3}+\delta_o}^{\frac{5\pi}{3}+\delta_o}\right]$$

$$b_n = -\frac{1}{n\pi}\left[\begin{array}{l}\left[\left[\cos\left(\frac{n\pi}{3}+n\delta_o\right)-\cos n\delta_o\right] + \left[\cos\left(\frac{3n\pi}{3}+n\delta_o\right)-\cos\left(\frac{2n\pi}{3}+n\delta_o\right)\right]\right] + \\ \left[\cos\left(\frac{5n\pi}{3}+n\delta_o\right)-\cos\left(\frac{4n\pi}{3}+n\delta_o\right)\right]\end{array}\right]$$

$$b_n = -\frac{1}{n\pi}\left[\begin{array}{l}\cos\dfrac{n\pi}{3}\cos n\delta_o - \sin\dfrac{n\pi}{3}\sin n\delta_o - \cos n\delta_o + \\[2mm] \cos\dfrac{3n\pi}{3}\cos n\delta_o - \sin\dfrac{3n\pi}{3}\sin n\delta_o + \\[2mm] -\left[\cos\dfrac{2n\pi}{3}\cos n\delta_o - \sin\dfrac{2n\pi}{3}\sin n\delta_o\right] + \\[2mm] \cos\dfrac{5n\pi}{3}\cos n\delta_o - \sin\dfrac{5n\pi}{3}\sin n\delta_o + \\[2mm] -\left[\cos\dfrac{4n\pi}{3}\cos n\delta_o - \sin\dfrac{4n\pi}{3}\sin n\delta_o\right]\end{array}\right]$$

$$b_n = -\frac{1}{n\pi}\left[\begin{array}{l}\cos\dfrac{n\pi}{3}\cos n\delta_o - \sin\dfrac{n\pi}{3}\sin n\delta_o - \cos n\delta_o + \cos n\pi\cos n\delta_o - \sin n\pi\sin n\delta_o + \\[2mm] -\cos\dfrac{2n\pi}{3}\cos n\delta_o + \sin\dfrac{2n\pi}{3}\sin n\delta_o + \cos\dfrac{5n\pi}{3}\cos n\delta_o - \sin\dfrac{5n\pi}{3}\sin n\delta_o \\[2mm] -\cos\dfrac{4n\pi}{3}\cos n\delta_o + \sin\dfrac{4n\pi}{3}\sin n\delta_o\end{array}\right]$$

167

$$b_n = -\frac{1}{n\pi}\begin{bmatrix} \cos\frac{n\pi}{3}\cos n\delta_o - \sin\frac{n\pi}{3}\sin n\delta_o - \cos n\delta_o + \cos n\pi\cos n\delta_o + \\ -\cos\frac{2n\pi}{3}\cos n\delta_o + \sin\frac{2n\pi}{3}\sin n\delta_o + \cos\frac{5n\pi}{3}\cos n\delta_o - \sin\frac{5n\pi}{3}\sin n\delta_o \\ -\cos\frac{4n\pi}{3}\cos n\delta_o + \sin\frac{4n\pi}{3}\sin n\delta_o \end{bmatrix}$$

$$b_n = -\frac{1}{n\pi}\begin{bmatrix} \cos\frac{n\pi}{3}\cos n\delta_o + \cos n\pi\cos n\delta_o - \cos\frac{2n\pi}{3}\cos n\delta_o \\ +\cos\frac{5n\pi}{3}\cos n\delta_o - \cos\frac{4n\pi}{3}\cos n\delta_o + \\ -\cos n\delta_o - \sin\frac{n\pi}{3}\sin n\delta_o + \sin\frac{2n\pi}{3}\sin n\delta_o + \\ -\sin\frac{5n\pi}{3}\sin n\delta_o + \sin\frac{4n\pi}{3}\sin n\delta_o \end{bmatrix}$$

$$b_n = -\frac{1}{n\pi}\begin{bmatrix} \left(\cos\frac{n\pi}{3} + \cos n\pi - \cos\frac{2n\pi}{3} + \cos\frac{5n\pi}{3} - \cos\frac{4n\pi}{3} - 1\right)\cos n\delta_o + \\ \left(-\sin\frac{n\pi}{3} + \sin\frac{2n\pi}{3} - \sin\frac{5n\pi}{3} + \sin\frac{4n\pi}{3}\right)\sin n\delta_o \end{bmatrix}$$

when n = 1:

$$b_1 = -\frac{1}{\pi}\begin{bmatrix} \left(\cos\frac{\pi}{3} + \cos\pi - \cos\frac{2\pi}{3} + \cos\frac{5\pi}{3} - \cos\frac{4\pi}{3} - 1\right)\cos\delta_o + \\ \left(-\sin\frac{\pi}{3} + \sin\frac{2\pi}{3} - \sin\frac{5\pi}{3} + \sin\frac{4\pi}{3}\right)\sin\delta_o \end{bmatrix}$$

$$b_1 = -\frac{1}{\pi}\begin{bmatrix} \left(\cos\frac{\pi}{3} - 1 + \cos\frac{\pi}{3} + \cos\frac{\pi}{3} + \cos\frac{\pi}{3} - 1\right)\cos\delta_o + \\ \left(-\sin\frac{\pi}{3} + \sin\frac{\pi}{3} + \sin\frac{\pi}{3} - \sin\frac{\pi}{3}\right)\sin\delta_o \end{bmatrix}$$

$$b_1 = 0$$

when n = 2:

$$b_2 = -\frac{1}{2\pi}\left[\begin{array}{l}\left(\cos\frac{2\pi}{3} + \cos 2\pi - \cos\frac{4\pi}{3} + \cos\frac{10\pi}{3} - \cos\frac{8\pi}{3} - 1\right)\cos n\delta_o + \\ \left(-\sin\frac{2\pi}{3} + \sin\frac{4\pi}{3} - \sin\frac{10\pi}{3} + \sin\frac{8\pi}{3}\right)\sin n\delta_o\end{array}\right]$$

$$b_2 = -\frac{1}{2\pi}\left[\begin{array}{l}\left(-\cos\frac{\pi}{3} + 1 + \cos\frac{\pi}{3} - \cos\frac{\pi}{3} + \cos\frac{\pi}{3} - 1\right)\cos 2\delta_o + \\ \left(-\sin\frac{\pi}{3} - \sin\frac{\pi}{3} + \sin\frac{\pi}{3} + \sin\frac{\pi}{3}\right)\sin 2\delta_o\end{array}\right] = 0$$

when n = 3:

$$b_3 = -\frac{1}{3\pi}\left[\begin{array}{l}\left(\cos\frac{3\pi}{3} + \cos n\pi - \cos\frac{6\pi}{3} + \cos\frac{15\pi}{3} - \cos\frac{12\pi}{3} - 1\right)\cos n\delta_o + \\ \left(-\sin\frac{3\pi}{3} + \sin\frac{6\pi}{3} - \sin\frac{15\pi}{3} + \sin\frac{12\pi}{3}\right)\sin n\delta_o\end{array}\right]$$

$$b_3 = -\frac{1}{3\pi}\left[\begin{array}{l}(\cos\pi + \cos 3\pi - \cos 2\pi + \cos\pi - \cos 2\pi - 1)\cos 3\delta_o + \\ (-\sin\pi + \sin\pi - \sin\pi + \sin 2\pi)\sin 3\delta_o\end{array}\right]$$

$$b_3 = -\frac{1}{3\pi}\left[(-1-1-1-1-1-1)\cos 3\delta_o\right]$$

$$a_3 = -\frac{6}{3\pi}\sin 3\delta_o, \quad b_3 = \frac{6}{3\pi}\cos 3\delta_o$$

Thus in *Case III,*

$$\alpha = \frac{1}{2} + \frac{6}{3\pi}\left[-\sin 3\delta_o \cos 3\theta + \cos 3\delta_o \sin 3\theta\right]$$

$$\alpha = \frac{1}{2} + \frac{2}{\pi}\left[\sin 3\theta \cos 3\delta_o - \cos 3\theta \sin 3\delta_o\right] \tag{5.90}$$

$$\alpha = \frac{1}{2} + \frac{2}{\pi}\left[\sin(3\theta - 3\delta_o)\right]$$

Figure 5.9. Waveform of the reference modulation signals with $\delta_o = 30^0$ showing the maximum and minimum values in the six sectors

Case IV: $\delta_o = 30^0$

The coefficient a_o is given by

$$a_o = \frac{1}{2\pi}\left[\int_0^{\frac{\pi}{3}-\delta_o} d\theta + \int_{\frac{2\pi}{3}-\delta_o}^{\frac{3\pi}{3}-\delta_o} d\theta + \int_{\frac{4\pi}{3}-\delta_o}^{\frac{5\pi}{3}-\delta_o} d\theta + \int_{\frac{6\pi}{3}-\delta_o}^{\frac{6\pi}{3}} d\theta\right] \qquad (5.91)$$

$$a_o = \frac{1}{2\pi}\left[[\theta]_0^{\frac{\pi}{3}-\delta_o} + [\theta]_{\frac{2\pi}{3}-\delta_o}^{\frac{3\pi}{3}-\delta_o} + [\theta]_{\frac{4\pi}{3}-\delta_o}^{\frac{5\pi}{3}-\delta_o} + [\theta]_{\frac{6\pi}{3}-\delta_o}^{\frac{6\pi}{3}}\right]$$

$$a_o = \frac{1}{2\pi}\begin{bmatrix} \left[\frac{\pi}{3}-\delta_o-0\right] + \left[\frac{3\pi}{3}-\delta_o-\left(\frac{2\pi}{3}-\delta_o\right)\right] + \\ \left[\frac{5\pi}{3}-\delta_o-\left(\frac{4\pi}{3}-\delta_o\right)\right] + \left[\frac{6\pi}{3}-\left(\frac{6\pi}{3}-\delta_o\right)\right] \end{bmatrix}$$

170

$$a_o = \frac{1}{2\pi}\left[\frac{\pi}{3} - \delta_o + \frac{\pi}{3} + \frac{\pi}{3} + \delta_o\right] = \frac{1}{2}$$

The coefficient a_n is given by

$$a_n = \frac{1}{\pi}\left[\begin{array}{l}\int_0^{\frac{\pi}{3}-\delta_o}\cos n\theta d\theta + \int_{\frac{2\pi}{3}-\delta_o}^{\frac{3\pi}{3}-\delta_o}\cos n\theta d\theta + \\[2mm] \int_{\frac{4\pi}{3}-\delta_o}^{\frac{5\pi}{3}-\delta_o}\cos n\theta d\theta + \int_{\frac{6\pi}{3}-\delta_o}^{\frac{6\pi}{3}}\cos n\theta d\theta\end{array}\right] \tag{5.92}$$

$$a_n = \frac{1}{n\pi}\left[\left[\sin n\theta\right]_0^{\frac{\pi}{3}-\delta_o} + \left[\sin n\theta\right]_{\frac{2\pi}{3}-\delta_o}^{\frac{3\pi}{3}-\delta_o} + \left[\sin n\theta\right]_{\frac{4\pi}{3}-\delta_o}^{\frac{5\pi}{3}-\delta_o} + \left[\sin n\theta\right]_{\frac{6\pi}{3}-\delta_o}^{\frac{6\pi}{3}}\right]$$

$$a_n = \frac{1}{n\pi}\left[\begin{array}{l}\left[\sin\left(\frac{n\pi}{3}-n\delta_o\right)-\sin n0\right] + \left[\sin\left(\frac{3n\pi}{3}-n\delta_o\right)-\sin\left(\frac{2n\pi}{3}-n\delta_o\right)\right] + \\[3mm] \left[\sin\left(\frac{5n\pi}{3}-n\delta_o\right)-\sin\left(\frac{4n\pi}{3}-n\delta_o\right)\right] + \left[\sin\frac{6n\pi}{3}-\sin\left(\frac{6n\pi}{3}-n\delta_o\right)\right]\end{array}\right]$$

$$a_n = \frac{1}{n\pi}\left[\begin{array}{l}\sin\frac{n\pi}{3}\cos n\delta_o - \cos\frac{n\pi}{3}\sin n\delta_o - \sin n0 + \\[3mm] \sin\frac{3n\pi}{3}\cos n\delta_o - \cos\frac{3n\pi}{3}\sin n\delta_o + \\[3mm] -\left[\sin\frac{2n\pi}{3}\cos n\delta_o - \cos\frac{2n\pi}{3}\sin n\delta_o\right] + \\[3mm] \sin\frac{5n\pi}{3}\cos n\delta_o - \cos\frac{5n\pi}{3}\sin n\delta_o \\[3mm] -\left[\sin\frac{4n\pi}{3}\cos n\delta_o - \cos\frac{4n\pi}{3}\sin n\delta_o\right] + \\[3mm] \sin\frac{6n\pi}{3} - \left[\sin\frac{6n\pi}{3}\cos n\delta_o - \cos\frac{6n\pi}{3}\sin n\delta_o\right]\end{array}\right]$$

$$a_n = \frac{1}{n\pi} \left[\begin{array}{l} \sin\dfrac{n\pi}{3}\cos n\delta_o - \cos\dfrac{n\pi}{3}\sin n\delta_o - \sin n0 + \\[2mm] \sin\dfrac{3n\pi}{3}\cos n\delta_o - \cos\dfrac{3n\pi}{3}\sin n\delta_o + \\[2mm] -\sin\dfrac{2n\pi}{3}\cos n\delta_o + \cos\dfrac{2n\pi}{3}\sin n\delta_o + \\[2mm] \sin\dfrac{5n\pi}{3}\cos n\delta_o - \cos\dfrac{5n\pi}{3}\sin n\delta_o + \\[2mm] -\sin\dfrac{4n\pi}{3}\cos n\delta_o + \cos\dfrac{4n\pi}{3}\sin n\delta_o + \\[2mm] \sin\dfrac{6n\pi}{3} - \sin\dfrac{6n\pi}{3}\cos n\delta_o + \cos\dfrac{6n\pi}{3}\sin n\delta_o \end{array} \right]$$

$$a_n = \frac{1}{n\pi} \left[\begin{array}{l} \sin\dfrac{n\pi}{3}\cos n\delta_o - \cos\dfrac{n\pi}{3}\sin n\delta_o - \sin n0 + \\[2mm] \sin n\pi \cos n\delta_o - \cos n\pi \sin n\delta_o + \\[2mm] -\sin\dfrac{2n\pi}{3}\cos n\delta_o + \cos\dfrac{2n\pi}{3}\sin n\delta_o + \\[2mm] \sin\dfrac{5n\pi}{3}\cos n\delta_o - \cos\dfrac{5n\pi}{3}\sin n\delta_o + \\[2mm] -\sin\dfrac{4n\pi}{3}\cos n\delta_o + \cos\dfrac{4n\pi}{3}\sin n\delta_o + \\[2mm] \sin 2n\pi - \sin 2n\pi \cos n\delta_o + \cos 2n\pi \sin n\delta_o \end{array} \right]$$

$$a_n = \frac{1}{n\pi} \left[\begin{array}{l} \sin\dfrac{n\pi}{3}\cos n\delta_o - \cos\dfrac{n\pi}{3}\sin n\delta_o - \cos n\pi \sin n\delta_o \\[2mm] -\sin\dfrac{2n\pi}{3}\cos n\delta_o + \cos\dfrac{2n\pi}{3}\sin n\delta_o + \\[2mm] \sin\dfrac{5n\pi}{3}\cos n\delta_o - \cos\dfrac{5n\pi}{3}\sin n\delta_o + \\[2mm] -\sin\dfrac{4n\pi}{3}\cos n\delta_o + \cos\dfrac{4n\pi}{3}\sin n\delta_o + \sin n\delta_o \end{array} \right]$$

$$a_n = \frac{1}{n\pi} \left[\begin{array}{l} \left(\sin\frac{n\pi}{3} - \sin\frac{2n\pi}{3} + \sin\frac{5n\pi}{3} - \sin\frac{4n\pi}{3} \right) \cos n\delta_o + \\ \left(-\cos\frac{n\pi}{3} - \cos n\pi + \cos\frac{2n\pi}{3} - \cos\frac{5n\pi}{3} + \cos\frac{4n\pi}{3} + 1 \right) \sin n\delta_o \end{array} \right]$$

when n = 1:

$$a_1 = \frac{1}{\pi} \left[\begin{array}{l} \left(\sin\frac{\pi}{3} - \sin\frac{2\pi}{3} + \sin\frac{5\pi}{3} - \sin\frac{4\pi}{3} \right) \cos\delta_o + \\ \left(-\cos\frac{\pi}{3} - \cos\pi + \cos\frac{2\pi}{3} - \cos\frac{5\pi}{3} + \cos\frac{4\pi}{3} + 1 \right) \sin\delta_o \end{array} \right]$$

$$a_1 = \frac{1}{\pi} \left[\begin{array}{l} \left(\sin\frac{\pi}{3} - \sin\frac{\pi}{3} - \sin\frac{\pi}{3} + \sin\frac{\pi}{3} \right) \cos\delta_o + \\ \left(-\cos\frac{\pi}{3} + 1 - \cos\frac{\pi}{3} - \cos\frac{\pi}{3} - \cos\frac{\pi}{3} + 1 \right) \sin\delta_o \end{array} \right]$$

$$a_1 = 0$$

when n = 2:

$$a_2 = \frac{1}{2\pi} \left[\begin{array}{l} \left(\sin\frac{2\pi}{3} - \sin\frac{4\pi}{3} + \sin\frac{10\pi}{3} - \sin\frac{8\pi}{3} \right) \cos 2\delta_o + \\ \left(-\cos\frac{2\pi}{3} - \cos 2\pi + \cos\frac{4\pi}{3} - \cos\frac{10\pi}{3} + \cos\frac{8\pi}{3} + 1 \right) \sin 2\delta_o \end{array} \right]$$

$$a_2 = \frac{1}{2\pi} \left[\begin{array}{l} \left(\sin\frac{\pi}{3} + \sin\frac{\pi}{3} - \sin\frac{\pi}{3} - \sin\frac{\pi}{3} \right) \cos 2\delta_o + \\ \left(\cos\frac{\pi}{3} - 1 - \cos\frac{\pi}{3} + \cos\frac{\pi}{3} - \cos\frac{\pi}{3} + 1 \right) \sin 2\delta_o \end{array} \right] = 0$$

when n = 3:

$$a_3 = \frac{1}{3\pi} \begin{bmatrix} \left(\sin\frac{3\pi}{3} - \sin\frac{6\pi}{3} + \sin\frac{15\pi}{3} - \sin\frac{12\pi}{3} \right)\cos 3\delta_o + \\ \left(-\cos\frac{3\pi}{3} - \cos 3\pi + \cos\frac{6\pi}{3} - \cos\frac{15\pi}{3} + \cos\frac{12\pi}{3} + 1 \right)\sin 3\delta_o \end{bmatrix}$$

$$a_3 = \frac{1}{3\pi} \begin{bmatrix} \left(\sin\pi - \sin 2\pi + \sin 5\pi - \sin 4\pi \right)\cos 3\delta_o + \\ \left(-\cos\pi - \cos 3\pi + \cos 2\pi - \cos 5\pi + \cos 4\pi + 1 \right)\sin 3\delta_o \end{bmatrix}$$

$$a_3 = \frac{1}{3\pi} \left[(1 + 1 + 1 + 1 + 1 + 1)\sin 3\delta_o \right]$$

$$a_3 = \frac{6}{3\pi}\sin 3\delta_o$$

The coefficient b_n is given by

$$b_n = \frac{1}{\pi} \begin{bmatrix} \int_0^{\frac{\pi}{3}-\delta_o} \sin n\theta d\theta + \int_{\frac{2\pi}{3}-\delta_o}^{\frac{3\pi}{3}-\delta_o} \sin n\theta d\theta + \\ \int_{\frac{4\pi}{3}-\delta_o}^{\frac{5\pi}{3}-\delta_o} \sin n\theta d\theta + \int_{\frac{6\pi}{3}-\delta_o}^{\frac{6\pi}{3}} \sin n\theta d\theta \end{bmatrix} \tag{5.93}$$

$$b_n = -\frac{1}{n\pi} \left[[\cos n\theta]_0^{\frac{\pi}{3}-\delta_o} + [\cos n\theta]_{\frac{2\pi}{3}-\delta_o}^{\frac{3\pi}{3}-\delta_o} + [\cos n\theta]_{\frac{4\pi}{3}-\delta_o}^{\frac{5\pi}{3}-\delta_o} + [\cos n\theta]_{\frac{6\pi}{3}-\delta_o}^{\frac{6\pi}{3}} \right]$$

$$b_n = -\frac{1}{n\pi} \begin{bmatrix} \left[\cos\left(\frac{n\pi}{3} - n\delta_o\right) - \cos n0 \right] + \left[\cos\left(\frac{3n\pi}{3} - n\delta_o\right) - \cos\left(\frac{2n\pi}{3} - n\delta_o\right) \right] + \\ \left[\cos\left(\frac{5n\pi}{3} - n\delta_o\right) - \cos\left(\frac{4n\pi}{3} - n\delta_o\right) \right] + \left[\cos\frac{6n\pi}{3} - \cos\left(\frac{6n\pi}{3} - n\delta_o\right) \right] \end{bmatrix}$$

174

$$b_n = -\frac{1}{n\pi}\left[\begin{array}{l}\cos\dfrac{n\pi}{3}\cos n\delta_o + \sin\dfrac{n\pi}{3}\sin n\delta_o - \cos n0 + \\[2mm] \cos\dfrac{3n\pi}{3}\cos n\delta_o + \sin\dfrac{3n\pi}{3}\sin n\delta_o + \\[2mm] -\left[\cos\dfrac{2n\pi}{3}\cos n\delta_o + \sin\dfrac{2n\pi}{3}\sin n\delta_o\right] + \\[2mm] \cos\dfrac{5n\pi}{3}\cos n\delta_o + \sin\dfrac{5n\pi}{3}\sin n\delta_o + \\[2mm] -\left[\cos\dfrac{4n\pi}{3}\cos n\delta_o + \sin\dfrac{4n\pi}{3}\sin n\delta_o\right] + \\[2mm] \cos\dfrac{6n\pi}{3} - \left[\cos\dfrac{6n\pi}{3}\cos n\delta_o + \sin\dfrac{6n\pi}{3}\sin n\delta_o\right]\end{array}\right]$$

$$b_n = -\frac{1}{n\pi}\left[\begin{array}{l}\cos\dfrac{n\pi}{3}\cos n\delta_o + \sin\dfrac{n\pi}{3}\sin n\delta_o - \cos n0 + \\[2mm] \cos n\pi\cos n\delta_o + \sin n\pi\sin n\delta_o + \\[2mm] -\cos\dfrac{2n\pi}{3}\cos n\delta_o - \sin\dfrac{2n\pi}{3}\sin n\delta_o + \\[2mm] \cos\dfrac{5n\pi}{3}\cos n\delta_o + \sin\dfrac{5n\pi}{3}\sin n\delta_o + \\[2mm] -\cos\dfrac{4n\pi}{3}\cos n\delta_o - \sin\dfrac{4n\pi}{3}\sin n\delta_o + \\[2mm] \cos 2n\pi - \cos 2n\pi\cos n\delta_o - \sin 2n\pi\sin n\delta_o\end{array}\right]$$

$$b_n = -\frac{1}{n\pi}\left[\begin{array}{l}\cos\dfrac{n\pi}{3}\cos n\delta_o + \sin\dfrac{n\pi}{3}\sin n\delta_o - 1 + \cos n\pi\cos n\delta_o + \\[2mm] -\cos\dfrac{2n\pi}{3}\cos n\delta_o - \sin\dfrac{2n\pi}{3}\sin n\delta_o + \cos\dfrac{5n\pi}{3}\cos n\delta_o + \sin\dfrac{5n\pi}{3}\sin n\delta_o \\[2mm] -\cos\dfrac{4n\pi}{3}\cos n\delta_o - \sin\dfrac{4n\pi}{3}\sin n\delta_o + 1 - \cos n\delta_o\end{array}\right]$$

$$b_n = -\frac{1}{n\pi}\left[\begin{array}{l} \cos\dfrac{n\pi}{3}\cos n\delta_o + \cos n\pi \cos n\delta_o - \cos\dfrac{2n\pi}{3}\cos n\delta_o + \\[2ex] \cos\dfrac{5n\pi}{3}\cos n\delta_o - \cos\dfrac{4n\pi}{3}\cos n\delta_o + \\[2ex] -\cos n\delta_o + \sin\dfrac{n\pi}{3}\sin n\delta_o - \sin\dfrac{2n\pi}{3}\sin n\delta_o + \\[2ex] \sin\dfrac{5n\pi}{3}\sin n\delta_o - \sin\dfrac{4n\pi}{3}\sin n\delta_o + 1 - 1 \end{array}\right]$$

$$b_n = -\frac{1}{n\pi}\left[\begin{array}{l} \left(\cos\dfrac{n\pi}{3} + \cos n\pi - \cos\dfrac{2n\pi}{3} + \cos\dfrac{5n\pi}{3} - \cos\dfrac{4n\pi}{3} - 1\right)\cos n\delta_o + \\[2ex] \left(\sin\dfrac{n\pi}{3} - \sin\dfrac{2n\pi}{3} + \sin\dfrac{5n\pi}{3} - \sin\dfrac{4n\pi}{3}\right)\sin n\delta_o \end{array}\right]$$

when n = 1:

$$b_1 = -\frac{1}{\pi}\left[\begin{array}{l} \left(\cos\dfrac{\pi}{3} + \cos\pi - \cos\dfrac{2\pi}{3} + \cos\dfrac{5\pi}{3} - \cos\dfrac{4\pi}{3} - 1\right)\cos\delta_o + \\[2ex] \left(\sin\dfrac{\pi}{3} - \sin\dfrac{2\pi}{3} + \sin\dfrac{5\pi}{3} - \sin\dfrac{4\pi}{3}\right)\sin\delta_o \end{array}\right]$$

$$b_1 = -\frac{1}{\pi}\left[\begin{array}{l} \left(\cos\dfrac{\pi}{3} - 1 + \cos\dfrac{\pi}{3} + \cos\dfrac{\pi}{3} + \cos\dfrac{\pi}{3} - 1\right)\cos\delta_o + \\[2ex] \left(\sin\dfrac{\pi}{3} - \sin\dfrac{\pi}{3} - \sin\dfrac{\pi}{3} + \sin\dfrac{\pi}{3}\right)\sin\delta_o \end{array}\right] = 0$$

when n = 2:

$$b_2 = -\frac{1}{2\pi}\left[\begin{array}{l} \left(\cos\dfrac{2\pi}{3} + \cos 2\pi - \cos\dfrac{4\pi}{3} + \cos\dfrac{10\pi}{3} - \cos\dfrac{8\pi}{3} - 1\right)\cos 2\delta_o + \\[2ex] \left(\sin\dfrac{2\pi}{3} - \sin\dfrac{4\pi}{3} + \sin\dfrac{10\pi}{3} - \sin\dfrac{8\pi}{3}\right)\sin 2\delta_o \end{array}\right]$$

$$b_2 = -\frac{1}{2\pi}\left[\begin{array}{l} \left(-\cos\dfrac{\pi}{3} + 1 + \cos\dfrac{\pi}{3} - \cos\dfrac{\pi}{3} + \cos\dfrac{\pi}{3} - 1\right)\cos 2\delta_o + \\[2ex] \left(\sin\dfrac{\pi}{3} + \sin\dfrac{\pi}{3} - \sin\dfrac{\pi}{3} - \sin\dfrac{\pi}{3}\right)\sin 2\delta_o \end{array}\right] = 0$$

176

when n = 3:

$$b_3 = -\frac{1}{3\pi}\left[\begin{array}{l}\left(\cos\frac{3\pi}{3} + \cos 3\pi - \cos\frac{6\pi}{3} + \cos\frac{15\pi}{3} - \cos\frac{12\pi}{3} - 1\right)\cos 3\delta_o + \\ \left(\sin\frac{3\pi}{3} - \sin\frac{6\pi}{3} + \sin\frac{15\pi}{3} - \sin\frac{12\pi}{3}\right)\sin 3\delta_o\end{array}\right]$$

$$b_3 = -\frac{1}{3\pi}\left[\begin{array}{l}\left(\cos\pi + \cos 3\pi - \cos 2\pi + \cos\pi - \cos 2\pi - 1\right)\cos 3\delta_o + \\ \left(\sin\pi - \sin\pi + \sin\pi - \sin 2\pi\right)\sin 3\delta_o\end{array}\right]$$

$$b_3 = -\frac{1}{3\pi}\left[\left(-1-1-1-1-1-1\right)\cos 3\delta_o\right]$$

$$a_3 = \frac{6}{3\pi}\sin 3\delta_o, \quad b_3 = \frac{6}{3\pi}\cos 3\delta_o$$

Thus in *Case IV*,

$$\alpha = \frac{1}{2} + \frac{6}{3\pi}\left[\sin 3\delta_o \cos 3\theta + \cos 3\delta_o \sin 3\theta\right]$$

$$\alpha = \frac{1}{2} + \frac{2}{\pi}\left[\sin 3\theta \cos 3\delta_o + \cos 3\theta \sin 3\delta_o\right] \tag{5.94}$$

$$\alpha = \frac{1}{2} + \frac{2}{\pi}\left[\sin\left(3\theta + 3\delta_o\right)\right]$$

Case V : $\delta_o = -30^0$

The coefficient a_o is given by

$$a_o = \frac{1}{2\pi}\left[\int_{\delta_o}^{\frac{\pi}{3}+\delta_o} d\theta + \int_{\frac{2\pi}{3}+\delta_o}^{\frac{3\pi}{3}+\delta_o} d\theta + \int_{\frac{4\pi}{3}+\delta_o}^{\frac{5\pi}{3}+\delta_o} d\theta\right] \tag{5.95}$$

177
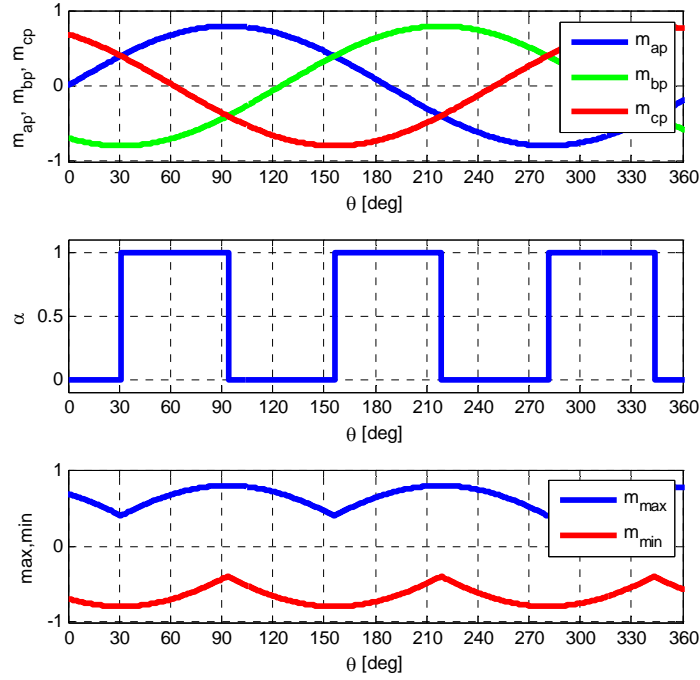
Figure 5.10.   Waveform of the reference modulation signals with $\delta_o = -30^0$ showing the maximum and minimum values in the six sectors

$$a_o = \frac{1}{2\pi}\left[[\theta]_{\delta_o}^{\frac{\pi}{3}+\delta_o} + [\theta]_{\frac{2\pi}{3}+\delta_o}^{\frac{3\pi}{3}+\delta_o} + [\theta]_{\frac{4\pi}{3}+\delta_o}^{\frac{5\pi}{3}+\delta_o}\right]$$

$$a_o = \frac{1}{2\pi}\left[\left[\frac{\pi}{3}+\delta_o-\delta_o\right] + \left[\frac{3\pi}{3}+\delta_o-\left(\frac{2\pi}{3}+\delta_o\right)\right] + \left[\frac{5\pi}{3}+\delta_o-\left(\frac{4\pi}{3}+\delta_o\right)\right]\right]$$

$$a_o = \frac{1}{2\pi}\left[\frac{\pi}{3}+\frac{\pi}{3}+\frac{\pi}{3}\right] = \frac{1}{2}$$

$$a_n = \frac{1}{\pi}\left[\int_{\delta_o}^{\frac{\pi}{3}+\delta_o}\cos n\theta d\theta + \int_{\frac{2\pi}{3}+\delta_o}^{\frac{3\pi}{3}+\delta_o}\cos n\theta d\theta + \int_{\frac{4\pi}{3}+\delta_o}^{\frac{5\pi}{3}+\delta_o}\cos n\theta d\theta\right]$$

178

$$a_n = \frac{1}{n\pi}\left[\left[\sin n\theta\right]_{\delta_o}^{\frac{\pi}{3}+\delta_o} + \left[\sin n\theta\right]_{\frac{2\pi}{3}+\delta_o}^{\frac{3\pi}{3}+\delta_o} + \left[\sin n\theta\right]_{\frac{4\pi}{3}+\delta_o}^{\frac{5\pi}{3}+\delta_o}\right]$$

$$a_n = \frac{1}{n\pi}\left[\begin{array}{l}\left[\sin\left(\frac{n\pi}{3}+n\delta_o\right)-\sin n\delta_o\right]+\left[\sin\left(\frac{3n\pi}{3}+n\delta_o\right)-\sin\left(\frac{2n\pi}{3}+n\delta_o\right)\right]+\\[2mm]\left[\sin\left(\frac{5n\pi}{3}+n\delta_o\right)-\sin\left(\frac{4n\pi}{3}+n\delta_o\right)\right]\end{array}\right]$$

$$a_n = \frac{1}{n\pi}\left[\begin{array}{l}\sin\frac{n\pi}{3}\cos n\delta_o + \cos\frac{n\pi}{3}\sin n\delta_o - \sin n\delta_o + \sin\frac{3n\pi}{3}\cos n\delta_o + \cos\frac{3n\pi}{3}\sin n\delta_o +\\[2mm]-\left[\sin\frac{2n\pi}{3}\cos n\delta_o + \cos\frac{2n\pi}{3}\sin n\delta_o\right]+\sin\frac{5n\pi}{3}\cos n\delta_o + \cos\frac{5n\pi}{3}\sin n\delta_o\\[2mm]-\left[\sin\frac{4n\pi}{3}\cos n\delta_o + \cos\frac{4n\pi}{3}\sin n\delta_o\right]\end{array}\right]$$

$$a_n = \frac{1}{n\pi}\left[\begin{array}{l}\sin\frac{n\pi}{3}\cos n\delta_o + \cos\frac{n\pi}{3}\sin n\delta_o - \sin n\delta_o + \sin\frac{3n\pi}{3}\cos n\delta_o + \cos\frac{3n\pi}{3}\sin n\delta_o +\\[2mm]-\sin\frac{2n\pi}{3}\cos n\delta_o - \cos\frac{2n\pi}{3}\sin n\delta_o + \sin\frac{5n\pi}{3}\cos n\delta_o + \cos\frac{5n\pi}{3}\sin n\delta_o\\[2mm]-\sin\frac{4n\pi}{3}\cos n\delta_o - \cos\frac{4n\pi}{3}\sin n\delta_o\end{array}\right]$$

$$a_n = \frac{1}{n\pi}\left[\begin{array}{l}\sin\frac{n\pi}{3}\cos n\delta_o + \cos\frac{n\pi}{3}\sin n\delta_o - \sin n\delta_o + \sin n\pi\cos n\delta_o + \cos n\pi\sin n\delta_o +\\[2mm]-\sin\frac{2n\pi}{3}\cos n\delta_o - \cos\frac{2n\pi}{3}\sin n\delta_o + \sin\frac{5n\pi}{3}\cos n\delta_o + \cos\frac{5n\pi}{3}\sin n\delta_o\\[2mm]-\sin\frac{4n\pi}{3}\cos n\delta_o - \cos\frac{4n\pi}{3}\sin n\delta_o\end{array}\right]$$

$$a_n = \frac{1}{n\pi} \begin{bmatrix} \sin\frac{n\pi}{3}\cos n\delta_o + \cos\frac{n\pi}{3}\sin n\delta_o + \cos n\pi\sin n\delta_o + \\[2mm] -\sin\frac{2n\pi}{3}\cos n\delta_o - \cos\frac{2n\pi}{3}\sin n\delta_o + \\[2mm] \sin\frac{5n\pi}{3}\cos n\delta_o + \cos\frac{5n\pi}{3}\sin n\delta_o - \sin\frac{4n\pi}{3}\cos n\delta_o + \\[2mm] -\cos\frac{4n\pi}{3}\sin n\delta_o - \sin n\delta_o \end{bmatrix}$$

$$a_n = \frac{1}{n\pi} \begin{bmatrix} \left(\sin\frac{n\pi}{3} - \sin\frac{2n\pi}{3} + \sin\frac{5n\pi}{3} - \sin\frac{4n\pi}{3}\right)\cos n\delta_o + \\[3mm] \left(\cos\frac{n\pi}{3} + \cos n\pi - \cos\frac{2n\pi}{3} + \cos\frac{5n\pi}{3} - \cos\frac{4n\pi}{3} - 1\right)\sin n\delta_o \end{bmatrix}$$

when n = 1:

$$a_1 = \frac{1}{\pi} \begin{bmatrix} \left(\sin\frac{\pi}{3} - \sin\frac{2\pi}{3} + \sin\frac{5\pi}{3} - \sin\frac{4\pi}{3}\right)\cos\delta_o + \\[3mm] \left(\cos\frac{\pi}{3} + \cos\pi - \cos\frac{2\pi}{3} + \cos\frac{5\pi}{3} - \cos\frac{4\pi}{3} - 1\right)\sin\delta_o \end{bmatrix}$$

$$a_1 = \frac{1}{\pi} \begin{bmatrix} \left(\sin\frac{\pi}{3} - \sin\frac{\pi}{3} - \sin\frac{\pi}{3} + \sin\frac{\pi}{3}\right)\cos\delta_o + \\[3mm] \left(\cos\frac{\pi}{3} - 1 + \cos\frac{\pi}{3} + \cos\frac{\pi}{3} + \cos\frac{\pi}{3} - 1\right)\sin\delta_o \end{bmatrix}$$

$$a_1 = 0$$

when n = 2:

$$a_2 = \frac{1}{2\pi} \begin{bmatrix} \left(\sin\frac{2\pi}{3} - \sin\frac{4\pi}{3} + \sin\frac{10\pi}{3} - \sin\frac{8\pi}{3}\right)\cos 2\delta_o + \\[3mm] \left(\cos\frac{2\pi}{3} + \cos 2\pi - \cos\frac{4\pi}{3} + \cos\frac{10\pi}{3} - \cos\frac{8\pi}{3} - 1\right)\sin 2\delta_o \end{bmatrix}$$

$$a_2 = \frac{1}{2\pi} \begin{bmatrix} \left(\sin\frac{\pi}{3} + \sin\frac{\pi}{3} - \sin\frac{\pi}{3} - \sin\frac{\pi}{3} \right)\cos 2\delta_o + \\ \left(-\cos\frac{\pi}{3} + 1 + \cos\frac{\pi}{3} - \cos\frac{\pi}{3} + \cos\frac{\pi}{3} - 1 \right)\sin 2\delta_o \end{bmatrix}$$

$$a_2 = 0$$

when n = 3:

$$a_3 = \frac{1}{3\pi} \begin{bmatrix} \left(\sin\frac{3\pi}{3} - \sin\frac{6\pi}{3} + \sin\frac{15\pi}{3} - \sin\frac{12\pi}{3} \right)\cos 3\delta_o + \\ \left(\cos\frac{3\pi}{3} + \cos 3\pi - \cos\frac{6\pi}{3} + \cos\frac{15\pi}{3} - \cos\frac{12\pi}{3} - 1 \right)\sin 3\delta_o \end{bmatrix}$$

$$a_3 = \frac{1}{3\pi} \begin{bmatrix} \left(\sin\pi - \sin 2\pi + \sin 5\pi - \sin 4\pi \right)\cos 3\delta_o + \\ \left(\cos\pi + \cos 3\pi - \cos 2\pi + \cos 5\pi - \cos 4\pi - 1 \right)\sin 3\delta_o \end{bmatrix}$$

$$a_3 = \frac{1}{3\pi} \left[(-1-1-1-1-1-1)\sin 3\delta_o \right]$$

$$a_3 = -\frac{6}{3\pi}\sin 3\delta_o$$

The coefficient b_n is given by

$$b_n = \frac{1}{\pi} \left[\int_{\delta_o}^{\frac{\pi}{3}+\delta_o} \sin n\theta d\theta + \int_{\frac{2\pi}{3}+\delta_o}^{\frac{3\pi}{3}+\delta_o} \sin n\theta d\theta + \int_{\frac{4\pi}{3}+\delta_o}^{\frac{5\pi}{3}+\delta_o} \sin n\theta d\theta \right] \qquad (5.96)$$

$$b_n = -\frac{1}{n\pi} \left[\left[\cos n\theta\right]_{\delta_o}^{\frac{\pi}{3}+\delta_o} + \left[\cos n\theta\right]_{\frac{2\pi}{3}+\delta_o}^{\frac{3\pi}{3}+\delta_o} + \left[\cos n\theta\right]_{\frac{4\pi}{3}+\delta_o}^{\frac{5\pi}{3}+\delta_o} \right]$$

$$b_n = -\frac{1}{n\pi}\left[\left[\left[\cos\left(\frac{n\pi}{3}+n\delta_o\right)-\cos n\delta_o\right]+\left[\cos\left(\frac{3n\pi}{3}+n\delta_o\right)-\cos\left(\frac{2n\pi}{3}+n\delta_o\right)\right]\right]+\left[\left[\cos\left(\frac{5n\pi}{3}+n\delta_o\right)-\cos\left(\frac{4n\pi}{3}+n\delta_o\right)\right]\right]\right]$$

$$b_n = -\frac{1}{n\pi}\left[\begin{array}{l}\cos\dfrac{n\pi}{3}\cos n\delta_o-\sin\dfrac{n\pi}{3}\sin n\delta_o-\cos n\delta_o+\\[2mm]\cos\dfrac{3n\pi}{3}\cos n\delta_o-\sin\dfrac{3n\pi}{3}\sin n\delta_o+\\[2mm]-\left[\cos\dfrac{2n\pi}{3}\cos n\delta_o-\sin\dfrac{2n\pi}{3}\sin n\delta_o\right]+\\[2mm]\cos\dfrac{5n\pi}{3}\cos n\delta_o-\sin\dfrac{5n\pi}{3}\sin n\delta_o+\\[2mm]-\left[\cos\dfrac{4n\pi}{3}\cos n\delta_o-\sin\dfrac{4n\pi}{3}\sin n\delta_o\right]\end{array}\right]$$

$$b_n = -\frac{1}{n\pi}\left[\begin{array}{l}\cos\dfrac{n\pi}{3}\cos n\delta_o-\sin\dfrac{n\pi}{3}\sin n\delta_o-\cos n\delta_o+\cos n\pi\cos n\delta_o-\sin n\pi\sin n\delta_o+\\[2mm]-\cos\dfrac{2n\pi}{3}\cos n\delta_o+\sin\dfrac{2n\pi}{3}\sin n\delta_o+\cos\dfrac{5n\pi}{3}\cos n\delta_o-\sin\dfrac{5n\pi}{3}\sin n\delta_o\\[2mm]-\cos\dfrac{4n\pi}{3}\cos n\delta_o+\sin\dfrac{4n\pi}{3}\sin n\delta_o\end{array}\right]$$

$$b_n = -\frac{1}{n\pi}\left[\begin{array}{l}\cos\dfrac{n\pi}{3}\cos n\delta_o-\sin\dfrac{n\pi}{3}\sin n\delta_o-\cos n\delta_o+\cos n\pi\cos n\delta_o+\\[2mm]-\cos\dfrac{2n\pi}{3}\cos n\delta_o+\sin\dfrac{2n\pi}{3}\sin n\delta_o+\cos\dfrac{5n\pi}{3}\cos n\delta_o-\sin\dfrac{5n\pi}{3}\sin n\delta_o\\[2mm]-\cos\dfrac{4n\pi}{3}\cos n\delta_o+\sin\dfrac{4n\pi}{3}\sin n\delta_o\end{array}\right]$$

$$b_n = -\frac{1}{n\pi}\left[\begin{array}{l} \cos\dfrac{n\pi}{3}\cos n\delta_o + \cos n\pi \cos n\delta_o - \cos\dfrac{2n\pi}{3}\cos n\delta_o + \\[2mm] \cos\dfrac{5n\pi}{3}\cos n\delta_o - \cos\dfrac{4n\pi}{3}\cos n\delta_o + \\[2mm] -\cos n\delta_o - \sin\dfrac{n\pi}{3}\sin n\delta_o + \sin\dfrac{2n\pi}{3}\sin n\delta_o + \\[2mm] -\sin\dfrac{5n\pi}{3}\sin n\delta_o + \sin\dfrac{4n\pi}{3}\sin n\delta_o \end{array}\right]$$

$$b_n = -\frac{1}{n\pi}\left[\begin{array}{l} \left(\cos\dfrac{n\pi}{3} + \cos n\pi - \cos\dfrac{2n\pi}{3} + \cos\dfrac{5n\pi}{3} - \cos\dfrac{4n\pi}{3} - 1\right)\cos n\delta_o + \\[2mm] \left(-\sin\dfrac{n\pi}{3} + \sin\dfrac{2n\pi}{3} - \sin\dfrac{5n\pi}{3} + \sin\dfrac{4n\pi}{3}\right)\sin n\delta_o \end{array}\right]$$

when n = 1:

$$b_1 = -\frac{1}{\pi}\left[\begin{array}{l} \left(\cos\dfrac{\pi}{3} + \cos\pi - \cos\dfrac{2\pi}{3} + \cos\dfrac{5\pi}{3} - \cos\dfrac{4\pi}{3} - 1\right)\cos\delta_o + \\[2mm] \left(-\sin\dfrac{\pi}{3} + \sin\dfrac{2\pi}{3} - \sin\dfrac{5\pi}{3} + \sin\dfrac{4\pi}{3}\right)\sin\delta_o \end{array}\right]$$

$$b_1 = -\frac{1}{\pi}\left[\begin{array}{l} \left(\cos\dfrac{\pi}{3} - 1 + \cos\dfrac{\pi}{3} + \cos\dfrac{\pi}{3} + \cos\dfrac{\pi}{3} - 1\right)\cos\delta_o + \\[2mm] \left(-\sin\dfrac{\pi}{3} + \sin\dfrac{\pi}{3} + \sin\dfrac{\pi}{3} - \sin\dfrac{\pi}{3}\right)\sin\delta_o \end{array}\right]$$

$$b_1 = 0$$

when n = 2:

$$b_2 = -\frac{1}{2\pi}\left[\begin{array}{l} \left(\cos\dfrac{2\pi}{3} + \cos 2\pi - \cos\dfrac{4\pi}{3} + \cos\dfrac{10\pi}{3} - \cos\dfrac{8\pi}{3} - 1\right)\cos n\delta_o + \\[2mm] \left(-\sin\dfrac{2\pi}{3} + \sin\dfrac{4\pi}{3} - \sin\dfrac{10\pi}{3} + \sin\dfrac{8\pi}{3}\right)\sin n\delta_o \end{array}\right]$$

$$b_2 = -\frac{1}{2\pi}\left[\begin{array}{l}\left(-\cos\frac{\pi}{3}+1+\cos\frac{\pi}{3}-\cos\frac{\pi}{3}+\cos\frac{\pi}{3}-1\right)\cos 2\delta_o +\\[2mm] \left(-\sin\frac{\pi}{3}-\sin\frac{\pi}{3}+\sin\frac{\pi}{3}+\sin\frac{\pi}{3}\right)\sin 2\delta_o\end{array}\right]$$

$$b_2 = 0$$

when n = 3:

$$b_3 = -\frac{1}{3\pi}\left[\begin{array}{l}\left(\cos\frac{3\pi}{3}+\cos n\pi-\cos\frac{6\pi}{3}+\cos\frac{15\pi}{3}-\cos\frac{12\pi}{3}-1\right)\cos n\delta_o +\\[2mm] \left(-\sin\frac{3\pi}{3}+\sin\frac{6\pi}{3}-\sin\frac{15\pi}{3}+\sin\frac{12\pi}{3}\right)\sin n\delta_o\end{array}\right]$$

$$b_3 = -\frac{1}{3\pi}\left[\begin{array}{l}(\cos\pi+\cos 3\pi-\cos 2\pi+\cos\pi-\cos 2\pi-1)\cos 3\delta_o +\\[2mm](-\sin\pi+\sin\pi-\sin\pi+\sin 2\pi)\sin 3\delta_o\end{array}\right]$$

$$b_3 = -\frac{1}{3\pi}\left[(-1-1-1-1-1-1)\cos 3\delta_o\right]$$

$$a_3 = -\frac{6}{3\pi}\sin 3\delta_o$$

$$b_3 = \frac{6}{3\pi}\cos 3\delta_o$$

Thus in *Case V*,

$$\alpha = \frac{1}{2}+\frac{6}{3\pi}\left[-\sin 3\delta_o\cos 3\theta+\cos 3\delta_o\sin 3\theta\right]$$

$$\alpha = \frac{1}{2}+\frac{2}{\pi}\left[\sin 3\theta\cos 3\delta_o-\cos 3\theta\sin 3\delta_o\right] \tag{5.97}$$

$$\alpha = \frac{1}{2}+\frac{2}{\pi}\left[\sin(3\theta-3\delta_o)\right]$$

Therefore, the general expression for α from the cases above given by

$$\alpha = \frac{1}{2} + \frac{2}{\pi}\left[\sin(3\theta + 3\delta_o)\right] \tag{5.98}$$

The maximum and minimum values found similarly.

For the maximum value:

$$a_o = \frac{1}{2\pi}\left[3\sqrt{3}\mathrm{M}\right] = \frac{3\sqrt{3}\mathrm{M}}{2\pi} \; ; \; a_1 = 0 \; ; \; b_1 = 0 \; ; \; a_2 = 0 \; ; \; b_2 = 0 \; ; \; a_3 = 0 \; ; \; b_3 = -\frac{3\sqrt{3}M}{8}$$

$$m_{max} = \frac{3\sqrt{3}\mathrm{M}}{2\pi} - \frac{3\sqrt{3}M}{8}\sin 3\theta \tag{5.99}$$

For the minimum value:

$$a_o = -\frac{1}{2\pi}\left[3\sqrt{3}\mathrm{M}\right] = -\frac{3\sqrt{3}\mathrm{M}}{2\pi} \; ; \; a_1 = 0 \; ; \; b_1 = 0 \; ; \; a_2 = 0 \; ; \; b_2 = 0 \; ; \; a_3 = 0 \; ; \; b_3 = -\frac{3\sqrt{3}M}{8}$$

$$m_{min} = -\frac{3\sqrt{3}\mathrm{M}}{2\pi} - \frac{3\sqrt{3}M}{8}\sin 3\theta \tag{5.100}$$

Substituting the values of α, m_{max} and m_{min} into the expression for the zero sequence modulation signal,

$$m_o = 1 - 2\alpha + (\alpha - 1)m_{max} - \alpha\, m_{min}$$

$$m_o = 1 - 2\alpha + (\alpha - 1)\left(\frac{3\sqrt{3}\mathrm{M}}{2\pi} - \frac{3\sqrt{3}M}{8}\sin 3\theta\right) - \alpha\left(-\frac{3\sqrt{3}\mathrm{M}}{2\pi} - \frac{3\sqrt{3}M}{8}\sin 3\theta\right)$$

$$m_o = 1 - 2\alpha - \left(\frac{3\sqrt{3}\mathrm{M}}{2\pi} - \frac{3\sqrt{3}M}{8}\sin 3\theta\right) + \frac{3\sqrt{3}\mathrm{M}}{2\pi}\alpha - \frac{3\sqrt{3}M}{8}\alpha\sin 3\theta + \frac{3\sqrt{3}\mathrm{M}}{2\pi}\alpha + \frac{3\sqrt{3}M}{8}\alpha\sin 3\theta$$

$$m_o = \begin{bmatrix} 1 - 2\alpha - \left(\dfrac{3\sqrt{3}M}{2\pi} - \dfrac{3\sqrt{3}M}{8}\sin 3\theta \right) + \dfrac{3\sqrt{3}M}{2\pi}\alpha + \\[3mm] \dfrac{3\sqrt{3}M}{2\pi}\alpha - \dfrac{3\sqrt{3}M}{8}\alpha\sin 3\theta + \dfrac{3\sqrt{3}M}{8}\alpha\sin 3\theta \end{bmatrix}$$

$$m_o = 1 - 2\alpha - \left(\dfrac{3\sqrt{3}M}{2\pi} - \dfrac{3\sqrt{3}M}{8}\sin 3\theta \right) + \dfrac{3\sqrt{3}M}{\pi}\alpha$$

$$m_o = 1 - 3\sqrt{3}M\left(\dfrac{1}{2\pi} - \dfrac{1}{8}\sin 3\theta \right) + \left(\dfrac{3\sqrt{3}M}{\pi} - 2 \right)\alpha$$

$$m_o = 1 - 3\sqrt{3}M\left(\dfrac{1}{2\pi} - \dfrac{1}{8}\sin 3\theta \right) + \left(\dfrac{3\sqrt{3}M}{\pi} - 2 \right)\left(\dfrac{1}{2} + \dfrac{2}{\pi}\left[\sin(3\theta + 3\delta_o) \right] \right)$$

$$m_o = 1 - 3\sqrt{3}M\left(\dfrac{1}{2\pi} - \dfrac{1}{8}\sin 3\theta \right) + \left(\dfrac{3\sqrt{3}M}{\pi} - 2 \right)\left(\dfrac{1}{2} + \dfrac{2}{\pi}\left[\sin(3\theta + 3\delta_o) \right] \right) \tag{5.101}$$

If the modulation signals have a phase angle θ_{eo}, then the maximum and minimum reference voltages is given by

$$m^*_{max} = \dfrac{3\sqrt{3}M}{2\pi} - \dfrac{3\sqrt{3}M}{8}\sin(3\theta + 3\theta_{eo}) \tag{5.102}$$

$$m^*_{min} = -\dfrac{3\sqrt{3}M}{2\pi} - \dfrac{3\sqrt{3}M}{8}\sin(3\theta + 3\theta_{eo}) \tag{5.103}$$

Now that the expressions for α, m^*_{max} and m^*_{min} in the 2-level converter are known, the corresponding expressions for the Nine-switch converter are found using (5.77) and (5.78).

5.2.2.4. **Generating switching pulses.** It has already been justified that the switching constraints of the Nine-switch converter is given by (5.1) as well as (5.41) if independent control of the two output voltages are required. With the modulation signals

186

defined by (5.70) and (5.71), the switching pulses can be generated by comparing with high frequency triangular carrier signal. But unlike in the simple comparison between one modulation signal and carrier signal, in the Nine-switch converter two modulations signals representing the upper and lower switches are compared with one triangular carrier as shown in Figure 5.11. The principle of generating the switching pulses to meet the dual objectives of satisfying the switching function constraint in (5.1) and (5.41) is given by

$$S_{ip} = \begin{cases} 1, & \text{when } M_{ip} \geq V_{tri} \\ 0, \text{every where else} \end{cases} \tag{5.104}$$

$$S_{in} = \begin{cases} 1, & \text{when } M_{in} \leq V_{tri} \\ 0, \text{every where else} \end{cases} \tag{5.105}$$
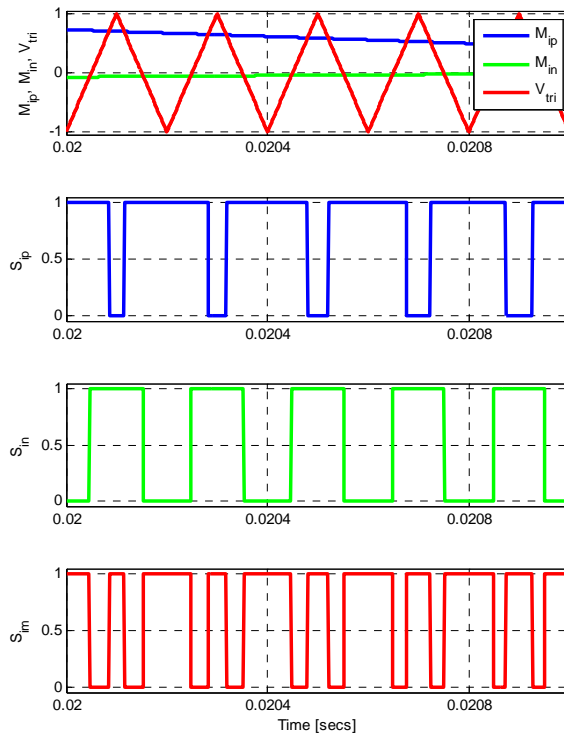
Figure 5.11.   Generation of device gate switching pulses

$$S_{ip} = 2 - S_{ip} - S_{in} \qquad (5.106)$$

where M_{ip}, M_{in} are, respectively, the modulation signals of the upper and bottom devices and V_{tri} is the high frequency triangular signal. M_{ip} is always greater than M_{in} and this has been made possible by the zero sequence voltage injection into the reference modulation signals.

5.2.3. Discontinuous PWM (DPWM)

5.2.3.1.Modulation principle. In discontinuous PWM methods for the 2-level converter, the zero sequence signals are used to modify the modulation signals clamping them to the positive or negative peak of the triangular carrier signal. The result is that the inverter phase legs are clamped to either the positive or negative DC rail for 120° portion of the fundamental period. In the most popular DPWM methods, the 120° clamping segment may be done in a single segment (120° DPWM) or divided into 2 or 4 separate segments (60° and 30° DPWM respectively).

Equation (5.37) represents the zero sequence voltages of the NSC. Variants of DPWMs may be achieved by eliminating either 1 or 2 of the 3 zero space vectors as shown in Table 5.13. This may be done in 2 ways; eliminate the same zero vector(s) throughout a switching cycle or alternately eliminate different zero space vector(s) during the fundamental period. For example, if only a single zero vector is to be applied, either mode *a(i)*, or *a(ii)* or *a(iii)* only is used in a switching cycle but not a combination of them. In the 2nd scenario of applying a single zero vector, *a(i)* , *a(ii)* , and *a(iii)* are.

188

Table 5.13. Zero voltage utilization (0 = unutilized zero vector; 1= utilized zero vector)

α	β	γ	Mode
0	0	1	*a(i)*
0	1	0	*a (ii)*
0	1	1	*b(i)*
1	0	0	*a (iii)*
1	0	1	*b(ii)*
1	1	0	*b(iii)*
1	1	1	*(c)*

alternately used within the switching cycle. Equation (5.107) and (5.108) may be used to implement the two scenarios

When (5.107) is used; only 1 zero vector is applied at a time but alternates between all 3 zero vectors within the fundamental period. However, if (5.108) is used, 1 or 2 zero vectors are alternately eliminated within the switching period.

$$
\left.\begin{aligned}
\alpha &= \frac{1}{2}[1 + \mathrm{sgn}((\cos 3(\omega_1 t + \delta_1)))] \\
\beta &= \frac{1}{2}[1 + \mathrm{sgn}((\cos 3(\omega_2 t + \delta_2)))](1 - \alpha) \\
\alpha &+ \beta + \gamma = 1
\end{aligned}\right\}
\tag{5.107}
$$

$$
\left.\begin{aligned}
\alpha &= \frac{1}{4}[1 + \mathrm{sgn}((\cos 3(\omega_1 t + \delta_1)))] \\
\beta &= \frac{1}{4}[1 + \mathrm{sgn}((\cos 3(\omega_2 t + \delta_2)))] \\
\alpha &+ \beta + \gamma = 1
\end{aligned}\right\}
\tag{5.108}
$$

In (5.107) and (5.108) sgn(X) is 1, 0 or -1 for $X > 0$, $X = 0$ and $X < 0$, respectively; ω_1, ω_2, are the frequencies of the reference voltages of *NSC1* and *NSC2* respectively; δ_1 and δ_2 are their corresponding modulation control angles. The modulation angle may be varied giving rise to infinite DPWM methods.

5.2.3.2.**IGBT Power Losses.** Power losses in the IGBT consist of both conduction and switching losses in the IGBT proper and the anti-parallel diode. Switching losses occur every time an IGBT is turned on or off and it is therefore sufficient to draw conclusions from observing the length of DC clamping in the DPWM techniques to compare their losses. However, not the same can be said about the conduction losses. The power loss expressions in the IGBT (P_{IGBT}) and anti-parallel diode (P_D) can be approximated as [99]:

$$P_{IGBT} = \frac{I_{CM}}{4\pi} \int_0^\pi \left(\frac{V_{CEN} - V_{CE0}}{I_{CN}} I_{CM} \sin^2 \varphi + V_{CE0} \sin \varphi \right)[1 + MF(\varphi + \theta)]d\varphi \tag{5.109}$$

$$P_D = \frac{I_{CM}}{4\pi} \int_0^\pi \left(\frac{V_{FN} - V_{F0}}{I_{CN}} I_{CM} \sin^2 \varphi + V_{F0} \sin \varphi \right)[1 - MF(\varphi + \theta)]d\varphi \tag{5.110}$$

where F represent the modulation function applied to the top, bottom or middle devices and are given respectively by:

$$F(\varphi_1 + \theta_1) = 2V_{jn}^* / V_{dc} + 2V_{n0} / V_{dc} = m_{ip} + m_{no}$$

$$F(\varphi_2 + \theta_2) = 2V_{km}^* / V_{dc} + 2V_{m0} / V_{dc} = m_{in} + m_{mo} \tag{5.111}$$

$$F(\varphi_1 + \theta_1, \varphi_2 + \theta_2) = 1 - (m_{ip} + m_{no} + m_{in} + m_{mo})$$

M is the magnitude of the modulation signal, I_{CM} is the maximum collector current, I_{CN} and V_{CEN} are the rated manufacturer's collector current and collector-to-emitter voltage, respectively; V_{CEO} is the threshold collector-to-emitter voltage, V_{FN} is the diode forward voltage at the rated current, V_{FO} is the diode threshold voltage, φ is the phase angle of the load current, θ is the load power factor angle.

Earlier in (5.77) and (5.78), it was found that the expressions of the normalized neutral voltages are:

$$m_{no} = m_{o1} + \alpha\left(m_{\max 2}^{*} - m_{\min 2}^{*}\right) \tag{5.112}$$

$$m_{mo} = m_{o2} + \beta\left(m_{\min 1}^{*} - m_{\max 2}^{*}\right) \tag{5.113}$$

The maximum and minimum modulation signals ($m_{\max}^{*}$ and $m_{\min}^{*}$) can be approximated using Fourier series resulting into the following expressions:

$$m_{\max 1}^{*} = \frac{3\sqrt{3}M_1}{2\pi} - \frac{3\sqrt{3}M_1}{8}\sin(3\varphi_1 + 3\varphi_{o1} + 3\theta_1) \tag{5.114}$$

$$m_{\min 1}^{*} = -\frac{3\sqrt{3}M_1}{2\pi} - \frac{3\sqrt{3}M_1}{8}\sin(3\varphi_1 + 3\varphi_{o1} + 3\theta_1) \tag{5.115}$$

$$m_{\max 2}^{*} = \frac{3\sqrt{3}M_2}{2\pi} - \frac{3\sqrt{3}M_2}{8}\sin(3\varphi_2 + 3\varphi_{o2} + 3\theta_2) \tag{5.116}$$

$$m_{\min 2}^{*} = -\frac{3\sqrt{3}M_2}{2\pi} - \frac{3\sqrt{3}M_2}{8}\sin(3\varphi_2 + 3\varphi_{o2} + 3\theta_2) \tag{5.117}$$

where φ_1 is the phase angle of the load current for the load being supplied by *NSC1*, φ_{o1} is the initial angle of the reference load voltage for *NSC1*, θ_1 is the power factor angle for *NSC1*; φ_2 is the phase angle of the load current for the load being supplied by *NSC2*, φ_{o2}

is the initial angle of the reference load voltage for *NSC2*, θ_2 is the power factor angle for *NSC2*; M_1 and M_2 are the modulation indices for *NSC1* and *NSC2* respectively.

5.2.3.3.**Analysis of IGBT Power Losses.** The Fourier approximation of α and β, assuming $\varphi_{o1} = \varphi_{o2} = 0°$, is given as :

$$\alpha = \frac{1}{2} + \frac{2}{\pi}[\sin(3\varphi_1 + 3\theta_1 + 3\delta_1)]$$

(5.118)

$$\beta = \left(\frac{1}{2} + \frac{2}{\pi}[\sin(3\varphi_2 + 3\theta_2 + 3\delta_2)]\right)$$

(5.119)

Substituting (5.114)-(5.119) into (5.112) and (5.113) as well as letting the two voltages references to be of equal frequency and amplitude for easy comparison of losses, the resulting normalized neutral voltage expressions are given by (5.120) and (5.121).

$$m_{no} = \begin{bmatrix} \frac{2}{\pi}\left(\frac{2\sqrt{3}M}{\pi} + \frac{3\sqrt{3}M}{\pi} - 2\right)\sin(3\varphi_1 + 3\theta_1 + 3\delta_1) + \\ \frac{3\sqrt{3}M}{8}\sin(3\varphi_1 + 3\theta_1) + \frac{3\sqrt{3}M}{\pi} \end{bmatrix}$$

(5.120)

$$m_{m0} = \begin{bmatrix} \left(-\frac{8}{\pi^2} + \frac{24\sqrt{3}}{\pi^3}M\right)\sin^2(3\varphi_1 + 3\theta_1 + 3\delta_1) + \\ \left(\frac{2}{\pi} - \frac{2\sqrt{3}}{\pi^2}M\right)\sin(3\varphi_1 + 3\theta_1 + 3\delta_1) + \\ +\frac{3\sqrt{3}}{8}M\sin(3\varphi_1 + 3\theta_1) - \frac{3\sqrt{3}}{2\pi}M + \\ +\frac{3\sqrt{3}}{\pi}\left(\frac{1}{2} + \frac{2}{\pi}[\sin(3\varphi_2 + 3\theta_2 + 3\delta_2)]\right) \end{bmatrix}$$

(5.121)

Substituting (5.120) and (5.121) into (5.111), the power loss expressions given in (5.109) and (5.110) after evaluating the integral expressions result into the conduction

192

power loss expressions given as in (5.122) - (5.127). In (5.122) - (5.127), the subscripts *igbt* and *d* refer the IGBT proper and the connected anti-parallel diode respectively; *p, m,* and *n* refer to the top, middle devices respectively.

From (5.122) - (5.127) it can be seen that at any given operating point, the IGBT conduction power losses are dependent on the device characteristics, the magnitude of the modulation signal, the power factor angle and the modulation control angle.

$$
P_{igbt,p} = \left[\begin{array}{l} V_{ce0}I_{cm}(4\pi + 6\sqrt{3}M_1^2 + \pi^2 M_1^2\cos(\theta_1))/(8\pi^2) \\ -(V_{ce0}-V_{cen})I_{cm}^2 \left(\begin{array}{l} (30\pi^3 + 64M_1\pi\cos(3\theta_1+3\delta_1) + 80M_1^2\pi^2\cos(\theta_1) \\ -192\sqrt{3}M_1^2\cos(3\theta_1+3\delta_1) + 45\pi^2\sqrt{3}M_1^2 + \\ -6\sqrt{3}M_1^2\pi^2\cos(3\theta_1)) \end{array} \right)/(240\pi^3 I_{cn}) \end{array} \right]
\tag{5.122}
$$

$$
P_{d,p} = \left[\begin{array}{l} -V_{f0}I_{cm}(-4\pi + 6\sqrt{3}M_1^2 + \pi^2 M_1^2\cos(\theta_1))/(8\pi^2) \\ -(V_{f0}-V_{fn})I_{cm}^2 \left(\begin{array}{l} (30\pi^3 - 64\pi4_1\cos(3\theta_1+3\delta_1) - 80M_1^2\pi^2\cos(\theta_1) + \\ 192\sqrt{3}M_1^2\cos(3\theta_1+3\delta_1) - 45\pi^2\sqrt{3}M_1^2 + + 6\sqrt{3}M_1^2\pi^2\cos(3\theta_1)) \end{array} \right)/(240\pi^3 I_{cn}) \end{array} \right]
\tag{5.123}
$$

$$
P_{igbt,n} = \left[\begin{array}{l} (V_{ce0}I_{cm}(560\pi M_1 - 1680\sqrt{3}M_1^2 + 140\pi^3 + 210\pi^2\sqrt{3}M_1^2 + \\ +16\pi M_1\cos(6\theta_1+6\delta_1) - 48\sqrt{3}M_1^2\cos(6\theta_1+6\delta_1) - 35\pi^4 M_1^2\cos(\theta_1)))/(280\pi^4) \\ -(I_{CM}^2(Vce0-Vcen)(30\pi^4 + 120\pi^2 M_1 - 80\pi^3 M_1^2\cos(\theta_1) + \\ -360\pi\sqrt{3}M_1^2 + +32\pi^2 M_1\cos(3\theta_1+3\delta_1) - -96\pi\sqrt{3}M_1^2\cos(3\theta_1+3\delta_1) + \\ +6\pi^3\sqrt{3}M_1^2\cos(3\theta_1) + +45\pi^3\sqrt{3}M_1^2))/(240\pi^4 I_{cn}) \end{array} \right]
\tag{5.124}
$$

$$P_{d,n} = \begin{bmatrix} (V_{f0}I_{cm}(-560\pi M_1 + 1680\sqrt{3}M_1^2 + 140\pi^3 - 210\pi^2\sqrt{3}M_1^2 + \\ + 16\pi M_1\cos(6\theta_1 + 6\delta_1) + 48\sqrt{3}M_1^2\cos(6\theta_1 + 6\delta_1) + \\ 35\pi^4 M_1^2\cos(z1)))/(280\pi^4) - (I_{cm}^2(V_{f0} - V_{fn})(30\pi^4 + 120\pi^2 M_1 + 80\pi^3 M_1^2\cos(\theta_1) + \\ + 360\pi\sqrt{3}M_1^2 + -32\pi^2 M_1\cos(3\theta_1 + 3\delta_1) + 96\pi\sqrt{3}M_1^2\cos(3\theta_1 + 3\delta_1) + \\ -6\pi^3\sqrt{3}M_1^2\cos(3\theta_1) - 45\pi^3\sqrt{3}M_1^2))/(240\pi^4 I_{cn}) \end{bmatrix} \tag{5.125}$$

$$P_{igbt,m} = \begin{bmatrix} (((I_{cm}V_{ce0}\pi^3)/2 + 6\sqrt{3}M_1^2 V_{ce0}I_{cm} + (\pi^3 M_1 V_{ce0}I_{cm})/2 + \\ -2\pi M_1 V_{ce0}I_{cm} - (2\pi M_1 V_{ce0}I_{cm}\cos(6\theta_1 + 6\delta_1))/35 + \\ (6\sqrt{3}M_1^2 V_{ce0}I_{cm}\cos(6\theta_1 + 6\delta_1))/35 - 3\sqrt{3}\pi^2 M_1^2 V_{ce0}I_{cm})/2)/\pi^4 + \\ -((\pi^4 V_{ce0}I_{cm}^2)/8 - (\pi^4 V_{cen}I_{cm}^2)/8 - (\pi^2 M_1 V_{ce0}I_{cm}^2)/2 \\ + (\pi^2 M_1 V_{cen}I_{cm}^2)/2 + (3\pi\sqrt{3}M_1^2 V_{ce0}I_{cm}^2)/2 - (3\pi\sqrt{3}M_1^2 V_{cen}I_{cm}^2)/2 + \\ + (\pi^4 M_1 V_{ce0}I_{cm}^2)/8 - (\pi^4 M_1 V_{cen}I_{cm}^2)/8 \\ -(2\pi^2 M_1 V_{ce0}I_{cm}^2\cos(3\theta_1 + 3\delta_1))/5 + (2\pi^2 M_1 V_{cen}I_{cm}^2\cos(3\theta_1 + 3\delta_1))/5 + \\ + (6\pi\sqrt{3}I_{cm}^2 M_1^2 V_{ce0}\cos(3\theta_1 + 3\delta_1))/5 - (6\pi\sqrt{3}M_1^2 V_{cen}I_{cm}^2\cos(3\theta_1 + 3\delta_1))/5 + \\ -(3\pi^3\sqrt{3}M_1^2 V_{ce0}I_{cm}^2)/8 + (3\pi^3\sqrt{3}M_1^2 V_{cen}I_{cm}^2)/8)/(\pi^4 I_{cn})) \end{bmatrix} \tag{5.126}$$

$$P_{d,m} = \begin{bmatrix} (((I_{cm}V_{f0}\pi^3)/2 - 6\sqrt{3}M_1^2 V_{f0}I_{cm} - (\pi^3 M_1 V_{f0}I_{cm})/2 + 2\pi M_1 V_{f0}I_{cm} + \\ + (2\pi M_1 V_{ce0}I_{cm}\cos(6\theta_1 + 6\delta_1))/35 + \\ -(6\sqrt{3}M_1^2 V_{f0}I_{cm}\cos(6\theta_1 + 6\delta_1))/35 + 3\sqrt{3}\pi^2 M_1^2 V_{f0}I_{cm})/2)/\pi^4 + \\ -((\pi^4 V_{ce0}I_{cm}^2)/8 - (\pi^4 V_{cen}I_{cm}^2)/8 + (\pi^2 M_1 V_{ce0}I_{cm}^2)/2 \\ -(\pi^2 M_1 V_{cen}I_{cm}^2)/2 - (3\pi\sqrt{3}M_1^2 V_{ce0}I_{cm}^2)/2 + (3\pi\sqrt{3}M_1^2 V_{cen}I_{cm}^2)/2 + \\ -(\pi^4 M_1 V_{ce0}I_{cm}^2)/8 + (\pi^4 M_1 V_{cen}I_{cm}^2)/8 + (2\pi^2 M_1 V_{ce0}I_{cm}^2\cos(3\theta_1 + 3\delta_1))/5 + \\ -(2\pi^2 M_1 V_{cen}I_{cm}^2\cos(3\theta_1 + 3\delta_1))/5 - (6\pi\sqrt{3}I_{cm}^2 M_1^2 V_{ce0}\cos(3\theta_1 + 3\delta_1))/5 + \\ (6\pi\sqrt{3}M_1^2 V_{cen}I_{cm}^2\cos(3\theta_1 + 3\delta_1))/5 + (3\pi^3\sqrt{3}M_1^2 V_{ce0}I_{cm}^2)/8 - (3\pi^3\sqrt{3}M_1^2 V_{cen}I_{cm}^2)/8)/(\pi^4 I_{cn})) \end{bmatrix} \tag{5.127}$$

Figures 5.12 – 5.14 show the IGBT conduction losses as functions of the power factor angle and collect current at I_{cm} = 24 A. The IGBT manufacturer's catalogue test parameters are taken from IXXY's IXGN60N60C2D2. Its electrical characterisitcs are: V_{cen} = 2.5 V, V_{fn} = 2.2 V, V_{ce0} = 1.8 V, and I_{cn} = 60 A. Figure 5.12(a) show the losses of the top devices using SV-PWM ($\alpha = \beta$ = 1/3). Figure 5.12 (b) shows the corresponding losses using α and β expressions in (1.118) and (1.119). Similar depiction of the conduction losses for the middle and bottom devices is shown in Figures 5.13 and 5.14 respectively. The power factor angle is varied from -90° to 90° and the plots show the variation of the total IGBT conduction losses with the power factor angle. It can be shown that the total losses are almost independent of the modulation control angle. The minimum and maximum losses occur at unity power factor leading and unity power factor lagging respectively. The plots show that there that in terms of conduction losses, the proposed DPWM scheme does not have any significant advantage compared to the SV-PWM. Observe that the conduction loss in the anti-parallel diode is fairly significant and it would be erroneous to neglect its contribution in thermal design analysis.

5.2.3.4.**Voltage stress on the switching devices.** It can be shown that when a device is turned-off, the voltage across it is equal to the input DC voltage, Vdc. As an example consider the condition following combination of switches on all three phases (a, b and c): Sap = 0, San = 1, Sbp = 1, Sbn = 0, Scp =1 and Scn = 1. This represents the state U1 of Figure 5.3(a). Furthermore, it should be noted that Sam = 1, Sbm = 1 and Scm = 0 for the constraint in (5.1) to be met. Under such circumstances, an observation of Figure 5.1 will reveal that with this state, the voltage across the switches Tap, Tam, Tbn and Tcm will be equal to Vdc, whereas the voltage across the other switches will be zero.

Conduction loss, top devices T_{ip} [W]:SVPWM

(a)

Conduction loss, top devices T_{ip} [W]:DPWM
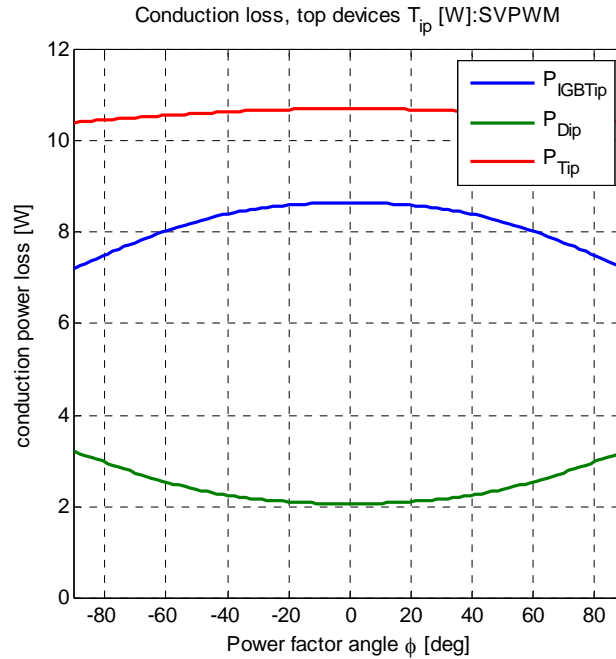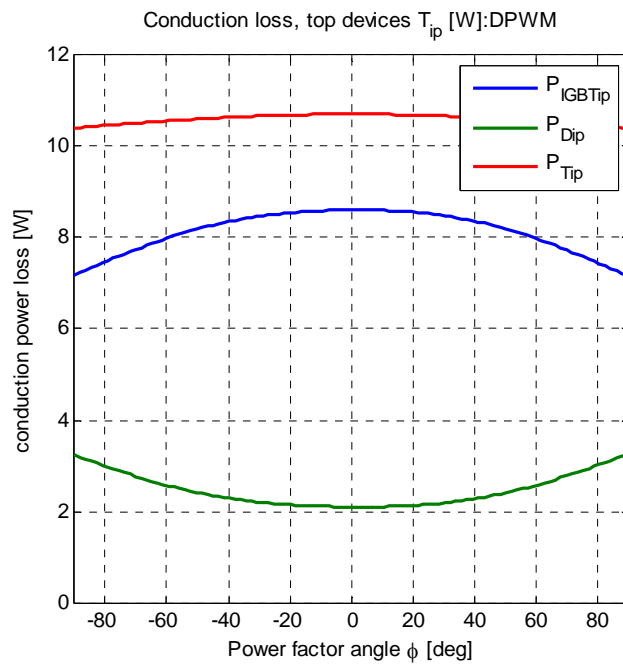
(b)

Figure 5.12.   IGBT conduction power losses of the top devices as a function of the power factor for (a) SV-PWM and (b) DPWM

Conduction loss, middle devices T_{im} [W]:SVPWM

(a)

Conduction loss, middle devices T_{im} [W]:DPWM
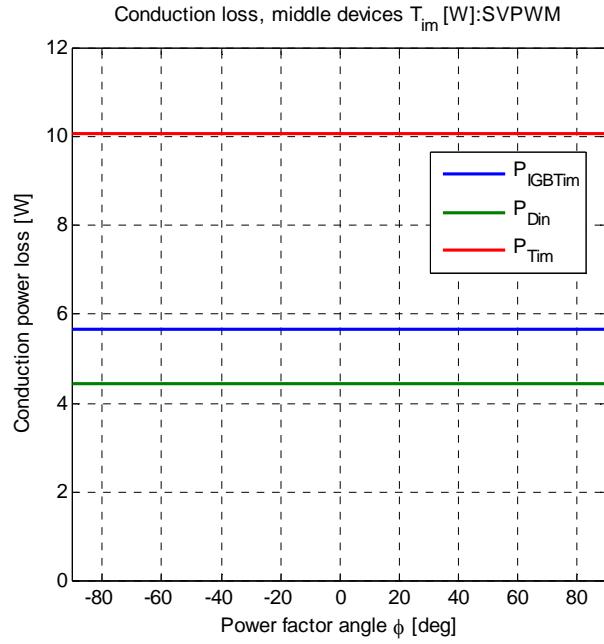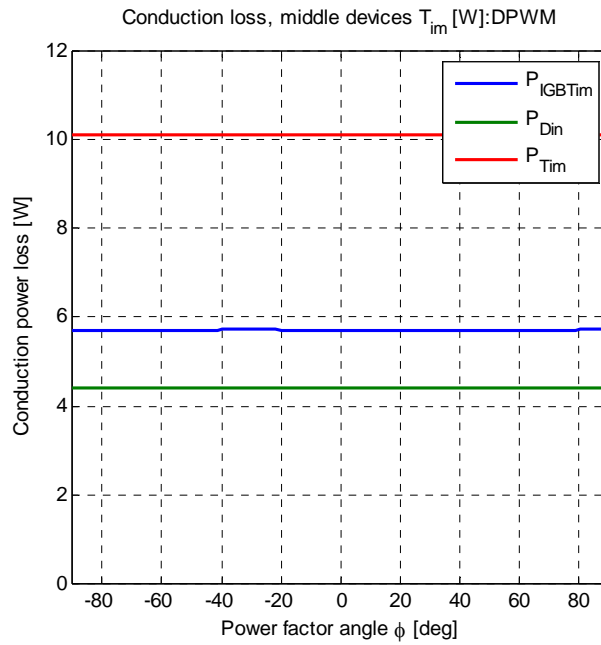
(b)

Figure 5.13.   IGBT conduction power losses of the middle devices as a function of the power factor for (a) SV-PWM and (b) DPWM

197
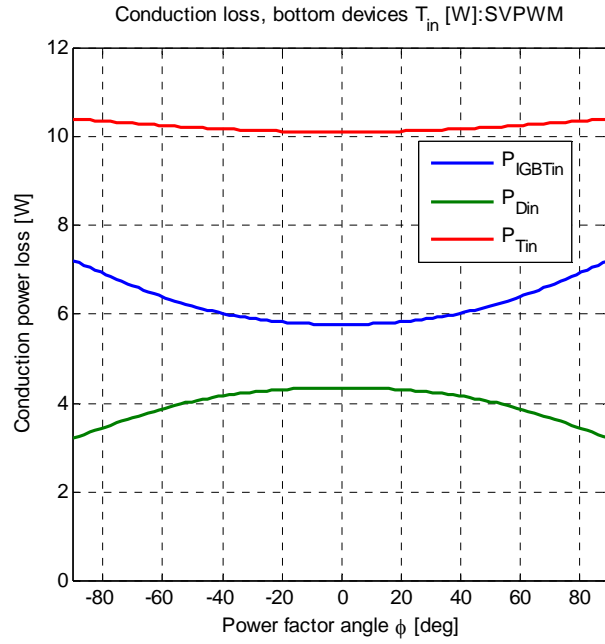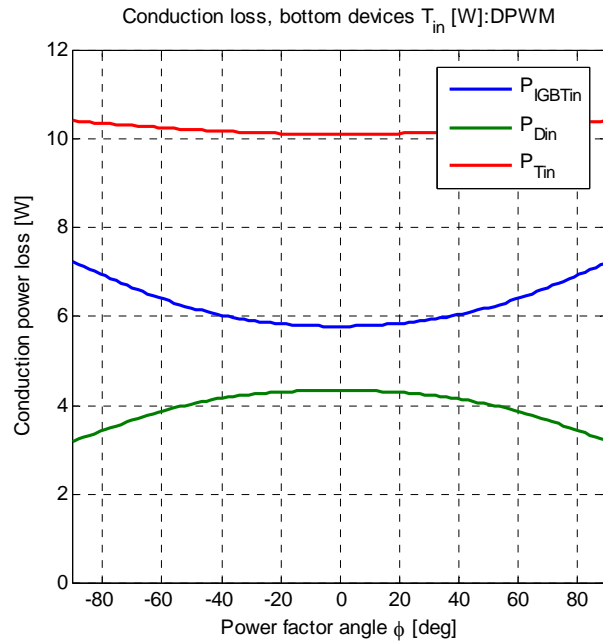
Figure 5.14.   IGBT conduction power losses of the bottom devices as a function of the power factor for (a) SV-PWM and (b) DPWM

Since at any particular switching condition, two switches will be on in one phase, using the per phase truth table, the voltage stress on each device in a leg can be determined in terms of the switching functions, as shown in Table 5.14 for phase 'a'. Figure 5.15 shows the simulation of the voltage stress on each device in a leg showing that the switching losses per cycle on the middle devices are about twice those of the top and bottom devices

Table 5.14. Calculating device voltage stress

State	S_{ip}	S_{im}	S_{in}	Device Voltage
1	0	1	1	$(1- S_{ip})V_{dc}$
2	1	0	1	$(1- S_{im})V_{dc}$
3	1	1	0	$(1- S_{in})V_{dc}$
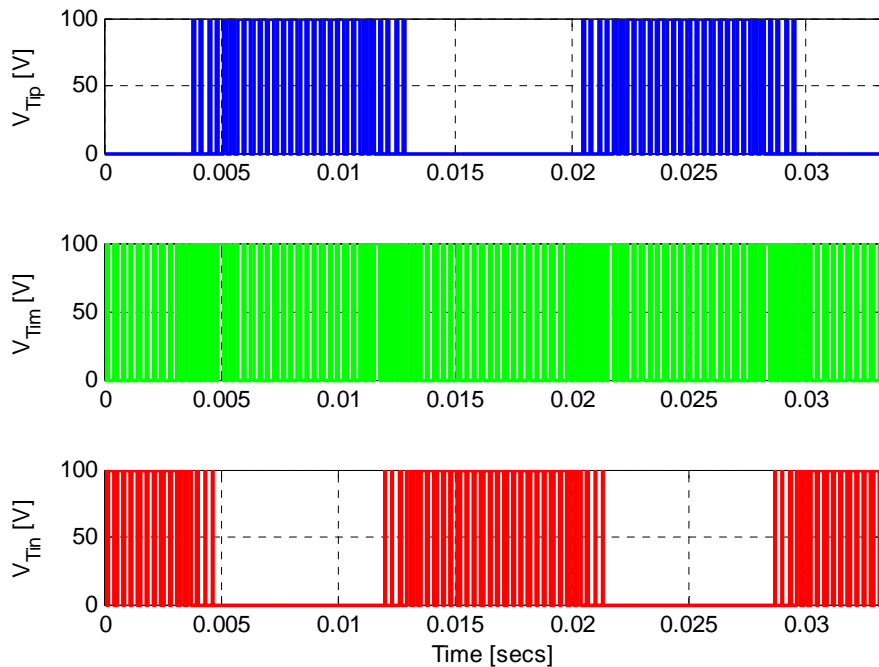
Figure 5.15.   Voltage stress on switching devices

5.3 Simulation and Experimental Results

Simulations were performed using Matlab/Simulink to validate the proposed PWM schemes. In the following simulations, the desired two sets of balanced 3-phase voltages, for phases '*abc*' and '*xyz*', respectively, to be synthesized are:

V_{an} = (50/√3) cos(2π60t), V_{bn} = (50/√3)cos (2π60t - 2π/3), V_{cn} = (50/√3)cos (2π60t + 2π/3); V_{xm} = (50/√3) cos (2π30t), V_{ym} = (50/√3)cos (2π30t -2π/3), V_{zm} = (50/√3) cos (2π30t +2π/3). The DC-link voltage of 100 V is used and therefore m_1 = m_2 = 1/√3, (where m_1 = peak($2V_{jn}/V_{dc}$) and m_2 = peak($2V_{km}/V_{dc}$) are the peaks of the reference modulation signals). The converter switching frequency chosen is 1 kHz. These simulations are performed for both SV-PWM and CB-PWM schemes.

5.3.1. SV- PWM

The implementation of the SV-PWM in MATLAB/Simulink consists of first identifying the sectors of the desired voltages to be synthesized. The time of application of active and zero vectors are then calculated and arranged according to the predefined switching pattern depicted in Figure 5.5. Figure 5.16 shows all the phase voltages for *NSC1* and *NSC2* produced using the proposed SV-PWM. The low frequency components of the synthesized voltages and the reference voltages have been superimposed. With α = β= γ = 1/3, Figure 5.16 shows that, the desired voltages have correctly been synthesized.
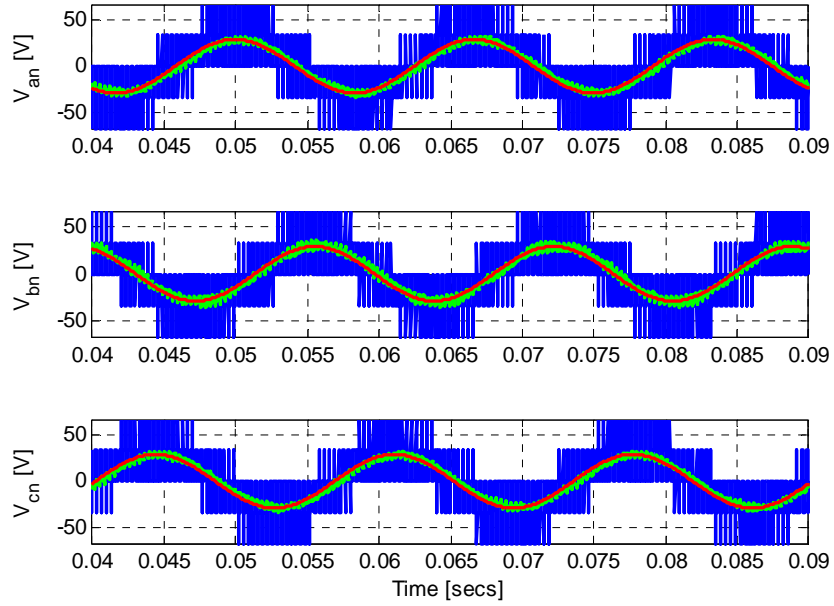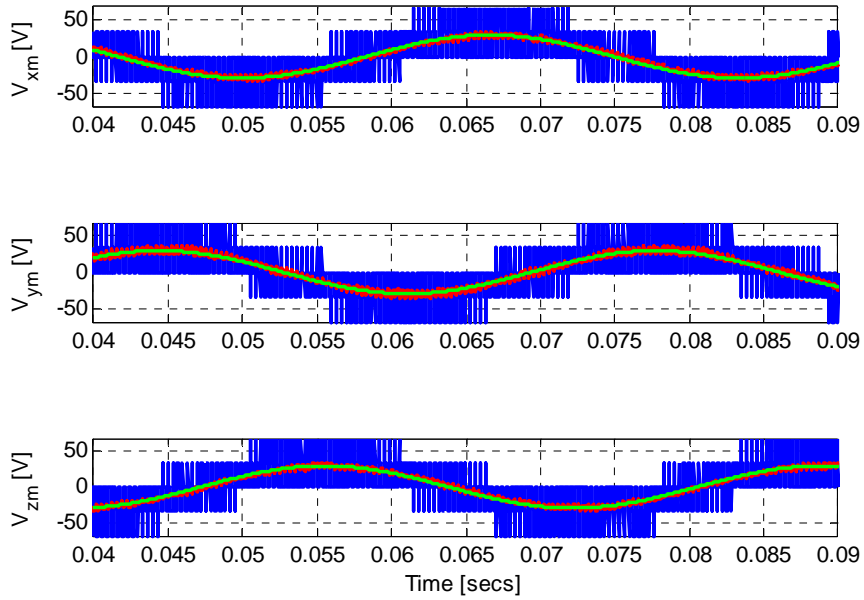
Figure 5.16.   Phase voltages with $\alpha = \beta = \gamma = 1/3$ for (a) *NSC1* output ($f_1 = 60$ Hz) and (b) *NSC2* output ($f_2 = 30$ Hz) using SV-PWM

5.3.2. Continuous CB-PWM (CPWM)

In general, there are three (3) zero vectors; and depending on the choice of the values for α, β and γ, all 3 zero vectors, or 2 zero vectors or 1 zero vector can be applied. Under all possibilities the sum of α, β and γ must be less than or equal to unity. For example when $\alpha = \beta = \gamma = 1/3$, the neutral voltages in (5.37) reduce to (5.128). This condition corresponds to the classical SV-PWM in the 2-level converter ($\alpha = \beta = \frac{1}{2}$).

$$\left.\begin{aligned} V_{n0} &= V_{dc}/6 - 1/3\,(2V_{max1} - V_{max2} + V_{min1} + V_{min2}) \\ V_{m0} &= -V_{dc}/6 - 1/3\,(V_{max1} + V_{max2} - V_{min1} + 2V_{min2}) \end{aligned}\right\} \tag{5.128}$$

Equation (5.37) represents the general DC offsets that must be added to the two sets of modulation signals so that the switching constraints are not violated. In particular if $\alpha = \beta = 0$ and $\gamma = 1$, the expressions in (5.37) reduce to (5.129) which are the same as those in [66] for discontinuous CB-PWM.

$$\left.\begin{aligned} V_{n0} &= V_{dc}/2 - V_{max1} \\ V_{m0} &= -V_{dc}/2 - V_{min2} \end{aligned}\right\} \tag{5.129}$$

Figure 5.17 shows the carrier based modulation signals corresponding to SV-PWM. The generated voltages are shown in Figure 5.18 with the low frequency components and reference voltages superimposed on each other. In the simulation, $\alpha = \beta = \gamma = 1/3$ (equivalent to SV-PWM) in (5.37) have been apportioned to synthesize the desired voltages. This equal apportioning of the zero vectors results in maximum voltage utilization for both *NSC1* and *NSC2*. By injecting the neutral voltages into the modulation scheme, the sum of the modulation indices is increased from unity to 1.155. The corresponding line-to-line voltages are shown in Figure 5.19
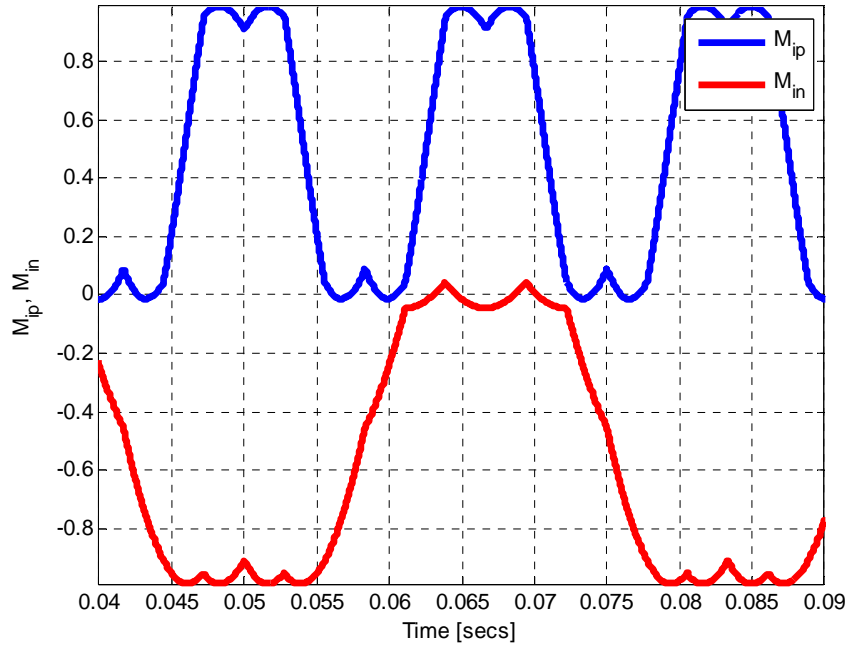
Figure 5.17. Modulation signals for top and bottom devices using continuous CB-PWM switches with $f_1 = 60$ Hz, $f_2 = 30$ Hz, and $\alpha = \beta = \gamma = 1/3$

5.3.3. Discontinuous CB-PWM (DPWM)

Figures 5.20 and 5.21 show the modulation signals of the proposed DPWM methods. In Figure 5.20(a), when $\gamma = 1$, both top and bottom signals are clamped to the peak of the triangular carrier, therefore there no switching losses during these clamped segments. However, if either $\alpha = 1$ or $\beta = 1$ as in Figures 5.20(b) and 5.20(c), only one set of signals experience the clamping. In other words, one set of modulation signals are continuous and the other discontinuous. Figure 2.21 shows the modulation signals when one or two of the 3 zero space vectors are alternately eliminated during the switching
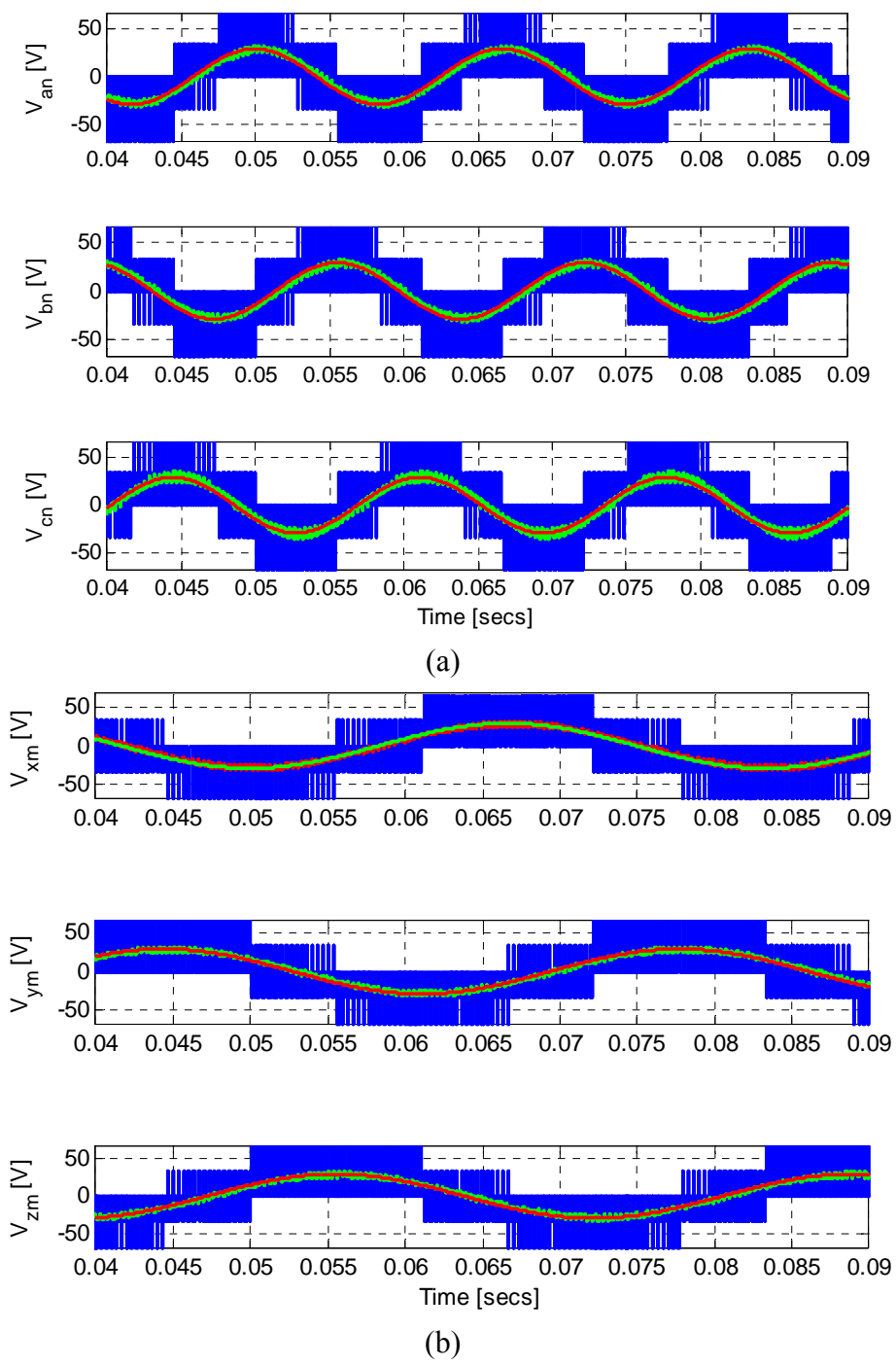
Figure 5.18.   Phase voltages with $\alpha = \beta = \gamma = 1/3$ for (a) *NSC1* output ($f_1 = 60$ Hz) and (b) *NSC2* output ($f_2 = 30$ Hz) using CPWM
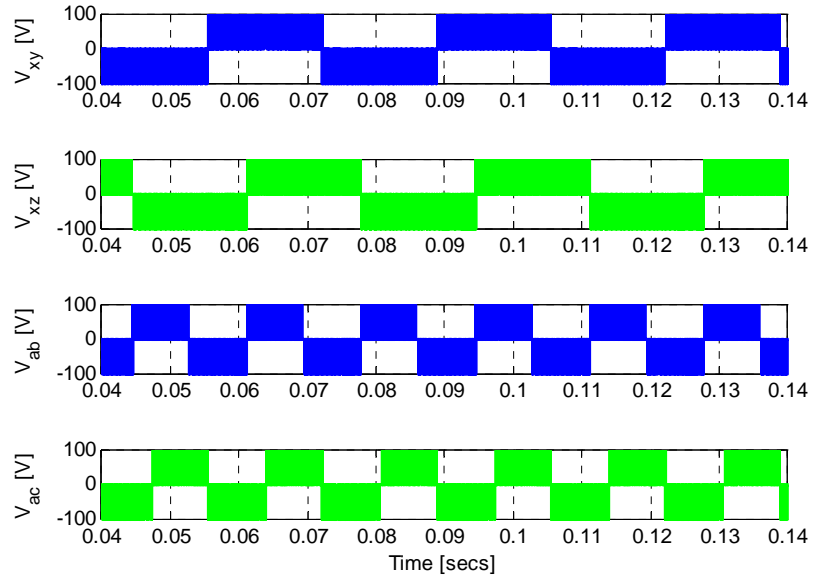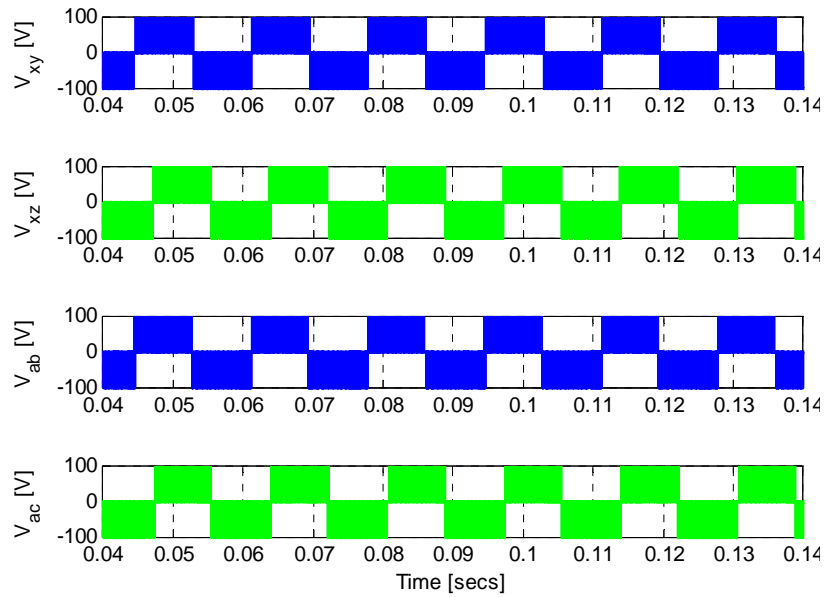
Figure 5.19. NSC line-to-line voltages with (a) $f_1 = 60$ Hz, $f_2 = 30$ Hz and(b) $f_1 = f_2 = 60$ Hz using CPWM

(a)

(b)

206
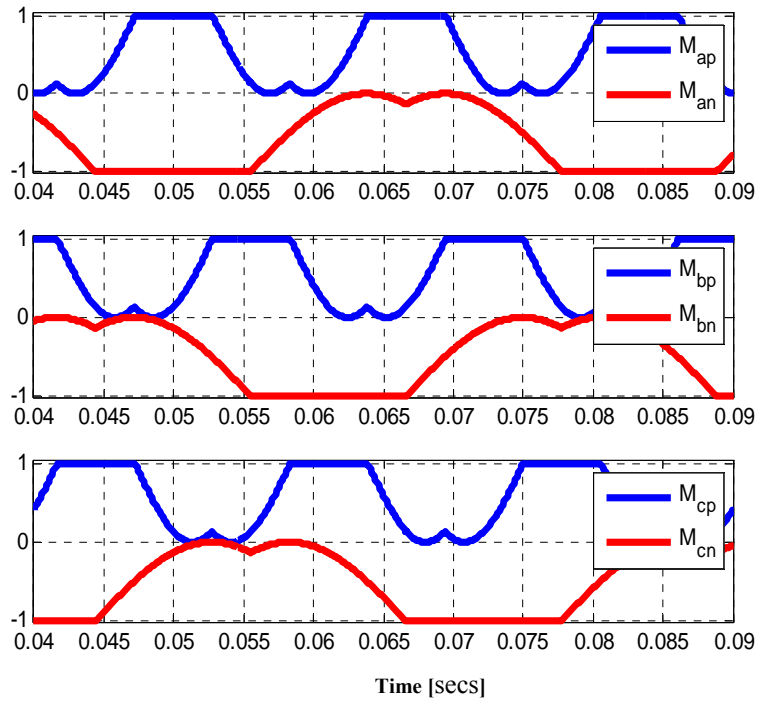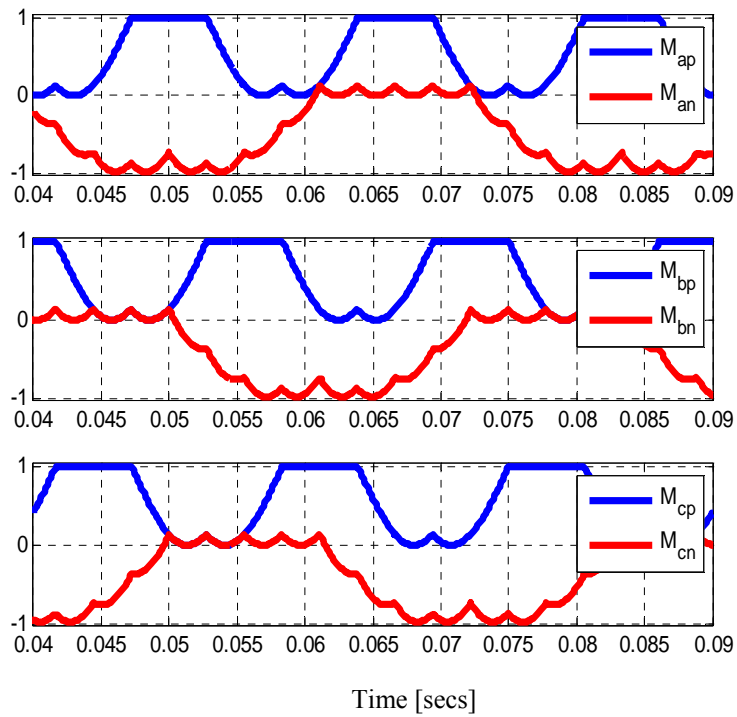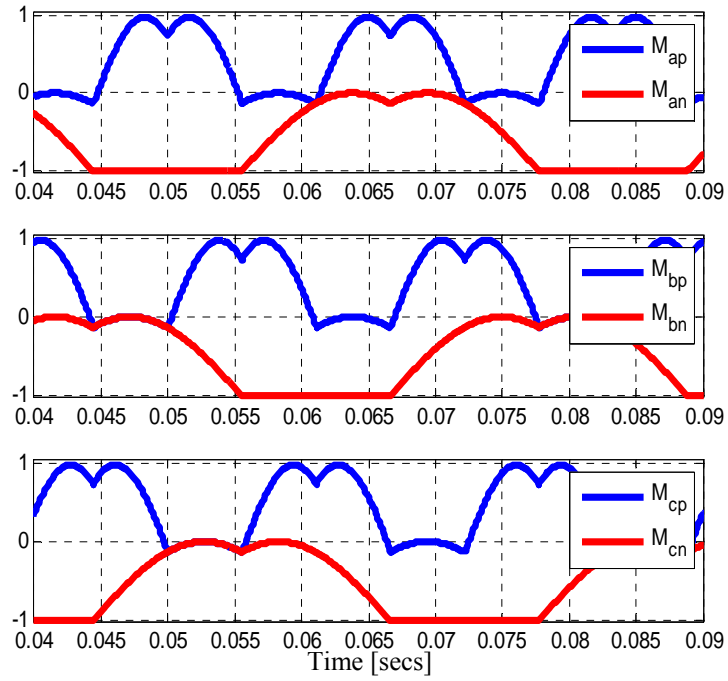
Figure 5.20. DPWM signals for (a) $\alpha = 0$, $\beta = 0$, $\gamma = 1$, (b) $\alpha = 0$, $\beta = 1$, $\gamma = 0$ and (c) $\alpha=1$, $\beta = 0$, $\gamma = 0$ with $f_1 = 60$ Hz, $f_2 = 30$ Hz, and $m_1 = m_2 = 1/\sqrt{3}$
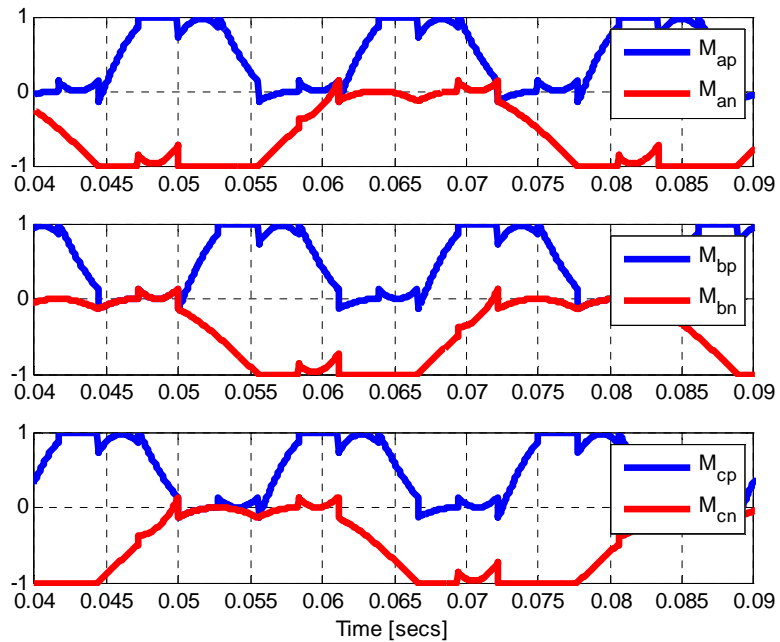
(a)
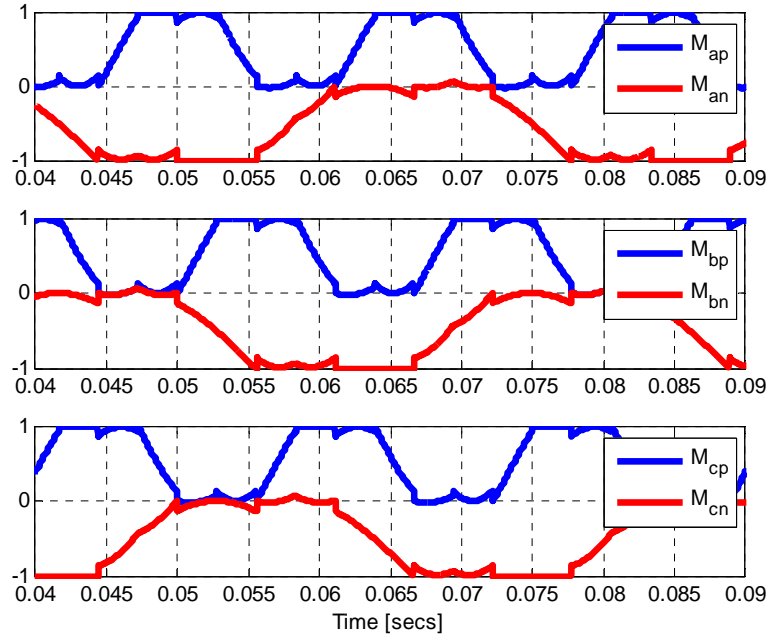
(b)

Figure 5.21.   DPWM modulation signals using (a) only one of α, β or, γ, and (b) only one and/or two of α, β, γ alternately in a switching cycle for $f_1 = 60$ Hz, $f_2 = 30$ Hz, $m_1 = m_2 = 1/\sqrt{3}$, , $\delta_1 = \delta_2 = 0^o$
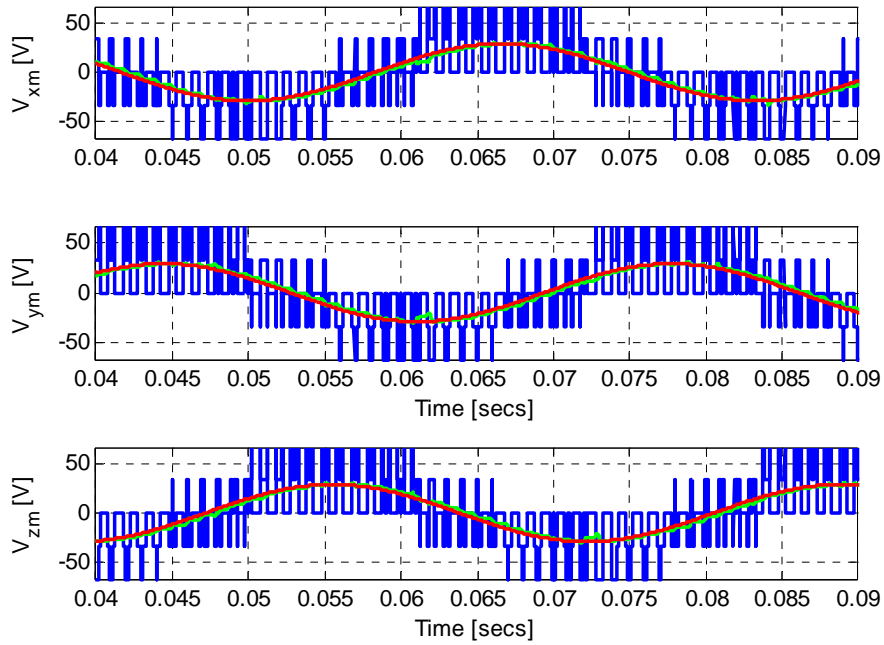
(a)
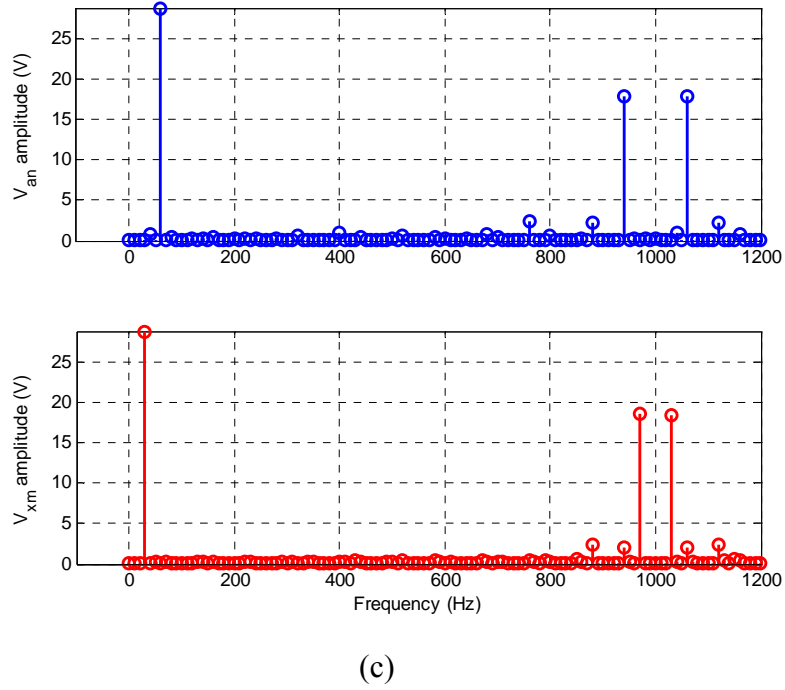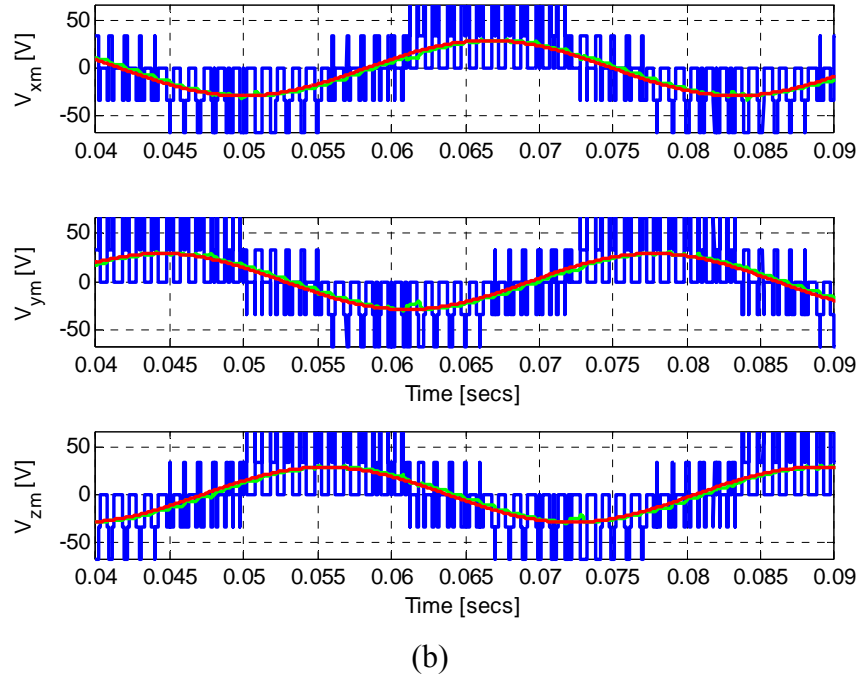
Figure 5.22. Phase voltages and harmonic spectra: (a) *NSC1* phase voltages V_{an}, V_{bn}, and V_{cn}, (b) *NSC2* phase voltages V_{xn}, V_{yn}, and V_{zm} and (c) the harmonic spectra of V_{an} and V_{xm} at the edge of linear modulation region ($m_1 = m_2 = 1/\sqrt{3}$, $f_1 = 60$ Hz, $f_2 = 30$ Hz, $\delta_1 = \delta_2 = 0^{\circ}$).

(a)

(b)

(c)
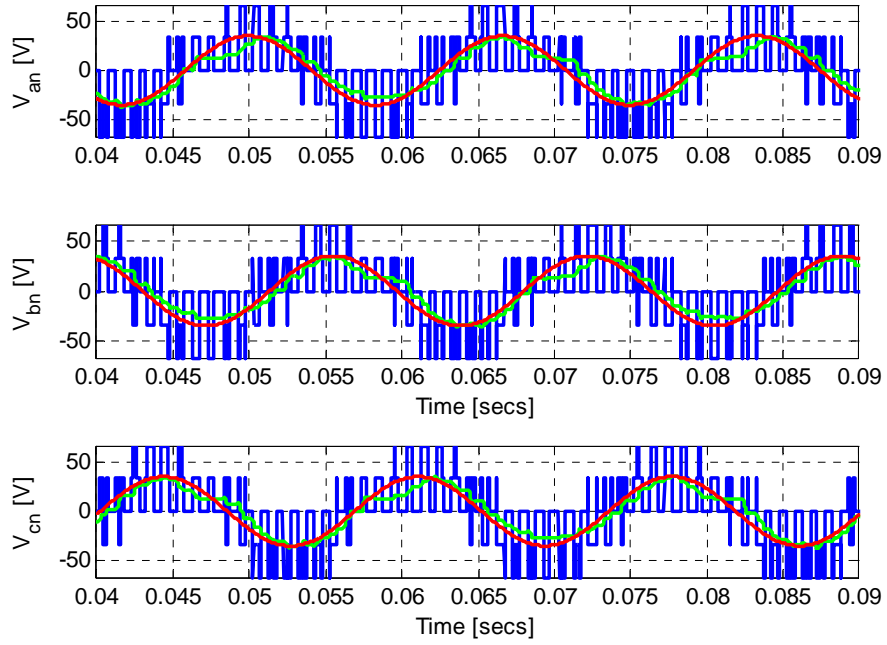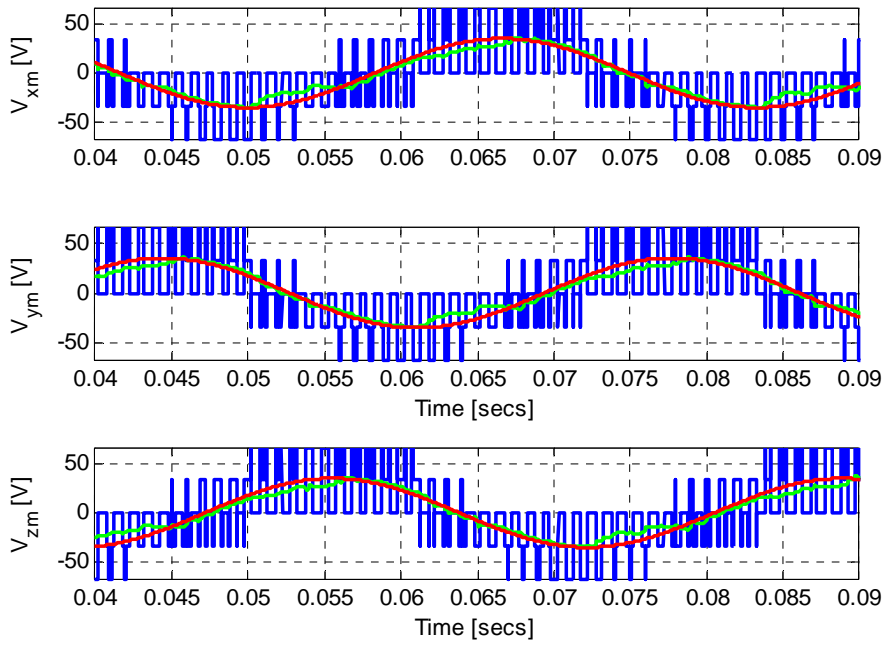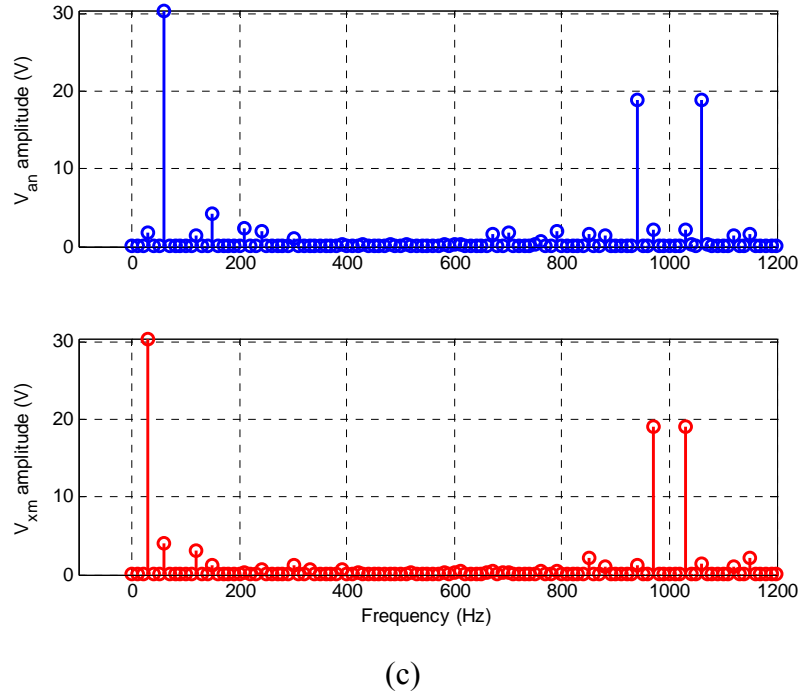
Figure 5.23. Phase voltages and harmonic spectra: (a) *NSC1* phase voltages V_{an}, V_{bn}, and V_{cn}, (b)) *NSC2* phase voltages V_{xn}, V_{yn}, and V_{zm} and (c) the harmonic spectra of V_{an} and V_{xm} in the over-modulation region ($m_1 = m_2 = 0.7$, $f_1 = 60$ Hz, $f_2 = 30$ Hz, $\delta_1 = \delta_2 = 0^o$).

cycle. Figure 5.22(a) and 5.22(c) show the phase voltages with the low frequency components of the synthesized voltages and the reference voltages superimposed on each other and their corresponding harmonic spectra in Figure 5.22(c). Observe that there are no low order harmonics and the dominant harmonics are centered on the converter switching frequency of 1k Hz, which are the same attributes observed in the conventional CPWM methods. The added advantage of using the DPWM methods is that the converter retains most of its characteristics as it moves into over-modulation. Figure 5.23 depict the phase voltages and the harmonic spectra when $\gamma = 0$ and $m_1 = m_2 = 0.7$. Observe that the gain in voltage magnitude is obtained at the expense of waveform quality and so as the

converter is operated deeper into the over-modulation region, the waveform degrades rapidly (see Figures 5.22(c) and 5.23(c)).

5.3.4. Common-Mode Voltages(CMVs)

The common mode voltage is the voltage difference between the neutral points of a load connected to the outputs of *NSC1* and *NSC2* and an arbitrary midpoint of the DC source. The NSC has 2 CMVs as shown in Figure 5. 1 and are expressed in terms of the switching functions of the top and bottom devices as:

$$V_{n0} = \frac{V_{dc}}{3}(S_{ap} + S_{bp} + S_{cp}) - \frac{V_{dc}}{2} \tag{5.130}$$

$$V_{m0} = -\frac{V_{dc}}{3}(S_{an} + S_{bn} + S_{cn}) + \frac{V_{dc}}{2} \tag{5.131}$$

Reference [106] shows that the CMV is highly dependent on the modulation method can only be reduced by avoiding the zero states. The simulations of the CMVs and their corresponding frequency spectra are shown in Figures 5.24 and 5.25 for CPWM and DPWM, respectively. The waveforms shown in Figure 5.25 apply $\delta_1 = 0$, $\delta_2 = 30^o$ and in such a case all three zero vectors are alternatively used. Observe that the FFT, Figure 5.25(b), is almost identical to that of the CPWM shown in Figure 5.24(b) but with reduced switching. There is no observed reduction in CMV because of the DPWM method used here simply alternates between different zero states intead of avoiding them altogeghter. However, the DPWM scheme used still has a superior performance in terms of the CMV compared to the CPWM method since switching losses are minimized while retaining identical frequency spectra as shown in Figures 5.24 (a) and 5.25 (b).
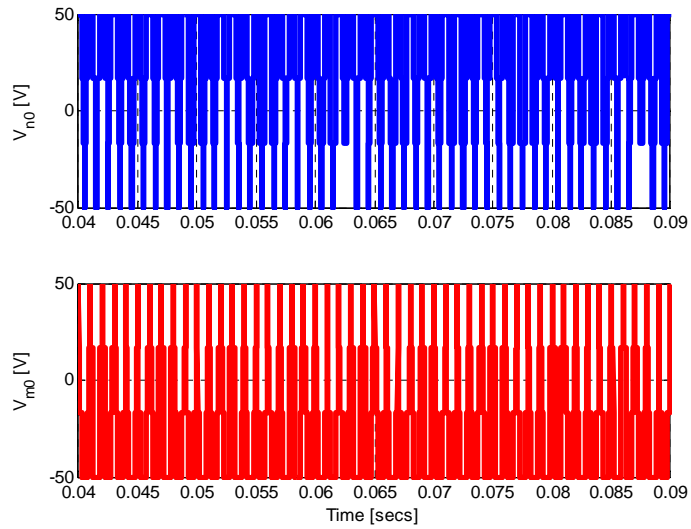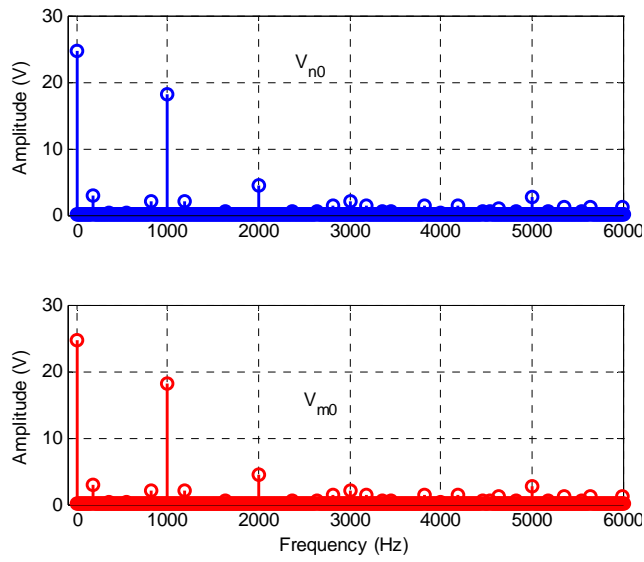
Figure 5.24. CMVs, V_{n0} and V_{m0} in (a) time domain and (b) FFT using CPWM with $\alpha = \beta = \gamma = 1/3$, $m_1 = m_2 = 1/\sqrt{3}$, $f_1 = f_2 = 60$Hz
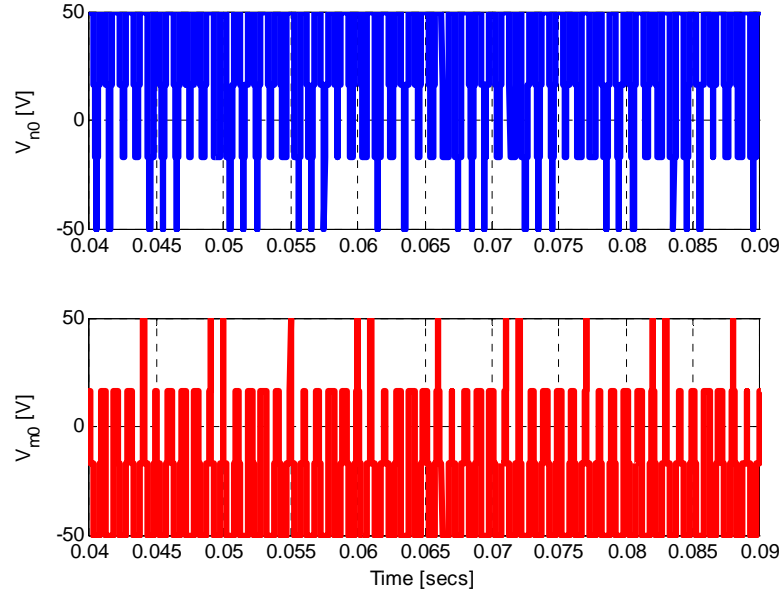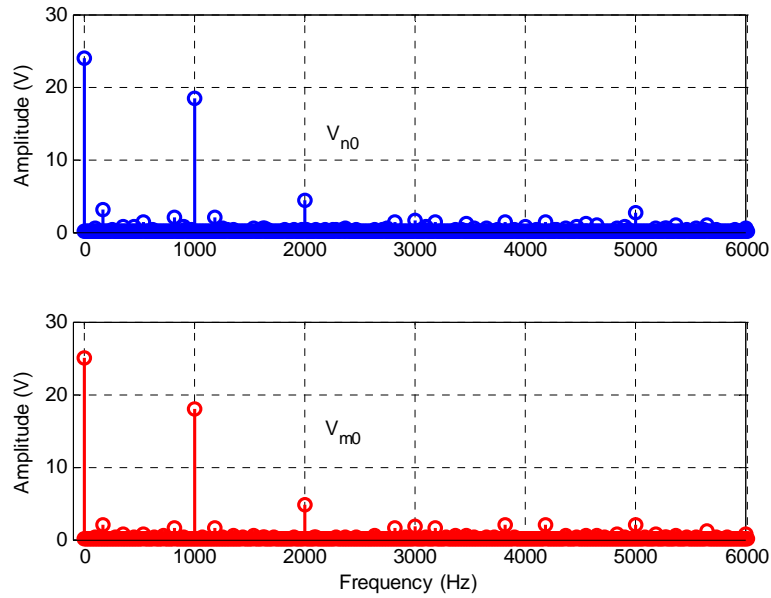
Figure 5.25. CMVs, V_{n0} and V_{m0} in (a) time domain and (b) FFT using DPWM, α, β, and γ defined by (5.107), $m_1 = m_2 = 1/\sqrt{3}$, $f_1 = f_2 = 60$Hz and $\delta_1 = 0$, $\delta_2 = 30^\circ$

Unlike in the conventional 2-level converter, the frequency spectra of the NSC show a large DC peak in addition to dominant peaks at the carrier frequency and its multiples. The appearance of this DC component can be explained by looking at the switching sequence in Figure 5.5. It is observed that the contributions of the zero sequence voltages by *NSC1* and *NSC2* on one another is always $+0.5V_{dc}$ and $-0.5V_{dc}$ respectively. Since the active switching states take a significant portion of the switching time, an effective DC component of the CMV appears. This a drawback of the converter, but in high frequency motor drive applications, the DC component produces negligible common-mode current since at low frequencies the common mode capacitance is effectively an open circuit.

5.3.5. Experimental Results

The assembled prototype of the NSC is shown in Figure 5.26. The gate PWM signals were generated using dSPACE ds1104 real-time controller. Using the assembled prototype, a 100V DC voltage was supplied to the converter with a balanced resistive load connected to the six phases in order to get access to the neutral point. However, the line-to-line voltages were measured at no-load. The experimental waveforms are shown in Figures 5.27-5.31. Figure 5.27 shows the matching experimental waveforms of the modulation signals of the upper and bottom switching devices, which are found to agree well with the simulation results in Figure 5.17.

Figure 5.28 and Figure 5.29 show the experimental waveform of the phase and line-to-line voltages corresponding to Figures 5.18 and 5.19 respectively. Observe that the two different frequencies have been produced and match well with simulation results. In Figures 5.30 and 5.31, the experimental waveforms of the phase and line-to-line voltages using the same frequency (60 Hz) for *NSC1* and *NSC2* are shown.

5.4 Summary

The space vector and a carrier-based modulation methodology for the NSC have been proposed. The generalized neutral voltages for the NSC have been derived for the first time in this research. Simulation results show that injecting these neutral voltages into the modulation signals would result in maximizing the NSC voltage capacity. The effect of neutral voltage injection on the CB-PWM scheme in particular is that the sum of the modulation indices is increased from unity to 1.155. The two 3-phase voltages have been correctly synthesized using both SV-PWM and CB-PWM modulation techniques. It has also been shown by simulation that the voltage stress on each device will be equal to the input dc voltage (V_{dc}), with the middle switching devices having about twice of the stress as that of either the top or bottom switching devices.
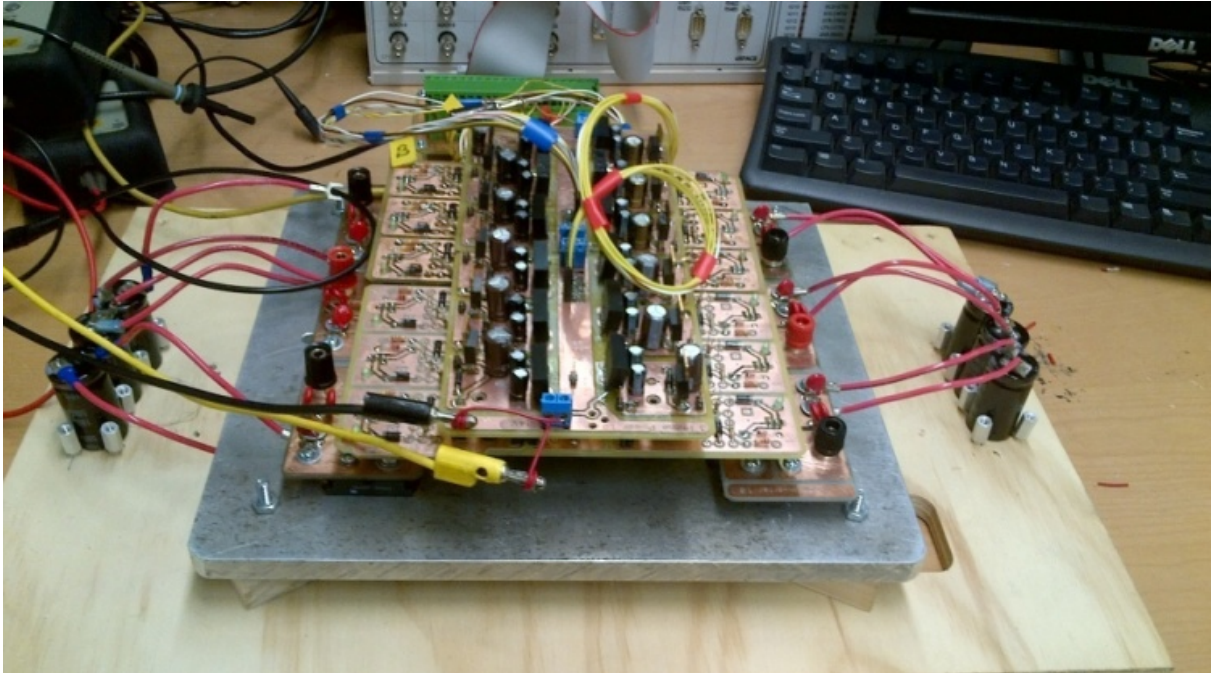
Figure 5.26.   Photogragh of prototype Nine-switch converter
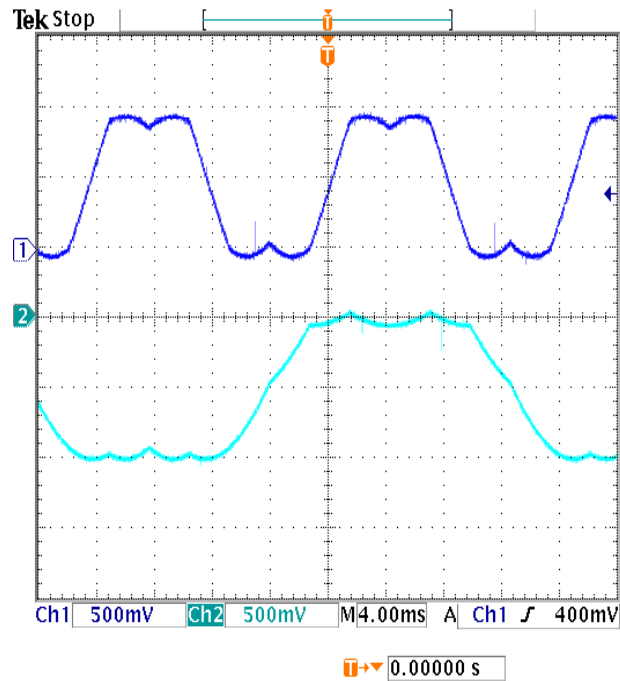
Figure 5.27.   CB-PWM signals of the upper and lower switches with f_1 = 60 Hz (Ch1), and f_2 = 30 Hz (Ch2), $\alpha = \beta = \gamma = 1/3$
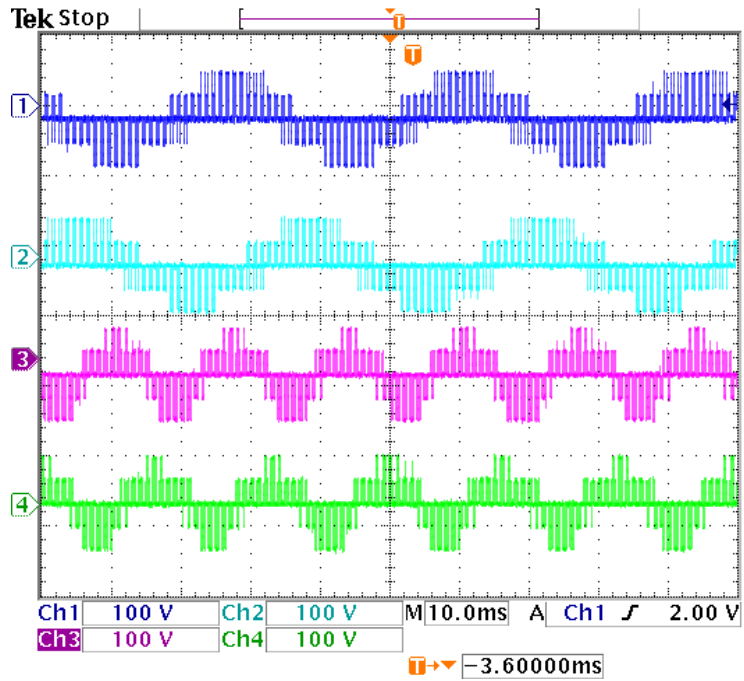
Figure 5.28. Phase voltages: Ch1, Ch2 - *NSC1* output (f_1 = 60 Hz) and for Ch3, Ch4 - *NSC2* output (f_2 = 30 Hz)
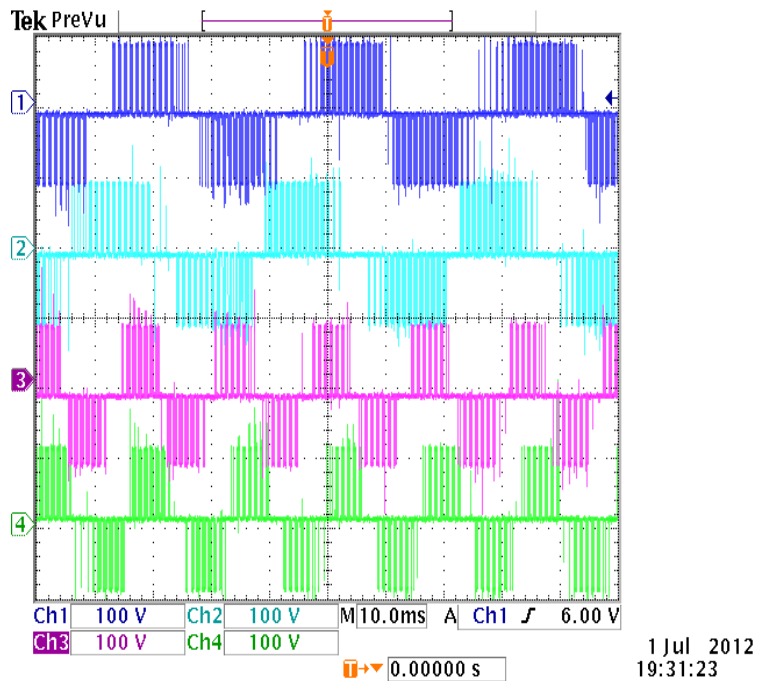
Figure 5.29. Line voltages: Ch1, Ch2 - *NSC1* output (f_1 = 60 Hz) and for Ch3, Ch4 - *NSC2* output (f_2 = 30 Hz)

218
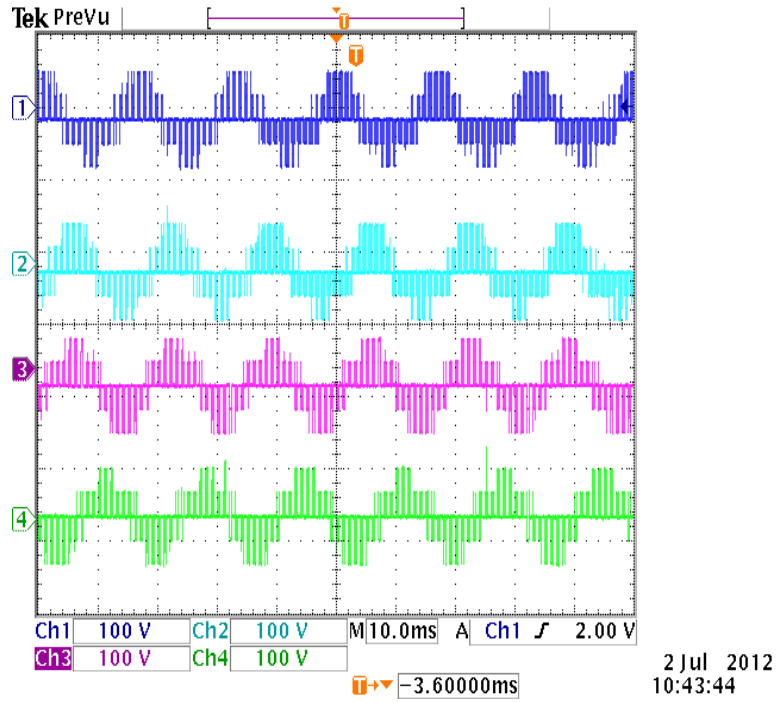
Figure 5.30.   Phase voltages: Ch1, Ch2 - *NSC1* output (f_1 = 60 Hz) and for Ch3, Ch4 - *NSC2* output (f_2 = 60 Hz)
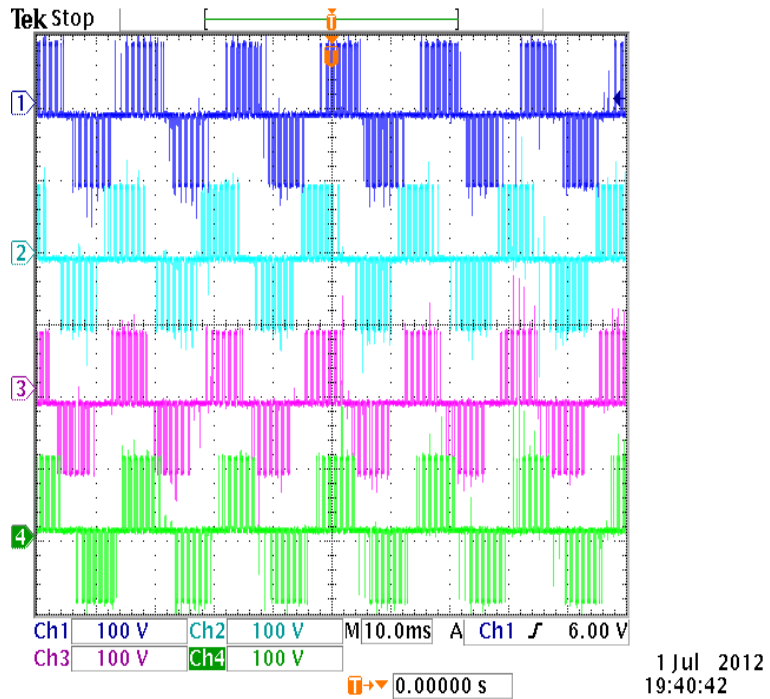
Figure 5.31.   Line voltages: Ch1, Ch2 - *NSC1* output (f_1 = 60 Hz) and for Ch3, Ch4 - *NSC2* output (f_2 = 60 Hz)

219

Different DC-clamping PWM methodologies for the Nine-switch converter have been proposed. The generalized neutral voltages for the NSC have been used to derive the generalized discontinuous PWM of the Nine-switch converter. Simulation results show that two sets of 3-phase voltages have been correctly synthesized by the proposed discontinuous PWM modulation techniques. It has also been shown, in this paper that, in fact, with an appropriate elimination of zero vectors, the converter's two sets of reference voltages may be controlled so that one operates in the continuous and the other in discontinuous PWM modes simultaneously. The DPWM methods have also shown to give good performance in the over-modulation region with its resultant increase in voltage gain and reduced IGBT power losses.

CHAPTER 6

GENERALIZED 3N+3-SWITCH CONVERTER

6.1 Introduction

The 3n+3-switch converter is a generalization of the Nine-switch converter introduced in Chapter 5 where 'n' is the number of 3-phase independent outputs. The concept of the 3n+3-switch converter was first introduced by Kominami and Fujimoto [42] but its modulation scheme has not been adequately studied. As is with most switch reduction converter topologies, a reduction in switch count is accompanied by some switching constraints as described in Chapter 5. In this chapter, the mathematical model of the 3n+3-converter is developed based on the Nine-switch converter and a 12-switch converter to be modeled in this chapter.

6.2 Structure and Switching Limitations

The topology of the generalized 3n+3-switch converter is shown in Figure 6.1 where 'n' is the number of 3-phase outputs. If n = 1; 2; or 3, a 6-switch, 9-switch or 12-switch converter is obtained as shown in Figures 6.2(a), (b), and (c) respectively. The 6-switch converter topology is same as the conventional 2-level converter whose operation
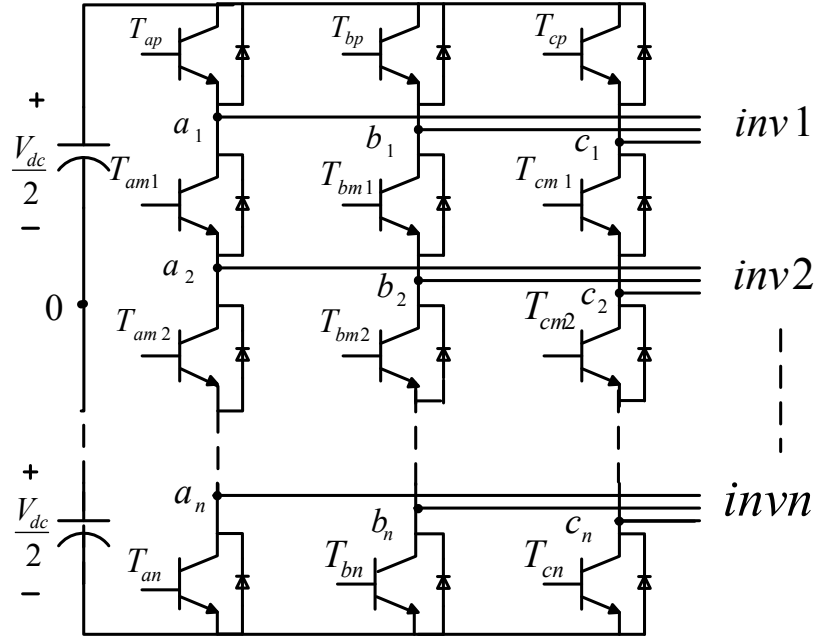
Figure 6.1. Schematic of proposed generalized 3n+3-converter

is well documented and there is no gain in reduced switch count. The Nine-switch converter has been investigated in Chapter 5 of this dissertation and the 12-switch converter is studied in this chapter.

Figure 6.2 (c) shows the structure of the proposed 12-switch converter, which is essentially an integration of three independent 2-level converters combined but differ in operational principle since some switching devices are being shared. The upper portion in Figure 6 (c) comprising the two topmost switching devices in each phase-leg (i.e., T_{ap}, T_{bp}, T_{cp} and T_{am1}, T_{bm1}, T_{cm1}), would henceforth be referred to as *Inv1*. The middle portion comprising the two inner devices in each phase-leg (i.e., T_{am1}, T_{bm1}, T_{cm1} and T_{am2}, T_{bm2}, T_{cm2}) is referred to as *Inv2* whereas *Inv3* comprise the two lower switching devices in each phase-leg (i.e., T_{am2}, T_{bm2}, T_{cm2} and T_{an}, T_{bn}, T_{cn}).
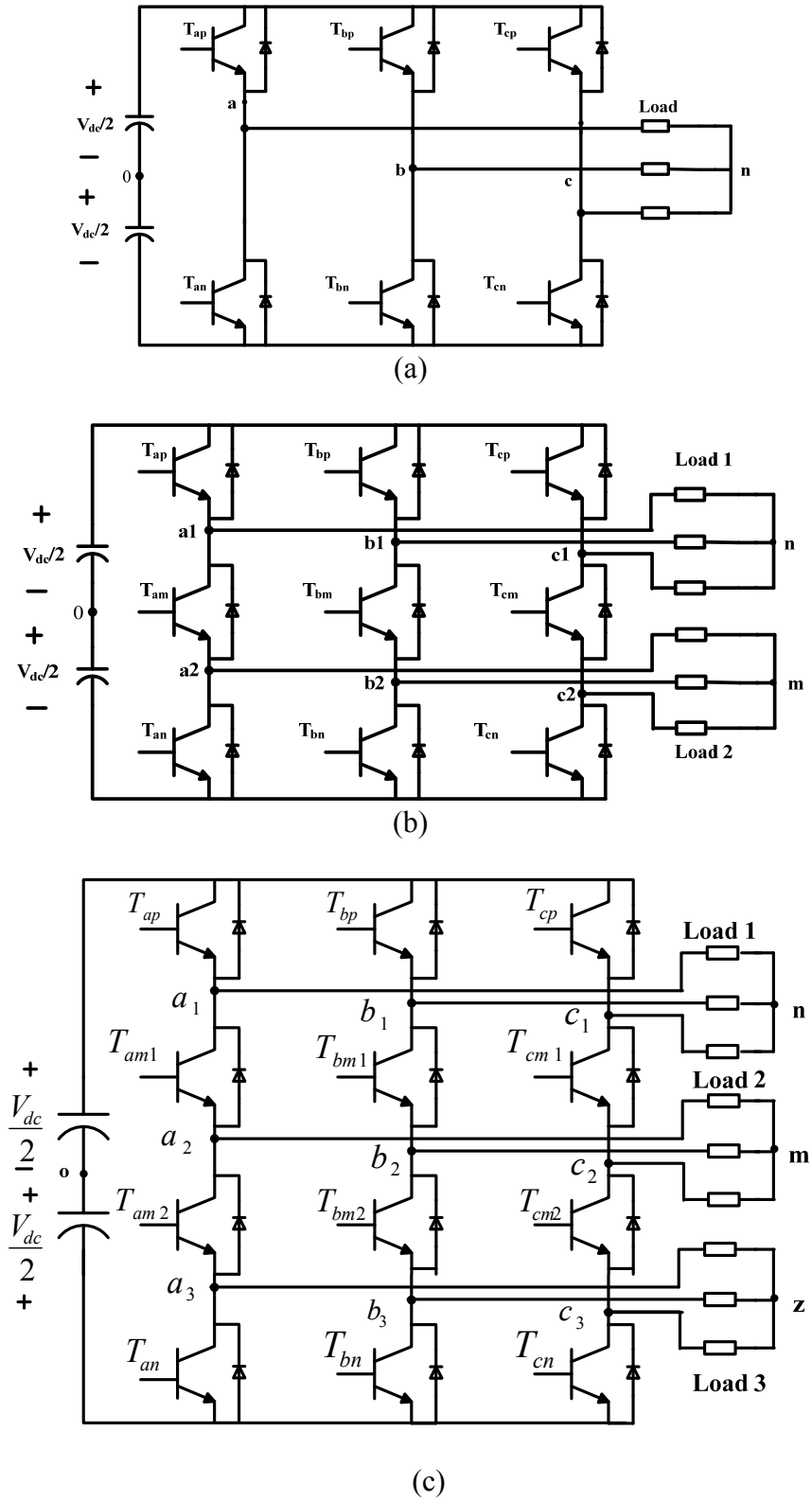
Figure 6.2. Schematic of (a) 6-switch, (b) Nine-switch, and (c) 12-switch converters

223

The upper-inner switching devices (T_{am1}, T_{bm1}, T_{cm1}) are shared between *Inv1* and *Inv2* whereas the lower-inner switches (T_{am2}, T_{bm2}, T_{cm2}) are shared between *Inv2* and *Inv3*. These sharing of switching devices of the '*three*' converters imposes some switching constraints that limit the amplitudes and frequencies of the three-phase voltages that can be synthesized. In the case of the Nine-switch converter, [41], [43], and [44] postulated that to ensure Kirchoff's voltage law (KVL) and Kirchoff's current law (KCL) were not violated during operation, the modulation signals of *Inv1* at any instant must always be greater than the modulation signals of *Inv2*. This has been accomplished in [41], [42], and [66] by adding 'appropriate' DC offsets to the two modulation signals so that they are separated from each other to satisfy the switching constraint. In Chapter 5, the zero sequence voltages of the Nine-converter were used to provide these offsets as well as determining the desired modulation strategy. A similar derivation would be done in this chapter for the 12-switch converter.

6.3 Modulation Techniques of the 12-Switch Converter

The analysis of the modulation strategies is similar to the Nine-switch converter discussed in Chapter 5. Space Vector Pulse-Width Modulation (SV-PWM) and Carrier-Based Pulse-Width Modulation (CB-PWM) methods for the 12-switch converter are investigated. In the 12-switch topology shown in Figure 6.2(c), there are four thousand and ninety-six ($2^{12} = 4096$) different possible switch combinations of all the 12 switching devices. However, KCL and KVL must be obeyed to prevent short-circuiting the power

supply and ensure current continuity. Thus, the following constraint on the switching functions must be satisfied:

$$S_{ip} + S_{im1} + S_{im2} + S_{in} = 3 \qquad\qquad (6.1)$$

where S_{ip}, S_{im1}, S_{im2}, S_{in} are respectively, the switching functions of the upper, upper-inner, lower-inner, and lower switching devices. These switching functions take a value of unity when the switch is conducting and zero when in the non-conducting mode. The subscripts $i = a, b, c$ refer to the output phase to which the switching device is connected; *p, m1, m2, n* refers to the upper, upper-inner, lower-inner, and lower switching devices of the converter leg, respectively. The switching function constraint equation, (6.1), reduces the feasible switching states to sixty-four (64) as listed in Table 6.1.

6.3.1. Space Vector Modulation of the 12-Switch Converter

The SV-PWM technique is a direct digital PWM method that calculates the conduction times of the switching devices to synthesize the desired voltage vector. From (6.1), it has been shown that there are sixty-four (64) feasible switching states of the 12-switch converter as given in Table 6.1. The procedure in deriving the SV-PWM scheme is outlined in the previous chapter but is repeated here for the sake of completeness. The procedure to obtain the SV-PWM scheme involves first transforming the converter voltages in the natural *abc* reference frame into stationary *qd0* reference using (6.2) [57].

Table 6.1. Feasible switching states of the 12-switch converter

State	S_{ap}	S_{am1}	S_{an}	S_{bp}	S_{bm1}	S_{bn}	S_{cp}	S_{cm1}	S_{cn}
1	0	1	1	0	1	1	0	1	1
2	0	1	1	0	1	1	1	0	1
3	0	1	1	0	1	1	1	1	0
4	0	1	1	0	1	1	1	1	1
5	0	1	1	1	0	1	0	1	1
6	0	1	1	1	0	1	1	0	1
7	0	1	1	1	0	1	1	1	0
8	0	1	1	1	0	1	1	1	1
9	0	1	1	1	1	0	0	1	1
10	0	1	1	1	1	0	1	0	1
11	0	1	1	1	1	0	1	1	0
12	0	1	1	1	1	0	1	1	1
13	0	1	1	1	1	1	0	1	1
14	0	1	1	1	1	1	1	0	1
15	0	1	1	1	1	1	1	1	0
16	0	1	1	1	1	1	1	1	1
17	1	0	1	0	1	1	0	1	1
18	1	0	1	0	1	1	1	0	1
19	1	0	1	0	1	1	1	1	0
20	1	0	1	0	1	1	1	1	1
21	1	0	1	1	0	1	0	1	1
22	1	0	1	1	0	1	1	0	1
23	1	0	1	1	0	1	1	1	0
24	1	0	1	1	0	1	1	1	1
25	1	0	1	1	1	0	0	1	1
26	1	0	1	1	1	0	1	0	1
27	1	0	1	1	1	0	1	1	0
28	1	0	1	1	1	0	1	1	1
29	1	0	1	1	1	1	0	1	1
30	1	0	1	1	1	1	1	0	1
31	1	0	1	1	1	1	1	1	0
32	1	0	1	1	1	1	1	1	1
33	1	1	0	0	1	1	0	1	1

Table 6.1 (Continued)

State	S_{ap}	S_{am1}	S_{an}	S_{bp}	S_{bm1}	S_{bn}	S_{cp}	S_{cm1}	S_{cn}
34	1	1	0	0	1	1	1	0	1
35	1	1	0	0	1	1	1	1	0
36	1	1	0	0	1	1	1	1	1
37	1	1	0	1	0	1	0	1	1
38	1	1	0	1	0	1	1	0	1
39	1	1	0	1	0	1	1	1	0
40	1	1	0	1	0	1	1	1	1
41	1	1	0	1	1	0	0	1	1
42	1	1	0	1	1	0	1	0	1
43	1	1	0	1	1	0	1	1	0
44	1	1	0	1	1	0	1	1	1
45	1	1	0	1	1	1	0	1	1
46	1	1	0	1	1	1	1	0	1
47	1	1	0	1	1	1	1	1	0
48	1	1	0	1	1	1	1	1	1
49	1	1	1	0	1	1	0	1	1
50	1	1	1	0	1	1	1	0	1
51	1	1	1	0	1	1	1	1	0
52	1	1	1	0	1	1	1	1	1
53	1	1	1	1	0	1	0	1	1
54	1	1	1	1	0	1	1	0	1
55	1	1	1	1	0	1	1	1	0
56	1	1	1	1	0	1	1	1	1
57	1	1	1	1	1	0	0	1	1
58	1	1	1	1	1	0	1	0	1
59	1	1	1	1	1	0	1	1	0
60	1	1	1	1	1	0	1	1	1
61	1	1	1	1	1	1	0	1	1
62	1	1	1	1	1	1	1	0	1
63	1	1	1	1	1	1	1	1	0
64	1	1	1	1	1	1	1	1	1

$$f_{qd0s} = K(\theta)f_{abcs} \tag{6.2}$$

$$K(\theta) = \frac{2}{3}\begin{bmatrix} \cos(\theta) & \cos(\theta - 2\pi/3) & \cos(\theta + 2\pi/3) \\ \sin(\theta) & \sin(\theta - 2\pi/3) & \sin(\theta + 2\pi/3) \\ 1/2 & 1/2 & 1/2 \end{bmatrix} \tag{6.3}$$

where

$f_{qd0s} = [f_{qs} \quad f_{ds} \quad f_{0s}]^T$, $f_{abcs} = [f_{as} \quad f_{bs} \quad f_{cs}]^T$ and f_{abcs} represent voltage, current or

flux linkage. The reference transformation angle is $\theta = 0^o$ to obtain the stationary

reference frame voltage vectors. To synthesize the desired 3-phase voltages, the natural

abc voltages are transformed into the *qd0* stationary reference frame voltages using (6.4)

– (6.6).

$$V_{qs}^* = \frac{2}{3}\left(v_{as} - \frac{1}{2}v_{bs} - \frac{1}{2}v_{cs} \right) \tag{6.4}$$

$$V_{qs}^* = \frac{2}{3}\left(-\frac{\sqrt{3}}{2}v_{bs} + \frac{\sqrt{3}}{2}v_{cs} \right) \tag{6.5}$$

$$V_{0s}^* = \frac{2}{3}\left(\frac{1}{2}v_{as} + \frac{1}{2}v_{bs} + \frac{1}{2}v_{cs} \right) \tag{6.6}$$

In terms of the switching functions, the voltage between the converter phase-leg and the

midpoint of the input dc voltage is given by

$$V_{j10} = \frac{V_{dc}}{2}(S_{ap} - S_{am1}S_{am2}S_{an}) \tag{6.7}$$

$$V_{j20} = \frac{V_{dc}}{2}(S_{ap}S_{am1} - S_{am2}S_{an}) \tag{6.8}$$

$$V_{j30} = \frac{V_{dc}}{2}(S_{ap}S_{am1}S_{am2} - S_{an}) \tag{6.9}$$

228

where j = a, b, c for phases a, b, and c respectively of the converter. Thus using (6.4) – (6.9), the *abc* and the corresponding *qd0* voltages for all 64 switching states can be calculated as listed in Tables 6.2.

The next step in the SV-PWM modeling process is to draw the space vector diagrams based on the *qd0* stationary voltages. In this dissertation, the positive q-axis is in the direction of the positive real-x axis and the positive d-axis is in the same direction as that of the imaginary axis of the complex plane. The 0-axis is assumed to be at the origin of the complex plane. Thus, based on Table 6.2, the converter *qd0* voltages can be plotted on the complex plane. Table 6.3 lists all the zero (or null) switching states and Table 6.4 lists that of the active switching states giving the angle of orientation in the complex plane. In the zero switching states, no energy is transferred to the load and vice versa, i.e., the converter serves as an open circuit between the input dc supply and the three loads.

The following observations can be made from Tables 6.3 and 6.4:

- Four zero states {1, 22, 43, and 64} are common to *Inv1*, *Inv2*, and *Inv3*.

- The rest of the zero states in *Inv1* are active states in *Inv2* and/or *Inv3*. The same can be said of the other zero states in *Inv2* and *Inv3*.

- There are some active states that are associated with only one of the three outputs. These are indicated in bold fonts in Table 6.4.

If we desire independent control of the three sets of 3-phase outputs (variable frequency and/or amplitude), two things need to be done:

- Eliminate all the zero states that are not common to all three outputs

- Secondly, in Table 6.4, eliminate all active states that appear more than once

229

Table 6.2. 12-switch converter *abc* and *qd0* stationary voltages using switching function for all feasible switching states

			Switching Functions							$*V_{dc}/2$	$*V_{dc}/2$	$*V_{dc}/2$	$*V_{dc}/2$	$*V_{dc}/2$	$*V_{dc}/2$	$*V_{dc}/2$	$*V_{dc}/2$	$*V_{dc}/2$	$*V_{dc}/6$	$*V_{dc}\sqrt{3}/6$	$*V_{dc}/6$	$*V_{dc}/6$	$*V_{dc}\sqrt{3}/6$	$*V_{dc}/6$	$*V_{dc}/6$	$*V_{dc}\sqrt{3}/6$	$*V_{dc}/6$
State	S_{ap}	S_{am1}	S_{an}	S_{bp}	S_{bm1}	S_{bn}	S_{cp}	S_{cm1}	S_{cn}	V_{a10}	V_{b10}	V_{c10}	V_{a20}	V_{b20}	V_{c20}	V_{a30}	V_{b30}	V_{c30}	V_{qs1}	V_{ds1}	V_{01}	V_{qs2}	V_{ds2}	V_{02}	V_{qs3}	V_{ds3}	V_{03}
1	0	1	1	0	1	1	0	1	1	-1	-1	-1	-1	-1	-1	-1	-1	-1	0	0	-3	0	0	-3	0	0	-3
2	0	1	1	0	1	1	1	0	1	-1	-1	1	-1	-1	-1	-1	-1	-1	-2	2	-1	0	0	-3	0	0	-3
3	0	1	1	0	1	1	1	1	0	-1	-1	1	-1	-1	1	-1	-1	1	-2	2	-1	-2	2	-1	-2	2	-1
4	0	1	1	0	1	1	1	1	1	-1	-1	1	-1	-1	1	-1	-1	-1	-2	2	-1	-2	2	-1	0	0	-3
5	0	1	1	1	0	1	0	1	1	-1	1	-1	-1	-1	-1	-1	-1	-1	-2	-2	-1	0	0	-3	0	0	-3
6	0	1	1	1	0	1	1	0	1	-1	1	1	-1	-1	-1	-1	-1	-1	-4	0	1	0	0	-3	0	0	-3
7	0	1	1	1	0	1	1	1	0	-1	1	1	-1	-1	1	-1	-1	1	-4	0	1	-2	2	-1	-2	2	-1
8	0	1	1	1	0	1	1	1	1	-1	1	1	-1	-1	1	-1	-1	-1	-4	0	1	-2	2	-1	0	0	-3
9	0	1	1	1	1	0	0	1	1	-1	1	-1	-1	1	-1	-1	1	-1	-2	-2	-1	-2	-2	-1	-2	-2	-1
10	0	1	1	1	1	0	1	0	1	-1	1	1	-1	1	-1	-1	1	-1	-4	0	1	-2	-2	-1	-2	-2	-1
11	0	1	1	1	1	0	1	1	0	-1	1	1	-1	1	1	-1	1	1	-4	0	1	-4	0	1	-4	0	1
12	0	1	1	1	1	0	1	1	1	-1	1	1	-1	1	1	-1	1	-1	-4	0	1	-4	0	1	-2	-2	-1

230

Table 6.2 (Continued)

State	S_{ap}	S_{am1}	S_{an}	S_{bp}	S_{bm1}	S_{bn}	S_{cp}	S_{cm1}	S_{cn}	V_{a10}	V_{b10}	V_{c10}	V_{a20}	V_{b20}	V_{c20}	V_{a30}	V_{b30}	V_{c30}	V_{qs1}	V_{ds1}	V_{01}	V_{qs2}	V_{ds2}	V_{02}	V_{qs3}	V_{ds3}	V_{03}
13	0	1	1	1	1	1	0	1	1	-1	1	-1	-1	1	-1	-1	-1	-1	-2	-2	-1	-2	-2	-1	0	0	-3
14	0	1	1	1	1	1	1	0	1	-1	1	1	-1	1	-1	-1	-1	-1	-4	0	1	-2	-2	-1	0	0	-3
15	0	1	1	1	1	1	1	1	0	-1	1	1	-1	1	1	-1	-1	1	-4	0	1	-4	0	1	-2	2	-1
16	0	1	1	1	1	1	1	1	1	-1	1	1	-1	1	1	-1	-1	-1	-4	0	1	-4	0	1	0	0	-3
17	1	0	1	0	1	1	0	1	1	1	-1	-1	-1	-1	-1	-1	-1	-1	4	0	-1	0	0	-3	0	0	-3
18	1	0	1	0	1	1	1	0	1	1	-1	1	-1	-1	-1	-1	-1	-1	2	2	1	0	0	-3	0	0	-3
19	1	0	1	0	1	1	1	1	0	1	-1	1	-1	-1	1	-1	-1	1	2	2	1	-2	2	-1	-2	2	-1
20	1	0	1	0	1	1	1	1	1	1	-1	1	-1	-1	1	-1	-1	-1	2	2	1	-2	2	-1	0	0	-3
21	1	0	1	1	0	1	0	1	1	1	1	-1	-1	-1	-1	-1	-1	-1	2	-2	1	0	0	-3	0	0	-3
22	1	0	1	1	0	1	1	0	1	1	1	1	-1	-1	-1	-1	-1	-1	0	0	3	0	0	-3	0	0	-3
23	1	0	1	1	0	1	1	1	0	1	1	1	-1	-1	1	-1	-1	1	0	0	3	-2	2	-1	-2	2	-1
24	1	0	1	1	0	1	1	1	1	1	1	1	-1	-1	1	-1	-1	-1	0	0	3	-2	2	-1	0	0	-3
25	1	0	1	1	1	0	0	1	1	1	1	-1	-1	1	-1	-1	1	-1	2	-2	1	-2	-2	-1	-2	-2	-1

Table 6.2 (Continued)

State	S_{ap}	S_{am1}	S_{an}	S_{bp}	S_{bm1}	S_{bn}	S_{cp}	S_{cm1}	S_{cn}	V_{a10}	V_{b10}	V_{c10}	V_{a20}	V_{b20}	V_{c20}	V_{a30}	V_{b30}	V_{c30}	V_{qs1}	V_{ds1}	V_{01}	V_{qs2}	V_{ds2}	V_{02}	V_{qs3}	V_{ds3}	V_{03}
26	1	0	1	1	1	0	1	0	1	1	1	1	-1	1	-1	-1	1	-1	0	0	3	-2	-2	-1	-2	-2	-1
27	1	0	1	1	1	0	1	1	0	1	1	1	-1	1	1	-1	1	1	0	0	3	-4	0	1	-4	0	1
28	1	0	1	1	1	0	1	1	1	1	1	1	-1	1	1	-1	1	-1	0	0	3	-4	0	1	-2	-2	-1
29	1	0	1	1	1	1	0	1	1	1	1	-1	-1	1	-1	-1	-1	-1	2	-2	1	-2	-2	-1	0	0	-3
30	1	0	1	1	1	1	1	0	1	1	1	1	-1	1	-1	-1	-1	-1	0	0	3	-2	-2	-1	0	0	-3
31	1	0	1	1	1	1	1	1	0	1	1	1	-1	1	1	-1	-1	1	0	0	3	-4	0	1	-2	2	-1
32	1	0	1	1	1	1	1	1	1	1	1	1	-1	1	1	-1	-1	-1	0	0	3	-4	0	1	0	0	-3
33	1	1	0	0	1	1	0	1	1	1	-1	-1	1	-1	-1	1	-1	-1	4	0	-1	4	0	-1	4	0	-1
34	1	1	0	0	1	1	1	0	1	1	-1	1	1	-1	-1	1	-1	-1	2	2	1	4	0	-1	4	0	-1
35	1	1	0	0	1	1	1	1	0	1	-1	1	1	-1	1	1	-1	1	2	2	1	2	2	1	2	2	1
36	1	1	0	0	1	1	1	1	1	1	-1	1	1	-1	1	1	-1	-1	2	2	1	2	2	1	4	0	-1
37	1	1	0	1	0	1	0	1	1	1	1	-1	1	-1	-1	1	-1	-1	2	-2	1	4	0	-1	4	0	-1
38	1	1	0	1	0	1	1	0	1	1	1	1	1	-1	-1	1	-1	-1	0	0	3	4	0	-1	4	0	-1

Table 6.2 (Continued)

State	S_{ap}	S_{am1}	S_{an}	S_{bp}	S_{bm1}	S_{bn}	S_{cp}	S_{cm1}	S_{cn}	V_{a10}	V_{b10}	V_{c10}	V_{a20}	V_{b20}	V_{c20}	V_{a30}	V_{b30}	V_{c30}	V_{qs1}	V_{ds1}	V_{01}	V_{qs2}	V_{ds2}	V_{02}	V_{qs3}	V_{ds3}	V_{03}
39	1	1	0	1	0	1	1	1	0	1	1	1	1	-1	1	1	-1	1	0	0	3	2	2	1	2	2	1
40	1	1	0	1	0	1	1	1	1	1	1	1	1	-1	1	1	-1	-1	0	0	3	2	2	1	4	0	-1
41	1	1	0	1	1	0	0	1	1	1	1	-1	1	1	-1	1	1	-1	2	-2	1	2	-2	1	2	-2	1
42	1	1	0	1	1	0	1	0	1	1	1	1	1	1	-1	1	1	-1	0	0	3	2	-2	1	2	-2	1
43	1	1	0	1	1	0	1	1	0	1	1	1	1	1	1	1	1	1	0	0	3	0	0	3	0	0	3
44	1	1	0	1	1	0	1	1	1	1	1	1	1	1	1	1	1	-1	0	0	3	0	0	3	2	-2	1
45	1	1	0	1	1	1	0	1	1	1	1	-1	1	1	-1	1	-1	-1	2	-2	1	2	-2	1	4	0	-1
46	1	1	0	1	1	1	1	0	1	1	1	1	1	1	-1	1	-1	-1	0	0	3	2	-2	1	4	0	-1
47	1	1	0	1	1	1	1	1	0	1	1	1	1	1	1	1	1	-1	0	0	3	0	0	3	2	2	1
48	1	1	0	1	1	1	1	1	1	1	1	1	1	1	1	1	1	-1	0	0	3	0	0	3	4	0	-1
49	1	1	1	0	1	1	0	1	1	1	-1	-1	1	-1	-1	-1	-1	-1	4	0	-1	4	0	-1	0	0	-3
50	1	1	1	0	1	1	1	0	1	1	-1	1	1	-1	-1	-1	-1	-1	2	2	1	4	0	-1	0	0	-3
51	1	1	1	0	1	1	1	1	0	1	-1	1	1	-1	1	-1	-1	1	2	2	1	2	2	1	-2	2	-1

Table 6.2 (Continued)

State	S_{ap}	S_{aml}	S_{an}	S_{bp}	S_{bml}	S_{bn}	S_{cp}	S_{cml}	S_{cn}	V_{a10}	V_{b10}	V_{c10}	V_{a20}	V_{b20}	V_{c20}	V_{a30}	V_{b30}	V_{c30}	V_{qs1}	V_{ds1}	V_{01}	V_{qs2}	V_{ds2}	V_{02}	V_{qs3}	V_{ds3}	V_{03}
52	1	1	1	0	1	1	1	1	1	1	-1	1	1	-1	1	-1	-1	-1	2	2	1	2	2	1	0	0	-3
53	1	1	1	1	0	1	0	1	1	1	1	-1	1	-1	-1	-1	-1	-1	2	-2	1	4	0	-1	0	0	-3
54	1	1	1	1	0	1	1	0	1	1	1	1	1	-1	-1	-1	-1	-1	0	0	3	4	0	-1	0	0	-3
55	1	1	1	1	0	1	1	1	0	1	1	1	1	-1	1	-1	-1	1	0	0	3	2	2	1	-2	2	-1
56	1	1	1	1	0	1	1	1	1	1	1	1	1	-1	1	-1	-1	-1	0	0	3	2	2	1	0	0	-3
57	1	1	1	1	1	0	0	1	1	1	1	-1	1	1	-1	-1	1	-1	2	-2	1	2	-2	1	-2	-2	-1
58	1	1	1	1	1	0	1	0	1	1	1	1	1	1	-1	-1	1	-1	0	0	3	2	-2	1	-2	-2	-1
59	1	1	1	1	1	0	1	1	0	1	1	1	1	1	1	-1	1	1	0	0	3	0	0	3	-4	0	1
60	1	1	1	1	1	0	1	1	1	1	1	1	1	1	1	-1	1	-1	0	0	3	0	0	3	-2	-2	-1
61	1	1	1	1	1	1	0	1	1	1	1	-1	1	1	-1	-1	-1	-1	2	-2	1	2	-2	1	0	0	-3
62	1	1	1	1	1	1	1	0	1	1	1	1	1	1	-1	-1	-1	-1	0	0	3	2	-2	1	0	0	-3
63	1	1	1	1	1	1	1	1	0	1	1	1	1	1	1	-1	-1	1	0	0	3	0	0	3	-2	2	-1
64	1	1	1	1	1	1	1	1	1	1	1	1	1	1	1	-1	-1	-1	0	0	3	0	0	3	0	0	-3

Table 6.3. Zero states for *Inv1*, *Inv2*, and *Inv3* located at the origin of space vector diagram

							Zero switching states									
	1	3	**22**	23	24	26	27	28	30	31	32	38	39	40	42	**43**
Inv1	44	46	47	48	54	55	56	58	59	60	62	**64**				
Inv2	1	2	5	6	17	18	21	**22**	**43**	44	47	48	59	60	63	**64**
	1	2	4	5	6	8	13	14	16	17	18	20	21	**22**	24	29
Inv3	30	32	**43**	49	50	52	53	54	56	61	62	**64**				

Table 6.4. Location of active switching states on space vector diagram (refer to Table 6.2)

Active switching states																	
Inv1						*Inv2*						*Inv3*					
0°	**60°**	**120°**	**180°**	**240°**	**-60°**	**0°**	**60°**	**120°**	**180°**	**240°**	**-60°**	**0°**	**60°**	**120°**	**180°**	**240°**	**-60°**
17	**18**	**2**	**6**	**5**	**21**	33	35	3	11	9	41	33	35	3	11	9	41
33	19	3	7	9	25	34	36	4	12	10	42	34	39	7	27	10	42
49	20	4	8	13	29	37	39	7	15	13	45	36	**47**	15	**59**	12	**44**
	34		10		37	38	40	8	16	14	46	37		19		25	
	35		11		41	49	51	19	27	25	57	38		23		26	
	36		12		45	50	52	20	28	26	58	40		31		28	
	50		14		53	53	55	23	31	29	61	45		51		57	
	51		15		57	**54**	**56**	**24**	**32**	**30**	**62**	46		55		58	
	52		16		61							**48**		**63**		**60**	

235

After eliminating these switching states as described above, an independent control of the converter frequencies and amplitudes is now possible since the active states of *Inv1, Inv2* and *Inv3* are chosen such that an active state applied to *Inv1* produces a zero state in *Inv2* and *Inv3* and vice versa [42]. There are then twenty-two (22) states as shown in Table 6.5 and the corresponding space vector diagrams are shown in Figure 6.3.

Any desired three, 3-phase voltage sets expressed in the stationary reference frame , V_{qd1}^*, V_{qd2}^* V_{qd3}^* may be synthesized from their respective immediate adjacent space vectors, V_{qda} , V_{qdb} , V_{qdc} , V_{qdd} , V_{qde} , and V_{qdf} respectively in addition to the zero vectors V_{qd01} , V_{qd02} , V_{qd03} and V_{qd04} as shown in Figures 6.3 and 6.4.

6.3.1.1.**Calculating time duration of active vectors.** The time intervals during which the adjacent active vectors are applied in order to synthezise any three reference output voltages V_{qd1}^* , V_{qd2}^* and V_{qd3}^* are derived below. For Inv1, define the two adjacent vectors for synthesizing V_{qd1}^* to be V_{qda} and V_{qdb} and the corresponding normalized switching time duration to be t_a , and t_b respectively, as shown in Figure 6.4(a).

Similarly, (V_{qdc} , V_{qdd}) and (V_{qde} , V_{qdf}) and their corresponding normalized time durations (t_c , t_d) and (t_e , t_f) can be used to synthesize V_{qd2}^* and V_{qd3}^* as shown in Figures 6.4(b) and (c) respectively. In addition, it is desired to inject the zero sequence vectors into the reference modulation signals.

Table 6.5. Switching states for independent control of *Inv1, Inv2,* and *Inv3*

State	S_{ap}	S_{am1}	S_{an}	S_{bp}	S_{bm1}	S_{bn}	S_{cp}	S_{cm1}	S_{cn}	V_{qs1} $*V_{dc}/6$	V_{ds1} $*V_{dc}\sqrt{3}/6$	V_{01} $*V_{dc}/6$	V_{qs2} $*V_{dc}/6$	V_{ds2} $*V_{dc}\sqrt{3}/6$	V_{02} $*V_{dc}/6$	V_{qs3} $*V_{dc}/6$	V_{ds3} $*V_{dc}\sqrt{3}/6$	V_{03} $*V_{dc}/6$
1	1	0	1	0	1	1	0	1	1	4	0	-1	0	0	-3	0	0	-3
2	1	0	1	0	1	1	1	0	1	2	2	1	0	0	-3	0	0	-3
3	0	1	1	0	1	1	1	0	1	-2	2	-1	0	0	-3	0	0	-3
4	0	1	1	1	0	1	1	0	1	-4	0	1	0	0	-3	0	0	-3
5	0	1	1	1	0	1	0	1	1	-2	-2	-1	0	0	-3	0	0	-3
6	1	0	1	1	0	1	0	1	1	2	-2	1	0	0	-3	0	0	-3
7	1	1	1	1	0	1	1	0	1	0	0	3	4	0	-1	0	0	-3
8	1	1	1	1	0	1	1	1	1	0	0	3	2	2	1	0	0	-3
9	1	0	1	1	0	1	1	1	1	0	0	3	-2	2	-1	0	0	-3
10	1	0	1	1	1	1	1	1	1	0	0	3	-4	0	1	0	0	-3
11	1	0	1	1	1	1	1	0	1	0	0	3	-2	-2	-1	0	0	-3
12	1	1	1	1	1	1	1	0	1	0	0	3	2	-2	1	0	0	-3
13	1	1	0	1	1	1	1	1	1	0	0	3	0	0	3	4	0	-1
14	1	1	0	1	1	1	1	1	0	0	0	3	0	0	3	2	2	1
15	1	1	1	1	1	1	1	1	0	0	0	3	0	0	3	-2	2	-1
16	1	1	1	1	1	0	1	1	0	0	0	3	0	0	3	-4	0	1
17	1	1	1	1	1	0	1	1	1	0	0	3	0	0	3	-2	-2	-1
18	1	1	0	1	1	0	1	1	1	0	0	3	0	0	3	2	-2	1
19	0	1	1	0	1	1	0	1	1	0	0	-3	0	0	-3	0	0	-3
20	1	0	1	1	0	1	1	0	1	0	0	3	0	0	-3	0	0	-3
21	1	1	0	1	1	0	1	1	0	0	0	3	0	0	3	0	0	3
22	1	1	1	1	1	1	1	1	1	0	0	3	0	0	3	0	0	-3
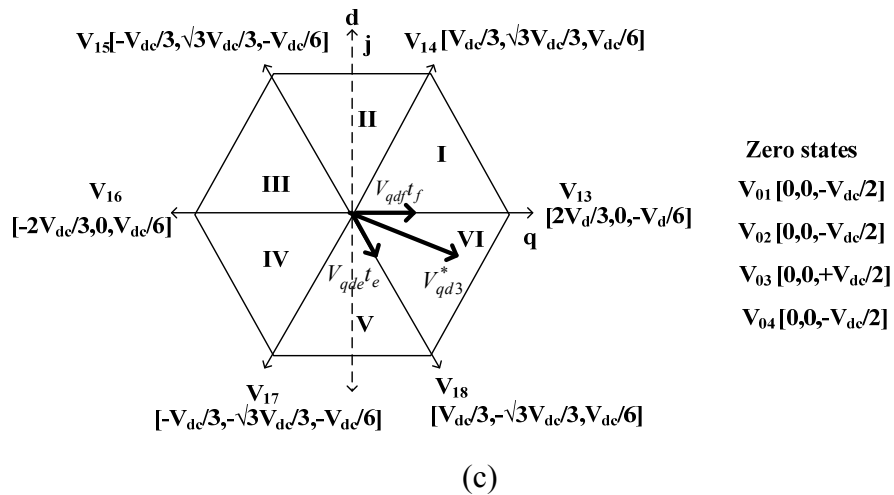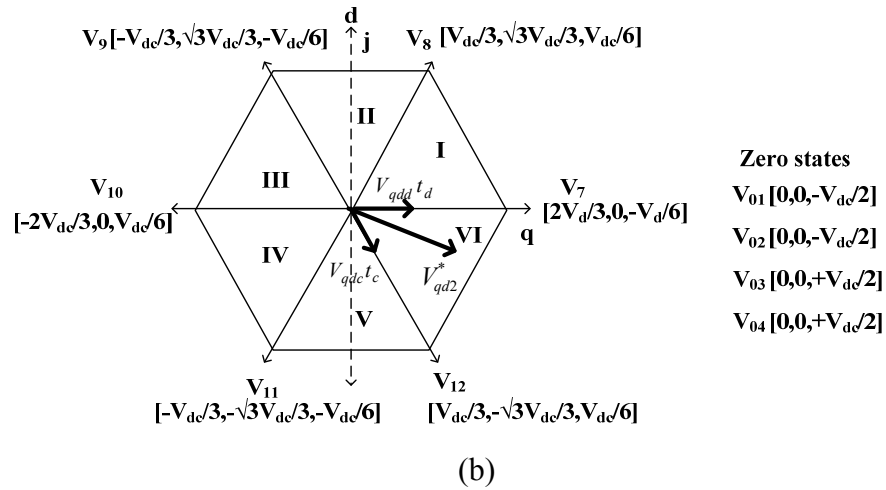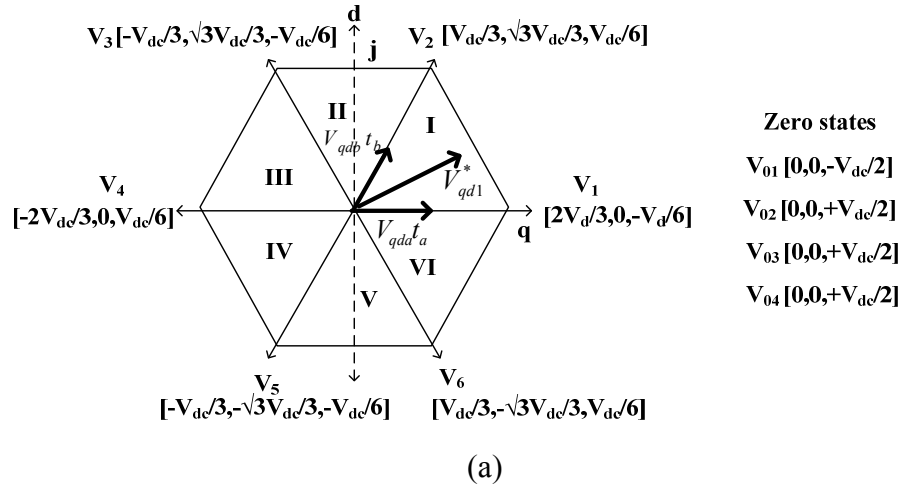
Figure 6.3. Voltage space vector diagrams for (a) *Inv1*, (b) *Inv2,* and (c) *Inv3* for selected switching states which ensures their independent control

238
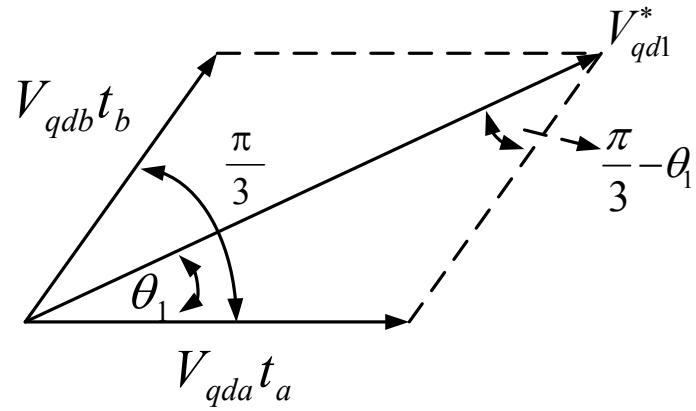
(a)
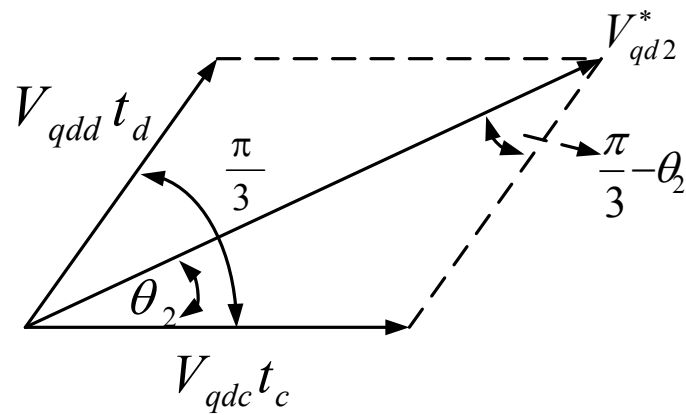
(b)
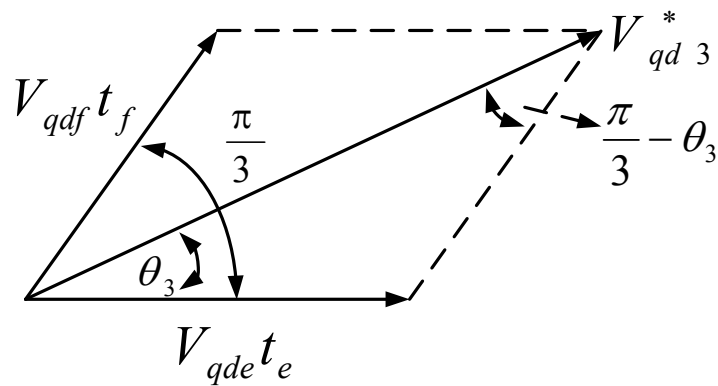
(c)

Figure 6.4. Synthesizing desired voltage for (a) V_{qd1}^* , (b) V_{qd2}^* , and (c) V_{qd3}^* using their immediate adjacent voltages vectors

Define the four zero sequence vectors and their corresponding normalized times as,

(V_{qd01}, V_{qd02}, V_{qd03}) and (t_{01}, t_{02}, t_{03} and t_{04}) respectively. Hence, the reference voltages

are given by

$$V^*_{qd1} = t_a V_{qda} + t_b V_{qdb} + t_{01} V_{qd01} + t_{02} V_{qd02} + t_{03} V_{qd03} + t_{03} V_{qd04} \qquad (6.10)$$

$$V^*_{qd2} = t_c V_{qdc} + t_d V_{qdd} + + t_{01} V_{qd01} + t_{02} V_{qd02} + t_{03} V_{qd03} + t_{03} V_{qd04} \qquad (6.11)$$

$$V^*_{qd3} = t_e V_{qde} + t_f V_{qdf} + t_{01} V_{qd01} + t_{02} V_{qd02} + t_{03} V_{qd03} + t_{03} V_{qd04} \qquad (6.12)$$

where

$$V^*_{qd1} = V^*_{q1} + j V^*_{d1} \qquad (6.13)$$

$$V^*_{qd2} = V^*_{q2} + j V^*_{d2} \qquad (6.14)$$

$$V^*_{qd3} = V^*_{q3} + j V^*_{d3} \qquad (6.15)$$

Substituting (6.13)-(6.15) into (6.10)-(6.12):

$$V^*_{qd1} = t_a \left(V_{qqa} + j V_{dda} \right) + t_b \left(V_{qqb} + j V_{ddb} \right) \qquad (6.16)$$

$$V^*_{qd2} = t_c \left(V_{qqc} + j V_{ddc} \right) + t_d \left(V_{qqd} + j V_{ddd} \right) \qquad (6.17)$$

$$V^*_{qd3} = t_e \left(V_{qqe} + j V_{dde} \right) + t_f \left(V_{qqf} + j V_{ddf} \right) \qquad (6.18)$$

Note that the zero vectors do not contribute to the output voltages. Therefore eliminating these, expanding and separating (6.16)-(6.18) into real and imaginary parts:

$$V^*_{q1} = t_a V_{qqa} + t_b V_{qqb} \qquad (6.19)$$

$$V^*_{d1} = t_a V_{dda} + t_b V_{ddb} \qquad (6.20)$$

$$V^*_{q2} = t_c V_{qqc} + t_d V_{qqd} \qquad (6.21)$$

240

$$V_{d2}^* = t_c V_{ddc} + t_d V_{ddd} \tag{6.22}$$

$$V_{q3}^* = t_e V_{qqe} + t_f V_{qqf} \tag{6.23}$$

$$V_{d3}^* = t_e V_{dde} + t_f V_{ddf} \tag{6.24}$$

This gives six (6) equations and six (6) unknowns and therefore the normalized active time durations of application of the active and zero vectors found by solving these equations simultaneously to obtain

$$t_a = \frac{V_{d1}^* V_{qqb} - V_{ddb} V_{q1}^*}{V_{dda} V_{qqb} - V_{ddb} V_{qqa}} \tag{6.25}$$

$$t_b = \frac{V_{q1}^* V_{dda} - V_{qqa} V_{d1}^*}{V_{dda} V_{qqb} - V_{ddb} V_{qqa}} \tag{6.26}$$

$$t_c = \frac{V_{d2}^* V_{qqd} - V_{ddd} V_{q2}^*}{V_{ddc} V_{qqd} - V_{ddd} V_{qqc}} \tag{6.27}$$

$$t_d = \frac{V_{q2}^* V_{ddc} - V_{qqc} V_{d2}^*}{V_{ddc} V_{qqd} - V_{ddd} V_{qqc}} \tag{6.28}$$

$$t_e = \frac{V_{d3}^* V_{qqf} - V_{ddf} V_{q3}^*}{V_{dde} V_{qqf} - V_{ddf} V_{qqe}} \tag{6.29}$$

$$t_f = \frac{V_{q3}^* V_{dde} - V_{qqe} V_{d3}^*}{V_{dde} V_{qqf} - V_{ddf} V_{qqe}} \tag{6.30}$$

The dwell times of the zero vectors are given by

$$t_0 = t_{01} + t_{02} + t_{03} + t_{04} = 1 - (t_a + t_b + t_c + t_d + t_e + t_f) \tag{6.31}$$

241

$$t_{01} = \alpha t_0$$
$$t_{02} = \beta t_0$$
$$t_{03} = \gamma t_0 \tag{6.32}$$
$$t_{04} = \mu t_0 = (1 - \alpha - \beta - \gamma)t_0$$
$$\alpha + \beta + \gamma + \mu = 1$$

where, α, β, γ, and μ are the utilization factors of the zero vectors V_{01}, V_{02}, V_{03} and V_{04}

respectively.

The three reference voltages, V_{qd1}^*, V_{qd2}^* and V_{qd3}^* may be written in complex form

as:

$$V_{qd1}^* = mag(V_{qd1}^*)\left[\cos\theta_1 + j\sin\theta_1\right]$$
$$\tag{6.33}$$
$$= mag(V_{qda})t_a + mag(V_{qdb})(\cos\pi/3 + j\sin\pi/3)t_b$$

$$V_{qd2}^* = mag(V_{qd2}^*)\left[\cos\theta_2 + j\sin\theta_2\right]$$
$$\tag{6.34}$$
$$= mag(V_{qdc})t_c + mag(V_{qdd})(\cos\pi/3 + j\sin\pi/3)t_d$$

$$V_{qd3}^* = mag(V_{qd3}^*)\left[\cos\theta_3 + j\sin\theta_3\right]$$
$$\tag{6.35}$$
$$= mag(V_{qde})t_e + mag(V_{qdf})(\cos\pi/3 + j\sin\pi/3)t_f$$

where $mag(\ )$ is the magnitude of the complex parameter, θ_1, θ_2, and θ_3 are the angles of

orientation of the reference voltages with respect to the lower immediate adjacent

vectors. Expanding (6.33)-(6.35) and comparing real and imaginary parts on both sides of

the equations, the normalized times are given by

$$t_a = \frac{\sqrt{3}}{V_{dc}} mag(V_{qd1}^*)\sin\left(\frac{\pi}{3} - \theta_1\right) \tag{6.36}$$

$$t_b = \frac{\sqrt{3}}{V_{dc}} mag(V_{qd1}^*)\sin(\theta_1) \tag{6.37}$$

$$t_c = \frac{\sqrt{3}}{V_{dc}} mag(V_{qd2}^*)\sin\left(\frac{\pi}{3} - \theta_2\right) \tag{6.38}$$

$$t_d = \frac{\sqrt{3}}{V_{dc}} mag(V_{qd2}^*)\sin(\theta_2) \tag{6.39}$$

$$t_e = \frac{\sqrt{3}}{V_{dc}} mag(V_{qd3}^*)\sin\left(\frac{\pi}{3} - \theta_3\right) \tag{6.40}$$

$$t_f = \frac{\sqrt{3}}{V_{dc}} mag(V_{qd3}^*)\sin(\theta_3) \tag{6.41}$$

6.3.1.2.**Constraint on modulation indices.** In the linear modulation region, the sum of the normalized active times must be less than or equal to unity as given by (6.42). Substituting the expressions of the active times given in (6.36) – (6.41) into (6.42), the resulting expression is given by (6.43).

$$t_a + t_b + t_c + t_d + t_e + t_f \leq 1 \tag{6.42}$$

$$\left[\begin{array}{l} \dfrac{\sqrt{3}}{V_{dc}} mag(V_{qd1}^*)\sin\left(\dfrac{\pi}{3} - \theta_1\right) + \dfrac{\sqrt{3}}{V_{dc}} mag(V_{qd1}^*)\sin\theta_1 + \\[2mm] \dfrac{\sqrt{3}}{V_{dc}} mag(V_{qd2}^*)\sin\left(\dfrac{\pi}{3} - \theta_2\right) + \dfrac{\sqrt{3}}{V_{dc}} mag(V_{qd2}^*)\sin\theta_2 \\[2mm] \dfrac{\sqrt{3}}{V_{dc}} mag(V_{qd3}^*)\sin\left(\dfrac{\pi}{3} - \theta_3\right) + \dfrac{\sqrt{3}}{V_{dc}} mag(V_{qd3}^*)\sin\theta_3 \end{array}\right] \leq 1 \tag{6.43}$$

Define the amplitude ratios k_1 and k_2 given by

$k_1 = \dfrac{mag(V_{qd2}^*)}{mag(V_{qd1}^*)}$ and $k_2 = \dfrac{mag(V_{qd3}^*)}{mag(V_{qd1}^*)}$. Substituting these ratios into (6.43):

243

$$
\left[
\begin{array}{l}
\dfrac{\sqrt{3}}{V_{dc}}mag(V_{qd1}^{*})\sin\left(\dfrac{\pi}{3}-\theta_1\right)+\dfrac{\sqrt{3}}{V_{dc}}mag(V_{qd1}^{*})\sin\theta_1+ \\[3mm]
\dfrac{\sqrt{3}}{V_{dc}}mag(k_1V_{qd1}^{*})\sin\left(\dfrac{\pi}{3}-\theta_2\right)+\dfrac{\sqrt{3}}{V_{dc}}mag(k_1V_{qd1}^{*})\sin\theta_2+ \\[3mm]
\dfrac{\sqrt{3}}{V_{dc}}mag(k_2V_{qd1}^{*})\sin\left(\dfrac{\pi}{3}-\theta_3\right)+\dfrac{\sqrt{3}}{V_{dc}}mag(k_2V_{qd1}^{*})\sin\theta_3
\end{array}
\right] \leq 1 \qquad (6.44)
$$

Solving for k_2

$$
\left[
\begin{array}{l}
\dfrac{\sqrt{3}}{V_{dc}}mag(V_{qd1}^{*})\sin\left(\dfrac{\pi}{3}-\theta_1\right)+\dfrac{\sqrt{3}}{V_{dc}}mag(V_{qd1}^{*})\sin\theta_1+\dfrac{\sqrt{3}}{V_{dc}}mag(k_1V_{qd1}^{*})\sin\left(\dfrac{\pi}{3}-\theta_2\right)+ \\[3mm]
\dfrac{\sqrt{3}}{V_{dc}}mag(k_1V_{qd1}^{*})\sin\theta_2+\dfrac{\sqrt{3}}{V_{dc}}mag(k_2V_{qd1}^{*})\sin\left(\dfrac{\pi}{3}-\theta_3\right)+\dfrac{\sqrt{3}}{V_{dc}}mag(k_2V_{qd1}^{*})\sin\theta_3
\end{array}
\right] \leq 1
$$

$$
\dfrac{\sqrt{3}}{V_{dc}}mag(k_2V_{qd1}^{*})\left(\sin\left(\dfrac{\pi}{3}-\theta_3\right)+\sin\theta_3\right) \leq \left[1-\dfrac{\sqrt{3}}{V_{dc}}mag(V_{qd1}^{*})\left(\begin{array}{l}\sin\left(\dfrac{\pi}{3}-\theta_1\right)+\sin\theta_1+ \\[3mm] +k_1\sin\left(\dfrac{\pi}{3}-\theta_2\right)+k_1\sin\theta_2\end{array}\right)\right]
$$

$$
k_2 \leq \dfrac{1}{\dfrac{\sqrt{3}}{V_{dc}}mag(k_2V_{qd1}^{*})\left(\sin\left(\dfrac{\pi}{3}-\theta_3\right)+\sin\theta_3\right)}\left[1-\dfrac{\sqrt{3}}{V_{dc}}mag(V_{qd1}^{*})\left(\begin{array}{l}\sin\left(\dfrac{\pi}{3}-\theta_1\right)+\sin\theta_1+ \\[3mm] +k_1\sin\left(\dfrac{\pi}{3}-\theta_2\right)+k_1\sin\theta_2\end{array}\right)\right]
$$

$$
k_2 \leq \dfrac{\left[\begin{array}{l}-(3mag(V_{qd1}^{*})\cos\theta_1-2V_{dc}+3mag(V_{qd1}^{*})k_1\cos\theta_2+ \\[2mm] +\sqrt{3}mag(V_{qd1}^{*})\sin\theta_1+\sqrt{3}mag(V_{qd1}^{*})k_1\sin\theta_2)\end{array}\right]}{mag(V_{qd1}^{*})(3\cos\theta_3+\sqrt{3}\sin\theta_3)} \qquad (6.45)
$$

The voltage ratio k_1 is dependent on the voltage angles θ_1, θ_2, and θ_3 for given amplitude of the reference voltage , $mag(V_{qd1}^{*})$. In the linear operating region, the

244

reference voltage vectors around the center of the hexagon, Figure 6.3, must lie on or within the boundary of the hexagon. For a given $mag(V_{qd1}^*)$, the combination of θ_1, θ_2 and θ_3 that gives the maximum allowed $mag(V_{qd2}^*)$ and $mag(V_{qd3}^*)$ gives the limiting value of the voltage ratios. In others words, the maximum value of k_2. Thus the modulation indices constraint can be determined by taking the partial derivatives of (6.45) with respect to θ_1, θ_2, and θ_3, and then setting the resulting expressions to zero. That is:

$$\frac{\partial k_2}{\partial \theta_1} = \frac{-(-3mag(V_{qd1}^*)sin\theta_1 + \sqrt{3}mag(V_{qd1}^*)cos\theta_1)}{mag(V_{qd1}^*)(3cos\theta_3 + \sqrt{3}sin\theta_3)}$$

Setting the partial derivative to zero,

$$\frac{\partial k_2}{\partial \theta_1} = \frac{3sin\theta_1 - \sqrt{3}cos\theta_1}{3cos\theta_3 + \sqrt{3}sin\theta_3} = 0$$

$$\Rightarrow 3sin\theta_1 - \sqrt{3}cos\theta_1 = 0 \text{ and } \theta_1 = a\tan\left(\frac{\sqrt{3}}{3}\right) = \frac{\pi}{6}.$$

Similarly, the partial derivative of k_2 with respect to θ_2 is given by

$$\frac{\partial k_2}{\partial \theta_2} = \frac{-(-3mag(V_{qd1}^*)k_1 sin(\theta_2) + \sqrt{3}mag(V_{qd1}^*)k_1 cos(\theta_2))}{mag(V_{qd1}^*)(3cos\theta_3 + \sqrt{3}sin\theta_3)}$$

$$\frac{\partial k_2}{\partial \theta_2} = \frac{k_1(3sin\theta_2 - \sqrt{3}cos\theta_2)}{3cos\theta_3 + \sqrt{3}sin\theta_3} = 0$$

$$\Rightarrow 3sin\theta_2 - \sqrt{3}cos\theta_2 = 0$$

Thus $\theta_2 = a\tan\left(\frac{\sqrt{3}}{3}\right) = \frac{\pi}{6}.$

Finally, the partial derivative of k_2 with respect to θ_3 :

$$\frac{\partial k_2}{\partial \theta_3} = \frac{\left[\begin{array}{l}-(3mag(V_{qd1}^*)\cos\theta_1 - 2V_{dc} + 3mag(V_{qd1}^*)k_1\cos\theta_2 + \\ +\sqrt{3}mag(V_{qd1}^*)\sin\theta_1 + \sqrt{3}mag(V_{qd1}^*)k_1\sin\theta_2)\end{array}\right]\left(3\sin\theta_3 - \sqrt{3}\cos\theta_3\right)}{mag(V_{qd1}^*)\left(3\cos\theta_3 + \sqrt{3}\sin\theta_3\right)^2} = 0 \qquad (6.46)$$

In (6.46), either or both of the product terms of the numerator can be zero. That is:

$$\left(3\sin\theta_3 - \sqrt{3}\cos\theta_3\right) = 0 \text{ or}$$

$- mag(V_{qd1}^*)(3\cos\theta_1 + \sqrt{3}\sin\theta_1 + 3k_1\cos\theta_2 + \sqrt{3}k_1\sin\theta_2) + 2V_{dc} = 0$. Since only the first

expression contains θ_3 , this expression is used to solve for θ_3 . That is:

$$3\sin\theta_3 - \sqrt{3}\cos\theta_3 = 0 \text{ and } \theta_3 = a\tan\left(\frac{\sqrt{3}}{3}\right) = \frac{\pi}{6}$$

Thus if $\theta_1 = \theta_2 = \theta_3 = \pi/6$, k_2 is maximized. That is:

$$k_{2,max} = k_2\left(\pi/6, \pi/6, \pi/6\right) = \frac{-\left[\begin{array}{l}(3mag(V_{qd1}^*)\cos(\pi/6) - 2V_{dc} + 3mag(V_{qd1}^*)k_1\cos(\pi/6) + \\ +\sqrt{3}mag(V_{qd1}^*)\sin(\pi/6) + \sqrt{3}mag(V_{qd1}^*)k_1\sin(\pi/6))\end{array}\right]}{mag(V_{qd1}^*)(3\cos(\pi/6) + \sqrt{3}\sin(\pi/6))}$$

$$k_{2,max} = k_2\left(\pi/6, \pi/6, \pi/6\right) = \frac{-\left[\begin{array}{l}(\frac{3\sqrt{3}}{2}mag(V_{qd1}^*) - 2V_{dc} + \frac{3\sqrt{3}}{2}mag(V_{qd1}^*)k_1 + \\ +\frac{\sqrt{3}}{2}mag(V_{qd1}^*) + \frac{\sqrt{3}}{2}mag(V_{qd1}^*)k_1)\end{array}\right]}{\frac{4\sqrt{3}}{2}mag(V_{qd1}^*)} \text{ and}$$

$$k_{2,max} = k_2\left(\pi/6, \pi/6, \pi/6\right) = \frac{V_{dc}}{\sqrt{3}mag(V_{qd1}^*)} - k_1 - 1 \qquad (6.47)$$

If the modulation indices are defined as:

246

$m_1 = \dfrac{2}{V_{dc}} mag(V_{qd1}^*)$, $\quad m_2 = \dfrac{2}{V_{dc}} mag(V_{qd2}^*)$, and $\quad m_3 = \dfrac{2}{V_{dc}} mag(V_{qd3}^*)$ then (6.47) can be

rewritten as:

$$\sqrt{3}\left(mag(V_{qd1}^*)k_1 + mag(V_{qd1}^*)k_2 + mag(V_{qd1}^*)\right) = V_{dc}$$

$$\sqrt{3}\left(mag(V_{qd2}^*) + m\,mag(V_{qd3}^*) + mag(V_{qd1}^*)\right) = V_{dc}$$

$$\frac{mag(V_{qd1}^*)}{V_{dc}} + \frac{mag(V_{qd2}^*)}{V_{dc}} + \frac{mag(V_{qd3}^*)}{V_{dc}} = \frac{1}{\sqrt{3}}$$

Thus, the constraint on the modulation indices is given by

$$m_1 + m_2 + m_3 \le \frac{2}{\sqrt{3}} \qquad (6.48)$$

6.3.1.3. **Switching sequence for 12-switch converter.** In general, the dwell times of the active vectors are less than unity when operating in the linear modulation region. The remaining time may then be filled by one or more of the zero vectors. The switching sequence adopted in this research is to place switching states in a sequence that minimizes switching loss by reducing the number of switching commutations.

For the 12-switch converter, there are two hundred and sixteen (216) possible sector combinations involving *Inv1*, *Inv2*, and *Inv3*. The brute way to obtain the switching sequence is to laboriously go through all 216 possible sector combinations and layout each sequence. A closer examination of the first eight (8) sector combinations given in Tables 6.6 – 6.13 however, show some pattern. Two important observations can be inferred from Tables 6.6 – 6.13; the positions of the four zero sequence states are the same and the positions of the active states in the sequence depend entirely on whether the sector is odd or even. From these observations, the 216 sector combinations can be categorized into eight (8) possible sector combinations involving *Inv1*, *Inv2*, and *Inv3*. If

247

each sector combination is represented by (n_1, n_2, n_3) where n_1, n_2, n_3 represent the sector numbers for *Inv1*, *Inv2*, and *Inv3* respectively, then the possible sector combinations given that an odd sector is represented as a '0' and an even sector as a '1' are (0,0,0), (0,0,1); (0,1,0); (0,1,1); (1,0,0); (1,0,1); (1,1,0), and (111). Table 6.14 gives a summary of the switching sequence for all 216 sector combinations. In this way, a lot of computational burden is saved since in a switching period, only sector combinations involved are checked and used for calculating the switching durations.

Table 6.6. Switching sequence table for sector (I, I, I)

	SVM#	S_{ap}	S_{am1}	S_{am2}	S_{an}	S_{bp}	S_{bm1}	S_{bm2}	S_{bn}	S_{cp}	S_{cm1}	S_{cm2}	S_{cn}	time
(I,I,I)														
V_{01}	19	0	1	1	1	0	1	1	1	0	1	1	1	t_{01}
V_a	1	1	0	1	1	0	1	1	1	0	1	1	1	t_a
V_b	2	1	0	1	1	0	1	1	1	1	0	1	1	t_b
V_{02}	20	1	0	1	1	1	0	1	1	1	0	1	1	t_{02}
V_c	7	1	1	0	1	1	0	1	1	1	0	1	1	t_c
V_d	8	1	1	0	1	1	0	1	1	1	1	0	1	t_d
V_{04}	22	1	1	0	1	1	1	0	1	1	1	0	1	t_{04}
V_e	13	1	1	1	0	1	1	0	1	1	1	0	1	t_e
V_f	14	1	1	1	0	1	1	0	1	1	1	1	0	t_f
V_{03}	21	1	1	1	0	1	1	1	0	1	1	1	0	t03

Table 6.7. Switching sequence table for sector (I, I, II)

	SVM#	S_{ap}	S_{am1}	S_{am2}	S_{an}	S_{bp}	S_{bm1}	S_{bm2}	S_{bn}	S_{cp}	S_{cm1}	S_{cm2}	S_{cn}	time
(I,I,II)														
V_{01}	19	0	1	1	1	0	1	1	1	0	1	1	1	t_{01}
V_a	1	1	0	1	1	0	1	1	1	0	1	1	1	t_a
V_b	2	1	0	1	1	0	1	1	1	1	0	1	1	t_b
V_{02}	20	1	0	1	1	1	0	1	1	1	0	1	1	t_{02}
V_c	7	1	1	0	1	1	0	1	1	1	0	1	1	t_c
V_d	8	1	1	0	1	1	0	1	1	1	1	0	1	t_d
V_{04}	22	1	1	0	1	1	1	0	1	1	1	0	1	t_{04}
V_f	15	1	1	0	1	1	1	0	1	1	1	1	0	t_f
V_e	14	1	1	1	0	1	1	0	1	1	1	1	0	t_e
V_{03}	21	1	1	1	0	1	1	1	0	1	1	1	0	t_{03}

Table 6.8. Switching sequence table for sector (I, II, I)

	SVM#	S_{ap}	S_{am1}	S_{am2}	S_{an}	S_{bp}	S_{bm1}	S_{bm2}	S_{bn}	S_{cp}	S_{cm1}	S_{cm2}	S_{cn}	time
(I,II,I)														
V_{01}	19	0	1	1	1	0	1	1	1	0	1	1	1	t_{01}
V_a	1	1	0	1	1	0	1	1	1	0	1	1	1	t_a
V_b	2	1	0	1	1	0	1	1	1	1	0	1	1	t_b
V_{02}	20	1	0	1	1	1	0	1	1	1	0	1	1	t_{02}
V_c	9	1	0	1	1	1	0	1	1	1	1	0	1	t_d
V_d	8	1	1	0	1	1	0	1	1	1	1	0	1	t_c
V_{04}	22	1	1	0	1	1	1	0	1	1	1	0	1	t_{04}
V_f	13	1	1	1	0	1	1	0	1	1	1	0	1	t_e
V_e	14	1	1	1	0	1	1	0	1	1	1	1	0	t_f
V_{03}	21	1	1	1	0	1	1	1	0	1	1	1	0	t_{03}

Table 6.9. Switching sequence table for sector (I, II, II)

	SVM#	S_{ap}	S_{am1}	S_{am2}	S_{an}	S_{bp}	S_{bm1}	S_{bm2}	S_{bn}	S_{cp}	S_{cm1}	S_{cm2}	S_{cn}	time
(I,II,II)														
V_{01}	19	0	1	1	1	0	1	1	1	0	1	1	1	t_{01}
V_a	1	1	0	1	1	0	1	1	1	0	1	1	1	t_a
V_b	2	1	0	1	1	0	1	1	1	1	0	1	1	t_b
V_{02}	20	1	0	1	1	1	0	1	1	1	0	1	1	t_{02}
V_c	9	1	0	1	1	1	0	1	1	1	1	0	1	t_d
V_d	8	1	1	0	1	1	0	1	1	1	1	0	1	t_c
V_{04}	22	1	1	0	1	1	1	0	1	1	1	0	1	t_{04}
V_f	15	1	1	0	1	1	1	0	1	1	1	1	0	t_f
V_e	14	1	1	1	0	1	1	0	1	1	1	1	0	t_e
V_{03}	21	1	1	1	0	1	1	1	0	1	1	1	0	t_{03}

Table 6.10. Switching sequence table for sector (II, I, I)

	SVM#	S_{ap}	S_{am1}	S_{am2}	S_{an}	S_{bp}	S_{bm1}	S_{bm2}	S_{bn}	S_{cp}	S_{cm1}	S_{cm2}	S_{cn}	time
(II,I,I)														
V_{01}	19	0	1	1	1	0	1	1	1	0	1	1	1	t_{01}
V_b	3	0	1	1	1	0	1	1	1	1	0	1	1	t_b
V_a	2	1	0	1	1	0	1	1	1	1	0	1	1	t_a
V_{02}	20	1	0	1	1	1	0	1	1	1	0	1	1	t_{02}
V_c	7	1	1	0	1	1	0	1	1	1	0	1	1	t_c
V_d	8	1	1	0	1	1	0	1	1	1	1	0	1	t_d
V_{04}	22	1	1	0	1	1	1	0	1	1	1	0	1	t_{04}
V_e	13	1	1	1	0	1	1	0	1	1	1	0	1	t_e
V_f	14	1	1	1	0	1	1	0	1	1	1	1	0	t_f
V_{03}	21	1	1	1	0	1	1	1	0	1	1	1	0	t_{03}

Table 6.11. Switching sequence table for sector (II, I, II)

	SVM#	S_{ap}	S_{am1}	S_{am2}	S_{an}	S_{bp}	S_{bm1}	S_{bm2}	S_{bn}	S_{cp}	S_{cm1}	S_{cm2}	S_{cn}	time
(II,I,II)														
V_{01}	19	0	1	1	1	0	1	1	1	0	1	1	1	t_{01}
V_b	3	0	1	1	1	0	1	1	1	1	0	1	1	t_b
V_a	2	1	0	1	1	0	1	1	1	1	0	1	1	t_a
V_{02}	20	1	0	1	1	1	0	1	1	1	0	1	1	t_{02}
V_c	7	1	1	0	1	1	0	1	1	1	0	1	1	t_c
V_d	8	1	1	0	1	1	0	1	1	1	1	0	1	t_d
V_{04}	22	1	1	0	1	1	1	0	1	1	1	0	1	t_{04}
V_f	15	1	1	0	1	1	1	0	1	1	1	1	0	t_f
V_e	14	1	1	1	0	1	1	0	1	1	1	1	0	t_e
V_{03}	21	1	1	1	0	1	1	1	0	1	1	1	0	t_{03}

Table 6.12. Switching sequence table for sector (II, II, I)

	SVM#	S_{ap}	S_{am1}	S_{am2}	S_{an}	S_{bp}	S_{bm1}	S_{bm2}	S_{bn}	S_{cp}	S_{cm1}	S_{cm2}	S_{cn}	time
(II,II,I)														
V_{01}	19	0	1	1	1	0	1	1	1	0	1	1	1	t_{01}
V_b	2	1	0	1	1	0	1	1	1	1	0	1	1	t_b
V_c	1	1	0	1	1	0	1	1	1	0	1	1	1	t_a
V_{02}	20	1	0	1	1	1	0	1	1	1	0	1	1	t_{02}
V_d	9	1	0	1	1	1	0	1	1	1	1	0	1	t_d
V_c	8	1	1	0	1	1	0	1	1	1	1	0	1	t_c
V_{04}	22	1	1	0	1	1	1	0	1	1	1	0	1	t_{04}
V_e	13	1	1	1	0	1	1	0	1	1	1	0	1	t_e
V_f	14	1	1	1	0	1	1	0	1	1	1	1	0	t_f
V_{03}	21	1	1	1	0	1	1	1	0	1	1	1	0	t_{03}

Table 6.13. Switching sequence table for sector (II, II, II)

	SVM#	S_{ap}	S_{am1}	S_{am2}	S_{an}	S_{bp}	S_{bm1}	S_{bm2}	S_{bn}	S_{cp}	S_{cm1}	S_{cm2}	S_{cn}	time
II,II,II														
V_{01}	19	0	1	1	1	0	1	1	1	0	1	1	1	t_{01}
V_b	2	1	0	1	1	0	1	1	1	1	0	1	1	t_b
V_c	1	1	0	1	1	0	1	1	1	0	1	1	1	t_a
V_{02}	20	1	0	1	1	1	0	1	1	1	0	1	1	t_{02}
V_d	9	1	0	1	1	1	0	1	1	1	1	0	1	t_d
V_c	8	1	1	0	1	1	0	1	1	1	1	0	1	t_c
V_{04}	22	1	1	0	1	1	1	0	1	1	1	0	1	t_{04}
V_f	15	1	1	0	1	1	1	0	1	1	1	1	0	t_f
V_e	14	1	1	1	0	1	1	0	1	1	1	1	0	t_e
V_{03}	21	1	1	1	0	1	1	1	0	1	1	1	0	t_{03}

Table 6.14. Summarized switching sequence for all possible sector combinations (0=odd sector; 1=even sector)

Switching Sequence	V^*_{qd1} in	V^*_{qd2} in	V^*_{qd2} in
V_{01}→V_a→V_b→V_{02}→V_c→V_d→V_{04}→V_e→V_f→V_{03}	0	0	0
V_{01}→V_a→V_b→V_{02}→V_c→V_d→V_{04}→V_f→V_e→V_{03}	0	0	1
V_{01}→V_a→V_b→V_{02}→V_d→V_e→V_{04}→V_e→V_f→V_{03}	0	1	0
V_{01}→V_a→V_b→V_{02}→V_c→V_d→V_{04}→ V_f→V_e→V_{03}	0	1	1
V_{01}→V_b→V_a→V_{02}→V_c→V_d→V_{04}→V_e→V_f→V_{03}	1	0	0
V_{01}→V_b→V_a →V_{02}→V_c→V_d→V_{04}→ V_f→V_e→V_{03}	1	0	1
V_{01}→V_b→V_a V_{02}→ V_d→V_e →V_{04}→V_e→V_f→V_{03}	1	1	0
V_{01}→V_b→V_a →V_{02}→V_d→V_e→V_{04}→ V_f→V_e→V_{03}	1	1	1

6.3.1.4.**Calculating the device turn-on times.** Similar to finding the switching sequence, the device turn on times may be calculated by going through all 216 possible sector combinations, finding the switching durations of the active states and the zero states and then summing them up to obtain the device turn-on time. However a close examination produces a simpler method. An example is given here on how to determine the turn-on times of the upper switches, represented as Tap, Tbp, and Tcp.

Since the switch turned-off periods (i.e., when $S_{ap} = S_{bp} = S_{cp} = 0$) do not contribute to T_{ap}, T_{bp} and T_{cp}, a closer examination of these may reveal some pattern. The information presented in Table 6.15 is extracted from Table 6.5 and categorizes all sectors in *Inv1*, *Inv2*, and *Inv3* into three groups. The first group of sectors referred to as *independent* sectors and represented by a '0' are all sectors that are completely unaffected by the active states with their switching functions $S_{ap} = S_{bp} = S_{cp} = 0$. The second group referred to here as *dependent* sectors and represented by a '1' are all sectors completely enclosed by the active states with $S_{ap} = S_{bp} = S_{cp} = 0$. The last group referred to as *partially dependent* sectors and represented by a '-1' are all sectors that are share a boundary with the active states where $S_{ap} = S_{bp} = S_{cp} = 0$.

For example, to find T_{ap}, refer to Table 6.5 and observe that $S_{ap} = 0$ for the switching states V_3, V_4, V_5 and V_{19}. Referring to the space diagram for *Inv1* which is redrawn in Figure 6.5 showing the three categories of sectors just described above. Note that in this example, only *Inv1* has its $S_{ap} = S_{bp} = S_{cp} = 0$ as shown in Tables 6.5 and 6.15. In summary, there are eight possible sector combinations involving these 3 groups of sectors in addition to a sector number being either odd or even as shown in Table 6.16.

Table 6.15. Switching states with switching functions $S_{ap} = S_{bp} = S_{cp} = 0$

	Inv1			Inv2			Inv3		
	S_{ap}	S_{bp}	S_{cp}	S_{ap}	S_{bp}	S_{cp}	S_{ap}	S_{bp}	S_{cp}
State	$V_3, V_4,$ V_5, V_{19}	$V_1, V_2, V_3,$ V_{19}	$V_1, V_5,$ V_6, V_{19}	V_{19}	V_{19}	V_{19}	V_{19}	V_{19}	V_{19}
Independent sectors = 0	I,VI	IV, V	II, III	All	All	All	All	All	All
dependent sectors = 1	III, IV	I, II	V, VI	none	none	none	none	none	none
Partially dependent sectors = -1	II, V	III, IV	I, IV	none	none	none	none	none	none
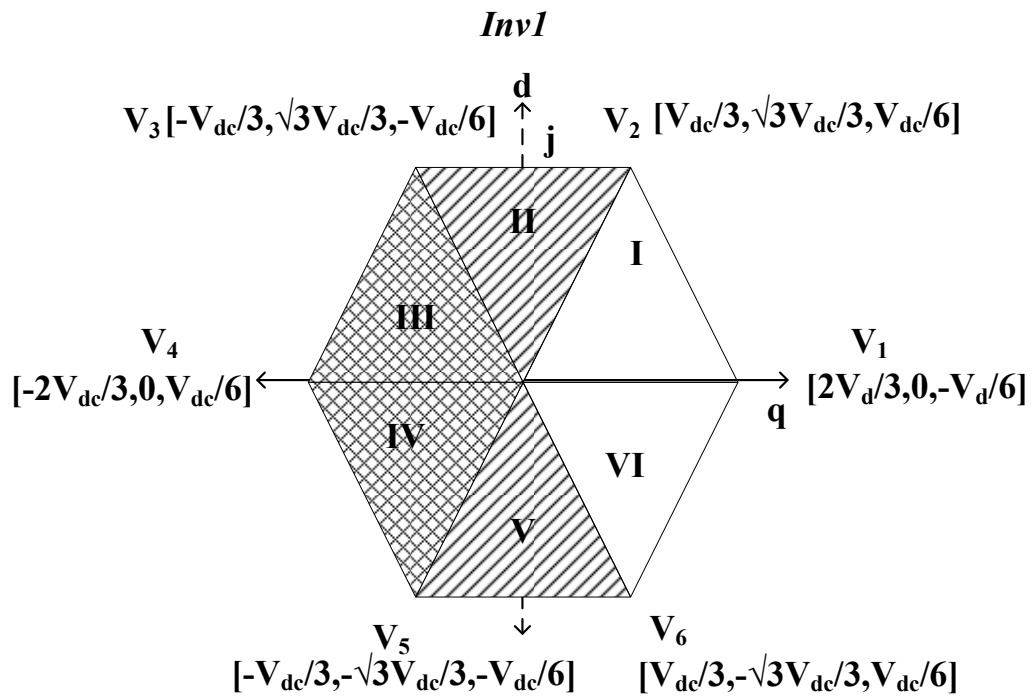
Figure 6.5. Space vector diagram of *Inv1* showing sector categorizations
Note: double cross shading depicts dependent sector, single cross shaping for partially dependent sectors and no shading for independent sectors

Table 6.16. Possible sector combinations based on Table 6.15 (0 = independent sector, 1 = dependent sector, and -1 = partially dependent)

Sector combinations			
n_1	n_2	n_2	$T_{ap} = T_{bp} = T_{cp} = t_{01} + t_{02} + t_{03} + t_{04} + t_a + t_b + t_c + t_d + t_e + t_f$
0	0	0	$t_{01} = 0$
0	1	0	$t_{01} = 0$
0	-1	0	$t_{01} = 0$
1	0	0	$t_0 = t_a = t_b = 0$
1	1	0	$t_0 = t_a = t_b = 0$
1	-1	0	$t_0 = t_a = t_b = 0$
-1	0	0	$t_0 = t_a = 0$ if n_1 is odd; $t_0 = t_b = 0$ if n_1 is even
-1	1	0	$t_0 = t_a = 0$ if n_1 is odd; $t_0 = t_b = 0$ if n_1 is even
-1	-1	0	$t_0 = t_a = 0$ if n_1 is odd; $t_0 = t_b = 0$ if n_1 is even

So the question is how do the above sector categorizations affect the device times T_{ap}, T_{bp} and T_{cp}? Table 6.16 shows the turn on times of the upper devices. Observe that all sectors in *Inv2* and *Inv3* are independent sectors and are shown not to affect the variations of T_{ap}, T_{bp} and T_{cp}. Tables 6.15 and 6.16 may be generalized for determining T_{am1}, T_{bm1}, T_{cm1} as well as T_{an}, T_{bn} and T_{cn}. In the case of T_{am1}, T_{bm1}, and T_{cm1}, the sectors of interest involves those in *Inv1* and *Inv2* (i.e. n_1 and n_2), whereas for T_{an}, T_{bn} and T_{cn}, only n_3 is of interest. The generalized algorithm of finding the device turn-on times is as follows:

1) Check the switching states that give $S_{ip} = 0$, $S_{im1} = 0$, or $S_{in} = 0$

2) Categorize all sectors in *Inv1*, *Inv2*, and *Inv3* into independent = 0, dependent = 1, and partially dependent = -1 sectors

3) If $S_{ip} = 0$, $S_{im1} = 0$ and $S_{in} = 0$, $t_{01} = 0$, $t_{02} = 0$, and $t_{03} = 0$ respectively

255

4) If n_1, n_2 or $n_3 = 1$(dependent),

    a.   For n_1, $t_a = t_b = 0$

    b.   For n_2, $t_c = t_d = 0$

    c.   For n_3, $t_e = t_f = 0$

5) If n_1, n_2 or $n_3 = -1$ (partially dependent),

    a.   If $n_1 =$ even, $t_b = 0$, otherwise $t_a = 0$

    b.   If $n_2 =$ even, $t_d = 0$, otherwise $t_c = 0$

    c.   If $n_2 =$ even, $t_e = 0$, otherwise $t_f = 0$

6) Sum the dwell times to obtain the corresponding device turn-on time

6.3.1.5.**Generalized neutral voltage (V_{no}, V_{mo}, V_{zo}).** It has been shown in [70] that the placement of the zero space vectors is the fundamental difference between different PWM strategies. In this research, it is assumed that all four (4) zero vectors are used in synthesizing the reference voltages with the utilization factors α, β, γ, and μ. The average neutral voltage can be approximated as:

$$V_{x0} >= V_{0a}t_a + V_{0b}t_b + V_{0c}t_c + V_{0d}t_d + V_{01}t_{01} + V_{02}t_{02} + V_{03}t_{03} \qquad (6.49)$$

Where $x = n$, m, or z; V_{0a}, V_{0b}, V_{0c}, V_{0d}, V_{0e}, and V_{0f} are the zero sequence components of the active voltage vectors V_a, V_b, V_c, V_d, V_e, and V_f respectively.

In synthesizing a desired voltage, it was shown earlier that all the feasible sector combinations can be grouped into 8 categories. Referring to Table 6.16 using one sector combination as a representation of each of the 8 sector combinations, the neutral voltages can be calculated in terms of the active and zero vector device dwell times t_a, t_b, t_c, t_d, t_e,

256

t_f, t_{01}, t_{02}, t_{03}, and t_{04}. Table 6.17 shows the expressions for the neutral voltages of the three outputs. They are shown to depend entirely on the sector numbers n_1, n_2 and n_3 and whether these are odd or even. This dependency gives rise to two expressions each for V_{no}, V_{mo} and V_{zo} as given in (6.50) – (6.52).

$$V_{no} = 3(-t_{01} + t_{02} + t_{03} + t_{04}) + \eta(t_a - t_b) + 3(t_c + t_d) + 3(t_e + t_f) \qquad (6.50)$$

$$V_{mo} = 3(-t_{01} - t_{02} + t_{03} + t_{04}) - 3(t_a + t_b) + \eta(t_c - t_d) + 3(t_e + t_f) \qquad (6.51)$$

$$V_{zo} = 3(-t_{01} - t_{02} + t_{03} - t_{04}) + 3(t_a + t_b) - 3(t_c + t_d) + \eta(t_e - t_f) \qquad (6.52)$$

where $\eta = +1$ for even sector number and $\eta = -1$ for odd sector number.

Table 6.17. Neutral voltages (V_{no}, V_{mo} and V_{zo}) for some selected sector combinations

n_1	n_2	n_3	V_{no}	V_{mo}	V_{zo}
I	I	I	$3(t_{02} - t_{01} + t_{03} + t_{04}) - t_a + t_b$ $+3(t_c + t_d + t_e + t_f)$	$3(t_{03} - t_{02} - t_{01} + t_{04}) - 3(t_a + t_b)$ $- t_c + t_d + 3(t_e + t_f)$	$3(t_{03} - t_{02} - t_{01} - t_{04}) - 3(t_a + t_b)$ $- 3(t_c + t_d) - t_e + t_f$
I	I	II	$3(t_{02} - t_{01} + t_{03} + t_{04}) - t_a + t_b$ $+3(t_c + t_d + t_e + t_f)$	$3(t_{03} - t_{02} - t_{01} + t_{04}) - 3(t_a + t_b)$ $- t_c + t_d + 3(t_e + t_f)$	$3(t_{03} - t_{02} - t_{01} - t_{04}) - 3(t_a + t_b)$ $- 3(t_c + t_d) + t_e - t_f$
I	II	I	$3(t_{02} - t_{01} + t_{03} + t_{04}) - t_a + t_b$ $+ 3(t_c + t_d + t_e + t_f)$	$3(t_{03} - t_{02} - t_{01} + t_{04}) - 3(t_a + t_b)$ $+ t_c - t_d + 3(t_e + t_f)$	$3(t_{03} - t_{02} - t_{01} - t_{04}) - 3(t_a + t_b)$ $- 3(tc + td) - te + tf$
I	II	II	$3(t_{02} - t_{01} + t_{03} + t_{04}) - t_a + t_b$ $+ 3(t_c + t_d + t_e + t_f)$	$3(t_{03} - t_{02} - t_{01} + t_{04}) - 3(t_a + t_b)$ $+ t_c - t_d + 3(t_e + t_f)$	$3(t_{03} - t_{02} - t_{01} - t_{04}) - 3(t_a + t_b)$ $- 3(t_c + t_d) + t_e - t_f$
II	I	I	$3(t_{02} - t_{01} + t_{03} + t_{04}) + t_a - t_b$ $+ 3(t_c + t_d + t_e + t_f)$	$3(t_{03} - t_{02} - t_{01} + t_{04}) - 3(t_a + t_b)$ $- t_c + t_d + 3(t_e + t_f)$	$3(t_{03} - t_{02} - t_{01} - t_{04}) - 3(t_a + t_b)$ $- 3(t_c + t_d) - t_e + t_f$
II	I	II	$3(t_{02} - t_{01} + t_{03} + t_{04} + t_a - t_b$ $+ 3(t_c + t_d + t_e + t_f)$	$3(t_{03} - t_{02} - t_{01} + t_{04}) - 3(t_a + t_b)$ $- t_c + t_d + 3(t_e + t_f)$	$3(t_{03} - t_{02} - t_{01} - t_{04}) - 3(t_a + t_b)$ $- 3(t_c + t_d) + t_e - t_f$
II	II	I	$3(t_{02} - t_{01} + t_{03} + t_{04}) + t_a - t_b$ $+ 3(t_c + t_d + t_e + t_f)$	$3(t_{03} - t_{02} - t_{01} + t_{04}) - 3(t_a + t_b)$ $+ t_c - t_d + 3(t_e + t_f)$	$3(t_{03} - t_{02} - t_{01} - t_{04}) - 3(t_a + t_b)$ $- 3(t_c + t_d) - t_e + t_f$
II	II	II	$3(t_{02} - t_{01} + t_{03} + t_{04}) + _{ta} - t_b$ $+ 3(t_c + t_d + t_e + t_f)$	$3(t_{03} - t_{02} - t_{01} + t_{04}) - 3(t_a + t_b)$ $+ t_c - t_d + 3(t_e + t_f)$	$3(t_{03} - t_{02} - t_{01} - t_{04}) - 3(t_a + t_b)$ $- 3(t_c + t_d) + t_e - t_f$

Table 6.18. Device switching times in terms of the line-to-line voltages

Sector	I	II	III	IV	V	VI
t_a	V_{ab1}/V_{dc}	V_{ac1}/V_{dc}	V_{bc1}/V_{dc}	V_{ba1}/V_{dc}	V_{ca1}/V_{dc}	V_{cb1}/V_{dc}
t_b	V_{bc1}/V_{dc}	V_{ba1}/V_{dc}	V_{ca1}/V_{dc}	V_{cb1}/V_{dc}	V_{ab1}/V_{dc}	V_{ac1}/V_{dc}
V_{max1}	V_{an1}	V_{bn1}	V_{bn1}	V_{cn1}	V_{cn1}	V_{an1}
V_{min1}	V_{cn1}	V_{cn1}	V_{an1}	V_{an1}	V_{bn1}	V_{bn1}
t_c	V_{ab2}/V_{dc}	V_{ac2}/V_{dc}	V_{bc2}/V_{dc}	V_{ba2}/V_{dc}	V_{ca2}/V_{dc}	V_{cb2}/V_{dc}
t_d	V_{bc2}/V_{dc}	V_{ba2}/V_{dc}	V_{ca2}/V_{dc}	V_{cb2}/V_{dc}	V_{ab2}/V_{dc}	V_{ac2}/V_{dc}
V_{max2}	V_{am2}	V_{bm2}	V_{bm2}	V_{cm2}	V_{cm2}	V_{am2}
V_{min2}	V_{cm2}	V_{cm2}	V_{am2}	V_{am2}	V_{bm2}	V_{bm2}

Referring to Table 6.17, the neutralized voltages in sector (I, I, I), are given by

$$V_{no} = 3(-t_{01} + t_{02} + t_{03} + t_{04}) - (t_a - t_b) + 3(t_c + t_d) + 3(t_e + t_f) \qquad (6.53)$$

$$V_{mo} = 3(-t_{01} - t_{02} + t_{03} + t_{04}) - 3(t_a + t_b) - (t_c - t_d) + 3(t_e + t_f) \qquad (6.54)$$

$$V_{zo} = 3(-t_{01} - t_{02} + t_{03} - t_{04}) - 3(t_a + t_b) - 3(t_c + t_d) - (t_e - t_f) \qquad (6.55)$$

In this sector combination, the active vectors dwell times in terms of the line-to-line voltages as in given Table 6.18 are:

$t_a = \dfrac{V_{ab1}}{V_{dc}}$, $t_b = \dfrac{V_{bc1}}{V_{dc}}$, $t_c = \dfrac{V_{ab2}}{V_{dc}}$, $t_d = \dfrac{V_{bc2}}{V_{dc}}$, $t_e = \dfrac{V_{ab3}}{V_{dc}}$, and $t_f = \dfrac{V_{bc3}}{V_{dc}}$. Substituting these

dwell times into (6.53) – (6.55), the expressions for the neutralized voltages can be rewritten in terms of the line-to-line voltages.

V_{no} is given by

$$V_{no} = 3(-\alpha t_0 + \beta t_0 + \gamma t_0 + (1 - \alpha - \beta - \gamma)t_0) - (t_a - t_b) + 3(t_c + t_d) + 3(t_e + t_f)$$

$$V_{no} = 3(1 - 2\alpha)t_0 - (t_a - t_b) + 3(t_c + t_d) + 3(t_e + t_f)$$

$$V_{no} = 3\,(1-2\alpha)\left(1-t_a-t_b-t_c-t_d-t_e-t_f\right)-\left(t_a-t_b\right)+3\left(t_c+t_d\right)+3\left(t_e+t_f\right)$$

$$V_{no} = \frac{V_{dc}}{2}-\alpha V_{dc}-\frac{V_{bc1}}{3}-\frac{2V_{ab1}}{3}+\alpha\left(V_{ab1}+V_{ab2}+V_{ab3}+V_{bc1}+V_{bc2}+V_{bc3}\right) \tag{6.56}$$

V_{mo} is given by

$$V_{mo} = 3(-\alpha t_0-\beta t_0+\gamma t_0+(1-\alpha-\beta-\gamma)t_0)-3\left(t_a+t_b\right)-\left(t_c-t_d\right)+3\left(t_e+t_f\right)$$

$$V_{mo} = 3\left((-\alpha-\beta+\gamma+(1-\alpha-\beta-\gamma))t_0\right)-3\left(t_a+t_b\right)-\left(t_c-t_d\right)+3\left(t_e+t_f\right)$$

$$V_{mo} = 3(1-2\alpha-2\beta)t_0-3\left(t_a+t_b\right)-\left(t_c-t_d\right)+3\left(t_e+t_f\right)$$

$$V_{mo} = 3(1-2\alpha-2\beta)\left(1-t_a-t_b-t_c-t_d-t_e-t_f\right)-3\left(t_a+t_b\right)-\left(t_c-t_d\right)+3\left(t_e+t_f\right)$$

$$V_{mo} = \left[\begin{array}{l}\dfrac{V_{dc}}{2}-\dfrac{2V_{ab2}}{3}-V_{bc1}-\dfrac{V_{bc2}}{3}-V_{ab1}+\alpha\left(V_{ab1}+V_{ab2}+V_{ab3}\right)+\beta\left(V_{ab1}+V_{ab2}+V_{ab3}\right)\\[2mm]+\alpha\left(V_{bc1}+V_{bc2}+V_{bc3}\right)+\beta\left(V_{bc1}+V_{bc2}+V_{bc3}\right)-\alpha V_{dc}-\beta V_{dc}\end{array}\right]$$

$$V_{mo} = \left[\begin{array}{l}\dfrac{V_{dc}}{2}\left(1-2(\alpha+\beta)\right)-\dfrac{2V_{ab2}}{3}-V_{bc1}-\dfrac{V_{bc2}}{3}-V_{ab1}+\\[2mm]+\ (\alpha+\beta)(V_{ab1}+V_{ab2}+V_{ab3})\\[2mm]+(\alpha+\beta)(V_{bc1}+V_{bc2}+V_{bc3})\end{array}\right] \tag{6.57}$$

And V_{zo} is given by

$$V_{zo} = 3(-\alpha t_{01}-\beta t_{02}+\gamma t_{03}-(1-\alpha-\beta-\gamma)t_{04})-3\left(t_a+t_b\right)-3\left(t_c+t_d\right)-\left(t_e-t_f\right)$$
$$V_{zo} = 3(2\gamma-1)t_0-3\left(t_a+t_b\right)-3\left(t_c+t_d\right)-\left(t_e-t_f\right)$$

$$V_{zo} = 3(2\gamma - 1)(1 - t_a - t_b - t_c - t_d - t_e - t_f) - 3(t_a + t_b) - 3(t_c + t_d) - (t_e - t_f)$$

$$V_{zo} = \frac{V_{dc}}{2}(2\gamma - 1) + \frac{V_{ab3}}{3} + \frac{2V_{bc3}}{3} - \gamma(V_{ab1} - V_{ab2} - V_{ab3} - V_{bc1} - V_{bc2} - V_{bc3}) \quad (6.58)$$

The phase 'b' voltages in terms of phase 'a' and 'c' can be written as:

$V_{b1} = -V_{a1} - V_{c1}, \; V_{b2} = -V_{a2} - V_{c2}, \; V_{b3} = -V_{a3} - V_{c3}$

In sector (I, I, I) , the maximum and minimum voltages are:

$V_{a1} = V_{max1}, \; V_{a2} = V_{max2}, \; V_{a3} = V_{max3},$

$V_{c1} = V_{min1}, \; V_{c2} = V_{min2}, \quad V_{c3} = V_{min3}$

Substituting the above definitions into (6.56) - (5.58), the neutral voltages are given as:

$$V_{no} = \begin{bmatrix} \frac{V_{dc}}{2}(1 - 2\alpha) - V_{max1} + \alpha(V_{max1} + V_{max2} + V_{max3}) + \\ -\alpha(V_{min1} + V_{min2} + V_{min3}) \end{bmatrix} \quad (6.59)$$

$$V_{mo} = \begin{bmatrix} \frac{V_{dc}}{2}(1 - 2\alpha - 2\beta) - V_{max2} - V_{max1} + V_{min1} + \\ +\alpha(V_{max1} + V_{max2} + V_{max3}) - \beta(V_{min1} + V_{min2} + V_{min3}) \end{bmatrix} \quad (6.60)$$

$$V_{zo} = \begin{bmatrix} \frac{V_{dc}}{2}(2\gamma - 1) - V_{min3} - \gamma(V_{max1} + V_{max2} + V_{max3}) + \gamma(V_{min1} + V_{min2} + V_{min3}) \end{bmatrix} \quad (6.61)$$

Similar mathematical manipulations for all other sector combinations all result in (6.59) – (6.61). These are therefore the generalized neutral voltages for the 12-switch converter.

6.3.2. Carrier-Based Pulse-Width Modulation (CB-PWM) of 12-Switch Converter

It has been was shown that there are eighteen (18) feasible active switching states and on per phase basis, three states can be identified as listed in Table 6.19 based on the switching function constraint.

Table 6.19. Per phase Truth Table for 12-switch converter

State	S_{ip}	S_{im1}	S_{im2}	S_{in}	V_{jo}	V_{ko}	V_{lo}
1	0	1	1	1	$-V_{dc}/2$	$-V_{dc}/2$	$-V_{dc}/2$
2	1	0	1	1	$V_{dc}/2$	$-V_{dc}/2$	$-V_{dc}/2$
3	1	1	0	1	$V_{dc}/2$	$V_{dc}/2$	$-V_{dc}/2$
4	1	1	1	0	$V_{dc}/2$	$V_{dc}/2$	$V_{dc}/2$

In Table 6.19, V_{jo}, V_{ko} and V_{zo} are the voltages between the inverter leg and the mid-point '0' of the dc supply for *Inv1*, *Inv2*, and *Inv3* respectively; $i = a, b, c$; $j = a_1, b_1, c_1$; $k = a_2, b_2, c_2$; $l = a_3, b_3, c_3$; V_{dc} is the dc-link voltage. The converter voltages are given as:

$$V_{jo} = V_{jn} + V_{no} = \frac{V_{dc}}{2}[S_{ip} - S_{im1}S_{im2}S_{in}] \tag{6.62}$$

$$V_{ko} = V_{km} + V_{mo} = \frac{V_{dc}}{2}[S_{ip}S_{im1} - S_{im2}S_{in}] \tag{6.63}$$

$$V_{lo} = V_{lz} + V_{zo} = \frac{V_{dc}}{2}[S_{ip}S_{im}S_{im2} - S_{in}] \tag{6.64}$$

Summing all the respective rows of (6.62), (6.63), and (6.64):

$$\sum_j V_{jo} = \sum_j V_{jn} + 3V_{no} \tag{6.65}$$

$$\sum_{k} V_{ko} = \sum_{k} V_{km} + 3V_{mo} \qquad (6.66)$$

$$\sum_{l} V_{lo} = \sum_{l} V_{Lz} + 3V_{zo} \qquad (6.67)$$

For balance load:

$$\sum_{j} V_{jn} = \sum_{k} V_{km} = \sum_{L} V_{Lz} = 0 \qquad (6.68)$$

$$V_{no} = \frac{1}{3}(V_{a1o} + V_{b1o} + V_{c1o}) \qquad (6.69)$$

$$V_{mo} = \frac{1}{3}(V_{a2o} + V_{b2o} + V_{c2o}) \qquad (6.70)$$

$$V_{zo} = \frac{1}{3}(V_{a3o} + V_{b3o} + V_{c3o}) \qquad (6.71)$$

Thus the 3-phase voltages of *Inv1* are given by

$$V_{a1n} = V_{a1o} - V_{no} = \frac{1}{3}(2V_{a1o} - V_{b1o} - V_{c1o}) \qquad (6.72)$$

$$V_{b1n} = V_{b1o} - V_{no} = \frac{1}{3}(-V_{a1o} + 2V_{b1o} - V_{c1o}) \qquad (6.73)$$

$$V_{c1n} = V_{c1o} - V_{no} = \frac{1}{3}(-V_{a1o} - V_{c1o} + 2V_{c1o}) \qquad (6.74)$$

The 3-phase voltages of *Inv2* are given by

$$V_{a2m} = V_{a2o} - V_{mo} = \frac{1}{3}(2V_{a2o} - V_{b2o} - V_{c2o}) \qquad (6.75)$$

$$V_{b2m} = V_{b2o} - V_{mo} = \frac{1}{3}(-V_{a2o} + 2V_{b2o} - V_{c2o}) \qquad (6.76)$$

263

$$V_{c2m} = V_{c2o} - V_{mo} = \frac{1}{3}(-V_{a2o} - V_{c2o} + 2V_{c2o})$$ (6.77)

And the 3-phase voltages of *Inv3* are given by

$$V_{a3z} = V_{a3o} - V_{zo} = \frac{1}{3}(2V_{a3o} - V_{b3o} - V_{c3o})$$ (6.78)

$$V_{b3z} = V_{b3o} - V_{mo} = \frac{1}{3}(-V_{a3o} + 2V_{b3o} - V_{c3o})$$ (6.79)

$$V_{c3z} = V_{c3o} - V_{zo} = \frac{1}{3}(-V_{a3o} - V_{c3o} + 2V_{c3o})$$ (6.80)

A look at the phase truth table above (see Table 6.19), shows the following relationship between the switching functions:

$$S_{ip} + S_{im1}S_{im2}S_{in} = 1$$ (6.81)

$$S_{ip}S_{im1}S_{im2} + S_{in} = 1$$ (6.82)

$$S_{ip}S_{im1} + S_{im2}S_{in} = 1$$ (6.83)

Substituting these expressions into (6.62) – (6.64):

$$V_{jo} = \frac{V_{dc}}{2}[2S_{ip} - 1]$$ (6.84)

$$V_{ko} = \frac{V_{dc}}{2}[2S_{ip}S_{im1} - 1]$$ (6.85)

$$V_{Lo} = \frac{V_{dc}}{2}[1 - 2S_{in}]$$ (6.86)

And the neutral voltages are:

$$V_{no} = \frac{V_{dc}}{3}\left[S_{ap} + S_{bp} + S_{cp}\right] - \frac{V_{dc}}{2} \qquad (6.87)$$

$$U_{mo} = \frac{V_{dc}}{3}\left[S_{ap}S_{am1} + S_{bp}S_{bm1} + S_{cp}S_{cm1}\right] - \frac{V_{dc}}{2} \qquad (6.88)$$

$$V_{zo} = \frac{V_{dc}}{2} - \frac{V_{dc}}{3}\left[S_{an} + S_{bn} + S_{cn}\right] \qquad (6.89)$$

The expressions for the switching functions, of the top and bottom devices can be obtained from (6.84) and (6.86). They are given respectively, by

$$S_{ip} = \frac{V_{jn}}{V_{dc}} + \frac{V_{n0}}{V_{dc}} + \frac{1}{2} \qquad (6.90)$$

$$S_{in} = \frac{1}{2} - \left[\frac{V_{lz}}{V_{dc}} + \frac{V_{zo}}{V_{dc}}\right] \qquad (6.91)$$

For the upper-inner devices, solving (6.85),

$$V_{ko} = \frac{V_{dc}}{2}\left[2S_{ip}S_{im1} - 1\right]$$

$$\frac{1}{V_{dc}}\left(V_{km} + V_{mo}\right) + \frac{1}{2} = S_{ip}S_{im1}$$

$$\frac{1}{V_{dc}}\left(V_{km} + V_{mo}\right) + \frac{1}{2} = S_{ip}S_{im1}$$

$$S_{ip} = \frac{V_{jn}}{V_{dc}} + \frac{V_{n0}}{V_{dc}} + \frac{1}{2} = \frac{2V_{jn} + 2V_{n0} + V_{dc}}{2V_{dc}}$$

$$S_{im1} = \left(\frac{V_{km}}{V_{dc}} + \frac{V_{mo}}{V_{dc}} + \frac{1}{2} \right) \frac{2V_{dc}}{2V_{jn} + 2V_{n0} + V_{dc}}$$

$$S_{im1} = \frac{2V_{km} + 2V_{mo} + V_{dc}}{2V_{jn} + 2V_{no} + V_{dc}} \tag{6.92}$$

This is a complicated expression. Alternatively define a new switching function

$$S_{ipm1} = S_{ip} S_{im1}$$

$$V_{ko} = \frac{V_{dc}}{2} \left[2S_{ipm1} - 1 \right]$$

$$\tag{6.93}$$

$$S_{ipm1} = \frac{V_{km}}{V_{dc}} + \frac{V_{mo}}{V_{dc}} + \frac{1}{2}$$

The relationship between the switching functions and the modulation signal may be approximated by

$$S_{ip} = 0.5(1 + M_{ip}) \tag{6.94}$$

$$S_{ipm1} = 0.5(1 + M_{ipm1}) \tag{6.95}$$

$$S_{in} = 0.5(1 - M_{in}) \tag{6.96}$$

Substituting (6.94), (6.95), and (6.96) into (6.90), (6.93), and (6.91) respectively, the expressions for the modulation signals are:

$$M_{ip} = \frac{2V_{jn}^*}{V_{dc}} + \frac{2V_{no}}{V_{dc}} \tag{6.97}$$

$$M_{ipm1} = \frac{2V_{km}^*}{V_{dc}} + \frac{2V_{mo}}{V_{dc}} \tag{6.98}$$

266

$$M_{in} = -\left(\frac{2V_{ln}^*}{V_{dc}} + \frac{2V_{zo}}{V_{dc}}\right)$$ (6.99)

where M_{ip}, M_{ipm1}, and M_{in} are respectively the modulation signals of the upper ,upper-inner , and lower devices; V_{jn}^* , V_{km}^* and V_{lz}^* are the reference inverter output voltages; V_{n0} , V_{m0} and V_{z0} are the neutral voltages of *Inv1*, *Inv2* , and *Inv3* respectively. The modulation signals obtained is a generalized one for the 12-switch converter as it is valid for same frequencies and/or amplitudes, different frequency and/or amplitudes for *Inv1*, *Inv2,* and *Inv3*.

The gate pulses of the devices are generated as in the case of the Nine-switch converter explained in Chapter 5. It has been shown that the switching constraint of the 12-switch converter is given by (6.1) as well as (6.81) – (6.83) if independent control of the three output voltages is required. With the modulation signals defined by (6.97) – (6.99), the switching pulses can be generated by comparing them with a high frequency triangular carrier signal. In this case, there are three modulation signals and one carrier as shown in Figure 6.6. The principle of the generating the switching pulses to meet the dual objectives of satisfying the switching function constraints are given by

$$S_{ip} = \begin{cases} 1, & \text{when } M_{ip} \geq V_{tri} \\ 0, \text{every where else} \end{cases}$$ (6.100)

$$S_{im1} = \begin{cases} 1, & \text{when } M_{im1} \geq V_{tri} \\ 0, \text{every where else} \end{cases}$$ (6.101)

$$S_{in} = \begin{cases} 1, & \text{when } M_{in} \le V_{tri} \\ \\ 0, \text{every where else} \end{cases} \qquad (6.102)$$

$$S_{im2} = 3 - S_{ip} - S_{im1} - S_{in} \qquad (6.103)$$

where M_{ip}, M_{im1} and M_{in} are, respectively, the modulation signals of the upper and bottom devices and V_{tri} is the high frequency triangular signal. Observe that $M_{ip} \ge M_{im1} \ge M_{in}$ and this has been made possible by the zero sequence voltage injection into the reference modulation signal.
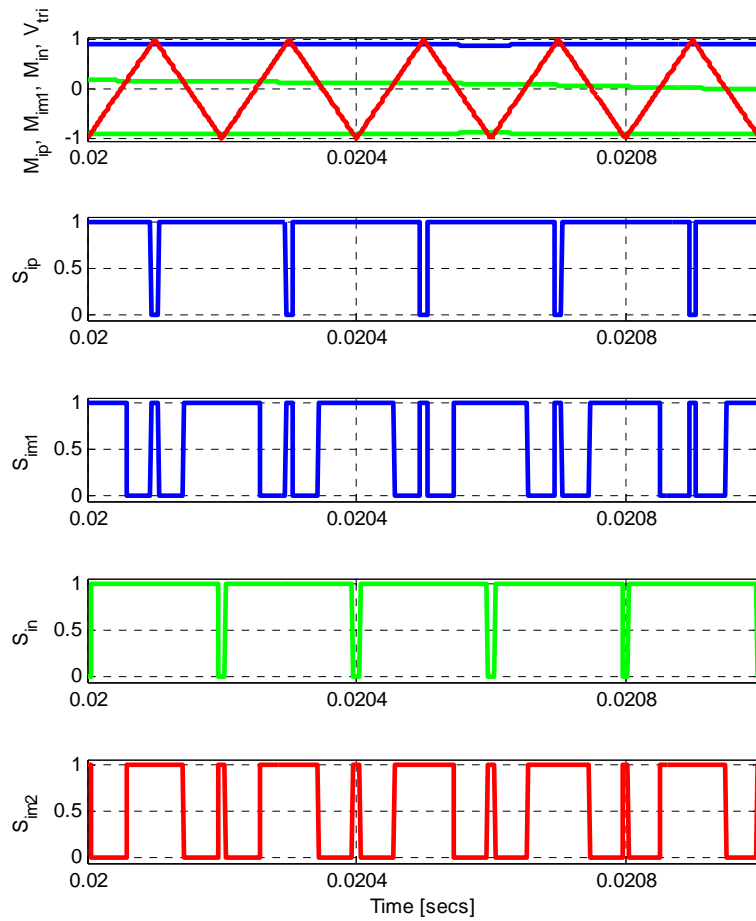
Figure 6.6. Generation of device gate switching pulses

6.3.3. Average input dc current

Applying KCL at node P in Figure 6.7, the average input dc current is given by

$$I_{dc} = I_A + I_B + I_C \qquad (6.104)$$

where I_A, I_B, and I_C are the average currents flowing through phase-leg 'a', 'b', and 'c' respectively. These phase-leg currents can be determined by averaging their values for each of the four switching states in Table 6.19 and their corresponding equivalent circuits in Figure 6.8.
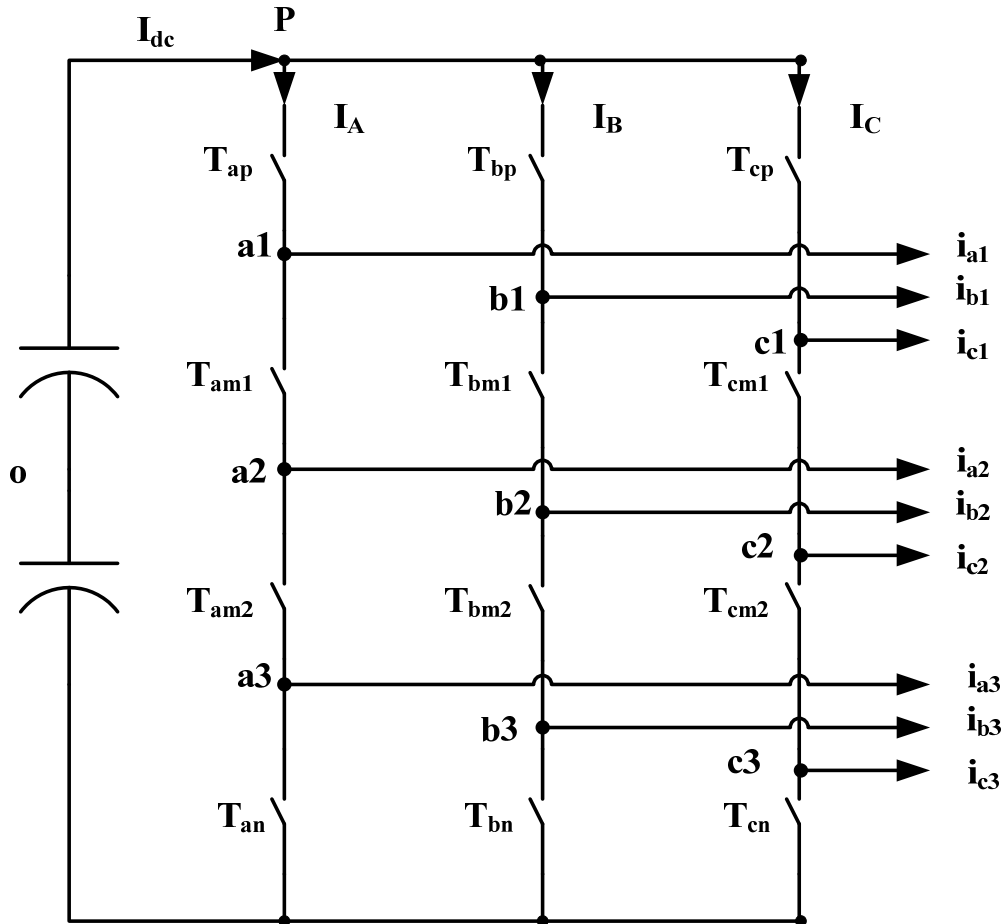
Figure 6.7. 12-switch converter currents

269
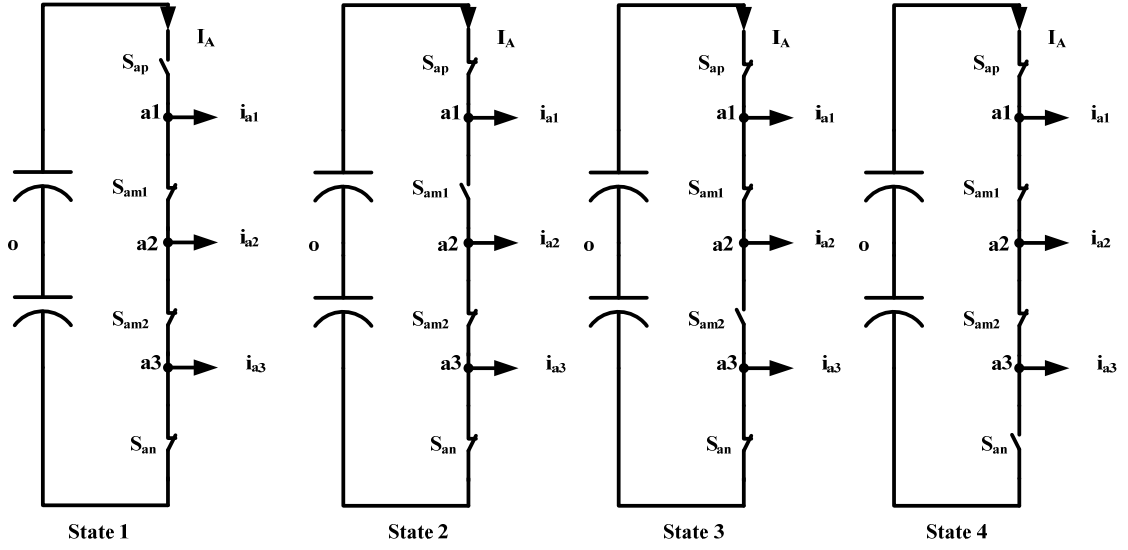
Figure 6.8. The four possible equivalent circuits for phase-leg 'a' of the 12-switch converter

Using phase-leg 'a' as an example, for switching state 1,

$$i_A = 0 \qquad (6.105)$$

For switching state 2:

$$i_A = S_{ap} i_{a1} \qquad (6.106)$$

For switching state 3:

$$i_A = S_{ap} S_{am1} (i_{a1} + i_{a2}) \qquad (6.107)$$

And for switching state 4:

$$i_A = S_{ap} S_{am1} S_{am2} (i_{a1} + i_{a2} + i_{a3}) \qquad (6.108)$$

Thus combining the values of i_A in all four switching states, its average value is given by

$$I_A = S_{ap} i_{a1} + S_{ap} S_{am1} (i_{a1} + i_{a2}) + S_{ap} S_{am1} S_{am2} (i_{a1} + i_{a2} + i_{a3}) \qquad (6.109)$$

Similar derivations can be made for phase-leg 'b' and 'c' resulting in the following expressions:

$$I_B = S_{bp}i_{b1} + S_{bp}S_{bm1}(i_{b1}+i_{b2}) + S_{bp}S_{bm1}S_{bm2}(i_{b1}+i_{b2}+i_{b3}) \qquad (6.110)$$

$$I_C = S_{cp}i_{c1} + S_{cp}S_{cm1}(i_{c1}+i_{c2}) + S_{cp}S_{cm1}S_{cm2}(i_{c1}+i_{c2}+i_{c3}) \qquad (6.111)$$

And the average input dc current is the sum of these phase-leg currents. That is:

$$I_{dc} = \begin{bmatrix} S_{ap}i_{a1} + S_{ap}S_{am1}(i_{a1}+i_{a2}) + S_{ap}S_{am1}S_{am2}(i_{a1}+i_{a2}+i_{a3}) + \\ S_{bp}i_{b1} + S_{bp}S_{bm1}(i_{b1}+i_{b2}) + S_{bp}S_{bm1}S_{bm2}(i_{b1}+i_{b2}+i_{b3}) + \\ S_{cp}i_{c1} + S_{cp}S_{cm1}(i_{c1}+i_{c2}) + S_{cp}S_{cm1}S_{cm2}(i_{c1}+i_{c2}+i_{c3}) \end{bmatrix} \qquad (6.112)$$

6.4 Simulation and Experimental Results

Simulations were performed using Matlab/Simulink to validate the proposed PWM schemes. In the following simulations, the reference voltages for *Inv1, Inv2,* and *Inv3* are balanced three-phase sinusoids with the following amplitudes and frequencies:

Inv1: amplitude $V_1 = \dfrac{0.5V_{dc}}{\sqrt{3}}$ and frequency $f_1 = 95$ Hz

Inv2: amplitude $V_2 = \dfrac{0.3V_{dc}}{\sqrt{3}}$ and frequency $f_2 = 60$ Hz

Inv3: amplitude $V_3 = \dfrac{0.2V_{dc}}{\sqrt{3}}$ and frequency $f_3 = 25$ Hz

The dc link voltage is V_{dc} is 100 V and the converter switching frequency chosen is 1 kHz. These simulations are performed for both SV-PWM and CB-PWM schemes. Table 6.20 gives the details of the three-phase R-L loads used in the simulation.

271

Table 6.20. Component parameters used in simulation

Symbol	Description	Value
L_{f1}	Upper load inductance	1.05 mH
R_1	Upper load resistance	0.3 ohm
L_{f2}	Middle load inductance	1.05 mH
R_2	Lower load resistance	0.3 ohm
L_{f3}	Lower load inductance	1.05 mH
R_3	Lower load resistance	0.3 ohm

6.4.1. SV- PWM

The implementation of the SV-PWM in MATLAB/Simulink consists of first identifying the sectors of the desired voltages to be synthesized. The time of application of active and zero vectors are then calculated and arranged according to the predefined switching pattern. Figure 6.9 show the device turn on times required to synthesize the reference voltages. For each phase, the device turn on times is calculated for only three of the four devices since the switching pulse for the fourth device can be obtained from the switching function constraint. The corresponding phase voltages are for *Inv1*, *Inv2,* and *Inv3* produced using the proposed SV-PWM ar e shown in Figures 6.10(a) – 6.10(c). The low frequency components of the synthesized voltages and the reference voltages have been superimposed. The dwell time for zero states is distributed equally among the four zero states (i.e. $\alpha = \beta = \gamma = \mu = \frac{1}{4}$). Figures 6.10(a) – 6.10(c) show that the desired voltages have correctly been synthesized.
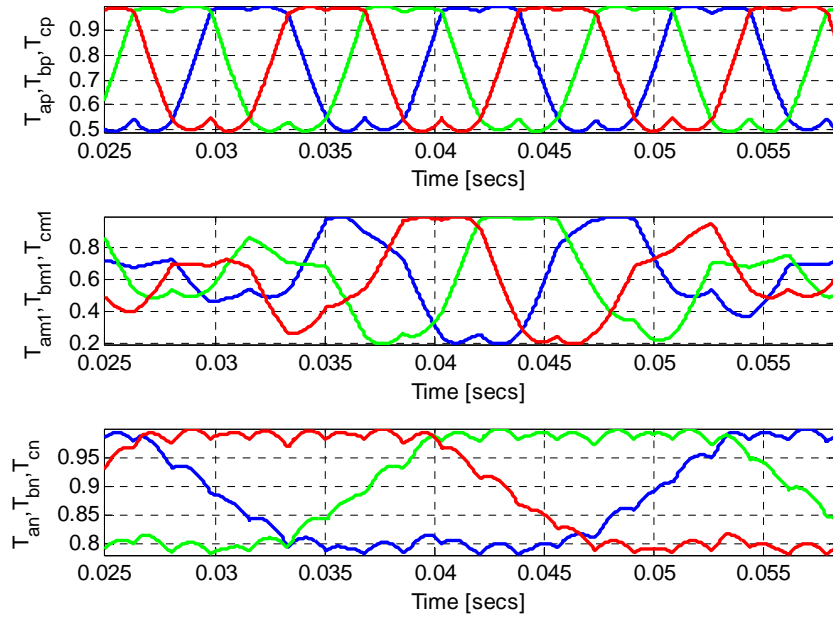
Figure 6.9. Device turn-on times for (a) T_{ip}, (b) T_{im1} and (c) T_{in} where $i = a, b, c$
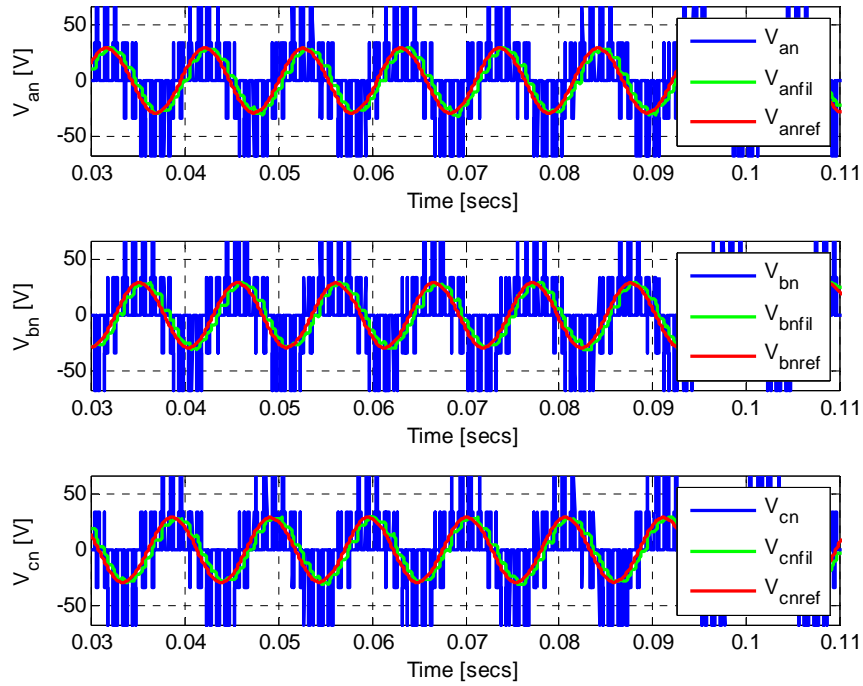
Figure 6.10 (a) Phase voltages with SV-PWM $(\alpha = \beta = \gamma = \mu = \frac{1}{4})$ for $f_1 = 95$ Hz
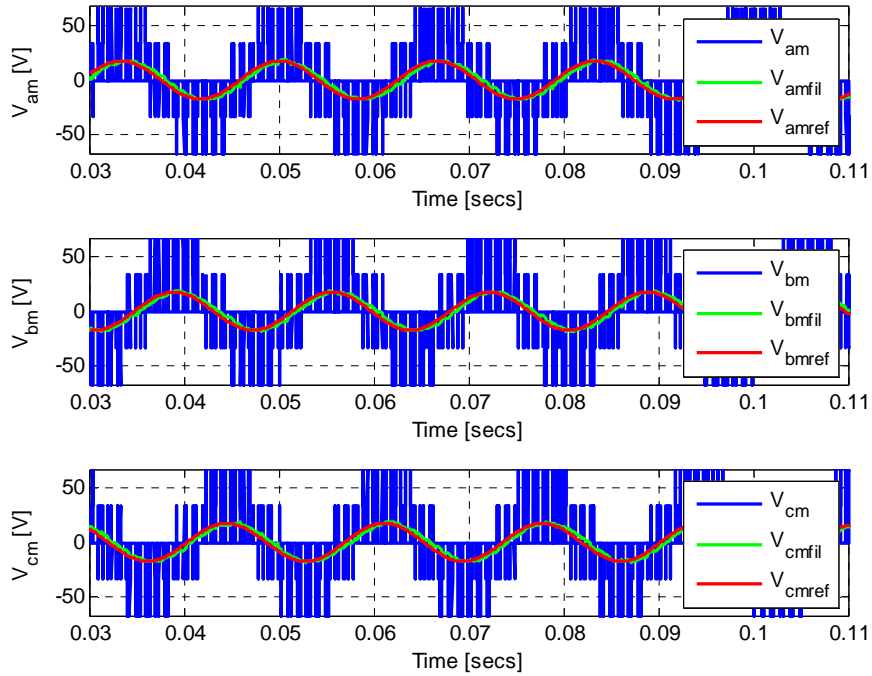
(b)
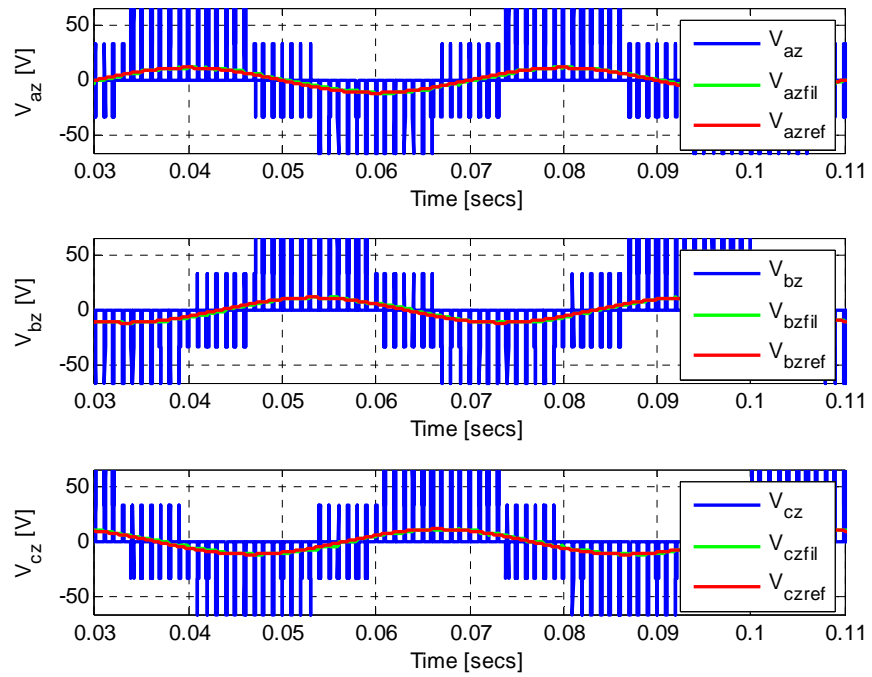
(c)

Figure 6.10. Phase voltages with SV-PWM $(\alpha = \beta = \gamma = \mu = \frac{1}{4})$ for (a) $f_1 = 95$ Hz, (b) $f_2 = 60$ Hz, and (c) $f_3 = 25$ Hz

274

6.4.2. Continuous CB-PWM (CPWM)

In general, there are four (4) zero vectors; and depending on the choice of the values for α, β, γ and μ, all four zero vectors, or three zero vectors or ,two zero vectors , or one zero vector can be applied. Under all possibilities, the sum of α, β, γ ,and μ must be less than or equal to unity. For example when $\alpha = \beta = \gamma = \mu = \frac{1}{4}$, the generalized neutral voltages corresponds to the classical SV-PWM in the 2-level converter when $\alpha = \beta = 1/2$.

The modulation signals with $\alpha = \beta = \gamma = \mu = \frac{1}{4}$ is illustrated in Figure 6.11. The corresponding phase voltages are shown in Figure 6.12. The generated voltages are shown with the low frequency components and reference voltages superimposed on each other showing that the desired voltages have been correctly synthesized. Figures 6.13 and 6.14 also depict the corresponding load currents and the input dc current of the converter.

Simulations were also performed for unbalanced voltages. The reference voltage unbalance in each of the three outputs was caused by reducing the amplitudes in phase 'b' and 'c' with respect to phase 'a'. Given that phase 'a' amplitude is m_a, phase 'b' and 'c' are respectively $m_b = 0.8m_a$ and $m_c = 0.5m_a$. The modulation signals showing the unbalance is illustrated in Figure 6.15 and the corresponding phase voltages, phase currents and input dc current are illustrated in Figures 6.16, 6.17, and 6.18 respectively.
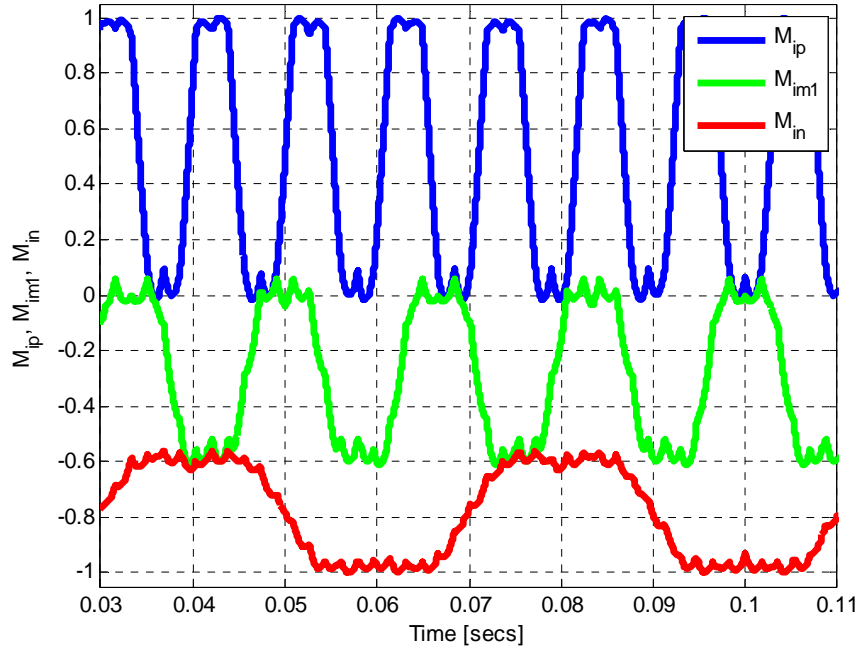
Figure 6.11.   Continuous CB-PWM modulation signals of the upper , upper-inner and lower switches with f_1 = 95 Hz, f_2 = 60 Hz and f_3 = 25 Hz, for $\alpha = \beta = \gamma = \mu = \frac{1}{4}$.
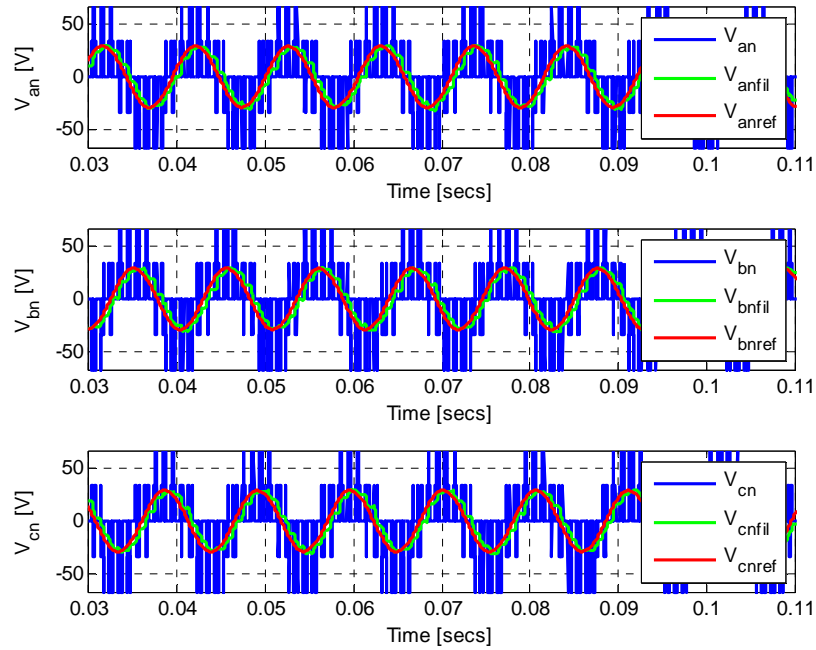
Figure 6.12 (a) Converter phase voltages with $\alpha = \beta = \gamma = \mu = \frac{1}{4}$ for *Inv1* output (f_1 = 95 Hz)
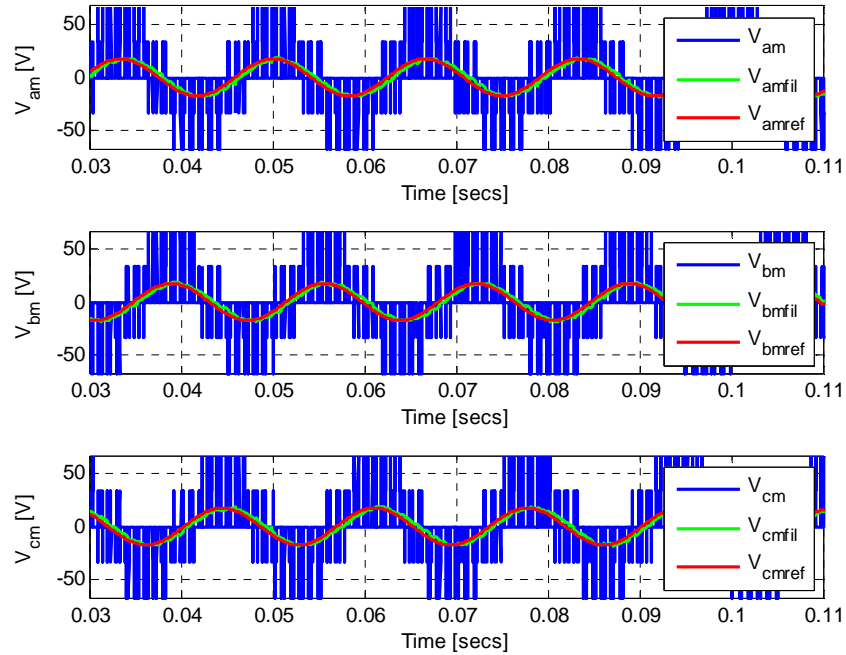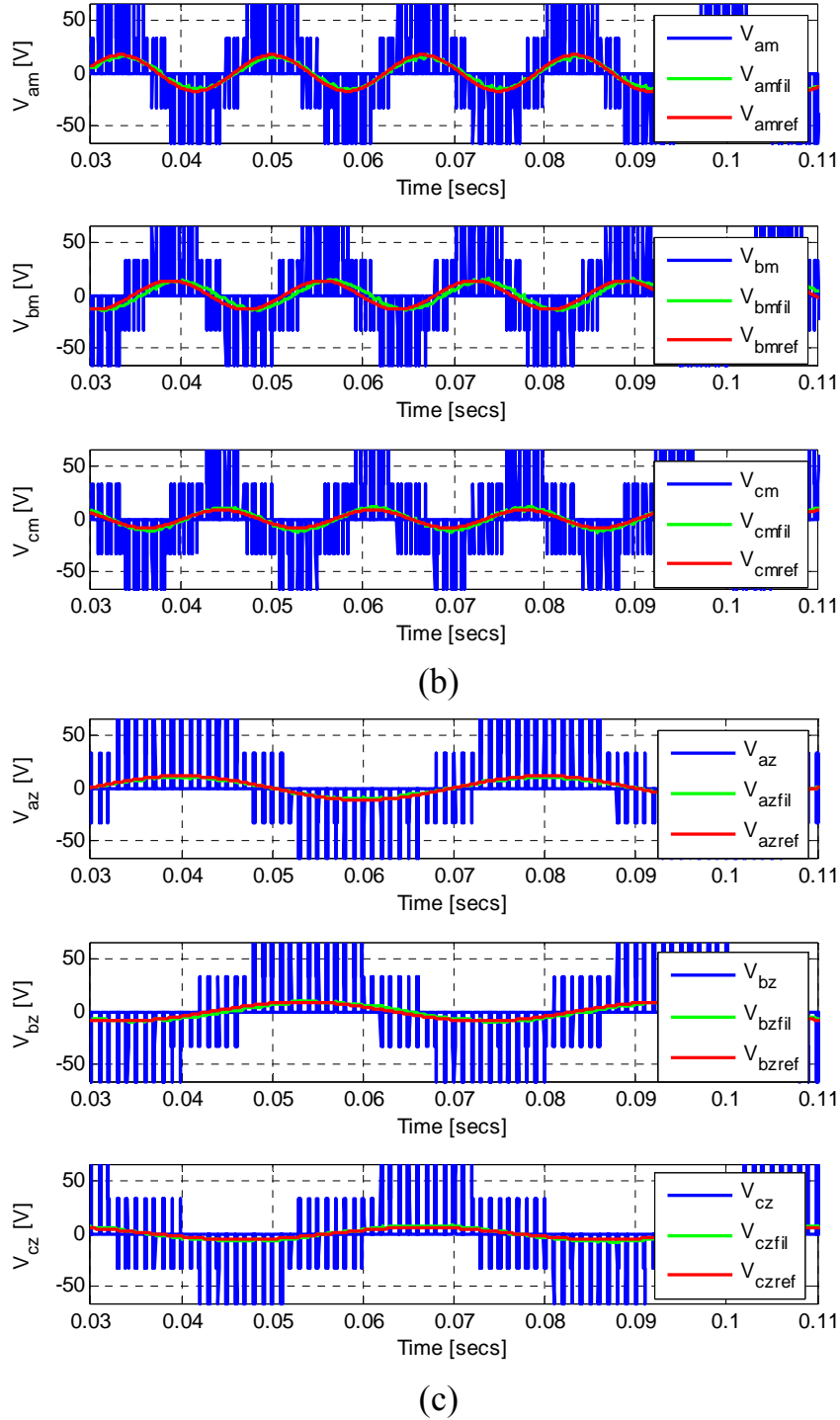
(b)
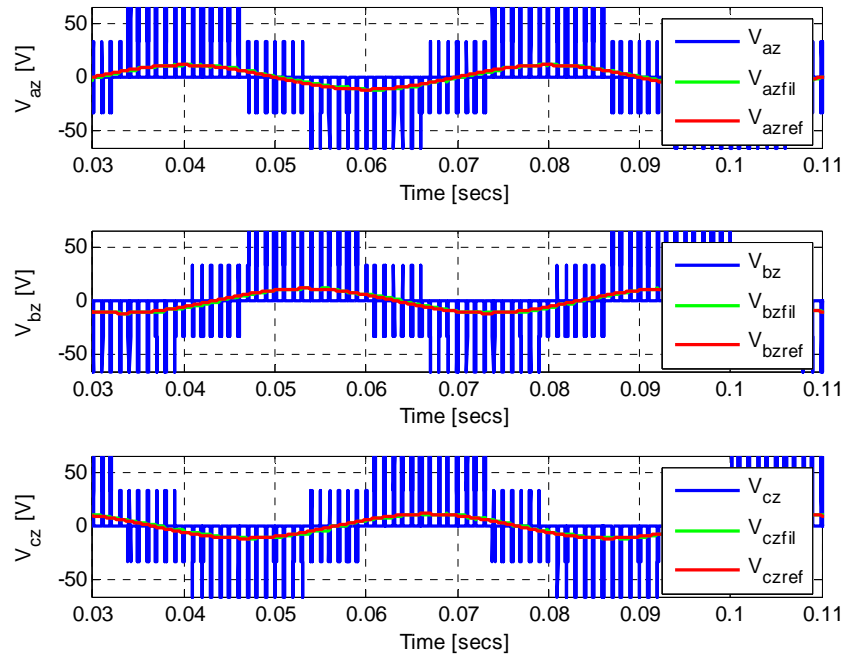
(c)

Figure 6.12.   Converter phase voltages with α = β= γ =μ= ¼ for (a) *Inv1* output (f₁ = 95 Hz)
and (b) *Inv2* output (f₂ = 60 Hz) and (c) *Inv3* output (f₂ = 25 Hz) using CPWM
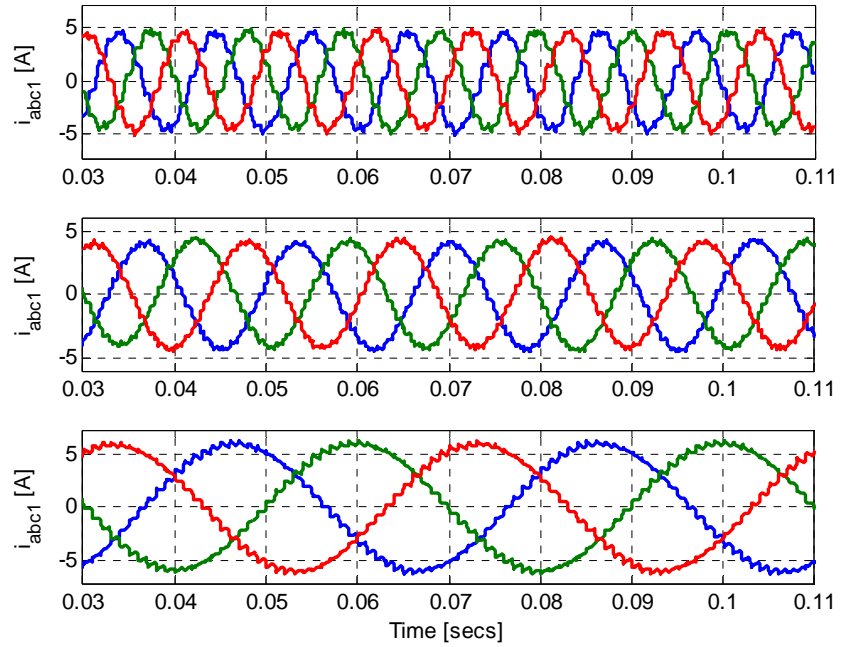
Figure 6.13.   Simulation results of the load currents
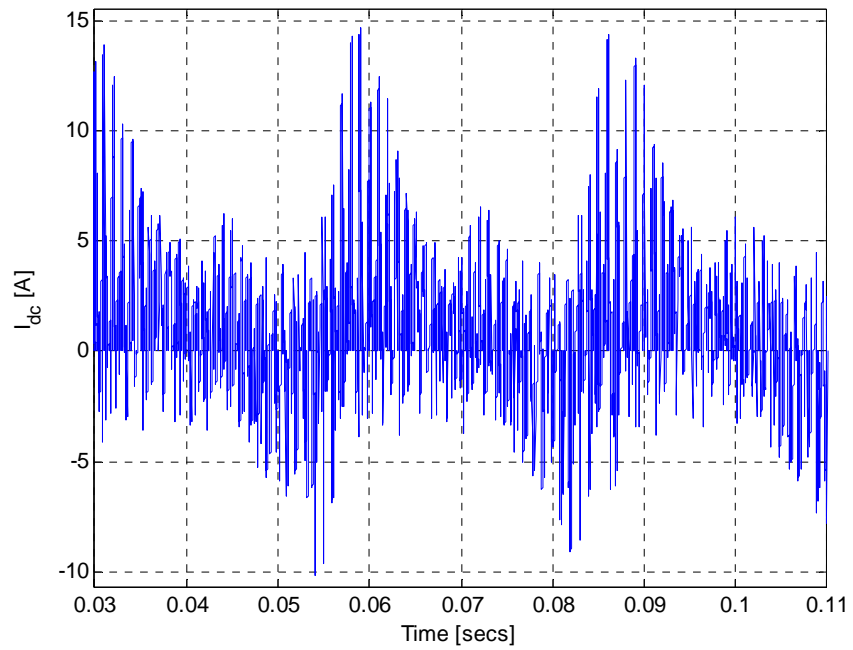
Figure 6.14.   Simulation results of the input dc current

278
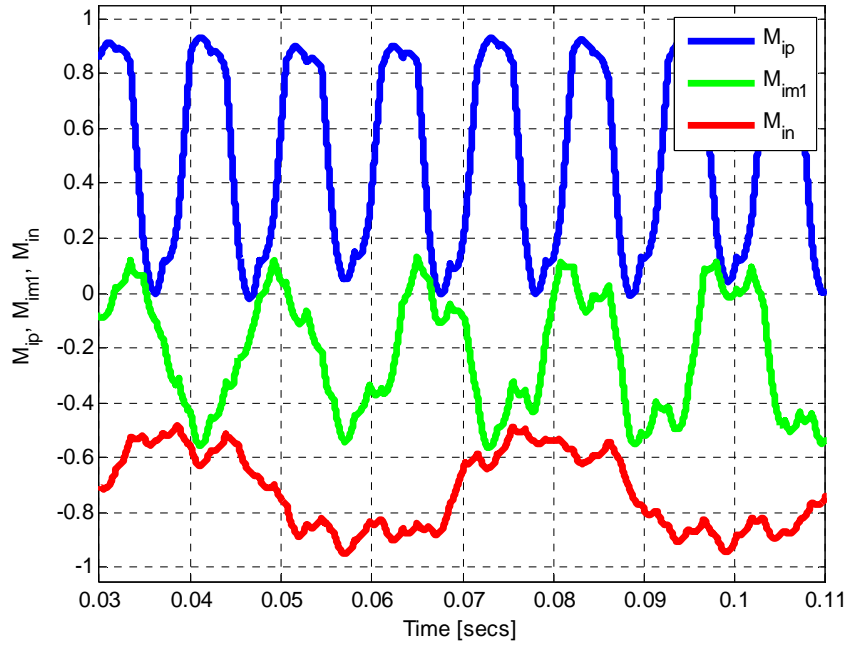
Figure 6.15. Unbalanced CPWM modulation signals of the upper , upper-middle and lower switches with $f_1 = 95$ Hz, $f_2 = 60$ Hz and $f_3 = 25$ Hz, $\alpha = \beta = \gamma = \mu = \frac{1}{4}$
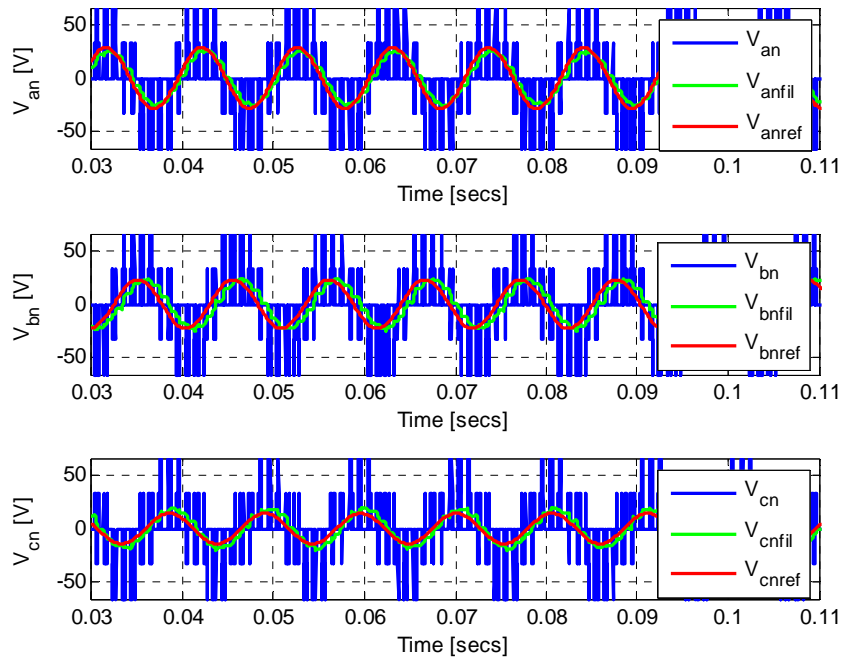
Figure 6.16 (a) Unbalanced converter phase voltages with $\alpha = \beta = \gamma = \mu = \frac{1}{4}$ for *Inv1* output ($f_1 = 95$ Hz)

Figure 6.16. Unbalanced converter phase voltages with α = β = γ = μ = ¼ for (a) *Inv1* output (f₁ = 95 Hz), (b) *Inv2* output (f₂ = 60 Hz) and (c) *Inv3* output (f₂ = 25 Hz) using CPWM
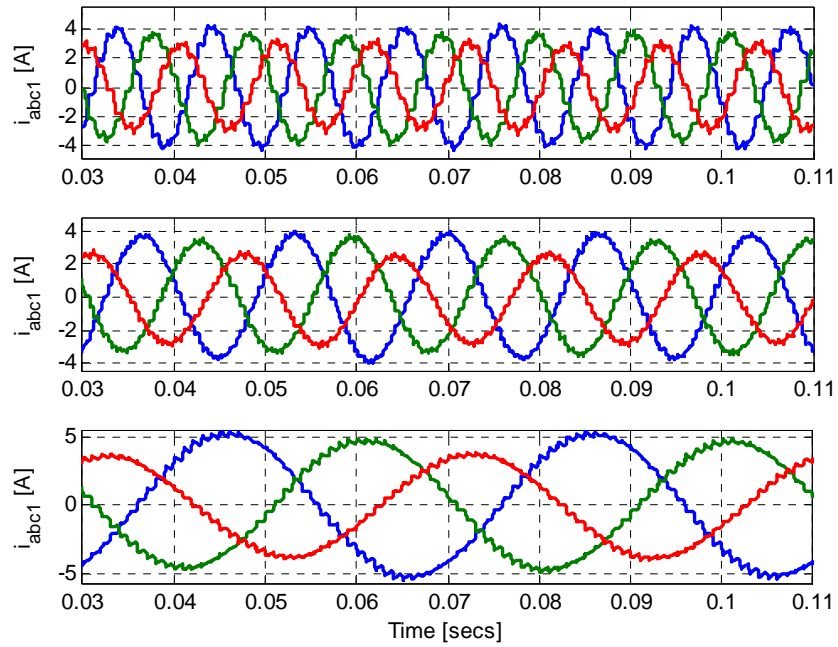
Figure 6.17.   Load currents for unbalanced reference voltages
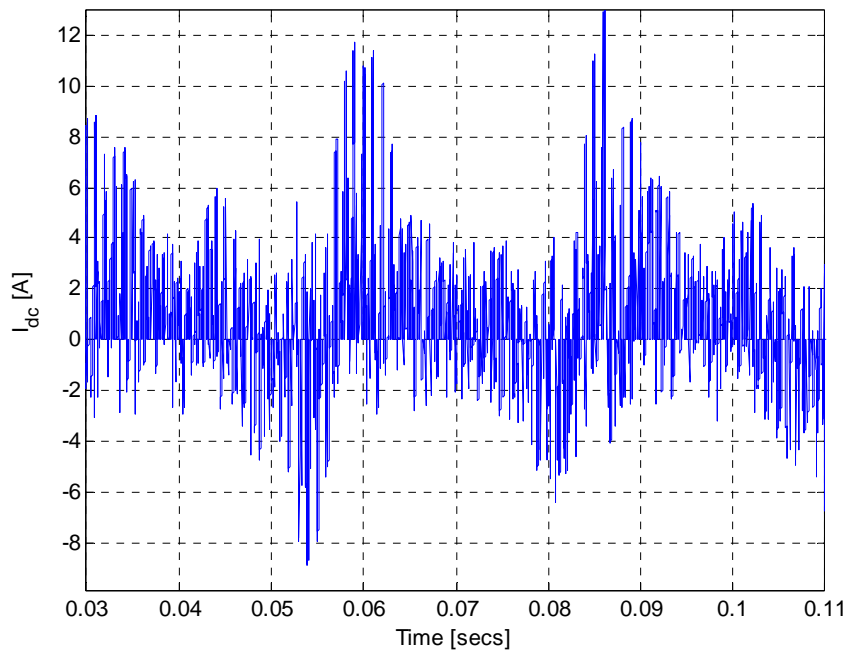
Figure 6.18.   Input dc current for unbalanced reference voltages

281

6.4.3. Discontinuous CB-PWM (DPWM)

There are infinite ways of producing discontionous PWM. For example, let α, β, γ, and μ be defined as follws:

$$\alpha = \frac{1}{8}\left[1 + \text{sgn}[\cos 3(\omega_1 t + \delta_1)]\right]$$

$$\beta = \frac{1}{8}\left[1 + \text{sgn}[\cos 3(\omega_2 t + \delta_2)]\right]$$

$$\gamma = \frac{1}{8}\left[1 + \text{sgn}[\cos 3(\omega_3 t + \delta_3)]\right]$$

$$\mu = 1 - (\alpha + \beta + \gamma)$$

(6.113)

Figure 6.19 shows the modulation signals with α, β, γ, and μ defined by (6.112). The corresponding three-phase voltages, currents and input dc current are shown in Figures 6.20, 6.21 and 6.22 respectively.
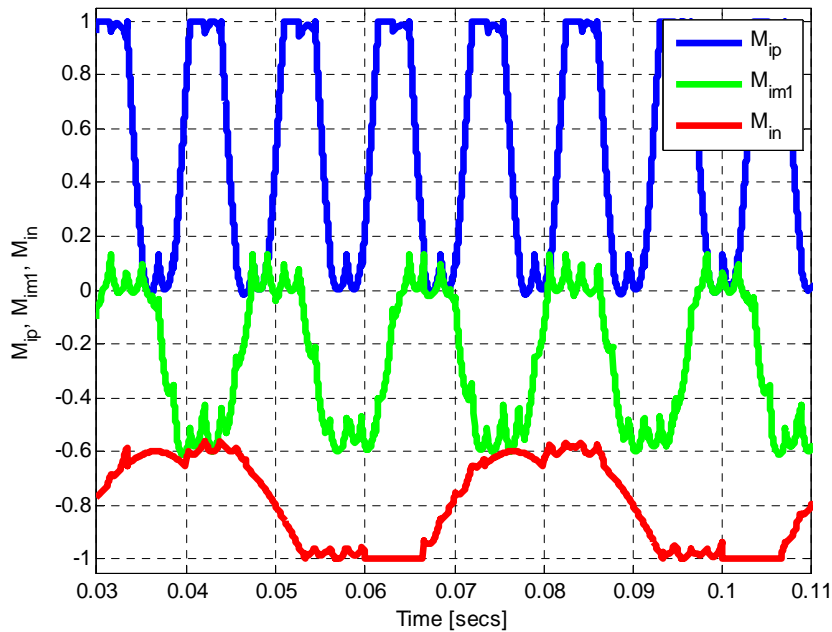
Figure 6.19. DPWM signals for the upper , upper-inner and lower switches with α, β, γ, and μ defined by (6.112), $f_1 = 95$ Hz, $f_2 = 60$ Hz and $f_2 = 25$ Hz)
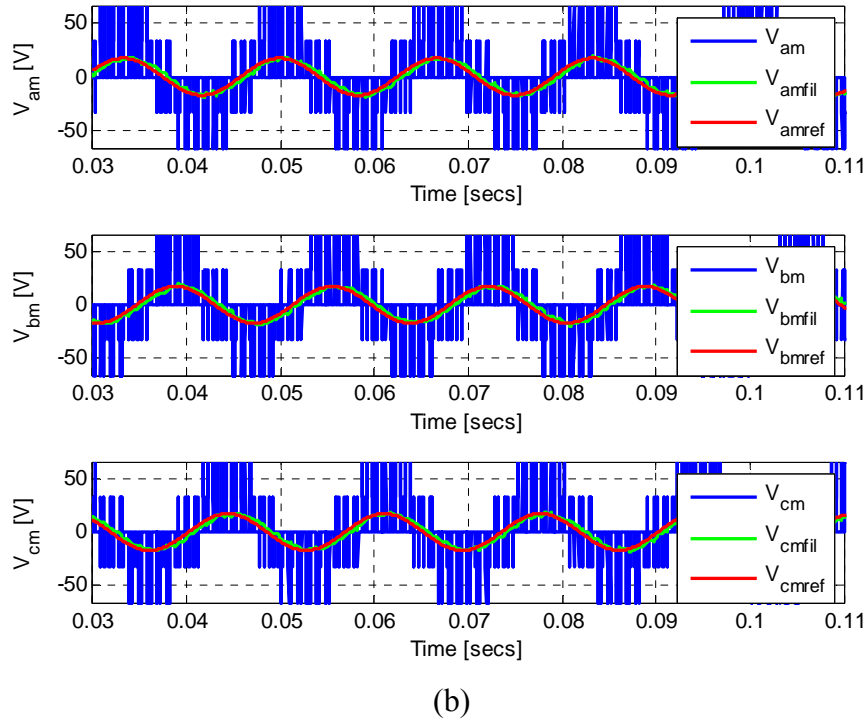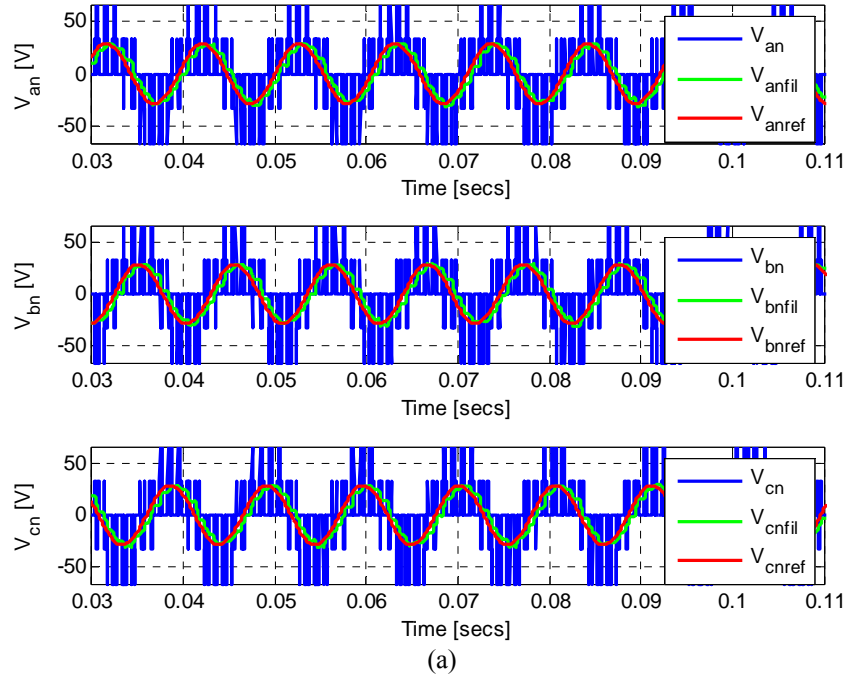
Figure 6.20. Phase voltages with α, β, γ, and μ defined by (6.112), (a) *Inv2* output ($f_1 = 95$ Hz), and (b) *Inv2* output ($f_2 = 60$ Hz)

(c)
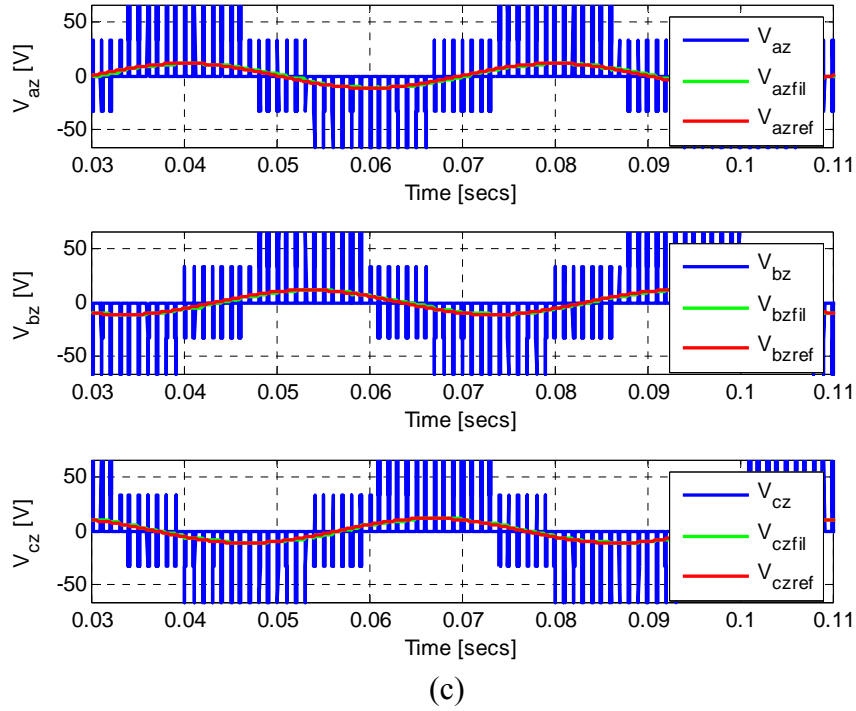
Figure 6.20.   Phase voltages with α, β, γ, and μ defined by (6.112) (a) *Inv1* output (f_1 = 95 Hz), (b) *Inv2* output (f_2 = 60 Hz) , and (c) *Inv3* output (f_1 = 25 Hz)
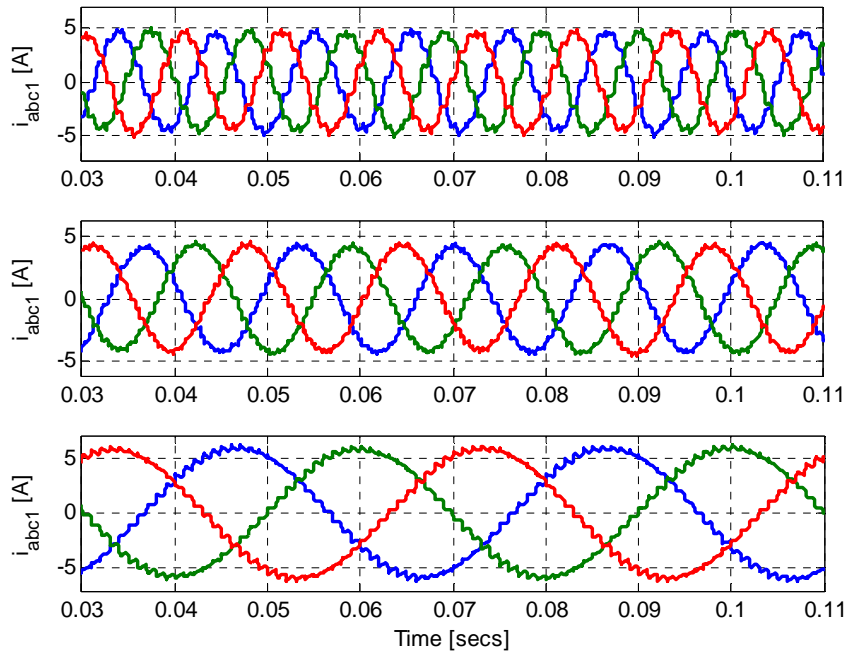
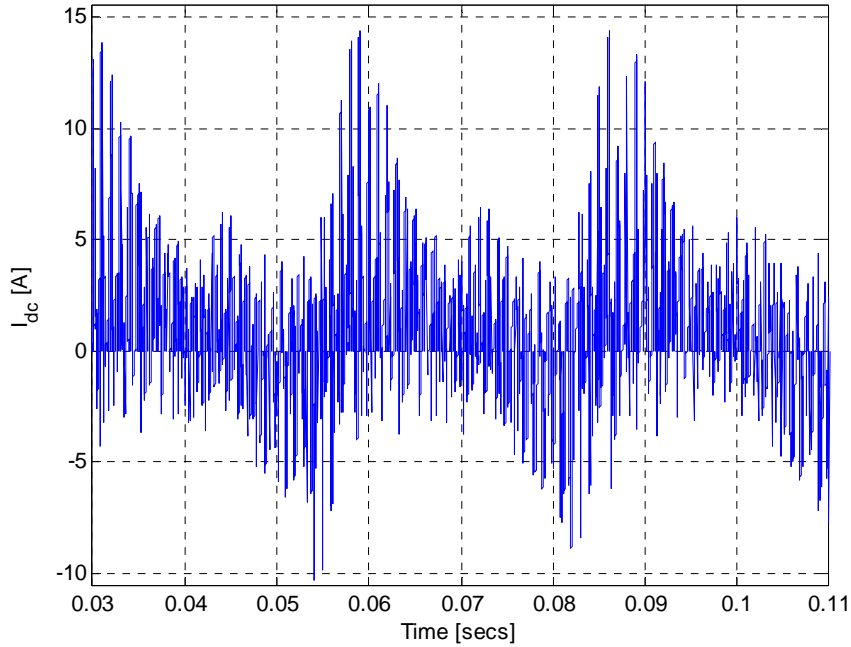Figure 6.21.   Load currents using discontinuous PWM

Figure 6.22.   Input dc current using discontinuous PWM

6.4.4. Experimental Results

The 12-switch converter was designed and built in the laboratory. Figure 5.26 shows its photograph. The converter was designed to be adaptable for both the Nine-switch and 12-switch converters. The gate PWM signals were generated using dSPACE ds1104 real-time controller. Using the assembled prototype, a 100V DC voltage was supplied to the converter and the line-to-line voltages were measured at no-load. Illustrative experimental waveforms using continuous PWM are shown in Figures 6.23-6.28.

Figure 6.23 shows the phase line-to-line voltages corresponding to three different frequencies (50 Hz, 60 Hz, and 25 Hz) but having the same amplitudes across all phases

285

and all three inverter outputs. In Figure 6.24, the frequency of *Inv1* is change to 95 Hz to illustrate the resulting waveform if the frequency range is increased. It is observed that as the frequencies varied widely, there is an accompanying mild degradation in the waveform quality. Figures 6.25 and 6.26 show the same waveforms as in Figures 6.23 and 6.24 but with an initial phase angle of -30 degrees in phase 'a'. In Figure 6.27, the amplitude unbalanced was applied to the individual phases in each of *Inv1, Inv2* and *Inv3* the converter has the ability to produced voltages at different frequencies and/or amplitudes. However, this comes with some limitation in the magnitude for the voltages that can be produced.

Finally, a three-phase inductive load of 1.05 mH and 0.3 ohm internal resistance is connected to *Inv1, Inv2*, and *Inv3*. Figures 6.28 (a) − (c), depict the experimental waveforms of the line-to-line voltage, phase voltage, the corresponding phase current and the input dc current for a 50 V dc input voltage. These compare to simulation results depicted in Figures 6.16 − 6.18. The phase current is sinusoidal but with a lot of harmonics. It has been observed in simulations that as the switching frequency increases, the current waveform becomes smoother. This could not be done because of the print step limitation in the ds1104.
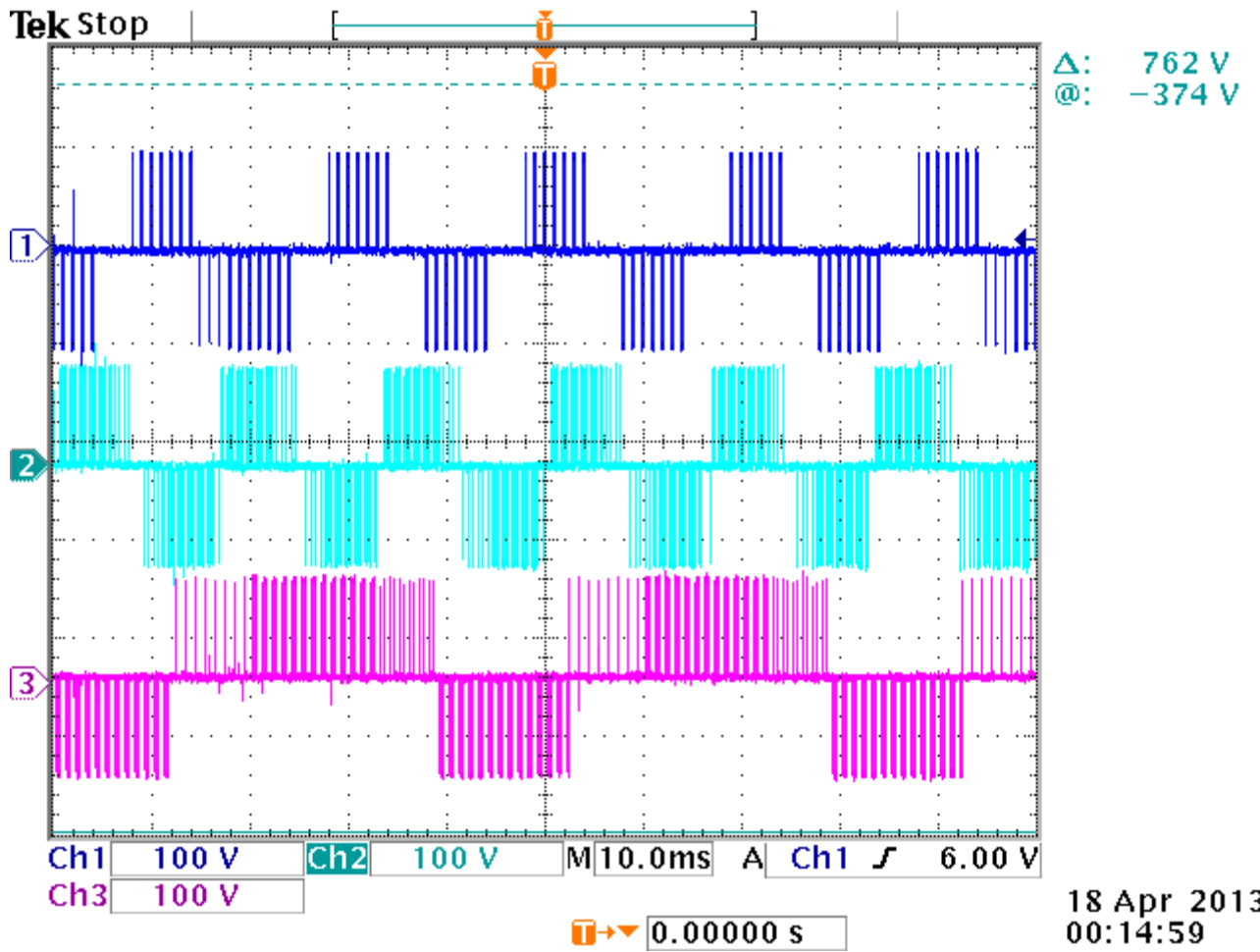
Figure 6.23.   Line-to-line voltages for *Inv1* (Ch1), *Inv2* (Ch2), and *Inv3* (Ch3) with frequencies 50 Hz, 60 Hz, and 25 Hz respectively and same amplitudes of $V_1 = V_2 = V_3 = 0.3V_{dc}/\sqrt{3}$.
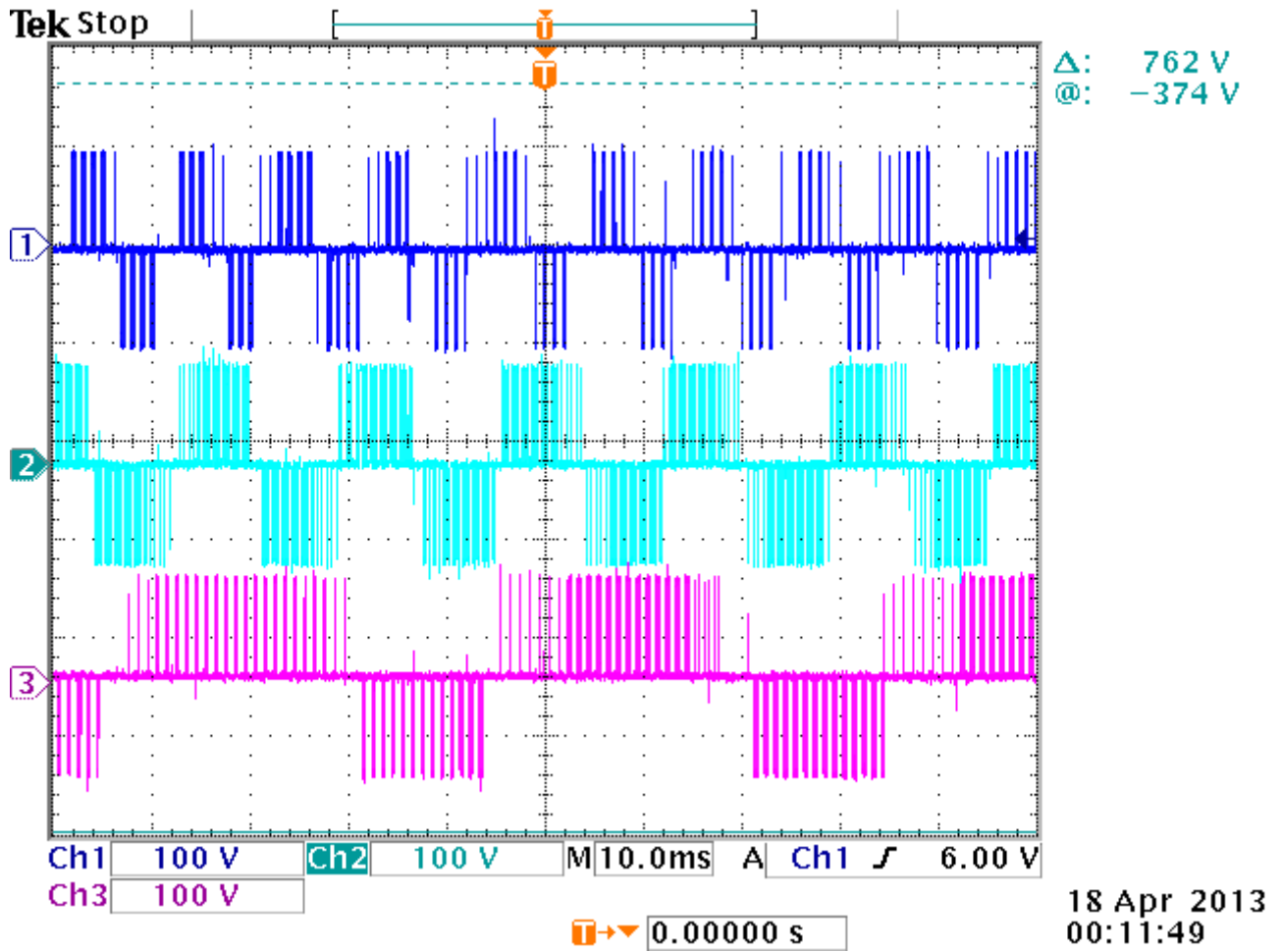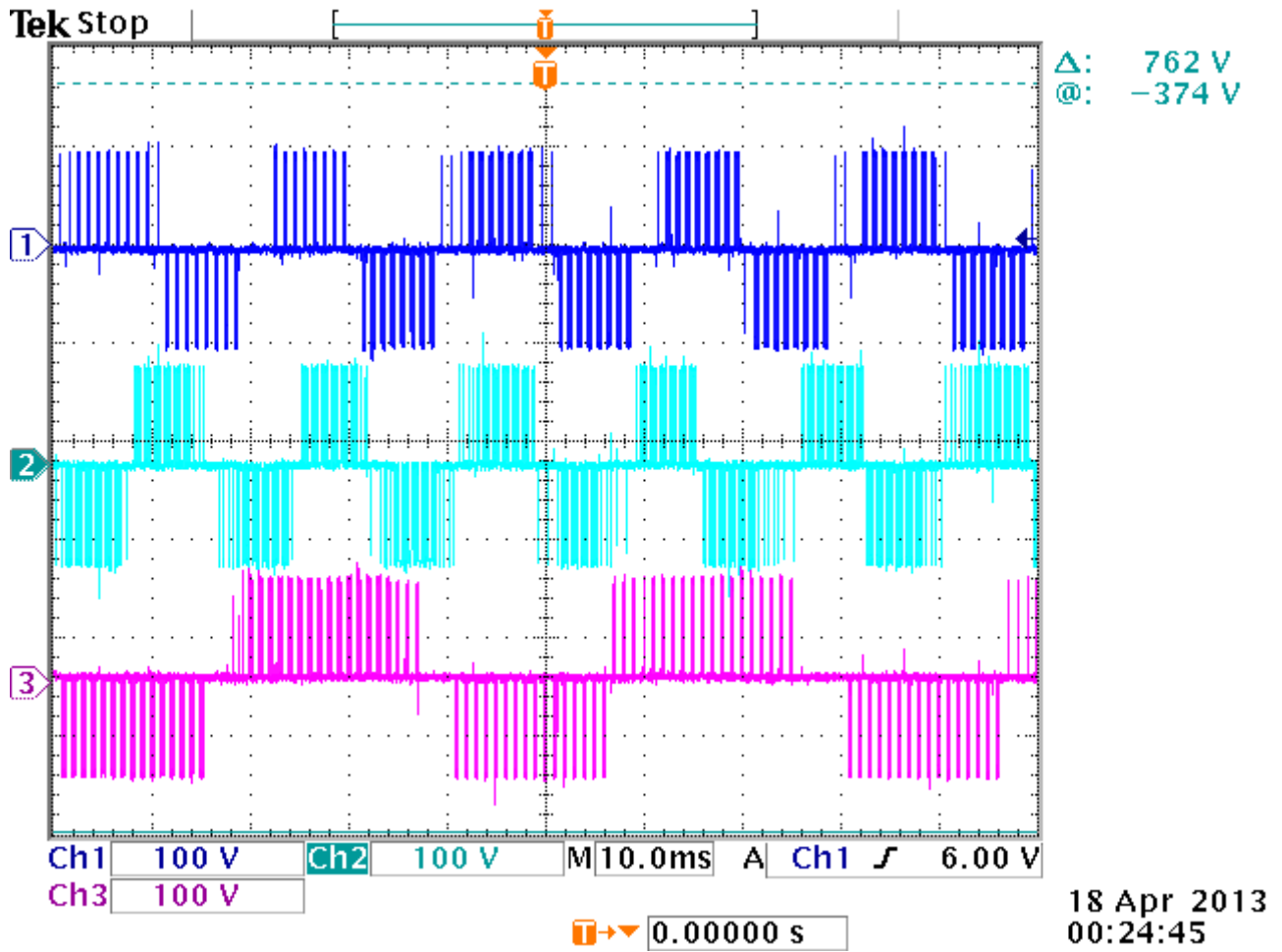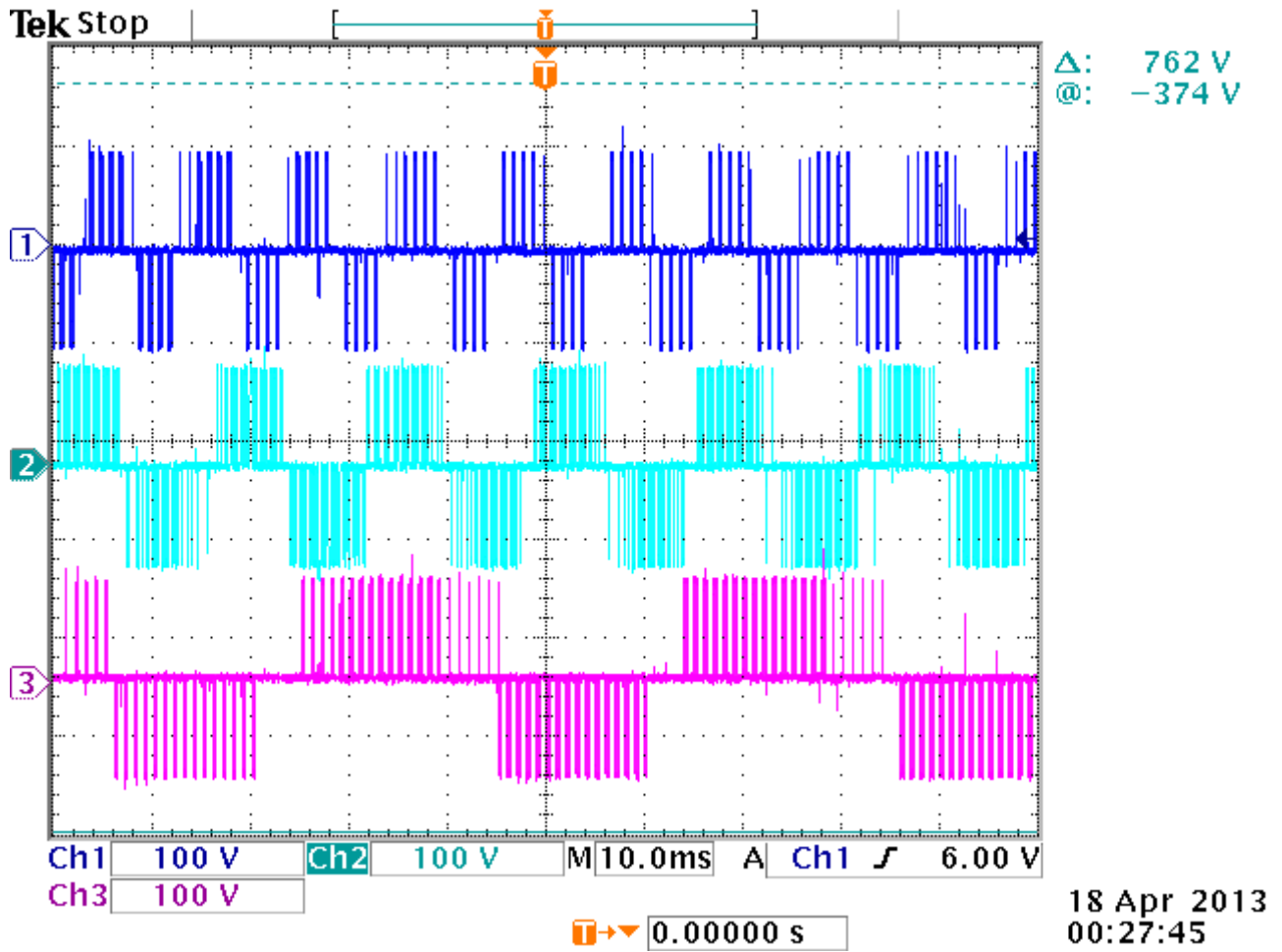
Figure 6.24.   Line-to-line voltages for *Inv1* (Ch1), *Inv2* (Ch2), and *Inv3* (Ch3) with frequencies 95 Hz, 60 Hz, and 25 Hz respectively and same amplitudes of $V_1 = V_2 = V_3 = 0.3V_{dc}/\sqrt{3}$.

Figure 6.25.   Line-to-line voltages for *Inv1* (Ch1), *Inv2* (Ch2), and *Inv3* (Ch3) with frequencies 50 Hz, 60 Hz, and 25 Hz respectively and same amplitudes of $V_1 = V_2 = V_3 = 0.3V_{dc}/\sqrt{3}$ and initial phase angle for phase 'a' of is -30 deg for all three outputs with the phases 'b' and 'c' having 0 deg initial phase angles
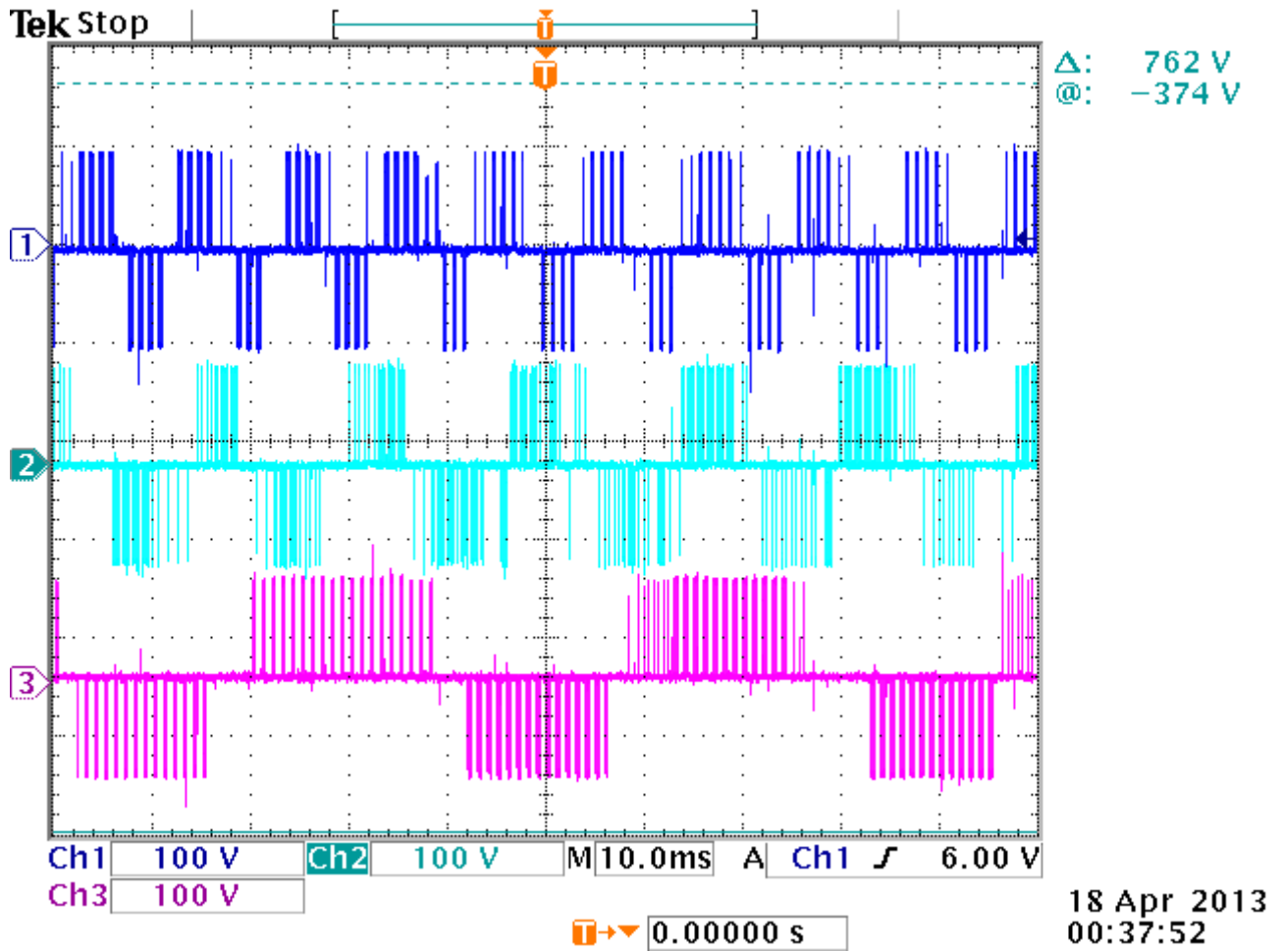
Figure 6.26.   Line-to-line voltages for *Inv1* (Ch1), *Inv2* (Ch2), and *Inv3* (Ch3) with frequencies 95 Hz, 60 Hz, and 25 Hz respectively and same amplitudes of $V_1 = V_2 = V_3 = 0.3V_{dc}/\sqrt{3}$ and initial phase angle for phase 'a' of is -30 deg for all three outputs with the phases 'b' and 'c' having 0 deg initial phase angles
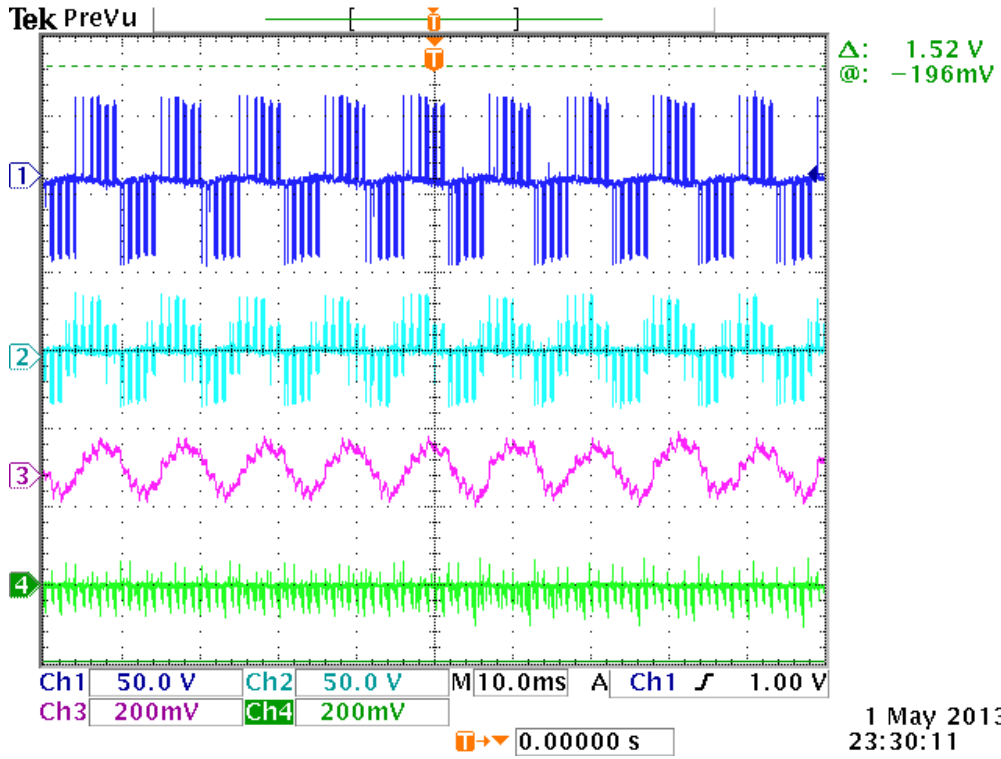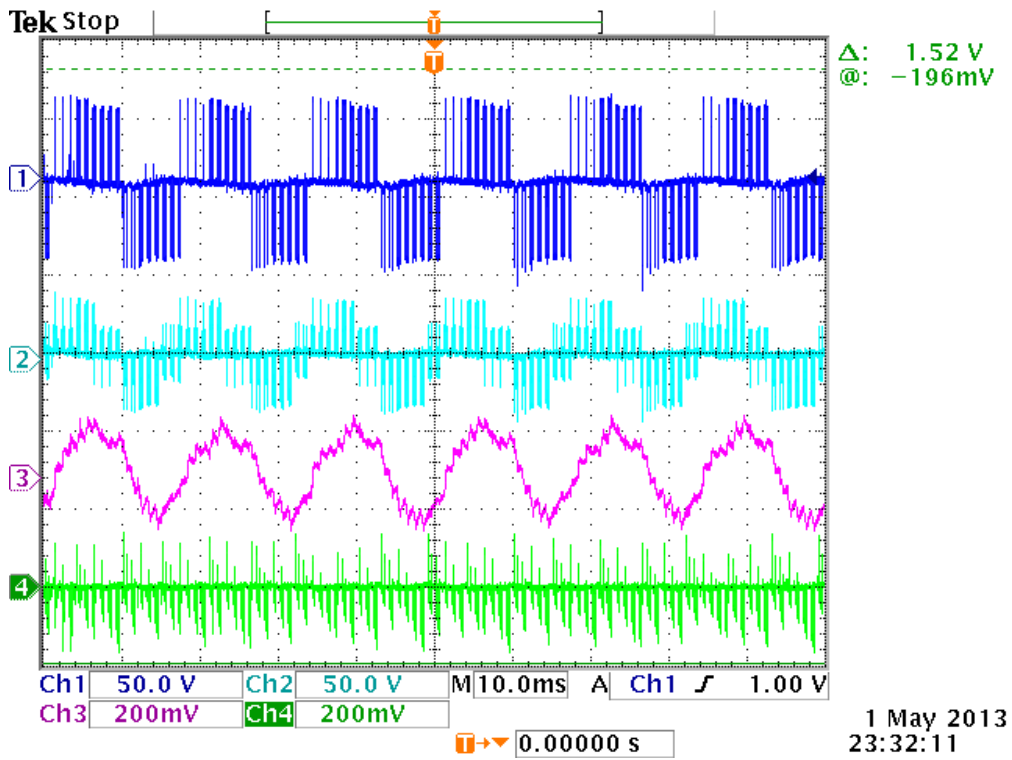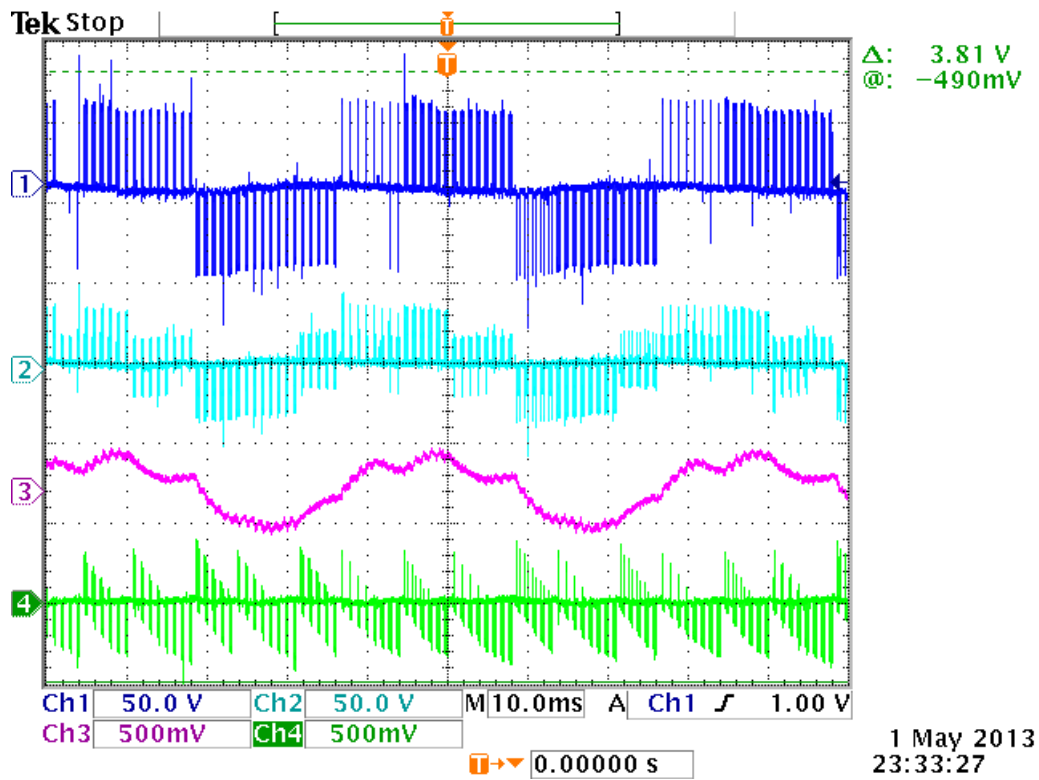
Figure 6.27.   Line-to-line voltages for *Inv1* (Ch1), *Inv2* (Ch2), and *Inv3* (Ch3) with frequencies 95 Hz, 60 Hz, and 25 Hz respectively and amplitude unbalance $V_1 = V_2 = V_3 = 0.3 V_{dc}/\sqrt{3}$, $V_{b1} = V_{b2} = V_{b3} = 0.8 V_{a1}$, and $V_{b1} = V_{b2} = V_{b3} = 0.5 V_{a1}$.

(a)

(b)

292

(c)

Figure 6.28.   Experimental waveforms of (a) *Inv1 ,* (b) *Inv2,* and (c) *Inv3* showing (Ch1) line-to-line voltage, (Ch2) phase voltage,   (Ch3) phase current, and (Ch4) input dc current with frequencies 95 Hz, 60 Hz, and 25 Hz respectively and balance amplitudes of $V_1 = V_2 = V_3 = 0.3V_{dc}/\sqrt{3}$.

6.5 Generalization for 3n+3-Converter

The structure of the generalized 3n+3-switch converter is shown in Figure 6.1. The converter can be used control *n* loads independently. From the models of both the Nine-switch converter in Chapter 5 and the 12-switch converter in this chapter, the following conclusions can be made as listed in Table 6.21.

An important property to generalize is the neutral voltages used for the carrier-based PWM. To this end, the neutral voltages for the Nine-switch, 12-switch are rewritten and the emerging pattern from these two converters is used to derive the corresponding expresions for a 15-switch and consequently, the 3n+3-switch converter. The neutral voltages for the topmost output for the 9-switch, 12-switch, 15-switch, and 3n+3-switch converters in terms of the active vevtors dwell times are:

Table 6.21. Generalizations for the 3n+3-switch from Nine- and 12-switch converters

Converter property	9-switch	12-switch	15-switch	3n+3-switch
Number of independent outputs	2	3	4	*n*
Number of devices in leg	3	4	5	*n+1*
Number of feasible states	27	64	125	$(n+1)^3$
Number of feasible states for independent control of outputs	15	22	29	*7n+1*
Number of independent active states	12	18	24	6*n*
Number of zero states	3	4	5	*n*+1
Sum of switching functions per phase-leg	2	3	4	*n*

$$V_{m10}^{9} = 3(-t_{01} + t_{02} + t_{03}) + \eta(t_{a1} - t_{b1}) + 3(t_{a2} + t_{b2}) \tag{6.114}$$

$$V_{m10}^{12} = 3(-t_{01} + t_{02} + t_{03} + t_{04}) + \eta(t_{a1} - t_{b1}) + 3(t_{a2} + t_{b2}) + 3(t_{a3} + t_{b3}) \tag{6.115}$$

$$V_{m10}^{15} = \left[\begin{array}{l} 3(-t_{01} + t_{02} + t_{03} + t_{04} + t_{05}) + \eta(t_{a1} - t_{b1}) + \\ 3(t_{a2} + t_{b2}) + 3(t_{a3} + t_{b3}) + 3(t_{a4} + t_{b4}) \end{array} \right] \tag{6.116}$$

$$V_{m10}^{3n+3} = \left[\begin{array}{l} 3(-t_{01} + t_{02} + t_{03} + ... + t_{n+1}) + \eta(t_{a1} - t_{b1}) + \\ 3(t_{a2} + t_{b2}) + 3(t_{a3} + t_{b3}) + ... + 3(t_{an} + t_{bn)}) \end{array} \right] \tag{6.117}$$

$$V_{m10}^{3n+3} = -3t_{01} + 3\sum_{k=2}^{n+1} t_{0k} + \eta(t_{a1} - t_{b1}) + 3\sum_{k=2}^{n} (t_{ak} + t_{bk})$$

where $\eta = \pm 1$ for even and odd sectors respectively.

Similarly, for the bottommost ouput, neutral voltages for the 9-switch, 12-switch, 15-switch, and 3n+3-switch converters in terms of the active vevtors dwell times are:

$$V_{mn0}^{9} = 3(-t_{01} + t_{02} - t_{03}) - 3(t_{a1} + t_{b1}) + \eta(t_{a2} - t_{b2}) \tag{6.118}$$

$$V_{mn0}^{12} = 3(-t_{01} - t_{02} + t_{03} - t_{04}) - 3(t_{a1} + t_{b1}) - 3(t_{a2} + t_{b2}) + \eta(t_{a3} - t_{b3}) \tag{6.119}$$

$$V_{mn0}^{15} = \left[\begin{array}{l} 3(-t_{01} - t_{02} - t_{03} + t_{04} - t_{05}) - 3(t_{a1} + t_{b1}) + \\ -3(t_{a2} + t_{b2}) - 3(t_{a3} + t_{b3}) + \eta(t_{a4} - t_{b4}) \end{array} \right] \tag{6.120}$$

$$V_{mn0}^{3n+3} = \left[\begin{array}{l} 3(-t_{01} - t_{02} - t_{03} - ... + t_{n} - t_{n+1}) - 3(t_{a1} + t_{b1}) + \\ -3(t_{a2} + t_{b2}) - 3(t_{a3} + t_{b3}) + ... + \eta(t_{an} + t_{bn)}) \end{array} \right] \tag{6.121}$$

$$V_{mn0}^{3n+3} = 3t_{0n} - 3\sum_{\substack{k=1 \\ (k \neq n)}}^{n+1} t_{0k} - 3\sum_{k=1}^{n-1} (t_{ak} + t_{bk}) + \eta(t_{an} - t_{bn})$$

The neutral voltage for inner outputs is not applicable to the 9-switch. However the 12-switch 15-switch and 3n+3-switch have one (1), two (2) and n-2 neutral voltages respectively. In terms of the active vectors dwell times these neutral voltages are given by

$$V_{m20}^{12} = 3(-t_{01} - t_{02} + t_{03} + t_{04}) - 3(t_{a1} + t_{b1}) + \eta(t_{a2} - t_{b2}) + 3(t_{a3} + t_{b3}) \tag{6.122}$$

$$V_{m20}^{15} = \begin{bmatrix} 3(-t_{01} - t_{02} - t_{03} + t_{04} + t_{05}) - 3(t_{a1} + t_{b1}) + \\ \eta(t_{a2} - t_{b2}) + 3(t_{a3} + t_{b3}) + 3(t_{a4} + t_{b4}) \end{bmatrix} \tag{6.123}$$

$$V_{m20}^{3n+3} = \begin{bmatrix} 3(-t_{01} - t_{02} - t_{03} - \ldots t_{n-1} + \ldots + t_{n+1}) + 3(t_{a1} + t_{b1}) + \\ \eta(t_{a2} - t_{b2}) + 3(t_{a3} + t_{b3}) + \ldots + 3(t_{an} + t_{bn}) \end{bmatrix}$$

$$V_{m20}^{3n+3} = -3\sum_{k=1}^{n-1} t_{0k} + 3\sum_{k=n}^{n+1} t_{0k} + \eta(t_{a2} - t_{b2}) + 3\sum_{\substack{k=1 \\ (k \neq 2)}}^{n} (t_{ak} + t_{bk}) \tag{6.124}$$

$$V_{mq0}^{3n+3} = -3\sum_{k=1}^{n-1} t_{0k} + 3\sum_{k=n}^{n+1} t_{0k} + \eta(t_{aq} - t_{bq}) + 3\sum_{\substack{k=1 \\ (k \neq 2)}}^{n} (t_{ak} + t_{bk})$$

Generalizing for the inner neutral voltages from (6.123)

$$V_{mq0}^{3n+3} = -3\sum_{k=1}^{n-1} t_{0k} + 3\sum_{k=n}^{n+1} t_{0k} + \eta(t_{aq} - t_{bq}) + 3\sum_{\substack{k=1 \\ (k \neq 2)}}^{n} (t_{ak} + t_{bk}) \tag{6.125}$$

where q (= 2, 3, 4, …, n-1) is the position of the output except the topmost or bottommost outputs.

Using the above expressions for the neutral voltages, the generalized neutral voltages may be derived using space vector modulation as outlined for the 9-switch and 12-switch converters. For a generalized 3n+3-switch converter, let the utilization of the zero vectors be $\alpha_1, \alpha_2, \alpha_3, \ldots \alpha_{n+1}$ and the corresponding normalized neutral voltages be

$m_{m1o}, m_{m2o}, m_{m3o}, \ldots m_{mno}$. For the Nine-switch converter $n = 2$ and the normalized neutral voltages were found in Chapter 5 to be:

$$m_{m1o} = 1 - 2\alpha_1 + (\alpha_1 - 1)m_{max1} + \alpha_1 m_{max2} - \alpha_1(m_{min1} + m_{min2})$$

$$m_{m1o} = 1 - 2\alpha_1 - m_{max1} + \alpha_1(m_{max1} + m_{max2}) - \alpha_1(m_{min1} + m_{min2}) \qquad (6.126)$$

$$m_{m1o} = 1 - 2\alpha_1 - m_{max1} + \alpha_1 \sum_{k=1}^{n}(m_{max\,k} - m_{min\,k})$$

$$m_{m2o} = 2\alpha_2 - 1 + (\alpha_2 - 1)m_{min2} + \alpha_2 m_{min1} - \alpha_2(m_{max1} + m_{max2})$$

$$m_{m2o} = 2\alpha_2 - 1 - m_{min2} + \alpha_2(m_{min1} + m_{min2}) - \alpha_2(m_{max1} + m_{max2}) \qquad (6.127)$$

$$m_{m2o} = 2\alpha_2 - 1 - m_{min2} + \alpha_2 \sum_{k=1}^{n}(m_{min\,k} - m_{max\,k})$$

where k = 1, 2, 3,…, n.

Similarly for the 12-switch converter with $n = 3$, the normalized neutral voltages were derived earlier in this chapter to be:

$$m_{m1o} = (1 - 2\alpha_1) + (\alpha_1 - 1)m_{max1} + \alpha_1(m_{max2} + m_{max3}) - \alpha_1(m_{min1} + m_{min2} + m_{min3})$$

$$m_{m1o} = (1 - 2\alpha_1) - m_{max1} + \alpha_1(m_{max1} + m_{max2} + m_{max3}) - \alpha_1(m_{min1} + m_{min2} + m_{min3}) \qquad (6.1$$

$$m_{m1o} = (1 - 2\alpha_1) - m_{max1} + \alpha_1 \sum_{k=1}^{n}(m_{max\,k} - m_{min\,k})$$

$$m_{m2o} = \begin{bmatrix} (1 - 2\alpha_1 - 2\alpha_2) - m_{\max 1} - m_{\max 2} + m_{\min 1} + \\ + (\alpha_1 + \alpha_2)(m_{\max 1} + m_{\max 2} + m_{\max 3}) + \\ - (\alpha_1 + \alpha_2)(m_{\min 1} + m_{\min 2} + m_{\min 3}) \end{bmatrix}$$

$$m_{m2o} = \begin{bmatrix} (1 - 2(\alpha_1 + \alpha_2)) + m_{\min 1} - m_{\max 1} - m_{\max 2} + \\ + (\alpha_1 + \alpha_2) \begin{bmatrix} m_{\max 1} + m_{\max 2} + m_{\max 3} + \\ - m_{\min 1} - m_{\min 2} - m_{\min 3} \end{bmatrix} \end{bmatrix} \qquad (6.1$$

$$m_{m2o} = \begin{bmatrix} 1 - 2(\alpha_1 + \alpha_2) + m_{\min 1} - m_{\max 1} - m_{\max 2} + \\ + (\alpha_1 + \alpha_2) \sum_{k=1}^{n} (m_{\max k} - m_{\min k}) \end{bmatrix}$$

$$m_{m3o} = 2\alpha_3 - 1 - m_{\min 3} - \alpha_3(m_{\max 1} + m_{\max 2} + m_{\max 3}) + \alpha_3(m_{\min 1} + m_{\min 2} + m_{\min 3})$$

$$\qquad (6.1$$

$$m_{m3o} = 2\alpha_3 - 1 - m_{\min 3} + \alpha_3 \sum_{k=1}^{n} (m_{\min k} - m_{\max k})$$

For the 15-switch converter, the four mormalized neutral voltages are found to be:

$$m_{m1o} = \begin{bmatrix} 1 - 2\alpha_1 - m_{\max 1} + \alpha_1(m_{\max 1} + m_{\max 2} + m_{\max 3} + m_{\max 4}) \\ - \alpha_1(m_{\min 1} + m_{\min 2} + m_{\min 3} + m_{\min 4}) \end{bmatrix}$$

$$\qquad ($$

$$m_{m1o} = \begin{bmatrix} 1 - 2\alpha_1 - m_{\max 1} & \alpha_1 \sum_{k=1}^{n} (m_{\max k} - m_{\min k}) \end{bmatrix}$$

$$m_{m2o} = \begin{bmatrix} 1 - 2(\alpha_1 + \alpha_2 + \alpha_3) - m_{\max 2} + \\ \alpha_1(m_{\max 1} + m_{\max 2} + m_{\max 3} + m_{\max 4}) + \alpha_2(m_{\max 1} + m_{\max 2} + m_{\max 3} + m_{\max 4}) + \\ \alpha_3(m_{\max 1} + m_{\max 2} + m_{\max 3} + m_{\max 4}) - \alpha_1(m_{\min 1} + m_{\min 2} + m_{\min 3} + m_{\min 4}) + \\ - \alpha_2(m_{\min 1} + m_{\min 2} + m_{\min 3} + m_{\min 4}) - \alpha_3(m_{\min 1} + m_{\min 2} + m_{\min 3} + m_{\min 4}) \end{bmatrix}$$

$$\qquad ($$

$$m_{m2o} = \begin{bmatrix} 1 - 2(\alpha_1 + \alpha_2 + \alpha_3) - m_{\max 2} + \alpha_1 \sum_{k=1}^{n} (m_{\max k} - m_{\min k}) + \\ \alpha_2 \sum_{k=1}^{n} (m_{\max k} - m_{\min k}) + \alpha_3 \sum_{k=1}^{n} (m_{\max k} - m_{\min k}) \end{bmatrix}$$

298

$$
m_{m3o} = \begin{bmatrix} 1 - 2(\alpha_1 + \alpha_2 + \alpha_3) - m_{\max 3} + \\ \alpha_1(m_{\max 1} + m_{\max 2} + m_{\max 3} + m_{\max 4}) + \alpha_2(m_{\max 1} + m_{\max 2} + m_{\max 3} + m_{\max 4}) + \\ \alpha_3(m_{\max 1} + m_{\max 2} + m_{\max 3} + m_{\max 4}) - \alpha_1(m_{\min 1} + m_{\min 2} + m_{\min 3} + m_{\min 4}) + \\ -\alpha_2(m_{\min 1} + m_{\min 2} + m_{\min 3} + m_{\min 4}) - \alpha_3(m_{\min 1} + m_{\min 2} + m_{\min 3} + m_{\min 4}) \end{bmatrix}
$$

$$
m_{m3o} = \begin{bmatrix} 1 - 2(\alpha_1 + \alpha_2 + \alpha_3) - m_{\max 3} + \alpha_1 \sum_{k=1}^{n}(m_{\max k} - m_{\min k}) + \\ \alpha_2 \sum_{k=1}^{n}(m_{\max k} - m_{\min k}) + \alpha_3 \sum_{k=1}^{n}(m_{\max k} - m_{\min k}) \end{bmatrix}
$$

$$
m_{m1o} = \begin{bmatrix} 1 - 2\alpha_1 - m_{\max 1} + \alpha_1(m_{\max 1} + m_{\max 2} + m_{\max 3} + m_{\max 4}) \\ -\alpha_1(m_{\min 1} + m_{\min 2} + m_{\min 3} + m_{\min 4}) \end{bmatrix}
$$

$$
m_{m1o} = \begin{bmatrix} 2\alpha_4 - 1 - m_{\min 4} - \alpha_4 \sum_{k=1}^{n}(m_{\max k} - m_{\min k}) \end{bmatrix}
$$

From the expressions above, the normalized neutral voltages for the upper and lower loads of the 3n+3-switch converter is easily deduced to be given by

$$
m_{m1o} = 1 - 2\alpha_1 - m_{\max 1} + \alpha_1 \sum_{k=1}^{n}(m_{\max k} - m_{\min k}) \tag{6.135}
$$

$$
m_{mno} = 2\alpha_n - 1 - m_{\min n} + \alpha_n \sum_{k=1}^{n}(m_{\min k} - m_{\max k}) \tag{6.136}
$$

The normalized neutral voltages of the inner devices that are obviously shared by two different outputs are a little more complicated and cannot be generalized from the 12- and 15-switch converters. This has been left for future work.

299

6.6 Summary

The space vector and a carrier-based modulation methodology for the 12-switch converter have been proposed. The generalized neutral voltages for the 12-switch and generalized 3n+3-switch converters have been derived for the first time. Simulation results show that injecting these neutral voltages into the modulation signals has a dual role; shaping the modulation scheme as well as ensure the switching function constraint of the converter is not violated. The modulation schemes proposed here is also applicable to the generalized 3n+3-converter. Simulation results show the validity of the proposed schemes. The simulation results are also corroborated by experimental results.

CHAPTER 7

SERIES VOLTAGE COMPENSATION FOR LVRT OF DFIG WIND TURBINE USING THE NINE-SWITCH CONVERTER

7.1 Principles of Series Compensation

The idea of series voltage compensation applied to Low Voltage Ride-Through (LVRT) for the DFIG wind turbine is derived from dynamic voltage restorers (DVRs) as used to protect sensitive loads from voltage disturbances from the supply side [80] − [86]. When a voltage sag (or swell) is detected, the DVR injects a compensating voltage in series with the ac supply line protecting loads connected downstream of the DVR. The DVR can also be used to compensate for harmonics in a polluted ac supply [81] and [82]. A typical DVR system is composed of a voltage source inverter (VSI), an injection transformer connected between the ac voltage line and the sensitive load, and a dc source as shown in Figure 7.1. [81].

DVRs are similar to uninterruptible power supplies (UPS) systems but unlike the UPS systems that must supply the total voltage and power to the sensitive load, the DVR is only required to compensate for the 'missing' voltage. The DVR power requirement is therefore much lower than a corresponding UPS system.

In DFIG wind turbine systems, the stator of the induction machine is directly connected to the grid and is very much at the mercy of any grid disturbances. This work follows from similar work done in [87] − [94] exploring the feature of the DVR's grid side converter. To differentiate the two grid side converters, the conventional grid side
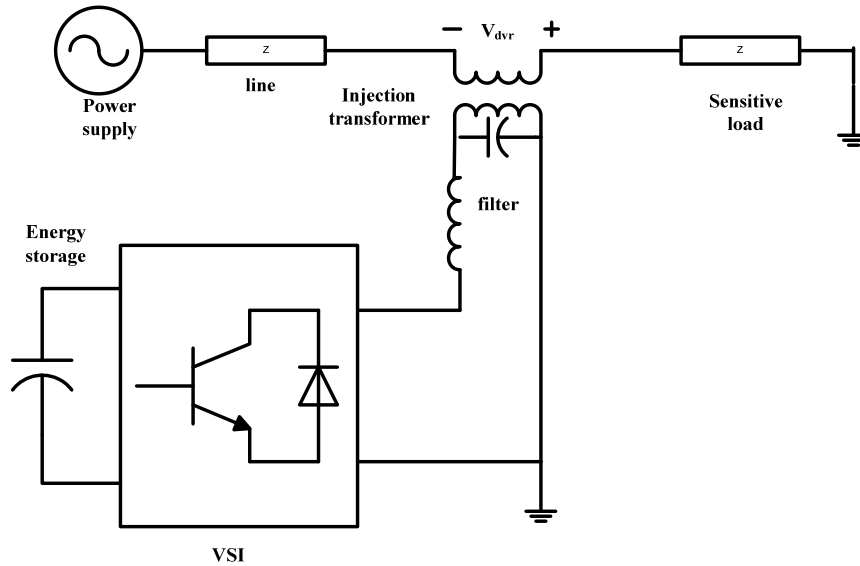
301

Figure 7.1. Typical application of a DVR to protect sensitive loads

converters, the conventional grid side converter which is connected in parallel with stator windings and grid connection is referred to as the Parallel Grid Side Converter (PGSC). It should be pointed out that the role of the SGSC though similar to the DVR used to protect sensitive loads, the SGSC is used in this application to keep the stator and rotor currents within their maximum permissible limits. A simplified block of the DFIG wind turbine system with the SGSC is shown in Figure 7.2.

Two main topologies of series voltage injection for the DFIG wind turbine LVRT have been proposed in literature namely transformer interfaced SGSC and (2) "stator neutral point" connected SGSC. In the transformer interfaced SGSC topology [87] – [94], the SGSC is connected via a three phase injection transformer in series with the main stator windings of the DFIG as shown in Figure 7.2. The machine neutral point is internally tied together as in a conventional DFIG. The SGSC, three phase injection
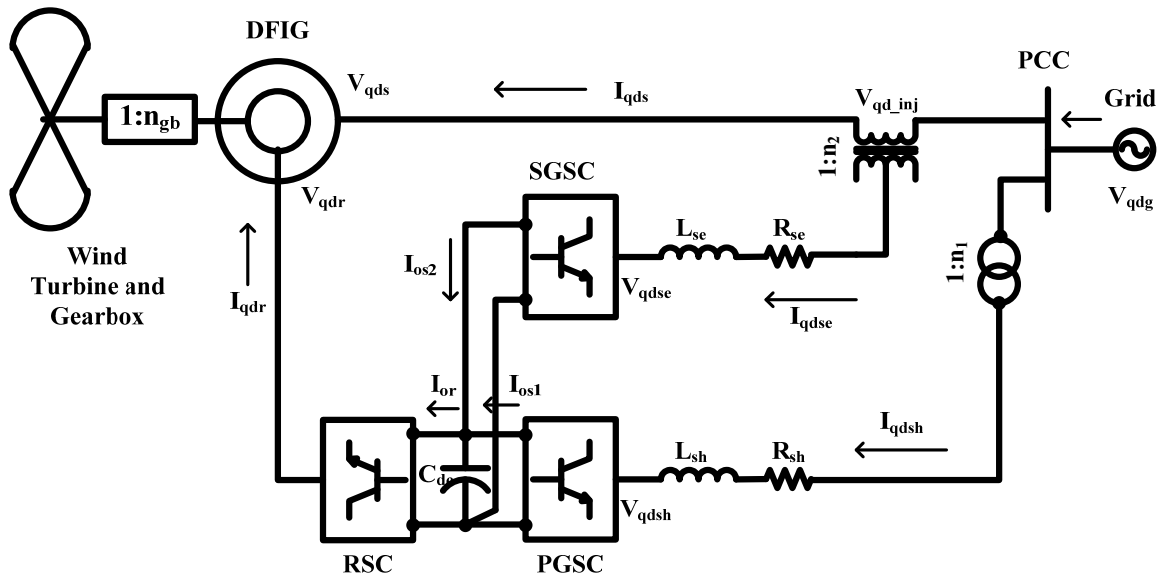
302

Figure 7.2. Schematic transformer interfaced DFIG wind turbine with PGSC and SGSC

transformer and inductive filter all share the same per unit current as the stator circuit of the DFIG.

Two main topologies of series voltage injection for the DFIG wind turbine LVRT have been proposed in literature namely transformer interfaced SGSC and "stator neutral point" connected SGSC. In the transformer interfaced SGSC topology [87] − [94], the SGSC is connected via a three phase injection transformer in series with the main stator windings of the DFIG as shown in Figure 7.2. The machine neutral point is internally tied together as in a conventional DFIG. The SGSC, three phase injection transformer and inductive filter all share the same per unit current as the stator circuit of the DFIG.

In the second type of series injection [33] − [35], the neutral point of the DFIG stator windings is opened up and is no longer connected internally. The three returns are instead brought out from the machine individually and connected directly to the SGSC.

This allows the SGSC to directly modify the net voltage applied to the stator windings without the use of an injection transformer. The drawback of this topology is that harmonics in the series voltage is directly injected into the stator windings, causing heating. In this dissertation, the injection transformer topology is adopted.

7.2 Modeling of Proposed System

The single line diagram of the proposed low voltage ride-through is shown in Figure 7.3. In this topology, the two (2) grid side converters in Figure 7.2 are replaced with the Nine-switch converter developed in Chapter 5. That is the two outputs of the Nine-switch converter serve the dual role of the PGSC and SGSC. The governing dynamic equations of the DFIG wind turbine have been derived in Chapter 3 except that this is without the series injection. For the sake of completeness, the overall dynamics are derived in this chapter. The dynamic equations in *qd* arbitrary reference frame applying Kirchhoff's' voltage and current laws (KVL and KCL) to Figure 7.3 are stated below. The convention adopted here assumes all currents directions as flowing into the induction machine as shown in Figure 7.3.

The DFIG stator and rotor voltage equations are given by

$$V_{qg} = V_{qs} + V_{qi} \tag{7.1}$$

$$V_{dg} = V_{ds} + V_{di} \tag{7.1}$$

$$V_{qs} = r_s I_{qs} + p\lambda_{qs} + \omega\lambda_{ds} \tag{7.2}$$

$$V_{ds} = r_s I_{ds} + p\lambda_{ds} - \omega\lambda_{qs} \tag{7.3}$$

$$V_{qr} = r_r I_{qr} + p\lambda_{qr} + (\omega - \omega_r)\lambda_{dr} \tag{7.4}$$

$$V_{dr} = r_r I_{dr} + p\lambda_{dr} - (\omega - \omega_r)\lambda_{qr} \tag{7.5}$$

where the stator and rotor flux linkages are defined as

$$\lambda_{qs} = L_s I_{qs} + L_m I_{qr} \tag{7.6}$$

$$\lambda_{ds} = L_s I_{ds} + L_m I_{dr} \tag{7.7}$$

$$\lambda_{qr} = L_m I_{qs} + L_r I_{qr} \tag{7.8}$$

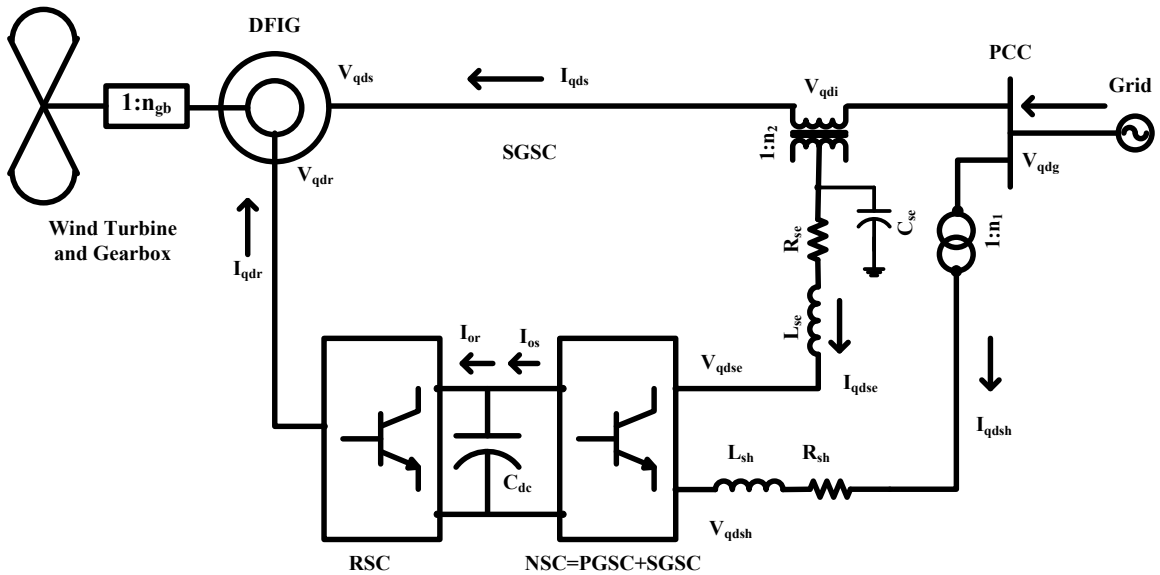$$\lambda_{dr} = L_m I_{ds} + L_r I_{dr} \tag{7.9}$$

Figure 7.3. Single-line diagram of a DFIG wind turbine with Nine-switch converter

The dynamic equations of the series injection assuming the injection transformer ratio n_2:

$$V_{qi} = n_2\left(r_{se}I_{qse} + L_{se}pI_{qse} + \omega L_{se}I_{dse} + V_{qse}\right)$$

(7.10)

$$V_{di} = n_2\left(r_{se}I_{dse} + L_{se}pI_{dse} - \omega L_{se}I_{qse} + V_{dse}\right)$$

(7.11)

$$I_{qs} = \frac{1}{n_2}\left(C_{se}pV_{qi} + \omega C_{se}V_{di} + I_{qse}\right)$$

(7.12)

$$I_{ds} = \frac{1}{n_2}\left(C_{se}pV_{di} - \omega C_{se}V_{qi} + I_{dse}\right)$$

(7.13)

The dynamic equations at the PGSC side assuming the transformer ratio, n_1:

$$V_{qg} = n_1\left(r_{sh}I_{qsh} + L_{sh}pI_{qsh} + \omega L_{sh}I_{dsh} + V_{qsh}\right)$$

(7.14)

$$V_{dg} = n_1\left(r_{sh}I_{dsh} + L_{sh}pI_{dsh} - \omega L_{sh}I_{qsh} + V_{dsh}\right)$$

(7.15)

The dc bus dynamics are:

$$C_{dc}pV_{dc} = I_{ose} + I_{osh} - I_{or}$$

(7.16)

$$I_{ose} = \frac{3}{4}\left(M_{qse}I_{qse} + M_{dse}I_{dse}\right)$$

(7.17)

$$I_{osh} = \frac{3}{4}\left(M_{qsh}I_{qsh} + M_{dsh}I_{dsh}\right)$$

(7.18)

$$I_{or} = \frac{3}{4}\left(M_{qr}I_{qr} + M_{dr}I_{dr}\right)$$

(7.19)

In (7.1) – (7.19), the subscripts q and d refer to q-axis and d-axis components; s, r, i, and g refer to variables associated with stator , rotor, series injection and grid circuits respectively; se and sh refer to variables associated the series - and parallel (shunt) grid side converter parameters respectively; $V_{qs}, V_{ds}, V_{qr}, V_{dr}, V_{qi}, V_{di}, V_{qg}, V_{dg}$ are respectively the q and d stator , rotor, series injected and grid voltages and $I_{qs}, I_{ds}, I_{qr}, I_{dr}, I_{qg}, I_{dg}$ are their corresponding currents; I_{qsh}, I_{dsh} represent the current injected into the grid via the parallel grid side converter; $\lambda_{qs}, \lambda_{ds}, \lambda_{qr}$ and λ_{dr} are the stator and rotor fluxes linkages; L_s, L_r, and L_m are respectively the machine stator , rotor , and magnetizing inductances; r_s and r_r are the stator and rotor resistances ; $L_{se}, L_{sh}, r_{se}, r_{sh}$ represent the series and shunt filter inductances and resistances; $M_{qse}, M_{dse}, M_{qsh}, M_{dsh}, M_{qr}$ and M_{dr} are the modulation indices of the series grid side, parallel grid side and rotor side converters respectively; V_{dc} is the DC link voltage and corresponding DC link capacitance is represented by C_{dc}; ω is the angular frequency of the arbitrary reference frame; ω_r is the rotor electrical speed; n_1, n_2 represent the transformer turn ratios of the parallel and series transformers respectively, and $p = d/dt$.

7.3 Steady State Characteristics

7.3.1. DFIG with SGSC only

The dynamic model of the DFIG wind turbine in Figure 7.3 without the PGSC is given by

$$V_{qs} = r_s I_{qs} + p\lambda_{qs} + \omega\lambda_{ds} = V_{qg} - V_{qi} \tag{7.20}$$

$$V_{ds} = r_s I_{ds} + p\lambda_{ds} - \omega\lambda_{qs} = V_{dg} - V_{di} \tag{7.21}$$

$$V_{qr} = r_r I_{qr} + p\lambda_{qr} + (\omega - \omega_r)\lambda_{dr} = M_{qr}\frac{V_{dc}}{2} \tag{7.22}$$

$$V_{dr} = r_r I_{dr} + p\lambda_{dr} - (\omega - \omega_r)\lambda_{qr} = M_{dr}\frac{V_{dc}}{2} \tag{7.23}$$

$$V_{qi} = n_2\left(r_{se} I_{qse} + L_{se} p I_{qse} + \omega L_{se} I_{dse} + M_{qse}\frac{V_{dc}}{2}\right) \tag{7.24}$$

$$V_{di} = n_2\left(r_{se} I_{dse} + L_{se} p I_{dse} - \omega L_{se} I_{qse} + M_{dse}\frac{V_{dc}}{2}\right) \tag{7.25}$$

$$C_{dc} p V_{dc} = \frac{3}{4}\left(M_{qse} I_{qse} + M_{dse} I_{dse} - M_{qr} I_{qr} - M_{dr} I_{dr}\right) \tag{7.26}$$

Substituting (7.24) and (7.25) into (7.20) and (7.21) respectively and rearranging, the complete dynamic equations for this model is given as follows:

308

$$V_{qg} = r_s I_{qs} + p\lambda_{qs} + \omega\lambda_{ds} + n_2\left(r_{se}I_{qse} + L_{se}pI_{qse} + \omega L_{se}I_{dse} + M_{qse}\frac{V_{dc}}{2}\right) \tag{7.27}$$

$$V_{dg} = r_s I_{ds} + p\lambda_{ds} - \omega\lambda_{qs} + n_2\left(r_{se}I_{dse} + L_{se}pI_{dse} - \omega L_{se}I_{qse} + M_{dse}\frac{V_{dc}}{2}\right) \tag{7.28}$$

$$V_{qr} = r_r I_{qr} + p\lambda_{qr} + \left(\omega - \omega_r\right)\lambda_{dr} = M_{qr}\frac{V_{dc}}{2} \tag{7.29}$$

$$V_{dr} = r_r I_{dr} + p\lambda_{dr} - \left(\omega - \omega_r\right)\lambda_{qr} = M_{dr}\frac{V_{dc}}{2} \tag{7.30}$$

$$C_{dc}pV_{dc} = \frac{3}{4}\left(M_{qse}I_{qse} + M_{dse}I_{dse} - M_{qr}I_{qr} - M_{dr}I_{dr}\right) \tag{7.31}$$

At steady state, all state variables are assumed to be constant and therefore their derivatives vanish from the model equations. Thus the steady state equations are as follows:

$$V_{qg} = r_s I_{qs} + \omega\lambda_{ds} + n_2\left(r_{se}I_{qse} + \omega L_{se}I_{dse} + M_{qse}\frac{V_{dc}}{2}\right) \tag{7.32}$$

$$V_{dg} = r_s I_{ds} - \omega\lambda_{qs} + n_2\left(r_{se}I_{dse} - \omega L_{se}I_{qse} + M_{dse}\frac{V_{dc}}{2}\right) \tag{7.33}$$

$$V_{qr} = r_r I_{qr} + \left(\omega - \omega_r\right)\lambda_{dr} = M_{qr}\frac{V_{dc}}{2} \tag{7.34}$$

$$V_{dr} = r_r I_{dr} - \left(\omega - \omega_r\right)\lambda_{qr} = M_{dr}\frac{V_{dc}}{2} \tag{7.35}$$

$$0 = \left(M_{qse}I_{qse} + M_{dse}I_{dse} - M_{qr}I_{qr} - M_{dr}I_{dr}\right) \tag{7.36}$$

Assuming that the grid voltage, rotor speed and DC link voltage are known quantities, there are eight (10) unknown variables $(I_{qs}, I_{ds}, I_{qse}, I_{dse}, I_{qr}, I_{dr}, M_{qr}, M_{dr}, M_{qse}, M_{dse})$, but

only five (5) equations. To solve for a steady state operating condition, three (5) constraints need to be specified.

Neglecting power losses, the real power transferred to the grid is equal to the wind turbine power. Constraints can also be placed on the reactive power transferred to the grid and that transferred by the series grid converter. That is:

$$P_g^* = P_m = \frac{3}{2}\left(V_{qg}I_{qs} + V_{dg}I_{ds}\right)$$
(7.37)

$$Q_g^* = \frac{3}{2}\left(-V_{dg}I_{qs} + V_{qg}I_{ds}\right)$$
(7.38)

$$Q_{se}^* = \frac{3}{2}\left(-V_{dse}I_{qse} + V_{qse}I_{dse}\right) = \frac{3}{2}\frac{V_{dc}}{2}\left(-M_{dse}I_{qse} + M_{qse}I_{dse}\right)$$
(7.39)

If the grid voltage is aligned with the q-axis, then the d-axis component of the grid voltage is zero. Thus the active and reactive powers in (7.37) and (7.38), reduces to:

$$P_g^* = P_m = \frac{3}{2}V_{qg}I_{qs}$$
(7.40)

$$Q_g^* = \frac{3}{2}V_{qg}I_{ds}$$
(7.41)

Therefore q- and d-axis stator currents can be found if the rotor speed (turbine power) and the reactive power injected into the grid are specified. Additionally, if the reactive power at the output of the series grid side converter is specified and assuming the series grid side converter filter capacitor $C_{se} = 0$, and $n_1 = n_2 = 1$, then $I_{qse} = I_{qse}$, $I_{dse} = I_{ds}$, an additional equation is obtained. Thus, (7.32) - (7.36) and (7.39) may be solved to obtain

the unknown variables $(I_{qr}, I_{dr}, M_{qr}, M_{dr}, M_{qse}, M_{dse})$. The steady-state characteristics of a 2 MW DFIG wind turbine are shown in Figures 7.4-7.10 assuming maximum power tracking below rated speed and rated power mode above rated speed. The parameters of the system are given in Appendix.

It can be observed that in most of the DFIG operating region, the induction machine's stator voltage is greater than the grid voltage as long as there is a voltage injected in series with the stator. This also affects other variables such as the stator and rotor flux linkages and currents. Note however that the analysis was arrived at assuming normal grid conditions. In the event of voltage sag for example, the magnitude of the grid is reduced and the series injection is then important.
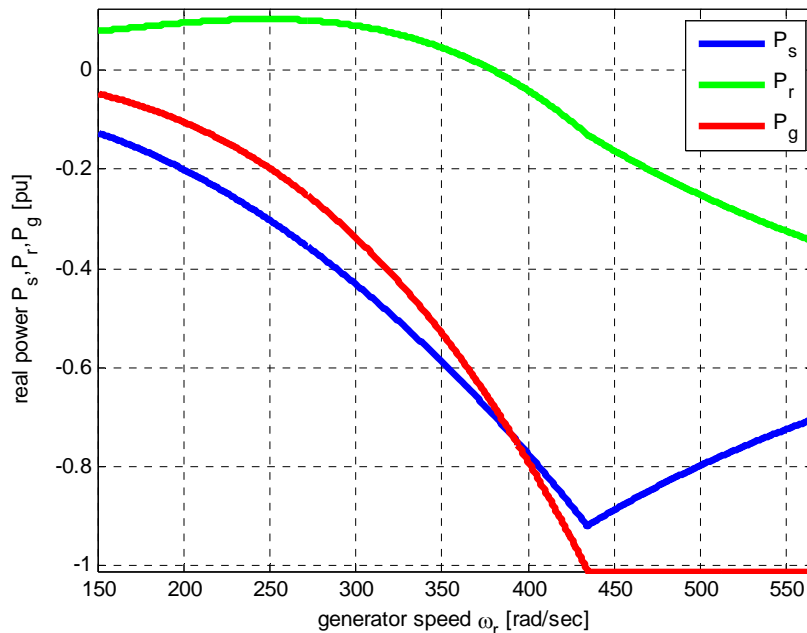

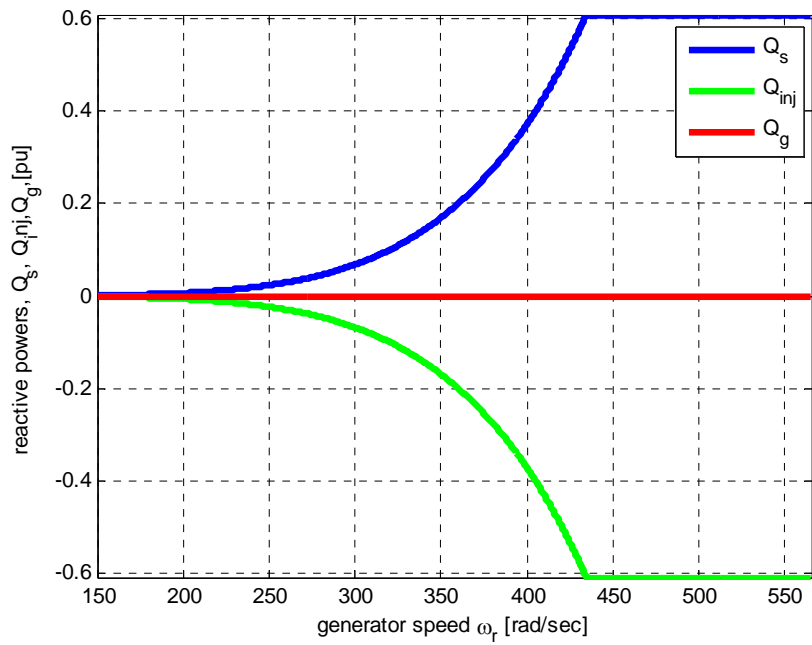Figure 7.4. Stator, rotor and total real powers at varying generator speed

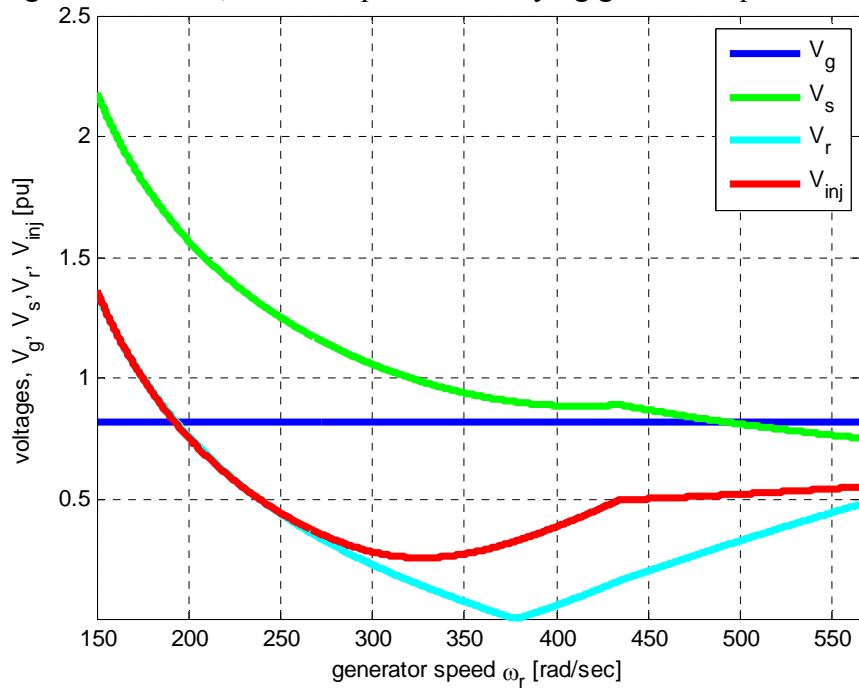Figure 7.5. Stator, rotor and powers at varying generator speed

Figure 7.6. Grid , stator , rotor and series injected voltage magnitudes at varying generator speed
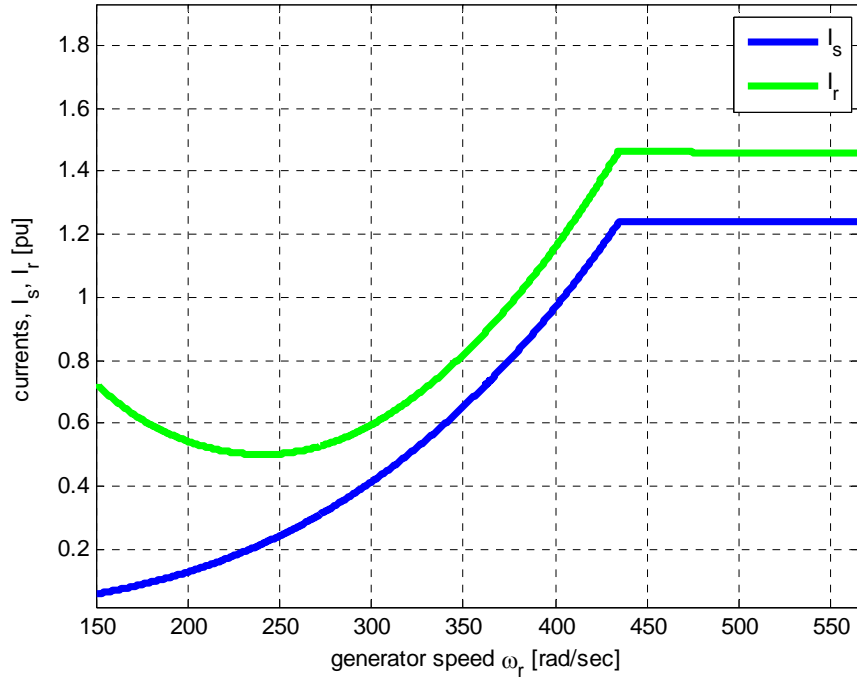
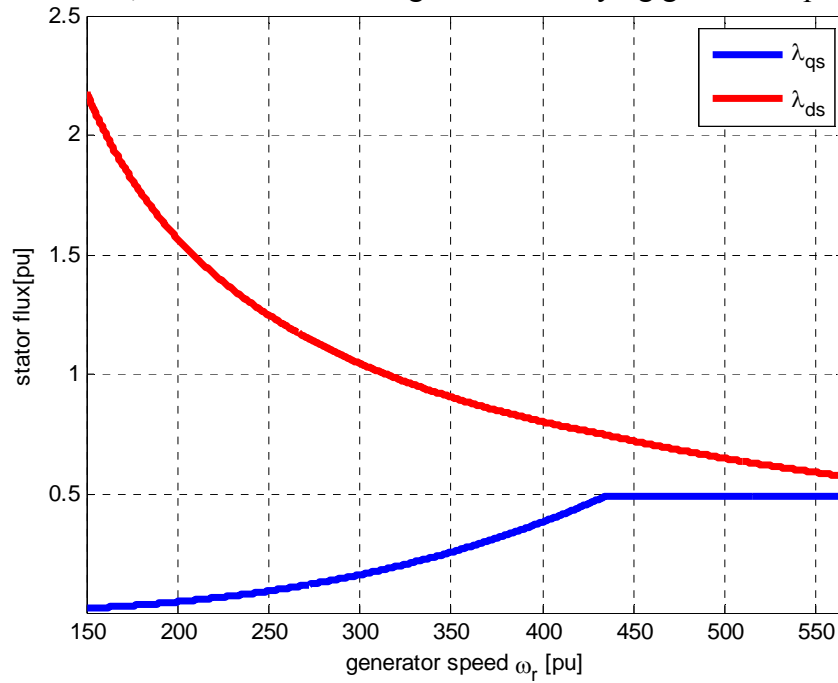Figure 7.7. Stator, and rotor current magnitudes at varying generator speed

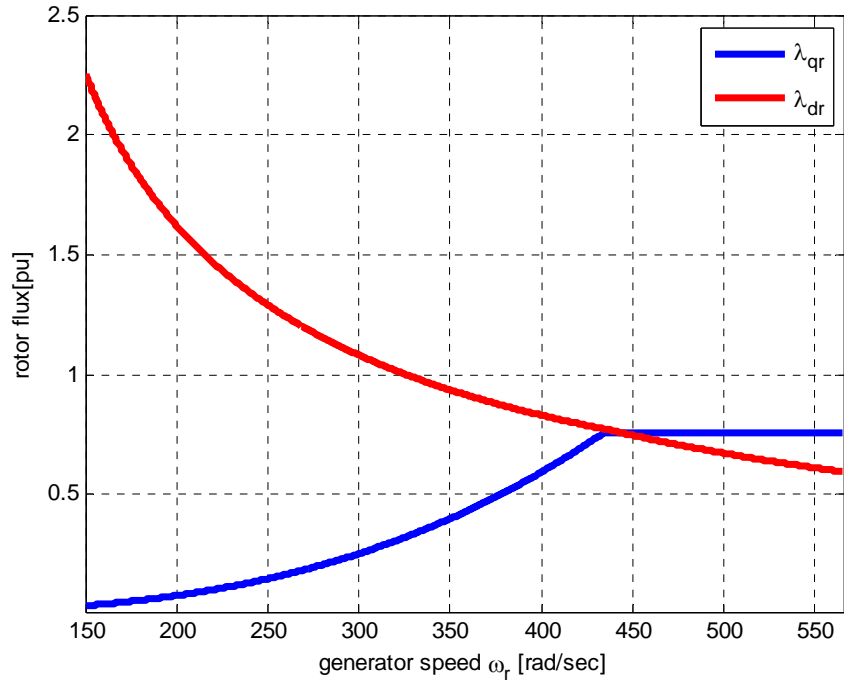Figure 7.8. DFIG stator q-d flux linkages
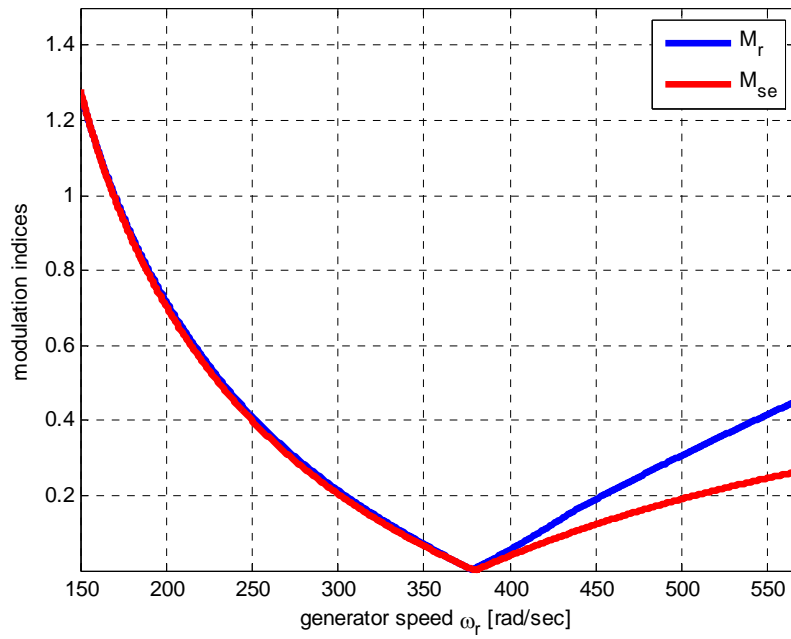
313

Figure 7.9. DFIG rotor q-d flux linkages

Figure 7.10.   Magnitude of the modulation indices for rotor and series grid side converters

314

7.3.2. DFIG with both Series and Parallel Grid Side Converters

In this subsection , the steady state characteristics of the entire system including the doubly fed induction machine, rotor side converter, and both grid side converters (series and shunt) are considered. The steady state equations when $C_{se} = 0$, $n_1 = n_2 = 1$ are given by

$$V_{qg} = r_s I_{qs} + \omega \lambda_{ds} + n_2 \left(r_{se} I_{qs} + \omega L_{se} I_{ds} + M_{qse} \frac{V_{dc}}{2} \right) \tag{7.42}$$

$$V_{dg} = r_s I_{ds} - \omega \lambda_{qs} + n_2 \left(r_{se} I_{ds} - \omega L_{se} I_{qs} + M_{dse} \frac{V_{dc}}{2} \right) \tag{7.43}$$

$$V_{qr} = r_r I_{qr} + \left(\omega - \omega_r \right) \lambda_{dr} = M_{qr} \frac{V_{dc}}{2} \tag{7.44}$$

$$V_{dr} = r_r I_{dr} - \left(\omega - \omega_r \right) \lambda_{qr} = M_{dr} \frac{V_{dc}}{2} \tag{7.45}$$

$$V_{qg} = r_{sh} I_{gsh} + \omega L_{sh} I_{dsh} + M_{qsh} \frac{V_{dc}}{2} \tag{7.46}$$

$$V_{dg} = r_{sh} I_{dsh} - \omega L_{sh} I_{qsh} + M_{dsh} \frac{V_{dc}}{2} \tag{7.47}$$

$$0 = \left(M_{qsh} I_{qh} + M_{dsh} I_{dh} + M_{qse} I_{qs} + M_{dse} I_{ds} - M_{qr} I_{qr} - M_{dr} I_{dr} \right) \tag{7.48}$$

In this case , there are seven (7) equations but ten (10) unknowns. Three (3) constraints are specifed in order to to determine an operating point. The active and reactive powers injected into the grid are considered known since the input turbine power is known and the about of reactive that needs to be injected into the grid can be specified

by the system operator. In addition the stator active power can be approximated knowing the slip. Finally, the reactive power injected by the parallel grid side converter into the grid and at the output of the series side converter may also be specified by the system operator. The above contraints leads to the following equations:

$$P_g^* = P_m = \frac{3}{2} V_{qg} I_{qs} \tag{7.49}$$

$$Q_g^* = \frac{3}{2} V_{qg} I_{ds} \tag{7.50}$$

$$P_s^* + P_{inj}^* = \frac{3}{2} V_{qg} I_{qs} \tag{7.51}$$

$$Q_{sh}^* = \frac{3}{2} V_{qg} I_{dsh} \tag{7.52}$$

$$Q_{se}^* = \frac{3}{2} \frac{V_{dc}}{2} \left(-M_{dse} I_{qs} + M_{qse} I_{ds} \right) \tag{7.53}$$

At this point, there are eight (8) equations and eight (8) unknowns variables $(I_{qr}, I_{dr}, M_{qr}, M_{dr}, M_{qse}, M_{dse}, M_{qsh}, M_{dsh})$ and there solutions can be found from these equations. Figures 7.11 – 7.20 shows the steady state characteristics of a 2 WM DFIG wind turbine systems whose parameters are given in appendix. The effect of the series injection is clearly observed in the stator voltage. The stator voltage is always greater than the grid voltage at all rotor speeds.
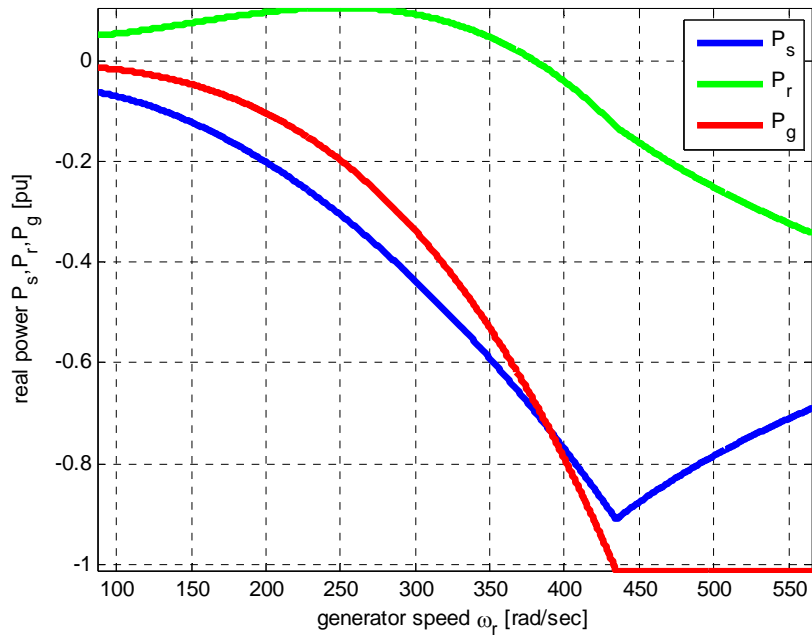
Figure 7.11.   Stator, rotor and total real powers at varying generator speed
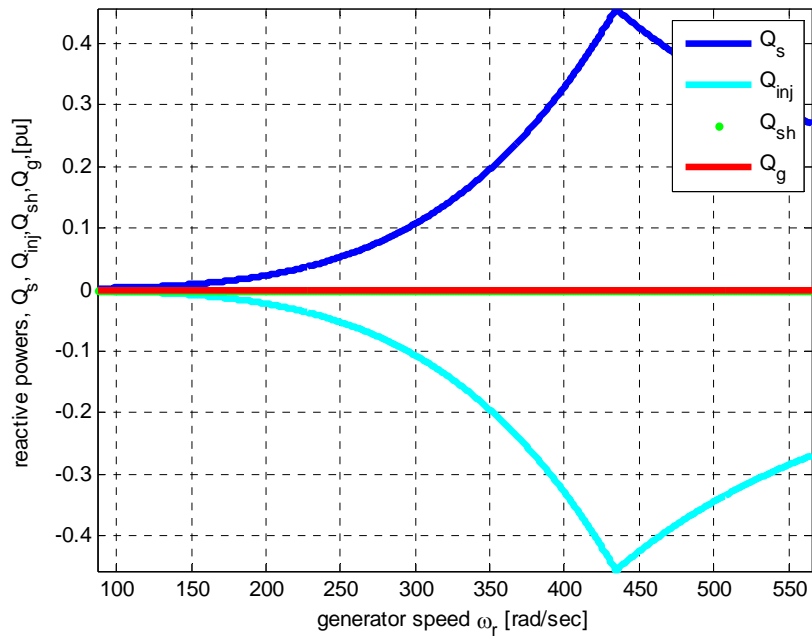
Figure 7.12.   Stator, rotor and powers at varying generator speed

317
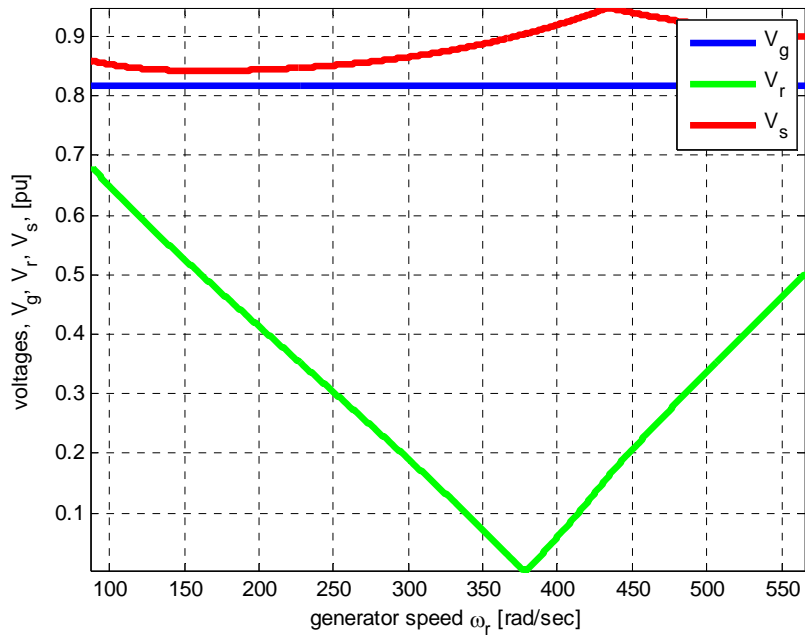
Figure 7.13.   Grid , stator , and rotor voltage magnitudes at varying generator speed
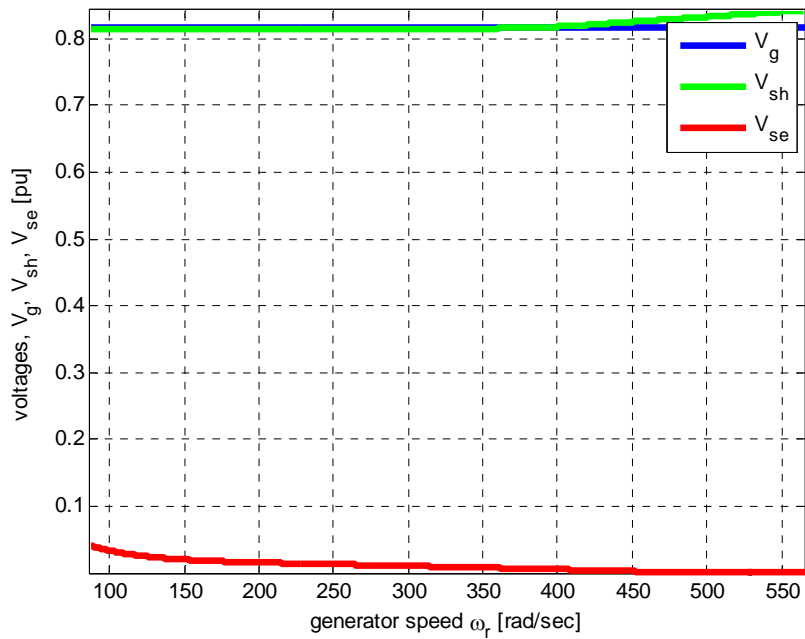
Figure 7.14.   Grid , shunt and series injected voltage magnitudes at varying generator speed
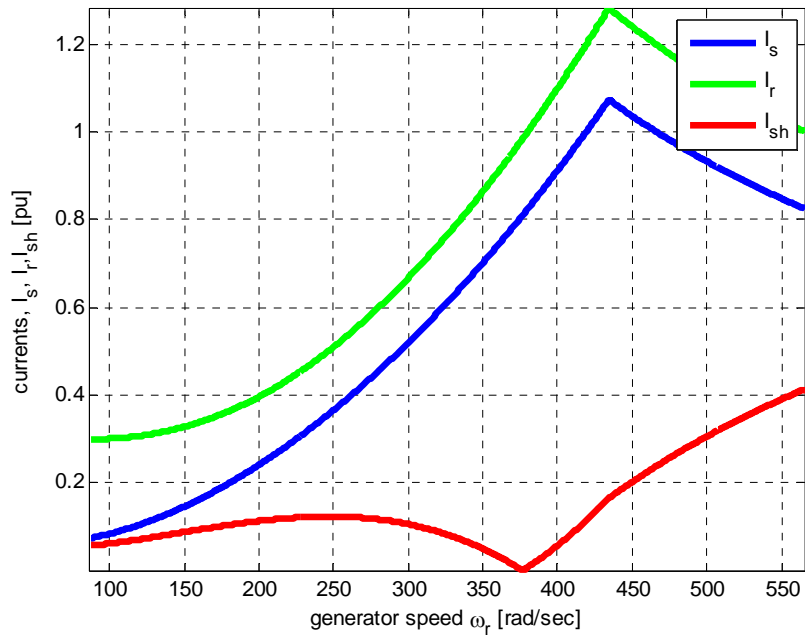
Figure 7.15.   Stator, rotor and shunt injected current magnitudes at varying generator speed
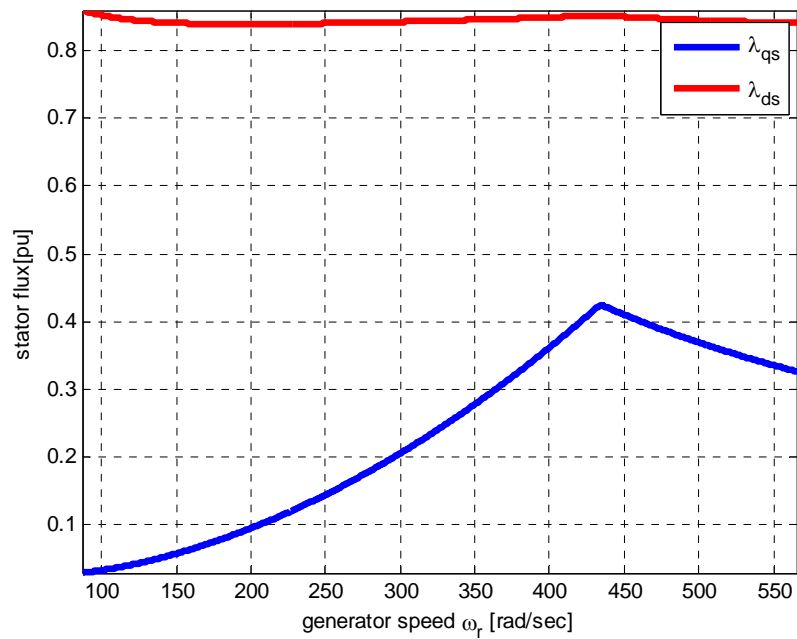
Figure 7.16.   DFIG stator q-d flux linkages
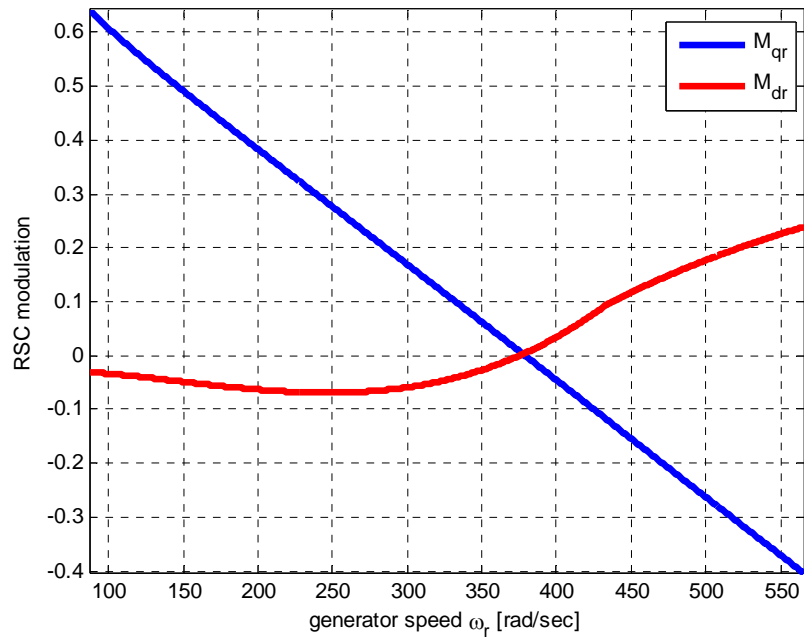
Figure 7.17.   *q-d* modulation indices for rotor side converters
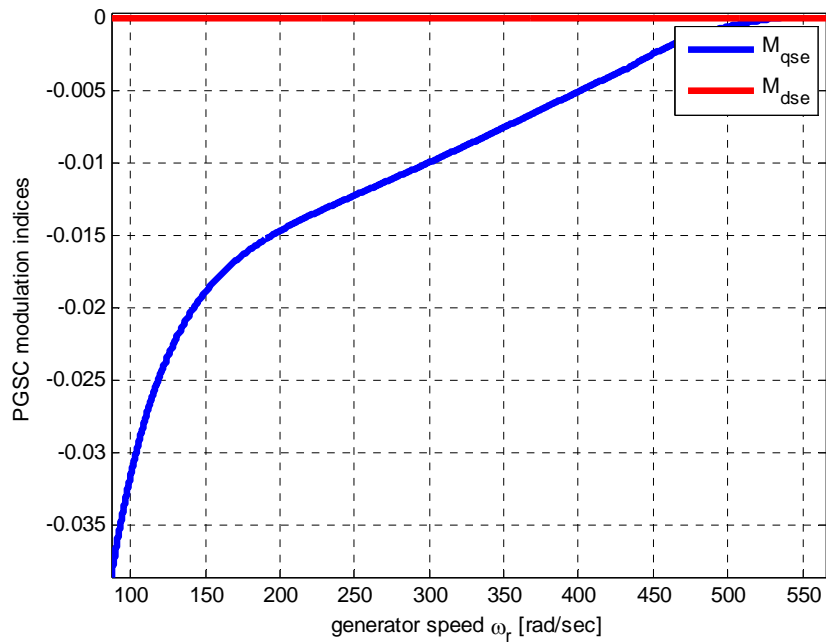
Figure 7.18.   q-d modulation indices for series grid side converter
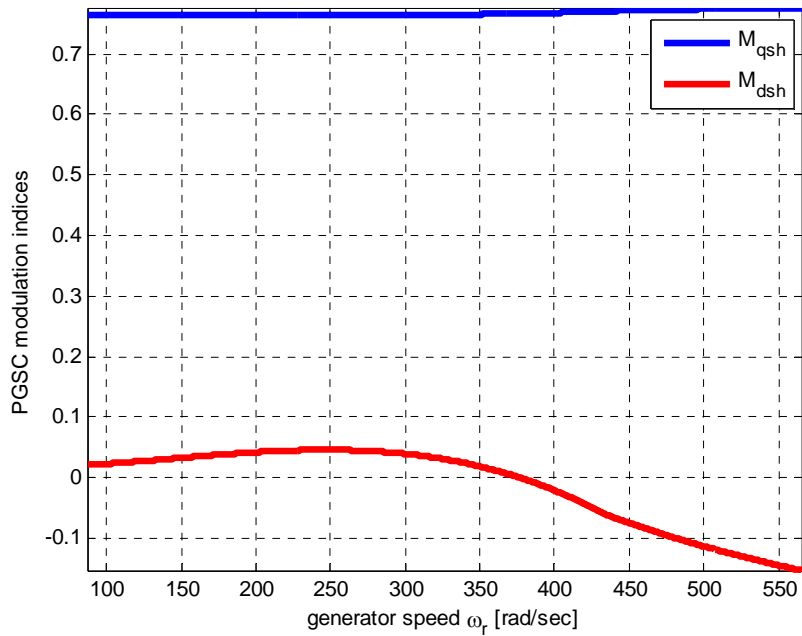
Figure 7.19.   *q-d* modulation indices for parallel grid side converter
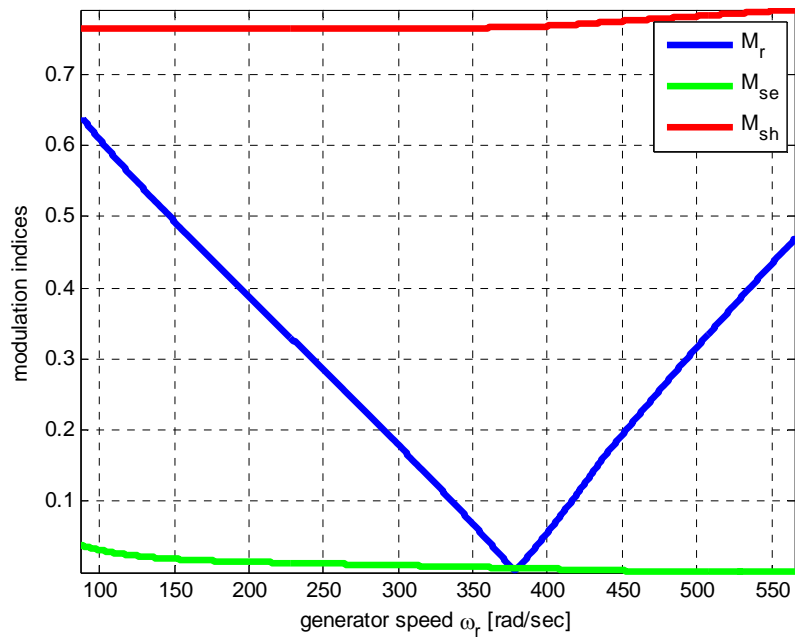
Figure 7.20.   Magnitude of the modulation indices for rotor ,series and parallel grid side converters

7.4 Proposed Control Strategy of DFIG for LVRT

Many researchers have explored the use of proportional resonant (PR) regulators for control of ac-dc converters using the stationary frame [88] – [94]. These PR regulators have been shown to offer fast dynamic response and zero steady-state tracking error for sinusoidal signals. This avoids the need to convert the system variables into the synchronous reference frame and the associated need for a Phase-Locked Loop (PLL) [88]. The following benefits of stationary frame controllers have been identified in literature [88]:

- Elimination of the PLL removes errors that would be brought upon by synchronization problems [90];

- Elimination of *abc-to-qd* and *qd-to-abc* frame transformations, thus significantly reducing overall computation burden [89];

- Improved response to unbalanced faults [93];

- Improved grid current waveforms when interface inductors are not perfectly balanced between the phases and

- Significant reduction in dc ripple under grid imbalance, leading to reduced dc capacitor sizing [94].

The above benefits are the primary reasons for the choice of this type of controller in this dissertation. In the following subsections, where appropriate, the PR controller would be used for the rotor side, parallel grid side, and series grid side converter regulators.

7.4.1. Rotor Side Converter (RSC) Control

In normal grid conditions, the control objective of the RSC is to regulate the stator active power (or generator torque) and reactive power injected into the grid. When a grid sag is detected, the stator power reference in normal grid conditions is disabled until sag event is cleared, and the reference stator power is scaled down according to the decrease in grid power [29]. In a worst case scenario of grid sag, no stator power is delivered to the grid; the dc-link has to absorb the full power of the generator and pitch angle control has to be activated to shed off some wind power.

When an unbalance sag event occurs, in addition to regulating the average active and reactive powers, their ripple components that appears due to the unbalanced needs to be regulated as well. From the DFIG equations (7.1)-(7.9), the stator currents and flux linkages can be expressed as:

$$I_{qs} = \frac{1}{L_s}\left(\lambda_{qs} - L_m I_{qr}\right) \tag{7.54}$$

$$I_{ds} = \frac{1}{L_s}\left(\lambda_{ds} - L_m I_{dr}\right) \tag{7.55}$$

$$\lambda_{qr} = \frac{L_m}{L_s}\lambda_{qs} + \sigma L_r I_{qr} \tag{7.56}$$

$$\lambda_{dr} = \frac{L_m}{L_s}\lambda_{ds} + \sigma L_r I_{dr} \tag{7.57}$$

where the leakage factor, σ is given by

$$\sigma = \left(1 - \frac{L_m^2}{L_s L_r}\right)$$

(7.58)

Eliminating the stator currents and rotor flux from the rotor voltage equations (7.4) and

(7.5), using (7.54)-(7.58), the rotor voltage equations may be rewritten as:

$$V_{qr} = r_r I_{qr} + \sigma L_r p I_{qr} + \frac{L_m}{L_s} p\lambda_{qs} + (\omega - \omega_r)\left(\frac{L_m}{L_s}\lambda_{ds} + \sigma L_r I_{dr}\right)$$

(7.59)

$$V_{dr} = r_r I_{dr} + \sigma L_r p I_{dr} + \frac{L_m}{L_s} p\lambda_{ds} - (\omega - \omega_r)\left(\frac{L_m}{L_s}\lambda_{qs} + \sigma L_r I_{qr}\right)$$

(7.60)

These two rotor voltage equations form the basis for the RSC current regulators.

7.4.1.1.**The torque and stator reactive power commands**. In the event of

unbalanced sag, the torque and reactive power can be resolved into positive and negative

sequence components as [95]:

$$T_{e+} = \frac{3}{2}\frac{P}{2}\text{Im}\left[\lambda_{qds+}^+ I_{qds+}'^+ + \lambda_{qds+}^+ I_{qds-}'^- e^{j2\omega_e t} e^{j(\varphi_+ - \varphi_-)}\right]$$

(7.61)

$$T_{e-} = \frac{3}{2}\frac{P}{2}\text{Im}\left[\lambda_{qds-}^- I_{qds-}'^- + \lambda_{qds-}^- I_{qds+}'^+ e^{-j2\omega_e t} e^{-j(\varphi_+ - \varphi_-)}\right]$$

(7.62)

$$Q_{s+} = \frac{3}{2}\text{Im}\left(V_{qds+}^+ I_{qds+}'^+ + V_{qds+}^+ I_{qds-}'^- e^{j2\omega_e t} e^{j(\varphi_+ - \varphi_-)}\right)$$

(7.63)

$$Q_{s-} = \frac{3}{2}\text{Im}\left(V_{qds-}^- I_{qds-}'^- + V_{qds-}^- I_{qds+}'^+ e^{-j2\omega_e t} e^{-j(\varphi_+ - \varphi_-)}\right)$$

(7.64)

where +, - in the subscripts refer to the positive and negative sequence components and in

superscripts refer to the positive and negative reference references respectively. The

variables with the apostrophe (') refer to complex conjugate, $f'_{qds} = f_{qs} + jf_{ds}$ where f is the general term for a voltage , current of flux linkages.

The torque and reactive power commands can be decoupled by using the stator flux orientation as described in Chapter 3. In the positive- and negative-sequence stator flux reference frames, respectively, both the positive and negative-sequence components of stator flux have imaginary parts only. That is:

$$\lambda^+_{qs+} = \lambda^-_{qs-} = 0 \qquad \lambda^+_{ds+} = \lambda_{s+} \qquad \lambda^-_{ds-} = \lambda_{s-} \tag{7.65}$$

If the voltages on the resistances are neglected, at steady state:

$$V^+_{qs+} = \omega_e \lambda^+_{ds+} \qquad V^-_{qs-} = \omega_e \lambda^-_{ds-} \qquad V^+_{ds+} = V^-_{ds-} = 0 \tag{7.66}$$

Thus, the positive and negative sequence torques and reactive powers are given by

$$T_{e+} = \frac{3}{2}\frac{P}{2}\left(\lambda^+_{ds+} I^+_{qs+}\right) \tag{7.67}$$

$$T_{e-} = \frac{3}{2}\frac{P}{2}\left(\lambda^-_{ds-} I^-_{qs-}\right) \tag{7.68}$$

$$Q_{s+} = \frac{3}{2}\omega_e\left(\lambda^+_{ds+} I^+_{ds+}\right) \tag{7.69}$$

$$Q_{s-} = \frac{3}{2}\omega_e\left(\lambda^-_{ds-} I^-_{ds-}\right) \tag{7.70}$$

Substituting (7.68)-(7.71) into (7.62)-(7.65), the generator torque and stator reactive are respectively:

$$
T_e = \begin{bmatrix} \dfrac{3}{2}\dfrac{P}{2}\left(\lambda^+_{ds+}I^+_{qs+} + \lambda^-_{ds-}I^-_{qs-}\right) + \\[2mm] +\left(\lambda^+_{ds+}I^-_{qs-} + \lambda^-_{ds-}I^+_{qs+}\right)\cos\!\left(2\omega_e t + \varphi_+ - \varphi_-\right) + \\[2mm] -\left(\lambda^+_{ds+}I^-_{ds-} - \lambda^-_{ds-}I^+_{ds+}\right)\sin\!\left(2\omega_e t + \varphi_+ - \varphi_-\right) \end{bmatrix}
\tag{7.71}
$$

$$
Q_s = \dfrac{3}{2}\omega_e \begin{bmatrix} \left(\lambda^+_{ds+}I^+_{ds+} - \lambda^-_{ds-}I^-_{ds-}\right) + \\[2mm] +\left(\lambda^+_{ds+}I^-_{ds-} - \lambda^-_{ds-}I^+_{ds+}\right)\cos\!\left(2\omega_e t + \varphi_+ - \varphi_-\right) + \\[2mm] +\left(\lambda^+_{ds+}I^-_{qs-} + \lambda^-_{ds-}I^+_{qs+}\right)\sin\!\left(2\omega_e t + \varphi_+ - \varphi_-\right) \end{bmatrix}
\tag{7.72}
$$

Similarly, the stator active power is given by

$$
P_s = \dfrac{3}{2}\omega_e \begin{bmatrix} \left(\lambda^+_{ds+}I^+_{qs+} - \lambda^-_{ds-}I^-_{qs-}\right) + \\[2mm] +\left(\lambda^+_{ds+}I^-_{qs-} - \lambda^-_{ds-}I^+_{qs+}\right)\cos\!\left(2\omega_e t + \varphi_+ - \varphi_-\right) + \\[2mm] +\left(-\lambda^+_{ds+}I^-_{ds-} - \lambda^-_{ds-}I^+_{ds+}\right)\sin\!\left(2\omega_e t + \varphi_+ - \varphi_-\right) \end{bmatrix}
\tag{7.73}
$$

From the torque and reactive power equations above, to minimize the ripples, the following equations should be satisfied:

$$
\lambda^+_{ds+}I^-_{qs-} + \lambda^-_{ds-}I^+_{qs+} = 0
\tag{7.74}
$$

$$
\lambda^+_{ds+}I^-_{ds-} - \lambda^-_{ds-}I^+_{ds+} = 0
\tag{7.75}
$$

Multiplying both sides of the above equations by $\lambda^+_{ds+}\lambda^-_{ds-}$ and rearranging:

$$\lambda_{ds+}^{+} I_{qs-}^{-} \lambda_{ds+}^{+} \lambda_{ds-}^{-} + \lambda_{ds-}^{-} I_{qs+}^{+} \lambda_{ds+}^{+} \lambda_{ds-}^{-} = 0$$

$$\left(\lambda_{ds+}^{+}\right)^2 \lambda_{ds-}^{-} I_{qs-}^{-} + \left(\lambda_{ds-}^{-}\right)^2 I_{qs+}^{+} \lambda_{ds+}^{+} = 0 \qquad (7.76)$$

$$\lambda_{ds-}^{-} I_{qs-}^{-} = -\left(\frac{\lambda_{ds-}^{-}}{\lambda_{ds+}^{+}}\right)^2 I_{qs+}^{+} \lambda_{ds+}^{+}$$

$$\lambda_{ds+}^{+} I_{ds-}^{-} \lambda_{ds+}^{+} \lambda_{ds-}^{-} - \lambda_{ds-}^{-} I_{ds+}^{+} \lambda_{ds+}^{+} \lambda_{ds-}^{-} = 0$$

$$\left(\lambda_{ds+}^{+}\right)^2 \lambda_{ds-}^{-} I_{ds-}^{-} - \left(\lambda_{ds-}^{-}\right)^2 I_{ds+}^{+} \lambda_{ds+}^{+} = 0 \qquad (7.77)$$

$$\lambda_{ds-}^{-} I_{ds-}^{-} = \left(\frac{\lambda_{ds-}^{-}}{\lambda_{ds+}^{+}}\right)^2 I_{ds+}^{+} \lambda_{ds+}^{+}$$

Substituting into (7.77) and (7.78) into (7.69) and (7.71), the references of the negative sequence torque and stator reactive power are given as:

$$T_{e-} = -\frac{3}{2}\frac{P}{2}\left(\frac{\lambda_{ds-}^{-}}{\lambda_{ds+}^{+}}\right)^2 I_{qs+}^{+} \lambda_{ds+}^{+}$$

$$T_{e-} = -\left(\frac{\lambda_{ds-}^{-}}{\lambda_{ds+}^{+}}\right)^2 T_{e+} \qquad (7.78)$$

$$Q_{s-} = \frac{3}{2}\omega_e\left(\frac{\lambda_{ds-}^{-}}{\lambda_{ds+}^{+}}\right)^2 I_{ds+}^{+} \lambda_{ds+}^{+}$$

$$Q_{s-} = \left(\frac{\lambda_{ds-}^{-}}{\lambda_{ds+}^{+}}\right)^2 Q_{s+} \qquad (7.79)$$

It is expected that in minimizing the torque, the stator active power is indirectly minimized too. This can be verified by finding the condition for minimizing the stator

active power ripples. From (7.74), to minimize the ripples in the stator active power, the following conditions must be met:

$$\left(\lambda_{ds+}^{+}I_{qs-}^{-} - \lambda_{ds-}^{-}I_{qs+}^{+}\right) = 0 \tag{7.80}$$

$$\left(-\lambda_{ds+}^{+}I_{ds-}^{-} - \lambda_{ds-}^{-}I_{ds+}^{+}\right) = 0 \tag{7.81}$$

These conditions are the same as in the previous case when using the torque and stator reactive power expressions. Thus only two controllers are required to minimize the ripples in generator torque, stator active and reactive powers.

7.4.1.2.**Speed controller.** The shaft speed dynamics assuming a one-mass DFIG wind turbine representation is given as:

$$p\omega_r = \frac{P}{2J}\left(T_{e+} + T_{e-} - T_L\right) \tag{7.82}$$

$$T_{e+} = \frac{3}{2}\frac{P}{2}\left(\lambda_{ds+}^{+}I_{qs+}^{+}\right) = -\frac{3}{2}\frac{P}{2}\frac{L_m}{L_s}\lambda_{ds+}^{+}I_{qr+}^{+} \tag{7.83}$$

Substituting the generator torque into the speed equation,

$$\begin{aligned}
p\omega_r &= \frac{P}{2J}\left(T_{e+} + T_{e-} - T_L\right) \\
p\omega_r &= \frac{P}{2J}\left(T_{e+} - \left(\frac{\lambda_{ds-}^{-}}{\lambda_{ds+}^{+}}\right)^2 T_{e+} - T_L\right) \\
p\omega_r &= \frac{P}{2J}\left(\eta T_{e+} - T_L\right) \\
p\omega_r &= -\frac{P}{2J}\left(\frac{3}{2}\frac{P}{2}\frac{L_m}{L_s}\eta\lambda_{ds+}^{+}I_{qr+}^{+} + T_L\right)
\end{aligned} \tag{7.84}$$

328

where T_L is the turbine mechanical torque and $\eta = 1 - \left(\dfrac{\lambda_{ds-}^-}{\lambda_{ds+}^+} \right)^2$.

The speed controller can be defined as:

$$p\omega_r = \sigma_{\omega r} = \left(k_{p\omega r} + \frac{k_{i\omega r}}{p} \right)\left(\omega_r^* - \omega_r \right)$$

$$p\omega_r = \sigma_\omega = \left(k_{p\omega r} + \frac{k_{i\omega r}}{p} \right)\omega_r^* - \left(k_{p\omega r} + \frac{k_{i\omega r}}{p} \right)\omega_r$$

$$\left(p + k_{p\omega r} + \frac{k_{i\omega r}}{p} \right)\omega_r = \left(k_{p\omega r} + \frac{k_{i\omega r}}{p} \right)\omega_r^*$$

(7.85)

$$\frac{\omega_r}{\omega_r^*} = \frac{p k_{p\omega r} + k_{i\omega r}}{p^2 + p k_{p\omega r} + k_{i\omega r}}$$

where $\sigma_{\omega r}$ is the output of the speed controller; $k_{p\omega r}$ and $k_{i\omega r}$ respectively are the proportional in integral gains of the PI controller. The PI controller gains, $k_{p\omega r}$ and $k_{i\omega r}$, are determined by comparing the denominator of the speed transfer function given by (7.86) to the Butterworth polynomial

$$p^2 + p k_{p\omega r} + k_{i\omega r} \equiv p^2 + \sqrt{2}\omega_{o\omega r}p + \omega_{o\omega r}^2$$

$$k_{p\omega r} = \sqrt{2}\omega_{o\omega r}, \quad k_{i\omega r} = \omega_{o\omega r}^2$$

(7.86)

Given that the switching frequency for all converters f_{sw} is 1 kHz, following from Chapter 3, the bandwidth frequency of the speed controller is chosen to be one hundred of the switching frequency [105]. That is:

$$\omega_{0\omega r} = \frac{\omega_{sw}}{100} \text{ where } \omega_{sw} = 2\pi f_{sw} = 6280 \text{ } rad/s.$$

From (7.86), the controller gains are:

$$k_{p\omega r} = \sqrt{2}\,\omega_{o\omega r} = \sqrt{2}(62.80) = 88.8126$$

$$k_{i\omega r} = \omega_{o\omega r}^2 = 62.8^2 = 3943.8$$

7.4.1.3.**Inner current control loops.** Under unbalanced grid voltage conditions, voltage, current and flux in the stationary reference frame fixed to the stator, contain ac quantities of both positive- and negative-sequence components at ω_e and $-\omega_e$ respectively. A resonant controller tuned at ω_e is capable of simultaneously regulating both the positive and negative sequence currents at ω_e and $-\omega_e$ in the stationary reference frame and providing zero steady-state error [101].

In this dissertation, a hybrid controller consisting of a proportional integral (PI) controller and a Resonant (Res) controller is used to achieve the above objective of simultaneous regulation of both positive and negative sequences variables. A general form of this hybrid controller here referred to as PI+Res controller is given as [89], [102], and [104]:

$$\text{PI} + \text{Res} = \left[k_p + \frac{k_i}{p} + \frac{pk_R}{p^2 + 2\omega_c p + (2\omega_e)^2} \right] \qquad (7.87)$$

where ω_c refers to the cut-off frequency introduced into the resonant controller to reduce its sensitivity against slight frequency variations at the resonant poles (5-15 rad/s is satisfactory in practice [102]).

From the rotor voltage equations in (7.59) and (7.60), the qd rotor current controllers can be defined as:

$$\sigma_{qr} = r_r I_{qr} + \sigma L_r p I_{qr} = \left[k_{pr} + \frac{k_{ir}}{p} + \frac{p k_{Rr}}{p^2 + 2\omega_{c1} p + (2\omega_e)^2} \right]\left(I_{qr}^* - I_{qr} \right) \tag{7.88}$$

$$\sigma_{dr} = r_r I_{dr} + \sigma L_r p I_{dr} = \left[k_{pr} + \frac{k_{ir}}{p} + \frac{p k_{Rr}}{p^2 + 2\omega_{c1} p + (2\omega_e)^2} \right]\left(I_{dr}^* - I_{dr} \right) \tag{7.89}$$

where σ_{qr} and σ_{dr} are the respectively the output of the q- and d-axis current controllers; k_{pr} and k_{ir} are respectively the proportional in integral gains of the PI controller and ω_{c1} is the corresponding cut-off frequency defined (7.87) for the current controller. The transfer functions of the actual to reference currents are:

$$\frac{I_{qr}}{I_{qr}^*} = \frac{I_{dr}}{I_{dr}^*} = \frac{k_{pr} + \dfrac{k_{ir}}{p} + \dfrac{p k_{Rr}}{p^2 + 2\omega_{c1} p + (2\omega_e)^2}}{r_r + \sigma L_r p + k_{pr} + \dfrac{k_{ir}}{p} + \dfrac{p k_{Rr}}{p^2 + 2\omega_{c1} p + (2\omega_e)^2}}$$

or

$$\frac{I_{qr}}{I_{qr}^*} = \frac{I_{dr}}{I_{dr}^*} = \frac{\left[\begin{array}{l} \left[p^3 + 2\omega_{c1} p^2 + (2\omega_e)^2 \right] p k_{pr} + \\ k_{ir}\left[p^3 + 2\omega_{c1} p^2 + (2\omega_e)^2 \right] + k_{Rr} p^2 \end{array} \right]}{\left[\begin{array}{l} \left[r_r + \sigma L_r p + k_{pr} \right]\left[p^3 + 2\omega_{c1} p^2 + (2\omega_e)^2 p \right] + \\ k_{ir}\left[p^2 + 2\omega_{c1} p + (2\omega_e)^2 \right] + k_{Rr} p^2 \end{array} \right]} \tag{7.90}$$

The denominator of this transfer function is a fourth order polynomial and the controller gains may be determined comparing this polynomial to the Butterworth polynomial. The fourth order Butterworth polynomial is given by

$$B(p) = \left(p^2 + 0.7654\omega_{n1}p + \omega_{n1}^2\right)\left(p^2 + 1.8478\omega_{n1}p + \omega_{n1}^2\right)$$

(7.91)

$$B(p) = p^4 + 2.6132\omega_{n1}p^3 + 3.4143\omega_{n1}^2p^2 + 2.6132\omega_{n1}^3p + \omega_{n1}^4$$

where ω_n is the controller bandwidth frequency.

Comparing the denominator of the transfer function (7.91) with the Butterworth fourth order polynomial (7.92), PI controller gains are:

$$D(p) = \begin{bmatrix} \sigma L_r p^4 + \left(r_r + k_{pr} + 2\omega_{c1}\sigma L_r\right)p^3 + \\ + \left[2\omega_{c1}\left(r_r + k_{pr}\right) + \left(2\omega_e\right)^2\sigma L_r + k_{ir} + k_{Rr}\right]p^2 \\ + \left[\left(2\omega_e\right)^2\left(r_r + k_{pr}\right) + 2\omega_{c1}k_{ir}\right]p + \left(2\omega_e\right)^2 k_{ir} \end{bmatrix}$$

(7.92)

$$\frac{r_r + k_{pr} + 2\omega_{c1}\sigma L_r}{\sigma L_r} = 2.6132\omega_{n1}$$

(7.93)

$$k_{pr} = 2.6132\omega_{n1}\sigma L_r - 2\omega_{c1}\sigma L_r - r_r$$

$$\frac{\left(2\omega_e\right)^2 k_{ir}}{\sigma L_r} = \omega_{n1}^4, \qquad \Rightarrow k_{ir} = \sigma L_r \frac{\omega_{n1}^4}{\left(2\omega_e\right)^2}$$

(7.94)

$$\frac{\left(2\omega_e\right)^2\left(r_r + k_{pr}\right) + 2\omega_{c1}k_{ir}}{\sigma L_r} = 2.6132\omega_{n1}^3$$

$$\left(2\omega_e\right)^2\left(r_r + k_{pr}\right) = 2.6132\omega_{n1}^3\sigma L_r - 2\omega_{c1}k_{ir}$$

(7.95)

$$\left(2\omega_e\right)^2\left(r_r + k_{pr}\right) = 2.6132\omega_{n1}^3\sigma L_r - 2\omega_{c1}\sigma L_r \frac{\omega_{n1}^4}{\left(2\omega_e\right)^2}$$

$$\left(2\omega_e\right)^2\left(r_r + k_{pr}\right) = 2.6132\omega_{n1}^3\left(2\omega_e\right)^2\sigma L_r - 2\omega_{c1}\sigma L_r\omega_{n1}^4$$

$$\frac{2\omega_{c1}(r_r + k_{pr}) + (2\omega_e)^2 \sigma L_r + k_{ir} + k_{Rr}}{\sigma L_r} = 3.4143\omega_{n1}^2$$

$$2\omega_{c1}(r_r + k_{pr}) + (2\omega_e)^2 \sigma L_r + k_{ir} + k_{Rr} = 3.4143\sigma L_r \omega_{n1}^2$$

$$k_{Rr} = 3.4143\sigma L_r \omega_{n1}^2 - 2\omega_{c1}(r_r + k_{pr}) - (2\omega_e)^2 \sigma L - k_{ir}$$

$$k_{Rr} = 3.4143\sigma L_r \omega_{n1}^2 - 2\omega_{c1}(2.6132\omega_{n1}\sigma L_r - 2\omega_{c1}\sigma L_r) - (2\omega_e)^2 \sigma L_r - \sigma L_r \frac{\omega_{n1}^4}{(2\omega_e)^2} \qquad (7.96)$$

$$k_{Rr} = \sigma L_r \left(3.4143\omega_{n1}^2 - (2\omega_{c1}2.6132\omega_{n1} - 2\omega_{c1}2\omega_{c1}) - (2\omega_e)^2 - \frac{\omega_{n1}^4}{(2\omega_e)^2} \right)$$

Using the 5 hp induction machine parameters and a switching frequency of 1 kHz, the band width frequency for the current loop is chosen to be one-tenth of the switching frequency. That is:

$\omega_{n1} = \frac{\omega_{sw}}{10} = 682.8 \text{ rad/s}$. In practice, ω_{c1} in the range of 5-15 rad/s is satisfactory [102]).

Thus using $\omega_{c1} = 5$ rad/s, the controller gains can be calculated using (7.93) – (7.96) and are shown in Table 7.22

Table 7.22. Rotor current controller gains

Controller gain		k_{pr}	k_{ir}	k_{Rr}
Rotor current	I_{qr}	4.86	872.84	1556.7
	I_{dr}	4.86	872.84	1556.7

7.4.2. Parallel Grid Side Converter Control [96]

The goal of the PGSC control is to regulate the dc link voltage in addition to regulating the reactive power injected into the grid from the rotor circuit. Under unbalanced voltage sag operating conditions, in addition to regulating the average dc link voltage and reactive power, the control strategy should minimize ripple in the dc-link voltage and harmonics in the filter currents.

7.4.2.1.DC-link controller. The DC-link dynamics is given by

$$C_{dc}pV_{dc} = \frac{3}{4}\left(M_{qse}I_{qse} + M_{dse}I_{dse} + M_{qsh}I_{qsh} + M_{dsh}I_{dsh}\right) - \frac{3}{4}I_{or} \tag{7.97}$$

In (7.97), if the term in the brackets is taken care of the the inner current control loop and the last term is taken as a disturbance, the DC-link voltage controller can be defined as:

$$C_{dc}pV_{dc} = \sigma_{V_{dc}} = \left(k_{pdc} + \frac{k_{idc}}{p}\right)\left(V_{dc}^* - V_{dc}^*\right) \tag{7.98}$$

The transfer function between the actual DC voltage and its reference is obtained as:

$$C_{dc}pV_{dc} = \sigma_{V_{dc}} = \left(k_{pdc} + \frac{k_{idc}}{p}\right)\left(V_{dc}^* - V_{dc}\right)$$

$$\left(C_{dc}p + k_{pdc} + \frac{k_{idc}}{p}\right)V_{dc} = \left(k_{pdc} + \frac{k_{idc}}{p}\right)V_{dc}^*$$

$$\frac{V_{dc}}{V_{dc}^*} = \frac{pk_{pdc} + k_{idc}}{C_{dc}p^2 + pk_{pdc} + k_{idc}}$$

$$\frac{V_{dc}}{V_{dc}^*} = \frac{\dfrac{1}{C_{dc}}\left(pk_{pdc} + k_{idc}\right)}{p^2 + \dfrac{1}{C_{dc}}pk_{pdc} + \dfrac{1}{C_{dc}}k_{idc}}$$

(7.99)

Comparing the denominator of (7.99) to a second order Butterworth polynomial, the controller gains are given by:

$$k_{pdc} = \sqrt{2}\omega_{odc}C_{dc} \text{ and } k_{idc} = \omega_{odc}^2 C_{dc}.$$

7.4.2.2.**PGSC power outer loop control.** To achieve of objective of regulating the reactive power and cancelling its ripples, four constrains must be satisfied [97]. These constraints are represented by a set of four linear equations in Positive and Negative Synchronous Reference Frames (PNSRF). That is:

$$P_{sh0} = \frac{3}{2}\text{Re}\left[V_{qdg+}I'_{qdg+} + V_{qdg-}I'_{qdg-}\right]$$

(7.100)

$$Q_{sh0} = \frac{3}{2}\text{Im}\left[V_{qdg+}I'_{qdg+} + V_{qdg-}I'_{qdg-}\right]$$

(7.101)

$$P_{c2} = 0 = \frac{3}{2}\text{Re}\left[V_{qdg+}I'_{qdg-}e^{j2\omega_e t} + V_{qdg-}e^{-j2\omega_e t}I'_{qdg+}\right]$$

(7.102)

$$P_{s2} = 0 = \frac{3}{2}\text{Im}\left[V_{qdg+}I'_{qdg-}e^{j2\omega_e t} + V_{qdg-}e^{-j2\omega_e t}I'_{qdg+}\right]$$

(7.103)

Where P_{sh0} and Q_{sh0} are the average components of the active and reactive powers injected into the grid from the parallel grid side converter; P_{c2} and P_{s2} are the ripple components of the active and reactive powers at the output terminals of the parallel grid side converter.

Equations (7.98) and (7.99) are related with the average active and reactive power regulation and (7.100) and (7.101) are used to nullify the oscillating components of the instantaneous active power at the output of the PGSC and regulate the dc link ripple to zero. Proposed control strategy of PGSC. The control is implemented in the stationary reference frame which has been demonstrated in [96] to be a much simpler control scheme than the ones implemented in PNSRF. The four constraint equations (7.100) – (7.103) are transformed into the stationary reference frame.

$$P_{sh0} = \frac{3}{2}(V^+_{\alpha sh+}I^+_{\alpha sh+} + V^+_{\beta sh+}I^+_{\beta sh+} + V^-_{\alpha sh-}I^-_{\alpha sh-} + V^-_{\beta sh-}I^-_{\beta sh-}) \tag{7.104}$$

$$Q_{sh0} = \frac{3}{2}(V^+_{\beta sh+}I^+_{\alpha sh+} - V^+_{\alpha sh+}I^+_{\beta sh+} + V^-_{\beta sh-}I^-_{\alpha sh-} - V^-_{\alpha sh-}I^-_{\beta sh-}) \tag{7.105}$$

$$P_{c2} = \frac{3}{2}\left[\begin{array}{l} (\cos^2 \omega t - \sin^2 \omega t)(V^-_{\alpha sh-}I^+_{\alpha sh+} + V^-_{\beta sh-}I^+_{\beta sh+} + V^+_{\alpha sh+}I^-_{\alpha sh-} + V^+_{\beta sh+}I^-_{\beta sh-}) \\ -(2\sin \omega t \cos \omega t)(V^-_{\beta sh-}I^+_{\alpha sh+} - V^-_{\alpha sh-}I^+_{\beta sh+} - V^+_{\beta sh+}I^-_{\alpha sh-} + V^+_{\alpha sh+}I^-_{\beta sh-}) \end{array} \right] = 0 \tag{7.106}$$

$$P_{s2} = \frac{3}{2}\left[\begin{array}{l} (\cos^2 \omega t - \sin^2 \omega t)(V^-_{\beta sh-}I^+_{\alpha sh+} - V^-_{\alpha sh-}I^+_{\beta sh+} - V^+_{\beta sh+}I^-_{\alpha sh-} + V^+_{\alpha sh+}I^-_{\beta sh-}) \\ +(2\sin \omega t \cos \omega t)(V^-_{\alpha sh-}I^+_{\alpha sh+} + V^-_{\beta sh-}I^+_{\beta sh+} + V^+_{\alpha sh+}I^-_{\alpha sh-} + V^+_{\beta sh+}I^-_{\beta sh-}) \end{array} \right] = 0 \tag{7.107}$$

To eliminate the oscillating components of the active power P_{c2} and P_{s2} must be zero. That is:

$$V^-_{\alpha sh-}I^+_{\alpha sh+} + V^-_{\beta sh-}I^+_{\beta sh+} + V^+_{\alpha sh+}I^-_{\alpha sh-} + V^+_{\beta sh+}I^-_{\beta sh-} = 0 \tag{7.108}$$

$$V^-_{\beta sh-}I^+_{\alpha sh+} - V^-_{\alpha sh-}I^+_{\beta sh+} - V^+_{\beta sh+}I^-_{\alpha sh-} + V^+_{\alpha sh+}I^-_{\beta sh-} = 0 \tag{7.109}$$

The current references can then be calculated as follows:

$$\frac{2}{3}\begin{bmatrix} P_{sh0} \\ Q_{sh0} \\ P_{c2} \\ P_{s2} \end{bmatrix} = \begin{bmatrix} V^+_{\alpha g+} & V^+_{\beta g+} & V^-_{\alpha g-} & V^-_{\beta g-} \\ V^+_{\beta g+} & -V^+_{\alpha g+} & -V^-_{\beta g-} & V^-_{\alpha g-} \\ V^-_{\alpha sh-} & V^-_{\beta sh-} & V^+_{\alpha sh+} & V^+_{\beta sh+} \\ V^-_{\beta sh-} & -V^-_{\alpha sh-} & -V^+_{\beta sh+} & V^+_{\alpha sh+} \end{bmatrix}\begin{bmatrix} I^+_{\alpha sh+} \\ I^+_{\beta sh+} \\ I^-_{\alpha sh-} \\ I^-_{\beta sh-} \end{bmatrix} \tag{7.110}$$

$$\begin{bmatrix} I^+_{\alpha sh+} \\ I^+_{\beta sh+} \\ I^-_{\alpha sh-} \\ I^-_{\beta sh-} \end{bmatrix} = \frac{2}{3} \cdot \begin{bmatrix} V^+_{\alpha g+} & V^+_{\beta g+} & V^-_{\alpha g-} & V^-_{\beta g-} \\ V^+_{\beta g+} & -V^+_{\alpha g+} & -V^-_{\beta g-} & V^-_{\alpha g-} \\ V^-_{\alpha sh-} & V^-_{\beta sh-} & V^+_{\alpha sh+} & V^+_{\beta sh+} \\ V^-_{\beta sh-} & -V^-_{\alpha sh-} & -V^+_{\beta sh+} & V^+_{\alpha sh+} \end{bmatrix}^{-1}\begin{bmatrix} P_{sh0} \\ Q_{sh0} \\ P_{c2} \\ P_{s2} \end{bmatrix} \tag{7.111}$$

$$\bar{I}^*_{\alpha\beta sh} = \bar{I}^{+*}_{\alpha\beta sh} + \bar{I}^{-*}_{\alpha\beta sh} \tag{7.112}$$

$$I^*_{\alpha sh} = I^{+*}_{\alpha sh+} + I^{-*}_{\alpha sh-} = \frac{\left[k_1 + k_3 + (k_2 - k_4)k_{pf}\right]2P_{sh0}}{3den} \tag{7.113}$$

$$I^*_{\beta sh} = I^{+*}_{\beta sh+} + I^{-*}_{\beta sh-} = \frac{\left[k_2 + k_4 + (k_3 - k_1)k_{pf}\right]2P_{sh0}}{3den} \tag{7.114}$$

where the superscript "*" means reference values, and

$$k_1 = V^+_{\alpha g+}\left(V^{+2}_{\alpha sh+} + V^{+2}_{\beta sh+}\right) + V^-_{\alpha g-}\left(V^+_{\beta sh+}V^-_{\beta sh-} - V^+_{\alpha sh+}V^-_{\alpha sh-}\right) - V^-_{\beta g-}\left(V^+_{\alpha sh+}V^-_{\beta sh-} + V^+_{\beta sh+}V^-_{\alpha sh-}\right) \tag{7.115}$$

$$k_2 = V^+_{\beta g+}\left(V^{+2}_{\alpha sh+} + V^{+2}_{\beta sh+}\right) - V^-_{\alpha g-}\left(V^+_{\alpha sh+}V^-_{\beta sh-} + V^+_{\beta sh+}V^-_{\alpha sh-}\right) + V^-_{\beta g-}\left(V^+_{\alpha sh+}V^-_{\alpha sh-} - V^+_{\beta sh+}V^-_{\beta sh-}\right) \tag{7.116}$$

$$k_3 = V_{\alpha g-}^{-}\left(V_{\alpha sh-}^{-2} + V_{\beta sh-}^{-2}\right) - V_{\alpha g+}^{+}\left(V_{\alpha sh+}^{+}V_{\alpha sh-}^{-} - V_{\beta sh+}^{+}V_{\beta sh-}^{-}\right) - V_{\beta g+}^{+}\left(V_{\alpha sh+}^{+}V_{\beta sh-}^{-} + V_{\beta sh+}^{+}V_{\alpha sh-}^{-}\right)$$ (7.117)

$$k_4 = V_{\beta g-}^{-}\left(V_{\alpha sh-}^{n2} + V_{\beta sh-}^{n2}\right) - V_{\alpha g+}^{+}\left(V_{\alpha sh+}^{+}V_{\beta sh-}^{-} + V_{\beta sh+}^{+}V_{\alpha sh-}^{-}\right) - V_{\beta g+}^{+}\left(V_{\beta sh+}^{+}V_{\beta sh-}^{-} - V_{\alpha sh+}^{+}V_{\alpha sh-}^{-}\right)$$ (7.118)

$$den = k_1 V_{\alpha g+}^{+} + k_2 V_{\beta g+}^{+} + k_3 V_{\alpha g-}^{-} + k_4 V_{\beta g-}^{-}$$ (7.119)

7.4.2.3.**Inner current loop.** The control is strategy is to minimize ripple in the dc-link voltage and harmonics in the filter currents. From (7.14) and (7.15), the output of the PGSC current contollers can be defined as:

$$\sigma_{qsh} = r_{sh}I_{qsh} + L_{sh}pI_{qsh}$$ (7.120)

$$\sigma_{qsh} = r_{sh}I_{qsh} + L_{sh}pI_{qsh}$$ (7.121)

Observe that (7.100) and (7.101) are equivalent to the RSC current controller outputs given respectively, in (7.88) and (7.89). Thus, the controller is designed similarly with the following substitutions:

$$r_r \rightarrow r_{sh}, \quad \sigma L_r \rightarrow L_{sh},$$

$$I_{qr} \rightarrow I_{qsh}, \quad \text{and} \quad I_{dr} \rightarrow I_{dsh}.$$

The bandwidth chosen is same as in the RSC current controller. That is:

$\omega_{n1} = 682.8\,\text{rad/s}$ and $\omega_{c1} = 5\,\text{rad/s}$. The controller gains can be calculated using (7.93) – (7.96) and are shown in Table 7.23

Table 7.23. PGSC current and DC-link controller gains

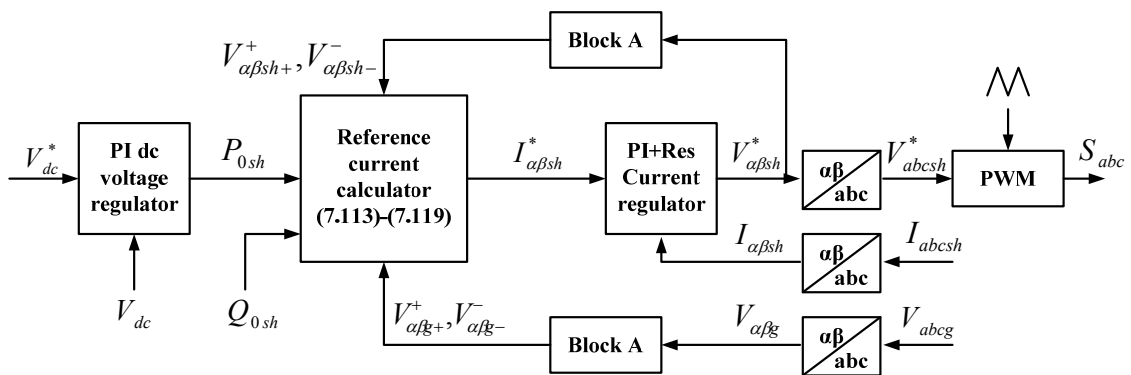| Controller gain		k_{psh}	k_{ish}	k_{Rsh}
Rotor current	I_{qsh}	15.9635	2741.6	4889.5
	I_{dsh}	15.9635	2741.6	4889.5
DC-link	V_{dc}	0.1	0.0001	N/A

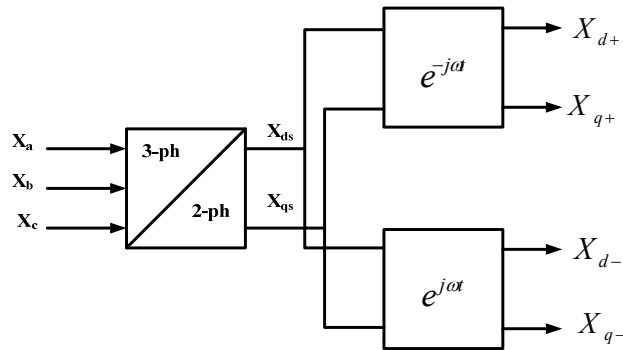Figure 7.21.   Block diagram of the proposed PGSC control scheme

Figure 7.22.   Block diagram of tranformation Block A in Figure 7.21 for sequential component extraction

The block diagram of the proposed control scheme is shown in Figure 7.21. It consists of the DC-link PI voltage regulator, reference current calculator, the PI+Res regulator and reference frame transformation blocks. The positive and negative sequence components of the converter voltages and grid voltages are obtained using the positive/negative sequence component extraction control block (block A) [98]. Block A as shown in Figure 7.22 involve two transformations; abc to stationary reference frame and to positive and negative synchronous reference frames. That is:

$$X_{ds} = \frac{1}{3}\left(2X_a - X_b - X_c\right), \quad X_{qs} = \frac{1}{\sqrt{3}}\left(X_b - X_c\right)$$

$$X_{d+} = X_{ds}\cos\theta_e - X_{qs}\sin\theta_e, \quad X_{q+} = X_{ds}\cos\theta_e + X_{qs}\sin\theta_e$$

$$X_{d-} = X_{ds}\cos\theta_e + X_{qs}\sin\theta_e, \quad X_{q-} = X_{ds}\cos\theta_e - X_{qs}\sin\theta_e$$

7.4.3. Series Grid Side Converter Control

There are two (2) main solutions found in literature namely stator flux control and SGSC voltage control. As the names suggest, the former uses the stator flux as the main control target whereas the latter targets the required series injection voltage required to compensate for the 'missing' grid voltage in the event of voltage sag. The description of the two control schemes are outlined below.

7.4.3.1. **Stator flux control[13].** The SGSC remains dormant during normal conditions to eliminate switching losses. When a sag event is detected, the SGSC engages and controls the total stator flux. The SGSC transitions from the dormant state to stator

340

flux control when the imbalance in the relationship between the stator flux and rotor EMF. Under normal grid voltage, $V_{qdi} = 0$ and $p\lambda_{qds} = 0$ at steady state and

$$\left| V_{qds} - r_s I_{qds} + j\omega_e \lambda_{qds} \right| = 0 \tag{7.122}$$

During a sag event, this equilibrium is disturbed as a nonzero flux derivative is produced. This forms the basis for detecting a sag event. That is

$$\left| V_{qds} - r_s I_{qds} + j\omega_e \lambda_{qds} \right| \geq \chi \pm \delta \tag{7.123}$$

where $\chi \pm \delta$ is a hysteretic threshold for engagement of the SGSC.

The objectives during a sag is to null where present, any negative sequence stator flux as well as the minimizing the effects of the dc flux. The positive sequence flux is also scaled in proportion to the remaining grid voltage. Thus the reference commands are given as:

$$\lambda_{qds}^{*+} = \frac{\lambda_{qds}}{j\omega_e}, \qquad \lambda_{qds}^{*-} = 0, \qquad \lambda_{sDC}^* = 0 \tag{7.124}$$

where λ_{sDC}^* is the reference DC component of the stator flux.

Flux controller (in stationary frame) is modeled from the stator voltage equations:

$$p\lambda_{qs} = \sigma_{\lambda q} = V_{qg} - V_{qi} - r_s I_{qs} \tag{7.125}$$

$$p\lambda_{ds} = \sigma_{\lambda d} = V_{dg} - V_{di} - r_s I_{ds} \tag{7.126}$$

Equations (7.125) and (7.126) can be rewritten in complex form as:

$$p\lambda_{qds} = \sigma_{\lambda qd} = V_{qdg} - V_{qdi} - r_s I_{qds}$$

where $\quad \lambda_{qds} = \lambda_{qs} + j\lambda_{ds}$, $\quad V_{qdg} = V_{qg} + jV_{dg}$, $\quad V_{qdi} = V_{qi} + jV_{di}$, $I_{qds} = I_{qs} + jI_{ds}$ and

$\sigma_{\lambda qd} = \sigma_{\lambda q} + j\sigma_{\lambda d}$.

Using a PI+RES controller tuned at flux frequency, it is possible to simultaneously regulate both the positive and negative sequence fluxes and providing a zero steady-state error. From (7.125) and (7.126), the controller can be modeled as:

$$p\lambda_{qs} = \sigma_{\lambda q} = \left[\begin{array}{c} k_{p\lambda q} + \dfrac{k_{i\lambda q}}{p} + \\ \dfrac{pk_{R\lambda q}}{p^2 + 2\omega_{c2}p + (2\omega_e)^2} \end{array} \right] \left(\lambda_{qs}^* - \lambda_{qs} \right) = V_{qg} - V_{qi} - r_s I_{qs} \qquad (7.127)$$

$$p\lambda_{ds} = \sigma_{\lambda d} = \left[\begin{array}{c} k_{p\lambda d} + \dfrac{k_{i\lambda d}}{p} + \\ \dfrac{pk_{R\lambda d}}{p^2 + 2\omega_{c2}p + (2\omega_e)^2} \end{array} \right] \left(\lambda_{ds}^* - \lambda_{ds} \right) = V_{qg} - V_{qi} - r_s I_{qs} \qquad (7.128)$$

The controller block diagram is shown in Figure 7.23. The flux controller gains can be found by finding the transfer function between the flux and its reference:
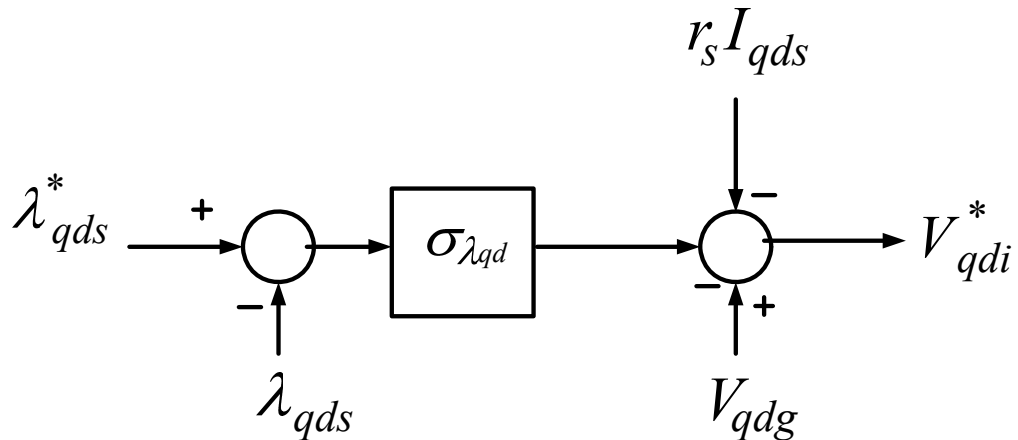

Figure 7.23.   Stator flux PI+Res controller

$$\frac{\lambda_{qs}}{\lambda_{qs}^*} = \frac{k_{p\lambda_q}p\left[p^2 + 2\omega_{c2}p + (2\omega_e)^2\right] + k_{i\lambda_q}\left[p^2 + 2\omega_{c2}p + (2\omega_e)^2\right] + p^2 k_{R\lambda_q}}{\left(p + k_{p\lambda_q}\right)p\left[p^2 + 2\omega_{c2}p + (2\omega_e)^2\right] + k_{i\lambda_q}\left[p^2 + 2\omega_{c2}p + (2\omega_e)^2\right] + p^2 k_{R\lambda_q}} \quad (7.129)$$

$$\frac{\lambda_{ds}}{\lambda_{ds}^*} = \frac{k_{p\lambda_d}p\left[p^2 + 2\omega_{c2}p + (2\omega_e)^2\right] + k_{i\lambda_d}\left[p^2 + 2\omega_{c2}p + (2\omega_e)^2\right] + p^2 k_{R\lambda_d}}{\left(p + k_{p\lambda_d}\right)p\left[p^2 + 2\omega_{c2}p + (2\omega_e)^2\right] + k_{i\lambda_d}\left[p^2 + 2\omega_{c2}p + (2\omega_e)^2\right] + p^2 k_{R\lambda_d}} \quad (7.130)$$

The denominator of the stator flux transfer function is of fourth order. Comparing the coefficients to a fourth order Butterworth polynomial, the controller gains are found as follows:

$$D(p) = \begin{bmatrix} p^4 + (k_{p\lambda} + 2\omega_{c2})p^3 + \\ + \left[(2\omega_e)^2 + 2\omega_{c2}k_{p\lambda} + k_{i\lambda} + k_{R\lambda}\right]p^2 + \\ + \left[(2\omega_e)^2 k_{p\lambda} + 2\omega_{c2}k_{i\lambda}\right]p + (2\omega_e)^2 k_{i\lambda} \end{bmatrix} \quad (7.131)$$

$$D(p) = \begin{bmatrix} \left(p + k_{p\lambda}\right)\left[p^3 + 2\omega_{c2}p^2 + (2\omega_e)^2 p\right] + \\ k_{i\lambda}\left[p^2 + 2\omega_{c2}p + (2\omega_e)^2\right] + p^2 k_{R\lambda} \end{bmatrix}$$

$$D(p) = \begin{bmatrix} p^4 + (k_{p\lambda} + 2\omega_{c2})p^3 + \\ + \left[(2\omega_e)^2 + 2\omega_{c2}k_{p\lambda} + k_{i\lambda} + k_{R\lambda}\right]p^2 + \\ + \left[(2\omega_e)^2 k_{p\lambda} + 2\omega_{c2}k_{i\lambda}\right]p + (2\omega_e)^2 k_{i\lambda} \end{bmatrix} \quad (7.132)$$

$$B(p) = p^4 + 2.6132\omega_{n2}p^3 + 3.4143\omega_{n2}^2 p^2 + 2.6132\omega_{n2}^3 p + \omega_{n2}^4$$

$$\left(k_{p\lambda} + 2\omega_{c2}\right) = 2.6132\omega_{n2} \Rightarrow k_{p\lambda} = 2.6132\omega_{n2} - 2\omega_{c2}$$

$$\left[\left(2\omega_e\right)^2 + 2\omega_{c2}k_{p\lambda} + k_{i\lambda} + k_{R\lambda}\right] = 3.4143\omega_{n2}^2$$

$$\Rightarrow k_{R\lambda} = 3.4143\omega_{n2}^2 - \left(2\omega_e\right)^2 - 2\omega_{c2}k_{p\lambda} - k_{i\lambda}$$

$$\left[\left(2\omega_e\right)^2 k_{p\lambda} + 2\omega_{c2}k_{i\lambda}\right] = 2.6132\omega_{n2}^3 \tag{7.133}$$

$$\Rightarrow \left(2\omega_e\right)^2 = \frac{1}{k_{p\lambda}}\left[2.6132\omega_{n2}^3 - 2\omega_{c2}k_{i\lambda}\right]$$

$$\left(2\omega_e\right)^2 k_{i\lambda} = \omega_{n2}^4 \Rightarrow k_{i\lambda} = \frac{\omega_{n2}^4}{\left(2\omega_e\right)^2}$$

Using the 5 hp induction machine parameters and a switching frequency of 1 kHz, the bandwidth frequency for the stator flux controller is chosen to be one-fifth bandwidth of the rotor current controller bandwidth. That is:

$\omega_{n2} = \omega_{n1} = 682.8\,\text{rad/s}$ and $\omega_{c1} = \omega_{c2} = 5\,\text{rad/s}$ is chosen. The controller gains are given in Table 7.24.

Table 7.24. Stator flux controller gains

Controller gain		$k_{p\lambda}$	$k_{i\lambda}$	$k_{R\lambda}$
Stator flux	λ_{qs}	672.0948	274160	488830
	λ_{ds}	672.0948	274160	488830

7.4.3.2.**Voltage control solution.** The effectiveness of this solution depends on how quickly a sag event is detected. In this dissertation the detection method uses the *rms* of the error vector. This algorithm is able to detect both symmetrical and asymmetrical sags as well as any associated phase jumps.

$$\left|V_{qd,error}\right| = \sqrt{\left(V_{qg} - V_{qg,ref}\right)^2 + \left(V_{dg} - V_{dg,ref}\right)^2} \geq V_{threshold} \tag{7.134}$$

The dynamic equations of series grid side in stationary reference frame is given by

$$V_{qi} = n_2\left(r_{se}I_{qse} + L_{se}pI_{qse} + V_{qse}\right) \tag{7.135}$$

$$V_{di} = n_2\left(r_{se}I_{dse} + L_{se}pI_{dse} + V_{dse}\right) \tag{7.136}$$

$$C_{se}pV_{qi} = n_2 I_{qs} - I_{qse} \tag{7.137}$$

$$C_{se}pV_{di} = n_2 I_{ds} - I_{dse} \tag{7.138}$$

Equations (7.135) to (7.138) can be used to model cassacaded voltage and current controllers. From (7.135) and (7.136), the current controller is modeled as follows:

$$L_{se}pI_{qse} + r_{se}I_{qse} = \sigma_{I_{qse}} = \left[\begin{array}{c} k_{pse} + \dfrac{k_{ise}}{p} + \\ \dfrac{pk_{Rse}}{p^2 + 2\omega_{c3}p + \left(2\omega_e\right)^2} \end{array}\right]\left(I_{qse}^* - I_{qse}\right) = \frac{1}{n_2}\left(V_{qi} - V_{qse}\right)$$

$$L_{se}pI_{dse} + r_{se}I_{dse} = \sigma_{I_{dse}} = \left[\begin{array}{c} k_{pse} + \dfrac{k_{ise}}{p} + \\ \dfrac{pk_{Rse}}{p^2 + 2\omega_{c3}p + \left(2\omega_e\right)^2} \end{array}\right]\left(I_{qse}^* - I_{qse}\right) = \frac{1}{n_2}\left(V_{di} - V_{dse}\right)$$

In its complex form, (7.139) and (7.140) is given by

$$L_{se} p I_{qdse} + r_{se} I_{qdse} = \sigma_{I_{qdse}} = \left[\frac{k_{pse} + \dfrac{k_{ise}}{p} +}{p^2 + 2\omega_{c3} p + (2\omega_e)^2} \right] \left(I_{qdse}^* - I_{qdse} \right) = \frac{1}{n_2} \left(V_{qdi} - V_{qdse} \right)$$

$$\frac{I_{qdse}}{I_{qdse}^*} = \frac{\left[k_{pse} + \dfrac{k_{ise}}{p} + \dfrac{pk_{Rse}}{p^2 + 2\omega_{c3} p + (2\omega_e)^2} \right]}{\left[L_{se} p + r_{se} + k_{pse} + \dfrac{k_{ise}}{p} + \dfrac{pk_{Rse}}{p^2 + 2\omega_{c3} p + (2\omega_e)^2} \right]}$$

$$\frac{I_{qdse}}{I_{qdse}^*} = \frac{\left[k_{pse} + \dfrac{k_{ise}}{p} + \dfrac{pk_{Rse}}{p^2 + 2\omega_{c3} p + (2\omega_e)^2} \right]}{\left[L_{se} p + r_{se} + k_{pse} + \dfrac{k_{ise}}{p} + \dfrac{pk_{Rse}}{p^2 + 2\omega_{c3} p + (2\omega_e)^2} \right]}$$

$$\frac{I_{qdse}}{I_{qdse}^*} = \frac{\left[p^3 + 2\omega_{c3} p^2 + (2\omega_e)^2 p \right] k_{pse} + k_{ise} \left[p^2 + 2\omega_{c3} p + (2\omega_e)^2 \right] + p^2 k_{Rse}}{\begin{array}{l} L_{se} \left[p^4 + 2\omega_{c3} p^3 + (2\omega_e)^2 p^2 \right] + \left(r_{se} + k_{pse} \right) \left[p^3 + 2\omega_{c3} p^2 + (2\omega_e)^2 p \right] + \\ k_{ise} \left[p^2 + 2\omega_{c3} p + (2\omega_e)^2 \right] + p^2 k_{Rse} \end{array}}$$

The denominator of the transfer function $\dfrac{I_{qdse}}{I_{qdse}^*}$ is simplified to

$$D(p) = \left[\begin{array}{l} p^4 + \left(2\omega_{c3} + \dfrac{r_{se} + k_{pse}}{L_{se}} \right) p^3 + \left[(2\omega_e)^2 + 2\omega_{c3} \dfrac{r_{se} + k_{pse}}{L_{se}} + \dfrac{k_{ise}}{L_{se}} + \dfrac{k_{Rse}}{L_{se}} \right] p^2 \\ + \left[(2\omega_e)^2 \dfrac{r_{se} + k_{pse}}{L_{se}} + 2\omega_{c3} \dfrac{k_{ise}}{L_{se}} \right] p + (2\omega_e)^2 \dfrac{k_{ise}}{L_{se}} \end{array} \right]$$

Comparing $D(p)$ with a 4th order Butterworth polynomial, the controller gains are given by

$$B(p) = p^4 + 2.6132\omega_{n3}p^3 + 3.4143\omega_{n3}^2p^2 + 2.6132\omega_{n3}^3p + \omega_{n3}^4$$

$$2\omega_{c3} + \frac{r_{se} + k_{pse}}{L_{se}} = 2.6132\omega_{n3}$$

$$\Rightarrow k_{pse} = L_{se}(2.6132\omega_{n3} - 2\omega_{c3}) - r_{se}$$

$$(2\omega_e)^2 + 2\omega_{c3}\frac{r_{se} + k_{pse}}{L_{se}} + \frac{k_{ise}}{L_{se}} + \frac{k_{Rse}}{L_{se}} = 3.4143\omega_{n3}^2$$

$$k_{Rse} = 3.4143\omega_{n3}^2 - \left[(2\omega_e)^2 L_{se} + 2\omega_{c3}(r_{se} + k_{pse}) + k_{ise}\right]$$

$$(2\omega_e)^2\frac{r_{se} + k_{pse}}{L_{se}} + 2\omega_{c3}\frac{k_{ise}}{L_{se}} = 2.6132\omega_{n3}^3$$

$$(2\omega_e)^2 = 2.6132\omega_{n3}^3\frac{L_{se}}{r_{se} + k_{pse}} - 2\omega_{c3}\frac{k_{ise}}{r_{se} + k_{pse}}$$

$$k_{ise} = \omega_{n3}^4(2\omega_e)^2 L_{se}$$

Similarly, from (7.137) and (7.138), the voltage controller is modeled as follows:

$$C_{se}pV_{qi} = \sigma_{vqi} = \left[\begin{array}{c} k_{pvi} + \dfrac{k_{ivi}}{p} + \\ \dfrac{pk_{Rvi}}{p^2 + 2\omega_{c4}p + (2\omega_e)^2} \end{array}\right](V_{qi}^* - V_{qi}) = \frac{n_2}{C_{se}}I_{qs} - I_{qse} \tag{7.139}$$

$$C_{se}pV_{di} = \sigma_{vdi} = \left[\begin{array}{c} k_{pvi} + \dfrac{k_{ivi}}{p} + \\ \dfrac{pk_{Rvi}}{p^2 + 2\omega_{c4}p + (2\omega_e)^2} \end{array}\right](V_{di}^* - V_{di}) = \frac{n_2}{C_{se}}I_{ds} - I_{dse} \tag{7.140}$$

In its complex form, (7.139) and (7.140) is given by

$$C_{se}pV_{qdi} = \sigma_{vqdi} = \left[\frac{k_{pvi} + \dfrac{k_{ivi}}{p} +}{\dfrac{pk_{Rvi}}{p^2 + 2\omega_{c4}p + (2\omega_e)^2}}\right](V_{qdi}^* - V_{qdi}) = \frac{n_2}{C_{se}}I_{qds} - I_{qdse}$$

The block diagram of the SGSC voltage controller is shown in Figure 7.24. The voltage controller gains are obtained from the voltage transfer function as follows:

$$\frac{V_{qi}}{V_{qi}^*} = \frac{\dfrac{1}{C_{se}}k_{pvi}p\left[p^2 + 2\omega_{c4}p + (2\omega_e)^2\right] + \dfrac{1}{C_{se}}k_{ivi}\left[p^2 + 2\omega_{c4}p + (2\omega_e)^2\right] + \dfrac{1}{C_{se}}p^2 k_{Rvi}}{\left[\begin{array}{l}p^4 + \dfrac{1}{C_{se}}(2\omega_{c4}C_{se} + k_{pvi})p^3 + \dfrac{1}{C_{se}}\left[(2\omega_e)^2 C_{se} + 2\omega_{c4}k_{pvi} + k_{ivi} + k_{Rvi}\right]p^2 \\ + \dfrac{1}{C_{se}}\left[(2\omega_e)^2 k_{pvi} + 2\omega_{c4}k_{ivi}\right]p + \dfrac{1}{C_{se}}(2\omega_e)^2 k_{ivi}\end{array}\right]} \tag{7.141}$$

$$D(p)\left[\begin{array}{l}p^4 + \dfrac{1}{C_{se}}(2\omega_{c4}C_{se} + k_{pvi})p^3 + \dfrac{1}{C_{se}}\left[(2\omega_e)^2 C_{se} + 2\omega_{c4}k_{pvi} + k_{ivi} + k_{Rvi}\right]p^2 \\ + \dfrac{1}{C_{se}}\left[(2\omega_e)^2 k_{pvi} + 2\omega_{c4}k_{ivi}\right]p + \dfrac{1}{C_{se}}(2\omega_e)^2 k_{ivi}\end{array}\right] \tag{7.142}$$

$$\frac{1}{C_{se}}(2\omega_{c4}C_{se} + k_{pvi}) = 2.6132\omega_{n4} \Rightarrow k_{pvi} = 2.6132\omega_{n4}C_{se} - 2\omega_{c4}C_{se}$$

$$\frac{1}{C_{se}}\left((2\omega_e)^2 C_{se} + 2\omega_{c4}k_{pvi} + k_{ivi} + k_{Rvi}\right) = 3.4143\omega_{n4}^2$$

$$\frac{1}{C_{se}}\left(\left(2\omega_e\right)^2 k_{pvi} + 2\omega_{c4}k_{ivi}\right) = 2.6132\omega_{n4}^3$$

$$\Rightarrow \left(2\omega_e\right)^2 = \frac{1}{k_{pvi}}\left(2.6132\omega_{n4}^3 C_{se} - 2\omega_{c4}k_{ivi}\right) \tag{7.143}$$

$$\frac{1}{C_{se}}\left(2\omega_e\right)^2 k_{iv} = \omega_{n4}^4 \Rightarrow k_{iv} = \frac{\omega_{n4}^4 C_{se}}{\left(2\omega_e\right)^2}$$

The controller gains are designed with bandwith of the current and voltage loops of

$\omega_{n3} = \omega_{n1} = 682.8\,\text{rad/s}$, $\omega_{n3} = \frac{1}{10}\omega_{n3}$ respectively and $\omega_{c3} = \omega_{c4} = 5\,\text{rad/s}$.
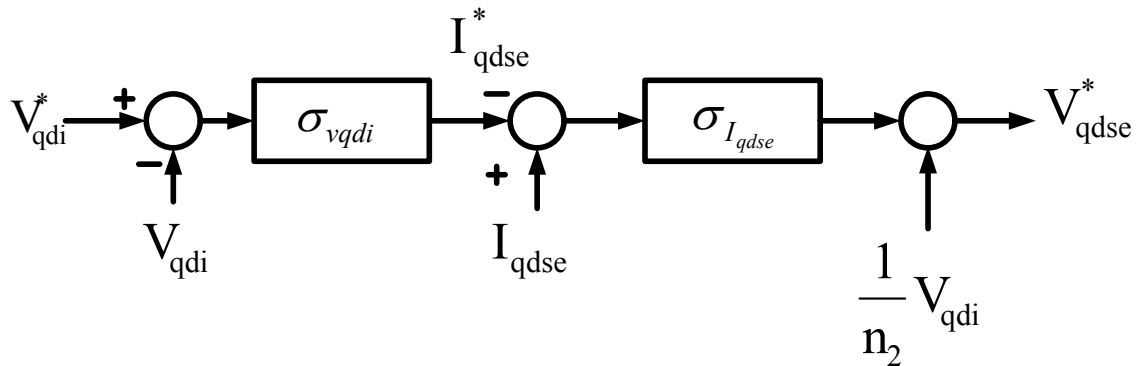
Figure 7.24.   Block diagram of SGSC voltage controller

Table 7.25. SGSC voltage controller gains

Controller gain		k_{pvse}	k_{ivse}	k_{Rvse}
SGSC current	I_{qse}	6.4209	2741.6	4985.5
	I_{dse}	6.4209	2741.6	4985.5
Controller gain		k_{pvi}	k_{ivi}	k_{Rvi}
SGSC voltage	V_{qi}	0.6013	0.1069	2170.7
	V_{di}	0.6013	0.1069	2170.7

7.5 System Simulation

To demonstrate the effectiveness of the proposed LVRT solution, Matlab/Simulink simulations of a 5hp DFIG wind turbine system with a Nine-switch converter as shown in Figure 7.3 were performed. The parameters of the proposed system are given in Appendix. In the simulations, the system performance is compared in the following situations:

  i.   Three-phase symmetrical voltage sag

 ii.   Two-phase voltage sag

iii.   One-phase to ground voltage sag

These sag events are simulated for 50% and 80% sags for 150 ms (between 2 to 2.15 seconds). The series injection command in these simulations was delayed for about ¼ of a cycle to mimic the practical implementation of the sag detection method. These simulation results are presented in Figures 7.25 – 7.31. In Figure 7.25, the series injection command is disabled to show the effect of 50% grid sag without the series compensation.

Observe that the stator and rotor currents during the sag more than quadruple compared to the pre-sag values. The currents increases are even worst at the inception of the sag. This is a very important observation especially for the power rating of SGSC. The dc-link voltage also fluctuates widely at the onset of the sag and at the point of sag clearance. To reduce the dc link capacitor rating as well as the SGSC, and injection transformer, the stator voltage need not be 100 percent compensated during the entire

period of the sag. This has been demonstrated decaying exponential series injection voltage [36] or ramp function injection method [31].

In Figures 7.26 – 7.31, the series voltage compensation actuator is enabled and as soon as the sag detection schemes detect that the stator voltage falls below 90% of its set value. In the simulations, the missing stator voltage is then supplied by the series injection. Notice that, the rotor currents and the dc link voltage now only vary slightly at the onset of the sag. The slight fluctuation is due to the fact the simulation has been done to mimic a practical implementation of the sag detection algorithm that has a time delay of approximately one-quarter of a cycle. The stator active and reactive powers also fluctuate slightly at the beginning of the sag but smoothen out before the end of the sag.
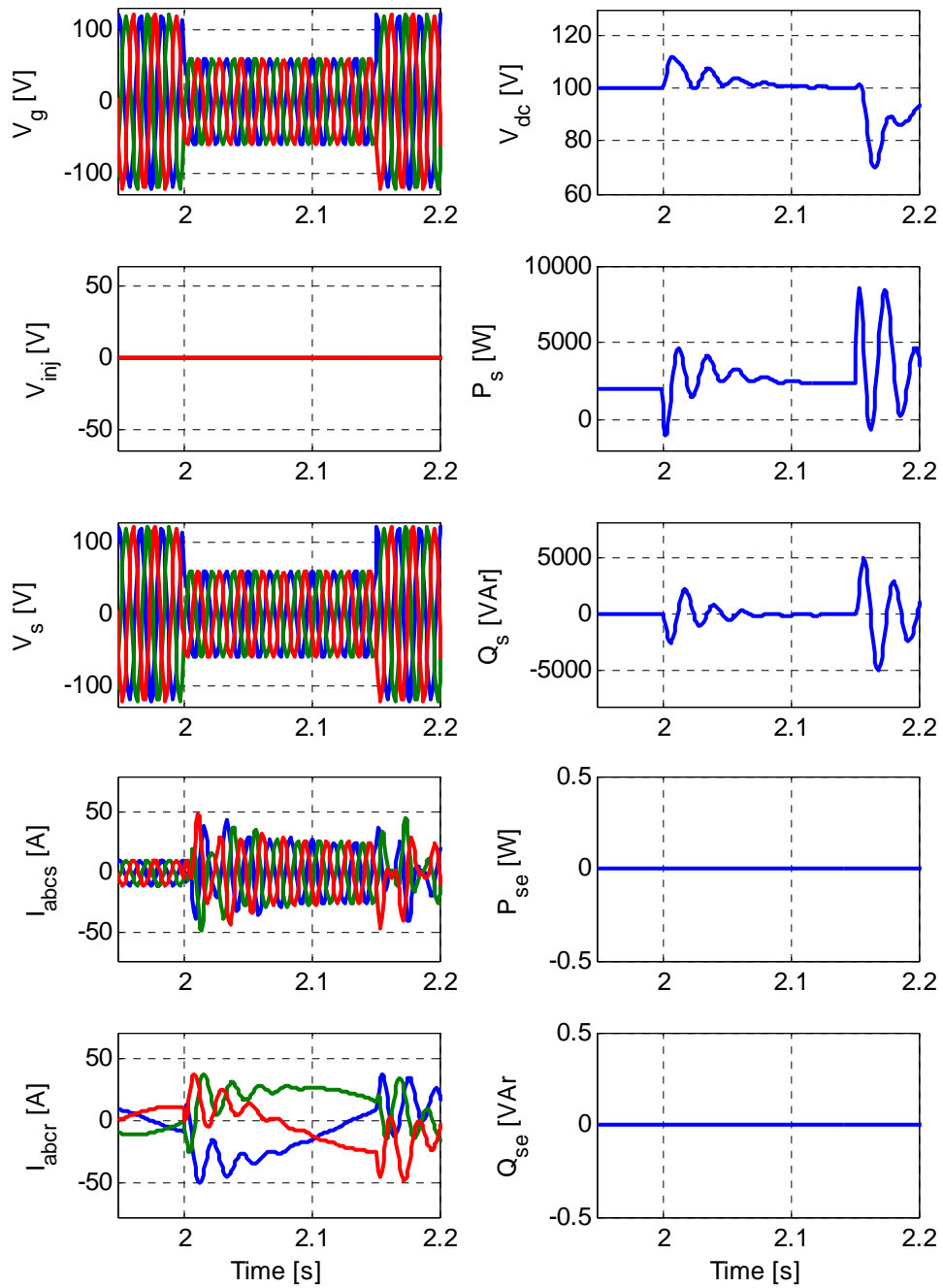
Figure 7.25.   Simulation of DFIG performance of a 5hp DFIG wind turbine without series injection to a 50%, 3-phase symmetrical sag
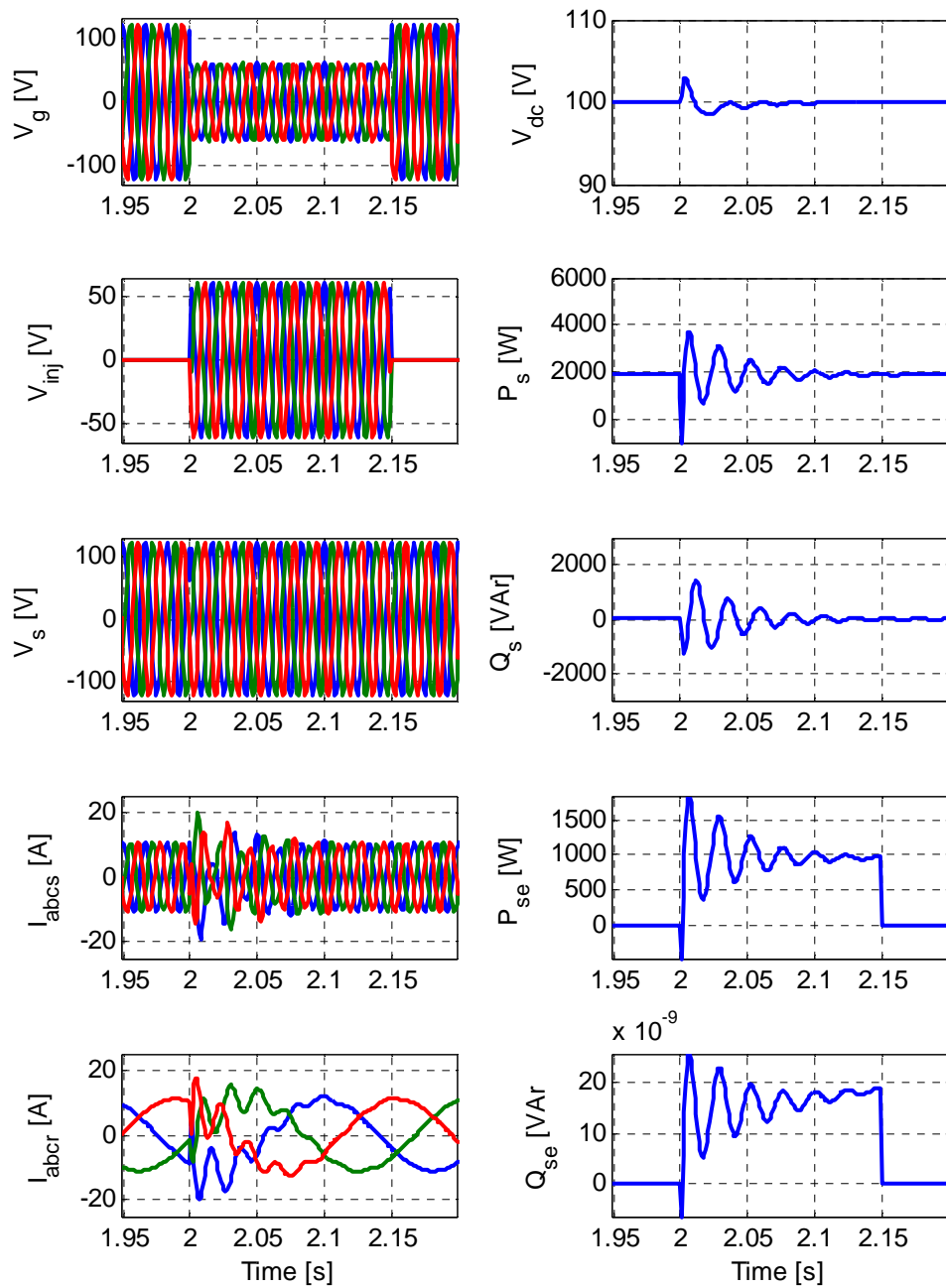
Figure 7.26.   Simulation of DFIG performance of a 5hp DFIG wind turbine with series
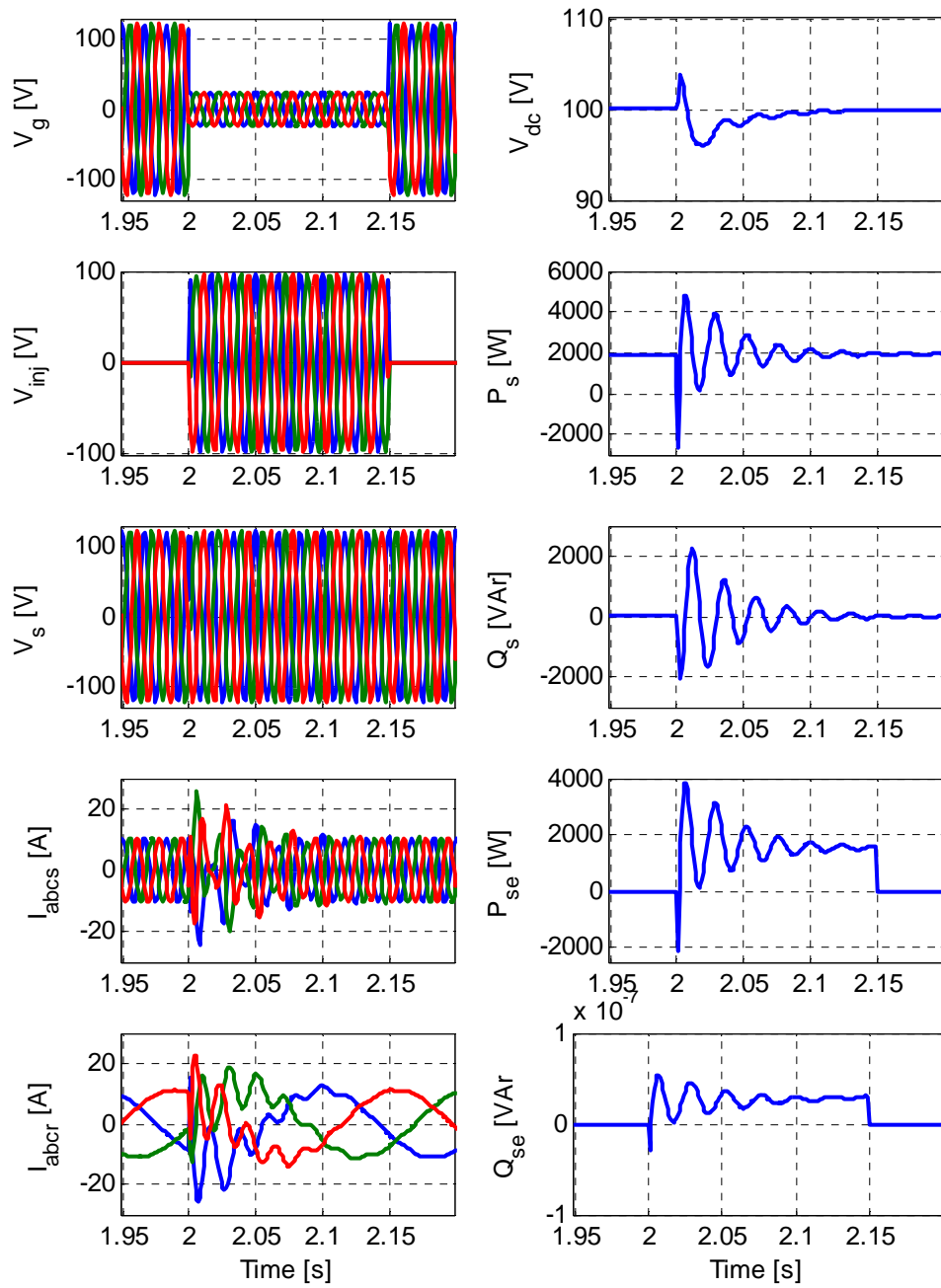injection to a 50%, 3-phase symmetrical sag

Figure 7.27.   Simulation of DFIG performance of a 5hp DFIG wind turbine with series injection to a 80%, 3-phase symmetrical sag
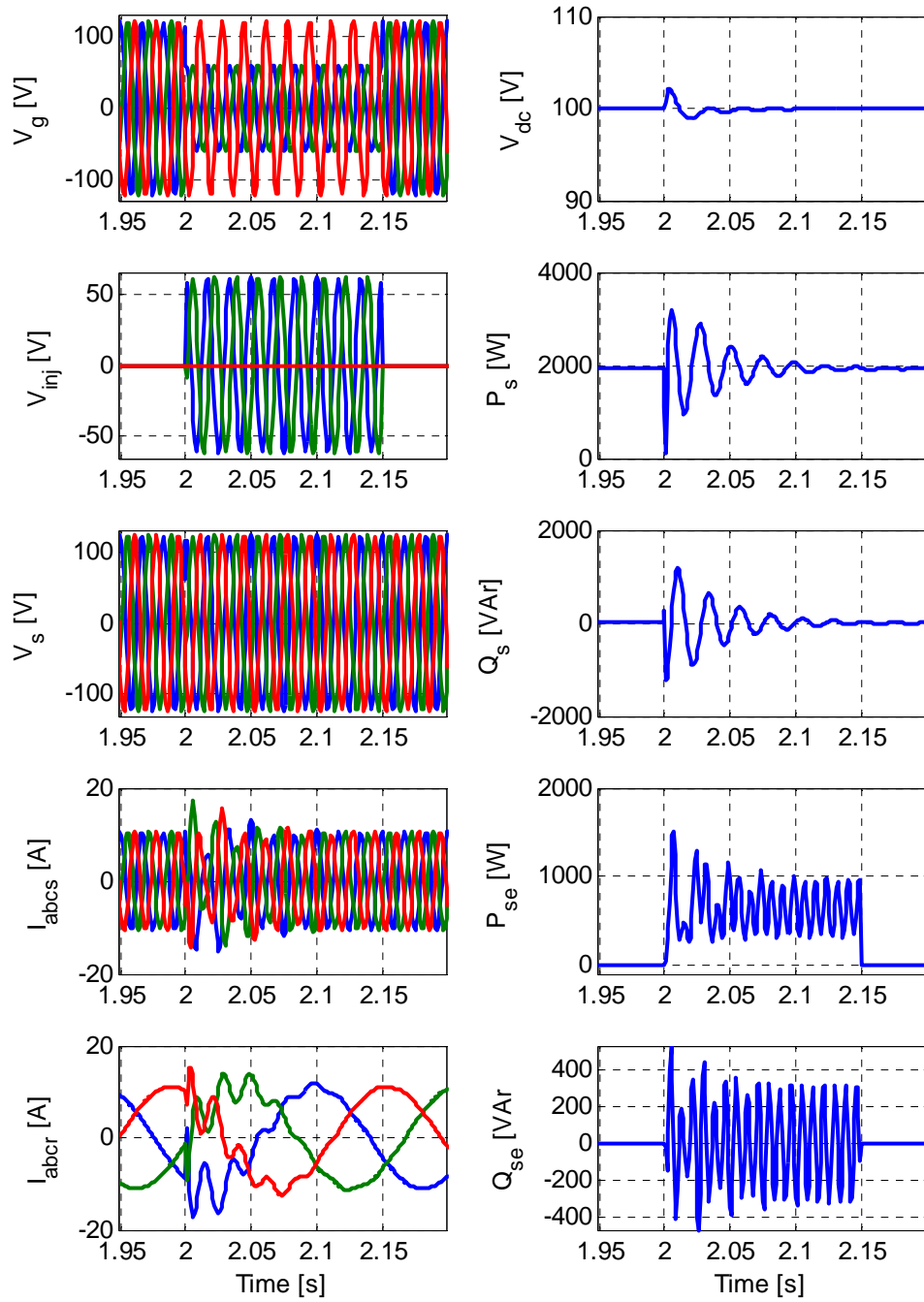
Figure 7.28. Simulation of DFIG performance of a 5hp DFIG wind turbine with series injection to a 50%, 2-phase sag
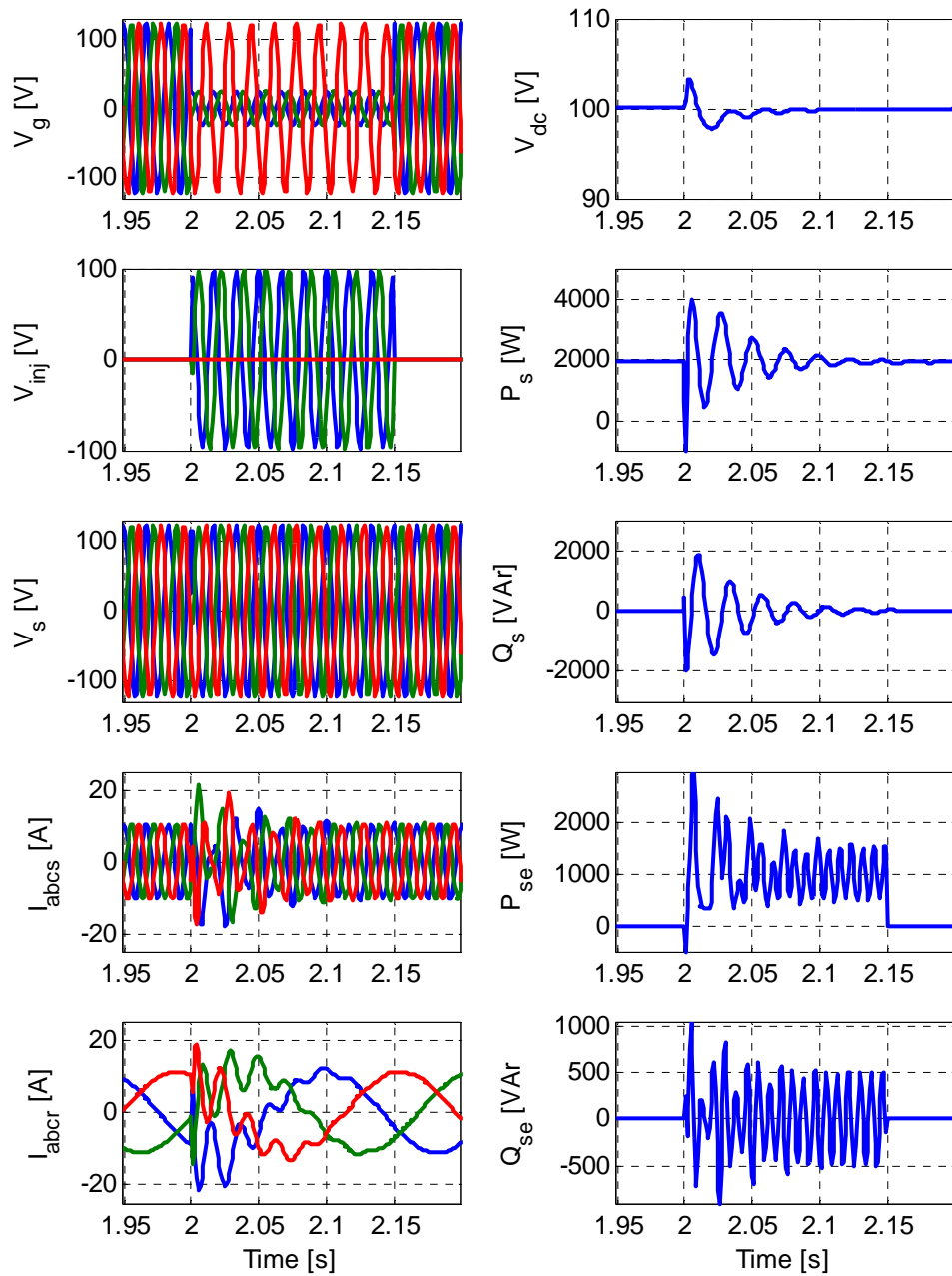
Figure 7.29.   Simulation of DFIG performance of a 5hp DFIG wind turbine with series injection to a 80%, 2-phase sag
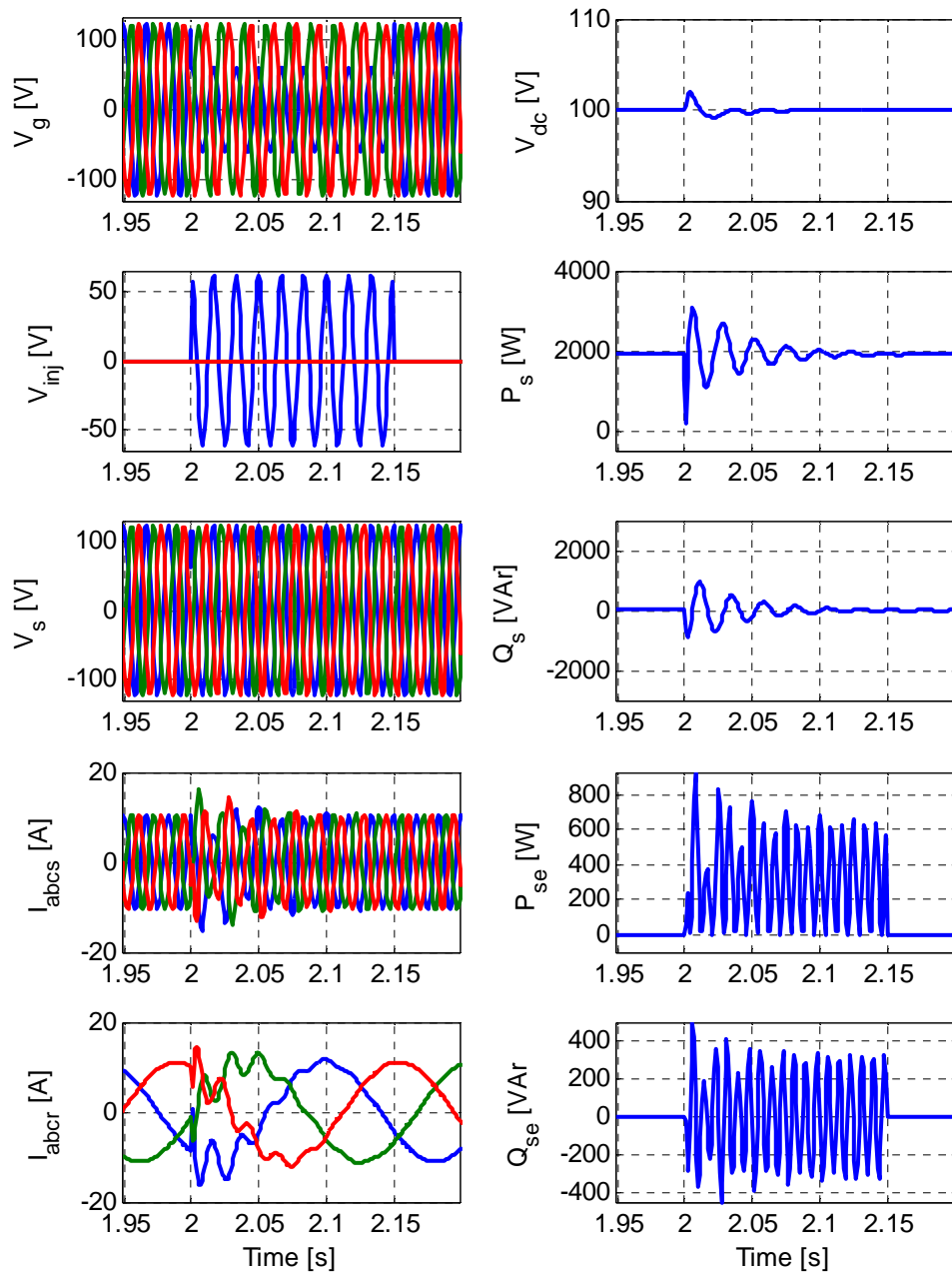
Figure 7.30.   Simulation of DFIG performance of a 5hp DFIG wind turbine with series injection to a 50%, 1-phase sag
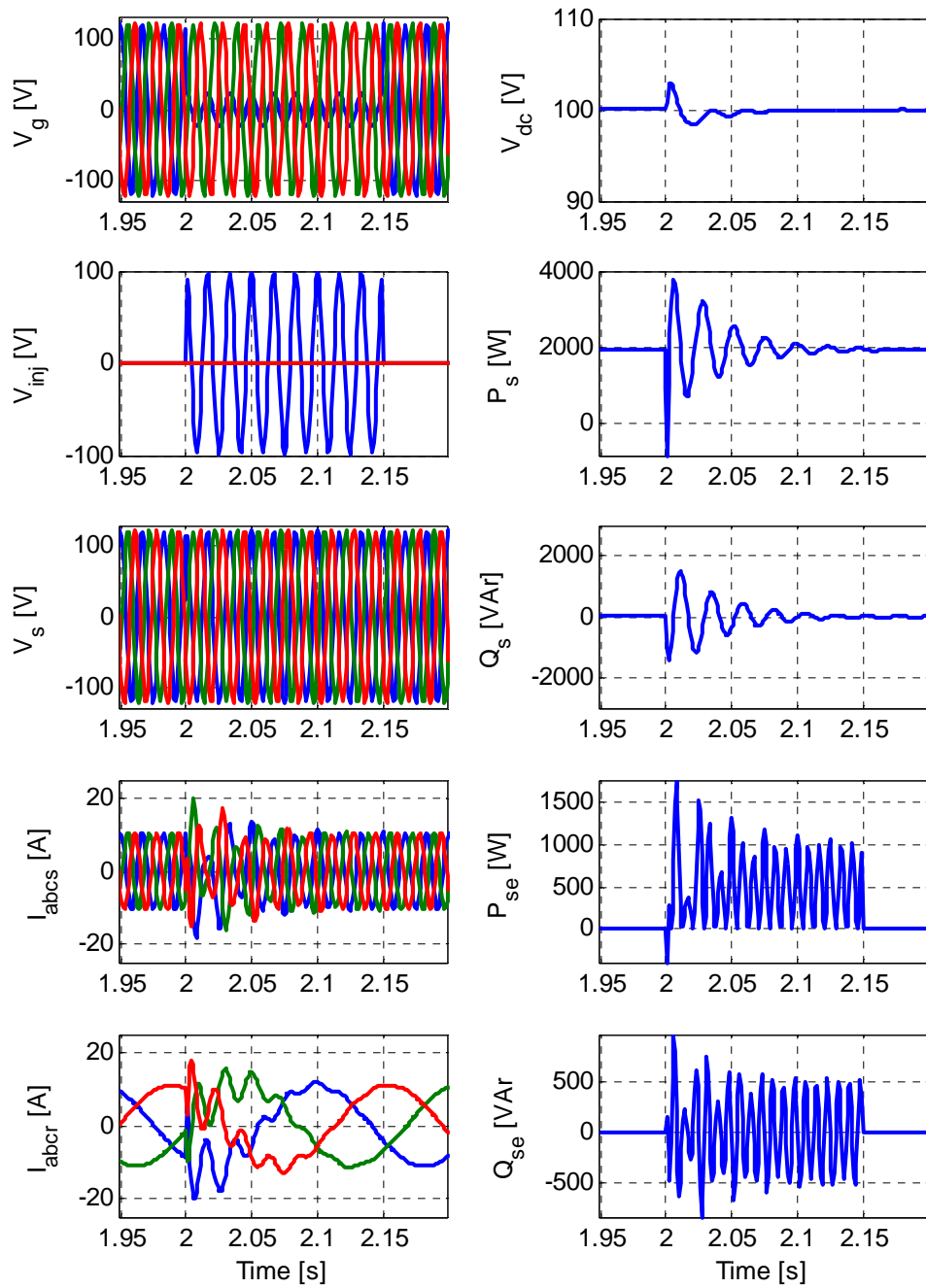
357

Figure 7.31.   Simulation of DFIG performance of a 5hp DFIG wind turbine with series injection to a 80%, 1-phase sag

7.6 Hardware Implementation

7.6.1. Experimental Setup

The overall experimental rig for the proposed low voltage ride-through is shown is given shown in Figure 7.32. A photograph of the laboratory setup is shown in Figure 7.33.

The setup consists of:

- A 5 kVa, 25 Amp three-phase Semikron voltage source converter

- A 5 kVA, 20 Amp Nine-switch converter designed and built in the laboratory

- The DFIG is a 5-hp, 6 pole, 60 Hz three-phase wound rotor induction machine

- A 5 hp, DC machine is used to emulate the wind turbine

- A laboratory dSPACE (DS1104) real-time interface controller is employed for generating the switching pulses to control the voltage source converter as well as for data acquisition and processing

- A desktop computer equipped with all necessary software packages such as MATLAB/Simulink and dSPACE Real Time Interface software

- Three auto transformers and three single-phase injection transformers

- Two diode rectifiers to provide dc power supply to the field and armature circuits of the dc machine

- Miscellaneous:

- ✓ Different interface circuits (the dead time; current and voltage sensors, inverter circuits) were designed and built for data acquisition as well as signal routing

- ✓ Some display, digital and analogue measuring equipment were be used at different stages of implementation
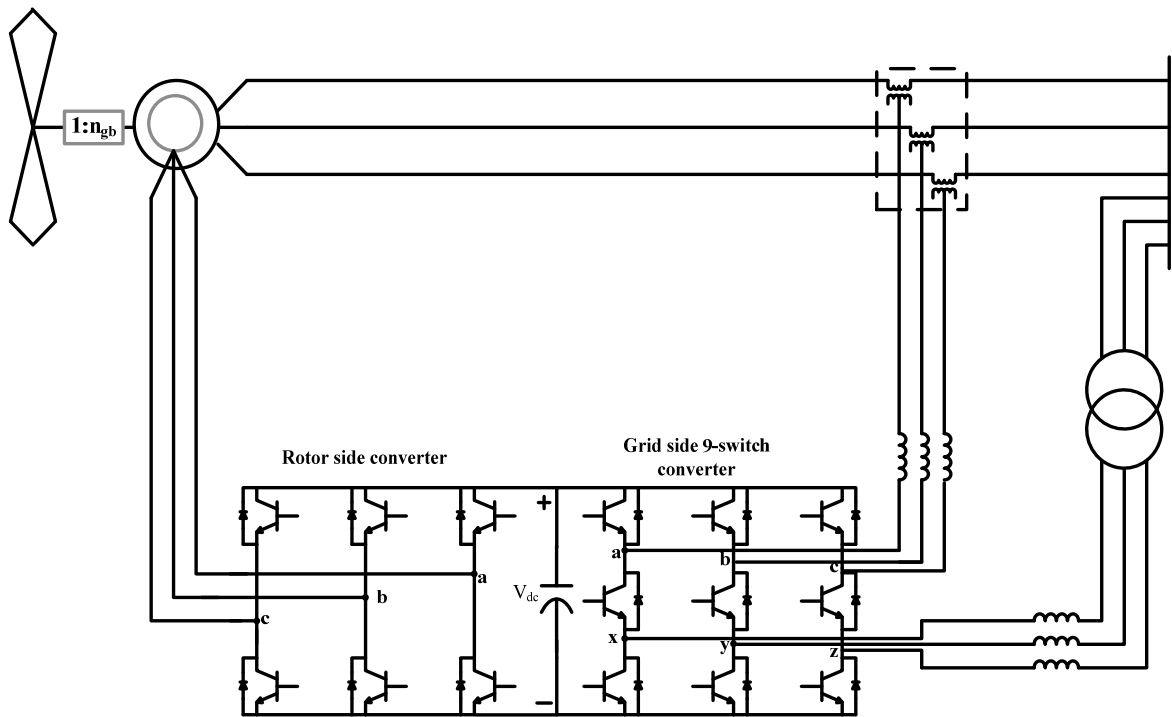

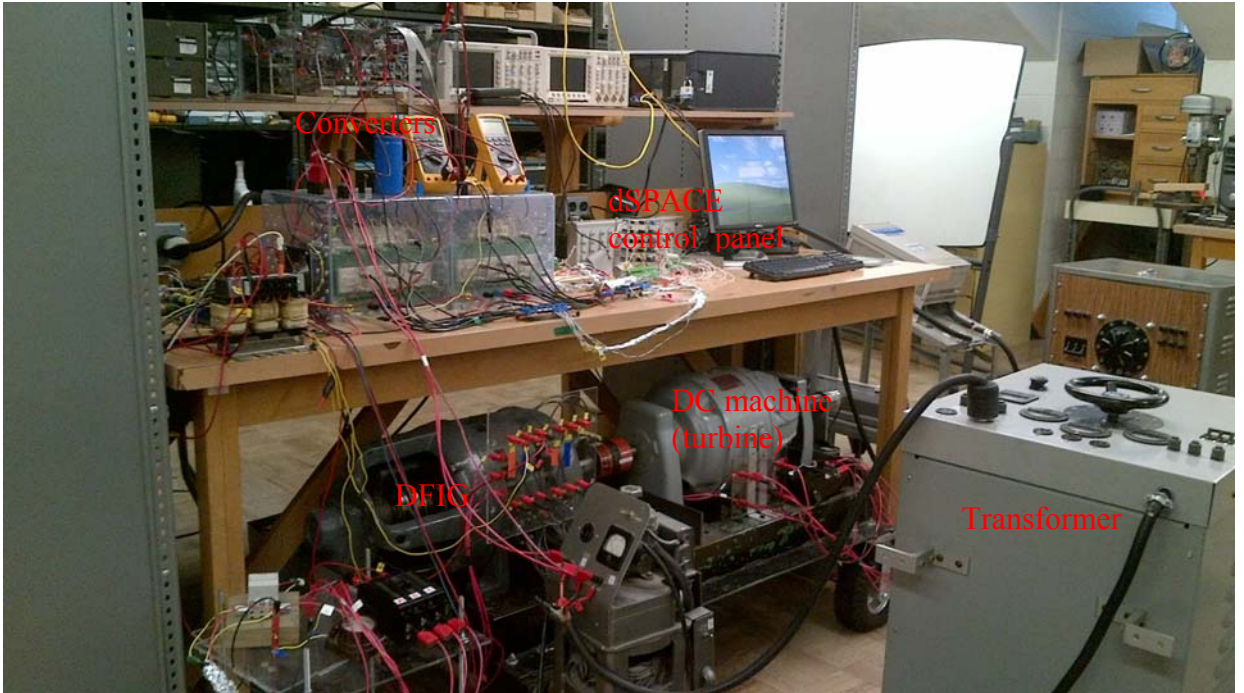Figure 7.32.   Block diagram of 5hp DFIG wind turbine experimental setup

Figure 7.33.   Photograph of laboratory 5hp DFIG wind turbine experimental setup

The rotor shaft of the 5-hp induction machine is mechanically coupled with the separately excited 5-hp dc machine. The rotor side converter is the Semikron converter whilst the Nine-switch serve the dual role of the parallel and grid side converters. The dSpace DS1104 card installed on the computer is used to acquire the grid line voltage, stator line voltages, stator and grid side converter filter currents, rotor position (and speed), and dc source voltage and processes them for the control algorithm.

7.6.2. Experimental Procedure

The DFIG is started in a soft procedure:

a) First turn on the driver power supply

b) *Pre-charge the DC link capacitor as follows:*

    i. Connect a three-phase resistive circuit between the GSC L-filter and the autotransformer output. Include a switch to disconnect these resistors after pre-charging is completed.

    ii. Using the uncontrolled diode rectifier on the GSC, and grid supply gradually increase the DC link voltage to a little below its required value.

    iii. Start DC machine and increase the rotor speed to some set value just below the reference speed. At this point release the RSC and allow the speed to reach the reference speed before releasing the PGSC to keep the DC link voltage constant and maintain the reactive power with the grid at zero.

c) Then turn on the grid switch gradually increase the voltage using an autotransformer

7.6.3. Experimental Results

Figure 7.34 shows the system voltages after a 50% three-phase symmetrical grid sag and subsequent series injection. It shows that the series injection output of the Nine-switch converter injects the missing grid voltage upon detection sag, protecting the stator and rotor circuits from overcurrents.
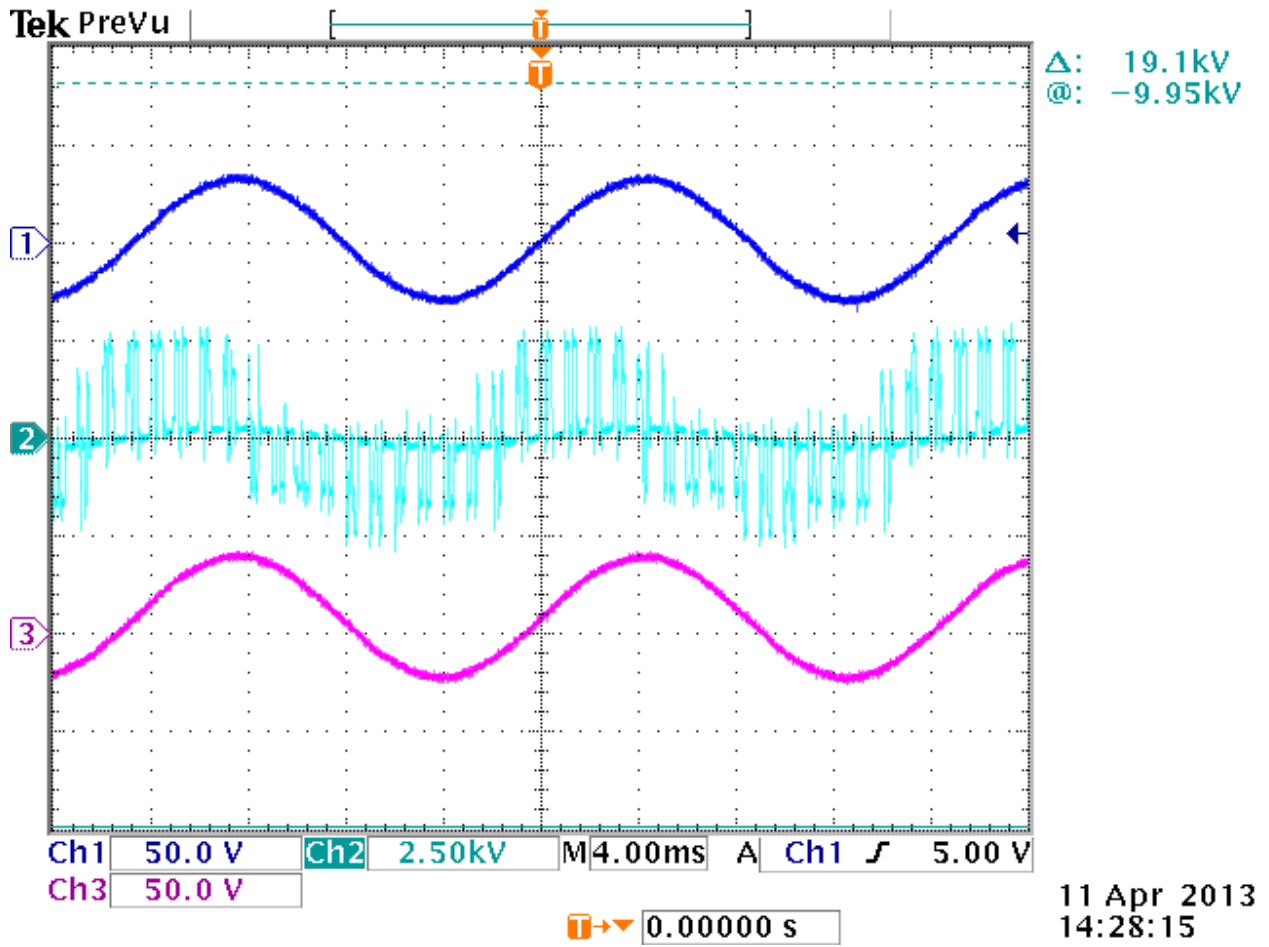
(a)

Figure 7.34.   Experimental waveform showing the closed loop line-to-line voltages: (Ch1) grid voltage, (Ch2) series injection voltage and (Ch3) stator voltage captured on a scope
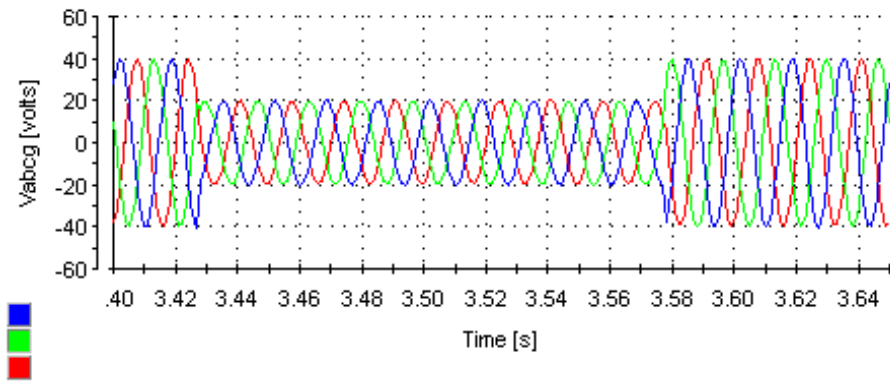
(b)

(c)

(d)

Figure 7.35.   Performace of the closed loop responcse for a 50% voltage sag (a) scope trace
(b) filtered grid voltage, (c) injected voltage, and (d) stator voltage in dSPCE controldesk

364
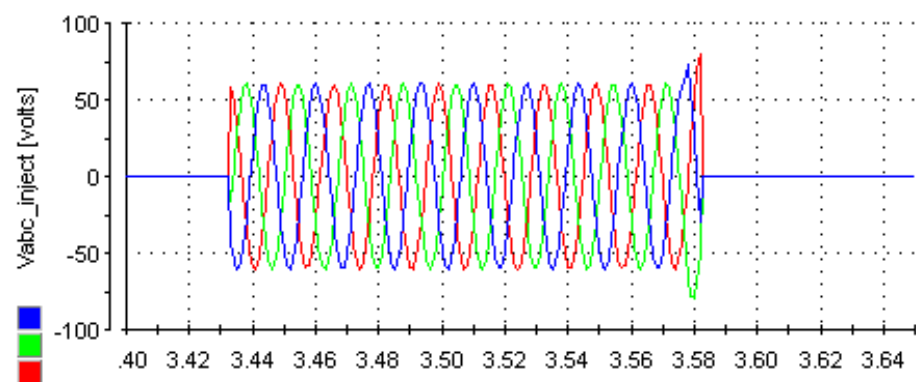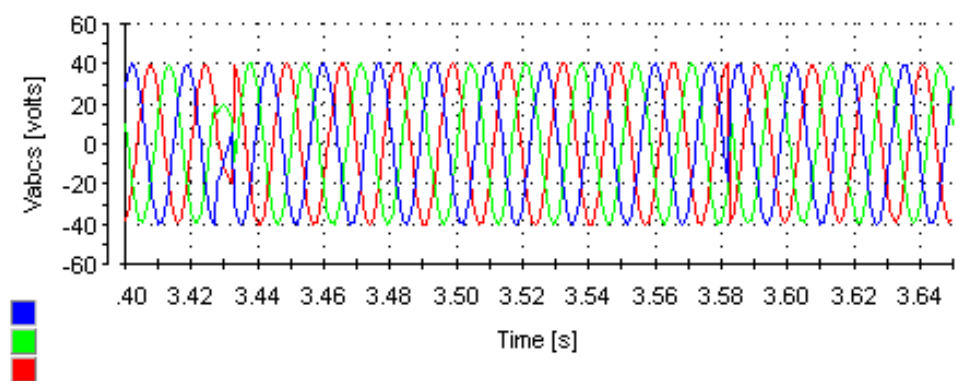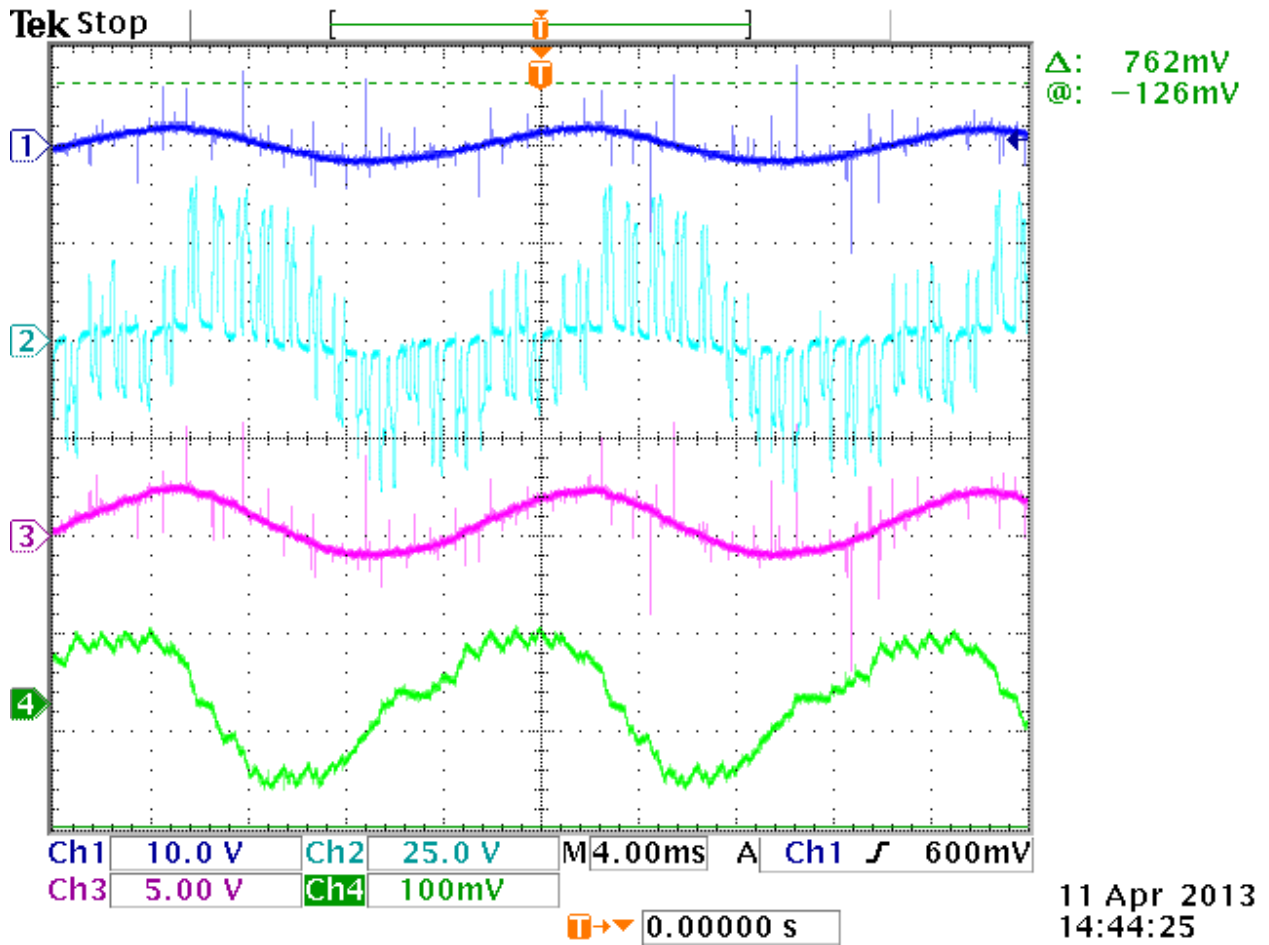
Figure 7.36.   Experimental waveform showing the line-to-line voltages: (Ch1) grid voltage, (Ch2) series injection voltage, (Ch3) stator voltage, (Ch4) PGSC filter phase 'a' current
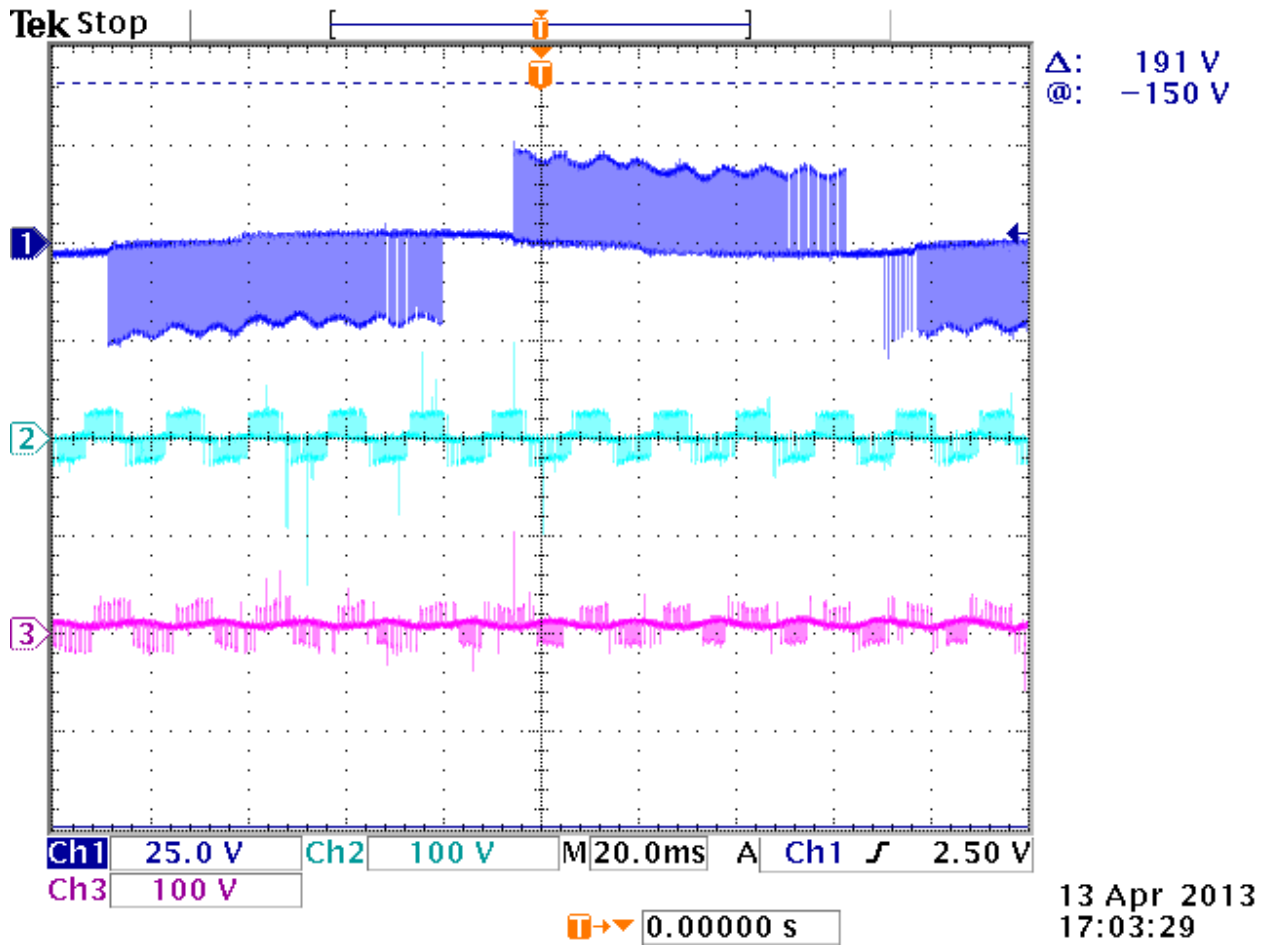
Figure 7.37.   Experimental waveform showing the line-to-line voltages: (Ch1) rotor voltage, (Ch2) series injection voltage, (Ch3) PGSC output voltage

In Figure 7.35, also depicted is the PGSC voltage and filter current injected into the grid. The rotor voltage is also shown. The stator active and reactive powers are shown in Figure 7.36 illustrating that about 2kW power is injected into the grid. The corresponding stator and rotor currents are shown in Figures 7.37 and 7.38 respectively.

Figure 7.38.   Experimental waveform showing stator active and reactive powers

Figure 7.39.   Experimental waveform showing stator qd-axis currents
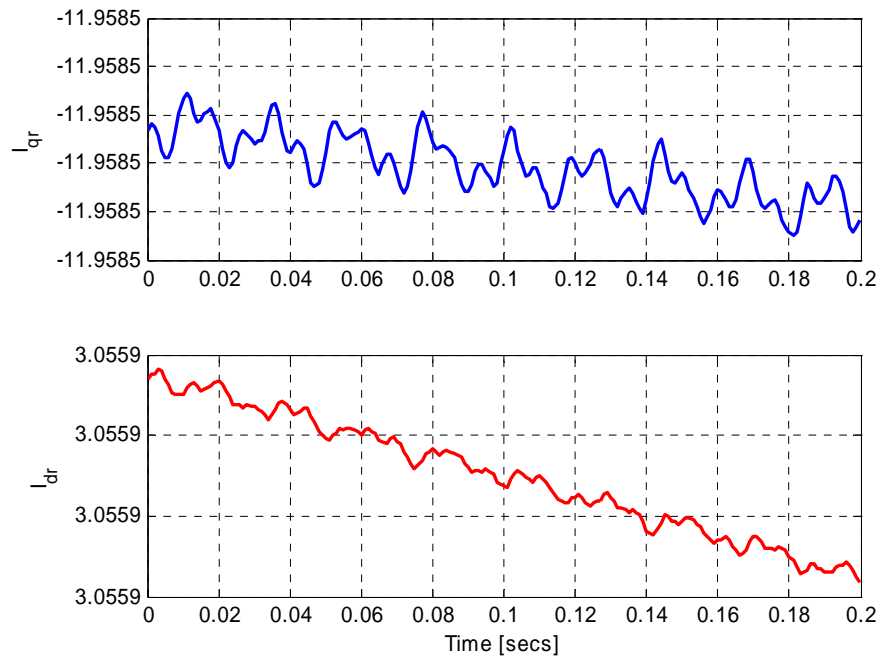
Figure 7.40.   Experimental waveform showing rotor qd-axis currents

CHAPTER 8

CONCLUSIONS AND FUTURE WORK

8.1 Introduction

This chapter presents the summary of this dissertation. A summary of the main chapters of the dissertation is given touching on key areas of each chapter compared to current state of the art. It also highlights major contributions made to the body knowledge. The chapter concludes with some suggestions for future work.
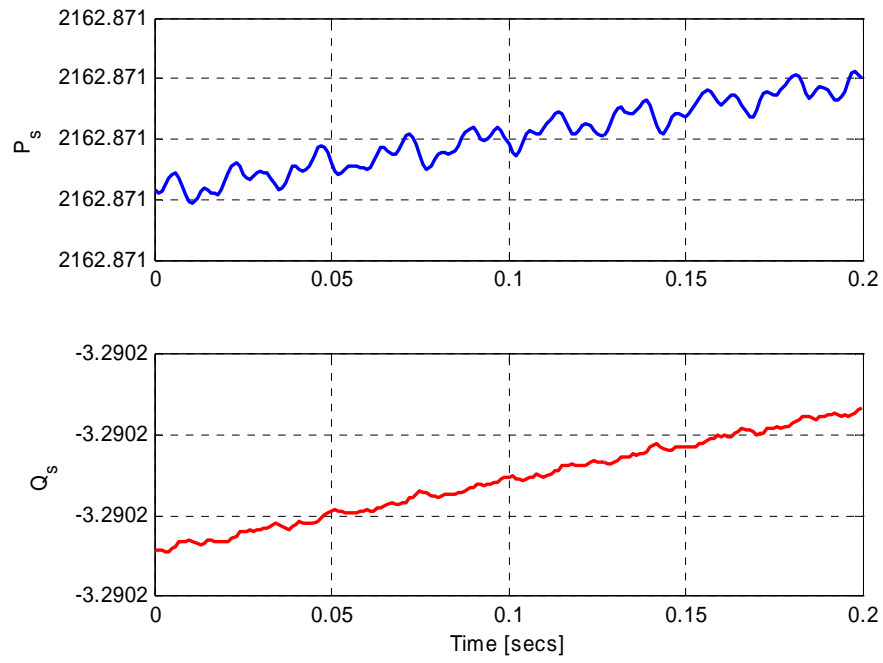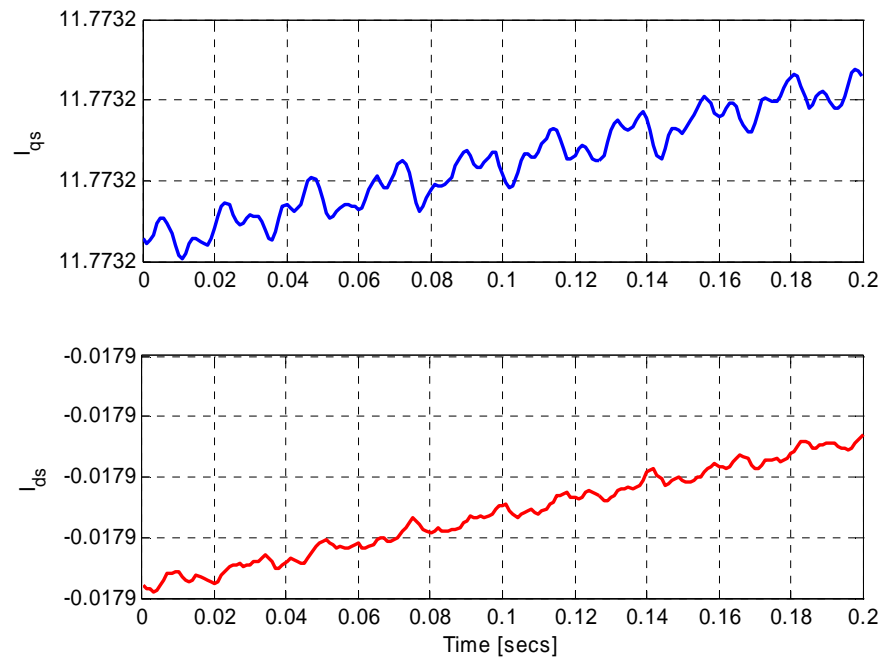
8.2 Conclusions

In chapter 3, the dynamic behavior of the doubly-fed induction generator based wind turbine is studied. This served to give a background to the state of the art control schemes for this type of wind energy conversion system. In particular, the vector control scheme based on the stator flux reference frame orientation is used for the rotor side and grid side converter controllers. These controllers are modeled in the synchronous reference frame. The steady state and dynamic simulations of the DFIG wind turbine system are also presented.

The generic expression for the intrinsic stability criteria of a variable-speed, variable-pitch DFIG-based wind turbine is derived in Chapter 4. The stability criteria obtained predicts the acceptable region of operation of the wind system when it is capturing maximum power at low to medium wind speeds, rated power at high wind speeds, and power regulation operation mode with more accuracy than conventional

methods. It reveals a narrower stability region than the conventional method for both maximum power tracking and rated power modes.

In the second part of this Chapter 4, the effect of rotor position error and machine parameter inaccuracies on a vector controlled DFIG turbine system is investigated. Results show that the error in rotor position has a significant effect on the stability of the entire system. Specifically, the system's eigenvalues related to the speed and power controllers crosses over to the right-hand plane when the slip angle error is at about 1.55 rad. This large error is known to occur when using hardware phase locked loop. It is also found that for a properly tuned controller gains, machine parameter inaccuracies do not affect the stability of the system but affects the placement of system poles in the left-hand plane.

In Chapter 5, space vector and carrier-based pulse-width modulation methodologies for the Nine-switch converter are proposed. The generalized neutral voltages for the converter were derived for the first time in this research and used to serve the dual role of separating the modulations signals of the upper and lower switching devices. This is required to prevent short-circuiting the input dc supply and ensuring independent control of its two outputs. In addition, the neutral voltages are also used to obtain different carrier-based modulation strategies, increasing the linear operating region of the converter.

The mathematical model of the 12-switch converter is presented in Chapter 6 as an extension of the Nine-switch converter presented in Chapter 5. The space vector and a carrier-based modulation schemes for the 12-switch converter are also proposed. Its generalized neutral voltages are also derived for the first time. Based on the models of the

370

Nine-switch and 12-switch converters, the model of the generalized 3n+3-switch converter is presented. Simulation results show that injecting these neutral voltages into the modulation signals has a dual role; shaping the modulation scheme as well as ensuring that the switching function constraints of the converter are not violated. Simulation results are presented to show the validity of the proposed schemes and corroborated by experimental results.

Chapter 7 proposes a low voltage ride-through solution for a grid-tied DFIG wind turbine using the Nine-switch converter to serve the dual role of a parallel grid side converter and series grid side converters. This ride-through solution is applicable for both balanced and unbalanced voltage sags at the grid interface. The principle of ride-through, sag detection, and controllers are described. The controllers are designed based on the stationary reference frame using a proportional plus a resonance controller. Operation is demonstrated through simulation and confirmed by experimentation using a laboratory scale 5-hp DFIG wind turbine.

8.3 Summary of Contributions

The summary of the major contributions of this dissertations are given below.

- Mathematical model of the Nine-switch converter capable of variable frequency and/or amplitude operation

- Mathematical model of the 12-switch converter and the generalized 3n+3-switch converter also capable of variable frequency and/or amplitude operation

- Space vector and carrier-based PWM schemes for the above converters

- DFIG wind turbine model and sources of steady-state instability

- The use of the Nine-switch converter's dual outputs for the parallel and series grid side converter to ride-through low voltage sags at the DFIG stator terminals

- Develop a proportional plus resonant controller to achieve robust voltage injection and ability to response to different types of voltage sages

- A laboratory scale prototype test to validate the proposed solution with the Nine-switch converter

8.4 Suggestions for Future Work

A single 5-hp DFIG may predict the behavior of a single MW turbine to a good degree but same cannot be said of a large wind farm with all the interactions between the units. Thus a more accurate model of the wind farm system will enable a more realistic performance evaluation of the SGSC.

The SGSC part of the Nine-switch converter is used only when the voltage at the terminals of the DFIG stator falls below a set reference. Since the sag events represent a tiny fraction of the operational time of the converter, the converter 'may' be underutilized most of the time. It should be worthwhile during normal operation conditions, to use the SGSC output for harmonic cancellation in a polluted network.

Another solution to utilizing the full potential of the Nine-switch converter at all times is to reconfigure the converter to act as the conventional two-level converter by changing the input modulations signals. For example, the inner two switching devices in each phase-leg may be considered as one device by supplying them with the same

372

modulation signal. This is possible if output of the SGSC is isolated from stator during normal grid conditions using a switch but closed during sag events.

The 12-switch converter may also be employed to replace the three converters namely; rotor side converter, parallel grid side converter and series grid side converter. This can be an interesting application since the different frequency and amplitude property would be at play.

Finally, to fully generalize the 3n+3-converter particularly the expressions for the neutral voltages of inner loads, the model for an 18-switch converter should be derived to provide sufficient information for generalization.

REFERENCES

[1]   J. Morren and S. W. H. de Haan, "Ride through of wind turbines with doubly-fed induction generator during a voltage dip," *IEEE Transactions on Energy Conversion*, vol. 20, no. 2, pp. 435–441, June, 2005.

[2]   European Wind Energy Association. Pure Power, wind energy targets for 2020 and 2030. Technical Report; 2011.

[3]   Energy Information Administration. International Energy Outlook. September, 2011 [Online]. Available: http://www.eia.gov/forecasts/ieo/pdf/0484(2011).pdf.

[4]   U.S. Federal Energy Regulatory Commission, Regulatory Order 661: *Interconnection for Wind Energy,* issued June 2, 2005.

[5]   U.S. Federal Energy Regulatory Commission, Regulatory Order 661-A: Interconnection for Wind Energy, Joint Report of the North American Electric Reliability Council and the American Wind Energy Association, 19 September, 2005.

[6]   M. Tsili and S. Papathanassiou, "A review of grid code technical requirements for wind farms," *IET Renewable Power Generation*, vol. 3, no. 3, pp. 308-332, September 2009.

[7]   ABB Products and services for wind turbines: Electrical drivetrain solutions and products for turbine subsystems [Online]. http://search.abb.com/library/Download

[8]   M. H. J. Bollen, "Characterisation of voltage dips experienced by three phase adjustable-speed drives," *IEEE Transactions on Power Delivery*, vol. 12, no. 4, pp. 1666-1671, October 1997.

[9]   M. H. J. Bollen, G. Olguin, and M. Martins, "Voltage dips at the terminals of wind power installations," *Wind Energy*, vol. 8, no. 3, pp. 307–318, July/September 2005.

[10]   S. Seman, J. Niiranen, and A. Arkkio, "Ride-Through Analysis of Doubly Fed Induction Wind-Power Generator Under Unsymmetrical Network Disturbance," *IEEE Transactions on Power Systems*, vol. 21, no. 4, pp. 1782-1789, November 2006.

[11]   J. Lopez, P. Sanchis, X. Roboam, and L. Marroyo, "Dynamic Behavior of the Doubly Fed Induction Generator During Three-Phase Voltage Dips," *IEEE Transactions on Energy Conversion*, vol. 22, no. 3, pp. 709-717, September 2007.

[12]   D. Xiang, L. Ran, P. J. Tavner, and S. Yang, "Control of a doubly fed induction generator in a wind turbine during grid fault ride-through," *IEEE Transactions on Energy Conversion*, vol. 21, no. 3, pp. 652-662, September 2006.

375

[13] P. S. Flannery, "Doubly Fed Induction Generator Wind Turbines with Series Grid Side Converter for Robust Voltage Sag Ride-Through," Ph.D. dissertation, University Of Wisconsin-Madison, 2008.

[14] T. Brekken and N. Mohan, "A novel doubly-fed induction wind generator control scheme for reactive power control and torque pulsation compensation under unbalanced grid voltage conditions," in *IEEE 34th Annual Power Electronics Specialist Conference (PESC 2003)*, vol. 2, pp. 760- 764 , 15-19 June 2003.

[15] T. K. A. Brekken and N. Mohan, "Control of a Doubly Fed Induction Wind Generator Under Unbalanced Grid Voltage Conditions," *IEEE Transactions on Energy Conversion*, vol. 22, no. 1, pp. 129-135, March 2007.

[16] M. Mohseni, S.M. Islam, and M. A. S. Masoum, "Impacts of Symmetrical and Asymmetrical Voltage Sags on DFIG-Based Wind Turbines Considering Phase-Angle Jump, Voltage Recovery, and Sag Parameters," *IEEE Transactions on Power Electronics*, vol. 26, no. 5, pp. 1587-1598, May 2011.

[17] I. Erlich, H. Wrede, and C. Feltes, "Dynamic Behavior of DFIG-Based Wind Turbines during Grid Faults," in *IEEE Power Conversion Conference (PCC 2007),* Nagoya, pp.1195-1200, 2-5 April 2007.

[18] M. Rodriquez, G. Abad, I. Sarasola, and A. Gilabert, "Crowbar control algorithms for doubly fed induction generator during voltage dips," in *IEEE European Conference on Power Electronics and Applications*, pp. 10, 2005.

[19] R. Lohde, S. Jensen, A. Knop, and F. W. Fuchs, "Analysis of three phase grid failure and Doubly Fed Induction Generator ride-through using crowbars," in *IEEE European Conference on Power Electronics and Applications*, pp.1-8, 2-5 September 2007.

[20] G. Pannell, D. J. Atkinson, and B. Zahawi, "Minimum-Threshold Crowbar for a Fault-Ride-Through Grid-Code-Compliant DFIG Wind Turbine," *IEEE Transactions on Energy Conversion*, vol. 25, no. 3, pp. 750-759, September 2010.

[21] C. Wessels and F. W. Fuchs, "Fault ride through of DFIG wind turbines during symmetrical voltage dip with crowbar or stator current feedback solution," *IEEE Energy Conversion Congress and Exposition (ECCE 2010),* pp. 2771-2777, 12-16 September 2010.

[22] F. K. A. Lima, A. Luna, P. Rodriguez, E. H. Watanabe, and F. Blaabjerg, "Rotor Voltage Dynamics in the Doubly Fed Induction Generator During Grid Faults," *IEEE Transactions on Power Electronics*, vol. 25, no. 1, pp. 118-130, January. 2010.

[23]   Z. Zhang, L. Xu, Y. Zhang, and B. Guan, "Novel rotor-side control scheme for Doubly Fed Induction Generator to ride through grid faults," in *IEEE Energy Conversion Congress and Exposition (ECCE 2010)*, pp. 3084-3090, 12-16 September 2010.

[24]   J. Liang, W. Qiao, and R. G. Harley, "Feed-Forward Transient Current Control for Low-Voltage Ride-Through Enhancement of DFIG Wind Turbines," *IEEE Transactions on Energy Conversion*, vol. 25, no. 3, pp. 836-843, September 2010.

[25]   X. Yan, G. Venkataramanan, P. S. Flannery, and Y. Wang, "Fault Tolerance of DFIG Wind Turbine with a Series Grid Side Passive Impedance Network," in *IEEE Industry Applications Society Annual Meeting*, pp.1-8, 4-8 October 2009.

[26]   X. Yan, G. Venkataramanan, P. S. Flannery, Y. Wang, Q. Dong, and B. Zhang, "Voltage-Sag Tolerance of DFIG Wind Turbine With a Series Grid Side Passive-Impedance Network," *IEEE Transactions on Energy Conversion*, vol. 25, no. 4, pp. 1048-1056, December 2010.

[27]   X. Yan, G. Venkataramanan, Y. Wang, Q. Dong, and B. Zhang, "Grid-Fault Tolerant Operation of a DFIG Wind Turbine Generator Using a Passive Resistance Network," *IEEE Transactions on Power Electronics*, vol. 26, no. 10, pp. 2896-2905, October 2011.

[28]   A. O. Ibrahim, T. H. Nguyen, D.-C. Lee, and S.-C. Kim, "Ride-through strategy for DFIG wind turbine systems using dynamic voltage restorers," in *IEEE Energy Conversion Congress and Exposition (ECCE 2009)*, pp.1611-1618, 20-24 September 2009.

[29]   A. O. Ibrahim, T. H. Nguyen, D.-C. Lee, S.-C. Kim, "A Fault Ride-Through Technique of DFIG Wind Turbine Systems Using Dynamic Voltage Restorers," *IEEE Transactions on Energy Conversion*, vol. 26, no. 3, pp. 871-882, September 2011.

[30]   Y. Liao, H. Li, and J. Yao, "Unbalanced-grid-fault ride-through control for a doubly fed induction generator wind turbine with series grid-side converter" *WSEAS Transactions on Circuits and Systems*, vol. 10, no. 2, pp. 69-82, February 2011.

[31]   S. Zhang, K.-J. Tseng, S. S. Choi, T. D. Nguyen, and D. L. Yao, "Advanced Control of Series Voltage Compensation to Enhance Wind Turbine Ride Through," *IEEE Transactions on Power Electronics*, vol. 27, no. 2, pp. 763-772, February 2012.

[32]   L. Zhang, P. C. Loh, and F. Gao, "An Integrated Nine-Switch Power Conditioner for Power Quality Enhancement and Voltage Sag Mitigation," *IEEE Transactions on Power Electronics*, vol. 27, no. 3, pp. 1177-1190, March 2012.

377

[33] A. Petersson, "Analysis modeling and control of doubly-fed induction generators for wind turbines," Ph.D. dissertation, Chalmers University of Technology, Gothenberg, Sweden, 2005.

[34] P. S. Flannery, G. Venkataramanan, "A Fault Tolerant Doubly Fed Induction Generator Wind Turbine Using a Parallel Grid Side Rectifier and Series Grid Side Converter," *IEEE Transactions on Power Electronics*, vol. 23, no. 3, pp. 1126-1135, May 2008.

[35] P. S. Flannery, G. Venkataramanan, "Unbalanced Voltage Sag Ride-Through of a Doubly Fed Induction Generator Wind Turbine With Series Grid-Side Converter," *IEEE Transactions on Industry Applications*, vol. 45, no. 5, pp. 1879-1887, September - October 2009.

[36] O. Abdel-Baqi and A. Nasiri, "Series Voltage Compensation for DFIG Wind Turbine Low-Voltage Ride-Through Solution," *IEEE Transactions on Energy Conversion*, vol. 26, no. 1, pp. 272-280, March 2011.

[37] O. Abdel-Baqi, A. Esmaili, and A. Nasiri, "Digital control of three-phase series converter for DFIG wind turbine low voltage ride-through solution," in 26th *IEEE Annual Applied Power Electronics Conference and Exposition*, pp. 946-951, 6-11 March 2011.

[38] T. Jimichi, H. Fujita, and H. Akagi, "Design and Experimentation of a Dynamic Voltage Restorer Capable of Significantly Reducing an Energy-Storage Element," *IEEE Transactions on Industry Applications*, vol. 44, no. 3, pp. 817-825, May-June 2008.

[39] J. G. Nielsen, M. Newman, H. Nielsen, and F. Blaabjerg, "Control and testing of a dynamic voltage restorer (DVR) at medium voltage level," *IEEE Transactions on Power Electronics*, vol. 19, no. 3, pp. 806–813, May 2004.

[40] E. K. K. Sng, S. S. Choi, and D. M. Vilathgamuwa, "Analysis of series compensation and DC-link voltage controls of a transformerless self-charging dynamic voltage restorer," *IEEE Transactions on Power Delivery*, vol. 19, no. 3, pp. 1511–1518, July 2004.

[41] K. Oka and K. Matsuse, "A Nine-switch inverter for driving two AC motors independently," *IEEJ Transactions on Electrical and Electronic Engineering*, vol. 2 , no. 1, pp. 92-96, 2007.

[42] T. Kominami, Y. Fujimoto, "A Novel Nine-Switch Inverter for Independent Control of Two Three-Phase Loads, "Pro*ceedings of the 42nd Annual Conference of IEEE Industry Applications Society on Industry Applications*, pp. 2346-2350, 23-27 September 2007.

[43] X. Liu, P. Wang, P. C. Loh, and F. Blaabjerg, "A Compact Three-Phase Single-Input/Dual-Output Matrix Converter," *IEEE Transactions on Industrial Electronics*, vol. 59, no. 1, pp. 6-16, January 2012.

[44] X. Liu, P. Wang, P. C. Loh, and F. Blaabjerg, "A Three-Phase Dual-Input Matrix Converter for Grid Integration of Two AC Type Energy Resources," *IEEE Transactions on Industrial Electronics*, vol. 60, no. 1, pp. 20-30, January 2013.

[45] C. Liu, B. Wu, N. R. Zargari, D. Xu, and J. Wang, "A Novel Three-Phase Three-Leg AC/AC Converter Using Nine IGBTs," *IEEE Transactions on Power Electronics*, vol. 24, no. 5, pp. 1151-1160, May 2009.

[46] H. Banakar, C. Luo, and B. T. Ooi, "Steady-state stability analysis of doubly-fed induction generator under decoupled P-Q control," *IEE Proceedings on Electrical Applications*, vol. 153, no. 2, pp. 300 - 306, March 2006.

[47] C.-H. Liu and Y.-Y. Hsu, "Effect of Rotor Excitation Voltage on Steady-State Stability and Maximum Output Power of a Doubly Fed Induction Generator," *IEEE Transactions on Industrial Electronics*, vol. 58, no. 4, pp. 1096-1109, April 2011.

[48] E. B. Muhando, T. Senjyu, A. Uehara, T. Funabashi, and C.-H. Kim, "LQG Design for Megawatt-Class WECS with DFIG Based on Functional Models' Fidelity Prerequisites," *IEEE Transactions on Energy Conversion*, vol. 24, no. 4, pp. 893-904, December 2009.

[49] P. Ledesma and J. Usaola, "Doubly fed induction generator model for transient stability analysis," *IEEE Transactions on Energy Conversion*, vol. 20, no. 2, pp. 388- 397, June 2005.

[50] R. Vepa, "Nonlinear, Optimal Control of a Wind Turbine Generator," *IEEE Transactions on Energy Conversion*, vol. 26, no. 2, pp. 468-478, June 2011.

[51] H. Geng and G. Yang, "Robust pitch controller for output power levelling of variable-speed variable-pitch wind turbine generator systems," *IET Renewable Power Generation*, vol. 3, no. 2, pp. 168-179, June 2009.

[52] C. Y. Tang, Y. Guo, and J. N. Jiang, "Nonlinear Dual-Mode Control of Variable-Speed Wind Turbines With Doubly Fed Induction Generators," *IEEE Transactions on Control Systems Technology*, vol. 19, no. 4, pp. 744-756, July 2011.

[53] N. A. Schinas, N. A. Vovos, and G. B. Giannakopoulos, "An Autonomous System Supplied only by a Pitch-Controlled Variable-Speed Wind Turbine," *IEEE Transactions on Energy Conversion*, vol. 22, no. 2, pp. 325-331, June 2007.

[54] M. Soliman, O. P. Malik, and D. T. Westwick, "Multiple Model Predictive Control for Wind Turbines with Doubly Fed Induction Generators," *IEEE Transactions on Sustainable Energy*, vol. 2, no. 3, pp. 215-225, July 2011.

[55] H. De Battista and R. J. Mantz, "Dynamical variable structure controller for power regulation of wind energy conversion systems," *IEEE Transactions on Energy Conversion*, vol. 19, no. 4, pp. 756-763, December 2004.

[56] L. Ran, D. Xiang, and J. L. Kirtley, "Analysis of Electromechanical Interactions in a Flywheel System with a Doubly Fed Induction Machine," in *Annual Meeting of IEEE Industry Applications Society (IAS 2010),* 2010, pp.1-8, Houston, 3-7th October 2010.

[57] P. Krause, O. Wasynczuk and S. D. Sudhoff, Analysis of Electric Machinery and Drive Systems, IEEE Press, Wiley-Interscience, John Wiley & Sons, Inc., New Jersey, 2002.

[58] R. V. Dukkipati and J. Srinivas, Textbook of Mechanical Vibrations, Prentice-Hall, New Delhi 2004.

[59] C. Lalanne, Mechanical Vibrations and Shock: Sinusoidal Vibration, CRC Press, March 2002.

[60] S. M. Muyeen, J. Tamura, and T. Murata, Stability Augumentation of a Grid-connected Wind Farm, Springer 2009.

[61] B. Friedland, Control System Design, An Introduction to State-Space Methods, Mc Graw – Hill, New York, 1995.

[62] K. Ogata, Modern Control Engineering, 2nd Ed., Prentice-Hall, London, 1990.

[63] N. P. Soe, D. M. Vilathgamuwa, and K.-S. Low, "Doubly Fed Induction Generator for wind energy generation using Nine-switch power converter," Pro*ceedings of 37th Annual Conference on Industrial Electronics Society* , pp. 3608-3613, 7-10 November 2011.

[64] M. Heydari, A. Y. Varjani, M. Mohamadian, and H. Zahedi, "A novel variable-speed wind energy system using permanent-magnet synchronous generator and Nine-switch AC/AC converter," Pro*ceedings IEEE 2nd Power Electronics, Drive Systems and Technologies Conference (PEDSTC 2011),* pp.5-9, 16-17 February 2011.

[65] E. C. dos Santos, C. B. Jacobina, and O. I. da Silva, "Six-phase machine drive system with Nine-switch converter," Pro*ceedings IEEE 37th Annual Conference on Industrial Electronics Society*, pp. 4204-4209, 7-10 November. 2011.

[66] F. Gao, L. Zhang, D. Li, P. C. Loh , Y. Tang, and H. Gao, "Optimal Pulsewidth Modulation of Nine-Switch Converter," *IEEE Transactions on Power Electronics*, vol. 25, no. 9, pp. 2331-2343, September 2010.

[67] S. M. D. Dehnavi, M. Mohamadian, A. Yazdian, and F. Ashrafzadeh, "Space Vectors Modulation for Nine-Switch Converters," *IEEE Transactions on Power Electronics*, vol. 25, no. 6, pp. 1488-1496, June 2010.

[68] S. M. Dehghan, M. Mohamadian, and M. A. E. Andersen, "Full space vectors modulation for Nine-switch converters including CF & DF modes," Proceedings IEEE 4th International Conference on Power Engineering and Optimization (PEOCO 2010), pp. 89-94, 23-24 June 2010.

[69] O. Ojo, "The generalized discontinuous PWM scheme for three-phase voltage source inverters," *IEEE Transactions on Industrial Electronics*, vol. 51, no. 6, pp. 1280- 1289, December 2004.

[70] D. G. Holmes and T.A. Lipo, Pulse Width Modulation for Power Converters: Principles and Practice (IEEE PressSeries on Power Engineering), Wiley-IEEE Press, 2003.

[71] A. M. Hava, R. J. Kerkman, and T. A. Lipo, "A high-performance generalized discontinuous PWM algorithm," *IEEE Transactions on Industry Applications*, vol. 34, no. 5, pp. 1059-1071, September/October 1998.

[72] H. Li and Z. Chen, "Transient Stability Analysis of Wind Turbines with Induction Generators Considering Blades and Shaft Flexibility," in 33rd Annual conference IEEE Industrial Electronics Society (IECON 2007), pp. 1604-1609, 5-8 November 2007.

[73] T. Noguchi, H. Tomiki, S. Kondo, and I. Takahashi, "Direct power control of PWM converter without power-source voltage sensors," *IEEE Transactions on Industry Applications*, vol. 34, no. 3, pp. 473-479, May/June 1998.

[74] J. Arbi, M. J.-B. Ghorbal, I. Slama-Belkhodja, and L. Charaabi, "Direct virtual torque control for doubly fed induction generator grid connection," *IEEE Transactions on Industrial Electronics*, vol. 56, no. 10, pp. 4163-4173, October. 2009.

[75] L. Xu and P. Cartwright, "Direct active and reactive power control of DFIG for wind energy generation," *IEEE Transactions on Energy Conversion*, vol. 21, no. 3, pp. 750–758, September 2006.

[76] R. Pena, J. C. Clare, and G. M. Asher, "Doubly fed induction generator using back-to-back PWM converters and its application to variable-speed wind-energy

generation," in *IEEE Proceedings on Electric Power Applications*, vol. 143, no. 3, pp. 231-341, May 1996.

[77]   Z. Wang, G.-J Li, Y. Sun, and B. T. Ooi, "Effect of Erroneous Position Measurements in Vector-Controlled Doubly Fed Induction Generator," *IEEE Transactions on Energy Conversion*, vol. 25, no. 1, pp. 59-69,March 2010.

[78]   M. S. Carmeli, F. Castelli-Dezza, M. Iacchetti, and R. Perini, "Effects of Mismatched Parameters in MRAS Sensorless Doubly Fed Induction Machine Drives," *IEEE Transactions on Power Electronics*, vol. 25, no. 11, pp. 2842-2851, November 2010.

[79]   S. Bolognani, L. Peretti, and M. Zigliotto, "Parameter Sensitivity Analysis of an Improved Open-Loop Speed Estimate for Induction Motor Drives," *IEEE Transactions on Power Electronics*, vol. 23, no. 4, pp. 2127-2135 ,July 2008.

[80]   C. Fitzer, M. Barnes, P. Green, "Voltage sag detection technique for a dynamic voltage restorer," *IEEE Transactions on Industry Applications*, vol. 40, no. 1, pp. 203-212, January-February 2004.

[81]   M. J. Newman, D. G. Holmes, J. G. Nielsen, and F. Blaabjerg, "A dynamic voltage restorer (DVR) with selective harmonic compensation at medium voltage level," *IEEE Transactions on Industry Applications*, vol. 41, no. 6, pp. 1744-1753, November-December 2005.

[82]   E. Babaei, M. F. Kangarlu, and M. Sabahi, "Mitigation of Voltage Disturbances Using Dynamic Voltage Restorer Based on Direct Converters," *IEEE Transactions on Power Delivery*, vol. 25, no. 4, pp. 2676-2683, October 2010.

[83]   J. G. Nielsen, F. Blaabjerg, "A detailed comparison of system topologies for dynamic voltage restorers," *IEEE Transactions on Industry Applications*, vol. 41, no. 5, pp. 1272-1280, September-October 2005.

[84]   F. Badrkhani S. Ajaei, S. Afsharnia, A. Kahrobaeian, and S. Farhangi, "A Fast and Effective Control Scheme for the Dynamic Voltage Restorer," *IEEE Transactions on Power Delivery*, vol. 26, no. 4, pp. 239-2406, October 2011.

[85]   F. B. Ajaei, S. Farhangi, and R. Iravani, "Fault Current Interruption by the Dynamic Voltage Restorer," *IEEE Transactions on Power Delivery*, vol. 28, no. 2, pp. 903-910, April 2013.

[86]   D. M. Vilathgamuwa, A. A. D. R. Perera, S. S. Choi, "Voltage sag compensation with energy optimized dynamic voltage restorer," *IEEE Transactions on Power Delivery*, vol. 18, no. 3, pp. 928-936, July 2003.

[87]   D. Ramirez, S. Martinez, C. A. Platero, F. Blazquez, and R. M. de Castro, "Low-Voltage Ride-Through Capability for Wind Generators Based on Dynamic Voltage Restorers," *IEEE Transactions on Energy Conversion*, vol. 26, no. 1, pp. 195-203, March 2011.

[88]   J.-W. G. Hwang, M. Winkelnkemper, and P. W. Lehn, "Design of an optimal stationary frame controller for grid connected ac-dc converters," Pro*ceedings. 32nd Annual Conference of IEEE Industrial Electronics Society*, France, November 2006, pp. 167–172.

[89]   D. N. Zmood, D. G. Holmes, and G. H. Bode, "Frequency-domain analysis of three-phase linear current regulators," *IEEE Transactions Industry Applications*, vol. 37, no. 2, pp. 601–610, March/April 2001.

[90]   D. N. Zmood and D. G. Holmes, "Stationary frame current regulation of PWM inverters with zero steady-state error," *IEEE Transactions Power Electronics*, vol. 18, no. 3, pp. 814–822, May 2003.

[91]   X. Yuan, W. Merk, H. Stemmler, and J. Allmeling, "Stationary-frame generalized integrators for current control of active power filters with zero steady-state error for current harmonics of concern under unbalanced and distorted operating conditions," *IEEE Transactions on Industry Applications*, vol. 38, no. 2, pp. 523–532, March/April 2002.

[92]   B. A. Francis and W. M. Wonham, "The internal model principle for linear multivariable regulators," Applied Mathematics and Optimization, vol. 2, no. 2, pp. 170–194, 1975.

[93]   F. Blaabjerg, R. Teodorescu, M. Liserre, and A. V. Timbus, "Overview of control and grid synchronization for distributed power generation systems," *IEEE Transactions on Industrial Electronics*, vol. 53, no. 5, pp. 1398–1409,October 2006.

[94]   J. G. Hwang, P. W. Lehn, and M. Winkelnkemper, "Control of gridconnected ac-dc converters with minimized dc link capacitance under unbalanced grid voltage condition," Pro*ceedings. IEEE European Conference on Power Electronics and Applications*, Aalborg, September 2007, pp. 1–10.

[95]   S. Z. Chen, N. C. Cheung, K. C.Wong, and J.Wu, "Integral sliding mode direct torque control of doubly-fed induction generators under unbalanced grid voltage," *IEEE Transactions on Energy Conversion*, vol. 25, no. 2, pp. 356–368, Jun. 2010.

[96]   D. Roiu, R.I. Bojoi, L.R. Limongi, and A. Tenconi, "New Stationary Frame Control Scheme for Three-Phase PWM Rectifiers Under Unbalanced Voltage Dips Conditions," *IEEE Transactions on Industry Applications*, vol. 46, no. 1, pp. 268-277, January-February 2010.

[97] Y. Suh and T. A. Lipo, "Control scheme in hybrid synchronous stationary frame for PWM AC/DC converter under generalized unbalanced operating conditions," *IEEE Transactions Industry Applications*, vol. 42, no. 3, pp. 825–835, May/June. 2006.

[98] J. Svensson, M. Bongiorno, and A. Sannino, "Practical Implementation of Delayed Signal Cancellation Method for Phase-Sequence Separation," *IEEE Transactions on Power Delivery*, vol. 22, no. 1, pp. 18,26, January 2007.

[99] F. Casanellas, "Losses in PWM inverters using IGBTs," *IEE Proceedings in Electric Power Applications*, vol. 141, no. 5, pp. 235-239, 1994.

[100] P. M. Kshirsagar, "PWM Strategies in Power Converters," M.S., Tennessee Technological University, Cookeville, 2003.

[101] J. Hu and Y. He, "Reinforced Control and Operation of DFIG-Based Wind-Power-Generation System Under Unbalanced Grid Voltage Conditions," IEEE Energy Conversion, IEEE Transactions on, vol.24, no.4, pp.905-915, Dec. 2009.

[102] Jiabing Hu, Hailiang Xu, Yikang He, "Coordinated Control of DFIG's RSC and GSC Under Generalized Unbalanced and Distorted Grid Voltage Conditions" IEEE Transactions on Industrial Electronics, vol. 60, no. 7, pp. 2808-2819, July 2013.

[103] J. Yao, H. Li, Z. Chen, X. Xia, X. Chen, Q. Li, and Y. Liao, "Enhanced Control of a DFIG-Based Wind-Power Generation System With Series Grid-Side Converter Under Unbalanced Grid Voltage Conditions," *IEEE Transactions on Power Electronics*, vol. 28, no. 7, pp. 3167-3181, July 2013.

[104] Y. Yan, M. Wang, Z.-F. Song, and C.-L. Xia, "Proportional-Resonant Control of Doubly-Fed Induction Generator Wind Turbines for Low-Voltage Ride-Through Enhancement," *Energies* vol. 5, no. 11, pp. 4758-4778, 2012.

[105] L. Harnefors and H-P. Lennart, "Model-based current control of AC machines using the internal model control method," *IEEE Transactions on Industry Applications* , vol. 34, no. 1, pp. 133-141, January/February 1998.

[106] N. O. Cetin and A. M. Hava, "Topology and PWM method dependency of high frequency leakage current characteristics of voltage source inverter driven AC motor drives," in *IEEE Energy Conversion Congress and Exposition (ECCE 2012)* , pp. 3430-3437, 15-20 September 2012.

APPENDIX

APPENDIX

A1. 5 hp wound rotor induction machine and 5hp DC machine

A 5 hp DC machine fed by a 3-phase diode bridge rectifier with a separated field winding also fed by a 3-phase diode rectifier is mechanically coupled to the induction machine as shown in Figure A1. Wind data of turbine torque and speed can be emulated and used as reference values to control the DC motor. The parameters of the two machines are given below.

Table A1: Induction Machine Parameters

5hp, 60Hz, 220–V line-line (rms), 6 pole wound-rotor	
Stator resistance (r_s)	4.24 Ω
Rotor referred resistance (r_r)	6.38 Ω
Stator leakage inductance (X_s)	44.05 Ω
Rotor referred leakage inductance (X_r)	42.02 Ω
Magnetizing inductance (X_m)	39.89 Ω

Table A2: Wind Turbine Parameters

Rated power ($P_{m,rated}$)	2238 W
Air density (ρ)	1.225 kg/m^3
Moment of inertia (J)	0.089 kgm^2
Blade radius (R)	1.25 m
Rated wind speed	12 m/s

The turbine power coefficient, C_p, has the following constants:
$c_1 = 0.5175$, $c_2 = 116$, $c_3 = 0.4$, $c_4 = 5$, $c_5 = 21$, $c_6 = 0.0068$, $c_7 = 0.08$, and $c_8 = 0.035$.

Table A3: Parameters of 2 MW DFIG for simulation

Parameters	Values
P_{rated}	2 WM
V_{base}(line-line)	690 Vrms
Z_{base}	0.231
ω_{base}	2π60
Stator leakage inductance	0.068 mH
Rotor leakage inductance	0.043 mH
Mutual Inductance	1.55 mH
Stator resistance	0.74 mΩ
Rotor resistance	0.74 mΩ
Series grid side filter inductance	0.030 mH
parallel grid side filter inductance	0.030 mH
dc-bus voltage	1100 V
dc-bus capacitor	25 mF

Table A4: Parameters of 2 MW wind turbine for simulation

Parameters	Values
P_{rated}	2 WM
Cut-in wind speed	3 m/s
Cut-out wind speed	25 m/s
Nominal wind speed	11 m/s
Gearbox ratio	80
Blade radius	44.18 m
Optimal power coefficient	0.4
Optimal tip speed ratio	8.0

VITA

Kennedy Adinbo Aganah was born in Kintampo, Brong-Ahafo Region of Ghana. He received his BSc. Mechanical Engineering from the Kwmae Nkrumah University of Science and Technoogy, Kumasi, Ghana, in 2002. He went on to graduate from Tuskegee University, Tuskegee Alabama with a Master of Science in Electrical Engineering in 2009. In the Fall of 2009, he joined Tennessee Technological University and is a candidate for Doctor of Philosophy in Engineering concentrating in Electrical Engineering.